Functional analysis of polyubiquitin chain linkage in genome maintenance

by

Tina Strauch
born 18.06.1993 in Gelnhausen

Dissertation

submitted for the degree of

Doctor of Natural Sciences (Dr. rer. nat.)

Institute of Molecular Biology

Department of Biology

Johannes Gutenberg University, Mainz

May 2024

Dean: Prof. Dr. Eckhard Thines

First Examiner:

Second Examiner:

Day of oral exam: 19.07.2024

Declaration

I, Tina Strauch, matriculation number 2710552, declare that the work presented in this thesis is my own. I confirm that any information or data that has been derived from other sources, either literally or analogously, are referred to and correctly cited in the thesis and that I have not used any sources or aids other than those specified. Finally, I declare that this work was not yet part of a study or examination in the same or a similar version.

_____ _____

(Place, date) (Signature)

Abstract

Ubiquitin is a small post-translational modifier involved in almost all cellular processes in eukaryotes. The versatility of ubiquitin as a signaling molecule derives mainly from its ability to form ubiquitin chains of varying topologies. This work was set up to deepen our knowledge of the so far poorly understood function-topology relationship of different ubiquitin linkages. Thereby, we focused on the two most studied linkages, K48 and K63, and their biological involvement. The first project of this thesis describes the characterization of a tool to study these specific ubiquitin chains, while the second project focuses on deciphering the role of a specific K63-linked ubiquitin chain in DNA damage bypass by investigating a potential reader of this specific ubiquitin code.

The first project "Specific binders for recognition, inhibition, and tracking of K48- and K63-polyubiquitin chain signaling" describes the design and characterization of specific affinity probes on the basis of designed ankyrin repeat proteins (DARPins) for the recognition, inhibition, or tracking of linkage-specific polyubiquitin signals for the two most extensively studied linkages, K48 and K63, *in vitro* and *in vivo*. DARPins are high-affinity binders that can, in contrast to conventional antibodies, be used *in vivo* due to their small size and simple structure. They were raised against K48- and K63-linked ubiquitin dimers from a library with randomized target interaction residues by our collaboration partners from the Plückthun group (University of Zürich). A screen of all hits yielded a panel of highly selective DARPins, which were characterized with respect to their selectivity and inhibitory effects on cell growth and (de-)ubiquitylation. The most suitable candidate per linkage was further investigated and compared to the commercially available TUBE (tandem-ubiquitin binding entities) with regard to their specificity and affinity. Crystal structures revealed their binding modes, explaining their properties. The anti-K48 and anti-K63 DARPins are suitable for diverse pull-down applications and retain their selectivity *in vivo* as demonstrated by mass spectrometry and co-localization with respective antibodies. Tagged with a fluorophore, these DARPins can be used as biological sensors to specifically track K48- and K63-polyubiquitin chains *in vivo*, enabling the monitoring of the dynamics and localization of specific ubiquitin conjugates in various pathways, including their involvement in aggresome formation and the DNA damage response. A combination of both linkage-specific DARPins yielded a K48-K63-branched ubiquitin chain sensor, which demonstrated its specificity *in vitro* and showed potential as a biosensor for *in vivo* applications.

The second part, entitled "Mechanistic analysis of the function of polyubiquitin chains in Exo1 recruitment for DNA damage bypass," endeavors to address the long-standing unresolved question of how the specific K63-linked ubiquitin chain on the Proliferating cell nuclear antigen (PCNA) initiates the DNA damage bypass pathway of template switching (TS). TS is the error-free pathway of the DNA damage bypass, which is critical to ensure complete and accurate duplication of the genome through DNA replication, thereby maintaining genome stability and avoiding potential carcinogenesis. TS and the K63-linked ubiquitylation as a starting signal have been known for approximately 20 years, yet no specific reader has been identified. We hypothesize that this reader could be the exonuclease Exo1, which has already been shown to be crucial for the TS pathway. Therefore, we investigated its direct interaction with PCNA and its ubiquitylated forms. A PCNA interaction motif in Exo1 was identified and characterized. We also set out to identify a ubiquitin binding domain by creating and analyzing the point mutants of a putative domain. Furthermore, the biological relevance of both motifs was studied to ascertain their involvement in the TS pathway.

Zusammenfassung

Ubiquitin ist eine posttranslationale Modifikation, die für zahlreiche Stoffwechselwege essentiell ist und daher fast alle zellulären Prozesse in Eukaryoten beeinflusst. Die Vielseitigkeit von Ubiquitin als Signalmolekül ergibt sich vor allem aus seiner Fähigkeit, Ubiquitinketten unterschiedlicher Topologien zu bilden. Ziel dieser Arbeit war es, unser Wissen über die bisher nur unzureichend verstandene Funktions-Topologie-Beziehung verschiedener Ubiquitin-Ketten zu erweitern. Der Schwerpunkt lag dabei auf den beiden am besten untersuchten Verknüpfungen, K48 und K63, und ihren biologischen Auswirkungen. Das erste Projekt dieser Arbeit beschreibt die Charakterisierung eines *tools* zur Untersuchung dieser spezifischen Ubiquitinketten, während sich das zweite Projekt auf die Entschlüsselung der Rolle einer spezifischen K63-verknüpften Ubiquitinkette im Prozess des *DNA damage bypass* konzentriert, indem ein potenzieller Leser dieses spezifischen Ubiquitin-Codes untersucht wird.

Das erste Projekt mit dem Titel „Spezifische Binder für die Detektion, Inhibition und Nachverfolgung von K48- und K63-Polyubiquitinketten-Signalen“ beschreibt die Entwicklung und Charakterisierung spezifischer Affinitätssonden für die Detektion, Inhibition und Nachverfolgung von spezifisch verlinkten Polyubiquitin-Signalen für die beiden am besten untersuchten Verknüpfungen K48 und K63, *in vitro* und *in vivo*. Die Sonden basieren auf designten Ankyrin-Repeat-Proteinen (DARPins) und können im Gegensatz zu herkömmlichen Antikörpern aufgrund ihrer geringen Größe und einfachen Struktur *in vivo* eingesetzt werden. Die DARPins wurden von unseren Kooperationspartnern aus dem Plückthun-Labor (Universität Zürich) gegen K48- und K63-verknüpfte Ubiquitindimere selektioniert. Eine Vorauswahl aller Kandidaten ergab eine Auswahl hochselektiver DARPins wurde im Hinblick auf ihre Selektivität und ihre Auswirkung auf das Zellwachstum und die (De-)Ubiquitinierungsreaktion charakterisiert. Der jeweils am besten geeignete Kandidat wurde näher untersucht und mit dem kommerziell erhältlichen TUBE (Tandem-Ubiquitin-Bindungseinheiten) hinsichtlich ihrer Spezifität und Affinität verglichen. Kristallstrukturen enthüllten die Bindungsmodi der DARPins und erklärten ihre Selektivität und *in vitro*-Eigenschaften. Die anti-K48- und anti-K63-DARPins eignen sich für verschiedene Pull-down-Anwendungen und können ihre Selektivität auch *in vivo* aufrechterhalten, wie durch Massenspektrometrie und Co-Lokalisierung mit den entsprechenden Antikörpern demonstriert werden konnte. Wenn diese Binder mit einem geeigneten Fluorophor kombiniert werden, können sie spezifisch K48- und K63-Polyubiquitinketten *in vivo* verfolgen. Dies ermöglicht die Überwachung der Lokalisierung und Dynamik der Ubiquitin-Signalübertragung in verschiedenen Prozessen, einschließlich ihrer Beteiligung an der Aggresombildung und der DNA-Schadensreparatur. Eine Kombination der beiden spezifischen DARPin ergab einen K48-K63-verzweigten Ubiquitin-Ketten-Sensor, der seine Spezifität *in vitro* unter Beweis stellte und als Grundlage für einen Biosensor für den *in vivo*-Einsatz geeignet ist.

Der zweite Teil mit dem Titel „Mechanistische Analyse der Funktion von Polyubiquitinketten bei der Rekrutierung von Exo1 im Pozess des *DNA damage bypass*“ befasst sich mit der seit langem ungelösten Frage, wie die spezifische K63-verknüpften Ubiquitinkette auf dem DNA-Ringklemmenprotein PCNA den *DNA damage bypass*-Signalweg des *template switching* (TS) einleitet. TS gilt als der fehlerfreie Signalweg des *DNA damage bypasses*, der für die vollständige und korrekte Vervielfältigung des Genoms durch DNA-Replikation von entscheidender Bedeutung ist. Dies stellt die Aufrechterhaltung der Genomstabilität sicher und vermeidet damit potenzielle Krebsentstehung. Obwohl TS und die K63-verknüpfte Ubiquitylierung als Startsignal etwa 20 Jahren bekannt sind, wurde bisher kein spezifischer Leser dieser Modifikation identifiziert. Wir stellen die Hypothese auf, dass es sich bei diesem Leser um die Exonuklease Exo1 handeln könnte, die sich bereits als entscheidend für den TS-Weg erwiesen hat. Daher haben wir ihre direkte Interaktion mit PCNA und ihren ubiquitylierten Formen untersucht. Es wurde ein PCNA-Interaktionsmotiv in Exo1 identifiziert und charakterisiert. Außerdem haben wir versucht, eine Ubiquitin-Binde-Domäne zu identifizieren, indem wir Punktmutanten einer mutmaßlichen Domäne erzeugten und analysierten. Darüber hinaus wurde die biologische Relevanz beider Motive untersucht, um ihre Beteiligung am TS-Signalweg zu ermitteln.

List of Content

List of Figures

List of Tables

List of Abbreviations

53BP1	p53-binding protein 1
AAD	Active adenylation domain
AMD	Age-related macular degeneration
Amp	Ampicillin
AMPK	AMP activated protein kinase
AMSH	Associated molecule with the SH3 domain of STAM
AP	Apurinic/Apyrimidinic (Abasic) site
APC	Anaphase-promoting complex
APE1	AP-endonuclease1
AQUA	Absolute quantification employing labeled ubiquitin standards
ATR	Ataxia Telangiectasia and Rad3 Related
BER	Base excision repair
BiFC	Bimolecular fluorescence complementation
BRCA1	Breast cancer 1
BRET	Bioluminescence resonance energy transfer
CDK	Cyclin-dependent kinases
Cm	Chloramphenicol
CUE	Coupling of ubiquitin conjugation to ER degradation
CV	Column volumes
DARPins	Designed ankyrin repeat proteins
DDR	DNA damage response
DDT	DNA damage tolerance
DIC	Differential Interference Contrast
DME	Diabetic macular edema
DMEM	Dulbecco's Modified Eagle Medium
DSB	DNA double-strand breaks
DUB	Deubiquitylases
DUIM	Double-sided ubiquitin-interacting motif
E1	Ubiquitin-activating enzyme
E2	Ubiquitin-conjugating enzyme
E3	Ubiquitin protein ligase
EGFR	Epidermal Growth Factor Receptor
EM	Electron microscopy
ER	Endoplasmic reticulum
F3H	Fluorescent three-hybrid
FA	Fanconi anemia
FBS	Fetal bovine serum
FCCH	First catalytic cysteine half-domains
FEN1	Flap-endonuclease 1
FRET	Förster resonance energy transfer
GAT	GGA and Tom1
Gen	Gentamycin
GFP	Green fluorescent protein
GLUE	Gramlike ubiquitin-binding in Eap45
GMP	Good Manufacturing Practice

HDR	Homology-directed repair
HECT	Homology to E6AP C-Terminus
HER2	Human epidermal growth factor receptor 2
HGF	Hepatocyte growth factor
Hip	Huntingtin interacting protein
HR	Homologous recombination
hTERT	Human telomerase reverse transcriptase subunit
HU	Hydroxyurea
HUWE1	HECT, UBA And WWE Domain Containing E3 Ubiquitin Protein Ligase 1
IBR	In-between RING
ICH	Immunohistochemistry
ICLs	Interstrand crosslinks
IMAC	Immobilized Metal Affinity Chromatography
IMB	Institute of Molecular Biology
IP	Immunoprecipitation
IR	Ionizing radiation
Kann	Kanamycin
LB	Lysogeny Broth
LDS	Lithium dodecyl sulfate
LIG3	DNA ligase 3
LLPS	Liquid-liquid phase seperation
LRR	Leucine-rich repeats
LUBAC	Linear ubiquitin chain assembly complex
MC	Mammalian cells
MIU/IUIM	Motif interacting with ubiquitin
MJD	Machado-Josephin domain
MMR	Mismatch repair
MS	Mass spectrometry
MVB	Multivesicular bodies
NC	Nitrocellulose
NEDD8	Neural-precursor-cell-expressed developmentally down-regulated 8
NEM	N-ethylmaleimide
NEMO	NF-κB essential modulator
NER	Nucleotide excision repair
NHEJ	Non-homologous end joining
NZF	Nuclear protein localization 4 zinc finger
OMM	Outer mitochondrial membrane
OPA	Ortho-phthalaldehyde
OTU	Ovarian tumor domain-containing proteases
PAHs	Polycyclic aromatic hydrocarbons
PAXX	Paralogue of XRCC4 and XLF
PBS	Phosphate buffered saline
PCNA	Proliferating cell nuclear antigen
PD	Pull-down
pEA	Predicted alignment error
PFA	Paraformaldehyde
PFU	PLAA family ubiquitin binding domain

PIP	PCNA-interacting protein
PIP3	Phosphatidylinositol(3)-phosphate
PLA	Proximity ligation assay
POI	Protein of interest
PORTs	Post-replicative repair territories
PPCF	Protein production core facility
PRA	Replication protein A
PRU	Pleckstrin-like receptor for ubiquitin
PTM	Post-translational modifications
RAD23B	UV excision repair protein Radiation sensitive 23B
RAP80	Receptor-associated protein 80
RBR	RING-between-RING
RFC	Replication factor C
RFU	Relative fluorescence units
RING	Really Interesting New Gene
RNF168	RING finger protein 168
RNF8	RING finger protein 8
ROS	Reactive oxygen species
RPMI	Roswell Park Memorial Institute
RT	Room temperature
SC	Synthetic complete
SCCH	Second catalytic cysteine half-domains
Sgs	Slow Growth Suppressor
SILAC	Stable isotope labeling by amino acids in cell culture
SIM	SUMO interaction motif
Smurf1	Smad ubiquitylation regulatory factor 1
SPR	Surface plasmon resonance
Srs2	Suppressor of Rad6 2
SSB	Single-strand breaks
SUMO	Small ubiquitin-like modifier
TAK1	TGFβ-activated kinase 1
TB	Tank blot
TBK1	TANK-binding kinase 1
TCA	Trichloroacetic acid
TLS	Translesion synthesis
TM	Transmembrane domain
TMT	Tandem mass tag
TS	Template switching
TUBE	Tandem-repeated ubiquitin binding entities
tUIM	Tandem ubiquitin-binding motifs
TXNIP	Thioredoxin interacting protein
U7BR	Ubc7 binding region
Ub	Ubiquitin
UBA	Ubiquitin-associated domain
UBAN	Ubiquitin binding in ABIN and NEMO
UBC	Ubiquitin-conjugating enzyme
UBD	Ubiquitin binding domain
UbI	Ubiquitin-like proteins

UbiCRest	Ubiquitin Chain Restriction
UBM	SH3, ubiquitin-binding motif
Ub-PSAQ	Ubiquitin-Protein standard absolute quantification
UBZ	Ubiquitin-binding zinc finger
UCH	ubiquitin C-terminal hydrolases
UEV	Ubiquitin E2 variant
UFD	Ubiquitin fusion degradation
UiFC	Ubiquitination-induced fluorescence complementation
UIM	Ubiquitin-interacting motif
UPS	Ubiquitin-proteasome system
VEGF	Vascular endothelial growth factor
VHS	Vps27/Hrs/STAM
VPS27	Vacuolar protein sorting-associated protein 27
XP	Xeroderma Pigmentosum
XRCC	X-ray repair cross-complementing protein
Y2H	Yeast two-hybrid
YFP	Yellow fluorescent protein
YP	Yeast Peptone
ZnF A20	Zinc finger in A20 protein
ZnF UBP	Zinc finger ubiquitin-binding protein
ZUP1	Zinc finger with UFM1-specific peptidase domain

1 Introduction

1.1 The ubiquitin system

1.1.1 The post-translational modifier ubiquitin

Proteins control all biological functions within a cell. In eukaryotes, almost all proteins undergo post-translational modifications (PTMs), which strongly increase the functional diversity of the proteome. PTMs are covalent modifications of proteins that occur after protein biosynthesis. Over 400 post-translational modifications are known to occur on a protein's N- or C-terminus, or on its amino acid side chains. These modifications can alter the properties, localization or fate of the protein. PTMs enable cells to rapidly, precisely, and economically regulate protein activity in response to environmental changes, without the need for time- and energy-consuming *de novo* protein synthesis. The range of eukaryotic PTMs is very broad, including direct amino acid modifications (e.g. deamidation), structural changes such as proteolytic cleavage of regulatory subunits or the covalent addition of small inorganic and organic groups (e.g. acetylation), complex molecules (e.g. glycosylation) or even entire proteins, such as ubiquitin.[1–4]

The modification of proteins through ubiquitylation was first discovered in 1977 by Goldknopf *et al.* in the case of histones.[5] Since then, the importance of ubiquitin as a modifier and the number of pathways in which it plays a role has continued to grow. It is now known to be involved in almost all pathways of eukaryotic cell biology. Therefore, it is not surprising that dysfunctions in ubiquitin signaling have been associated with various diseases, including cancer, neurodegenerative diseases, immunological disorders, and inflammatory diseases.[6]

1.1.2 The structure and properties of ubiquitin

Ubiquitin (Ub) is an 8.6 kDa small globular protein that consists of a single polypeptide chain of 76 amino acid residues. As its name implies, it is expressed ubiquitously and is present in all eukaryotic cells. The importance of ubiquitin is highlighted by its high evolutionary conservation within species. With only three different residues, ubiquitin is almost invariant from yeast to human, leading to a sequence identity of 96%. Ubiquitin is one of the most abundant proteins in a cell, present at approximately 10^8 copies per cell, amounting to up to 5% of all proteins.[7–10]

Ubiquitin is encoded by four genes and expressed as either a polymeric linear fusion protein consisting of four or more identical ubiquitin units in a head-to-tail configuration or as single N-terminal ubiquitin moieties fused to the large or small ribosomal polypeptides L40 and S27. The precursors of ubiquitin moieties are processed into mature monomeric ubiquitin, maintaining the constant cellular pool of free ubiquitin, together with recycled ubiquitin from ubiquitin conjugates.[11–13]

The monomeric ubiquitin's secondary structure comprises a 5-stranded mixed β-sheet, a short 3_{10}-helix, and a 3.5-turn α-helix. This forms a compact, hydrophobic β-grasp fold, except for a flexible six-residue C-terminal tail (Figure 1.1A). This tail contains the canonical conjugation motif LRGG, which is essential for the covalent linkage to target proteins. A group of proteins that share the β-grasp fold are commonly known as ubiquitin-like proteins (UbL). The two most extensively studied members of this group are NEDD8 (neural-precursor-cell-expressed developmentally down-regulated 8) and SUMO (Small ubiquitin-like modifier).[9–11]

Ubiquitin is a stable protein that can withstand protease digestion, changes in pH, and temperature fluctuations due to its compact structure and tightly packed hydrogen bonds. The N-terminal region is tightly constrained, making it inaccessible for degradation.[11, 14]

Characteristic features of ubiquitin are its hydrophobic surface patches (Figure 1.1B), including the Ile44 patch, which is recognized by the proteasome and most ubiquitin binding domains (UDB), and consists of Leu8, Ile44, Val70, and His68. Another hydrophobic surface, centered on Ile36 and involving the two leucines Leu71 and Leu73 of the ubiquitin tail, mediates interactions between ubiquitins and serves as the recognition signal for HECT E3s.[11, 15] The hydrophobic patch Phe4, composed of Gln2, Phe4, and Thr12 residues, plays a crucial role in yeast cell division and ubiquitin-mediated protein trafficking. Furthermore, the divergence between the Phe4 patch of ubiquitin and its closest relative, Nedd8, is a critical feature of the ubiquitin surface that enables deubiquitylases to distinguish between these homologs.[16, 17] Higher eukaryotes possess a 3D motif known as the TEK box, which includes Lys6, Lys11, Thr12, Thr14, and Glu34. This motif is required *inter alli* for mitotic degradation.[18, 19]

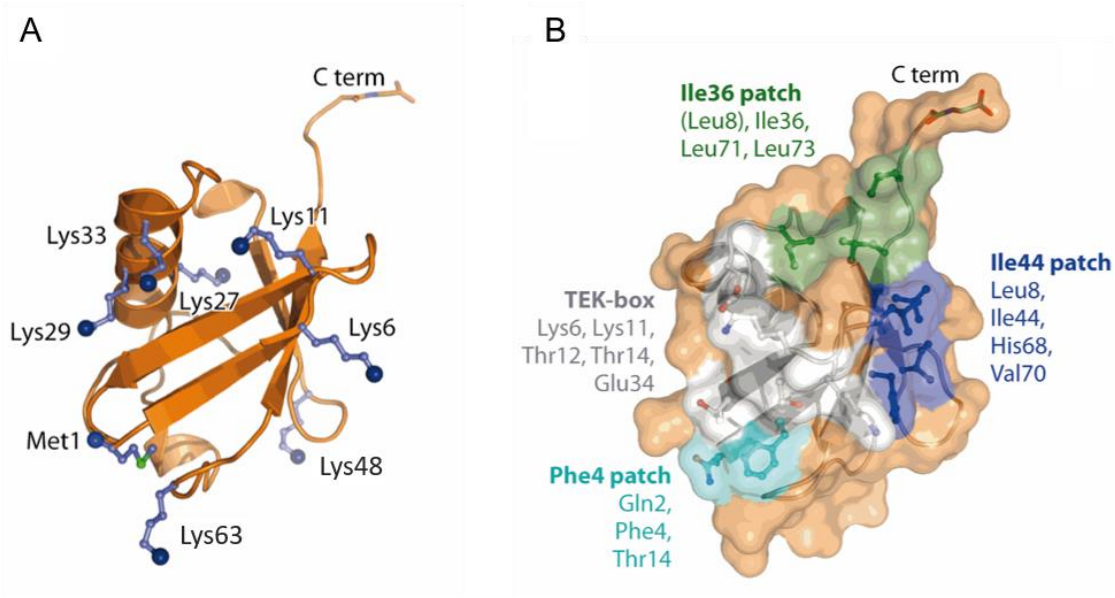

Figure 1.1: Structure of ubiquitin. (A) Structure of ubiquitin in ribbon representation (orange), indicating the C-terminal (C term) tail, and in blue, the seven Lys residues and Met1 used in ubiquitin chain formation. (B) Surface representation of ubiquitin (orange), with the hydrophobic patches: Ile44 (blue), Ile36 (green), Phe4 (cyan), and TEK-box (white) highlighted. (Figure adapted from Komander and Rape, 2012) [9]

Ubiquitin is attached to target proteins via an isopeptide bond between the glycine on the flexible C-terminus of ubiquitin and predominantly the ε-amino group of a substrate lysine residue. In recent years, there has been evidence for ubiquitylation events on other amino acids such as serine, cysteine, threonine, or N-terminal methionine.[20] Ubiquitin itself contains seven internal lysine residues and an N-terminal methionine (Figure 1.1A), which provide free amino groups. This enables ubiquitin-ubiquitin isopeptide-linkages, leading to the formation of differently linked polyubiquitin chains. All possible linkages coexist in mammalian cells. It has been demonstrated that specifically-linked ubiquitin chains activate distinct signaling pathways. This suggests that ubiquitin modification can function as a code for storing and transmitting information and therefore, can be referred to as 'ubiquitin code'.[9]

1.1.3 The ubiquitin code

There are several ways in which ubiquitin can modify a target protein. The first one is through the attachment of a single ubiquitin moiety, known as monoubiquitylation. A substrate can also carry multiple monoubiquitin moieties, referred to as multi-monoubiquitylation. Additionally, ubiquitin can be ubiquitylated itself, resulting in ubiquitin chains. These ubiquitin chains can be always linked via the same ubiquitin residue (homotypic chains) or via different residues of ubiquitin, resulting in heterogeneous mixed chains. In addition, a single ubiquitin can have multiple lysine residues ubiquitylated, resulting in branched ubiquitin chains. The diversity of ubiquitin signaling is further increased by post-translational modifications of ubiquitin itself. Thereby phosphorylation and acetylation, as well as linkages of ubiquitin to other Ubls, have been identified as regulatory mechanisms. The multifaceted ubiquitin modifications result in distinct conformations that lead to specific changes in the substrates fate and properties, provoking different cellular responses.[9, 21, 22]

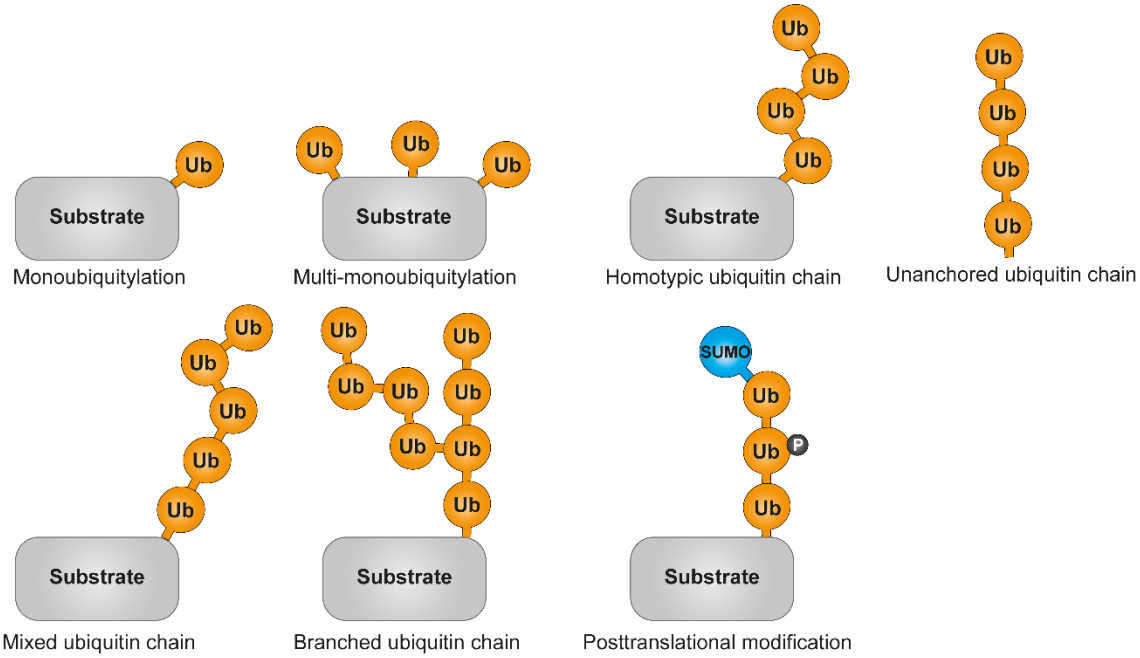

Figure 1.2: The different topologies of ubiquitylation. Different conformations of ubiquitin moieties (orange) bound to a substrate (grey) or as free chains. SUMO is depicted in blue and phosphorylation in black.

The ubiquitin system is a highly dynamic modification that is regulated by over 1,000 proteins in human cells. This large group of writers, readers, and erasers collaboratively regulate the various forms of the first layer of the ubiquitin code, resulting in a highly tunable signaling capacity.[21]

1.1.4 Writers of the ubiquitin code

The ubiquitin code is written by a cascade of enzymatic reactions known as the ubiquitylation cascade, which results in the covalent attachment of ubiquitin to the designated substrate or ubiquitin itself. This cascade comprises three classes of enzymes known as writers: a ubiquitin-activating enzyme (E1), a ubiquitin-conjugating enzyme (E2), and a ubiquitin protein ligase (E3).[9]

The initial step is ATP-dependent, whereby the Gly76 of ubiquitin is activated by adenylation at the carboxyl group (Figure 1.3). Afterwards, the active site cysteine of E1 can induce a nucleophilic attack, releasing AMP and covalently bind ubiquitin, resulting in a high-energy thioester. Subsequently, the activated ubiquitin is transferred to the active site cysteine of an E2 by transthioesterification. The next step in the ubiquitylation cascade depends on the type of E3 enzyme. There are three different classes of ubiquitin ligases: RING (Really Interesting New Gene)/U-box, HECT, and RING-between-RING (RBR). In the case of the latter two HECT/RBR E3s, ubiquitin is first transferred to the active site cysteine of the E3 via transthioesterification and then to the substrate, while for RING/U-Box E3s, ubiquitin is directly transferred from the E2 to the substrate.[23–25]

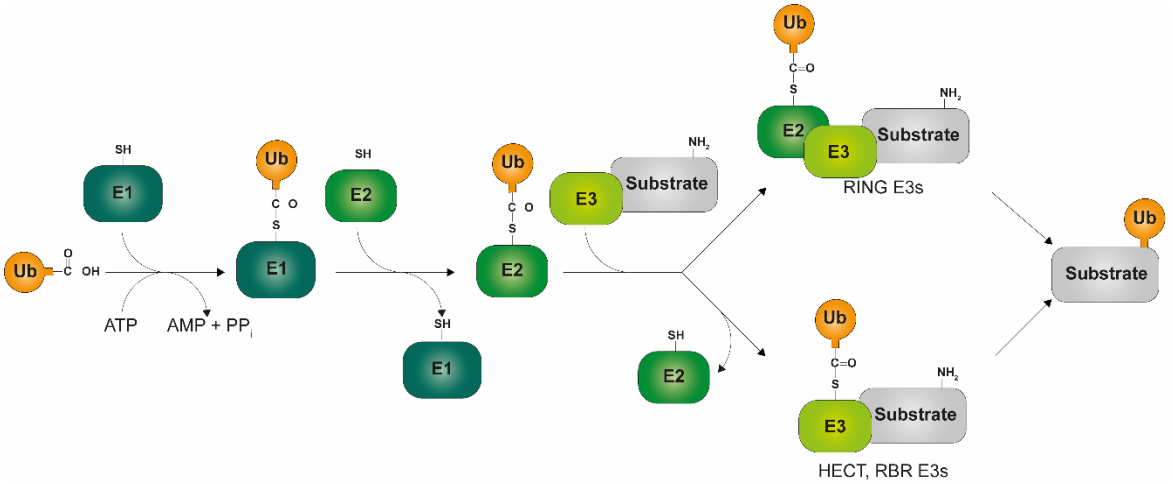

Figure 1.3: The ubiquitylation cascade. Free ubiquitin (Ub, orange) is activated in an ATP-dependent manner by the formation of a thioester linkage between E1 (dark green) and the carboxyl terminus of ubiquitin. Ubiquitin is transferred to an E2 (green), which associates with E3s (light green) subsequently. For HECT/RBR domain E3s, ubiquitin is transferred to the active-site cysteine of the E3 followed by transfer to the substrate (grey). For RING E3s ubiquitin is directly transferred from the E2 to the substrate.

The ubiquitin ligation machinery is hierarchical, with the human genome encoding two E1s (one in budding yeast), approximately 40 E2s (11 in budding yeast), and over 600 different E3s (60-100 in budding yeast).[23, 26, 27]

1.1.4.1 Ubiquitin-activating enzymes

In most species, the ubiquitylation cascade is initiated by a single E1 enzyme, which activates ubiquitin for the downstream cascade. E1 enzymes are monomeric proteins with a size of 110-120 kDa. E1 enzymes from different species exhibit a highly conserved structure and transfer mode. For instance, the sequence of human UBE1 and yeast UBA1 shows an identity of 96%.[28]

The E1 is composed of four building blocks (Figure 1.4A). The interaction between ubiquitin and the E1 occurs through the Ile44 patch of ubiquitin, which is in contact with the hydrophobic surface of the active adenylation domain (AAD), the 4HB, and the two residues Phe283 and Ala284 (Figure 1.4). Additionally, a contact side was found between the TEK box and the first and second catalytic cysteine half-domains (FCCH/SCCH). The recruitment of the positively charged E2 is mediated by the C-terminal ubiquitin fold domain (UFD), which is negatively charged.[28, 29]

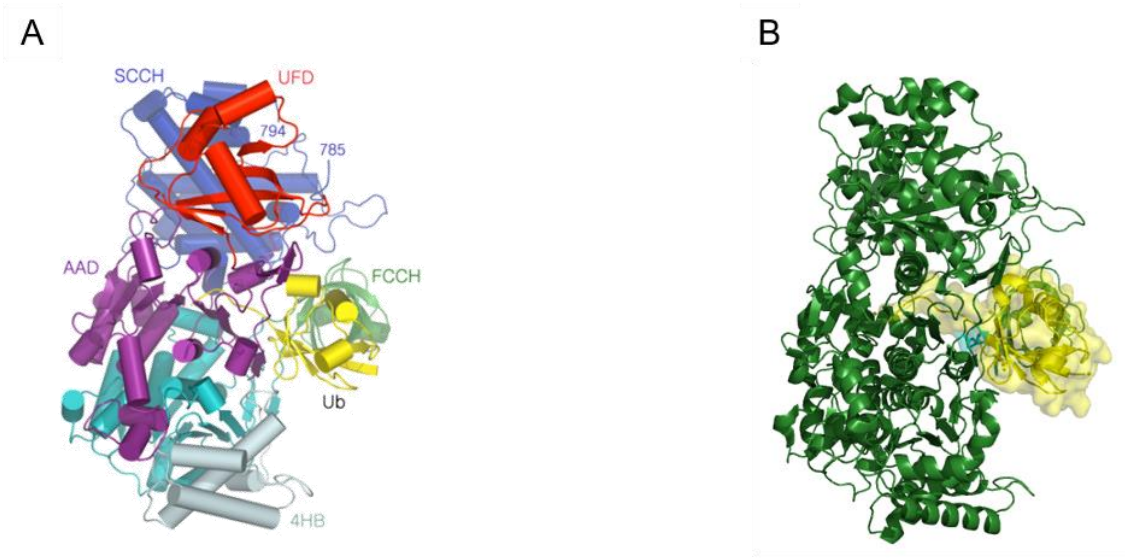

Figure 1.4: Schematic assembly of E1 UBA1 and its interaction with ubiquitin. (A) Cartoon representation of the UBA1-Ub complex with α-helices as cylinders and β-strands as curved arrows. The six domains of UBA1 are colored as follows: IDA in cyan, AAD in purple, FCCH in green, SCCH in blue, UFD in red and the 4HB domain in pale cyan. Ub is displayed in yellow. (Figure from Lee and Schindelin, 2008)[28] (B) Crystal structure showing the interaction of ubiquitin (yellow, ribbon and surface representation) with the human E1 UBA1 (dark green, ribbon representation). In cyan the residues of the Ile44 patch are marked. [PDB: 3CMM]

E1 enzymes are highly efficient, with a catalytic turnover rate of 1-2 s^{-1} for the E1-Ub formation. This allows for the production of sufficient ubiquitin for downstream reactions, despite the concentration of E1 being lower than that of the total E2 pool. The affinity between free E1 and E2 is low, but increases significantly after ubiquitin and ATP loading, with K_D values in the subnanomolar to nanomolar range. The two enzymes are only attached during the transthioesterification process, and then the affinity is lost after ubiquitin transfer, enabling one E1 to rapidly charge multiple E2s.[28, 30–32]

1.1.4.2 Ubiquitin-conjugating enzymes

In the second step of the ubiquitylation cascade, the E1 transfers the ubiquitin moiety to the active site cysteine residue of the E2. This residue is located in the highly conserved 150-200 amino acid ubiquitin-conjugating catalytic (UBC) fold domain, which contains the catalytic properties and molecular determinants of E2-interaction specificity with E1 and E3 enzymes. Additionally, certain E2 enzymes possess N- or C-terminal extensions that aid in substrate interaction or specific E3 enzyme binding. E3 binding sites frequently coincide with those of E1 to ensure the completion of one cycle before commencing the next.[33–35]

There are two types of E2 enzymes: class I E2 initiate ubiquitylation, while class II E2 elongate an existing ubiquitin chain. Some E2 enzymes, like human UBE2R1 (Cdc34), can perform both functions and initiate and elongate K48-linked ubiquitin chains. UBE2R1 is a good example of how E2 enzymes are not just simple carriers of activated ubiquitin, but also play a central role in the ubiquitin transfer process and can even determine the linkage specificity. This is true for E2 enzymes that interact with RING E3s or no E3 at all.[36–38]

The transfer of ubiquitin by E2 depends on the stability of the E2-Ub donor conjugate in the closed conformation. In this conformation, the tail of the distal ubiquitin is locked in position for the nucleophilic attack. This is achieved through contact between the hydrophobic Ile44 patch of the distal ubiquitin and the α2 helix of the E2.[39]

The E2 Ubc13 is unique in its function of exclusively generating K63-linked chains, and is used for this purpose in this work. It forms a heterodimeric ubiquitin-conjugating enzyme complex with the non-catalytic E2-like interaction partner Mms2. Mms2 stabilizes the closed conformation of Ubc13 and non-covalently binds the proximal ubiquitin on its Ile44 patch. This positions its lysine 63 in a way that faces the active site of the charged Ubc13, thereby enabling specific chain elongation.[40–43]

In this study, K48-linked ubiquitin chains were synthesized using either the E2-E3-pair Ubc7 and Cue1 or the human UBE2K.

Ubc7 is a 165 amino acid, 18.5 kDa E2 protein that plays a crucial role in ER degradation in yeast. It consists almost entirely of the conserved core domain, but additionally has an acidic loop (12-13 residues) near the active-site cysteine that interacts with the donor ubiquitin, allowing Ubc7 to synthesize ubiquitin chains without an E3. It thereby exclusively assembles K48-linked polyubiquitin chains.[44–46]

The human E2 UBE2K, also referred to as E2-25K or Huntingtin interacting protein (Hip), is a class II E2 enzyme, which preferentially synthesizes K48-linked chains on ubiquitylated substrates in the absence of an E3 enzyme. The positioning of the proximal ubiquitin is determined by residues adjacent to the active site, including the Ile44 patch. This unique feature makes UBE2K the only non-E3-dependent E2 enzyme that does not require acidic insertion or dimerization. Like its yeast homolog Ubc1, UBE2K features a C-terminal ubiquitin-associated (UBA) domain, which interacts preferably with K63-linked ubiquitin chains, indicating that UBE2K facilitates the selective assembly of K48-K63-branched ubiquitin chains.[47–49]

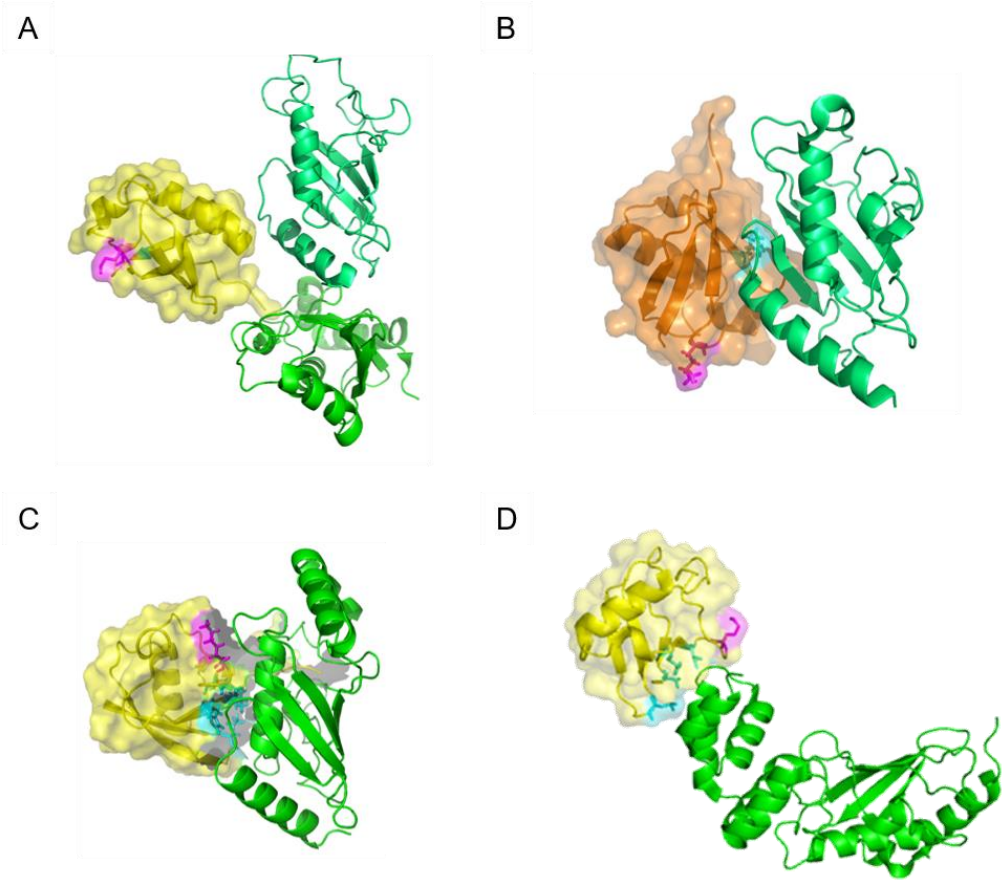

Figure 1.5: Binding of specific E2s to ubiquitin. (A) Crystal structure of Ubc13 and Mms2 (green and lime) with the distal ubiquitin. [PDB: 2GMI] (B) Crystal structure of Mms2 (lime) with the proximal ubiquitin [PDB: 1ZGU]. (C) Alpha-fold modeling of interaction between Ubc7 (green) [PDB: 2UCZ] and ubiquitin [PDB: 1UBQ]. Graph for the predicted alignment error (pAE) see Appendix Figure 6.15. (D) Crystal structure showing the interaction of UBE2K (green) and ubiquitin. [PDB: 3K9P]. In all structures the distal ubiquitin is shown in yellow, the proximal ubiquitin in orange. The Ile44 patch is marked in cyan and in magenta the K63/K48 residues are marked, respectively.

1.1.4.3 Ubiquitin protein ligases

The ubiquitin protein ligases are the largest and most diverse group in the ubiquitylation cascade. They catalyze the last step of the process by transferring ubiquitin to the substrate's amino-group, binding both the loaded E2 and the substrate. They are responsible for substrate specificity and play an essential role in determining specificity in ubiquitin-dependent signaling. The ubiquitin ligases can be classified into three main families based on their mechanism and conserved structural domains.[9, 50, 51]

The RING (Really Interesting New Gene) E3 family is the largest class of E3s, with over 600 different representatives in humans and 47 in budding yeast. These E3s lack an active site cysteine residue and mediate the direct transfer of ubiquitin from the E2 to the substrate by binding both the E2-Ub-thioester and the substrate simultaneously. Therefore, the E2 determines the linkage specificity in these cases by orienting the acceptor ubiquitin. Canonical RING domains are characterized by a conserved cross-brace zinc binding region in their N-terminus and can exist as monomers or form multimers.[51, 52] The related U-box E3 family, which includes 21 human and 2 yeast representatives identified so far, lacks the metal ion binding region, and is instead held by hydrogen bonds and salt bridges. However, it functions through a similar mechanism as the RING E3s.[50, 53, 54]

The second largest class is the HECT (Homology to E6AP C-Terminus) E3 family, consisting of approximately 30 representatives in humans and five in budding yeast. Unlike the RING E3s, HECT E3s contain an active site cysteine residue and catalyze the transfer of ubiquitin from the E2 to the HECT domain. Subsequently, a lysine residue from the substrate protein quickly attacks the HECT-Ub thioester. The 350 amino acid catalytic HECT domain contains two crucial domains: the C-lobe, which harbors the active site cysteine and determines the chain type specificity by specific interaction with the distal ubiquitin, and the approximately 250 residue N-lobe, which contains the E2 binding site.[52, 55–59]

The RBR (RING in Between RING) E3s are the smallest group of E3. They contain three domains: a RING1 connected by an in-between RING (IBR) domain to a RING-like domain. Mechanistically, RBRs are RING/HECT hybrids. They use the RING domain to recruit the ubiquitin-charged E2, but then transfer ubiquitin to the active cysteine of the RING-like domain. RBR E3s determine the linkage specificity. One prominent example is the LUBAC complex, which synthesizes M1-linked ubiquitin chains.[60–62]

For the synthesis of specifically linked K63 or K48 ubiquitin chains, the RING-finger E3 Pib1 or the Ubc7 activator Cue1 were used, respectively.

Pib1, the Phosphatidylinositol(3)-phosphate (PIP3) binding protein 1, is composed of two domains (Figure 1.6A): the FYVE domain, which binds the membrane-associated PIP3, and the E3 RING domain.[63] Our group member Renz *et al*. discovered that Pib1 selectively interacts with the heterodimeric E2 complex Ubc13/Mms2, which was previously only known to interact with the E3 Rad5 in budding yeast. This E2-E3 pair catalyzes the formation of K63-linked ubiquitin chains at internal membranes, suggesting a role for Ubc13/Mms2 in regulating membrane protein sorting. Additionally, the observation that the discharge of the Ubc13 thioester occurs preferentially onto ubiquitin but not free lysines indicates that Pib1 has a chain extension activity.[64]

The coupling of ubiquitin conjugation to the endoplasmic reticulum (ER) degradation protein 1 (Cue1) is not a ubiquitin ligase *per se*, but as part of the ERAD E3 complex, it recruits and stabilizes the K48-specific E2 Ubc7. This leads to an increased affinity of Ubc7 to its RING E3s Hrd1 and Doa10, stimulating the formation of K48-linked polyubiquitin chains.[65–67] It has also been shown to catalyze the formation of K48-linked ubiquitin chains by Ubc7 *in vitro*.[68] Cue1 contains three domains (Figure 1.6B): a transmembrane domain (TM), the C-terminal Ubc7 binding region (U7BR), and the CUE, which binds nascent K48-linked polyubiquitins. This results in the stabilization of the chain and a progressive acceleration of the elongation reaction with increasing chain length.[69]

Figure 1.6: Domain structure Pib1 (A) and Cue1 (B).[64, 69]

1.1.5 Readers of the ubiquitin code

In order for the ubiquitin code to elicit a specific effect, it must be read and translated into a cellular response. This is done by so-called readers, which include a wide variety of proteins, all of which contain at least one ubiquitin binding domain (UBD). These small domains, which range in size from 20-150 amino acids, possess diverse structures that enable them to interact with various ubiquitin topologies. They can be categorized into over 20 different families of UBDs. These were grouped into several subfamilies based on their structure and are summarized in Table 1.1. This table also contains information about the specific ubiquitin surface they interact with, the type of ubiquitin they bind, and examples of each class.[70, 71]

Table 1.1: Overview of UBDs grouped by structure. Abbreviations: mUb= monoubiquitin, pUb =polyubiquitin, UBL =ubiquitin-like domain, (>K48)= predominant binding to K48-linked pUb.[71]

Structure	UBD	Ub surface	Type of Ub binding	Examples
Single or multiple α-helix	Ubiquitin-interacting motif (UIM)	Ile44	mUb, pUb (K48, K63), UBL	S5a, VPS27, USP28
	Double-sided ubiquitin-interacting motif (DUIM)	Ile44	mUb	Hrs
	Motif interacting with ubiquitin (MIU/IUIM)	Ile44	mUb	Rabex-5
	VPS27/Hrs/STAM (VHS)	Ile44	mUb	STAM, Hrs
	Ubiquitin binding in ABIN and NEMO (UBAN)	Ile44, Phe4, linker	Met1-diUb	NEMO, optineurin, ABIN1-3
Three-helix bundle	Ubiquitin-associated (UBA) domain	Ile44	mUb, pUb (>K48), UBL	PLIC1/2, USP5, UBC1
	Coupling of ubiquitin conjugation to endoplasmic reticulum degradation (CUE)	Ile44	mUb	Cue2, VPS9
	GGA and Tom1 (GAT)	Ile44	mUb	GGA3, TOM1
Zinc fingers	Nuclear protein localization 4 zinc finger (NZF)	Ile44	mUb, pUb (K63)	Npl4, VPS36, HOIP
	Zinc finger in A20 protein (ZnF A20)	Asp58	mUb, pUb (K63)	A20, Rabex-5
	Zinc finger ubiquitin-binding protein (ZnF UBP)	Leu8, Ile36, tail	pUb (unanchored)	USP5, HDAC6, BRAP2
	Ubiquitin-binding zinc finger (UBZ)	Ile44	mUb, pUb	Polymerase η/κ, FAN1
Pleckstrin-homology fold	Gramlike ubiquitin-binding in Eap45 (GLUE)	Ile44	mUb	EAP45
	Pleckstrin-like receptor for ubiquitin (PRU)	Ile44	mUb, pUb (K48), UBL	Rpn13

Continued on next page

Table 1.1: Overview of UBDs grouped by structure.

Ubiquitin-conjugating-like structure	Ubiquitin E2 variant (UEV)	Ile44	mUb	VPS23, TSG101, Mms2
	Ubiquitin-conjugating enzyme (UBC)	Ile44	mUb	UbcH5C
Other	SH3, ubiquitin-binding motif (UBM)	Ile44	mUb	Sla1, CIN85
	PLAA family ubiquitin-binding domain (PFU)	Ile44	mUb, pUb	Doa1, PLAA
	Jab1/MPN	Ile44	mUb	Prp8p
	WD40 repeat β-propeller	Ile44	mUb	Doa1, UFD3

As Table 1.1 shows, UBDs are present in various enzymes, including the ligation machinery, DUBs, and multiple receptors. The majority of UBDs interact non-covalently with the hydrophobic patch around Ile44, making their binding to monoubiquitin mutually exclusive. This may restrain a ubiquitin signal to induce multiple processes, which could cause discordance in the cell.[15, 71]

UBDs typically have a low affinity for monoubiquitin, with K_D values in the high micromolar range.[72–74] Therefore, multiple UBDs are often present in a single protein or proteins oligomerize to enhance binding affinity and selectivity. Additionally, ubiquitin receptors typically have additional structures and features that regulate their localization, oligomerization, activity, or binding of additional UBD-containing proteins to increase the local concentrations of UBDs. A lot of UBDs were shown to bind monoubiquitin *in vitro* but interact with selective ubiquitin chains *in vivo*. The linkage specificity is achieved either by domains that specifically recognize the linker region between two ubiquitin moieties or by linkage-specific avidity.[15, 71] This avidity is achieved by detecting the spatial distribution and positioning of the individual moieties in a specifically linked ubiquitin chain. They do so by interacting with the hydrophobic patches, which are positioned differently depending on the linkage of the moieties. For example, this has been demonstrated in the case of receptor-associated protein 80 (RAP80), which contains multiple ubiquitin-interacting motifs (UIMs) that are connected by a specific linker. This linker allows for the proper positioning of the UBDs within an ubiquitin dimer that is linked via K63.[75]

1.1.6 Erasers of the ubiquitin code

Ubiquitylation is often used as a rapid response to cellular stress or changes in cell state and thus it is important to remove ubiquitin to prevent constant signaling when it is no longer needed. This is accomplished by specific proteases called deubiquitylases (DUBs), which act as antagonists to the ligation machinery. The interplay between these two competing enzymatic systems balances the ubiquitylation state of a protein and enables the highly dynamic nature of the ubiquitin system.[76, 77]

In mammalian cells, approximately 100 different DUBs are encoded (23 in *S. cerevisiae*). These can be differentiated based on their mechanism, into cysteine proteases and metalloproteases (the JAMM family). The former is the larger and better-studied group, with over 80 members, and can be broken down into six evolutionarily conserved families: the ubiquitin-specific processing proteases (USP), the ovarian tumor domain-containing proteases (OTU), the Machado-Josephin domain (MJD) DUBs, the ubiquitin C-terminal hydrolases (UCH), the MINDY domain family, as well as the recently discovered zinc finger with UFM1-specific peptidase domain (ZUP1) family, named after its founding protein member.[76–78]

All DUBs in this class of cysteine proteases utilize a catalytic triad composed of Asp-His-Cys to catalyze the hydrolysis of the ubiquitin linkages. In contrast, the metalloproteases of the JAMM family use the combination of a catalytic serine and a Zn^{2+} cofactor conjugated by two histidines.[77, 79–82] This ensures a stable pool of free ubiquitin, which is fed by two sources: activated precursor ubiquitin and recycling ubiquitin from degenerated protein. DUBs are required for both sources. The precursors UBA52, UBA80, UBB, and UBC are processed by the DUBs UCHL3, USP9X, USP7, USP5, and Otulin/Gumby/FAM105b, while ubiquitin is spared from proteasomal degradation through the action of the proteasome-associated DUBs POH1/Rpn11, USP14, and UCH37.[13, 83, 84]

DUB activity is regulated at various levels through expression, subcellular location, protein-protein interaction, or post-translational modifications. The mode of action varies between different DUBs, while some process the ubiquitin chain by gradually clipping it down from the end, others specifically cleave monoubiquitin from a particular substrate, and some cleave off the entire ubiquitin chain *en bloc*.[77, 85] Some DUBs, especially IsoT, also cleave unanchored ubiquitin chains to restore the free ubiquitin pool.[86] At least 1/3 of active DUBs exhibit some level of specificity, often for a particular linkage. Several of these linkage-specific DUBs are highly represented, such as the K48-linkage-specific OTUB1 or the M1-specific OTULIN. JAMM DUBs were shown to often prefer K63-linked ubiquitin chains, such as the associated molecule with the SH3 domain of STAM (AMSH). These linkage-specific DUBs can be used to analyze the ubiquitin chain architecture of a protein by examining the band pattern of DUB-treated samples through parallel electrophoretic analysis. This technique, known as Ubiquitin Chain Restriction (UbiCRest), also enables insights into the architecture of heterotypic chains.[76, 77, 87]

Several deubiquitinating enzymes (DUBs) have been shown to be essential for cell viability. They play a key role in critical signaling pathways, including proteasomal degradation, genome stability and immunology. DUBs are also involved in multiple diseases such as cancer and neurodegenerative diseases, making them an interesting therapeutic target. Inhibiting DUBs related to protein degradation could lead to a decreased level of the protein. However, although many small-molecule DUB inhibitors have been reported, only a few demonstrate good specificity. Therefore, it is essential to gain a better understanding of the specificity and differences of DUBs.[76, 88, 89]

As the function and binding sites of the K63-specific DUB AMSH and the K48-specific OTUB1 are important for this work they are described hereafter.

AMSH is a member of the human JAMM family that specifically cleaves K63-linked polyubiquitin chains. It consists of two parts: the C-terminal half, which contains the DUB domain, and achieves selectivity via an insertion loop that enables binding to the proximal ubiquitin when linked via K63 (Figure 1.7A), and the N-terminal half, which interacts with clathrin and proteins on the endosomes, explaining its role in endocytic cargo trafficking.[90–92]

OTUB1 is a 271-amino acid protein that belongs to the OTU family and contains their typical papain fold with the active-site cysteine (Figure 1.7B). It is a human DUB that can cleave NEDD8, but preferably cleaves K48-linked ubiquitin chains. OTUB1 functions in immune response, RNA processing, cell adhesion, and DNA damage repair.[93–95]

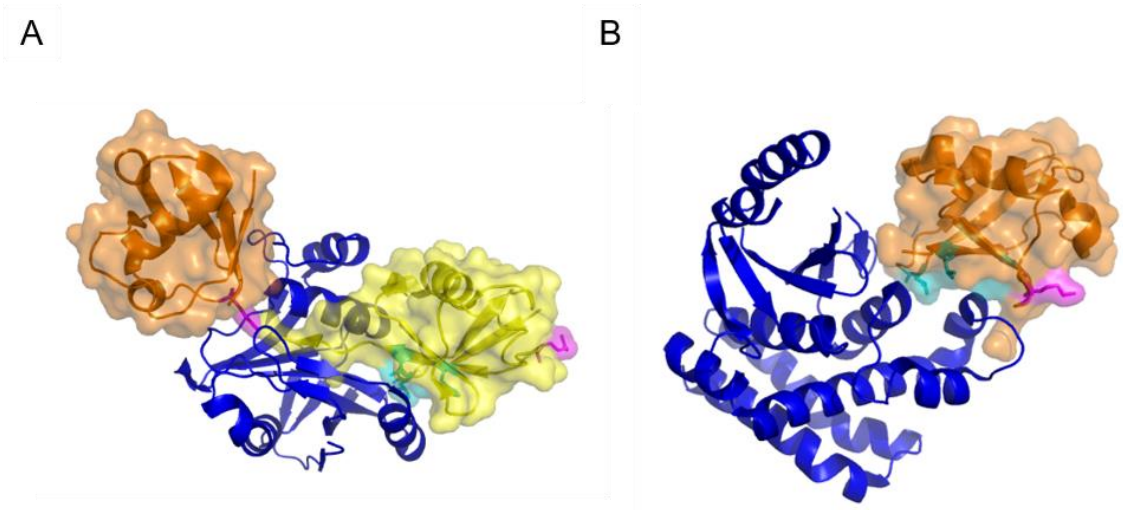

Figure 1.7: Binding of specific DUBs to ubiquitin. Crystal structure of the DUB (blue, ribbon representation) AMSH (A, PDB: 2ZNV) or OTUB1 (B, PDB: 4I6L) with ubiquitin (B) or the K63-linked ubiquitin dimer (A). The distal ubiquitin is marked in yellow, the proximal in orange, the Ile44 patch in cyan and the K48/K63-residue is marked in magenta.

1.1.7 Functions of the ubiquitin code

Ubiquitylation, which was initially understood only as a proteasomal degradation signal, is now known as one of the most versatile protein modification systems. Ubiquitin has a total cellular concentration of up to 85 µM and can take on a multitude of different topologies, triggering diverse signaling pathways.[21, 96]

More than half of the ubiquitin pool was shown to be present in the form of monoubiquitylated proteins, with half of these modifications occurring on histones, making H2A the most abundant ubiquitylated protein overall. Thus ubiquitin is essential for regulating nucleosome dynamics and transcription.[96–99] Monoubiquitylation can occur at specific residues, for instance, the attachment of ubiquitin to residue K164 of Proliferating-Cell-Nuclear-Antigen (PCNA), which plays a crucial role in DNA damage response.[100, 101] Furthermore, monoubiquitylation also stimulates a variety of signaling pathways outside of the nucleus. For example, it impairs the interaction of EGFR (Epidermal Growth Factor Receptor) signaling with the endocytic machinery, it changes the localization of proteins and triggers the internalization of plasma membrane proteins.[102, 103]

As many ubiquitylated substrates have multiple accessible lysine residues, multiple lysines can be ubiquitylated, resulting in multi-monoubiquitylation. One example is EGFR, for which its endocytic uptake is regulated by multi-monoubiquitylation.[9, 104]

Ubiquitin moieties that are not bound as monoubiquitin to a substrate are either present as free ubiquitin inside the cell or form ubiquitin chains linked via the seven internal lysine residues or the N-terminal methionine of ubiquitin. These chains make up 10-20% of the total ubiquitin pool.[96, 105]

1.1.7.1 Ubiquitin chains

The distribution of linkages within this ubiquitin chain fraction varies greatly depending on the species, cell line, cell cycle, and differentiation.[97] In unsynchronized U2OS cells, for example 55% of the ubiquitin chains were linked via K48, 27% via K63, 9% via K11, 5% via K29, and 2% via K6. Another mass spectrometry method (Ub-PSAQ) found that in HEK293 cells, 83% were linked via K48, 12% via K63, 5% via K11, and the remaining linkages were all below 1%.[96, 106] In *S. cerevisiae* the most abundant linkage was also K48, followed by either K11 or K63, depending on the cell state and analysis. One study showed that approximately 29% of all ubiquitin-ubiquitin linkages are linked through K48, followed by 28% of K11 linkages and 16% through K63. The less abundant remaining topologies include K6 at 11%, K27 at 9%, and approximately 3% each for K29 and K33.[107, 108] Overall, it can be concluded that in most cell types, K48 and K63 are the most abundant linkages and are thus referred to as canonical linkages.

Polyubiquitin chains were shown to be present in two conformations depending on their linkage: a closed or compact conformation, in which adjacent moieties interact with each other or an open conformation, in which no interference except for the linkage itself was found. The closed conformation was initially observed in solution for dimers and tetramers linked via K48. The buried hydrophobic interface is caused by an interaction of their two Ile44 patches. However, this conformation is not rigid, and an open conformation is also observed under physiological conditions, allowing the binding of DUBs that interact with the Ile44 patch.[9, 109–111] Molecular modeling predicts that diubiquitin linked via K6, K11, and K27 can also oscillate between these two conformations.[112] In contrast, for the other linkages (M1, K29, K33, and K63), it was shown that they are unable to form such contacts. Therefore, they are found in an open conformation, which provides a high degree of conformational freedom and available hydrophobic patches for UBDs.[109, 113]

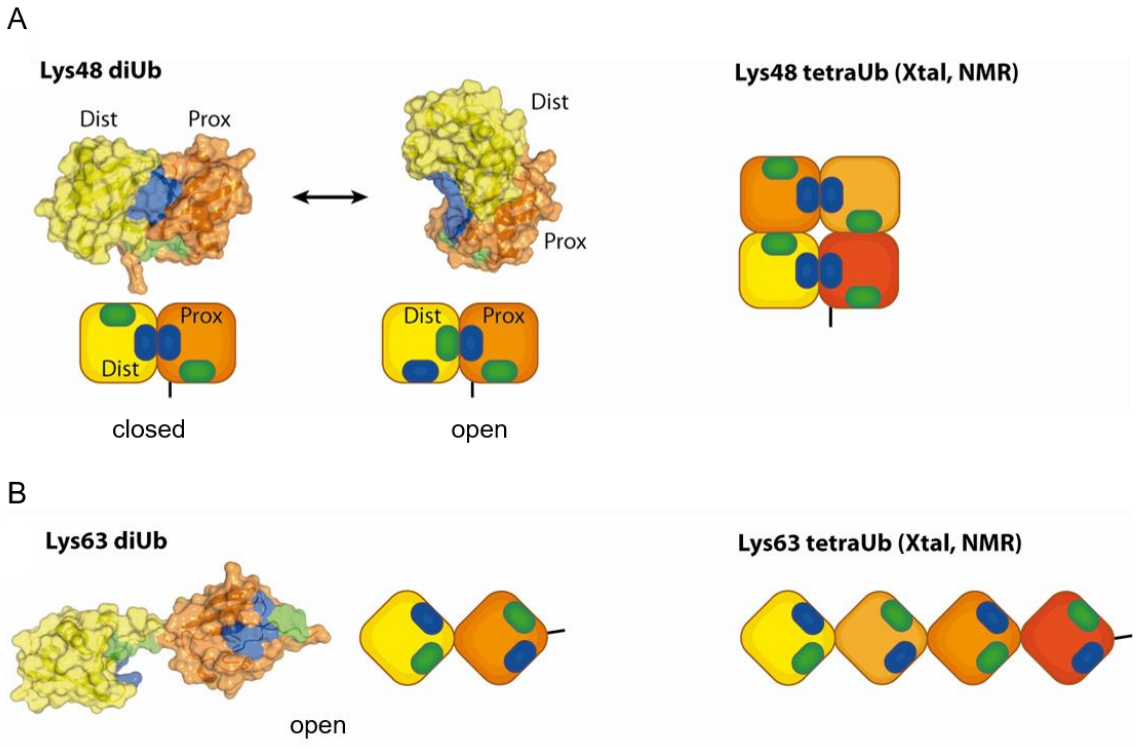

Figure 1.8: Open and closed conformations of ubiquitin chains. Ubiquitin dimers linked via K48 (A) and K63 (B) are shown with the distal (Dist) ubiquitin in yellow and the proximal (Prox) ubiquitin in orange. Alongside a schematic representation of the ubiquitin dimers and tetramers indicating the Ile44 (blue) and Ile36 (green) patches. (Figure adapted from Komander and Rape, 2012)[9]

1.1.7.1.1 K48-linked ubiquitin chains

The K48-linkage is the most abundant type of ubiquitin linkages and was the first one for which a biological function was described. In the 1980s, research by Hershko and Ciechanover identified ubiquitin as the canonical signal for protein degradation by the proteasome.[114–117] It has been proven that degradation based on this K48-linked ubiquitin signal is essential for cell viability of *S. cerevisiae*.[118] It was initially suggested that only K48-linked ubiquitin chains longer than tetramers feature an effective signal for 26S proteasomal degradation. However, more recent studies have shown that two diubiquitin modifications are superior to longer K48-linked ubiquitin chains. Therefore, the understanding has shifted from a defined degradation signal to a ubiquitin threshold model, in which the signal is determined by the local concentration of ubiquitin rather than the length of the chain.[21, 119, 120] Proteins that shall be ubiquitylated for degradation are identified by various signals, including the PEST sequence, N-degrons or cyclin destruction boxes.[3, 121, 122]

Despite its predominant role as a degradation signal, some studies postulate additional non-degradative functions for K48-linked ubiquitin chains, for example, in transcription factor regulation or translesion.[123–125]

1.1.7.1.2 K63-linked ubiquitin chains

K63-linked ubiquitin chains are the second most abundant chains in mammalian cells.[96, 126] They function in a variety of predominantly non-degradative roles, often through the regulation of protein-protein interactions.[9]

Their most prominent role is in DNA repair, where they act as a recruitment signal for different DNA repair factors. DNA double-strand breaks (DSB) trigger the RING finger protein 8 (RNF8)/RNF168-mediated K63-linked polyubiquitylation of histones, leading to the recruitment of first RAP80 and then a range of genome caretaker proteins and their associated factors, including p53-binding protein 1 (53BP1) and Breast cancer 1 (BRCA1). K63-linked polyubiquitylation of the DNA sliding clamp PCNA by Rad5 initiates the error-free damage bypass in yeast and fork reversal in human cells.[101, 127–129]

Another field in which K63-linked ubiquitin chains play a crucial role in yeast and human cells is endocytosis and intracellular trafficking. They are identified in multivesicular bodies (MVB), on plasma membrane endocytic cargoes such as EGFR, and on proteins viral for the budding process. Additionally, they function as a general sorting signal for the autophagy system.[130–134] In addition, K63-linked ubiquitin chains were shown to play a role in inflammation and immune response by kinase activation leading to NF-κB activation.[135, 136]

1.1.7.1.3 Non-canonical linkages

Compared to K48- and K63-linked ubiquitin chains, our understanding of atypical ubiquitin linkages is still limited. However, as more powerful methods for their analysis are developed (see section 1.1.8), our knowledge is constantly increasing.[137] This subchapter will provide a brief review of the known roles related to non-canonical ubiquitin linkages.

M1-linked ubiquitin chains are the only chains that are not bound via an isopeptide bond, but by a peptide bond between the C-terminal carboxyl group of one ubiquitin and the N-terminal amino group of the other ubiquitin, resulting in a head-to-tail fusion.[138] M1-linked ubiquitin chains, also referred to as linear chains, have only been identified in higher eukaryotes, but do not seem to be enzymatically produced in budding yeast.[139] The linear ubiquitin chain assembly complex (LUBAC) is the only E3 complex identified so far to form M1-linked ubiquitin chains using its two RBR proteins, HOIL1 and HOIP, along with the structural complex SHARPIN. M1-linked ubiquitin chains play a role in inflammatory and immunity signaling by ubiquitylating NEMO (NF-κB essential modulator). In combination with K63-linked chains, they thereby effectively activate NF-κB signaling.[17, 140–144] Furthermore, linear chains have been reported to be involved in the regulation of cell death, viral nucleotide receptor sensing, T- and B-cell development, mitophagy and protein quality control mechanisms in relation to cancer and autoimmune diseases, offering linear ubiquitin chains as a novel drug target.[145–149]

K6-linked ubiquitin chains were first identified to function in mitophagy, which is the autophagic processing of damaged mitochondria. In this process, damaged outer mitochondrial membrane (OMM) proteins are ubiquitylated by the RBR E3 Parkin. This process is antagonized by the K6-selective, mitochondrial DUB USP30 or USP8.[150–154] Another condition that has been shown to lead to the build-up of K6-linked polyubiquitin is DNA damage. Here, the BRCA1/BARD1 complex forms K6-linked chains in response to replication stress and DSB repair.[155–157]

Another E3 ligase which has been shown to assemble K6-linked ubiquitylated species is HUWE1 (HECT, UBA and WWE domain containing E3 ubiquitin protein ligase 1). Interestingly, K6-linkages accumulate upon inhibition of p97 but not proteasome, suggesting their non-degradative role in p97-mediated transactions. It is necessary to further clarify whether this can serve as a proteasomal degradation signal, as demonstrated for Mfn2, or if it has other functions.[158–160] Additionally, K6-linked ubiquitin chains have been found to play a role in various other pathways, including the antiviral immune response, the quality control pathway at stalled ribosomes, and protein stabilization. This highlights the functional multiplexity of this type of ubiquitylation.[137, 161–164]

K11-linked ubiquitin chains are primarily understood as an additional proteasome degradation signal associated with cell cycle regulation. These chains are assembled by the E2 UBE2S in conjugation with the anaphase-promoting complex (APC/C). Studies have shown that K11-linked ubiquitin chains often accompany K48-linked ubiquitin chains, and the efficacy of the degradation signal increases significantly when K11-K48 branched ubiquitin chains are present.[21, 137, 165–167] Also several non-degradative roles of K11-linked ubiquitin chains have been proposed including immune response and DNA damage response (DDR).[168, 169]

K27-linked ubiquitin chains play a significant role in innate immunity by regulating IRF pathways and NF-κB through TANK-binding kinase 1 (TBK1) and TGFβ-activated kinase 1 (TAK1). Additionally, these chains are conjugated to H2A histones by RNF168, providing a recruitment platform for DDR proteins upon DSBs.[137, 170–172]

K29-linked ubiquitin chains are associated with proteasomal degradation. In *S. cerevisiae* K29-ubiquitylation by Ufd4 initiates the ubiquitin fusion degradation (UFD) pathway, a pathway that degrades proteins that are C-terminally fused to an uncleavable ubiquitin moiety. Similar to K11-linkage, the signal strength of K29-linked ubiquitin chains is increased by additional modification with K48-linked polyubiquitin by Ufd2.[173–175] K29-linked ubiquitylation has been implicated in neurodegenerative disorders such as Parkinson's disease and Huntington's disease. They have been found along with the E3 TRAF6 in the post-mortem brains of Huntington's disease patients and it was shown that TRAF6 promotes the aggregation of mutant DJ-1 and α-synuclein in Parkinson's through K29-linked ubiquitin chains.[176, 177] Furthermore, in mammalian cells it has been shown, that the E3 ligase Smurf1 (Smad ubiquitylation regulatory factor 1) modifies Axin, a scaffold protein, involved in the degradation of β-catenin, with nondegradable K29-linked ubiquitin chains, thereby repressing Wnt/β-catenin signaling.[178]

K33-linked ubiquitin chains are the least studied type of ubiquitin chains.[137] They have been associated with negative regulation of T-cell antigen receptor and AMP activated protein kinase (AMPK)-related protein kinase, as well as with post-Golgi trafficking. In this process, K33-linked ubiquitylation recruits its substrate to the trans-Golgi network.[179–181] Another substrate that has been found to be K33-polyubiquitylated is XRCC1, which leads to the activation of base excision repair (BER).[182]

1.1.7.1.4 Branched ubiquitin chains

Around 20 years ago, branched ubiquitin chains were first described, adding a new layer of complexity to the ubiquitin code.[107] It has since been shown that 5-20% of all ubiquitin chains are branched, and that some linkages predominantly exist in form of heterotypic or branched chains.[144, 183–185] The abundance of these chains can change in response to the cellular state and has been found to increase up to 50% upon general protease inhibition, demonstrating that these conjugates play an important role in cellular signaling.[183, 186] The function of branched ubiquitin chains has long remained unknown due to the lack of appropriate tools and methodologies. However, with the development of new, specific research methods, more and more functions of branched ubiquitin chains are being discovered.[187, 188]

Branched ubiquitin chains contain at least one ubiquitin moiety modified on at least two sites. These chains can be synthesized either by an enzyme specific to multiple linkages, such as NleL, which produces K6-K48-branched chains, or by two different E3s ubiquitylating the substrate. Therefore, the first ligase attaches the first specifically linked ubiquitin chain, which the second E3 recognizes and then branches off conjugates of a distinct topology. This second method appears to be the more prevalent scenario. An example of this is the UFD pathway described above (section 1.1.7.1.3).[174, 175, 188–190] There were also some DUBs found that preferentially cleave branched ubiquitin chains, such as UCH37, leaving the first homotypic chain intact. This results in an edited, but not completely terminated, ubiquitin signal.[188, 191]

Branched ubiquitin chains encode signals that differ in quantity and quality from homotypic chains.[192] They can lead to additional or branch-specific effectors being recruited (Figure 1.9) and thus result into the combination of signals and thereby pathways, to the enhancement of one signal or to the switch from one to a completely different signal. Branched ubiquitin chains provide a higher local concentration of ubiquitin near the attachment site. This can result in an enhanced signal due to an avidity effect, where multiple ubiquitin effectors bind to the receptor or due to amplified affinity of one effector, which harbors multiple UBDs.[144, 166, 193–195] The branching point can also form a new binding surface that leads to the recruitment of a certain effector, as proposed for the K11-K48-branch point bound by the proteasomal subunit Rpn1.[196] Branching can also block DUB activity, thereby enhancing and prolonging a signal (Figure 1.9). This was demonstrated for the regulatory role of K48-K63-branched chains in the NF-κB signaling pathway. This pathway is negatively regulated by the actions of two DUBs: CYLD and A20, which disrupt the initial K63-linked chains, leading to the cessation of NF-κB-dependent signaling. However, in the presence of interleukin-1β, the E3 ligase HUWE1 adds K48-linked chains onto the pre-existing K63-linked chains, resulting in the formation of K48-K63-branched chains. These branched chains do not lead to the degradation of the TRAF6 substrate, instead they confer resistance to digestion by CYLD, resulting in the continued existence of the K63-linked ubiquitin chain and, thus, a prolonged activation of the signaling pathway.[106, 187]

Following branched combinations were found inside cells: K11-K48, K29-K48, K48-K63, K6-K48, M1-K63, K6-K11, K27-K29, K29-K33, K11-K63. However, not all of them have been found to be functionally relevant so far.[187, 188] As relevant for this work the functions of K48-K63-branched ubiquitin chains will be elaborated in the following paragraph.

K48-K63-branched ubiquitin chains were shown to be formed by the ubiquitin-conjugating enzyme UBE2K and ubiquitin ligases HUWE1 and UBR5. In addition to the non-proteolytic role of K48-K63-branched chains described above for the regulation of NF-κB signaling, degradative functions have also been reported.[48, 106, 195] In a recent study the proapoptotic protein TXNIP (Thioredoxin interacting protein) was used as a prototype to gain insights into K48-K63 branched chain assembly and its impact on the substrate's fate. The study found that the E3 ITCH or WWP1 initially formed a K63-linked ubiquitin chain, which then recruited the K48-specific ubiquitin ligases UBR5 or HUWE1. The assembly of K48-K63-branched chains resulted in the targeting of the substrate for proteasomal degradation, which is not the outcome for the K63-linked ubiquitin chains alone, indicating a switch of signals.[195] Additionally, it has been shown that branched chains are substrates of p97. P97 is a segregase that unfolds proteins and prepares them for proteasomal degradation. This may even increase the rate of degradation of branched chains.[186, 197, 198]

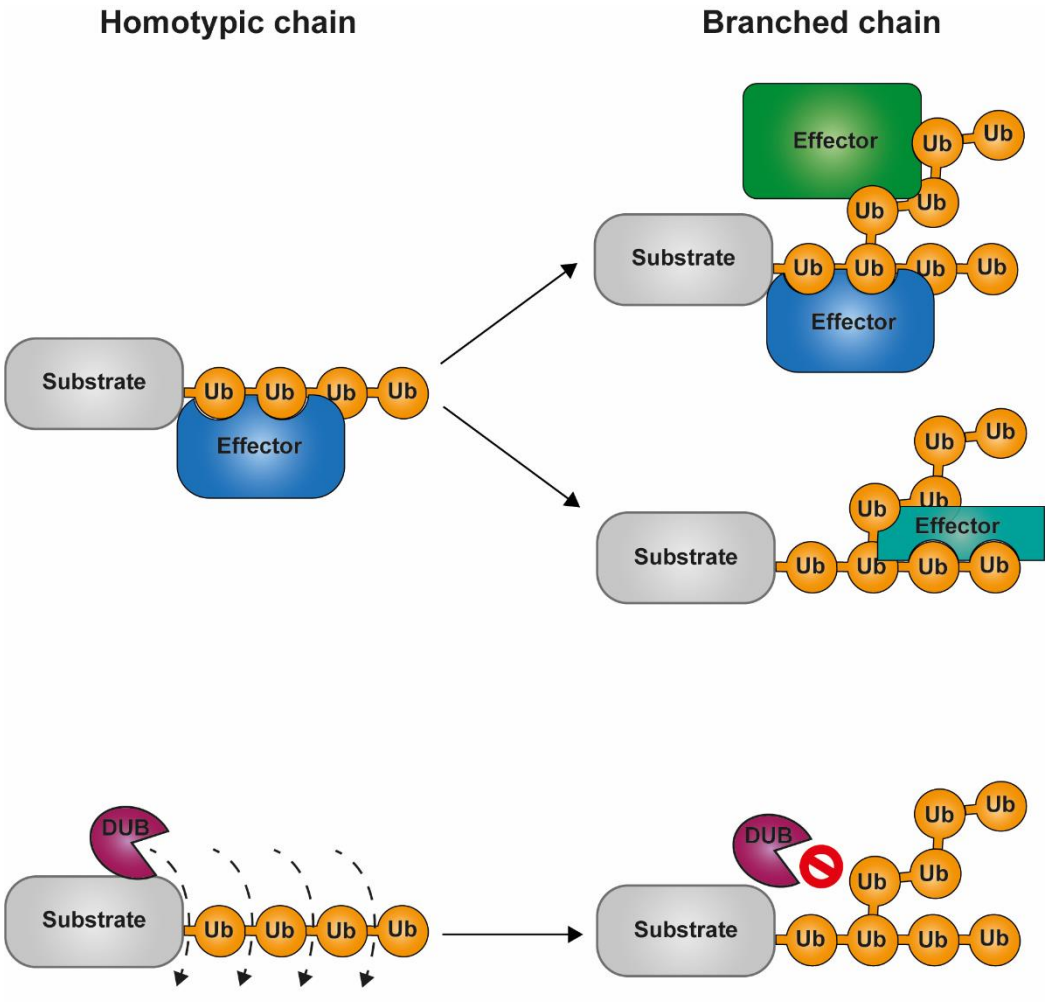

Figure 1.9: Functional outputs of branched ubiquitin chains. Branching leads to an altered recognition or processing by effectors or DUBs, thereby chageing the functional output of the signal. (Figure based on Wang *et al.* 2020.)[192]

1.1.8 Analysis and recognition tools for ubiquitylation

In recent years, a rising number of sophisticated tools have been developed to provide insights into quantitative composition and identify distinct linkage types, including branched ubiquitin chains. These tools range from *in vitro* techniques such as ubiquitin mutants and mass spectrometry approaches to linkage-specific antibodies, newly developed recognition tools, and linkage-specific binders. The following subsections will provide an overview of the most common analysis tools for studying linkage-specific ubiquitin signaling.

1.1.8.1 Ubiquitin mutants

To study the linkage of a certain ubiquitin chain or the enzyme responsible for its creation, a straightforward approach is to use lysine to arginine mutants (KxR) or single lysine mutants (Kx-only). If a certain KxR mutant shows a loss of ubiquitin chain formation compared to the wild-type, it indicates that the chain is linked via this mutated lysine. A partial reduction suggests that multiple linkages are formed.[188, 199]

1.1.8.2 Mass spectrometry methods

Among the various tools available to study the ubiquitin code, mass spectrometry-based approaches have had the most profound impact on identifying ubiquitin chain linkages and modifications. A typical workflow combines enrichment steps of the labeled analyte with one or more types of mass spectrometry (MS) detection. Label-free methods have also been developed that allow reliable quantification if a sufficient number of replicates are performed.[21, 200, 201]

The detection of ubiquitylated proteins by MS relies on identifying a specific peptide-adduct left on the substrate after digestion with specific peptidases. The most commonly used peptidase is trypsin, which cleaves the peptide bound between R74 and G75 of the C-terminal tail of ubiquitin, leaving a specific GG-motive on the residue to which the ubiquitin was linked. The peptides received are called 'ubiquitin remnant-containing peptides' and can be identified by MS through the shift of 114.04 Da, which corresponds to the mass of the diglycine adduct. This allows for the identification of the substrate residues that were ubiquitylated and the identification of the ubiquitin residues through which an ubiquitin chain was linked. In rare cases, trypsin may cleave between the penultimate R72 and L73, resulting in an LRGG adduct with a monoisotopic mass of 383.23 Da. Other peptidases, such as Lys-C and Glu-C, have also been used, leaving longer peptide fragments.[202–204]

To enrich the signal, earlier studies required the expression of tagged ubiquitin moieties, enabling isolation by pull-downs. However, this is no longer necessary due to the development of a monoclonal antibody against the GG-motif. This allows for a pull-down after trypsin digestion, enabling a global ubiquitin-proteome analysis without overexpression.[107, 205, 206]

The fragments of ubiquitin conjugates can be detected and quantitatively analyzed by MS. Two types of measurements must be distinguished: relative and absolute quantification.[200] Relative abundance measurements can detect modifications and determine how they change in response to perturbations, but they do not provide general stoichiometry information.

The two primary label-based relative MS techniques are tandem mass tag (TMT) labeling, which is used for samples that cannot be metabolically labeled, and stable isotope labeling by amino acids in cell culture (SILAC), which is a metabolic, *in vivo* labeling procedure that mostly uses labeled lysine and/or arginine.[207–209] Two major targeted approaches are widely used for absolute quantification: absolute quantification employing labeled ubiquitin standards (AQUA) and Ubiquitin-Protein standard absolute quantification (Ub-PSAQ). AQUA uses a set of 18 isotopically heavy ubiquitin peptides with defined performance parameters as an internal standard. Ub-PSAQ is a combination of differential affinity chromatography and stable isotope-labeled free ubiquitin, mono- and polyubiquitylated conjugate as standards. This method allows for precise measurement of the concentrations of free ubiquitin, monoubiquitin, or ubiquitin chains in cell extracts.[96, 210, 211]

These MS measurements are all 'bottom-up' approaches, which have the limitation that they cannot integrate multiple signaling events on a single protein. For example, branched ubiquitin chains that are not at adjacent lysine residues in the same peptide remain undetected.[21, 200] Since this disadvantage is a result of peptidase digestion, which is the basis for all these approaches, the introduction of an R54A mutation resulted in a peptide that contained both the K48 and K63 residues. This allowed for the identification of K48-K63-branched ubiquitin chains and showed that nearly 20% of all K63-linkages are branched via K48.[106]

However, this mutation approach is limited to the detection of K48-K63-branched ubiquitin chains and cannot be easily transferred to other branching types due to the potentially large distance and the prevalence of additional trypsin sites. Therefore, middle-down MS approaches with incomplete trypsinization are used, where trypsin only cuts between R74 and G75 but no other site. This ensures that branching points remain as Ub1-74 with two di-Gly motifs and can therefore be detected by the respective mass shift. However, the chain linkage at the branched point remains unidentified, requiring more specific workflows.[188, 190, 192] Another powerful method for studying branched chains is the Ub-clipping approach, which uses an engineered viral protease Lb^{pro*} that incompletely removes ubiquitin from substrates, leaving the GlyGly moiety attached to the modified residue. Lb^{pro*}-generated ubiquitin moieties from chains also retain the GlyGly-modified residues, allowing the quantification of branch-point ubiquitins by their multiple GlyGly-modification.[183]

While MS has provided valuable insights into the ubiquitin landscape, it has limitations in capturing spatial information, cell-to-cell variations, and rapid changes. Furthermore, MS requires sophisticated instruments and is labor-intensive, as all methods require extensive in-depth analysis.[21, 200, 212]

1.1.8.3 Linkage-selective binders

1.1.8.3.1 Antibodies and nanobodies

A wide range of general ubiquitin antibodies are commercially available. In the last 15 years antibodies against specifically linked ubiquitin chains have been introduced to the market. The first linkage-specific antibodies, K48 and K63, were developed by Newton *et al.* in 2008 using a combination of a minimalist diversity phage library and *in vitro* selection methods.[212] In subsequent years, antibodies against all other linkages were developed, enabling the enrichment and analysis of these specific linkage types.[165, 213–217] Additionally, a bispecific antibody was developed for the recognition of K11-K48-branched ubiquitin chains and used to identify substrates modified with this chain type.[186] Selective antibodies have proven useful for a variety of techniques, including Western blotting, ELISA, and immunoprecipitation (IP). However, their use *in vivo* is very limited because they cannot be introduced to living cells or expressed in most of them, due to the complex maturation process required for their correct folding.[168]

One alternative tool that can be expressed inside cells is the so-called nanobody. Nanobodies consist of single-chain V_HH antibody regions and are therefore small and monomeric.[218] Recently, nanobodies that detect K48- and K63-linked ubiquitin chains were published.[219] Additionally, a nanobody for the detection of K48-K63-branched ubiquitin chains was presented in a pre-print.[220] These nanobodies were primarily used to isolate proteins decorated with specific ubiquitin chains and subsequently analyze them via MS.[220]

1.1.8.3.2 Affimers

Another scaffold that has been used to create linkage-specific binders is affimers. Affimers are 12 kDa non-antibody scaffold proteins based on a cysteine fold with randomizable surface loops (Figure 1.10A).[221] They were raised against the atypical K6 and K33-linkages, showing a good affinity *in vitro*. Crystal structures of the affimers with their respective ubiquitin dimers revealed their binding mode. It has been shown that two affimers dimerize with each moiety interacting through its surface loops with the Ile44 patch of one ubiquitin moiety (Figure 1.10B&C). They thereby use the principle of naturally occurring UBDs to recognize the defined distance and relative orientations of the specifically linked ubiquitin dimer, rather than the linkage itself.[160]

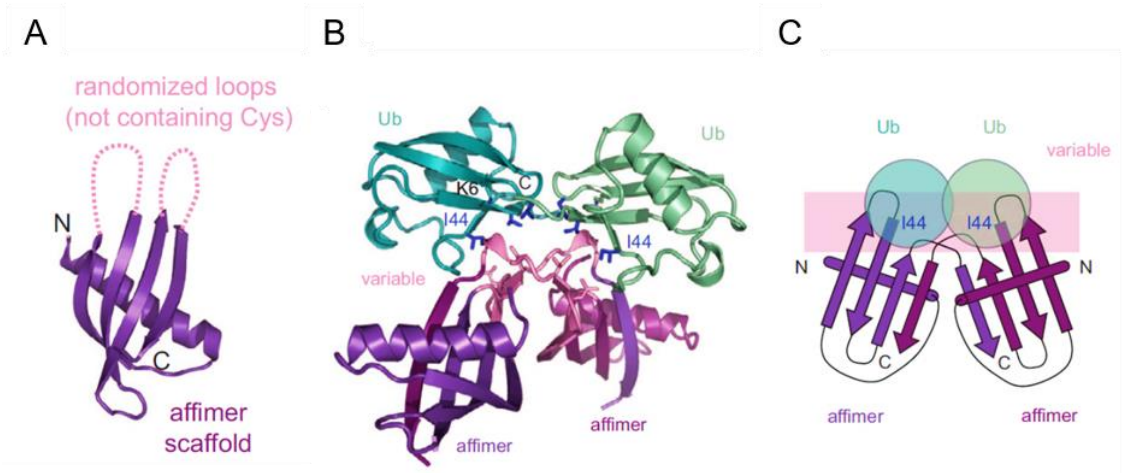

Figure 1.10: Structure of the K6-specific affimer with K6-linked diubiquitin. (A) General structure of the affimer scaffold. (B, C) Crystal (B) and schematic structure (C) of the K6-affimer bound to a K6-linked ubiquitin dimer. (Figure adapted from Michel *et al*, 2017)[160]

The affimer against K6 demonstrated good specificity and was utilized to identify proteins ubiquitylated with this linkage. Furthermore, it revealed the involvement of K6-linked ubiquitin chains in DDR and p97 metabolism. The K33-affimer exhibited cross-reactivity with K11-linkaged ubiquitin chains. However, Michel *et al.* provided tools for the recognition of atypical ubiquitin chains with properties comparable to antibodies and demonstrated their usefulness in both *in vitro* and *in vivo* applications.[158, 160] Additionally, affimers specific for K48-linked ubiquitin dimers are commercially available, but they are not further described besides their use in ELISA.[222]

1.1.8.3.3 UBDs and TUBEs

A method for recognizing and isolating ubiquitin is based on the use of naturally occurring UBDs. Initially, full-length proteins like GST-tagged human S5a were used to enrich ubiquitylated proteins from tissues.[223] Later, purified UBDs were used for the isolation and detection of ubiquitin chains in cell extracts. However, the weak K_D of a single UBD often complicates the capture.[224, 225] A high-affinity UBD from the human pathogen *Orientia tsutsugamushi* was recently identified. This UBD could be valuable for efficiently detecting especially monoubiquitylated proteins.[226]

Hjerpe *et al.* have taken a different approach to address the issue of low K_D by multimerizing UBDs. They developed tandem-repeated ubiquitin binding entities (TUBE) based on up to five UBA domains from the proteins UBQLN1 (TUBE1) or HR23A (TUBE2). These domains are connected by flexible polyglycine linkers in a single amino acid chain. The TUBEs were shown to recognize tetraubiquitins with 100-1,000 times higher affinity than monoubiquitin, while maintaining the same affinity to monoubiquitin as single UBAs. TUBEs can effectively purify polyubiquitin conjugates from native cell extracts and are suitable for immunoprecipitation. The high efficacy of enrichment is primarily due to their specificity and secondarily to their function as molecular traps, as TUBEs were shown to protect ubiquitin chains from DUBs and recognition, such as by the proteasome.[227] The subsequent step was to engineer the UBDs and linkers to achieve linkage specificity. Thus, the next TUBE was based on the highly K63-linkage-selective tandem ubiquitin-binding motifs (tUIM).

It was demonstrated that the length of the linker is crucial for the linkage selectivity of the construct. Therefore, when the naturally occurring UIMs from VPS27 (Vacuolar protein sorting-associated protein 27) and RAP80 were linked by a helical seven-alanine linker, the UIMs were spaced at precise distances to dock each UIM to one ubiquitin in a K63-linked chain. The anti-K63 TUBE resulting from RAP80 binds K63-linked polyubiquitin with a K_D as low as 6.9 nM. It exhibits a 1,000-fold preference over K48-linked ubiquitin chains and a 23,000-fold preference over linear chains.[75, 228, 229]

The TUBEs have been commercialized by Life Sensors and can be bought recombinantly attached to different tags. TUBEs are most commonly used as affinity-purification reagents for polyubiquitylated proteins, but they have also been shown to be useful for immunoblot applications, monitoring total cellular ubiquitin in an ELISA format, FRET-based high-throughput screens for monitoring E3 or DUB activity, or as a sensor to determine the localization of K63-modified proteins.[225, 228, 229]

However, the TUBEs also have some limitations that must be kept in mind. Due to their structure, TUBEs show a good affinity for polyubiquitin chains but have a low ability to isolate monoubiquitylated proteins. As natural occurring receptors use a limited set of residues on ubiquitin, simultaneous binding of another UBD or DUB is mostly excluded. Therefore, the TUBEs mask the respective ubiquitin chain and inhibit ubiquitin-dependent cellular processes. This results in an accumulation of ubiquitin chains in cells, which can enrich otherwise unstable conjugates but also distort the ubiquitylation landscape. Additionally, it has been demonstrated that the concentration of this tool inside the cell and on the bead surface must be carefully controlled to avoid off-target binding.[225, 228]

The LifeSensor collection also includes an anti-K48-TUBE, which in its second generation has an affinity of approximately 20 nM for the K48-linkage, while for other linkages an affinity over 2µM is stated.[230] Additionally, an anti-M1 TUBE has been added, which exhibits high selectivity for M1-linked ubiquitin chains over K48- and K63-linked polyubiquitin chains.[231]

Non-TUBE sensors based on UBDs include the GFP (Green fluorescent protein)-tagged single UBAN domain of NEMO, which was utilized to visualize M1-ubiquitylation, or the NZF domain of TAB2 to detect K63-linked chains in mammalian cells.[232] One approach used to image K48-linked ubiquitin chains inside the cell is ubiquitination-induced fluorescence complementation (UiFC).[233] UiFC is based on bimolecular fluorescence complementation (BiFC), where two non-fluorescent fragments of a normally fluorescent protein, such as mVenus, a yellow fluorescent protein (YFP) variant, are fused to two proteins of interest. If these proteins come into close proximity, the two fragments can reconstitute and emit a fluorescent signal.[234] For the UiFC, three tandem UIM domains of epsin1 were fused to the two fragments of Venus, enabling the imaging of K48 ubiquitylation dynamics in presynaptic assembly and differentiation.[233, 235, 236]

Qin *et al.* combined the unspecific 2UBA domains, the K48-specific 2UIM, or the K63-specific NFZ with their previously developed F3H (fluorescent three-hybrid) to determine the ubiquitylation status of a specific protein in live cells. The protein is anchored at a defined subcellular structure, and the recruitment of the mCherry-tagged probes was visualized. To enhance the signal-to-noise ratio, a BiFC approach was combined with the protein of interest (POI) and the respective UBD each containing one half of the fluorescent protein. This was recruited to a GBP-lacI bound lacO if the POI was ubiquitylated with the respective linkage, thus enabling monitoring of the dynamics of ubiquitylation on proteins such as HP1β, PCNA, and p53, but at a non-natural localization.[237]

1.2 DARPins

For centuries, biomedical research has relied on antibodies for biological assays. However, they have several shortcomings, such as their large and complex quaternary structures, which result in low tissue penetration and their inability to be expressed in prokaryotes like *E.coli*. Two classes of antibody alternatives have emerged: recombinantly generated immunoglobulin derivatives, such as nanobodies, and synthetically designed non-immunoglobulin binders that rely on different protein scaffolds. All of these scaffolds meet the requirements for an antibody alternative, possessing a relatively low molecular weight allowing them to be expressed *in vivo* and containing 10-20 positions that are usually randomizable so that they can be raised against different targets.[238–241]

One prominent example of the latter is the designed ankyrin repeat proteins (DARPins). They offer a promising solution to the problems associated with antibody use and were therefore chosen as the basis of this work.

1.2.1 Structure and properties

DARPins are based on natural repeat proteins, which consist of a number of repeating structural modules, commonly found in eukaryotes. These proteins have been linked to a diverse set of cellular functions based on their ability to mediate protein-protein interactions. Interestingly, in some jawless vertebrates, a family of leucine-rich repeats (LRR) is found in proteins that function in the adaptive immune system, demonstrating the potential of these proteins to function in an antibody-like manner.[242–244]

Ankyrin repeat proteins are a family known for their ability to bind with high specificity to a wide range of proteins. This diversity is primarily due to their unique tertiary structure, which consists of tightly packed repeats of 33 amino acids each. Each repeat forms a structural unit composed of a β-turn followed by two antiparallel α-helices (Figure 1.11C).[241, 245, 246] These repeating modules are stacked on top of each other and interactions between adjacent modules create a stable and compact fold with an elongated shape. This results in a large surface-to-volume ratio (Figure 1.1D).[247–249] Typically, 4-6 repeats are used to create a right-hand solenoid structure, although up to 29 consecutive repeats have been found in a single protein.[241, 250]

Overall, the structural similarity and properties lead to the concept that families like the ankyrins can be generalized to gain highly diverse and specific proteins as an alternative to antibody-based scaffolds. This principle has been applied for different scaffolds like the armadillo repeat proteins or α- helicoidal repeat proteins, but the DARPins have proven to be the most advanced class for a range of biochemical and biomedical applications.[241, 251, 252]

For the DARPin library creation conserved framework residues were identified from naturally occurring ankyrin repeats and were fixed, while surface residues potentially interacting with the target were randomized (Figure 1.11). The use of cysteine residues, to eliminate disulfide formation, as well as proline and glycine, which act as helix-breakers, was avoided.[253] It was demonstrated that repeat units can be exchanged, deleted, or inserted without destroying the tertiary structure as long as the hydrophobic interfaces between the repeats are present.[254]

To ensure soluble protein expression and shield the hydrophobic core from the hydrophilic environment, N- and C-terminal hydrophilic capping repeats were introduced. In the original design, both caps were based on the natural guanine-adenine-binding protein. However, the C-Cap was redesigned to achieve better packing, resulting in higher thermodynamic stability. This new cap also offers additional randomizable residues to create a larger interaction surface (Figure 1.11).[241, 255] Following these principles, libraries in the N2C (two internal repeats) or N3C (three internal repeats) format were created. The structures that are available confirmed the library design, as an average of 75% of the randomized positions contact the target.[239, 256]

The advantages of DARPins over conventional antibodies are their small and stable size. Each module has a size of approximately 3.5 kDa, resulting in a molecular weight range of 14-21 kDa for the N2C and N3C DARPins. This is one-tenth the size of a standard IgG monoclonal antibody, which provides benefits for pharmacokinetic properties and enables greater tissue penetration. DARPins can be concentrated to high levels without aggregation and exhibit excellent thermodynamic properties, heat stability, and storage stability. The elimination half-lives of DARPins are predicted to range from hours to days. They can be readily expressed in the cytoplasm of *E. coli*, where they can account for up to 30% of total cell protein and yield 1 g/L by simple shake-flask expression. The subsequent purification process is straightforward and can be performed under Good Manufacturing Practice (GMP) regulations. DARPins can be used singly or as conjugates to chemical moieties, ranging from PEG to radioactive labels or other proteins, making them versatile targeting vehicles.[241, 257–260]

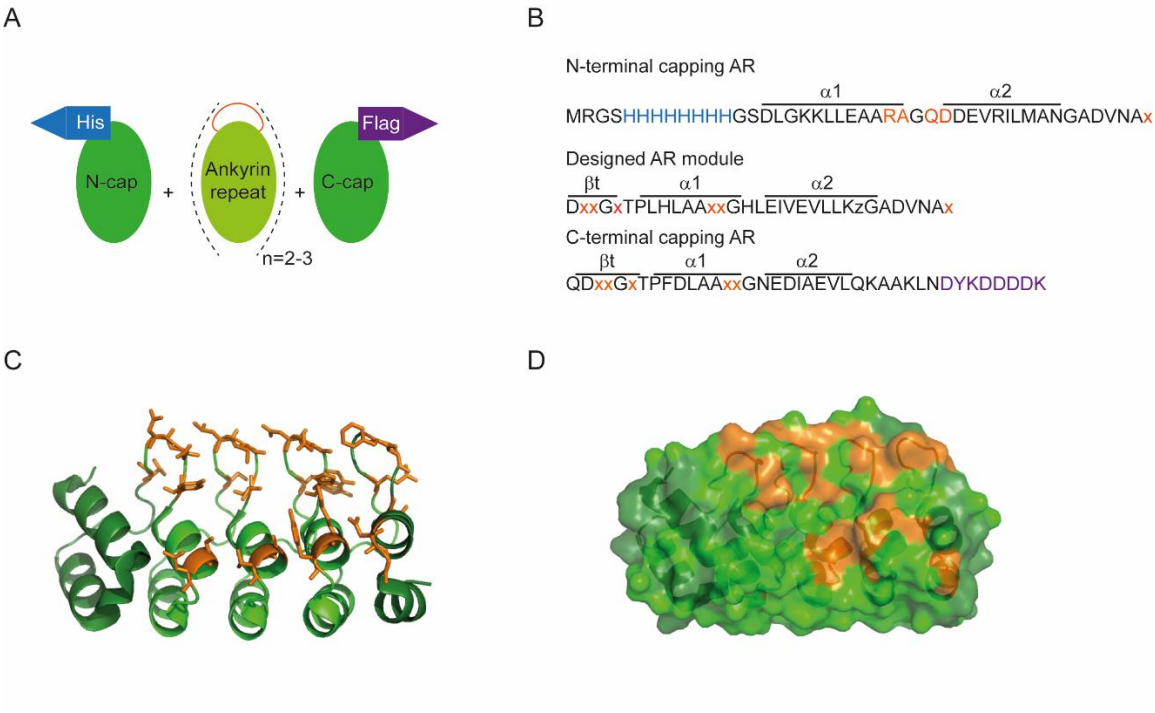

Figure 1.11: DARPin composition and structure. (A,B) Schematic representation (A) and sequences (B) of the build-up of the DARPins. The secondary structure elements of the ankyrin repeats (AR) are indicated above the sequence. A DARPin is created by assembling an N-terminal capping AR (dark green) containing a His_6-Tag, marked in blue, varying numbers of the designed AR module (green), and a C-terminal capping AR (dark green) with a Flag-tag (purple). The randomizable residues are marked in orange, the residue "z" is a randomized framework residue, which can be an asparagine, histidine, or tyrosine. (C, D) Ribbon (C) and surface (D) representation of a three variable module DARPin (E3_5, PDB: 1MJ0) Colors as in (A).

1.2.2 Selection by ribosome display

The generated synthetic DARPin library can be screened for binding candidates against virtually any target using most displays and selection methods originally developed for the selection of recombinant antibodies.[239] Various assays, such as the SNAP display, the signal recognition particle phage display, and the yeast-surface assay, have been successfully used to raise DARPin binders.[261–263] However, the majority of selections have been carried out by a ribosome display. Thus, this experimental setup will be further described in more detail.[264, 265]

Theoretically the DARPin library can consist of 5.2×10^{15} and 3.8×10^{23} for N2C and N3C binders, respectively. In the ribosome display, 10^{12}–10^{14} can be used, limited by the number of ribosomes present *in vitro*, which is still a magnitude higher than display methods based on transformation efficiency.[264–267]

The DARPin library is used as a DNA library in the form of a PCR fragment encoding the DARPin without a stop-codon. In the first step, each member of the library pool is transcribed *in vitro* from the double-stranded DNA into mRNA. Since the mRNAs do not contain a stop-codon, the ribosomes remain intact, generating stable ribosomal complexes that link the phenotype (DARPin) with the genotype (translated mRNA). In the next step, the ribosomal complexes are incubated with the immobilized target. Interacting DARPins are bound, while unbound or non-specifically bound DARPins are washed off. To liberate the mRNAs encoding potential target-specific DARPins, the specific bound complexes are destabilized with *S. cerevisiae* RNA. The eluted mRNAs are then reversely transcribed into double-stranded DNA and subsequently amplified by PCR. These amplified DNA fragments can then either be used as the template for *in vitro* transcription into mRNA for another selection round or can be subcloned into an expression vector to purify and characterize the specific binders (Figure 1.12).[264, 265, 268]

The ribosome display method has a key feature in its intrinsic PCR, which allows for easy manipulation through the introduction of additional mutations using DNA shuffling and/or error-prone PCR. This feature enables the convenient incorporation of a diversification step and allows for true directed evolution by enabling refinement and affinity maturation.[241, 269] The ribosome display approach was used to produce a variety of DARPins with high affinities to multiple proteins, including cytokines, growth factors, and intracellular kinases.[240, 270–272]

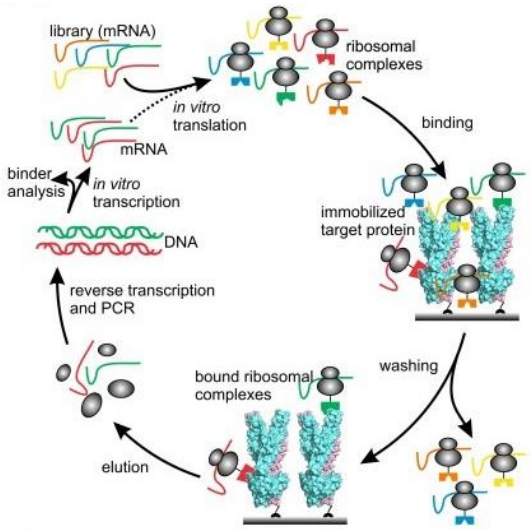

Figure 1.12: Schematic representation of the DARPin selection via ribosome display. Ribosome units are shown in grey spheres. The immobilized target protein is shown in cyan and pink. For detailed description see text above. (Figure from Seeger *et al.*, 2012)[268]

1.2.3 Range of applications

DARPins have a high affinity in the pM-nM range and a high specificity, allowing them to distinguish even small changes such as phosphorylation, different isoforms, and epitopes. This makes them useful for a wide range of applications, which can be grouped in three fields: biomedical research, diagnostics, and therapeutics. In biomedical research, DARPins serve mainly as chaperones and biosensors.[241, 273, 274]

As DARPins have good biophysical properties and the ability to readily crystallize, they are ideal candidates for chaperones, proteins that stabilize a particular conformation of their target and thus allow crystallization of also complex biological macromolecules. Over 50 crystal structures of specific DARPins in complex with their respective targets in the Protein Data Bank (https://www.rcsb.org/) demonstrate this function.[239, 275, 276] In some cases, optimizations were made to improve crystallization. For example, Seeger *et al.* created a second generation of DARPins in which apolar residues in the randomizable areas were reduced. Instead, they used more tyrosines and tryptophanes, which were shown to mediate strong protein-protein interactions.[277, 278] In another approach, crystallization was further enhanced by adding a C-terminal domain that allowed for rigid domain-domain fusion with TEM-1 β-lactamase, which enhanced protein-protein interactions and dominated the crystal structure.[279]

Biosensors are used to visualize molecules in living cells, providing information about their localization, trafficking, functionality, and interactions. DARPins, which can be functionally expressed in the cytoplasm unlike antibodies, have been shown to be valuable tools for approaches where a fluorescent label cannot be easily fused to a protein of interest. One special interest is to monitor PTMs on proteins.[239, 260, 280] For example, DARPins were raised against non-phosphorylated and double-phosphorylated ERK2 (mitogen-activated protein kinase extracellular signal-regulated kinase). The phosphorylation status was checked using a bioluminescence resonance energy transfer (BRET) approach. Additionally, DARPins conjugated to a dye that is activated upon binding were used to study patterns of ERK2 activation in living cells.[273, 281]

Antibodies still dominate the field of diagnostic, but recent studies have shown that some DARPins can offer similar sensitivity with higher specificity compared to their corresponding, FDA-approved antibodies, making them a viable alternative. One particular target for which DARPin recognition was shown to be useful is the human epidermal growth factor receptor 2 (HER2), which can be utilized in immunohistochemistry (IHC) of breast cancer tissue to identify patients suitable for anti-HER2 therapy. Additionally, anti-HER2 DARPins have also been labeled for use in tomography measurements, allowing monitoring of the progression. Tests in mice look promising, showing the potential of DARPins in this field.[239, 282, 283]

DARPins have been tested in various therapeutic approaches, including the treatment of allergic asthma. In this scenario, DARPins were used as IgE inhibitors and demonstrated high efficacy in inhibiting proinflammatory mediators, requiring a much lower dose than the respective antibody in pre-clinical experiments.[284, 285] However, the primary therapeutic area in which DARPins have been tested thus far is oncology. EGFR-bispecific DARPins inhibit the overexpressed receptor, thereby inhibiting proliferation in the cell model.[286] Another DARPin was raised to be an effective pan-HER inhibitor and was shown to serve as an alternative to the antibody, which often faces resistance.[287, 288] Additionally, DARPins were shown to be useful as building block for chemical drug condensates and as targeting molecules for delivering specific loads, such as siRNA or adenoviruses, with high selectivity for a particular cell type.[239, 289–291]

In 2007, the first DARPin-based drug was developed, which was clinically tested. This drug called Abicipar Pegol, was a vascular endothelial growth factor (VEGF)-binding DARPin and was tested for the treatment of diabetic macular edema (DME) and age-related macular degeneration (AMD). In these diseases, the cytokine VEGF-A stimulates angiogenesis and vascular hyperpermeability, which ultimately leads to a loss of vision. The antibody fragment ranibizumab, which targets VEGF, also inhibits this pathway. However, due to its low half-life and bioavailability, it must be administered intravitreally on a monthly basis, which can be burdensome for patients. Therefore, a more potent candidate with high aqueous solubility and stability was sought to provide a prolonged ocular half-life. Abicipar was shown to be safe for use in patients, even in high-concentration formulations, and has a longer half-life of two weeks, reducing injection frequency by 60%. It effectively neutralizes VEGF-A, leading to an improvement in vision for the patients in trial II. However, in 2020, the FDA rejected Abicipar for AMD due to increased intraocular inflammation. The company Molecular partners demonstrated in another phase II trial that the observed inflammation rates were due to impurities and a modified process decreased them drastically. However, AbbVie Inc. has terminated its collaboration with Molecular Partners for this component, making the further progression of this candidate uncertain.[239, 292–301]

After the first clinical trial proved the safety and efficacy of local dosing, several other candidates, mainly in the oncology field, were investigated. One such candidate was the dual DARPin inhibitor against the two growth factors VEGF and hepatocyte growth factor (HGF), which showed reduced invasion and metastasis in mouse models. Due to their small size, DARPins are prone to renal clearance when administered intravenously. Therefore, they must be modified either by PEGylation or, as in this case, through an additional binding site with serum albumin to prolong their half-life. In a phase I study, this led to a half-life of 2 weeks for the tested DARPin. The DARPin also demonstrated a safety profile comparable to that of the adequate antibodies, as well as low EC_{50} and good cellular potency. It is currently being tested in phase II in combination with the antibody bortezomib for the treatment of multiple myeloma.[259, 292, 302–304] Additionally, there are two other oncology drugs currently in clinical trials: UMP0317 for solid tumors and MPO533 for acute myeloid leukemia.[305]

During the COVID pandemic, a DARPin-based drug called ensovibep was also tested, but its development was stopped due to its lack of improvement compared to established treatments.[306] Since their development 20 years ago, DARPins have been widely used as research tools and have shown potential in diagnostic and therapeutic approaches, while for therapeutic use further innovations are still required.

1.3 Genome stability

DNA is the source of genetic information needed to build an organism, and its maintenance is essential for the perpetuation of life. However, the genome is constantly threatened by various endogenous and exogenous factors. Each human cell experiences 10,000-100,000 DNA lesions per day, threatening the integrity of the genome. Unrepaired or mutated lesions can cause genome instability and lead to diseases such as cancer or premature aging.[307–310]

The following sections describe the types of DNA damage a cell encounters and the many mechanisms that have evolved to maintain genetic information and ensure the delivery of intact genetic material to the next generation.

1.3.1 Types of DNA damage

DNA damage can be caused by both endogenous and exogenous factors and can take different forms depending on the trigger.

A prominent source of endogenous DNA damage is the replication process, where ~3 x 10^9 bases must be copied for each replication step. Errors occur at a rate of 10^{-6} to 10^{-8} per cell per replication, resulting in base mismatches, insertions or deletions.[307, 311, 312]

However, most of the endogenous DNA damage is caused by chemically activated DNA that undergoes hydrolytic, oxidative, or alkylating reactions. These reactions can occur spontaneously or can be induced by reactive oxygen species (ROS) or reactive nitrogen species (RNS), alkylating agents, or by X-rays. Spontaneous deamination can lead to the formation of uracil from cytidine and thereby alternate the coding sequence. The best known example of oxidative DNA damage is the oxidation of guanine at C8 (8-oxoG, Figure 1.13A). Alkylation reactions occur mainly as methylation of purine bases, leading, for example, to the formation of N7-methylguanine (Figure 1.13B). For repair, these two modified bases are removed from the DNA by DNA glycosylases, resulting in the formation of abasic sites (Figure 1.13C). However, abasic sites can also occur spontaneously, leading to almost 10,000 abasic sites per human cell per day, posing a threat to genomic stability.[313] Together with abasic sites, single-strand breaks (SSBs) are one of the most common DNA lesions. They can be caused by ROS activity on the DNA backbone, as an intermediate of base excision repair (BER, section 1.3.2) or as an intermediate of DNA replication.[307, 314]

In contrast to small base modifications such as oxidation or methylation, larger compounds can be also covalently attached to DNA bases, resulting in distortion of the DNA helix. Bulky adducts are typically caused by polycyclic aromatic hydrocarbons (PAHs), such as benzo[a]pyrene, a compound found in tobacco smoke but also in grilled meat. It is metabolized to a highly reactive epoxide that reacts with primarily guanine residues to form the adduct dG-BPDE (Figure 1.13D). Another type of DNA damage that distorts the DNA helix is DNA cross-linking. These can be either intra- or interstrand. Intrastrand crosslinks in the form of pyrimidine dimers (Figure 1.13E) and photoproducts are primarily caused by UV light. Interstrand crosslinks (ICLs) are covalent bonds between two complementary DNA strands that interfere with DNA replication and transcription. Interstrand crosslinks are primarily induced by chemicals such as the chemotherapy drug cisplatin (Figure 1.13F).[307, 314–316]

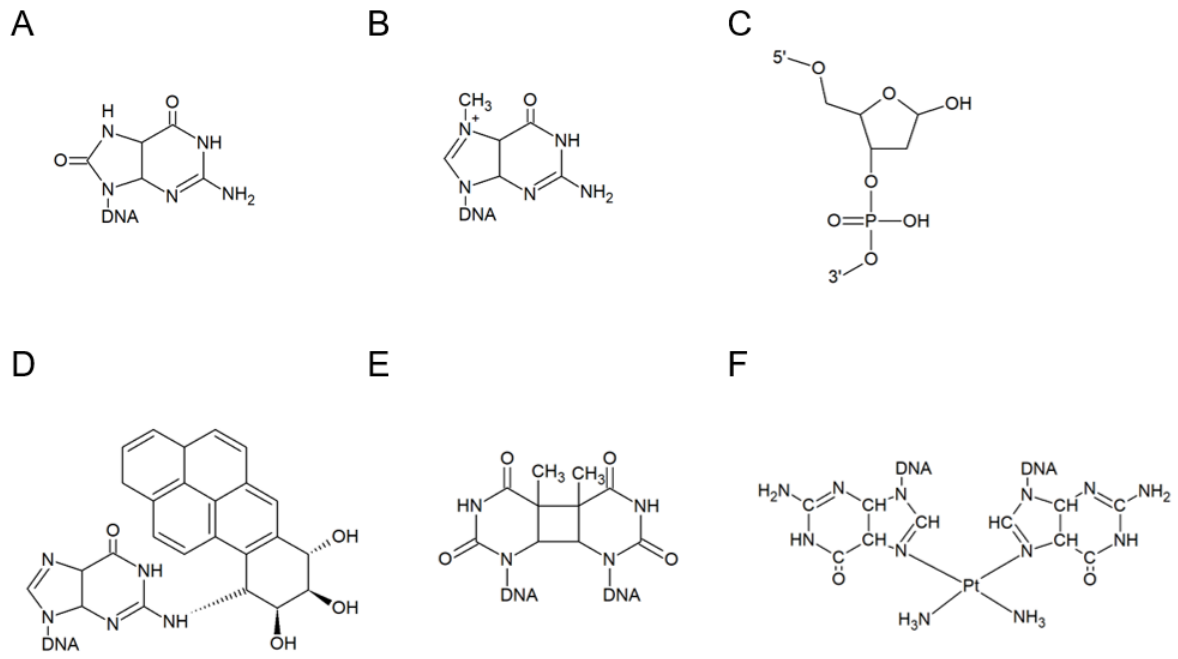

Figure 1.13: Structures of DNA lesions. (A) 8-oxoguanine (B) N7-methylguanine (C) Abasic site (D) dG-BPDE (E) Thymidine dimer (F) DNA crosslink by cis-platin.

Intrastrand crosslinks can lead to one of the most damaging structures, double-strand breaks (DSBs). A single DSB has been shown to be sufficient to kill a cell. They are mostly caused by ionizing radiation (IR), but can also be caused by certain chemicals, by two SSBs in opposite DNA strands in close proximity, or by inhibition of topoisomerase TOP2.[307, 317]

1.3.2 DNA damage repair

To maintain genome stability, cells have developed a multitude of different repair mechanisms to deal with all these different types of possible DNA lesions.

To correct replication errors such as base mismatch, insertion, or deletions, the cell uses a pathway called DNA mismatch repair (MMR). MMR contributes to replication fidelity by at least 100-fold and is highly conserved. In mammalian cells, two main MutS Homolog heterodimer complexes recognize mismatched bases: MutSα and MutSβ. MutSα identifies single base pair mismatches and small insertion/deletions, while MutSβ recognizes larger changes. The recognition of an error results in a conformational change of the complex. This leads to the recruitment of nucleases such as Exo1, which remove an area of approximately 150 nt surrounding the mismatch. The gap is subsequently filled by DNA polymerase δ and DNA ligase.[308, 318, 319]

Small, but mostly highly mutagenic, alterations like oxidative or alkylated bases are corrected by the base excision repair (BER). In this process, one of the eleven known damage-specific DNA glycosylases recognizes and removes the damaged base by cleaving the N-glycosidic bond between the aberrant base and the deoxyribose, resulting in the formation of an abasic site (AP). Different types of DNA glycosylases create gaps of varying sizes, which are then processed through either short-patch-repair or long-patch-repair. During short-patch-repair, PARP-1 and 2 bind to the AP, leading to the recruitment of AP-endonuclease1 (APE1). The APE1 enzyme processes the AP site by cleaving the DNA backbone 5' to the abasic site. This allows DNA polymerase β to insert the missing nucleotide, followed by ligation by DNA ligase 3 (LIG3) mediated by XRCC1 (X-ray repair cross-complementing protein 1). Long-patch BER mainly relies on gap-filling by polymerase δ/ε, which is associated with proliferating cell nuclear antigen (PCNA). The displaced 5'-flap is removed by the Flap-endonuclease 1 (FEN1) before DNA ligase I mediates the ligation. BER is also capable of repairing SSBs.[307, 314, 320, 321]

Bulky and helix-distorting lesions such as photoadducts and intrastrand crosslinks are repaired by the nucleotide excision repair (NER) pathway. Eukaryotes have two NER pathways: global genome NER (GG-NER) and transcription-coupled NER (TC-NER), with the latter being active in transcribed genes. The two pathways differ mainly in the mechanism of DNA lesion recognition. In GG-NER the DNA is scanned for lesions by XPC (Xeroderma Pigmentosum, complementation group C) in complex with RAD23B (UV excision repair protein Radiation sensitive 23B) protein and CETN2 (Centrin 2). In contrast, TC-NER is initiated when RNA polymerase II stalls at a DNA lesion. When a lesion is detected by either mechanism, the 10-subunit complex transcription initiation factor II H (TFIIH) is recruited. This complex contains the XPD helicase (Xeroderma Pigmentosum group D), which unwinds the DNA. The DNA is then stabilized by XPA (Xeroderma Pigmentosum group A) and RPA (replication protein A). Subsequently, the two endonucleases XPG (Xeroderma Pigmentosum group G) and XPF-ERCC1 (Xeroderma Pigmentosum group F) make an incision 3' and 5' to the damage and excise a 24-32 nucleotide DNA fragment containing the damaged lesion. The final steps of gap filling and ligation are carried out by PCNA, RFC (replication factor C), POL δ, POL ε, or POL κ, and the DNA ligase I or XRCC1–LIG3. In total, the NER process requires the coordinated action of around 30 proteins.[307, 308, 314]

The highly dangerous interstrand crosslinks (ICLs) are repaired by the Fanconi anemia (FA) pathway. The pathway is initiated during DNA replication when replication fork stalls, as the DNA cannot be further unwound due to the crosslink. This is recognized by FANCM in complex with FAAP24-MHF1-MHF2, which leads to the remodeling of the replication fork and activates ATR. This also results in the assembly of the FA core complex, which consists of eight FANC proteins (FANCA, FANCB, FANCC, FANCE, FANCF, FANCG, FANCL, and FANCM) and three associated proteins (FAAP20, FAAP24, and FAAP100). The phosphorylated FANCI-FAND2 heterodimer is monoubiquitylated by FANCL, which recruits various endonucleases, including XPF-ERCC1, to cleave the DNA and unhook the lesion. TLS polymerases (POL ι, POL κ, POL ν , and REV1) use the uncut leading strand as a template for further DNA synthesis, bypassing the lesion. Subsequently, the lagging strand invades the newly synthesized strand mediated by RAD51 and gets complimented by homologous recombination (HR).[307, 316, 322, 323]

To repair double-strand breaks (DSBs), the cell has evolved multiple mechanisms. DSBs are recognized and marked by kinases, including ATM (Ataxia telangiectasia mutated), which leads to the phosphorylation of the histone variant H2AX and triggers an extensive chromatin response. This results in the formation of a complex ubiquitin code at the site, mediated by the E3s RNF8 (RING finger protein 8) and RNF168 (RING finger protein 168), as well as the BRCA1-A complex containing a DUB activity. The ubiquitin code initiates the pathway choice through the major players 53BP1 and BRCA1. The appropriate repair pathway is chosen depending on the cell cycle phase, the type of lesion, and the chromatin surrounding the DSB. The following section describes the two main mechanisms in more detail.[308, 324–327]

The primary pathway in mammalian somatic cells for repairing DNA breaks is the resection-independent pathway known as non-homologous end joining (NHEJ). This pathway is active in all cell cycle phases except for M phase. NHEJ is initiated by the persistent binding of the Ku70-Ku80 dimer, which binds to the two ends of the DNA break and protects them from end-resection. The C-terminal domain of Ku80 recruits DNA-PKs, and depending on the break, the nuclease Artemis, along with the DNA polymerases Pol μ and γ. The DNA-PK complex is formed, which can perform minimal end processing if necessary. Next, XRCC4 (X-ray repair cross-complementing protein 4), XRCC4-like factor (XLF), the paralogue of XRCC4 and XLF (PAXX) and DNA ligase IV are recruited to directly seal the break, recovering genome integrity. However, the direct sealing during NHEJ carries the risk of insertions or deletions.[308, 324, 328–333]

In contrast, the homology-directed repair (HDR) pathway ensures a scarless resolution of DNA lesions by using the sister chromatid as a template. This pathway is restricted to late G2 and S phases. To initiate this pathway, the MRN complex forms at both ends of the DSB. CtIP interacts with the MRN complex and recruites and activates the nucleases within the MRN complex, which performs short-term resection. During this process, Ku70-80 is ubiquitylated with K48-linked ubiquitin chains and removed with the help of VCP, antagonizing the NHEJ pathway. The removal of the Ku70-80 dimer enables Exo1 and Dna2 to perform long-term resection, aided by the BLM helicase (Bloom syndrome protein). This long-term resection produces a long 3' single-strand DNA overhang, which is quickly coated with RPA for protection. RPA is phosphorylated and replaced by the DNA recombinase RAD51, which mediates the homologous sequence search on the sister chromatid by invading duplex DNA and facilitating base pairing with complementary homologous DNA sequences. Further factors that play a crucial role in this process are the BRCA1-BARD1 complex, BRCA2 and PALB2 that acts as a mediator between the two BRCA proteins. After identification of a homologous sequence, a Holliday junction is formed by strand exchange. RAD51 is removed, and DNA Pol δ synthesizes the new complementary DNA. In the last step, DSB ends are re-ligated, resulting in a highly accurate and error-free DNA double strand.[308, 334–341]

1.3.3 DNA damage bypass

If DNA damage sites are not repaired prior to replication they pose a high risk to the maintenance of genetic information. Damaged DNA bases function as roadblock for the replication machinery and are a primary source of replication stress, a condition that slows down or stalls replication forks and/or DNA synthesis.[342] Even a single damaged base cannot be repaired by BER or NER once the strands separate for replication because there is no complementary strand available as a template. Excision of this base would lead to a strand break and could induce cell death. Cells have therefore evolved mechanisms to ensure DNA replication in the presence of DNA damage, called DNA damage bypass or DNA damage tolerance (DDT). These mechanisms ensure complete replication and generation of a complementary undamaged strand without removing the actual damage, which can be repaired by subsequent BER or NER reaction after the DNA is back to its double-strand conformation.[343, 344]

In eukaryotes, there are two main pathways conserved: the error-prone translesion synthesis (TLS) and the error-free template switching (TS). The pathway choice is dictated by the ubiquitylation status of PCNA.[101, 345] The following sections will describe this reaction and the subsequent pathways in more detail, focusing on the processes and proteins involved in *S. cerevisiae*, the organism used in this work.

1.3.3.1 Post-translation modifications of PCNA

PCNA is a homotrimeric DNA clamp that functions as a processivity factor for DNA polymerase δ during unperturbed DNA synthesis.[346] In case a replication fork encounters a lesion or experiences stress due to other reasons, helicases and polymerases may uncouple, leading to the exposure of ssDNA. This is quickly covered by RPA, signaling the recruitment of the E2/E3 complex Rad6/Rad18. This complex attaches a single ubiquitin moiety to PCNA at the conserved residue K164, initiating TLS. In yeast, the mutation of the acceptor lysine K164 to an arginine completely abolished damage-induce mutagenesis, demonstrating the essentiality of monoubiquitylation of PCNA for TLS.[101]

The K63-specific, heterodimeric E2 Ubc13/Mms2, together with the E3 Rad5, can extend the monoubiquitin on PCNA into a K63-linked ubiquitin chain in budding yeast. This polyubiquitylation triggers DNA damage bypass via template switching and is vital for yeast cell survival after MMS and UV damage.[345, 347] Two Rad5 homologs (HLTF and SHPRH) have been characterized in mammalian cells.[348, 349] However, both have been found to be non-essential for PCNA polyubiquitylation. It is suggested that ubiquitin ligase RFWD3 triggers polyubiquitylation of PCNA, but further clarification is needed.[350] The TS pathway seems to be conserved and is also activated by K63-polyubiquitylation on PCNA in human cells. However, there is a high redundancy of TS and TLS. Additionally, K63-linked ubiquitin chains on PCNA have also been shown to trigger another pathway called fork reversal and have been linked to fork protection of stalled replication forks in mammalian cells.[351–353] Whether fork reversal can be considered a mode of template switching, where DNA synthesis takes place at the regressed arm, is still a matter of debate. Additional ubiquitylation sites on PCNA and additional E3 ligases have been identified, but their biological functions are not yet fully understood.[354–357] To remove ubiquitylation of PCNA and switch off DNA damage bypass, specialized DUBs are recruited. In yeast, this is done by Ubp10, while in humans, USP1 was reported to perform this function.[100, 358]

In addition to ubiquitylation, PCNA can also be SUMOylated, mainly in S-phase or as a result of high doses of damage. SUMO is conjugated to K164 and to a lesser extent K127 by the E2 SUMO conjugating enzyme Ubc9 and the E3 SUMO ligases Siz1 and Siz2, respectively.[359–361] Although SUMOylation and ubiquitylation target the same site on PCNA, they do not compete. In contrast, Rad18-dependent ubiquitylation is enhanced after binding to SUMOylated PCNA via its SIM (SUMO interaction motif).[360, 362] SUMOylation also supports error-free DDT by recruiting the helicase suppressor of Rad6 2 (Srs2) to dismantle Rad51 filaments and prevent unstrained homologous recombination (HR).[363, 364] Preventing SUMOylation of PCNA will lead to loss of HR inhibition and enhanced salvage recombination. This explains the suppressed damage sensitivity of yeast mutants that prevent SUMOylation and lack DNA damage bypass factors.[345, 365]

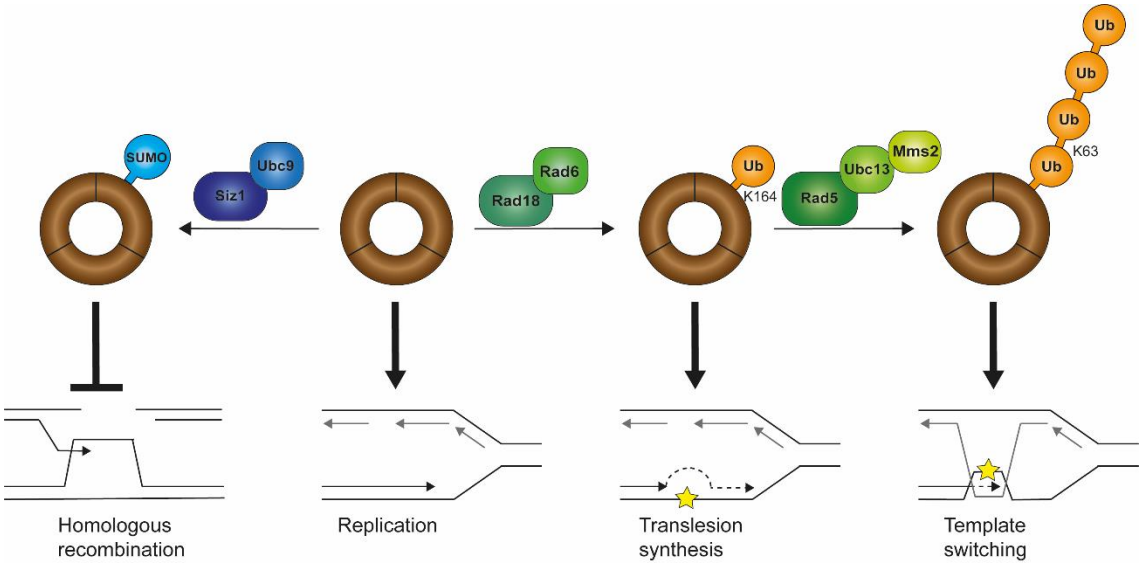

Figure 1.14: Post-translational modifications of PCNA and their consequences. PCNA (brown circle) can be SUMOylated (blue), mono- or polyubiquitylated (orange) by the specific E2 and E3s (green and blue). Unmodified PCNA is a processivity factor for DNA replication. SUMOylation of PCNA blocks homologous recombination, monoubiquitylation initiates translation synthesis, while polyubiquitylation triggers the template switching pathway.

1.3.3.2 Translesion synthesis

Translesion synthesis is performed by TLS polymerases, special damage-tolerant DNA polymerases that substitute for the stalled DNA polymerase. TLS polymerases are highly conserved, with three representatives in *S. cerevisiae*: REV1, DNA Pol ζ, and DNA Pol η. In vertebrates, there has been a large expansion of TLS polymerases, with eleven members in human cells. These are distributed in four families (Y, B, X and A) and PrimPol.[307, 343, 366] Most TLS polymerases have domains for interacting with ubiquitin (UBDs) and PCNA (PIP-box), which recruit them to the stalled fork upon PCNA monoubiquitylation.[367, 368] They lack processivity and proofreading exonuclease activity, and have a more relaxed catalytic pocket than the replicative DNA polymerases ε and δ, allowing them to accommodate modified DNA bases. This process enables replication across the lesion, but it also leads to a higher mutagenesis rate.[366, 369] The error rate during TLS depends on several factors, including the TLS polymerase's characteristics, the lesion's matching, and the DNA sequence context.[307, 370, 371] If all of these factors align, certain polymerases can bypass specific lesions in an error-free manner, such as Pol η, which can synthesize error-free over CPDs, thus this polymerase is crucial for the cellular response to UV damage.[372, 373]

TLS is often performed in a two-step process. First, an 'inserter' TLS enzyme incorporates a nucleotide across the DNA lesion. This often results in imperfect pairing for many DNA lesions, which cannot be extended by the replicative DNA polymerases, necessitating the use of a second extender TLS polymerase. This function is usually fulfilled by Pol ζ. Both processes are orchestrated by REV1, which has a unique scaffolding function and a binding site for PIP-containing polymerases such as Pol η, Pol ι or Pol κ and one for Pol ζ.[374–378]

Besides the examples of error-free synthesis across lesions by TLS polymerases, TLS is often mutagenic. However, this is a lesser evil for the cell than the persistence of a replication blockage, which may result in fork collapse, DSBs and cell death. Nevertheless, due to its mutagenic potential, TLS must be tightly regulated. For instance, it has been shown that ubiquitylation of Pol η inhibits its interaction with PCNA, preventing its function in undamaged cells. Upon various DNA-damaging agents this monoubiquitylation is downregulated to ensure availability of Pol η for TLS.[379] The metalloprotease Spartan also recognizes monoubiquitylated PCNA and recruits p97 to extract the TLS polymerase Pol η to prevent excessive TLS.[380] To terminate TLS after DNA lesion bypass, PCNA is modified with the UbL ISG15 by the ISG15 E3 EFP, which binds to monoubiquitylated PCNA. ISGylated PCNA then recruits the DUB USP10, which deubiquitylates PCNA and releases Pol η from PCNA.[381]

1.3.3.3 Template switching

Next to TLS, there is also a second arm of the Rad6-induced damage bypass that employs a recombination-like mechanism using the newly synthesized sister chromatid as a template. Thus, this error-free DNA damage bypass pathway is called template switching. The usage of the undamaged sister chromatid as a template ensures a complete replication without the loss of genetic information.[382, 383]

Initially, a fork reversal mechanism was proposed, but later the recombination-like invasion mechanism was discovered. In this mechanism, the blocked nascent strand invades the opposite homologous duplex and uses the sister chromatid as a template. This mechanism is supported by 2D gel analysis, which identified X-shaped structures as Holliday junctions between sister chromatids. These structures were observed in an environment of replication stress proximal to replication forks.[365, 382, 384–386] Later, these structures were also visualized by electron microscopy (EM), which showed a post-replicative gap filling model and revealed the nature of many key players.[387]

The formation of the X-structures is dependent on Rad6, Rad18, Ubc13-Mms2, and Rad5. In *S. cerevisiae*, these proteins activate the pathway by K63-linked PCNA polyubiquitylation. However, it is still not well understood how this signal directly initiates the error-free DNA damage bypass.[345, 385, 386]

To facilitate strand invasion, the gap is expanded by the 5'-3' exonuclease Exo1 and the helicase Pif1, which unwinds the 3' junction and generates a 3' flap (Figure 1.15). Exo1 is proposed to be recruited by the checkpoint clamp 9-1-1 (Rad9, Hus1, and Rad1; Ddc1, Mec3, and Rad17 in yeast), which is a critical factor in promoting TS and a sensor for checkpoint activation.[388–390]

Subsequently, the gap region anneals to the homologous duplex strand, forming a three-stranded DNA structure that allows the newly synthesized strand from the undamaged double-strand to serve as a template for new synthesis. This synthesis is mainly conducted by DNA Pol δ, which was shown to have an enhanced activity upon binding to PCNA with Pif1. The synthesis results in the formation of a double Holliday junction-like intermediate, where the two newly synthesized strands and the two parental strands anneal to each other, respectively.[365, 391] This structure is dissolved by the conserved RecQ helicase Sgs1 (Slow Growth Suppressor, BLM in humans), along with Top3 and Rmi1 (Figure 1.15).[365, 384]

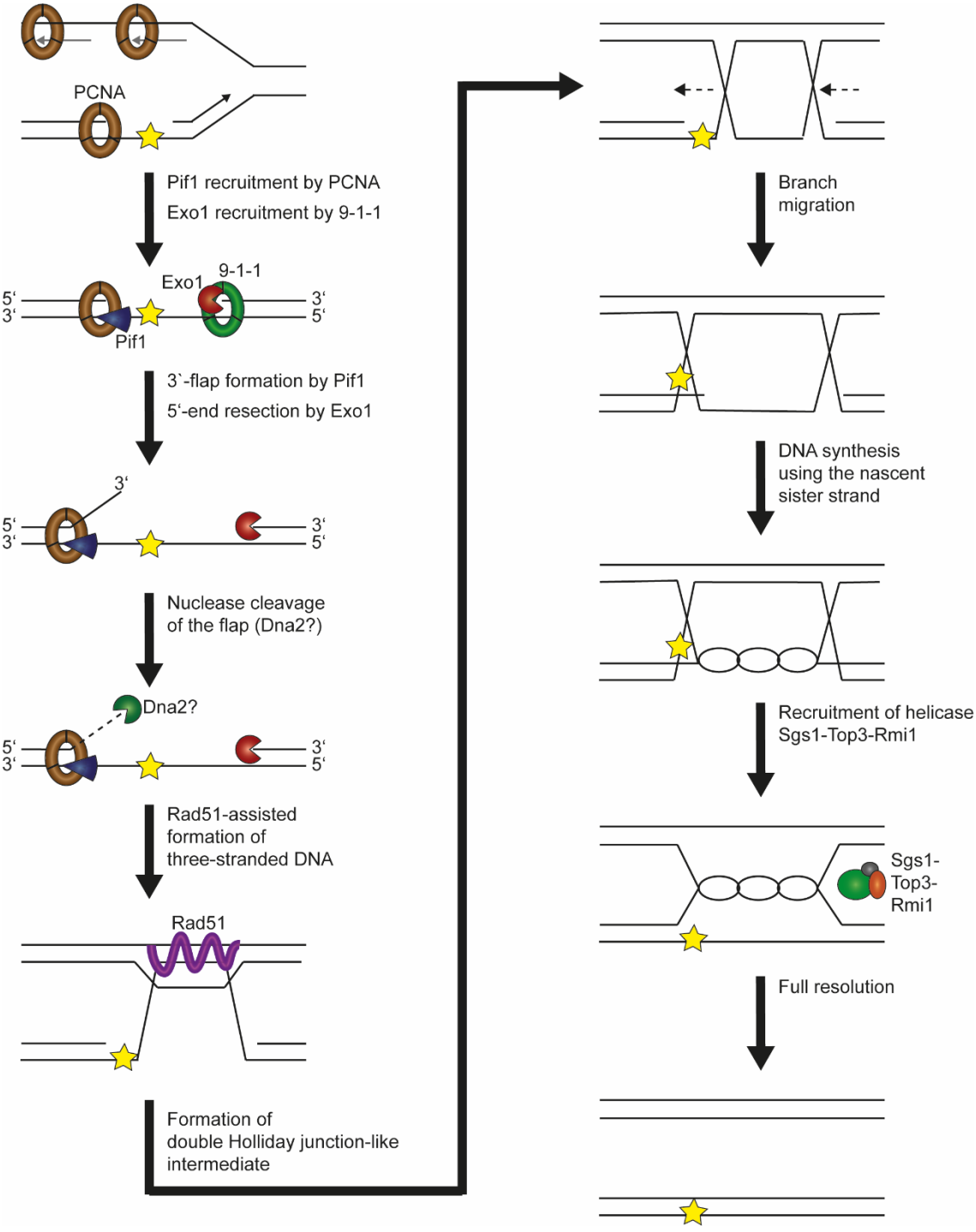

Figure 1.15: Proposed model of template switching. Description in text above. (Based on García-Rodrígues *et al*, 2018 and Branzei and Szakal, 2016.)[365, 390]

Although many factors involved in TS are also known for their function in HR, such as Rad51, Rad52, Rad55-57, and the Shu complex, the genetic pathway differs between the two.[365, 389, 392] Overall, there are still some unresolved questions regarding the pathway and regulation of TS. It is not fully understood how the pathway choice is determined, whether the individual parts of the heterotrimeric PCNA carry more than one modification, or how dynamic the ubiquitylation on PCNA is. However, the main unresolved question pertains to the mechanism by which K63-linked polyubiquitin chains on PCNA trigger TS.[365, 393] Some proteins, such as Mgs1/WRNIP1 or ZRANB3 have been reported to interact preferentially with polyubiquitylated PCNA. Mgs1, however, does not genetically belong to the TS pathway, and no homologs of ZRANB3 exist in yeast. Therefore, the translation of the polyubiquitylated PCNA signal into the TS pathway remains unclear. [352, 390, 394–396]

1.3.3.4 Salvage recombination

Even in the absence of the ubiquitin-dependent pathways, cells can mediate damage bypass through a mechanism called salvage recombination. This is a Rad18-independent DDT recombination pathway that mechanistically equals the homologous recombination pathway. During S phase, it is inhibited by SUMOylation of PCNA, which recruits the anti-recombinogenic helicase Srs2. It preferably acts in later cell cycle phases like G2/M phase. Thus, it is believed to deal with lesions that escaped the TS pathway. This delayed timing also reflects the potential toxicity of HR-mediated fork rescue, making it desirable for genome maintenance to postpone this mechanism as a last resort.[365, 397, 398]

1.3.3.5 Post-replicative repair

Multiple lines of evidence have shown that DNA damage bypass in yeast and mammalian cells is not restricted to the site of the replication fork, but can also work on post-replicative gaps. These daughter strand gaps, regions of ssDNA flanked by dsDNA, on both strands accumulate behind the fork when replication is carried out in the presence of DNA damage.[399–401] Therefore, DNA synthesis must be recommenced via repriming. In budding yeast, this process is mediated by Pol α/Primase and is coordinated with the fork movement by being coupled to the replicative helicase movement.[365, 402, 403] Repriming does not repair the damage but only allows the replication fork to continue past the lesion, leaving behind gaps that need to be repaired post-replicatively via the DNA damage bypass mechanisms TLS and TS. These gaps were shown to be the preferential initiation points of TS compared to the free 3'-termini found at the forks. This supports the idea that DNA damage bypass predominantly operates post-replicatively, mainly in the G2/M phase, accompanied by a cell cycle arrest. This was supported by the finding that TS and TLS factors can be limited to G2/M phase without significantly affecting genome stability.[365, 390, 399–401]

Wong *et al*. demonstrated that post-replicative repair occurs outside of known repair centers, such as nuclear pores, the nuclear periphery, or intra-nuclear quality control (INQ) centers. They defined the term PORTs (post-replicative repair territories) for these repair regions, which are in close proximity to replication centers. Overall, it seems that delaying DNA damage bypass is advantageous when repriming is possible, as it prevents stalling of genome replication progression and reduces the need for coordination of complex DNA structures and proteins. Therefore, DNA damage bypass is predominantly temporally and spatially segregated from ongoing replication.[404]

1.4 Exo1

A protein that has been mentioned already in the mechanism of template switching and MMR is the 5'-3' exonuclease Exo1. As it will be a main focus of this work, the structure and functions of *S. cerevisiae* Exo1 are characterized in more detail below.

Exonuclease 1 is a member of the Rad2 family of structure-specific nucleases. In addition to its 5'-3'double-stranded DNA exonuclease activity, it possesses a 5'flap endonuclease activity. Exo1 exhibits a strong preference for blunt-ended, 5'recessed termini, and DNA nicks and catalyzes the removal of mononucleotides from 5'ends, thereby producing 3'single-stranded tails.[405, 406] Exo1 was first described in 1991 by Philippe Szankasi and Gerald R. Smith in *S. pombe*, but has been shown to be evolutionarily well-conserved.[407] Therefore, the expression of human EXO1 can complement several defects in the *exo1Δ* strain, despite its low identity of 28.4%.[408]

Exo1 can be structurally divided into two parts: the N-terminal nuclease domain and the unstructured C-terminal region. The N-terminal catalytic domain, which is conserved among other Rad2 family members, consists of two subunits: the N-terminal (aa18-96) and internal (aa-123-257) subunits.[409, 410] The unstructured C-terminus has been shown to mediate multiple protein-protein interactions. The interaction between Mlh1 and Exo1 was found to be mediated by the so-called MIP-box located at aa443-448.[411–413] The interaction with Msh2 is mediated by two regions called SHIPs in the region of aa571-702 (Figure 1.16).[414, 415]

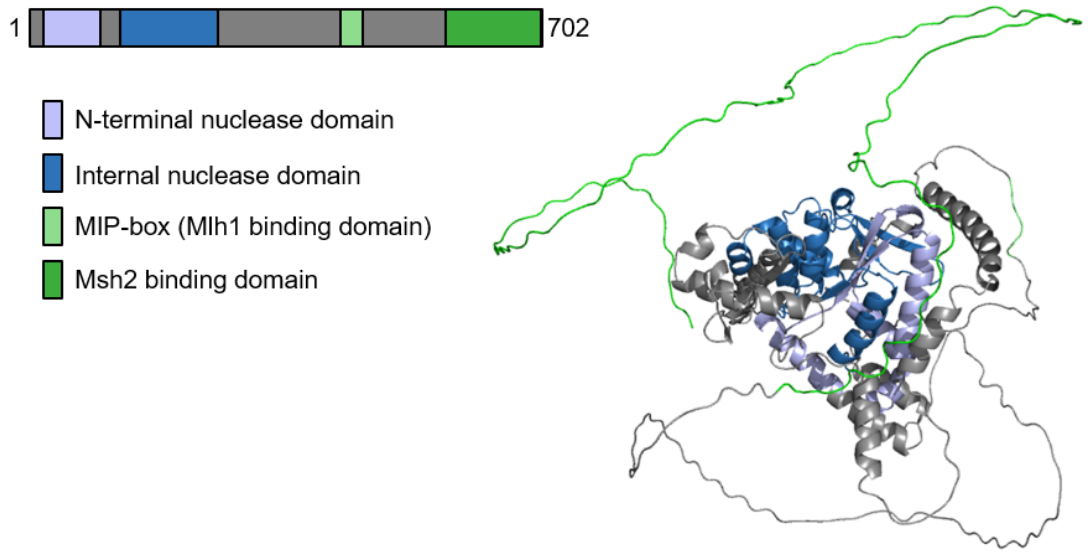

Figure 1.16: Structure and domains of *S. cerevisiae* Exo1. Schematic representation and Alpha-fold predicted structure (https://alphafold.ebi.ac.uk/entry/P39875) of the Exo1 protein and its domains.

Two additional motives in human EXO1 have been described: a PIN domain in the N-terminus that facilitates the recruitment of EXO1 to poly(ADP-ribose)ylated DNA double-strand breaks and a PCNA-interacting protein box (PIP-box) located in its C-terminus (786-802), mediating a direct interaction with PCNA. This interaction has been shown to enhance EXO1 activity during DNA resection.[416–418]

Exo1 is involved in various pathways for DNA metabolism and repair, including DSB repair, mitotic and meiotic recombination, MMR, replication stress response, Okazaki fragment maturation, response to UV damage, and telomere processing and maintenance.[409] Therefore, it is not surprising that *exo1Δ* in budding yeast exhibits synthetic lethality with a wide range of genes involved in oncology.[419] EXO1 has been identified as a target for mutations during oncogenesis itself and is utilized as a prognostic biomarker for various carcinomas.[420, 421]

Exo1 plays a significant role in the repair of DNA double-strand breaks through the initiation of recombination (HR) by resecting the double-stranded DNA breaks to generate a 3′ single-stranded DNA tail. Exo1 often performs long-term resection and extends the 3' single-stranded DNA tail that was created by the initial short-term resection by the MRX-complex (Mre11-Rad50-Xrs2) and Sae2. It has been demonstrated that long-term resection by Exo1 is redundant with the combined action of Sgs1 and Dna2. However, this resection in the absence of Exo1 is reduced.[422–426]

Another pathway in which Exo1 functions in the 5'-3' end resection on a DSB to initiate recombination is mitotic and meiotic recombination. However, it has been shown that Exo1 also has additional functions in this process: it is required for the removal of DNA after strand invasion, and it promotes inter-homologue crossover via the Msh4/Msh5 pathway. In *S. cerevisiae*, intergenic crossovers were reduced 1.5–2-fold in *exo1Δ* strains.[426–431] However, the precise role of Exo1 in crossover resolution during meiosis is not yet known. It has been shown that its exonuclease activity is not required, thus a structural role is proposed.[426] The importance of Exo1 for meiotic recombination is evident from its 5-fold increase in activity during meiosis, observed not only in *S. cerevisiae* but also in *S. pombe* and Drosophila.[432] However, deletion of Exo1 in *S. cerevisiae* only results in a modest loss of spore viability and an increase in chromosome nondisjunction, suggesting a backup mechanism.[428, 429] In contrast, $Exo1^{-/-}$ mice are sterile due to defects in spermatogenesis and oocyte production caused by the inability to progress through meiosis II.[433, 434]

Exo1 also functions in mismatch repair by excising the daughter strand after mismatch recognition (see section 1.3.2). However, a deletion of EXO1 only causes a small increase in the mutation rate (~1%), suggesting again a redundancy.[435] There are now at least two known MMR pathways: one Exo1-dependent and one Exo1-independent. The pathways start identically with the recognition of the mismatch by Msh2-Msh6, the recruitment of Mlh1-Pms1 and PCNA, and the DNA nicking by Mlh1-Pms1. In Exo1-dependent MMR, Exo1 cleaves the area surrounding the mismatch. The recruitment of Exo1 via its MIP-box is essential for this function. The mechanism of the Exo1-independent pathway is not fully understood. It is suggested that it requires strand displacement synthesis by Pol δ combined with flap cleavage of Rad27, excision by another nuclease, possibly MRE11, or additional DNA nicking by Mlh1-pms1, proposing even more than one independent pathway.[409, 436, 437] It was shown that the Exo1-dependent MMR is the more frequently used and faster one, and thus might be more important one *in vivo*.[409, 438]

Soon after the discovery of Exo1's role in MMR, an independent role for Exo1 in DNA damage tolerance was proposed. It was found that Exo1 deletion has an epistatic effect on the MMS sensitivity with the deletion of Mms2, thus functioning in the error-free DNA damage bypass pathway.[439] As explained in section 1.3.3.3, it functions in widening the gaps to allow recombination. Research has demonstrated that the yeast 9-1-1 complex enhances the Exo1 function in DNA end resection and that Exo1 can effectively compensate for the absence of Pif1 in this pathway.[388, 390]

Exo1 appears to function as back-up mechanisms of Rad27 in Okazaki fragment processing. In unperturbed conditions, the endonuclease Rad27 (FEN1 in humans) cleaves off the RNA primer-containing flap. In a strain lacking functional Rad27, Exo1 compensated for its phenotype by promoting strand displacement and/or removal of DNA flap structures. Additionally, it has been proposed that the 5' flap endonuclease activity plays a role in resolving DNA intermediates formed during replication and recombination. However, studies have shown that Exo1's flap activity on 5' flaps is most efficient on flaps that are only 1 or 2 nucleotides long and gets quite weaker for nucleotides longer than 20. This suggests that Exo1 has a weak structure-specific endonuclease activity that works in concert with a more potent 5' to 3' exonuclease activity.[408, 417, 427, 440, 441]

Additional functions for Exo1 have been shown in the repair of UV damage by an NER-independent pathway, in line with its increased expression after UV light, and in the maintenance of uncapped telomeres.[442–444] The widening of NER gaps outside of S-phase by Exo1 and Pif1 has been shown to contribute to checkpoint activation.[387, 445] Also, after DSBs Exo1, together with the Mre11 complex, functions in the activation of the Mec1 checkpoint signaling.[446] For human EXO1, an additional 5'-3' RNase H activity during Ribonucleotide excision repair and a function in immunoglobulin maturation have been proposed.[408, 441, 447]

Exo1 contributes to genome maintenance through its various functions. However, excessive degradation can lead to elevated genome instability, so the function of Exo1 needs to be tightly regulated. This regulation occurs through protein-protein interactions, such as the binding of CtIP (the human analog to yeast Sae2), which inhibits EXO1 nuclease activity, and through post-translational modification. Additionally, it has been shown that EXO1 is regulated during the cell cycle, and based on *in vitro* experiments, it was suggested that the C-terminal domain may function as an auto-inhibitory domain.[410, 448, 449]

The regulation of EXO1 via post-translational modification has been extensively characterized in humans. However, some modifications have also been discovered in yeast, such as damage-induced phosphorylation of Exo1, which leads to its interaction with 14-3-3 proteins. The stability of human EXO1 is regulated via phosphorylation by ATR and cyclin-dependent kinases (CDKs) 1 and 2.[448, 450–452] García-Rodríguez *et al* have shown, that by checkpoint activation, Exo1 also activates a negative feedback loop via the checkpoint kinase Rad53. Rad53 phosphorylates Exo1, inhibiting its activity and preventing excessive degradation and large-scale genome instability.[453]

Polyubiquitylation of EXO1, presumably linked via K6 and K33 by the SCF ligase, was observed after exposure to UV light and DNA damaging agents. Additionally, proteasomal degradation of EXO1 was observed after replication stress. Acetylation and SUMOylation sites were identified, but their specific roles are not yet known. In general, PTMs mostly promote the extinction of DNA processing activity, even though they are mainly located outside of the catalytic domain, thus they probably function through inhibiting or promoting protein-protein interactions instead of conformational changes.[155, 448, 454, 455]

1.5 Aims of this work

Ubiquitin is a post-translational modifier involved in almost all cellular processes in eukaryotes. Its versatility as a signaling molecule is due to its ability to occur in various topologies, including monoubiquitylation and ubiquitin chains linked via eight different residues, as well as mixed and branched ubiquitin chains. However, the function-topology relationship of specifically linked ubiquitin chains is still poorly understood. Among others, this is due to the lack of tools that can track linkage-specific polyubiquitin signals *in vivo* in a specific and independent manner.

The first part of this work aims to address this issue by developing linkage-specific affinity probes for the recognition, inhibition and tracking of linkage-specific polyubiquitylation for the two most studied linkages, K48 and K63, both *in vitro* and *in vivo*. Our tool is based on DARPins, which are synthetic scaffold proteins and have emerged as powerful tools as, unlike conventional antibodies, these specific, high-affinity binders can be used *in vivo* due to their small size and simple structure. DARPins against K48- and K63-linked ubiquitin dimers were raised from a library with randomized target interaction residues. This work aims to identify suitable candidates for both linkages and to characterize them regarding their binding properties, selectivity, and inhibitory effects. The specific affinity probes are then investigated for their usability in pull-down approaches and as sensors to specifically recognize and track K48-, K63-, as well as K48-K63-branched polyubiquitin chains *in vivo*, enabling us to monitor the dynamics and localization of these ubiquitin signals.

Ubiquitylation also regulates numerous pathways and factors involved in the DNA damage response. One crucial process is the ubiquitylation of PCNA, which determines the pathway choice of DNA damage bypass. However, although the K63-specific polyubiquitylation of PCNA, which triggers error-free template switching, has been known for over 20 years, the direct reader of this modification is still unknown.

Yeast two-hybrid screens conducted in our lab have suggested an interaction between PCNA and the exonuclease Exo1, which is enhanced upon ubiquitylation of PCNA. The second part of this work aims to reproduce this interaction, determine its nature and quantify the preferential binding of Exo1 to polyubiquitylated over unmodified PCNA. The domains in Exo1 that mediate this interaction shall be identified and characterized and the biological impact of this interaction is investigated.

2 Materials and Methods

2.1 Reagents

2.1.1 Chemicals

Unless indicated differently, chemicals used in this study were purchased from Sigma-Aldrich (Merck) or Thermo Fisher Scientific.

BioTrend: IPTG, ultrapure

Carl Roth: Acetic acid glacial, acetone, 96% and 99.5% ethanol, isoproanol, imidazole

Enzo Life Sciences: MG132 (Proteasome inhibitor)

Life Technologies: SYBR Safe DNA Stain

New England Biolabs: Quick load 100 bp or 1 kb DNA ladder, dNTPs, 10x CutSmart reaction buffer for restriction enzymes

Promega: 5x Green GoTaq reaction buffer, FuGENE® HD Transfection Reagent

Qiagen: Ni-NTA Agarose, QIAquick Gel Extraction Kit (250)

Roche: cOmplete Protease Inhibitor Cocktail

Sigma-Aldrich: Duolink® In Situ PLA® Probe Anti-Rabbit PLUS/Anti-Mouse MINUS, Duolink® In Situ Detection Reagents Red

Takara Bio: 2x DNA ligation kit

2.1.2 Proteins and peptides

Table 2.1: Commercial proteins used in this work.

Protein	Supplier
Apyrase	New England Biolabs
Bovine serum albumin (BSA)	Sigma-Aldrich
Di-ubiquitin (K6-linked)	Biomol
Di-ubiquitin (K11-linked)	Biozol
Di-ubiquitin (K27-linked)	Biozol
Di-ubiquitin (K29-linked)	Biomol
Di-ubiquitin (K33-linked)	Biomol
DpnI (1000 cU/ 50 µL)	Core Facility Protein Production, IMB
FastAP Thermosensitive Phosphatase	Thermo Fisher Scientific
Poly FLAG Peptide	Absource Diagnostics
Gibson assembly 2X master mix	Core Facility Protein Production, IMB
HF- DNA Polymerase	Core Facility Protein Production, IMB
His-3C Protease	Core Facility Protein Production, IMB
His-TEV Protease	Core Facility Protein Production, IMB

Continued on next page

Table 2.1: Commercial proteins used in this work.

K48-TUBE HF Flag	Tebu-bio
K63-TUBE Flag	Tebu-bio
LR clonase 4x master mix	Core Facility Protein Production, IMB
Prescission protease	Core Facility Protein Production, IMB
Restriction enzymes (5-20 kU / mL)	New England Biolabs
Sm Nuclease (>15 kU/ 60 µL)	Core Facility Protein Production, IMB
T4 DNA Ligase	Core Facility Protein Production, IMB
Takara DNA ligase mix	Clontech/Takara
Taq DNA polymerase (500 cU /100 µL)	Core Facility Protein Production, IMB
Tetra-ubiquitin chains (K48-linked)	R&D Systems
Tetra-ubiquitin chains (K63-linked)	R&D Systems
Ubiquitin (1 mg/mL)	Sigma Aldrich

2.1.3 Antibodies

Table 2.2: Primary antibodies used in this study.

ID	Name	Species	Source	Dilution
17	c-Myc	Rabbit pAb	Santa Cruz	1:2000
37	Exo1	Goat pAb	Santa Cruz	1:2000
40	Flag	Rabbit pAb	Sigma	1:2000
42	Flag M2	Mouse mAb	Sigma	1:2500
49	GFP	Mouse mAb	Roche	1:2000
51	GFP	Rabbit pAb	Invitrogen	1:2000
56	GST	Mouse mAb	Santa Cruz	1:5000
70	His	Mouse mAb	Sigma	1:5000
76	mCherry	Mouse mAb	-	1:2000
99	Myc	Mouse mAb	IMB-PPCF	1:2000
126	PCNA (Pol30, yeast)	Rabbit pAb	-	1:2500
150	Pol30	Rabbit serum	Francis CRICK Institute	1:2000
190	RFP (6G6)	Mouse mAb	ChromoTek	1:1000
260	Ubiquitin	Rabbit pAb	Dako	1:5000
261	Ubiquitin (VU-1)	Mouse mAb	Tebu-bio	1:1000
262	Ubiquitin (K48-selective, Apu2)	Rabbit mAb	Millipore	1:1000
263	Ubiquitin (K63-selective, HWA4C4)	Mouse mAb	Enzo	1:1000
265	Ubiquitin (P4D1)	Mouse mAb	CST	1:2500
266	Ubiquitin (FK2)	Mouse mAb	Biotrend	1:2000
298	Myc-Tag	Mouse mAb	Merck	1:2000
369	Ubiquitin	Rabbit pAb	CST	1:1000
431	G3BP1	Mouse mAb	Abcam	1:1000
432	Ubiquitin (E4I2J)	Rabbit mAb	CST	1:2000
442	Ubiquitin (#1002A)	Rabbit mAb	Bio-Tachne	1:2000
450	Ubiquitin (K63-specific, D7A11)	Rabbit mAb	CST	1:1000
458	Ubiquitin (K48-specific)	Rabbit pAb	CST	1:1000

Table 2.3: Secondary antibodies used in this study.

ID	Name	Species	Source	Dilution
55	Goat 800CW	Donkey	Licore	1:10,000
92	Mouse 800 CW	Donkey	Licore	1:10,000
96	Mouse HRP	Goat	Pierce	1:10,000
154	Rabbit 680LT	Donkey	Licore	1:10,000
155	Rabbit 800CW	Goat	Licore	1:10,000
156	Rabbit HRP	Goat	Pierce	1:10,000

2.2 Media and solutions

For the production of all media and solutions mentioned below sterile demineralized water was used.

2.2.1 Media for bacterial cells

All *E.coli* stains were grown on Lysogeny Broth (LB) plates or in liquid LB medium, both prepared by the IMB media laboratory. For selection antibiotics were added to the medium and agar plates for *E. coli* cultivation. The used antibiotics and their concentrations are summarized in Table 2.4.

Table 2.4: Antibiotics used in this work.

Antibiotic	Stock concentration (mg/ mL)	Final concentration (mg/L)
Ampicillin (Amp)	100	100
Kanamycin (Kan)	30	30
Chloramphenicol (Cm)	34	34
Gentamycin (Gen)	10	10

2.2.2 Media for yeast cells

Yeast Peptone (YP) medium, YPD plates, 4% (w/v) water-agar and 20% (w/v) glucose were prepared by the IMB media laboratory. Other growth media were prepared according to following recipes.

Synthetic complete (SC) powder:

36.7 g of the dropout powder were mixed with 0.5 g adenine, 2 g histidine, 4 g leucine, 2 g tryptophan and 2 g uracil overnight. Specific SC stocks were prepared by omitting the relevant amino acid.

2.5x SC medium:

4.25 g of yeast nitrogen base (without amino acids and ammonium sulfate), 12.5 g of ammonium sulfate and 5 g of the SC-powder (complete or depleted by one or several amino acids used for selection) were mixed in 1 L of water, afterwards stirred for 30 min and autoclaved.

1x SC medium:

200 mL of 2.5x SC medium, 250 mL of distilled water and 50 mL of 20% (w/v) sugar (glucose, raffinose or galactose) were mixed.

SC medium agar:

200 mL of 2.5x SC medium, 250 mL of 4% molten water-agar and 50 mL of 20% (w/v) glucose or galactose were mixed. For testing the growth under stress condition certain stressors (section 2.8.5) were added in indicated concentrations to the still warm mixture before this was poured into sterile plates.

2.2.3 Media for mammalian cells

HeLa cells were cultured in Dulbecco's Modified Eagle Medium (DMEM) supplemented with 2 mM L-glutamine, 100 U/ml penicillin, 100 µg/ml streptomycin and 10% (v/v) Fetal bovine serum (FBS). RPE1 cells were grown in RPMI 1640 medium with the same supplements. For seclection 2 µg/ml puromycin were added to the medium.

2.2.4 Buffers and Solutions

The solutions listed in the following were prepared by the IMB media laboratory according to general recipes: 0.5 M EDTA pH 8.0, 1 M KCl, 2 M $MgCl_2$, 5 M NaCl, 5x Phosphate buffered saline (PBS), 10x SDS running buffer, 1 M Tris(hydroxymethyl)aminomethane (Tris)-HCl pH 6.8, 1M Tris-HCl pH 7.5, 10x wet transfer buffer. The ingredients of the buffers prepared in our laboratory are listed hereafter.

4x Laemmli buffer:

250 mM Tris-HCl pH 6.8, 10% (w/v) SDS, 0.1% (w/v) bromophenol blue, 10% (v/v) glycerol. Freshly supplemented with 100 mM dithiothreitol (DTT)

6x DNA loading buffer:

50% (w/v) sucrose, 0.1% (w/v) bromophenol blue, 0.1% (w/v) xylene cyanol F in 1x TE

Blocking solution:

5% (w/v) skim milk powder in 1x PBS-T

HBS-EP buffer

0.01 M HEPES pH 7.4, 0.15 M NaCl, 3 mM EDTA, 0.005% v/v Surfactant P20

HT DNA solution:

Herring testes DNA Type XIV (Sigma) was dissolved and vigorously sonicated in TE buffer (10 mg/mL), phenol/chloroform extracted, precipitated with ethanol and resuspended in TE buffer before boiling at 95°C for 5 min. Afterwards the solution was quickly incubated on ice for 5 min and stored at 4°C.

HU buffer:

8 M hydroxyurea (HU), 5% (w/v) SDS, 200 mM Tris-HCl pH 6.8, 1 mM EDTA, 0.1% (w/v) bromophenol blue, 50 mM DTT

LiT buffer:

10 mM Tris-HCl, pH 7.4, 100 mM lithium acetate, autoclaved

LiT/PEG buffer:

50% (w/v) PEG 3350 in LiT buffer, autoclaved

MC lysis buffer:

100 mM Tris-HCl, pH 8.0, 0.15 M NaCl, 5 mM EDTA, 1% IGEPAL, 0,5% Triton-X100

MC dilution buffer:

100 mM Tris-HCl, pH 8.0, 0.15 M NaCl, 5 mM EDTA

MES running buffer:

50 mM MES hydrate, 50 mM Tris-HCl pH 7.3, 0.1% (v/v) SDS, 1 mM EDTA

MOPS running buffer:

50 mM MOPS, 50 mM Tris-HCl PH 7.7, 0.1% (v/v) SDS, 1 mM EDTA

NaOH/β−ME solution:

925 mL of 2 M NaOH and 75 mL of β-Mercaptoethanol (ME)

PBST-T:

1x PBS, 0.1% (v/v) Tween20

Ponceau S solution:

0.1% (w/v) Ponceau S in 5% (v/v) acetic acid

RIPA buffer:

50 mM Tris-HCl pH 7.5, 150 mM NaCl, 1% IGEPAL CA-630, 0.5% Sodium deoxycholate, 0.1% SDS, 2.5 mM $MgCl_2$

SORB buffer:

10 mM Tris-HCl pH 8.0, 1 mM EDTA pH 8.0, 100 mM lithium acetate,1 M Sorbitol, autoclaved

Trans-Blot Turbo buffer:

1x Trans-Blot Turbo buffer (Bio-Rad), 20% ethanol

Ubiquitylation buffer:

40 mM HEPES pH 7.4, 8 mM magnesium acetate, 50 mM NaCl

Zymolyase buffer

1.2 M Sorbitol, 100 mM $K_xH_xPO_4$ pH 6.5

2.2.4.1 Buffers for protein purification and assays

AEX buffer A

50 mM Tris pH 6.5, 1 mM EDTA

AEX buffer B

50 mM Tris pH 6.5, 1 mM EDTA, 1M NaCl

Amylose buffer A

25 mM Tris pH 7.4, 300 mM NaCl, 1 mM EDTA, 1 mM DTT

Exo1 PD buffer

1x PBS, 0.1% Triton X-100, 1 mM DTT

GF-buffer

50 mM HEPES pH 7.4, 150 mM NaCl, 10 %(v/v) Glycerol, 1 mM DTT

GST-lysis buffer

50 mM HEPES pH 7.5, 150 mM NaCl, 1 mM DTT

GST- buffer A

25 mM Tris pH 8.5, 200 mM NaCl, 1 mM DTT

IEX A:

50 mM TRIS pH 7.6

IEX B:

50 mM TRIS pH 7.6, 1M NaCl

IMAC A:

50 mM TRIS pH 8.0, 300 mM NaCl, 15 mM Imidazol, 1 mM DTT

IMAC B:

50 mM TRIS pH 8.0, 300 mM NaCl, 300/500 mM Imidazol, 1 mM DTT

MC dilution buffer

100 mM Tris-HCl pH 8.0, 150 mM NaCl, 5 mM EDTA

MC PD buffer

100 mM Tris-HCl pH 8.0, 150 mM NaCl, 5 mM EDTA, 0.05%(v/v) IGEPAL

2x PD buffer:

100 mM HEPES pH 7.5, 100 mM NaCl, 2%(v/v) Glycerol, 2%(v/v) Triton X-100

2x PD buffer high salt:

100 mM HEPES pH 7.5, 1 M NaCl, 2%(v/v) Glycerol, 2%(v/v) Triton X-100

Sf9 lysis buffer

50 mM Tris pH 7.5, 1m M DTT, 1mM EDTA

Storage buffer:

1x PBS, 10% Glycerol, 1 mM DTT

TEV cleavage buffer:

10 mM Tris pH 7.5, 150 mM NaCl, 1mM EDTA,1mM DTT

10x Ubi buffer

400 mM HEPES pH 7.4, 80 mM $Mg(CH_3COO)_2$, 500 mM NaCl

Ubi A buffer:

25 mM NaAc pH 4.5

Ubi B buffer:

25 mM NaAc pH 4.5, 1 M NaCl

Ulp1 cleavage buffer:

50 mM Tris-HCl pH 8, 150 mM NaCl, 1 mM DTT, 0.5 mM EDTA

Yeast lysis buffer

50 mM HEPES pH 7.4, 150 mM NaCl, 1 mM DTT, 10%(v/v) Glycerol

Yeast PD buffer

50 mM TRIS pH 7.5, 150 mM NaCl, 10% (v/v) Glycerol, 1 mM DTT, 5 mM EDTA, 0.1%(v/v) NP-400, 0.05%(v/v) TX-100

2.3 Microorganisms

2.3.1 Bacterial strains

Table 2.5: Bacterial strains used in this study.

ID	Name	Genotype	Purpose	Supplier
3	Bl21 (DE3)	B F– dcm ompT hsdS(rB – mB –) gall(DE3)	Standard expression	Novagen
4	Bl21 (DE3) pLys S	B F– dcm ompT hsdS(rB – mB –) gal l(DE3) [pLysS CamR]*	Expression of toxic proteins	Novagen
5	BL21-Codonplus DE3 RIL-(Codon +)	B F– ompT hsdSB(rB-mB) dcm+ TetR gal l(DE3) endA Hte [argU ileY leuW CamR]	Expression of proteins with rare codons: AGA, AGG,AUA, CUA	Stratagene
14	Top Ten F’	F– mcrA Δ(mrr-hsdRMS-mcrBC) φ80lacZΔM15 ΔlacX74 recA1 araD139 Δ(ara-leu)7697 galU galK λ– rpsL(StrR) endA1 nupG	Standard cloning	Invitrogen
16	XL1-blue	recA1 endA1 gyrA96 thi-1 hsdR17 supE44 relA1 lac [F’ proAB lacIqZDM15 Tn10 (Tetr)]	Standard cloning, DARPin expression	Stratagene (University Zurüch)
18	ccdB Survival 2	F-mcrA Δ(mrr-hsdRMSmcrBC) Φ80lacZΔM15 ΔlacX74 recA1 araΔ139 Δ(ara-leu)7697 galU galK rpsL (StrR) endA1 nupG fhuA::IS2	Cloning of ccdB containing vectors	Invitrogen
25	Rosetta™ 2 (DE3) pLysS	F- ompT hsdSB(rB- mB-) gal dcm (DE3) pLysSRARE2 (CamR)	Expression of proteins with rare codons: AGA, AGG, AUA, CUA, GGA, CCC, and CGG	Novagen
26	DH10 EmBacY	F-mcrA Δ(mrr-hsdRMS-mcrBC) Φ80lacZΔM15 ΔlacX74 recA1 endA1 araD139 Δ(ara, leu)7697 galU galK λ-rpsL nupG	Bacmid generation via Tn7 transposition according to Bac-to-Bac protocol from invitrogen, modified bacmid: YFP under polyhedrin promotor control plus loxP site.	PPCF, IMB

2.3.2 Yeast strains

Table 2.6: *S. cerevisiae* strains used in this study.

ID	Name	Genotype	Back-ground	Source
3	DF5	*his3-Δ200, leu2-3,2-112, lys2-801, trp1-1(am), ura3-52*	DF5	Stefan Jentsch
195	PJ69-4A	*trp1-901, leu2-3,112, ura3-52, his3-200, gal4Δ, gal80Δ, LYS2::GAL1-HIS3, GAL2-ADE2, met2::GAL7-lacZ*	PJ	Philip James
2260	pdr5Δ	*his3-Δ200, leu2-3,2-112, lys2-801, trp1-1(am), ura3-52, pdr5::KanMX*	DF5	Shengkai Zhao
2821	W303 RAD5+	*leu2-3,112 trp1-1 can1-100 ura3-1 ade2-1 his3-11,15*	W303	Liz Colby
3887	rad18	*RAD5 bar1::LoxP rad18::HPH*	W303	Cheng-Fu Kao
3921	Exo1-9myc	*his3-Δ200, leu2-3,2-112, lys2-801, trp1-1(am), ura3-52, EXO1-9myc::hphNT1*	DF5	Nestor Garcia
3962	pol32 exo1	*his3-Δ200, leu2-3,2-112, lys2-801, trp1-1(am), ura3-52, pol32::KanMX exo1Δ::natNT2*	DF5	Nestor Garcia
4040	smc6–56–13MYC exo1	*ade2–1 can1–100 ura3–1 his3–11,15 leu2–3,112 trp1–1 rad5–535, smc6–56–13MYC::KanMX, RAD5+, exo1Δ::hphNT1*	W303	Nestor Garcia
4043	W303 RAD5+ exo1	*leu2-3,112 trp1-1 can1-100 ura3-1 ade2-1 his3-11,15, exo1Δ::hphNT1*	W303	Nestor Garcia
4044	W303 RAD5+ ubc13	*leu2-3,112 trp1-1 can1-100 ura3-1 ade2-1 his3-11,15, ubc13Δ::natNT2*	W303	Nestor Garcia
4116	exo1	*his3-Δ200, leu2-3,2-112, lys2-801, trp1-1(am), ura3-52, exo1Δ::natNT2*	DF5	Nestor Garcia
4302	exo1-PIP2	*his3-Δ200, leu2-3,2-112, lys2-801, trp1-1(am), ura3-52, exo1-PIP2::His3MX*	DF5	Nestor Garcia
4304	pol32 exo1-PIP2	*his3-Δ200, leu2-3,2-112, lys2-801, trp1-1(am), ura3-52, pol32::KanMX, exo1-PIP2::His3MX*	DF5	Nestor Garcia
4306	W303 RAD5+ exo1-PIP2	*leu2-3,112 trp1-1 can1-100 ura3-1 ade2-1 his3-11,15, exo1-PIP2::His3MX*	W303	Nestor Garcia
4308	smc6–56–13MYC exo1-PIP2	*ade2–1 can1–100 ura3–1 his3–11,15 leu2–3,112 trp1–1 rad5–535, smc6–56–13MYC::KanMX, RAD5+, exo1-PIP2::His3MX*	W303	Nestor Garcia
5077	W303 RAD5+ doa4	*leu2-3,112 trp1-1 can1-100 ura3-1 ade2-1 his3-11,15, doa4 ::natNT2*	W303	This study
5791	DF5 TetO7-GFP	*his3-Δ200, leu2-3,2-112, lys2-801, trp1-1(am), URA::yIp211-TetO7-GFP*	DF5	This study

Continued on next page

Table 2.6: *S. cerevisiae* strains used in this study.

5792	DF5 TetO7-DARPin_E3_5-Flag-GFP	*his3-Δ200, leu2-3,2-112, lys2-801, trp1-1(am), URA::yIp211-TetO7-DARPin_E3_5_GFP*	DF5	This study
5793	DF5 TetO7-DARPin_Ub_K48_A1-Flag-GFP	*his3-Δ200, leu2-3,2-112, lys2-801, trp1-1(am), URA::yIp211-TetO7-DARPin_Ub_K48_A1-Flag-GFP*	DF5	This study
5794	DF5 TetO7-DARPin_Ub_K63_G1-Flag-GFP	*his3-Δ200, leu2-3,2-112, lys2-801, trp1-1(am), URA::yIp211-TetO7-DARPin_Ub_K63_G1-Flag-GFP*	DF5	This study
5795	pdr5Δ TetO7-GFP	*his3-Δ200, leu2-3,2-112, lys2-801, trp1-1(am), pdr5::KanMX, URA::yIp211-TetO7-GFP*	DF5	This study
5796	pdr5Δ TetO7-DARPin_E3_5-Flag-GFP	*his3-Δ200, leu2-3,2-112, lys2-801, trp1-1(am), pdr5::KanMX, URA::yIp211-TetO7-DARPin_E3_5_GFP*	DF5	This study
5797	pdr5Δ TetO7-DARPin_Ub_K48_A1-Flag-GFP	*his3-Δ200, leu2-3,2-112, lys2-801, trp1-1(am), pdr5::KanMX, URA::yIp211-TetO7-DARPin_Ub_K48_A1-Flag-GFP*	DF5	This study
5798	pdr5Δ Pab1-mCherry	*his3-Δ200, leu2-3,2-112, lys2-801, trp1-1(am), ura3-52, pdr5::KanMX Pab1-mcherry::NAT*	DF5	This study
5803	pdr5Δ TetON-2xNES-DARPIN-E3_5-Flag-GFP	*his3-Δ200, leu2-3,2-112, lys2-801, trp1-1(am), pdr5::KanMX, URA::YIp211-TetON-2xNES-DARPIN-E3.5-Flag-GFP*	DF5	This study
5804	pdr5Δ TetON-2xNES-DARPin-Ub K48 A1-Flag-GFP	*his3-Δ200, leu2-3,2-112, lys2-801, trp1-1(am), pdr5::KanMX, URA::YIp211-TetON-2xNES-DARPin-Ub K48 A1-Flag-GFP*	DF5	This study
5805	pdr5Δ TetON-2xNES-DARPin-Ub K63 G1-Flag-GFP	*his3-Δ200, leu2-3,2-112, lys2-801, trp1-1(am), pdr5::KanMX, URA::YIp211-TetON-2xNES-DARPin-Ub K63 G1-Flag-GFP*	DF5	This study
5806	pdr5Δ Pab1-mCherry TetO7-DARPin_E3_5-Flag-GFP	*his3-Δ200, leu2-3,2-112, lys2-801, trp1-1(am), ura3-52, pdr5::KanMX, Pab1-mcherry::NAT, URA::yIp211-TetO7-DARPin_E3_5_GFP*	DF5	This study
5807	pdr5Δ Pab1-mCherry TetO7-DARPin_Ub_K48_A1-Flag-GFP	*his3-Δ200, leu2-3,2-112, lys2-801, trp1-1(am), ura3-52, pdr5::KanMX, Pab1-mcherry::NAT, URA::yIp211-TetO7-DARPin_Ub_K48_A1-Flag-GFP*	DF5	This study

Continued on next page

Table 2.6: *S. cerevisiae* strains used in this study.

5808	pdr5Δ Pab1-mCherry TetO7-DARPin_Ub_K63_G1-Flag-GFP	*his3-Δ200, leu2-3,2-112, lys2-801, trp1-1(am), ura3-52, pdr5::KanMX, Pab1-mcherry::NAT, URA::yIp211-TetO7-DARPin_Ub_K63_G1-Flag-GFP*	DF5	This study
5815	pdr5Δ Pab1-GFP	*his3-Δ200, leu2-3,2-112, lys2-801, trp1-1(am), ura3-52, pdr5::KanMX, Pab1-GFP::NAT*	DF5	This study
5816	pdr5Δ Pab1-GFP DARPin K48 A1-mRuby	*his3-Δ200, leu2-3,2-112, lys2-801, trp1-1(am), ura3-52, pdr5::KanMX, Pab1-GFP::NAT, URA::YIp128-TET-DARPin_K48_A1-Flag-mRuby2*	DF5	This study
5817	pdr5Δ Pab1-GFP DARPin K63 G1-mRuby	*his3-Δ200, leu2-3,2-112, lys2-801, trp1-1(am), ura3-52, pdr5::KanMX, Pab1-GFP::NAT, URA::YIp128-TET-DARPin_K63_G1-Flag-mRuby2*	DF5	This study
5818	pdr5Δ Pab1-GFP DARPin E3_5-mRuby	*his3-Δ200, leu2-3,2-112, lys2-801, trp1-1(am), ura3-52, pdr5::KanMX, Pab1-GFP::NAT, URA::YIp128-TET-DARPin_E3_5-Flag-mRuby2*	DF5	This study
5823	Exo1-His6-FLAG	*ura3-52, trp1, leu2Δ1, his3-Δ200, pep4::HIS3, prb1Δ1.6R, can1, GAL10-Exo1-His6-FLAG*	RDKY 1293	D. Kolodner
5824	pol32 exo1-UBD	*his3-Δ200, leu2-3,2-112, lys2-801, trp1-1(am), ura3-52, pol32::KanMX, exo1-UBD::his3MX*	DF5	This study
5825	pol32 exo1-PIP2-UBD	*his3-Δ200, leu2-3,2-112, lys2-801, trp1-1(am), ura3-52, pol32::KanMX, exo1-PIP2-UBD::his3MX*	DF5	This study
5826	smc6–56–13MYC exo1-UBD	*ade2–1 can1–100 ura3–1 his3–11,15 leu2–3,112 trp1–1 rad5–535, smc6–56–13MYC::KanMX, RAD5+, exo1-UBD::His3MX*	W303	This study
5827	smc6–56–13MYC exo1-PIP2-UBD	*ade2–1 can1–100 ura3–1 his3–11,15 leu2–3,112 trp1–1 rad5–535, smc6–56–13MYC::KanMX, RAD5+, exo1-PIP2-UBD::His3MX*	W303	This study
5828	exo1-UBD	*his3-Δ200, leu2-3,2-112, lys2-801, trp1-1(am), ura3-52, exo1-UBD::His3MX*	DF5	This study
5829	exo1-PIP2-UBD	*his3-Δ200, leu2-3,2-112, lys2-801, trp1-1(am), ura3-52, exo1-PIP2-UBD::His3MX*	DF5	This study
5830	W303 Rad5+ exo1-UBD	*ade2–1 can1–100 ura3–1 his3–11,15 leu2–3,112 trp1–1 rad5–535, RAD5+, exo1-UBD::His3MX*	W303	This study

Continued on next page

Table 2.6: *S. cerevisiae* strains used in this study.

5831	W303 Rad5+ exo1-PIP2-UBD	*ade2–1 can1–100 ura3–1 his3–11,15 leu2–3,112 trp1–1 rad5–535, RAD5+, exo1-PIP2-UBD::His3MX*	W303	This study
5832	exo1-9Myc	*his3-Δ200, leu2-3,2-112, lys2-801, trp1-1(am), ura3-52, exo1-9Myc::His3MX*	DF5	This study
5833	exo1-PIP2 9Myc	*his3-Δ200, leu2-3,2-112, lys2-801, trp1-1(am), ura3-52, exo1-PIP2 9Myc::His3MX*	DF5	This study
5834	exo1-PIP1 9Myc	*his3-Δ200, leu2-3,2-112, lys2-801, trp1-1(am), ura3-52, exo1-PIP1 9Myc::His3MX*	DF5	This study
5835	exo1-PIP1 PIP2 9Myc	*his3-Δ200, leu2-3,2-112, lys2-801, trp1-1(am), ura3-52, exo1-PIP1 PIP2 9Myc::His3MX*	DF5	This study

2.3.3 Mammalian cell lines

Table 2.7: Mammalian cell lines used in this study.

ID	Name	Antibiotics	Source
120	RPE-1 FRT	Blasticidin, Zeocin, G418	Jonathon Pines
36	HeLa	-	CR-UK Cell Services
343	RPE-1-pDEST-YFP-DARPin-E3_5-Puro	Puromycin	P. Elleringmann
344	RPE-1-pDEST-YFP-DARPin-K48-A1-Puro	Puromycin	P. Elleringmann
344	RPE-1-pDEST-YFP-DARPin-K48-G2-Puro	Puromycin	P. Elleringmann
346	RPE-1-pDEST-YFP-DARPin-K48-E4-Puro	Puromycin	P. Elleringmann
347	RPE-1-pDEST-YFP-DARPin-K63-D2-Puro	Puromycin	P. Elleringmann
348	RPE-1-pDEST-YFP-DARPin-K63-G3-Puro	Puromycin	P. Elleringmann
349	RPE-1-pDEST-YFP-DARPin-K63-D1-Puro	Puromycin	P. Elleringmann
350	RPE-1-pDEST-YFP-DARPin-K63-C3-Puro	Puromycin	P. Elleringmann
351	RPE-1-pDEST-YFP-DARPin-K63-E3-Puro	Puromycin	P. Elleringmann
352	RPE-1-pDEST YFP-Rx3-Puro	Puromycin	P. Elleringmann
376	RPE-1-pDEST-YFP-DARPin-K48-C3-Puro	Puromycin	P. Elleringmann
378	RPE-1-pDEST-YFP-DARPin-K48-H1-Puro	Puromycin	P. Elleringmann
379	RPE-1-pDEST-YFP-DARPin-K48-H3-Puro	Puromycin	P. Elleringmann
405	RPE1-FlpIn-Venus_C-term_DARPin-Ub K63 G1-Flag_P2A_Venus_N-term_DARPin-Ub K48 A1-Flag	Puromycin	This study
406	RPE1-FlpIn-Venus_C-term_DARPin-E3_5_P2A_Venus_N-term_DARPin-Ub K48 A1-Flag	Puromycin	This study

2.4 Oligonucleotides

The used oligonucleotides are identified with an ID regarding the internal nomenclature of the Ulrich laboratory. The details for all used oligonucleotides are summarized in Table 2.8.

Table 2.8: Oligonucleotides used in this study. Sdm = site-directed mutagenesis

ID	Name	Sequence	Use	Created by
701	T7 terminator	GCTAGTTATTGCTCAGCGG	Sequencing	H.Ulrich
1892	GFP tag test down	CAAGTCTGCCATGCCAGAAGG	Sequencing	H.Ulrich
1893	GFP tag test up	CCTTCTGGCATGGCAGACTTG	Sequencing	H.Ulrich
1981	pQE down	AATAGATTCAATTGTGAGCGG	Sequencing	H.Ulrich
2346	T7 promotor	TAATACGACTCACTATAGGG	Sequencing	H.Ulrich
2347	GST FWD seq primer	ATGTTGTATGACGCTCTTGATG	Sequencing	H.Ulrich
2866	mCherry test_rv	CTTGGTCACCTTCAGCTTG	Sequencing	H.Ulrich
4149	MBP_seq_fw	GATGTCCGCTTTCTGGTATG	Sequencing	H.Ulrich
4997	BglII-Darpin-for	GCAAAGATCTGCAAATGGGATCC GACCTGGGTAAGAAAC	Restriction cloning	V. Tröster
5275	Flag_AgeI overhangs_fw	CCGGTGACTACAAGGATGACGAC GACAAGA	Adaptor	This study
5276	Flag_AgeI overhangs_rv	CCGGTCTTGTCGTCGTCATCCTTG TAGTCA	Adaptor	This study
5324	Ubiquitin_ +1bp_fw	TGCAGATCTTCGTCAAGACG	PCR cloning	This study
5325	Ubiquitin_ -1bp_rv	CCACCTCTTAGTCTTAAGACAAG	PCR cloning	This study
5416	Ubiquitin_gibson_fw	GGAGATATACATTATGCAGATCTT CGTCAAGACGTTAACC	Gibson cloning	This study
5417	Ubiquitin_gibson_rv	AAATCTGCATACCACCTCTTAGTC TTAAGACAAGATGT	Gibson cloning	This study
5418	pET30-Ub_gibson_fw	AAGAGGTGGTATGCAGATTTTCGT CAAGACTTTGACCGG	Gibson cloning	This study
5419	pET30-Ub_gibson_rv	AAGATCTGCATAATGTATATCTCC TTCTTAAAGTTAAACAAAATTATT TCTAGAGGGG	Gibson cloning	This study
5440	Exo1_301_fw _XhoI	CGACTCGAGCTGTACTTGAAAGAT ACCGAAA	PCR cloning	This study

Continued on next page

Table 2.8: Oligonucleotides used in this study. Sdm = site-directed mutagenesis

5441	pMACS-BAC_gibson_fw	TTTATAAAGGTAAATAAGGCGCGCCAAGCTTGT	Gibson cloning	This study
5442	pMACS-BAC_gibson_rv	TATAGGGGACATAGCCATGGCGCCCGAT	Gibson cloning	This study
5443	GST_gibson_fw	CCATCGGGCGCCATGGCTATGTCCCCTATACTAGGTTATTGGA	Gibson cloning	This study
5444	Exo1_gibson_rv	TCGACAAGCTTGGCGCGCCTTATTTACCTTTATAAACAAATTGGGAAAGC	Gibson cloning	This study
5498	Exo1_300_rv_NotI	CGTACGCGGCCGCTTACGGAATTTCATTCAAGCTCACTA	PCR cloning	This study
5503	Flag_AscI overhangs_fw	CGCGCCGACTACAAGGATGACGACGACAAGGGG	Adaptor	This study
5504	Flag_AscI overhangs_rv	CGCGCCCCTTGTCGTCGTCATCCTTGTAGTCGG	Adaptor	This study
5554	pFastBac polyhedrin promotor seq for	GTATTTTACTGTTTTCGTAACAG	Sequencing	This study
5555	pFastBac seq rev	GTTTCAGGTTCAGGGGG	Sequencing	This study
5622	pFastBac1_Gibson_M-Exo1_Flag_fw	AATTTGTTTATAAAGGTAAAGATTACAAGGATGACGACGA	Gibson cloning	This study
5623	pFastBac1_Gibson_M-Exo1_Flag_rv	TCGGTATCTTTCAAGTACAGCATGGCTCGAGACTGCAGG	Gibson cloning	This study
5624	Exo1 C-term_Gibson_wo_stop_fw	GCCTGCAGTCTCGAGCCATGCTGTACTTGAAAGATACCGAAAGTAAAAGAAAAAGAC	Gibson cloning	This study
5625	Exo1 C-term_Gibson_wo_stop_rv	TCGTCGTCATCCTTGTAATCTTTACCTTTATAAACAAATTGGGAAAGCAAGGAGA	Gibson cloning	This study
5631	Pab1_tagging_fw_S3	CTGCCTATGAGTCTTTCAAAAAGGAGCAAGAACAACAAACTGAGCAAGCTCGTACGCTGCAGGTCGAC	Tagging of Pab1 with mCherry	This study
5632	Pab1_tagging_rv_S2	AAGATGATAAGTTTGTTGAGTAGGGAAGTAGGTGATTACATAGAGCATTAATCGATGAATTCGAGCTCG	Tagging of Pab1 with mCherry	This study
5633	Pab1 test- C	GTCAGTAGTTTCGGAGTTGATGTTT	Test PCR	This study

Continued on next page

Table 2.8: Oligonucleotides used in this study. Sdm = site-directed mutagenesis

5634	Pbp1_tagging_fw_S3	ATCAAACTAGCCACCATGGCCACCATAATAGTAGTACCAGTGGCCATAAATCGTACGCTGCAGGTCGAC	Tagging of Pbp1 with mCherry	This study
5635	Pbp1_tagging_rv_S2	GCATGAATTTATTACTATATATTGCTTTTTCTGACGTGCTTCCTTCACTACATCGATGAATTCGAGCTCG	Tagging of Pbp1 with mCherry	This study
5636	Pbp1 test-C	ATGGCCATAGTAGAAATTACCATCA	Test PCR	This study
5637	Edc3_tagging_fw_S3	TCCAAAACTGTGATCTTTTCGTCACTGACGGGTCCCTGCTATTAGATTTGTCGTACGCTGCAGGTCGAC	Tagging of Edc3 with mCherry	This study
5638	Edc3_tagging_rv_S2	GTATGCTTATACGTATGTATCCAGTTTAGGCTAAAGTAATTCTTGGTTTACATCGATGAATTCGAGCTCG	Tagging of Edc3 with mCherry	This study
5639	Edc3 test-C	GTGTAACAAACAGCGAGGATCTACT	Test PCR	This study
5716	pFastBac1_M-Exo1_Flag_Gibson_fw	ACGATGGTAAAAATCAAATCGATTACAAGGATGACGACGATAAGTAACTCG	Gibson cloning	This study
5717	pFastBac1_M-Exo1_330_Flag_Gibson_rv	AATTTGTGCTCTCTGTTGGCCATGGCTCGAGACTGCAGG	Gibson cloning	This study
5718	pFastBac1_M-Exo1_450_Flag_Gibson_rv	TCCACAACAGTCATGGAGGGCATGGCTCGAGACTGCAG	Gibson cloning	This study
5719	Exo1_630_wo_stop_Gibson_rv	TCGTCGTCATCCTTGTAATCGATTTGATTTTTACCATCGTTATCGTCGCAA	Gibson cloning	This study
5720	Exo1_330_wo_stop_Gibson_fw	GCCTGCAGTCTCGAGCCATGGCCAACAGAGAGCACAAATTACAG	Gibson cloning	This study
5721	Exo1_450_wo_stop_Gibson_fw	GCCTGCAGTCTCGAGCCATGCCCTCCATGACTGTTGTGGAAA	Gibson cloning	This study
5792	DARPin_NdeI_fw	ATTATTATTCATATGAGATCCGACCTGGGTAAGAAA	PCR cloning	This study
5793	DARPin_EcoRI_rv	GCAGAATTCCTTAGCAGCTTTCTGCAGAA	PCR cloning	This study
5794	Exo1_402_XhoI_rv	CCGCTCGAGTTAATCCAATTTTGTCATTTTTTGGAA	PCR cloning	This study
5795	Exo1_403_ClaI_fw	GGAATCGATGATCATAACCCAAAAGTTGCAAAT	PCR cloning	This study
5796	Exo1_360_XhoI_rv	CCGCTCGAGTTAGGCTAGAGGTTGGTGAAAATC	PCR cloning	This study
5797	Rx3_NdeI_fw	ATTATTATTCATATGGGCGGCAGCGGCCTCGAG	PCR cloning	This study

Continued on next page

Table 2.8: Oligonucleotides used in this study. Sdm = site-directed mutagenesis

5798	Rx3_EcoRI_rv	GCAGAATTCAGAAGGCCGGCAACTATTCAGAC	PCR cloning	This study
5833	pFastBac_with_Flag-tag_Exo1_402_Gibson_fw	AAAAAATGACAAAATTGGATGATTACAAGGATGACGACGATAAGTAACTCG	Gibson cloning	This study
5834	Exo1_402_Gibson_wo_stop_rv	TCGTCGTCATCCTTGTAATCATCCAATTTTGTCATTTTTTGGAAGAACGAT	Gibson cloning	This study
5839	pFastBac1_M-Exo1_402_Flag_Gibson_rv	GCAACTTTTGGGTTATGATCCATGGCTCGAGACTGCAGG	Gibson cloning	This study
5840	Exo1_402_wo_stop_Gibson_fw	GCCTGCAGTCTCGAGCCATGGATCATAACCCAAAAGTTGCAAATAACATCCA	Gibson cloning	This study
5841	Myc-Ub I44A fw	AAAGATTGGCATTTGCCGGTAAGCAGCTCGA	Sdm	This study
5842	Myc-Ub I44A rv	CCGGCAAATGCCAATCTTTGTTGATCAGG	Sdm	This study
5843	Myc-Ub L8A fw	CAAGACGGCAACCGGTAAAACCATAACTCT	Sdm	This study
5844	Myc-Ub L8A rv	TTACCGGTTGCCGTCTTGACGAAGATCTGCA	Sdm	This study
5870	Exo1 I345S A346E fw	TGCATTTAAAATCAGAACAAGGTGACTTGAATCCATATGA	Sdm	This study
5871	Exo1 I345S A346E rv	AGTCACCTTGTTCTGATTTTAAATGCAAGTGGTGAT	Sdm	This study
5872	Exo1_301_NcoI_fw	GCAACCATGGATCTGTACTTGAAAGATACCGAAAGTAAAA	PCR cloning	This study
5890	DARPin_MBP_Gibson_fw	TTCTGCAGAAAGCTGCTAAGAAAACTGAAGAAGGTAAACTGGTAATCTGGA	Gibson cloning	This study
5891	DARPin_MBP_Gibson_rv	AGTTTACCTTCTTCAGTTTTCTTAGCAGCTTTCTGCAGAACTTCAG	Gibson cloning	This study
5892	MBP_Avi_Gibson_fw	CCCTGAAAGACGCGCAGACTTTCGGTCTGAACGATATCTTCGAAGCT	Gibson cloning	This study
5893	MBP_Avi_Gibson_rv	AAGATATCGTTCAGACCGAAAGTCTGCGCGTCTTTCAGG	Gibson cloning	This study
5900	DARPin_BamHI_fw	GGGATCCATGGGCTCAGACCTGGGTAAGAAACTGC	PCR cloning	This study
5901	Flag_PacI_rv	TGTTAATTAACTTGTCGTCGTCATCCTTGTA	PCR cloning	This study
5946	Exo1 I345S A346G rv	AGTCACCTTGTCCTGATTTTAAATGCAAGTGGTGAT	Sdm	This study

Continued on next page

Table 2.8: Oligonucleotides used in this study. Sdm = site-directed mutagenesis

5947	Exo1 I345S A346G fw	TGCATTTAAAATCAGGACAAGGT GACTTGAATCCATATGA	Sdm	This study
5960	Ubiquitin_NcoI_fw	GGCGCCATGGTTATGCAGATCTTC GTCAAGAC	PCR cloning	This study
5961	Ubiquitin_NotI_rv	GCGGCCGCTTCCACCTCTTAGTCT TAAGACAAG	PCR cloning	This study
5962	Ubiquitin_HindIII_rv	CCGCAAGCTTTCATCCACCTCTTA GTCTTAA	PCR cloning	This study
5987	DARPin_KpnI_fw	GGGGTACCCCGACCTGGGTAAGA AACT	PCR cloning	This study
5988	DARPin_XhoI_rv	CCGCTCGAGTCAATTAAGCTTAGC AGCTTTCTGCAG	PCR cloning	This study
5989	E3_5_XhoI_rv	CCGCTCGAGTTAATTAAGCTTTTG CAGGATTTCAGC	PCR cloning	This study
5990	Rx3_KpnI_fw	GGGGTACCAGATGACCGAGGAGG AG	PCR cloning	This study
5991	Rx3_XhoI_rv	CCGCTCGAGTTTAAGAAGGCCGG CAACTAT	PCR cloning	This study
6088	9Myc_vector_Gibson_fw	GCCGCGGATCTGCCGGTCTCCCTG CAGCCAAGCTAATTCCG	Gibson cloning	This study
6089	9Myc_vector_Gibson_rv	GGAAGAAGACCTTGGATACCGTC GACTTTTAAGCTAGTGGATCCG	Gibson cloning	This study
6090	Exo1_His_Gibson_fw	CCACTAGCTTAAAAGTCGACGGT ATCCAAGGTCTTCTTCCTCAGTTA AAGCC	Gibson cloning	This study
6091	Exo1_His_Gibson_rv	GGAATTAGCTTGGCTGCAGGGAG ACCGGCAGATCC	Gibson cloning	This study
6092	9Myc-Exo1_integration_fw	ACCACATTAAAATAAAAGGAGCT CGAAAAAACTGAAAGGCGTAGAA AGGATGTCCGGTTCTGCTGCTA	Integration of Exo1 mutant alleles	This study
6144	Exo1 SDM H342A fw	AGATCACCACTTGGCTTTAAAAAT TGCTCAAGGTG	Sdm	This study
6145	Exo1 SDM H342A rv	CTTGAGCAATTTTTAAAGCCAAGT GGTGATCTATATCGT	Sdm	This study
6146	Exo1 SDM I391A fw	AAAGTCAAACCAGCAGAATCGTT CTTCCAAAAAATGAC	Sdm	This study
6147	Exo1 SDM I391A rv	TGGAAGAACGATTCTGCTGGTTTG ACTTTGGC	Sdm	This study
6148	Exo1 SDM F394A F395A fw	AGTCAAACCAATAGAATCGGCCG CCCAAAAAATGACAAAATTGG	Sdm	This study
6149	Exo1 SDM F394A F395A rv	GTCATTTTTTGGGCGGCCGATTCT ATTGGTTTGACTTTGGC	Sdm	This study

Continued on next page

Table 2.8: Oligonucleotides used in this study. Sdm = site-directed mutagenesis

6181	9Myc_Gibson_fw	AATTTGTTTATAAAGGTAAAGAATTCATGTCCGGTTCTGCTG	Gibson cloning	This study
6182	9Myc_Gibson_rv	CTCCATGTCGCTGGCCGGGTTGCAGGGAATGATCGTTCCACTTT	Gibson cloning	This study
6183	pFA-Exo1_Gibson_fw	TGGAACGATCATTCCCTGCAACCCGGCCAGCGAC	Gibson cloning	This study
6184	pFA-Exo1_His_Gibson_rv	GCAGAACCGGACATGAATTCTTTACCTTTATAAACAAATTGGGAAAGCAAGGAGATAGA	Gibson cloning	This study
6256	Exo1_321_NcoI_fw	GCAACCATGGATATACACAGAGAAACTCAGAAAAAGCAAA	PCR cloning	This study
6257	Exo1_402_NcoI_fw	GCAACCATGGATGATCATAACCCAAAAGTTGCAAAT	PCR cloning	This study
6281	K48_DARPinA1_ sdm_site 1_W36A_W38A_fw	AACGACACTGCAGGTGCAACTCCGCTGCACCTGGC	Sdm	This study
6282	K48_DARPinA1_ sdm_site 1_W36A_W38A_rv	GGTGCAGCGGAGTTGCACCTGCAGTGTCGTTAGCGTTAAC	Sdm	This study
6283	K48_DARPin_A1_sdm_site 2_W101A L102A fw	CGCTCAGGACGCAGCAGGTGCTACTCCGTTCGAC	Sdm	This study
6284	K48_DARPin_A1_sdm_site 2_W101A L102A rv	TAGCACCTGCTGCGTCCTGAGCGTTAACGTCAGCGC	Sdm	This study
6285	K48_DARPin_A1_sdm_site 3_W112A fw	GACCTGGCTGCTGCAGTTGGTAACGAGGACATC	Sdm	This study
6286	K48_DARPin_A1_sdm_site 3_W112A rv	GTTACCAACTGCAGCAGCCAGGTCGAACGGA	Sdm	This study
6294	Exo1_361_NcoI_fw	GCAACCATGGATAACAGAGAGCACAAATTACAGCTG	PCR cloning	This study
6480	Exo1_integration_fw	ACCACATTAAAATAAAAGGAGCTCGAAAAAACTGAAAGGCGTAGAAAGGCGGATCCCCGGGTTAATTAA	mutagenesis	This study
6481	Exo1_301_PacI_fw	GGATTAATTAAATGCTGTACTTGAAAGATACCGAAAGTAAAAG	Cloning	This study
6482	Exo1_300_AscI_rv	CCGGGCGCGCCTTACGGAATTTCATTCAAGCTCACTATT	Cloning	This study

Continued on next page

Table 2.8: Oligonucleotides used in this study. Sdm = site-directed mutagenesis

6483	Exo1_402_AscI_rv	CCGGGCGCGCCTTAATCCAATTTTGTCATTTTTTGGAAGAACG	Cloning	This study
6484	Exo1_630_AscI_rv	CCGGGCGCGCCTTAGATTTGATTTTTACCATCGTTATCGTCG	Cloning	This study
6506	Exo1_sdm_A346F_fw	TGCATTTAAAAATTTTTCAAGGTGACTTGAATCCATATGA	Sdm	This study
6507	Exo1_sdm_A346F_rv	AGTCACCTTGAAAAATTTTTAAATGCAAGTGGTGAT	Sdm	This study
6508	Exo1_sdm_A346D_fw	ATTTAAAAATTGATCAAGGTGACTTGAATCCAT	Sdm	This study
6509	Exo1_sdm_A346D_rv	GTCACCTTGATCAATTTTTAAATGCAAGTGGT	Sdm	This study
6510	Exo1_sdm_A346R_fw	GCATTTAAAAATTCGTCAAGGTGACTTGAATCCATAT	Sdm	This study
6511	Exo1_sdm_A346R_rv	GTCACCTTGACGAATTTTTAAATGCAAGTGGT	Sdm	This study
6512	Exo1_sdm_D334A_fw	AAATTGTTCATTTCGCTGACGATATAGATCACCACTT	Sdm	This study
6513	Exo1_sdm_D334A_rv	GTGATCTATATCGTCAGCGAAATGAACAATTTGCTTTT	Sdm	This study
6514	Exo1_sdm_Y353A_fw	ACTTGAATCCAGCTGATTTTCACCAACCTCTAGC	Sdm	This study
6515	Exo1_sdm_Y353A_rv	GTTGGTGAAAATCAGCTGGATTCAAGTCACCTTGAG	Sdm	This study
6664	mVenus-N-term_TEV_BamHI_fw	ATATAGGATCCGAGAACCTGTACTTTCAGGGTGTGAGCAAGGGCGAGGAG	PCR cloning	This study
6665	mVenus-N-term_BamHI_rv	ATATAGGATCCGGCGGTGATATAGACGTTGTG	PCR cloning	This study
6666	mVenus-N-term_L20_BamHI_rv	TAGGATCCTGTAGCGCCAGATGTGCCACCTTCAGATCCGCCACCTTCAGAACCGCCAGCACCAGAAGCGGCGGTGATATAGACGTTGTG	PCR cloning	This study
6667	mVenus-C-term_TEV_BamHI_fw	ATATAGGATCCGAGAACCTGTACTTTCAGGGTGACAAGCAGAAGAACGGCATC	PCR cloning	This study
6668	mVenus-C-term_BamHI_rv	ATATAGGATCGGATCCTTTGTACAGCTCGTCCAT	PCR cloning	This study
6669	mVenus-C-term_L20_BamHI_rv	TATAGGATCCTGTAGCGCCAGATGTGCCACCTTCAGATCCGCCACCTTCAGAACCGCCAGCACCAGAAGCGTACAGCTCGTCCATGCC	PCR cloning	This study

Continued on next page

Table 2.8: Oligonucleotides used in this study. Sdm = site-directed mutagenesis

6696	mVenus-N-term_MC_Gibson_fw	CTCTGTTAAAGCAAGCAGGAGACGTGGAAGAAAACCCCGGTCCTGTGAGCAAGGGCGAGG	Gibson cloning	This study
6697	DARPin-Flag_MC_Gibson_rv	CTCTAGACTCGAGCGGCCGCGTCACTTGTCGTCGTCATCCTTGTA	Gibson cloning	This study
6698	mVenus-C-term_MC_Gibson2_fw	GTTTAAACTTAAGCTTCCACCATGGACAAGCAGAAGAACGGCATC	Gibson cloning	This study
6699	DARPin-Flag_MC_Gibson2_rv	GCTTGCTTTAACAGAGAGAAGTTCGTGGCTCCGCTTCCCTTGTCGTCGTCATCCTTGTAG	Gibson cloning	This study
6700	pcDNA5_FRT_TO_Gibson_fw	GGTGGAAGCTTAAGTTTAAACGC	Gibson cloning	This study
6701	pcDNA5_FRT_TO_Gibson_rv	CGGCCGCTCGAGTCTAGAG	Gibson cloning	This study
6822	mVenus N-term HindIII fw	GATCAAGCTTGTGAGCAAGGGCGAGGAG	PCR cloning	This study
6823	L20 nVenus N-term HindIII fw	TCAAGCTTGCTTCTGGTGCTGGCGGTTCTGAAGGTGGCGGATCTGAAGGTGGCACATCTGGCGCTACAGTGAGCAAGGGCGAGGAG	PCR cloning	This study
6824	mVenus-N-term Stop HindIII rv	CCAAGCTTAGGCGGTGATATAGACGTTGTGGC	PCR cloning	This study
6872	Exo1 delta8 fw	ATTTCGACGACGATATAGATCAAGGTGACTTGAATCCATA	PCR cloning	This study
6873	Exo1 delta8 rv	TATGGATTCAAGTCACCTTGATCTATATCGTCGTCGAAATGAACA	PCR cloning	This study
7088	HindIII_2xFlag_anneal_fw	AGCTTGACTACAAGGATGACGACGACAAGGACTACAAGGATGACGACGACAAGG	Linker	This study
7089	HindIII_2xFlag_anneal_rw	AGCTCCTTGTCGTCGTCATCCTTGTAGTCCTTGTCGTCGTCATCCTTGTAGTCA	Linker	This study
7173	K63-DARPin_G1_site1_W48A_fw	GCTATGGACGAAGCAGGTCAGACTCCGCTGCAC	Sdm	This study
7174	K63-DARPin_G1_site1_W48A_rv	AGCGGAGTCTGACCTGCTTCGTCCATAGCGTTAAC	Sdm	This study

Continued on next page

Table 2.8: Oligonucleotides used in this study. Sdm = site-directed mutagenesis

7175	K63-DARPin_G1_site2_W83A_fw	GACCTGTTCAGTGCAACTCCGTTCGACCTGGCT	Sdm	This study
7176	K63-DARPin_G1_site2_W83A_rv	TCGAACGGAGTTGCACTGAACAGGTCCTGAGCGT	Sdm	This study
7177	K63-DARPin_G1_site2a_F81A_S82A_W83A_fw	GCTCAGGACCTGGCAGCAGCAACTCCGTTCGACCTGGC	Sdm	This study
7178	K63-DARPin_G1_site2a_F81A_S82A_W83A_rv	AGGTCGAACGGAGTTGCTGCTGCCAGGTCCTGAGCGTTAAC	Sdm	This study
7179	K63-DARPin_G1_site3_W91A_W92A_fw	GACCTGGCTGCTGCAGCAGGTAACGAGGACATCGCTGA	Sdm	This study
7180	K63-DARPin_G1_site3_W91A_W92A_rv	GATGTCCTCGTTACCTGCTGCAGCAGCCAGGTCGAACGGA	Sdm	This study
7232	K63-DARPin_G1_site1_W48A_fw-1	AACGCTATGGACGAAGCAGGTCAGACTCCGCTG	Sdm	This study
7233	K63-DARPin_G1_site1_W48A_rv-1	CAGCGGAGTCTGACCTGCTTCGTCCATAGCGTT	Sdm	This study

2.5 Plasmids

The used plasmids will be termed in this work with the internally used ID. The following Table 2.9 states this ID together with the construct, the resistance, the construction, the use and the source for each of the used plasmids.

Table 2.9: Plasmids used in this study.

ID	Name	Resistance	Use	Construction	Source
684	pET-Ubi(K63R)	Amp	Expression of Ubi(K63R) in *E. coli*		H. Ulrich
685	pET-Ubi(74)	Amp	Expression of Ubi(74) in *E. coli*		H. Ulrich
872	pET11a-Myc-Ubi	Amp	Bacterial expression of Myc-ubiquitin		D. Huttner
2458	pGEX-Cue1	Amp	Expression of Cue1		Max Delbrück T. Sommer lab
2715	pGEX-2TK-SMT3-Ub-PCNA	Amp	*E.coli* expression of Ub-PCNA	Gibson assembly: vector p246 o3167 & o3170 fragment p2107 o3168 & o3169	S. Batke
2731	pET28-His-Ulp1	Kan	*E.coli* expression of catalytic domain of Ulp1		S. Batke
2806	pET30-His-TEV-Ubc13	Kan	Vector for bacterial expression of His-TEV-Ubc13	Insert: p250 pQE-Ubc13 Cloning via BamHI/PstI	C. Renz
2807	pET30-His6-TEV-Mms2	Kan	Vector for bacterial expression of His-TEV-Mms2	Insert: p255 pQE-Mms2 Cloning via BamHI/PstI	C. Renz
3360	pET30-Ub-Ub-AviTag-His6	Kan		Bacterial expression of Ub-Ub-AviTag-His6	C. Renz
3365	pMAL-TEV-Ubc7-His6	Amp	Vector for bacterial expression of MBP-TEV-Ubc7-His6	PCR: oHU4055/4056 on p3355 Cloning: via FseI/AscI in pMal-TEV2-FA-His6	C. Renz
3456	pOPINK-OTUB1	Kan		Bacterial expression of His6-GST-OTUB1	addgene #61420 D. Komander
3830	pMAL_TEV2_Exo1(301-702)_His6	Amp	Expression of MBP-Exo1 C-terminal fragment (301-702)-His in *E.coli*	PCR of Exo1 C-term from genomic DNA using o4410 and o4401, digested with FseI/AscI and inserted into FseI/AscI of p3554	N. García-Rodríguez

Continued on next page

Table 2.9: Plasmids used in this study.

3836	pMAL_TEV2_Exo1-PIP1_His6	Amp	Expression of MBP-Exo1-PIP1 mutant in *E. coli*	Site-directed mutagenesis of plasmid 3829 using o4473 and o4474	N. García-Rodríguez
3837	pMAL_TEV2_Exo1-PIP2_His6	Amp	Expression of MBP-Exo1-PIP2 mutant in *E. coli*	Site-directed mutagenesis of plasmid 3829 using o4475 and o4476	N. García-Rodríguez
3982	pET11a-Myc-Ub-Ub	Amp	Vector for bacterial expression of Myc-Ub-Ub	Insert: p3360, AgeI Vector: p872, AgeI	T. Strauch master thesis
4318	pET11a-Myc-6Ub	Amp	Vector for bacterial expression of Myc-Ub-Ub	Insert: p3360, AflII Vector: p3982, AflII	T. Strauch master thesis
4412	pQIq-MRGS-8His-DARPin-Ub K48 A1-Flag	Amp	Vector for bacterial expression of DARPin		Jonas Schaefer, DARPin CF Zuerich
4413	pQIq-MRGS-8His-DARPin-Ub K48 G2-Flag	Amp	Vector for bacterial expression of DARPin		Jonas Schaefer, DARPin CF Zuerich
4414	pQIq-MRGS-8His-DARPin-Ub K48 E4-Flag	Amp	Vector for bacterial expression of DARPin		Jonas Schaefer, DARPin CF Zuerich
4415	pQIq-MRGS-8His-DARPin-Ub K63 F2-Flag	Amp	Vector for bacterial expression of DARPin		Jonas Schaefer, DARPin CF Zuerich
4416	pQIq-MRGS-8His-DARPin-Ub K63 D2-Flag	Amp	Vector for bacterial expression of DARPin		Jonas Schaefer, DARPin CF Zuerich
4417	pQIq-MRGS-8His-DARPin-Ub K63 G3-Flag	Amp	Vector for bacterial expression of DARPin		Jonas Schaefer, DARPin CF Zuerich
4418	YEp195-Gal-DARPin-Ub K48 A1	Amp URA	Expression of anti-K48-linked Ub DARPin A1 in yeast	Cut- and paste cloning with BamHI and HindIII: clone fragment from p4412 into p3645	This study
4419	YEp195-Gal-DARPin-Ub K48 G2	Amp URA	Expression of anti K48-linked Ub DARPin G2 in yeast	Cut- and paste cloning with BamHI and HindIII: clone fragment from p4413 into p3645	This study

Continued on next page

Table 2.9: Plasmids used in this study.

4420	YEp195-Gal-DARPin-Ub K48 E4	Amp URA	Expression of anti K48-linked Ub DARPin E4 in yeast	Cut- and paste cloning with BamHI and HindIII: clone fragment from p4414 into p3645	This study
4421	YEp195-Gal-DARPin-Ub K63 F2	Amp URA	Expression of anti K63-linked Ub DARPin F2 in yeast	Cut- and paste cloning with BamHI and HindIII: clone fragment from p4415 into p3645	This study
4422	YEp195-Gal-DARPin-Ub K63 D2	Amp URA	Expression of anti K63-linked Ub DARPin D2 in yeast	Cut- and paste cloning with BamHI and HindIII: clone fragment from p4416 into p3645	This study
4423	YEp195-Gal-DARPin-Ub K63 G3	Amp URA	Expression of anti K63-linked Ub DARPin G3 in yeast	Cut- and paste cloning with BamHI and HindIII: clone fragment from p4417 into p3645	This study
4424	pEGFP-DARPin-Ub K48 A1	Kan	Expression of GFP-fused anti K48-linked Ub DARPin A1 in mammalian cells	Cut- and paste cloning with BamHI/BglII and HindIII: clone fragment from p4412 into p1475	This study
4425	pEGFP-DARPin-Ub K48 E4	Kan	Expression of GFP-fused anti K48-linked Ub DARPin E4 in mammalian cells	Cut- and paste cloning with BamHI/BglII and HindIII: clone fragment from p4414 into p1475	This study
4427	pEGFP-DARPin-Ub K63 D2	Kan	Expression of GFP-fused anti K63-linked Ub DARPin D2 in mammalian cells	Cut- and paste cloning with BamHI/BglII and HindIII: clone fragment from p4416 into p1475	This study
4428	pEGFP-DARPin-Ub K63 G3	Kan	Expression of GFP-fused anti K63-linked Ub DARPin G3 in mammalian cells	Cut- and paste cloning with BamHI/BglII and HindIII: clone fragment from p4417 into p1475	This study
4570	pEGFP-DARPin-Ub K48 G2	Kan	Expression of GFP-fused anti K48-linked Ub DARPin G2 in mammalian cells	Cut- and paste cloning with BamHI/BglII and HindIII: clone fragment from p4413 into p1475	This study

Continued on next page

Table 2.9: Plasmids used in this study.

4580	pET30-SMT3-Exo1-AviTag-His6	Kan	Expression of SMT3-Exo1-AviTag-His6 in *E.coli*	Gibson assembly: Vector: p3224 digested with NdeI and EcoRI Insert: PCR with oligos o5261 and o5262	This study
4610	pET15b_His6-SMT3-Flag-Exo1	Amp	Expression of His-SMT3-Flag-Exo1 in E.coli	Cut vector with AgeI ligate with annealed oligos 5675 and 5676 containing the Flag-Tag and AgeI sites	This study
4617	pQIq-MRGS-8His-DARPin-UbK63 G1-Flag	Amp	Vector for bacterial expression of DARPin		Jonas Schaefer, DARPin CF Zuerich
4618	pQIq-MRGS-8His-DARPin-UbK63 C3-Flag	Amp	Vector for bacterial expression of DARPin		Jonas Schaefer, DARPin CF Zuerich
4619	pQIq-MRGS-8His-DARPin-UbK63 E3-Flag	Amp	Vector for bacterial expression of DARPin		Jonas Schaefer, DARPin CF Zuerich
4621	YEp195-Gal-DARPin-UbK63 G1	Amp URA	Expression of anti K63-linked Ub DARPin G1-2 in yeast	Cut- and paste cloning with BamHI and HindIII: clone fragment from p4617 into p3645	This study
4622	YEp195-Gal-DARPin-UbK63 C3	Amp URA	Expression of anti K63-linked Ub DARPin C3-2 in yeast	Cut- and paste cloning with BamHI and HindIII: clone fragment from p4618 into p3645	This study
4623	YEp195-Gal-DARPin-UbK63 E3	Amp, URA	Expression of anti K63-linked Ub DARPin E3-2 in yeast	Cut- and paste cloning with BamHI and HindIII: clone fragment from p4619 into p3645	This study
4624	pEGFP-DARPin-UbK63 G1	Kan	Expression of GFP-fused anti K63-linked Ub DARPin G1-2 in mammalian cells	Cut- and paste cloning with BamHI/BglII and HindIII: clone fragment from p4617 into p1475	This study
4625	pEGFP-DARPin-UbK63 C3	Kan	Expression of GFP-fused anti K63-linked Ub DARPin C3-2 in mammalian cells	Cut- and paste cloning with BamHI/BglII and HindIII: clone fragment from p4618 into p1475	This study

Continued on next page

Table 2.9: Plasmids used in this study.

4626	pEGFP-DARPin-UbK63 E3	Kan	Expression of GFP-fused anti K63-linked Ub DARPin E3-2 in mammalian cells	Cut- and paste cloning with BamHI/BglII and HindIII: clone fragment from p4619 into p1475	This study
4681	pMACS-BAC-Exo1 D173A	Amp	Expression of His6-Exo1 D173A in insect cells using the Baculovirus system	Mutagenesis: oHU4811/4812 on p3823	This study
4719	pGEX6P1-Exo1 (301-702)	Amp	Vector for bacterial expression of GST-Exo1 (301-702)	Cut- and paste cloning: Vector: p3866; digested with XhoI and NotI Insert: p3830; PCR with o4050 + o5440; digestion with XhoI and NotI	This study
4721	pMACS-BAC-GST-Exo1	Amp, Gentamycin	Bacmid production in DH10 Bac *E.coli*, virus production and protein expression (GST-Exo1) in insect cells (SF9, Hi5)	Gibson cloning: vector p3258: PCR with o5441+ o5442 insert p3866: PCR with o5443 +o5444	This study
4722	pMACS-BAC-GST-Exo1 D173A	Amp, Gentamycin	Bacmid production in DH10 Bac *E.coli*, virus production and protein expression (GST-Exo1 D173A) in insect cells (SF9, Hi5)	Gibson cloning: vector p3258: PCR with o5441+ o5442 insert p3910: PCR with o5443 +o5444	This study
4723	pMACS-BAC-GST-Exo1 (301-702)	Amp, Gentamycin	Bacmid production in DH10 Bac E.coli, virus production and protein expression (GST-Exo1 (301-702)) in insect cells (SF9, Hi5)	Gibson cloning: vector p3258: PCR with o5441+ o5442 insert p4719: PCR with o5443 +o5444	This study
4751	pGEX6P1-Exo1 (1-300)	Amp	Vector for bacterial expression of GST-Exo1 (1-300)	Cut- and paste cloning: Vector: p3866; digested with XhoI &NotI Insert: p3840; PCR with o4049+o5498; digestion with XhoI &NotI	This study
4769	YEp195-Gal-Flag-Rx3(A7)-Ub K63	Amp URA	Expression of anti K63-linked Ub TUBE Flag-Rx3 (A7) in yeast	Cut- and paste cloning with BamHI and HindIII: clone fragment from p2666 into p3645	This study

Continued on next page

Table 2.9: Plasmids used in this study.

4771	pMAL_TEV2_Exo1_Flag-His6	Amp	Vector for bacterial expression of Exo1-Flag-His6	Cut vector with AscI ligate with annealed oligos 5503 and 5504 containing the Flag-Tag and AscI sites	This study
4772	pFASTBac Exo1-Flag-His6	Amp, Gentamycin	Bacmid production in DH10 Bac *E.coli*, virus production and protein expression (Exo1-Flag-His6) in insect cells (SF9, Hi5)	Cut- and paste cloning with NcoI and HindIII: clone fragment from p4771 into p4770	This study
4773	pFastBac1_Exo 1-Flag	Amp, Gentamycin	Bacmid production in DH10 Bac *E.coli*, virus production and protein expression (Exo1-Flag) in insect cells (SF9, Hi5)		P. Cejka, IRB, USI, CH
4774	pFastBac1_Exo 1-Flag D173A	Amp, Gentamycin	Bacmid production in DH10 Bac *E.coli*, virus production and protein expression (Exo1-Flag D173A) in insect cells (SF9, Hi5)		P. Cejka, IRB, USI, CH
4777	pRS425-Exo1-His6-Flag	Amp, LEU	Expression of Exo1-His6-Flag in yeast		R. Kolodner
4884	YIp211-TetO7-DARPin-Ub K48 A1-Flag-GFP	Amp, URA	Integration of anti K48-linked Ub DARPin A1 in yeast	Amplify DARPin K48 A1 with oHU 5117 and 4997 on p4418, vector: p4480 Digest with BamHI	This study
4889	YIp211-TetO7-DARPin-Ub K63 G1-Flag-GFP	Amp, URA	Integration of anti K63-linked Ub DARPin G1 in yeast	Amplify DARPin K63 G1 with oHU 5117 and 4997 on p4621 vector: p4480 Digest with BamHI	This study
4940	pFastBac1_Exo 1 (301-702)-Flag	Amp, Gentamycin	Bacmid production in DH10 Bac *E.coli*, virus production and protein exprression (Exo1(301-702)-Flag) in insect cells (SF9, Hi5)	Gibson cloning: vector p4773: PCR with o5622+ o5623 insert p4719: PCR with o5624 +o5625	This study
5060	pET-11a-MycUbi K48R	Amp	Vector for bacterial expression of MycUbi K48R	Site-directed mutagenesis using primers oHU4455 and oHU4456 on plasmid p872	This study

Continued on next page

Table 2.9: Plasmids used in this study.

5061	pET-11a-MycUbi K63R	Amp	Vector for bacterial expression of MycUbi K63R	Site-directed mutagenesis using primers oHU4457 and oHU4458 on plasmid p872	This study
5062	YIp211-TetON-2xNES-DARPin-Ub K48 A1-Flag-GFP	Amp, URA	Expression of anti K48-linked Ub DARPin A1 in yeast, cytoplasmic localisation	Amplfiy DARPin from p4884 with oHU5604/5605. Cut insert with BglII and p4486 with BamHI before ligation.	This study
5067	pGEX6P1-3C-PIP-E3(K63)	Amp	Vector for bacterial expression of GST-3C-PIP-E3(K63)	Cut- and paste cloning: Vector: p2889; digested with SalI and BamHI Insert: p2452; digested with SalI and BamHI	This study
5090	pFastBac1_Exo 1 (360-630)-Flag	Amp, Gentamycin	Bacmid production in DH10 Bac *E.coli*, virus production and protein exprression (Exo1(360-630)-Flag) in insect cells (SF9, Hi5)	Gibson cloning: vector p4940: PCR with o5716+ o5717 insert p3707: PCR with o5720 +o5719	This study
5107	pFastBac1_Exo 1 (301-630)-Flag	Amp, Gentamycin	Bacmid production in DH10 Bac *E.coli*, virus production and protein exprression (Exo1(301-630)-Flag) in insect cells (SF9, Hi5)	Cut- and paste cloning with SmaI and Hind III vector p4940; insert 5090	This study
5124	pGBD-EXO1(301-450)	Amp, TRP	Yeast- two-hybrid	PCR of EXO1(301-450 aa) on p3286 using oligos oHU4252 and oHU4383, digested with ClaI/XhoI and cloned into pGBD-C1 (p194) cutted with ClaI/SalI of	This study
5125	pGBD-EXO1(301-402)	Amp, TRP	Yeast- two-hybrid	PCR of EXO1(301-402 aa) on p3286 using oHU4252 & oHU5794, digested with ClaI/XhoI and cloned into pGBD-C1 (p194) cutted with ClaI/SalI of	This study

Continued on next page

Table 2.9: Plasmids used in this study.

5126	pGBD-EXO1(301-360)	Amp, TRP	Yeast- two-hybrid	PCR of EXO1(301-360 aa) on p3286 using oHU4252 & oHU5796, digested with ClaI/XhoI and cloned into pGBD-C1 (p194) cutted with ClaI/SalI of	This study
5127	pGBD-EXO1(403-630)	Amp, TRP	Yeast- two-hybrid	PCR of EXO1(403-630 aa) on p3286 using oHU5795 & oHU4330, digested with ClaI/XhoI and cloned into pGBD-C1 (p194) cutted with ClaI/SalI of	This study
5165	pEGFP- Flag-Rx3(A7)-Ub K63	Kan	Expression of GFP-fused anti K63-linked Ub Rx3 (TUBE) in mammalian cells	Cut- and paste cloning with BamHI/BglII and HindIII: clone fragment from p4769 into p1475	This study
5166	pET30-DARPin Ub K48 A1-AviTag-His6	Kan	Vector for bacterial expression of biotinylated anti K48-linked Ub DARPin A1	Cut- and paste cloning Amplify DARPin insert from p4424 using o5792 and o5793; digest with NdeI and EcoRI vector: p3224 digest with NdeI and EcoRI	This study
5180	pET30-DARPin Ub K63 G1-AviTag-His6	Kan	Vector for bacterial expression of biotinylated anti K63-linked Ub DARPin G1	Cut- and paste cloning Amplify DARPin insert from p4624 using o5792 and o5793; digest with NdeI and EcoRI vector: p3224 digest with NdeI and EcoRI	This study
5187	pFastBac1_Exo 1 (301-402)-Flag	Amp, Gentamycin	Bacmid production in DH10 Bac *E.coli*, virus production and protein exprression (Exo1(301-402)-Flag) in insect cells (SF9, Hi5)	Gibson cloning: vector p4940: PCR with oligos o5623 + 5833 insert p5125: PCR with oligos o5624 + 5834	This study

Continued on next page

Table 2.9: Plasmids used in this study.

5213	pENTR4-Exo1 301-402	Kan	Gateway cloning	PCR amplification of pHU5125 using oHU5872 and oHU5794. Cloning into 1788 digested with NcoI and XhoI.	This study
5214	pET-His-3C-Exo1 301-402	Amp	Expression of His-3C-Exo1 301-402	Gateway cloning: p5213 into 5211	This study
5215	pET-His-GST-3C-Exo1 301-402	Amp	Expression of His-GST-3C-Exo1 301-402	Gateway cloning: p5213 into 5037	This study
5217	pET-His-MBP-3C-Exo1 301-402	Amp	Expression of His-MBP-3C-Exo1 301-402	Gateway cloning: p5213 into 5033	This study
5261	pET-His-MBP-3C-Exo1 301-402 I345S A346G	Amp	Expression of His-MBP-3C-Exo1 301-402 I345S A346G	sdm using oligos oHU5946 and oHU5947	This study
5262	YIp128-TET-DARPin K48 A1-Flag-mRuby2	Amp, LEU	Dox-inducible expression of DARPin K48 A1-Flag-mRuby2	Cut- and paste cloning: Amplify DARPin from p4884 with oHU5900 and 590, digestion with PacI and BamHI vector p4860: digestion with PacI and BamHI;	This study
5266	YIp128-TET-DARPin K63 G1-Flag-mRuby2	Amp, LEU	Dox-inducible expression of DARPin K63 G1-Flag-mRuby2	Cut- and paste cloning: Amplify DARPin from p4889 with oHU5900 and 590, digestion with PacI and BamHI vector p4860: digestion with PacI and BamHI;	This study
5283	pET-His-MBP-3C-Exo1 301-402 PIP2	Amp	Expression of His-MBP-3C-Exo1 301-402 PIP2	sdm using oligos oHU4475 and oHU4476	This study
5284	pET-His-MBP-3C-Exo1 301-402 PIP2 I345S A346G	Amp	Expression of His-MBP-3C-Exo1 301-402 PIP2 I345S A346G (UBD mt)	sdm using oligos oHU5946 and oHU5947 on p5283	This study
5292	pET-His-TEV-YFP-Ubiquitin	Amp	Vector for bacterial expression of His-YFP-Ubiquitin (for FRET-assay)	Cut- and past cloning vector: p5210 insert: p872 PCR with o500 and o585 digestion with BamHI	This study

Continued on next page

Table 2.9: Plasmids used in this study.

5293	pET30a-His-TEV-ECFP-Ubiquitin	Kan	Vector for bacterial expression of His-ECFP-Ubiquitin (for FRET-assay)	Cut- and past cloning vector: p4876 digestion with BamHI and HindIII insert (Ub): p872 PCR with o5962 and o1888 and then digestion with BamHI and HindIII	This study
5295	pFA-HIS-Exo1-PIP2 UBD	Amp His	Introduction of Exo1-PIP2 UBD into yeast	site-directed mutagenesis PCR: template p3852 oligos o5946 and o5947	This study
5296	pGBD-EXO1 UBD	Amp Trp	Yeast- two-hybrid	site-directed mutagenesis PCR: template p3286 oligos o5946 and o5947	This study
5297	pFA-HIS-Exo1-UBD	Amp His	Introduction of Exo1-UBD into yeast	PCR using plasmid 5296 and oligos 4607 and 4306, digested with PacI/AscI and cloned into PacI/AscI of plasmid 233	This study
5301	pENTR4-DARPin E3_5	Kan	Gateway cloning	PCR amplification of pHU3680 using oHU5987 and oHU5989. Cloning into vector pHU1788, both digested with KpnI and XhoI.	This study
5352	pET-His-GST-3C-Exo1 301-402 PIP2	Amp	Expression of His-GST-3C-Exo1 301-402 PIP2	sdm using oligos oHU4475 and oHU4476	This study
5353	pET-His-GST-3C-Exo1 301-402 UBD	Amp	Expression of His-GST-3C-Exo1 301-402 UBD	sdm using oligos oHU5946 and oHU5947	This study
5354	pET-His-GST-3C-Exo1 301-402 UBD PIP2	Amp	Expression of His-GST-3C-Exo1 301-402 UBD PIP2	sdm using oligos oHU4475 and oHU4476	This study
5401	pET-His-MBP-3C-Exo1 301-402 I345S A346E	Amp	Expression of His-MBP-3C-Exo1 301-402 PIP2 I345S A346E (UBD2 mt)	sdm using oligos oHU5870 and oHU5871 on p5217	This study

Continued on next page

Table 2.9: Plasmids used in this study.

5402	pET-His-GST-3C-Exo1 301-402 UBD2 (I345S A346E)	Amp	Expression of His-GST-3C-Exo1 301-402 UBD2	sdm using oligos oHU5870 and oHU5871 on 5215	This study
5415	pET-His-MBP-3C-Exo1 301-402 H342A (UBD3)	Amp	pET-His-MBP-3C-Exo1 301-402 AmpR H342A (UBD3)	sdm using oligos oHU6144 and oHU6145 on p5217	This study
5416	pET-His-MBP-3C-Exo1 301-402 F394A F395A (PIP2-2)	Amp	pET-His-MBP-3C-Exo1 301-402 F394A F395A (PIP2-2 mutant)	sdm using oligos oHU6148 and oHU6149 on p5217	This study
5417	pET-His-MBP-3C-Exo1 301-402 I391A (PIP2-1)	Amp	pET-His-MBP-3C-Exo1 301-402 I391A (PIP2-1 mutant)	sdm using oligos oHU6146 and oHU6147 on p5217	This study
5449	pFA-HIS-Exo1-9Myc-PIP2	Amp His	Introduction of Exo1-9Myc PIP2 into yeast	Gibson cloning: vector p3852: PCR with o6183 + 6184 insert p5197: PCR with o6181 + 6182	This study
5450	pFA-HIS-Exo1-9Myc-UDB	Amp His	Introduction of Exo1-9Myc UBD into yeast	Gibson cloning: vector p5297: PCR with o6183 + 6184 insert p5197: PCR with o6181 + 6182	This study
5451	pFA-HIS-Exo1-9Myc-PIP2 UDB	Amp His	Introduction of Exo1-9Myc PIP2 UBD into yeast	Gibson cloning: vector p5295: PCR with o6183 + 6184 insert p5197: PCR with o6181 + 6182	This study
5452	pFA-HIS-Exo1-9Myc	Amp His	Introduction of Exo1-9Myc into yeast	Cut- and paste cloning: vector p5449 digested with Nsi and Blg II insert p3866 (Exo1 wt): digested Nsi and Blg II	This study
5481	pET-His-GST-3C-Exo1 301-402 H342A (UBD3)	Amp	Bacterial expression of His-GST-3C-Exo1 301-402 H342A (UBD3)	sdm using oligos oHU6144 and oHU6145 on p5215	This study
5482	pET-His-GST-3C-Exo1 301-402 F394A F395A (PIP2-2)	Amp	Bacterial expression of His-GST-3C-Exo1 301-402 F394A F395A (PIP2-2)	sdm using oligos oHU6148 and oHU6149 on p5215	This study
5483	pET-His-GST-3C-Exo1 301-402 I391A (PIP2-1)	Amp	Bacterial expression of His-GST-3C-Exo1 301-402 I391A (PIP2-1)	sdm using oligos oHU6146 and oHU6147 on p5215	This study

Continued on next page

Table 2.9: Plasmids used in this study.

5525	pQIq-MRGS-8His-DARPin-Ub K48 A1-FLAG W36A W38A	Amp	Expression of His-DARPin-Ub K48 A1-FLAG W36A W38A (site 1 mutant)	sdm using oligos oHU6281 and oHU6282 on p4412	This study
5526	pQIq-MRGS-8His-DARPin-Ub K48 A1-FLAG W101A L102A	Amp	Expression of His-DARPin-Ub K48 A1-FLAG W101A L102A (site 2 mutant)	sdm using oligos oHU6283 and oHU6284 on p4412	This study
5527	pQIq-MRGS-8His-DARPin-Ub K48 A1-FLAG W122A	Amp	Expression of His-DARPin-Ub K48 A1-FLAG W122A (site 3 mutant)	sdm using oligos oHU6285 and oHU6286 on p4412	This study
5528	pENTR4-Exo1 301-360	Kan	Gateway cloning	PCR amplification of pHU5124 using oHU5872 and oHU5796. Cloning into 1788 digested with NcoI and XhoI.	This study
5529	pENTR4-Exo1 301-450	Kan	Gateway cloning	PCR amplification of pHU5124 using oHU5872 and oHU4383. Cloning into 1788 digested with NcoI and XhoI.	This study
5530	pENTR4-Exo1 361-402	Kan	Gateway cloning	PCR amplification of pHU5124 using oHU6294 and oHU5794. Cloning into 1788 digested with NcoI and XhoI.	This study
5531	pENTR4-Exo1 361-450	Kan	Gateway cloning	PCR amplification of pHU5124 using oHU6294 and oHU4383. Cloning into 1788 digested with NcoI and XhoI.	This study
5532	pENTR4-Exo1 402-450	Kan	Gateway cloning	PCR amplification of pHU5124 using oHU6257 and oHU4383. Cloning into 1788 digested with NcoI and XhoI.	This study
5533	pQIq-MRGS-8His-DARPin-Ub K48 C3-Flag	Amp	Vector for bacterial expression of DARPin		Jonas Schaefer, DARPin CF Zuerich

Continued on next page

Table 2.9: Plasmids used in this study.

5534	pQIq-MRGS-8His-DARPin-Ub K48 F3-Flag	Amp	Vector for bacterial expression of DARPin		Jonas Schaefer, DARPin CF Zuerich
5535	pQIq-MRGS-8His-DARPin-Ub K48 H1-Flag	Amp	Vector for bacterial expression of DARPin		Jonas Schaefer, DARPin CF Zuerich
5536	pQIq-MRGS-8His-DARPin-Ub K48 H3-Flag	Amp	Vector for bacterial expression of DARPin		Jonas Schaefer, DARPin CF Zuerich
5555	pET-His-GST-3C-Exo1 301-360	Amp	Expression of His-GST-3C-Exo1 301-360	Gateway cloning: p5528 into 5037	This study
5556	pET-His-GST-3C-Exo1 301-450	Amp	Expression of His-GST-3C-Exo1 301-450	Gateway cloning: p5529 into 5037	This study
5557	pET-His-GST-3C-Exo1 361-402	Amp	Expression of His-GST-3C-Exo1 361-402	Gateway cloning: p5530 into 5037	This study
5558	pET-His-GST-3C-Exo1 361-450	Amp	Expression of His-GST-3C-Exo1 361-450	Gateway cloning: p5531 into 5037	This study
5559	pET-His-GST-3C-Exo1 402-450	Amp	Expression of His-GST-3C-Exo1 402-450	Gateway cloning: p5532 into 5037	This study
5560	pET-His-MBP-3C-Exo1 301-360	Amp	Expression of His-MBP-3C-Exo1 301-360	Gateway cloning: p5528 into 5033	This study
5561	pET-His-MBP-3C-Exo1 301-450	Amp	Expression of His-MBP-3C-Exo1 301-450	Gateway cloning: p5529 into 5033	This study
5562	pET-His-MBP-3C-Exo1 361-402	Amp	Expression of His-MBP-3C-Exo1 361-402	Gateway cloning: p5530 into 5033	This study
5563	pET-His-MBP-3C-Exo1 361-450	Amp	Expression of His-MBP-3C-Exo1 361-450	Gateway cloning: p5531 into 5033	This study
5564	pET-His-MBP-3C-Exo1 402-450	Amp	Expression of His-MBP-3C-Exo1 402-450	Gateway cloning: p5532 into 5033	This study
5593	pET-His-GST-3C-Exo1 301-402 PIP1	Amp	Expression of His-GST-3C-Exo1 301-402 with mutations in PIP1	sdm using oligos oHU4473 and oHU4474	This study
5621	pFA-HIS-Exo1-9Myc-PIP1	Amp His	Introduction of Exo1-9Myc PIP1 into yeast	sdm with o4473 and o4474 on p5452	This study
5622	pFA-HIS-Exo1-9Myc-PIP1 PIP2	Amp His	Introduction of Exo1-9Myc PIP1 PIP2 into yeast	sdm with o4473 and o4474 on p5449	This study

Continued on next page

Table 2.9: Plasmids used in this study.

5634	pET-His-GST-3C-Exo1 301-402 PIP1 PIP2	Amp	Expression of His-GST-3C-Exo1 301-402 PIP1 PIP2	sdm using oligos oHU4473 and oHU4474 on p5352	This study
5655	pET-His-MBP-3C-Exo1 301-402 A346D	Amp	Bacterial expression of His-MBP-3C-Exo1 301-402 A346D	sdm using oligos oHU6508 and oHU6509 on p5217	This study
5656	pET-His-MBP-3C-Exo1 301-402 A346F	Amp	Bacterial expression of His-MBP-3C-Exo1 301-402 A346F	sdm using oligos oHU6506 and oHU6507 on p5217	This study
5657	pET-His-MBP-3C-Exo1 301-402 A346R	Amp	Bacterial expression of His-MBP-3C-Exo1 301-402 A346R	sdm using oligos oHU6510 and oHU6511 on p5217	This study
5658	pET-His-GST-3C-Exo1 301-402 A346D	Amp	Bacterial expression of His-GST-3C-Exo1 301-402 A346D	sdm using oligos oHU6508 and oHU6509 on p5215	This study
5659	pET-His-GST-3C-Exo1 301-402 A346F	Amp	Bacterial expression of His-GST-3C-Exo1 301-402 A346F	sdm using oligos oHU6506 and oHU6507 on p5215	This study
5660	pET-His-GST-3C-Exo1 301-402 A346R	Amp	Bacterial expression of His-GST-3C-Exo1 301-402 A346R	sdm using oligos oHU6510 and oHU6511 on p5215	This study
5663	pFA-HIS-Exo1-1-300	Amp His	Introduction of Exo1-1-300 into yeast	PCR using plasmid 3698 and oligos 4607 and 6482, digested with PacI/AscI and cloned into PacI/AscI of plasmid 233	This study
5664	pFA-HIS-Exo1 301-702	Amp His	Introduction of Exo1 301-702 into yeast	PCR using plasmid 3700 and oligos 4306 and 6481, digested with PacI/AscI and cloned into PacI/AscI of plasmid 233	This study
5665	pFA-HIS-Exo1 301-630	Amp His	Introduction of Exo1 301-630 into yeast	PCR using plasmid 3705 and oligos 6481 and 6484, digested with PacI/AscI and cloned into PacI/AscI of plasmid 233	This study
5666	pFA-HIS-Exo1 301-402	Amp His	Introduction of Exo1 301-402 into yeast	PCR using plasmid 5125 and oligos 6481 and 6483, digested with PacI/AscI and cloned into plasmid 233	This study

Continued on next page

Table 2.9: Plasmids used in this study.

5708	pFA-HIS-Exo1-9Myc A346D	Amp	Introduction of pFA-HIS-Exo1-9Myc A346D into yeast	sdm using oligos oHU6508 and oHU6509 on p5452	This study
5709	pFA-HIS-Exo1-9Myc A346F	Amp	Introduction of pFA-HIS-Exo1-9Myc A346F into yeast	sdm using oligos oHU6506 and oHU6507 on p5452	This study
5710	pFA-HIS-Exo1-9Myc A346R	Amp	Introduction of pFA-HIS-Exo1-9Myc A346R into yeast	sdm using oligos oHU65010 and oHU6511 on p5452	This study
5754	pET3a-Ub K48R_new	Amp	Bacterial expression of UbK48R	Site-directed mutagenesis: o4455/o4456 on p3598	C. Renz
5808	pQIq-MRGS-8His-TEV-mVenus (155-238)_DARPin-Ub K63 G1-Flag	Amp	Vector for bacterial expression of His-TEV-mVenus (155-238)_DARPin-Ub K63 G1-FLAG for BiFC	Cut- and paste cloning Amplify mVenus insert (155-238) from p5292 using o6667 and o6668 ; vector: p4617 digest with BamHI	This study
5809	pQIq-MRGS-8His-TEV-mVenus (155-238)_L20_DARPin-Ub K63 G1-Flag	Amp	Vector for bacterial expression of His-TEV-mVenus (155-238)_L20_DARPin-Ub K63 G1-FLAG for BiFC	Cut- and paste cloning Amplify mVenus insert (155-238) from p5292 using o6667 and o6669; vector: p4617 digest with BamHI	This study
5816	pQIq-MRGS-8His-TEV-mVenus (1-154)_DARPin-Ub K48 A1-Flag	Amp	Vector for bacterial expression of His-TEV-mVenus (1-154)_DARPin-Ub K48 A1-FLAG for BiFc	Cut- and paste cloning Amplify mVenus insert (1-154) from p5292 using o6664 and o6665 ; vector: p4412 digest with BamHI	This study
5889	pDEST_TO_YFP-DARPin K48 A1	Amp Hygro	generation of stable cell lines expressing YFp-tagged DARpin K48 A1 via FRT-site/flipase-mediated integration	LR cloning with p1803 and p5303	This study
5890	pDEST_TO_YFP-DARPin K63 G1	Amp Hygro	generation of stable cell lines expressing YFp-tagged DARPin K63 G1 via FRT-site/flipase-mediated integration	LR cloning with p1803 and p5308	This study

Continued on next page

Table 2.9: Plasmids used in this study.

5891	pDEST_TO_YFP-DARPin E3_5	Amp Hygro	generation of stable cell lines expressing YFP-tagged DARPin E3_5 via FRT-site/flipase-mediated integration	LR cloning with p1803 and p5301	This study
6006	pET-His-MBP-3C-Exo1 301-402 delta8	Amp	Bacterial expression of His-MBP-3C-Exo1 301-402 delta8	sdm using oligos oHU6872 and oHU6873 on p5217	This study
6007	pQIq-MRGS-8His-TEV-mVenus (1-154)_DARPin-E3_5-Flag	Amp	Vector for bacterial expression of His-TEV-mVenus (1-154)_DARPin-E3_5-FLAG for BiFc	Cut- and paste cloning Amplify mVenus insert (1-154) from p5292 using o6664 and o6665 ; vector: p3680 digest with BamHI	This study
6008	pQIq-MRGS-8His-TEV-mVenus (155-238)_DARPin-Ub E3_5-Flag	Amp	Vector for bacterial expression of His-TEV-mVenus (155-238)_DARPin-E3_5-FLAG for BiFC	Cut- and paste cloning Amplify mVenus insert (155-238) from p5292 using o6667 and o6668 ; vector: p3680 digest with BamHI	This study
6009	pcDNA5_FRT_TO_Venus_C-term_DARPin-Ub K63 G1-Flag_P2A_Venus_N-term_DARPin-Ub K48 A1-Flag	Amp Hygro	Overexpression of Venus_C-term_DARPin-Ub K63 G1-Flag and Venus_N-term_DARPin-Ub K48 A1-Flag separated by P2A site in mammalian cells	Gibson assembly vector p5643: linearized with o6700 and o6701 insert 1: o6696 and o6697 on p5816 insert 2: o6698 and o6699 on p5808	This study
6010	pcDNA5_FRT_TO_Venus_C-term_DARPin-E3_5_P2A_Venus_N-term_DARPin-Ub K48 A1-Flag	Amp Hygro	Overexpression of Venus_C-term_DARPin-E3_5-Flag and Venus_N-term_DARPin-Ub K48 A1-Flag separated by P2A site in mammalian cells	Gibson assembly vector p5643: linearized with o6700 and o6701 insert 1: o6696 and o6697 on p5816 insert 2: o6698 and o6699 on p6008	This study
6011	pcDNA5_FRT_TO_Venus_C-term_DARPin-Ub K63 G1-Flag_P2A_Venus_N-term_DARPin-E3_5-Flag	Amp Hygro	Overexpression of Venus_C-term_DARPin-Ub K63 G1-Flag and Venus_N-term_DARPin-E3_5-Flag separated by P2A site in mammalian cells	Gibson assembly vector p5643: linearized with o6700 and o6701 insert 1: o6696 and o6697 on p6007 insert 2: o6698 and o6699 on p5808	This study

Continued on next page

Table 2.9: Plasmids used in this study.

6101	pQIq-MRGS-8His-DARPin-Ub K48 A1-Flag W36A W38A W122A	Amp	Expression of His-DARPin-Ub K48 A1-FLAG W36A W38A W122A (site 1+3 mutant)	sdm using oligos oHU6285 and oHU6286 on p5525	This study
6102	pQIq-MRGS-8His-DARPin-Ub K48 A1-Flag W36A W38A W101A L102A W122A	Amp	Expression of His-DARPin-Ub K48 A1-FLAG W36A W38A W101A L102A W122A (site 1,2 & 3 mutant)	sdm using oligos oHU6283 and oHU6284 on p6101	This study
6150	pQIq-MRGS-8His-DARPin-Ub K63 G1-FLAG W48A	Amp	Expression of His-DARPin-Ub K63 G1-FLAG W48A (site 1 mutant)	sdm using oligos oHU7173 and oHU7174 on p4617	This study
6151	pQIq-MRGS-8His-DARPin-Ub K63 G1-FLAG W83A	Amp	Expression of His-DARPin-Ub K63 G1-FLAG W83A (site 2 mutant)	sdm using oligos oHU7175 and oHU7176 on p4617	This study
6152	pQIq-MRGS-8His-DARPin-Ub K63 G1-FLAG F81A S82A W83A	Amp	Expression of His-DARPin-Ub K63 G1-FLAG F81A S82A W83A (site 2a mutant)	sdm using oligos oHU7177 and oHU7178 on p4617	This study
6153	pQIq-MRGS-8His-DARPin-Ub K63 G1-FLAG W91A W92A	Amp	Expression of His-DARPin-Ub K63 G1-FLAG W91A W92A (site 3 mutant)	sdm using oligos oHU7179 and oHU7180 on p4617	This study
6154	pQIq-MRGS-8His-DARPin-Ub K63 G1-FLAG F81A S82A W83A W91A W92A	Amp	Expression of His-DARPin-Ub K63 G1-FLAG F81A S82A W83A W91A W92A (site2a+ 3 mutant)	sdm using oligos oHU7177 and oHU7178 on p6153	This study
6155	pQIq-MRGS-8His-DARPin-Ub K63 G1-FLAG W48A F81A S82A W83A W91A W92A	Amp	Expression of His-DARPin-Ub K63 G1-FLAG W48A F81A S82A W83A W91A W92A (site 1 + 2a + 3 mutant)	sdm using oligos oHU7173 and oHU7174 on p6154	This study

2.6 Methods for DNA modification and analysis

2.6.1 Determination of DNA concentration

For the determination of DNA concentrations, UV-VIS spectroscopy was used, as according to the Beer-Lambert law, the absorption A_{260} is proportional to the concentration of the absorbing DNA (c_{DNA}).

$$A_{260} = c_{\mathrm{DNA}} \cdot \varepsilon_{260\mathrm{nm}} \cdot d \tag{1.1}$$

Factor *d* thereby represents the length of the optical path, it was in this case given as 1 cm. The extinction coefficient for double-stranded DNA at a wavelength of 260 nm ($\varepsilon_{260\mathrm{nm}}$) amounts to 0.02 $\frac{\mu L}{ng \cdot cm}$, so the concentration was received in the unit $\frac{ng}{\mu L}$. For measuring 1.5 µL of the sample was pipetted on the optical path of the spectrophotometer (NanoDrop2000, Thermo Scientific or DeNovix DS-11, Biozym) after blanking with the respective buffer solution.

2.6.2 Agarose gel electrophoresis

For the separation of DNA fragments and the control of PCR products an agarose gel electrophoresis was used. Agarose gels were prepared by dissolving 1% (w/v) agarose in 1x TBE buffer, supplemented with SYBR Safe DNA stain (Invitrogen). The DNA sample was mixed 5:1 with the 6x DNA loading dye, afterwards loaded on the agarose gel and run for 25—30 min at 100 V in TBE buffer. In order to estimate the size of the DNA fragments the 1 kbp or 100 bp DNA ladder (NEB) was loaded on each gel for comparison. As the SYBR Safe DNA stain binds to DNA and absorbs blue light[456] the blue-light table of the FusionFX-7 imaging system was used for visualization.

2.6.3 Polymerase chain reaction

Amplification of DNA fragments was conducted using polymerase chain reaction (PCR). The reaction was performed using the homemade high-fidelity (HF) polymerase (Core Facility Protein Production, IMB) or the Phusion® HF DNA polymerase (NEB) according to the manufacturer's protocol. The reaction was composed of 10-50 ng of DNA, 1x HF-buffer, 0.5 µM forward and reverse primer, 200 µM dNTPs and 1U DNA polymerase, filled up to 50 µL with nuclease-free water. For some reactions 1-3% of DMSO was added to aid in the denaturation especially for templates with GC-rich content.[457]

The reaction was performed in a Professional TRIO cycler (Biometra) using following temperature protocol: First an initial denaturation step at 98°C for 30 s was performed, followed by 30-35 cycles of 98°C for 10 s (denaturation), 50-72°C (according to the oligo's melting temperature) 30 s of annealing and an extension step at 72°C for 30 s/kbp of the according amplicon. The PCR was finished with a final extension step at 72°C for 5 min.

PCR reactions were cleaned up using the GeneJET PCR purification kit (Thermo Fisher Scientific) or the QIAquick Gel Extraction Kit (Qiagen) according to the manufacturer's instructions.

2.6.4 Site-directed mutagenesis

In order to introduce point mutations into a plasmid, intergenic primers (forward and reverse) were designed carrying the desired nucleotide mutations. With these primers a PCR was conducted using the homemade HF-Polymerase, the high fidelity polymerases Pfu Turbo or Pfu Ultra (all Agilent) as described in 2.6.3 and according to their respective manufacturer protocol.

To remove the template DNA, 1x CutSmart buffer (NEB) and 0.5 µL DpnI restriction nuclease (20 U/µl) were added, and the mixture was incubated at 37°C for 1-16 h. The product was purified using the MiniElute PCR Purification Kit (Qiagen) according to the manufacturer's instruction and transformed into chemically competent Top10 cells (see section 2.7.1).

2.6.5 Restriction cloning

Restriction cloning was used to clone a gene of interest into a different plasmid backbone. This approach requires the same or compatible restriction sites in both fragments. The plasmids or PCR products (1-2 µg) were digested by the corresponding endonuclease (5-20 U) in 1xCutSmart Buffer at 37°C for 3-16 h. If the vector was linearized by cleavage with only one restriction enzyme a dephosphorylation step was added to inhibit recircularization. Therefore the 5'-phosphate of the vector backbone was cleaved by adding 1 U Fast AP (Thermo Fisher Scientific) for 1–2 h at 37°C to the mixture. Subsequently, the DNA fragments were separated by agarose gel electrophoresis, and the desired fragment was purified using the QIAquick gel extraction kit (Qiagen) according to the manufacturer's instructions. For DNA ligation 50 ng of the vector and the insert DNA fragment were combined in a molar ratio of 1:3. The solution was filled up with demineralized water to a volume of 5 µL and the same volume of 2x Takara's ligation solution was added to ligate the compatible DNA fragments at 16°C for 30-60 min. For defining ligation efficiency, a negative control without insert was prepared by replacing the missing volume with demineralized water. The ligation mix was transformed into chemically competent Top10 cells (section 2.7.1).

2.6.6 Gibson assembly

The Gibson Assembly reaction is used to seamlessly and restriction-enzyme independent construct synthetic and natural genes and plasmids by joining together DNA fragments containing ~20 nt long overlapping ends. These fragments are amplified by PCR (compare section 2.6.3) with respective primers and then mixed in a stoichiometric manner in a total volume of 10 µL with 10 µL of the homemade 2x Gibson assembly master mix (Core Facility Protein Production, IMB) containing the T5 exonuclease, the Phusion DNA polymerase and the Taq Ligase. The reaction mix was incubated at 50°C for 1 h and transformed into chemically competent Top10 cells (section 2.7.1).[458]

2.6.7 Gateway cloning

Invitrogen Gateway cloning was used for inserting a fragment into multiple vectors or *vice versa* having different fragments which need to be inserted into the same vector. In a one-step reaction, 100 ng of a Gateway entry vector, containing the fragment of interest, and 100 ng of a Gateway destination vector were mixed in 7.5 µL. 2.5 µL of the 4x LR clonase mix (Core Facility Protein Production, IMB) were added and the mixture was incubated for 1 h at room temperature. The reaction was transformed into ccdB-susceptible, competent *E.coli* cells (section 2.7.1).

2.6.8 Colony PCR

For screening clones for positive insertion of the desired fragment, a colony PCR was conducted. In the ideal case, primers were used, one of which binds to the vector and one to the desired insert in order to obtain a PCR product only if cloning was successful. Multiple clones were screened by stirring a single clone in a PCR mix, containing 250 µM dNTPs, 250 nM forward and revers primer and 0.5 U Taq polymerase in 1x Green buffer. The PCR protocol included a denaturation step at 95°C for 10 min followed by 35 cycles of 95°C for 30 s (denaturation), 50-72° C (according to the oligo's melting temperature) for 30 s (annealing) and 72°C for 30 s per kbp of the amplified DNA fragment (extension). The reaction was completed by a final extension step at 72 °C for 4 min. The product was analyzed by agarose gel electrophoresis. Positive clones were checked by sequencing.

2.6.9 DNA sequencing

DNA sequencing was conducted by the company StarSEQ (Mainz, Germany). Samples were prepared by mixing 400–700 ng of purified plasmid DNA and 1 µL of the sequencing primers (10 µM) in a total volume of 7 µL.

The received sequencing results were analyzed using SnapGene® 4.1.9, GSL Biotech LLC.

2.7 Methods for working with *E. coli*

2.7.1 Transformation using chemically competent cells

All competent *E. coli* strains listed in Table 2.5 were transformed by a heat shock method. The aliquot of chemically competent bacteria was thawn on ice. Then 50-100 ng DNA were added to 50 µL of cells and incubated on ice for 15-30 min before the heat shock at 42°C for 45-60 s was performed. Cells were incubated on ice for 5 minutes. For samples using ampicillin as a selection marker, cells were dissolved directly in 100 µL of LB medium and plated onto LB agar plates containing ampicillin. All plasmids with other antibiotic resistances for selection required a regeneration phase prior to plating. For this, 900 µL of LB medium was added to the transformation mix and the sample was incubated at 37°C for 45-60 min. The cells were pelleted at 3000x g (RT, 3 min), resuspended in 100 µL LB medium and plated on an LB agar plate containing the appropriate antibiotics. Plates were incubated overnight at 37°C.

2.7.2 Isolation of plasmid DNA

To receive the desired plasmids, a single bacterial clone of the transformation was picked, and 5 mL of LB medium supplemented with the appropriate antibiotic were inoculated. After incubation overnight (37°C, 180–200 rpm), the cells were harvested by centrifugation (4000 rpm, 10 min, room temperature (RT)) and purified using the Thermo Scientific GeneJET Plasmid Miniprep kit following the manufacturer's protocol.

2.7.3 *E. coli* cultivation and protein expression

For cultivation, all transformed *E. coli* strains were grown in LB medium supplemented with the appropriate antibiotic at 37°C.

For protein expression, the *E. coli* culture was grown in two steps. The preculture of 5-100 mL LB medium with the appropriate antibiotics (Table 2.4) was inoculated with a clone from the transformation plate and incubated overnight at 37°C and 180-225 rpm. For the main culture the next day, the preculture was diluted 1:50 in a (baffled) flask to a final volume of 0.25-8 L. The culture was incubated at 37°C and 180-200 rpm until the optical density at 600 nm (OD_{600}) reached a value of 0.6-0.8. A negative sample was taken for later analysis by SDS-PAGE and expression was started by induction with 0.1-1 mM IPTG.

The protein was expressed for 3-5 hours at 37°C or overnight at 16-18°C while shaking (180-200 rpm). After expression, another sample was taken with the same OD_{600} as the negative sample. The culture was harvested by centrifugation (5,000 rpm, 20 min, RT, Sorvall RC 6+), the supernatant was discarded, and the pellet was either directly lysed or frozen at -20°C for storage.

2.7.4 Cell lysis

For lysis, the cell pellet was resuspended in the appropriate lysis buffer (section 2.2.4) supplemented with the required additives such as protease inhibitors (1x), magnesium chloride (2 mM), SN nuclease (1:2500) or Triton X100 (0.1%). Two methods were used for cell disruption, depending on the construct. For the ultrasonic method, the samples were sonicated for 1-3 min at 40-50% duty cycle and 3 4 output power (Branson Sonifier S-250A) using the 5 or 9 mm tip depending on the sample volume. For more sensitive constructs, cells were mechanically lysed using the high-pressure cell disruptor TS-T240 (Constant Systems). *E. coli*'s were lysed by 2 rounds at a pressure of 180 bar.

The remaining cellular components were then separated by centrifugation (40,000 x g, 20 min, 4°C). A sample of the supernatant was taken for further analysis by SDS-PAGE and the supernatant was further purified.

2.8 Methods for working with yeast

2.8.1 Yeast cultivation

Yeast strains with an integrated construct were grown in YPD or SC complete media with 2% (w/v) glucose unless otherwise stated. Yeast strains containing an episomal expression plasmid were grown in SC media lacking the corresponding amino acid. All strains were grown at 30°C with shaking at 200-220 rpm. For protein expression driven by the GAL promoter, yeasts were first grown overnight in the respective medium containing 2% (w/v) raffinose and 0.2% (w/v) glucose and then transferred to medium supplemented with 2% (w/v) galactose and 0.1% (w/v) glucose to induce gene expression. For expression mediated by a tet-promoter 0.5-2 ng/µL doxycylcine was added to induce gene expression for the indicated amount of time.

2.8.2 Yeast transformation

For yeast transformation with episomal vectors, the yeast strain was pre-cultured overnight, then diluted to OD_{600}=0.2 and grown to exponential phase (OD_{600}= 0.5-0.7). 1 mL of cell suspension per construct was harvested at 8000 rpm for 2 minutes (RT). The cell pellet was first washed with 500 µL sterile ddH_2O and then with 200 µL SORB. The pellet was resuspended in 50 µL SORB/HT-ssDNA mixture (45 µL SROB + 5 µL HT-ssDNA) and 50-100 ng plasmid DNA was mixed in. 300 µL LiT/PEG was added and the sample was incubated for 30 min at room temperature. Then 38.9 µL DMSO was added and a heat shock was performed for 10 min at 42°C in a water bath. Finally, the cells were pelleted again by centrifugation at 4000 rpm for 2 min at RT and resuspended in 1 mL ddH_2O. 150 µL of the cell suspension was plated onto selective plates and grown at 30°C for 2-4 days.

For integrative plasmids, a similar protocol was used with the following adaptations: 5 mL yeast cells in logarithmic growth phase were used per construct, the volumes used for the wash steps were increased 10-fold to 5 mL ddH_20 and 2 mL SORB, but the cells were still resuspended in 50 µL SORB/HT-ssDNA mixture at the end. 500-1000 ng linearized DNA were added.

This linearized DNA could be a plasmid containing the gene of interest, which was cut with a restriction enzyme in the selection marker to allow integration or a product of a PCR-based tagging or knock out approach, where the gene of interest or a knock-out cassette was amplified by PCR primers containing homology overhangs for the integration area.[459] The heat shock was performed as described above. The final pellet was resuspended in only 100 µL water and the whole suspension was plated on appropriate plates. When antibiotic selection was used, cells needed an additional recovery step before plating, so cells were incubated in 1 mL YPD for 3 h at 30°C, before centrifugation and plating.

2.8.3 Yeast colony PCR

To verify successful integration into the *S. cerevisiae* genome, a colony PCR was performed. Single colonies from the transformation plate were replated onto selective plates and grown overnight. 2-3 colonies from these plates were resuspended in 50 µL of 20 mM NaOH. The suspension was heated at 95°C for 15 min, vortexed for 1 min and centrifuged (1 min, 13,000 rpm, RT) to remove insoluble debris. 25 µL of the supernatant was diluted with 25 µL of NF-ddH_2O. 2 µL of this mixture were used for PCR amplification, mixed with 0.5 µL forward and reverse primer each, 0.5 µL 10 mM dNTPs, 5 µL 5x green GoTaq buffer, 0.25 µL home-made Taq polymerase and filled up to 25 µL with NF-H_2O. The reaction was performed in the Professional TRIO 48 cycler (Biometra) with the following temperature program: initial denaturation at 95°C for 4 min, 35 cycles of 30 s at 95°C, 30 s at 55°C and 1 min/kb 72°C, and then finalized with an extension at 72°C for 5 min. The PCR product was subsequently analyzed by agarose gel separation.

2.8.4 Preparation of total yeast protein extract

Yeast extract was in this study used for two purposes: as input material for the pull-downs testing the specificity of the DARPins or for looking at expression levels of certain constructs.

When whole cell lysate was required as input sample, cultures were grown in the desired volume to an OD_{600} of 1-2. The culture was then harvested by centrifugation (5000 rpm, 15 min, RT). The pellets were either frozen or dissolved directly in 400 µL of yeast lysis buffer supplemented with 1× protease inhibitor and 10 mM of the deubiquitinase inhibitors N-ethylmaleimide (NEM) and ortho-phthalaldehyde (OPA). The mixture was transferred to tubes equipped with small matrix beads, which disrupted the cells by collisions induced by the three-dimensional movement of the FastPrep24 machine. 10-15 rounds of 40 s each were performed with 2 min breaks in between. Then 0.1% Triton X-100 was added and the samples were incubated for 15 min at 4°C. The lysate was separated from the beads by centrifugation (2000 x g, 2 min, 4°C) and finally the yeast extract was separated from the cell components by another centrifugation step at higher speed (14,000 rpm, 20 min, 4°C) to receive the clean protein lysate.

To check the expression levels of proteins inside yeast cells, they were enriched by the TCA (trichloroacetic acid) method. A sample of 1 mL (OD_{600} = 0.7-1) was collected by centrifugation at 16,000 xg for 15 min at RT. The cell pellet was resuspended in 1 mL ice-cold water. Then 150 µL of a mixture of ice-cold NaOH and β-mercaptoethanol (1.85 M NaOH+ 7.5% (v/v) β-mercaptoethanol) was added and incubated for 15 min on ice. 150 µL ice-cold 55% (w/v) TCA was added and samples were incubated for further 10 min before centrifugation at 21,000 xg for 10 min at 4°C. The supernatant was removed by aspiration and a further short centrifugation (21,000 xg, 1 min, 4°C) ensured that all residual liquid was removed. The pellet was resuspended in 1x NuPage buffer supplemented with DTT and the sample was heated to 65°C for 10 min before analysis by SDS-PAGE and Western blot.

2.8.5 Spot assay

Spot assays can be used to monitor the growth and viability of yeast strains with specific modifications, such as knock-out or expression of a particular protein, under basal and stress conditions, providing valuable insights into the function of certain proteins in specific stress responses.

Therefore, OD_{600}= 0.16 of an exponentially growing culture was serially diluted four times (1:5) in sterile ddH_2O in a 96-well plate. Using the Replica Plater for 96-Well Plate (Sigma-Aldrich), these dilutions were plated on the respective plates supplemented if indicated with stressors (see below). Unless otherwise stated, plates were incubated at 30°C for 2-4 days. The plates were scanned with the Epson Scan Perfection V700 Photo using the "Epson scan" software with following settings: positive film, 8-bit grayscale, 600 dpi.

Following stressors in indicated concentrations were added to freshly prepared plates for the spot assay:

NaCl: 0.1 M, 0.5 M, 0.75 M, 1 M, 1.25 M

Sorbitol: 0.5 M, 0.75 M, 1 M, 1.5 M

MMS (v/v): 0.0025 %, 0.005 %, 0.01 %, 0.02 %

Tunicamycin: 0.0625 µg/mL, 0.125 µg/mL, 0.15 µg/mL, 0.2 µg/mL, 0.25 µg/mL

2.8.6 Yeast two-hybrid assay

A yeast two-hybrid assay can provide insight whether two proteins interact with each other, as only then the respective yeast cell grows.[460, 461] The reporter yeast strain PJ69-4A (ID 195) was transformed (compare section 2.8.2) with plasmids carrying one gene of interest fused to the GAL4 activation (AD) and one fused to the DNA-binding domain (BD). They were plated on SC-plates lacking leucine and tryptophane and incubated at 30°C for 2-3 days.

For the spot assay, 4-6 colonies of each strain were resuspended in 500 µL sterile water and vortexed. 5 µL of each strain was spotted onto SC agar plates lacking specific amino acids (SC Trp-Leu-, SC Trp-Leu-His-, SC Trp-Leu-His-Ade-) and grown at 30°C for 4-5 days.

The presence of both yeast two-hybrid plasmids was confirmed by growth on plates lacking leucine and tryptophan. Positive interactions between the candidate proteins were determined by growth on plates lacking leucine, tryptophan and histidine.

2.8.7 Microscopy

To monitor expression and localization of proteins in live-cells by microscopy, 200 µL of culture, in the exponential growth phase unless otherwise stated, was transferred to a concanavalin A-coated glass bottom chamber coverslip (Ibidi). After a brief incubation, the cells were washed three times with medium and then released into fresh SC medium supplemented with doxycycline or the indicated drug, if necessary. Imaging was performed with a wide-field DeltaVision Elite system (GE Healthcare) equipped with a 60x oil immersion objective (NA=1.42), InsightSSITM solid-state illumination, Scientific CMOS camera, SoftWoRxTM software, and a build-in deconvolution algorithm. For each image, Z-stacks of 21 steps (step size = 0.2 mm) were acquired, each time taking an image with the optimized filters for each fluorescent dye as well as a Differential Interference Contrast (DIC) image as a whole cell image.

2.8.8 Proximity ligation assay

The proximity ligation assay (PLA) is a method for the *in situ* detection of protein-protein interactions. It is a type of ELISA in which the two target proteins are detected by specific primary antibodies from different species, and these two antibodies are then bound by two secondary antibodies coupled to an oligonucleotide (PLA probe). If the two probes and thus the two oligonucleotides are in close proximity (<16 nm), they can hybridize. After the addition of a ligase, a closed circular DNA template is formed, which allows rolling circle amplification by the added DNA polymerase. The final step, which allows detection by microscopy, is the addition of fluorochrome-labeled oligos that hybridize to repetitive sequences in the amplicons.[462–464]

1 OD_{600} of exponential yeast cells were harvested and fixed by resuspension in 4% formaldehyde in 100 mM potassium phosphate buffer, pH 6.4, for 10-20 minutes at room temperature. The pellet was then washed twice with 100 mM potassium phosphate buffer pH 6.5 and resuspended in 100 mM potassium phosphate buffer pH 7.4 for storage. For spheroplasting, the cells were centrifuged, the buffer discarded, and the pellet resuspended in 200 µL of zymolyase buffer containing 10 mM DTT. The suspension was incubated for 10 min at RT, then the cells were centrifuged and resuspended in 100 µL of the same buffer supplemented with 2 µL 10 mg/mL Zymolyase 100 T. With gentle shaking, the cells were incubated at 30°C for 15-30 min. During this time, spheroplast formation was monitored by sensitivity to SDS lysis. The OD_{600} of 10 µL cell suspension in 500 µL 1% SDS was measured, a value around 0 indicating spheroplasty. Spheroplasts were washed twice with zymolyase buffer and resuspended in 150 µL of the same buffer.

The 12-well microscope slide (speciatly printed microscope slides, epredia) was prepared as follows: after cleaning with water and 70% ethanol, 8 µL of 0.1% polylysine was pipetted into each well and allowed to sink in for 5-10 min at RT. The slide was then washed three times with ddH_2O and air dried. 10 µL of spheroplasted cells were pipetted into the wells and incubated for 5-10 min at RT. The supernatant was aspirated and the slide was immersed in ice-cold methanol for 6 min, then immediately submerged in acetone for 30 s before being air dried.

The cells were further permeabilized with 1% Triton X-100 in PBS for 15 min. Subsequently, they were blocked with PLA blocking solution containing 0.5% Triton X-100 for 30 min. The specific primary antibody was diluted (1:100) in antibody diluent containing 0.5% Triton X-100, and 10 µL of this antibody solution was added per well. The slide was incubated in a humidity chamber for 1-3 hours. Prior to incubation with 10 µL of commercial PLA secondary antibodies (1:5, Duolink® In Situ PLA® Probe Anti-Rabbit PLUS/Anti-Mouse MINUS, Sigma-Aldrich), it was washed twice for 5 min with PBS-T. The slide with the secondary antibody was also incubated in a humidity chamber at 37°C for 1 h. Then, it was washed twice for 5 min with PLA Wash Buffer A (Sigma-Aldrich). For ligation, the ligase was diluted in 1x ligation buffer (stock: 5x) with 0.2% Triton X-100. This mixture was applied to the slide and incubated for 30 min at 37°C in a humidity chamber. The slide was washed twice for 2 min with PLA Wash Buffer A, 10 µL of the amplification mixture (1:80 diluted polymerase in 1x amplification stock with 0.2% Triton X-100) was added per well and incubate for 100 minutes at 37°C in a humidity chamber. For ligation, the ligase was diluted in 1x ligation buffer (stock: 5x) with 0.2% Triton X-100. This mixture was applied to the slide and incubated again for 30 min at 37°C in a humidity chamber. The slide was washed twice for 2 min with PLA Wash Buffer A and 10 µL of the amplification mixture (1:80 diluted polymerase in 1x amplification stock with 0.2% Triton X-100) was added per well for 100 min at 37°C (humidity chamber). The slide was washed once with PLA Wash B (Sigma-Aldrich) for 1 min and then rinsed with water. Duolink In Situ Mounting Medium (Sigma-Aldrich), which already contains DAPI, was used for mounting the samples, which was then afterwards sealed with coverslips. The samples were kept in the dark at 4°C until imaging. Imaging was performed following the procedure described in section 2.8.7.

2.9 Methods for working with mammalian cells

2.9.1 Mammalian cell culture

HeLa cells were cultured in Dulbecco's Modified Eagle Medium (DMEM), RPE-1 cells in Roswell Park Memorial Institute (RPMI-1640) medium, both supplemented with 10% Fetal Bovine Serum (FBS), 1% penicillin/ streptomycin (Pen/Strep) and 2 mM L-glutamine at 37°C with 5% CO_2 and 85% humidity in the Forma Steri-Cult CO_2 incubator (Thermo Scientific).

2.9.1.1 Cell thawing and freezing

To thaw cells, a cryovial containing the frozen cells was rapidly thawed in a pre-warmed water bath at 37°C. The cell suspension was added dropwise to a petri dish containing the appropriate medium. Then the cells were allowed to attach overnight before the medium was exchanged the next day.

For freezing, cells in the exponential growth phase were washed with Dulbecco's phosphate-buffered saline (DPBS) and then detached with 0.05% trypsin-EDTA-phenol red (Gibco). Cells were mixed with the appropriate medium and centrifuged at 300xg for 3 minutes. They were then resuspended in a mixture of 10% DMSO in complete growth medium and distributed in cryovials. They were stored in a CoolCell Freeing Container in the -80°C freezer for one to two days before being transferred to the -150°C freezer for long-term storage.

2.9.1.2 Cell passing and counting

When cells reached 80-100% confluence, they were split. For this purpose, the old medium was removed, the cells were washed with pre-warmed DPBS and then detached by incubation with 0.05% trypsin-EDTA-phenol red for 5-7 min at 37°C. Trypsin was neutralized by adding at least a 2-fold excess of complete growth medium. A portion of this cell suspension was transferred to a new dish and diluted 1:5 to 1:15 with fresh growth medium.

When an accurate cell count was required, the cell number was determined after trypsination using the TC20 Automated Cell Counter (Bio-Rad) according to the manufacturer's instructions.

2.9.2 Transient transfection

To transiently transfect plasmid DNA into HeLa cells, they were grown to 60-80% confluence. For a 10 cm dish, a mixture of 3 µg plasmid DNA with 9 µL Fugene HD reagent in 510 µL Opti-MEM medium was incubated for 10 min at room temperature. The cells were washed with DPBS and 10 mL of fresh medium without Pen/Strep was added. The transfection solution was added dropwise. After 24 hours, the medium was changed to complete growth medium.

2.9.3 Creation of stable cell lines via Flp-In integration

For stable integration of the DARPin constructs into RPE-1 cells, the Flp-In system was used. Therefore, a mixture of 2.7 µg Flp recombinase expression vector (pOG44, ID 1809) and 0.3 µg of target plasmid was transfected into RPE1 hTERT FlpIn TREX cells (ID 120) as described above in section 2.9.2. 48 hours after transfection, the antibiotic (puromycin or hydromycin) was added to a final concentration of 2-10 µg/mL. Cells were monitored over the next few weeks and the medium was replaced with fresh antibiotic-containing medium every 2-3 days until antibiotic-resistant colonies appeared. The cells were trypsinized and cultured according to the standard protocol (section 2.9.1).

2.9.4 Colony formation assay

To test the viability of a cell line, a colony formation assay was performed. Approximately 300 cells were seeded in a 10 cm dish. To monitor the effect of DARPin expression, six plates per cell line were seeded; in half of the plates, DARPin expression was induced by the addition of 2 ng/µL doxycyline. Cells were cultured for 7-10 days and then stained with crystal violet blue (Sigma Aldrich) for 15 minutes at RT. The plates were then washed with deionized water and dried at RT overnight, before the colonies were counted manually.

2.9.5 Mammalian cell lysate

For checking the expression of the DARPins, or as input samples for pull-downs, whole cell lysates were needed. To gain this, cells were washed with DPBS and the 1-2 mL of ice-cold DPBS was added to a 15 cm dish. The cells were collected with a cell scraper, transferred in an Eppendorf tube and centrifuged at 5000 rpm for 1 min. The DPBS was removed and cell pellets frozen and stored at -80°C.

For lysis the cell pellet was resuspended in 100-650 µL RIPA or MC lysis buffer, supplemented with 1x protease inhibitor, 1:2500 Sm Nuclease, 5 mM NEM and 2 mM OPA. The suspension was incubated on ice for 30 min and then centrifuged at full speed for 30 min (4°C). The supernatant was collected and the concentration determined using the Protein Assay Dye Reagent (Bio-Rad) according to the manufacturer's instructions.

2.9.6 Microscopy

For immunofluorescence analysis, cells were grown to ~90% confluency on coverslips. After the indicated treatments or induction of expression by doxycycline for the indicated times, cells were fixed with 4% paraformaldehyde (PFA) for 10 minutes and permeabilized with 0.25% Triton X-100 in PBS for 10 minutes at room temperature. They were then blocked in 3% BSA blocking solution for 1 hour and incubated with primary antibody overnight at 4°C. Coverslips were washed three times for 5 min with PBS and incubated with secondary antibodies and (1:10,000) Hoechst in PBS for 1 h at RT. Coverslips were then again washed three times for 5 min with PBS and mounted with PoLong™ Diamond Antifade Mountant (Invitrogen).

Images were captured using an inverted widefield microscope AF7000 (Leica) equipped with a 63x/1.4 oil objective (Leica) and LAS AF software. Images were analyzed using FIJI.

2.9.7 Analyzing protein recruitment to laser-induced stripes

To enable live-cell imaging after laser-induced DNA damage, approximately 200,000 RPE-1 cells with the stably integrated DARPin constructs were seeded in 1 mL medium in 35 mm glass-bottomed ibidi dishes. They were grown overnight and DARPin expression was induced the next day by 2 ng/mL doxycycline for 24 hours.

Microradiography and imaging were performed using a Visitron spinning disc microscope (60x1.2 Water objective, Yokogawa) equipped with an environmentally controlled (37°C, 5% CO_2) microscope stage to fit the 35 mm dish and allow time course analysis. The discs were fixed on this stage and irradiated with an ablation UVA laser (355 nm, pulsed) along a dedicated line within the nucleus. An image was taken before and during damage and then every 15 s for 15-60 min. Images were processed using FIJI.

2.10 Methods for protein analysis

2.10.1 Determination of protein concentration

Like the concentration of DNA (compare section 2.6.1), the concentration of purified proteins can be calculated based on a spectrophotometric measurement because aromatic residues such as phenylalanines, tyrosines, tryptophanes, and histidines absorb light at 280 nm.[465] The extinction coefficient of proteins thus depends on the abundance of these residues and was calculated using the ExPASy ProtParam online tool (https://web.expasy.org/protparam/) or the built-in function in Snapgene (GSL Biotech LLC). OD_{280} was measured with the NanoDrop2000 (Thermo Scientific or DeNovix DS-11, Biozym) and the concentration was calculated according to the Beer-Lambert law (Formular 1.1) using the Nanodrop software.

2.10.2 SDS gel electrophoresis

To analyze the abundance and purity of a protein, proteins were separated according to their electrophoretic mobility by SDS-polyacrylamide gel electrophoresis (SDS-PAGE). Samples were prepared in 1x lithium dodecyl sulfate (LDS) buffer with 100 mM DTT and heated to 95°C for 5-10 min for denaturation, before loading onto the gel along with the pre-stained PagePuler (Theromo Scientific) as a marker for size estimation.

In this work, either 4-15% Criterion TGX Stain-Free Protein gels (Bio-Rad) with 1x SDS buffer or NuPAGE 4-12% BT gels (Invitrogen) with 1x MOPS or 1x MES buffer were used. These were clamped into the appropriate chamber and filled with running buffer to the required mark. Electrophoresis was started by applying a constant voltage of 200 V or 160 V for 30-65 min respectively until the running front reached the end of the gel. The gel was stained by incubation in InstantBlue Ultrafast Protein Stain on a tilt shaker. For destaining, the gel was washed several times with deionized water.

2.10.3 Western blot

The principle of Western blotting is the combination of protein separation by electrophoresis and protein analysis by immunoassay. After separation by electrophoresis (see section 2.10.2), the proteins were transferred to a nitrocellulose (NC) membrane. Two methods were used for blotting, as described in the following subchapters. After completion of the blotting process, the membrane was blocked by incubation in 5% milk in PBS-T on a shaker for at least 30 min at room temperature to prevent unspecific binding of the subsequently added primary antibody. This primary antibody, specific for the protein of interest or its tag, was added at a dilution of 1:1000-1:5000 (Table 2.2) in blocking solution and the membrane was incubated either 1-2 h at room temperature or overnight at 4°C with constant shaking.

Unbound antibody was removed by two PBS-T washes for 10 min each, and a secondary antibody (Table 2.3) raised against the species of the first antibody was added for 1 h at RT with constant shaking. The membrane was washed twice with PBS-T for 10 min and then once with PBS. The secondary antibody used for detection was either conjugated to horseradish peroxidase (HRP) or fluorescently labeled. In the case of fluorescently labeled antibodies, the blot was scanned directly on an Odyssey Licor scanner, whereas blots with secondary antibodies conjugated to HRP had to be developed using Amersham's ECL Select Western blotting detection reagent according to the manufacturer's protocol. Proteins were then detected using the Fusion FX 7 (Vilber Lourmat).

2.10.3.1 Western blotting by wet transfer

This first Western blotting method was used specifically for sensitive proteins and detection methods. The membrane and Whatman filter papers, tailored to the size of the gel, were equilibrated for at least 5 min in tank blot (TB) buffer. The sandwich was assembled between a gel holder cassette in the following order: gel holder cassette (white side), sponge, Whatman paper, membrane, gel, another Whatman paper, and another sponge before closing the cassette with its black side. The cassette was placed vertically in the tank blot chamber (Bio-Rad) and the chamber was filled with TB buffer to the mark and cooled with a cooling unit. A voltage of 100 V was applied for 100 min at 4°C.

2.10.3.2 Western blotting by Trans-Blot Turbo system

Using Bio-Rad's Trans-Blot® Turbo™ System according to the manufacturer's protocol, blotting time was reduced to 12 minutes at 25 V. This dramatic reduction in blotting time made it the preferred method for most blots in this work. For this method, all membranes and filters were incubated in the pre-cooled turboblot buffer. The blot was then constructed similarly to the wet blot: filter-membrane-gel-filter. In contrast to the wet blot, the resulting sandwich was not mounted between a gel holder cassette, but directly horizontally in the device chamber. This chamber was inserted into the Trans-Blot Turbo system and a voltage of 25 V was applied for 5-12 min, depending on the size of the protein of interest (smaller proteins require shorter transfer times).

2.11 Protein purification

2.11.1 Purification of DARPins

His-tagged DARPin constructs were expressed in BL21 DE3 cells with 1 mM IPTG for 4 h at 37°C. After harvesting, cell pellets were resuspended in IMAC (Immobilized Metal Affinity Chromatography) A buffer (5 mL/g wet pellet). 1x protease inhibitor and 0.1% Triton-X100 were added, and the cells were lysed by sonication (Branson sonifier, 5 mm tip, 2 min, 3-4, 50%). The lysate was cleared by centrifugation (Sorvall RC 6+, 18,400 rpm, 25 min, 4°C) and equilibrated NiNTA-agarose was added (1 mL/L expression). The suspension was incubated for 60-90 minutes at 4°C. The beads were washed three times with five column volumes (CV) of IMAC A buffer and eluted five times with one CV of IMAB B buffer containing 500 mM imidazole. The elutions were pooled and analyzed by SDS-PAGE together with the samples taken during purification. For using the DARPins in pull-down assays, purity of most samples was sufficient. For more sensitive assays, the DARPins were further purified by gel filtration (S75 Increase 10/300 GL, 0.5 mL/min) in storage buffer. The protein-containing fractions were pooled, concentrated, aliquoted and stored at -80°C.

2.11.1.1 Purification of biotinylated DARPins

Biotinylated DARPins were required for SPR measurements. Biotinylation was achieved either by co-expression of Avi-tagged DARPins and BirA in competent Rosetta pLysS cells containing the BirA plasmid or by subsequent biotinylation of the purified Avi-tagged DARPin using purified BirA. For co-expression, 50 µM biotin was added at the same time as expression was induced with 0.1 mM IPTG. The proteins were expressed at 30°C for 6 h. The cells were then harvested and DARPins were purified as described above (section 2.11.1).

For biotinylation of purified Avi-tagged DARPins, the DARPins were expressed and purified as described above and then biotinylated *in vitro*. Therefore, 40 µM of the DARPins were incubated overnight at 4°C with 10 mM ATP, 10 mM MgOAc, 50 µM biotin and 2.5 µg BirA in 250 µL Bicine buffer pH 8.0.

To verify the degree of biotinylation, 0.2-0.5 µg of DARPin in 1x LDS were heated to 95°C for 10 min. The sample was cooled to room temperature and 1 µL streptavidin (1 mg/mL in PBS) was added. The mixture was incubated for 30 min at RT and then analyzed by SDS-PAGE in comparison to a sample without streptavidin. The level of biotinylation was quantified by comparing the intensity bands of this control to the streptavidin-containing sample using Image-J software.

2.11.2 Purification of ubiquitin variants

To enable ubiquitin dimer and chain formation *in vitro*, wild-type as well as several ubiquitin variants (Myc-tag, AviHis-tagged, HisCFP/HisYFP-tagged, Ub-74) and mutants (K48R, K63R) were purified using a similar protocol.

Ubiquitin constructs were expressed in Rosetta™ 2(DE3)pLysS cells with 1 mM IPTG. Cells were resuspended in Ubi A buffer, lysed by sonication (Brandson sonifier, 5 mm tip, 2x1-2 min, 3-4, 40-50%). The lysate was cleared by centrifugation (Sorvall RC 6+, 18,400 rpm, 25 min, 4°C) and in a first purification step the heat-stable proteins were purified by heating the sample to 68°C for 30 min. The solution was then cooled on ice for 30 min and cleared by centrifugation.

AviHis and HisCFP/HisYFP-tagged ubiquitin were subsequently purified by IMAC as described for the DARPins (section 2.10.2) and eluted with IMAC B containing 300 mM imidazole.

The wild-type and Myc-tagged ubiquitin mutants were purified by size exclusion chromatography (Superdex 75 Increase, 0.5 mL/min or Superdex 75 pg, 1 mL/min) in GF-buffer.

The ubiquitin mutants K48R and K63R as well as Ub-74 were purified in a two-step procedure by cation exchange chromatography using the HiTrap SP 5 mL column with Ubi A and B buffer (5 mL/min) and then by size exclusion chromatography using the Superdex75 pg column (0.75 mL/min) in GF-buffer.

Proteins were aliquoted, snap frozen and stored at -80°C for further use.

2.11.2.1 Purification of ubiquitin dimers

Ubiquitin dimers were linked enzymatically (section 2.12.1.1) and purified by heat denaturation. No further purification was required for pull-down approaches. For crystallography and SPR measurements, dimer formation was stopped with 1 mM EDTA and 5 mM DTT. The pH of the reaction was adjusted to 4.5 with 2 M acetic acid, the sample was cleared by centrifugation and diluted in 50 mL Ubi-A buffer. The dimer was then purified using cation exchange chromatography with Ubi A and Ubi B buffer (MonoS, 0.75 mL/min or ResourceS 2 mL/min). The dimer fractions were pooled, rebuffered in GF-buffer and snap frozen at -80°C.

2.11.3 Purification of ubiquitin writers and erasers

For ubiquitin dimer and chain formation or deconjugation linkage-specific E2, E3s and DUBs were purified. All constructs were expressed in BL21-Codonplus DE3RIL-(Codon +) cells using 0.5 mM IPTG for 5-16 h at 18°C.

2.11.3.1 Purification of Ubc7

Cell pellets after MBP-TEV-Ubc7-His6 expression were resuspended in IMAC A (35 mL/L expression) and lysed using the Cell Disruptor TS2 (2 throughputs, 26.5 kPsi). 0.1% Triton X-100, 1x protease inhibitor cocktail, 2 mM $MgCl_2$ and 1:2500 Sm Nuclease were added and incubated for 30 min at 4°C. The lysate was cleared by centrifugation (Sorvall RC 6+, 18,400 rpm, 25 min, 4°C) and IMAC was performed using 1 mL of equitized NiNTA beads per 1 L culture. Protein was eluted five times with 1 CV and rebuffered to TEV cleavage buffer. The concentration was adjusted to 1 mg/mL and the MBP-tag was cleaved by GST-labeled TEV (CFPP, IMB) in a 1:10 ratio by incubation overnight at 4°C. A second IMAC was performed analogously to the first and the purity was checked by SDS-PAGE. If purification was insufficient, ion exchange chromatography was performed using HiTrap Q 5 mL with IEX A and B buffer.

2.11.3.2 Purification of Cue1

Cells expressing GST-Cue1were harvested and resuspended in 25 mL/L GST lysis buffer. They were lysed using the Cell Disruptor TS2 followed by incubation with TritonX-100 and Sm nuclease analogously to the Ubc7 construct (see 2.11.3.1). 1 mL of equilibrated GSH-beads were added to the supernatant and incubated for 2.5 h at 4°C. After three wash steps with 5 mL GST-lysis buffer, the GST-labeled protein was eluted with 3 x 3 CV GST-lysis buffer containing 50 mM glutathione. The elutions were concentrated to 500 µL and purified by gel filtration (S200 Increase, .5 mL/min) in GF-buffer.

2.11.3.3 Purification of Ubc13 and Mms2

His-TEV-Ubc13 and His-TEV-Mms2 were purified analogously to Ubc7 (section 2.11.3.1) with the difference that His-tagged TEV (PPCF, IMB) was used and that at the second IMAC not the elution but the flow-through contained the desired protein. It was collected and subjected to gel filtration (S75 Increase, 0.5 mL/min) in GF-buffer.

2.11.3.4 Purification of PIP-E3(63)

PIP-E3(63) is an enzyme, developed in our laboratory by Wegmann *et al.*, that can specifically ubiquitylate Ub-PCNA with K63-linked ubiquitin chains.[466] This construct was used to test the selectivity of Exo1 towards K63-ubiquitylated PCNA *in vitro*. For easier, animal-friendly purification, the construct was recloned with a PreScisson cleavage site and purified as follows. GST-3C-PIP-E3(63) was lysed and coupled to GSH beads according to the protocol used for GST-Cue1 (see 2.11.3.2). Prior to elution, the beads were washed first with GST-lysis buffer supplemented with 0.05% Triton X-100, and then twice with a high-salt containing 1 M NaCl GST-lysis buffer, and then again with the regular GST-lysis buffer. The protein was eluted with the GST-lysis buffer supplemented with 50 mM glutathione, diluted to 15 mg/mL, and the GST tag was cleaved by adding PreScission in a 1:100 ratio overnight. A reverse GST affinity purification with 500 µL beads removed the GST-tag and gel filtration (S75 Increase, 0.5 mL/min) in GF-buffer yielded the untagged protein.

2.11.3.5 Purification of OTUB1

GST-OTUB1 was purified as previously described by Mevissen *et al.*[467] Briefly, 1.5 mL of GSH-Sepharose (GE Healthcare) was equilibrated and added to the cell lysate. The suspension was incubated at 4°C for 3 hours. The flow-through was separated by centrifugation (1,000 x g, 3 min, 4°C). The beads were washed 3 times with 10 mL high salt buffer (500 mM NaCl) and 2 times with low-salt (200 mM NaCl) GST buffer A before 100 µL GST-tagged PreScission was added to the beads in 10 mL of low-salt buffer. This mixture was incubated overnight at 4°C to cleave the GST tag on the resin and release the protein. The protein was diluted in GST buffer A and subjected to anion-exchange chromatography (HiTrap Q 1 mL, NaCl gradient 50-500 mM).

2.11.4 Purification of Ub-PCNA

For the ubiquitylation reaction on PCNA, a clean ubiquitin moiety as a fusion to PCNA without any tag was required. Since this alone was difficult to purify, the construct His-Smt3-Ub-PCNA was expressed in Codon+ cells with 0.2 mM IPTG overnight at 18°C. With the same conditions His-Ulp1 was expressed, the protease that allows the cleavage of the SMT3-tag without any remnant. Cells were resuspended in IMAC A buffer and lysed by high-pressure cell disruption (Cell Disruptor TS2, 2 throughputs, 26.5 kPsi). Subsequently, 1x protease inhibitor, 2 mM $MgCl_2$, 0.1% Triton X100 and 1:2500 Sm nuclease were added and incubated for 30 min at 4°C before the lysate was cleared by centrifugation (Sorvall RC 6+, 18,400 rpm, 25 min, 4°C). The supernatant of both proteins was subjected to IMAC using the HisTrap 5 mL (5 mL/min, elution gradient 15-500 mM imidazole). His-Ulp1 was further purified by gel filtration (Superdex S75 Increase, 0.5 mL/min) in Ulp cleavage buffer. His-SMT3-Ub-PCNA was further purified by anion exchange (HiTrapQ 5 mL, 5 mL/min) and rebuffered to AEX buffer A pH 6.5. The two purified constructs were then combined in a ratio 1:10 PCNA to Ulp1 to cleave the His-SMT3 tag of Ub-PCNA overnight at 16°C. The remaining His-Ulp1 was aliquoted, snap-frozen and stored at -80°C. A reverse IMAC using the HisTrap 5 mL was used to separate the Ub-PCNA from the tag, the flow-through was concentrated and subjected to gel filtration (S200 pg, 1 mL/min) in storage buffer for final purification.

2.11.5 Purification of Exo1 fragments

2.11.5.1 Purification of MBP-tagged Exo1 constructs

All His-MBP tagged Exo1 constructs ranging from full length to the smallest fragment aa301-aa360 and its mutants were expressed and purified using the following protocol. Constructs were expressed in 1-4 L Codon+ *E. coli* cells with 0.5 mM IPTG overnight at 18°C. Cells were harvested and cell pellets were resuspended in 25-50 mL IMAC A buffer /L expression and lysed using the Cell Disruptor TS2 (2 throughputs, 26.5 kPsi). The lysate was then incubated with 1x protease inhibitor cocktail, 2 mM $MgCl_2$, 0.1% Triton X100 and 1:2,500 Sm nuclease for 30 min at 4°C and cleared by centrifugation (Sorvall RC 6+, 18,400 rpm, 25 min, 4°C). The total lysate was subjected to IMAC using the HisTrap 5mL (5 mL/min, elution gradient 15-500 mM imidazole) and protein-containing fractions were pooled, concentrated and rebuffered to amylose buffer A. Then, for a second purification step, amylose beads 1 mL /L expression were equilibrated in amylose buffer A and added to the protein. The mixture was incubated for 2 h at 4°C, washed three times with 2.5 CV amylose buffer A, and eluted with amylose buffer A containing 10 mM maltose. The elution was concentrated and subjected to gel filtration (S200 Increase, 0.5 mL/min) in storage buffer.

His-MBP, which was used as a negative control for the pull-down assays was purified using the same procedure.

2.11.5.2 Purification of GST-tagged Exo1 constructs

GST-tagged Exo1 constructs were purified analogously to MBP-tagged constructs (see section 2.11.5.1). The only difference was that GSH-beads were used for the second purification step instead of amylose beads. 1 mL beads were added per 1 L expression and incubated for 2.5 h at 4°C in GST lysis buffer. The beads were also washed with this buffer and proteins were eluted three times with 3 CV GST lysis buffer supplemented with 75 mM glutathione. The elutions were concentrated and subjected to gel filtration in the same manner as the MBP-tagged constructs.

2.11.5.3 Purification of Exo1 from Sf9 cells

Since longer fragments of Exo1 were difficult to purify from *E. coli*, the expression vector system was switched to baculovirus, which has been shown to be ideal for the high-yield production of complex eukaryotic proteins in insect cells (Sf9 cells)[468, 469] and was already used for the expression Exo1 constructs by other groups.[470, 471] The expression of Flag-tagged Exo1 constructs was performed in and with the help of the Protein Production Core Facility (IMB, Mainz) according to manufacturer instructions (Bac-to-Bac Baculovirus® expression system, Life Technologies).[468] In short, a stock of baculovirus-infected insect cells (BIIC) was diluted in 20-100 mL growth medium (GIBCO SF-900 II SFM, Hyclone). This suspension was added to 200-1000 L of uninfected Sf9 cells respectively at a density of approximately 0.9 x 10^6 cells/mL, and the cells were maintained at a density of 1x 10^6 cells/mL until they stopped proliferating (day of proliferation arrest = dpa). Cells were harvested 24-48 hours after dpa. As control uninfected Sf9 cells were used.

Sf9 cell pellets were lysed as previously described by Cejka and Kowalczykowski.[472] Briefly, cells were re-suspended in 3 pellet volumes of Sf9 lysis buffer supplemented with 1x protease inhibitor cocktail, 1 mM PMSF and 30 µg/mL leupeptin and incubated for 20 minutes at 4°C. Then, 2 pellet volumes of ice-cold 50% glycerol was added to the sample before 5M NaCl was added dropwise to the solution until 6.5% was reached. The solution was incubated for 30 min at 4°C with gentle agitation and then cleared by centrifugation (10,000 g, 4°C, 15 min). For purification, 50 µL Flag beads /100 mL expression culture were added and incubated for 2 h at 4°C. Proteins were washed twice with Sf9 lysis buffer A supplemented with 350 mM NaCl and three times with Exo1 PD buffer (1x PBS, 0.1% Triton X100, 1 mM DTT) and then used directly for interaction assays (section 2.13.3.1) or were eluted with 3x 3 CV Flag peptide (0.4 µg/µL).

2.12 Enzymatic assays

2.12.1 Enzymatic formation of specific ubiquitin linkages

Enzymatic formation of specifically linked ubiquitin chains is a common tool and has been reported previously.[473] To generate different ubiquitin linkages, highly selective enzymes were used. For K48-linked polyubiquitin, the specific enzyme UBE2K or the combination of Ubc7 and Cue1 was used. K63-linkages were obtained using the combination of the E2 pair Ubc13/Mms2 and Pib1 (Pib1RING+100aa, purified by Dr. Christian Renz) as E3.

2.12.1.1 Enzymatic formation of ubiquitin dimers

Ubiquitin dimers were formed by using a capping mutant that cannot be extended by a mutation of the specific lysine residue (KxR) in combination with a ubiquitin with a blocked (Ub-AviHis) or truncated C-terminus (Ub-74) that cannot be transferred to another ubiquitin. For pull-down assays, the reaction was performed in 1x Ubi buffer with 25 µM of the two ubiquitin substrates, 0.05 µM E1 (His-Uba1, PPCF, IMB) and 1-4 µM Ubc13/Mms2 or 20 µM UBE2K as E2. The reaction was started with 1 mM ATP and incubated overnight at the appropriate temperature.

To obtain a pure product for methods such as SPR or crystallography, the reaction volume (500 µL- 5 mL) was increased to allow subsequent purification (section 2.11.2.1). The reaction was performed with 250-1000 µM of each ubiquitin variant and 10 mM ATP, while the enzyme concentrations stayed the same.

2.12.1.2 Enzymatic formation of free ubiquitin chains

Free ubiquitin chain formation was performed in 1x Ubi buffer with 0.05 µM E1 (His-Uba1, PPCF, IMB), 2 µM E2 and 0.5 µM E3. 8 µM wild-type ubiquitin and 2-4 µM capping mutant (Ub K48R/K63R) were used to reduce chain length. For more equal detection and comparison in the pull-down assays, these mutants sometimes contained a Myc-tag. The reaction mixture was started by adding 30 µM ATP and incubated at 30°C / 37°C for 1-16 h, depending on the origin and activity of the enzymes used.

2.12.1.3 Enzymatic formation of ubiquitin chains on PCNA

To obtain specifically linked ubiquitin chains on PCNA, tailor-made E3s containing a PCNA interaction motif (PIP-box) and a linkage-specific E3 were used (designed in our laboratory by Wegmann *et al*.)[466] Reactions were performed in 1x Ubi buffer in 50-400 µL scale. 0.1 µM E1 (His-Uba1, PPCF, IMB), 2 µM E2 and 1 µM PIP-E3 were used with 2 µM Ub-PCNA and 5 µM wild-type ubiquitin. The reaction was started with 100 µM ATP and incubated for 40 min at 30°C.

2.12.2 Monitoring ubiquitin chain formation and deconjugation

2.12.2.1 Ubiquitylation assay

To test the effect of the DARPins on ubiquitin chain formation, a reaction was set up using the same concentrations also used for free chain formation (Section 2.12.1.2). Prior to incubation, the reaction mixture was split and 8 - 40 µM selective DARPin or TUBE were added to the reaction mixture. One sample was left without DARPin as a negative control. Samples were incubated according to the enzyme properties at 30°C or 37°C and 10 µL samples were taken at different time points to monitor the progress of chain formation.

2.12.2.2 Deubiquitylation assay

The effect of DARPins was also tested on the deconjugation of ubiquitin chains by specific DUBs. For this purpose, untagged ubiquitin chains were generated as described in section 2.12.1.2. The reaction was stopped by the addition of 20 mM EDTA. A t=0 sample was taken and 8-40 µM DARPins/TUBEs were added to the obtained chain mixture. One sample was left without DARPin as a negative control. After incubation for 30 min, 2-10 µM of the specific DUBs were added, the mixture was incubated at 37°C and samples were collected after 10 and 20 min.

2.12.2.3 FRET assay

For a more quantitative analysis of the inhibitory effect of the DARPins on chain conjugation and deconjugation, a FRET-based approach was employed. Therefore, 1 µM ubiquitin moieties labeled with CFP or YFP were used.

To monitor ubiquitin chain formation in the presence of DARPins, the reaction was performed in a black 384-well plate in 1xUbi buffer containing 0.1 µM E1 (His-Uba1, PPCF, IMB), 2 µM Ubc7 or Ubc13/Mms2 and 1 µM E3: Cue1 or Pib1 for the formation of K48- or K63-linked ubiquitin chains, respectively. 1-4 µM DARPin were added and chain formation was initiated by the addition of 30 µM ATP. The reaction was incubated at 30°C for 2-5 h in the Tecan (Spark® 20M) and the fluorescence signal for CFP (Excitation (Ex) 430 nm, Emission (Em) 485, gain 42, z-position 19800) and YFP-FRET (Ex 430 nm, Em 535 nm, gain 37, z-position 19800) was recorded every 1-5 min. The ratio of YFP/CFP signal was calculated (YFP/CFP signal), the values of the negative control without ATP were subtracted and the mean of three replicates and the standard deviation were calculated and plotted against the time using GraphPadPrism 8.3.

For the quantification of the DARPin effect on chain deconjugation, the chain formation reaction described above was performed in the absence of DARPins for 2 h (K63-linked) or 5 h (K48-linked) at 30°C. The reaction was then stopped by the addition of apyrase (25 U/µL) or 20 mM EDTA and divided into as many wells as the number of DARPins to be measured in triplicates, plus the negative control without ATP and the positive control without DAPRin. The DARPins were added in a concentration of 1-4 µM together with the linkage specific DUBs OTUB1 (15 µM) or AMSH (8 µM). The reaction was prepared on ice and started by incubation at 30°C in the Tecan (Spark® 20M). The fluorescence signals were measured over the course of 2-3 h and the measurements were processed as described above for the chain conjugation assay.

2.12.2.4 IC_{50} determination

For the most specific DARPins the concentrations which lead to 50% inhibition, called IC_{50} (inhibitory concentration) values were determined for their effect on ubiquitin chain conjugation and deconjugation. Therefore, the effect of increasing concentrations (0.015625-8 µM) of DARPin was measured and plotted analogously to the procedure described in section 2.12.2.3.

The slope of the graphs obtained in the first 60 min was calculated with Excel (Microsoft office, 2016) and translated into the residual activity of the writers and erasers by setting the slope of the sample without DARPin to 100%. The activity and the corresponding logarithmic concentrations were plotted and the IC_{50} value was determined using GraphPad Prism 8.3.

2.12.2.5 BiFC measurements

In this approach, the anti-K48 and anti-K63 DARPin each equipped with one half of the fluorophore Venus were tested as a sensor based on bimolecular fluorescence complementation (BiFC) for the formation of K48-K63-branched ubiquitin chains. Therefore, samples were prepared in which only K48, only K63, a mixture of both homogeneous ubiquitin chains, or the K48-K63-branched ubiquitin chains were synthesized. The synthesis of the K63-linked ubiquitin chains was conducted according to the procedure described in section 2.12.1.2. Two samples were prepared with 2 µM K48R K63R ubiquitin as a capping mutant, in one sample 4 µM wild-type ubiquitin, and in the other sample 4 µM of K48R ubiquitin served as the main ubiquitin source. The latter K63-linked ubiquitin chains could then be used in a reaction with parallel K48-linked ubiquitin chain synthesis without branched ubiquitin chains being formed. The aforementioned chains were utilized as a foundation for the mixed and branched chain samples. In contrast, the other samples contained reaction mixture for the formation of homogeneous K48- or K63-linked ubiquitin chains. The samples were prepared in 1x Ubi buffer and the composition of all samples is summarized in Table 2.8.

Table 2.10: Composition BiFC samples.

Sample	Composition
K48-linked ubiquitin chains	0.05 µM E1 (His-Uba1, PPCF, IMB) 2 µM Ubc7 4 µM Cue1 4 µM Ub K63R
K63-linked ubiquitin chains	0.05 µM E1 (His-Uba1, PPCF, IMB) 2 µM Ubc13/Mms2 0.5 µM Pib1 4 µM Ub K48R
K48-linked and K63-linked ubiquitin chain mixture	2 µM K63-linked ubiquitin chains consisting of K48R ubiquitin 2 µM Ubc7 4 µM Cue1 2 µM Ub K63R
K48-K63-branched ubiquitin chains	2 µM K63-linked wild-type ubiquitin chains 10 µM UBE2K 2 µM Ub K63R

The reaction was prepared in triplicates in a black 384-well plate on ice and 0.25 µM of nYFP-DARPin-Ub K48 A1 and cYFP-DARPin-Ub K63 G1 each were added to each sample. Additionally a negative control with just the two DARPins was prepared and all reactions were initiated by the addition of 15-30 µM ATP. The time-dependent changes in BiFC fluorescence were quantified using an excitation wavelength of 485 nm and an emission wavelength of 535 nm at 37 °C every 10 min for 5 h by a TECAN Spark 20M multimode microplate reader.

2.13 Analysis methods for protein interactions

2.13.1 DARPin *in vitro* pull-down assay

In order to test the specificity of the DARPins for their respective linkage, pull-downs with differently linked ubiquitin dimers, tetramers and chains were performed. Briefly, 100 µL of 3-5 µM Flag-tagged DARPins were bound by incubation for 60-90 min at 4°C with equilibrated 15 µL resin slurry (1:1) of anti-Flag M2 conjugated agarose magnetic beads in PD buffer. After three washes with 500 µL PD buffer, the DARPin-bead mixture was incubated for 90 min at 4°C with the protein of interest, in this case 100 µL of 0.2-4 µM specifically linked ubiquitin dimers, tetramers or chains. The flow through was discarded and the beads were washed 3-4 times with PD buffer to remove any remaining unspecifically bound proteins. For higher washing efficiency in the ubiquitin chain pull-downs, three washing steps with high salt PD buffer (500 mM NaCl) were included. The proteins were eluted from the beads by heating to 95°C for 5 min in 15 µL 1x LDS buffer. The total elution and 10% of the input were analyzed by Western blot against ubiquitin directly or the Myc-tag of ubiquitin dimers or chains.

2.13.2 Pull-downs from whole cell extract

To test the affinity and specificity of the DARPins in a non-exclusive system, pull-downs were performed from cell lysates of different origins. Lysates from *S. cerevisiae* (section 2.8.4) and human HeLa cells (section 2.9.5) were prepared as described in the corresponding sections. These lysates were adjusted to a protein concentration of 2 mg/mL in yeast PD buffer or MC dilution buffer, respectively, supplemented with 1× protease inhibitor cocktail, 1 mM NEM, and 1 mM OPA. 1 mL of this lysate was incubated with 0.25-1 µM DARPins for 90-120 min at 4°C. 15 µL of equilibrated and blocked (30 min, 1 mg/mL BSA, 4°C) Flag-agarose beads were added per sample and incubated for a further 60-90 min at 4°C. The beads were washed three times with the appropriate PD buffer and the DARPins were eluted together with their interaction partners either by boiling in 1x LDS or by incubation with 15-30 µL of Flag-peptides (0.4 mg/mL) for 15 min.

2.13.3 Pull-down assays with Exo1 constructs

100 µL of MBP- or GST-tagged Exo1 constructs at a concentration of 2-5 µM in Exo1 PD buffer were coupled to pre-blocked (1 mg/mL BSA, 30 min, 4°C) 20 µL amylose or GSH beads, respectively, by incubation for 2 h at 4°C. The beads were washed 5 times with 500 µL Exo1 PD buffer and incubated with 100 µL of 0.2 µM PCNA or Ub-PCNA, 0.4 µM polyubiquitylated PCNA or 0.2-1 µM specifically linked ubiquitin dimers or tetramers for 90 min at 4°C. Beads were washed twice with Exo1 PD buffer, twice with PD buffer containing 0.5% Triton X-100, and twice again with Exo1 PD buffer before elution in 15 µL 1x LDS by heating to 95°C for 5 min.

2.13.3.1 Direct pull-down assays of Exo1 constructs

2.13.3.2 from cell lysate

Longer Exo1 fragments were difficult to purify and not very stable when stored at -80°C. Therefore, pull-downs were performed with the Exo1 protein directly coupled to the corresponding beads after cell lysis. The Flag-tagged Exo1 constructs from Sf9 cells were coupled to pre-blocked (1 mg/mL BSA, 30 min, 4°C) Flag-beads (50 µL/ 100 mL culture) by incubating the suspension for 2 h at 4°C. The beads were then washed twice with Sf9 lysis buffer A supplemented with 350 mM NaCl and three times with Exo1 PD buffer. The beads were split so that ~20 µL flag beads were used per PD and incubated with the respective analyte at the same concentration as for the clean pull-downs (Section 2.13.3) for 90 min at 4°C. The beads were then washed analogously and proteins were eluted in 1x LDS by heating to 95°C for 5 min.

2.13.4 Surface Plasmon Resonance

Surface plasmon resonance (SPR) experiments were performed on a Biacore X100 system, equlitbrated at 25°C in HBS-EP buffer using a streptavidin (SA) sensor chip and biotinylated DARPins as immobilized target with a density of 1000 RU. The different ubiquitin conjugates were injected for 180 s at a flow rate of 30 µL/min in increasing concentration (factor 2x), with the highest concentration ranging from 1.5 µM to 50 µM.

The Biacore X100 Control Software version 2.0.2 was used for data acquisition and the Biacore X100 Evaluation version 2.0.2 for data analysis. Affinity and kinetic data (K_D, k_{on} and k_{off}) for the DARPins were obtained using the fitting tool (1:1 binding model) of the Biacore X100 evaluation software version 2.0.2 and is reported as the mean of three independent experiments with corresponding standard deviations.

2.14 Mass spectrometry

The pull-downs for the analysis by mass spectrometry were conducted as described previously for the other pull-downs from cell lysate (section 2.13.2). The following steps were performed in the Proteomics CF, IMB, Mainz.

2.14.1 Enzymatic protein digestion of DARPin and TUBE pull-downs

Eluted pull-down samples were processed using the SP3 clean-up approach.[474] The proteins were then digested using trypsin overnight at 37°C. The resultant peptide solution was purified by solid phase extraction in C_{18} StageTips.[475]

2.14.2 GlyGly-modified peptide enrichment from HeLa cells

The following procedures were performed as described previously in Wegann *et al*.[466] Proteins (1 mg) from HeLa whole cell lysate were precipitated in acetone at -20°C overnight. The protein pellet was resolubilized in 8 M urea/2 M thiourea containing 10 mM HEPES pH 8. Following reduction by 1 mM DTT and alkylation by 5.5 mM chloroacetamide in the dark, the urea concentration was diluted to 2 M using 50 mM Tris pH 8. Proteins were then digested by trypsin (protein:enzyme ratio of 100:1) at room temperature overnight. Following desalting in C_{18} Sep-Pak columns (Waters), peptides were eluted in 50% acetonitrile. Afterwards, the acetonitrile was evaporated in a centrifugal evaporator. The resultant peptide solution was then adjusted with IAP buffer to reach 50 mM MOPS–NaOH (pH 7.2), 10 mM Na_2HPO_4, 50 mM NaCl (1x IAP buffer). Thereafter, the peptides were incubated with the PTMScan Ubiquitin Branch Motif (K-ε-GG) Immunoaffinity Beads (Cell Singaling) at 4°C overnight. Following sequential washes in 1x IAP buffer and water, peptides were eluted in 0.15% TFA and desalted in C_{18} StageTips.

2.14.3 Liquid chromatography tandem mass spectrometry

Peptides were analyzed using an Orbitrap Exploris 480 mass spectrometer (Thermo Fisher Scientific) coupled to EASY-nLC 1200 UHPLC system (Thermo Fisher Scientific). Peptides were separated in an in-house packed 60-cm analytical column (inner diameter: 75 µm; ReproSil-Pur 120 C_{18}-AQ 1.9-µm silica particles, Dr. Maisch GmbH) by online reversed-phase chromatography through a 90-min gradient of 2.4-32% acetonitrile with 0.1% formic acid at a nanoflow rate of 250 nl/min. The eluted peptides were sprayed directly by electrospray ionization into the mass spectrometer. Mass spectrometry measurement was conducted in data-dependent acquisition mode using a top15 method with one full scan (resolution: 60,000, scan range: 300-1650 m/z, target value: 3×10^6, maximum injection time: 40 ms) followed by 15 fragmentation scans via higher energy collision dissociation (HCD; normalised collision energy 30%; resolution: 15,000, target value: 1×10^5, maximum injection time: 40 ms, isolation window: 1.4 m/z). Only precursor ions of +2 to +6 charge state were selected for fragmentation scans. Additionally, precursor ions already isolated for fragmentation were dynamically excluded for 25 s.

2.14.4Mass spectrometry data processing

Mass spectrometry raw data files were processed using MaxQuant software (version 2.1.3.0).[476] MS/MS mass spectra were searched using Andromeda search engine[477] against a target-decoy database containing the forward and reverse protein sequences of UniProt *H. sapiens* reference proteome (101,761 entries; release 2022_03), together with the sequences of the corresponding DARPin and TUBE proteins, the triple FLAG peptide and a default list of common contaminants. Trypsin/P specificity was assigned.

Methionine oxidation, protein N-terminal acetylation, carbamidomethylation of cysteine, N-ethylmaleimide (NEM) derivatized cysteine and GlyGly remnant at lysine residue were chosen as variable modifications. A maximum of 2 missed cleavages were tolerated. The minimum peptide length was set to be 7 amino acids. False discovery rate (FDR) was set to 1% at both peptide and protein levels. The intensities of peptide evidences associated with each detected GlyGly (K) site were summed. These summed intensities of GlyGly (K) sites were then used for linkage type analysis.

2.15 Crytallography

The crystallography was performed by Lee Armstrong and Anna Perez in the group of Yogesh Kulathu (University of Dundee, UK).

Purified DARPins were incubated with an equimolar concentration of ubiquitin dimer for one hour on ice. The reaction was then loaded onto a HiLoad Superdex 75 16/600 column (Cytiva) and eluted in SEC buffer (20 mM Tris pH 7.5, 150 mM NaCl). Peak fractions were analysed by SDS-PAGE and concentrated using an Amicon ultra centrifugal filter to a final concentration of 12.2 mg/mL. Crystals grew at 20˚C in sitting drops containing a 1:1 ratio of protein (200-500 µL) to mother liquor (200-500 µL) which contained 0.1 M sodium acetate pH 4.6, 2.4 M sodium malonate. Crystals were frozen in cryoprotectant consisting of mother liquor supplemented with 20% glycerol.

All diffraction data were collected on the ID23-2 and ID30-B beamline, respectively, at the European Synchrotron Radiation Facility (ESRF, Grenoble, France). Structures were solved by molecular replacement (Phaser) using the structure of ubiquitin (PDB: 1UBQ) and an AlphaFold models of the DARPin as the search models.

3 Results and Discussion I

Specific binders for recognition, inhibition and tracking of K48- and K63-polyubiquitin chain signaling

3.1 Background and aim of this project

Ubiquitin is a post-translational modifier involved in almost all cellular processes in eukaryotes. The versatility of ubiquitin as a signaling molecule is mainly derived from its ability to form ubiquitin chains linked via different residues leading to different topologies (see section 1.1.3). Depending on the linkage, polyubiquitin chains can trigger a multitude of biological outcomes, suggesting that the topology of ubiquitin chains acts as a signaling code- the so-called ubiquitin code.[9] While there is an increasing understanding of which type of ubiquitin modifications are present in cells, the function-topology relationship of specifically linked ubiquitin chains is still poorly understood. As Swatek and Komander have stated: the words of this code, being distinctly modified ubiquitin moieties, are known, now the grammar (length, mixtures, branches etc.) needs to be studied.[21] This grammar and the encoded meaning are still largely unknown, in part due to the lack of independent tools that can clearly distinguish linkage-specific ubiquitylation, especially *in vivo*.

To address this issue, this project aims to develop independent affinity probes for the recognition, inhibition, or tracking of linkage-specific polyubiquitin signals for the two most studied linkages, K48 and K63, *in vitro* and *in vivo*. Furthermore, this thesis aims to develop a K48-K63-branched ubiquitin chain sensor by combining the K48- and K63-selective probe.

As a tool for this, a new class of synthetic scaffold proteins was chosen: designed ankyrin repeat proteins (DARPins), which have emerged as powerful tools in recent years. DARPins provide a stable, highly modifiable scaffold, exhibit high-affinity and high specificity towards their target and, unlike conventional antibodies, can be used *in vivo* due to their small size and simple structure. Therefore, they have proven to be a useful scaffold for specific targeting and as biosensors.[241, 273, 478] Our collaboration partners from the Plückthun group in Zürich raised DARPins against K48- and K63-linked ubiquitin dimers from a library with randomized target interaction residues. By three rounds of ribosome display, a total of 52 DARPins (29 for the K48-linkage and 23 for the K63-linkage) were identified, representing the starting point of my Master thesis, which I conducted from October 2018 to April 2019 in the group of Prof Helle Ulrich, at the Institute of Molecular Biology (IMB) in Mainz.[479]

During this period, the candidates received from Zürich were primarily screened for their selectivity towards their respective ubiquitin linkage *in vitro* using interaction assays with differently linked ubiquitin dimers and chains. Three anti-K48 DARPins (K48 A1, K48 G2, K48 E4) were identified and their selectivity was demonstrated to be superior to that of the commercially available anti-K48 TUBE (LifeSensors). For the anti-K63 DARPins, three candidates (K63 A1, K63 D2, K63 G3) were selected for further investigation based on their preferential binding to K63-linked ubiquitin chains.

These anti-K63 DARPins showed a comparable selectivity to the anti-K63 TUBE (LifeSensors) and initial inhibition assays revealed that the selected anti-K63 DARPins also exhibited similar inhibitory effects on K63-polyubiquitylation to the anti-K63 TUBE, with a lower impact on chain deconjugation. This suggests that the anti-K63 DARPins function as molecular traps and shield K63-ubiquitin chains *in vivo*. Two of the anti-K48 DARPins demonstrated a slight inhibitory effect on K48-linked ubiquitin chain formation and deconjugation comparable to the impact of the anti-K48 TUBE. At the same time, anti-K48 DARPin G2 did not affect the formation or deconjugation of K48-linked ubiquitin chains and, therefore, seemed a promising candidate for a non-inhibitory *in vivo* sensor.[479]

Since no highly selective anti-K63 DARPin was identified during my master thesis, this project started with a new set of 28 DARPins, which were selected in a second round of ribosome displays against K63-linked ubiquitin dimers, again performed by Jonas Schäfer, Plückthun laboratory, University of Zürich.

Following the identification of the most promising candidates for both linkages based on their *in vivo* selectivity, all the DARPins were subjected to further characterization with respect to their selectivity and specificity *in vitro* and *in vivo*, as well as their inhibitory effect on ubiquitylation and cell growth. Based on these results, the most suitable candidates for a biosensor per linkage were chosen and further tested for their binding properties. The binding sites of these DARPins were revealed by crystallography, in collaboration with the Yogesh Kulathu group (University of Dundee, UK).

Using (live-cell) microscopy the usage of the DARPins as biosensors in yeast and mammalian cells was analyzed. Co-localization experiments with biological markers revealed the involvement of K48- or K63-linked polyubiquitin chains in different cellular processes and responses (e.g. stress granules, aggresomes or DNA damage). Additionally, a combination of an anti-K48 and an anti-K63 DARPin with a split-YFP was tested as a sensor for K48-K63-branched ubiquitin chains *in vitro* and *in vivo*.

Overall, this broad characterization results in well-studied high-affinity tools that will be useful in a wide range of applications from pull-downs to live-cell imaging, allowing the investigation of the involvement of K48- and K63-linked ubiquitin chains, as well as their heterotypic chains, in various processes *in vitro* and *in vivo*, thus helping to further decipher the ubiquitin code.

3.2 Results

3.2.1 Selection of specific DARPins against K48- and K63-linked ubiquitin

To identify selective DARPins for K48- and K63-linked ubiquitin chains, they were raised and screened as depicted in Figure 3.1 below.

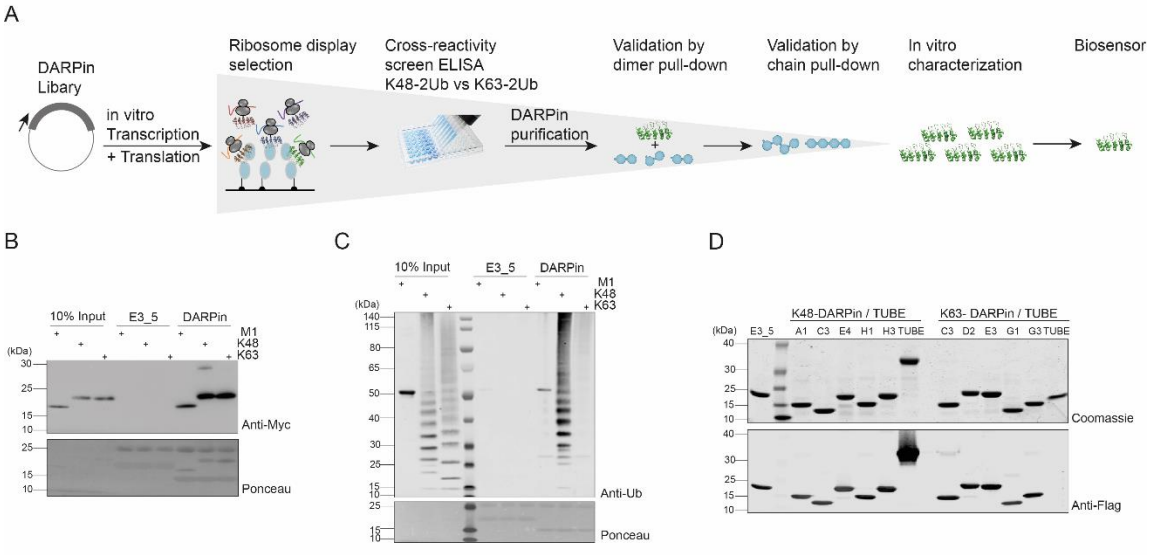

Figure 3.1: Selection process yielded five specific DARPins per linkage. (A) Schematic of the anti-K48 and anti-K63 DARPin selection and validation process. DARPins depicted in green, ubiquitin in light blue. (B, C) Exemplary pull-down to validate selectivity of the DARPins for their respective ubiquitin dimer (B) or chains (C) in comparison to the non-binding control DARPin (E3_5). Flag-pull-down with the Flag-tagged DARPins and Myc-tagged ubiquitin dimers (B) or untagged ubiquitin chains (B), specifically linked via M1, K48 and K63, was performed and analyzed by Western blotting against the Myc-tag of the ubiquitin dimers (B) or against ubiquitin directly (C). Staining with Ponceau served as loading control. (D) As quality and equal loading control all five selected anti-K48 and anti-K63 DARPins with their respective TUBE and the non-binding control DARPin (E3_5) were analyzed with a Coomassie-stained gel and an anti-Flag Western blot.

The first two steps of the ribosome display and ELISA screen for cross-reactivity were conducted by our collaboration partners from the Plückthun laboratory, University of Zürich. After receiving the pre-selected DARPins for the K48- and K63-linkage, the DARPins were expressed and purified by IMAC before being tested on their specificity by pull-down assay with M1, K48- or K63-linked Myc-tagged ubiquitin dimers as exemplified in Figure 3.1B.

Only DARPins that demonstrated high affinity for the ubiquitin dimer containing the linkage against which they were raised were subjected to further validation through a pull-down assay with K48- or K63-linked polyubiquitin chains, as well as a linear hexaubiquitin (Figure 3.1C). The five most selective candidates for each linkage (Figure 3.1D) from this assay were then further characterized and compared with the corresponding commercial TUBE. Based on their selectivity and inhibitory properties, one candidate for each linkage was chosen for further characterization and usage as a biosensor *in vivo* (Figure 3.1A).

When comparing the DARPins and TUBEs on the Coomassie and anti-Flag Western blot, it is evident that although all DARPins and TUBEs were loaded at the same concentration (see Coomassie Figure 3.1D), the anti-K63 TUBE is not visible on the Western blot. This may be due to its small size of 9 kDa[229] making it smaller than all DARPins (12-20 kDa). Although it runs a bit higher due to its linear design, it has been shown that small molecules are poorly transferred due to too-rapid transfer and lack of retention by the transfer membrane.[480] However, since higher molecular weight proteins such as specifically linked ubiquitin chains were often the main focus of interest, the blotting could not always be optimized for the low molecular weight TUBE. Therefore, even when the same concentrations were used, it shows less in some loading controls.

The following two subchapters describe the screening and selection process to identify the five most selective DARPin candidates per linkage.

3.2.1.1 Identification of three new promising anti-K63 DARPin candidates

The primary screen, performed during the time of my master thesis[479] did not lead to the identification of an anti-K63 DARPin that maintained its specificity when exposed to longer M1- or K48-linked ubiquitin chains. As a result, a new set of 28 DARPins was raised in Zürich against a K63-linked ubiquitin dimer. All 28 anti-K63 DARPins obtained from this second ribosome display were purified and tested in a first screen by pull-downs of specific ubiquitin dimers linked via M1, K48 or K63. As some general anti-ubiquitin antibodies were shown to detect certain linkages better than others, all dimers were tagged with a Myc-tag to ensure equal detection.[481] The individual DARPins are named after the well of the 96-well plate in which they were delivered. Figure 3.2 shows the result for all K63-DARPins. For clarity, only the relevant gel section is displayed, while the complete gel images and the corresponding Ponceau staining are enclosed in Appendix Figure 6.1.

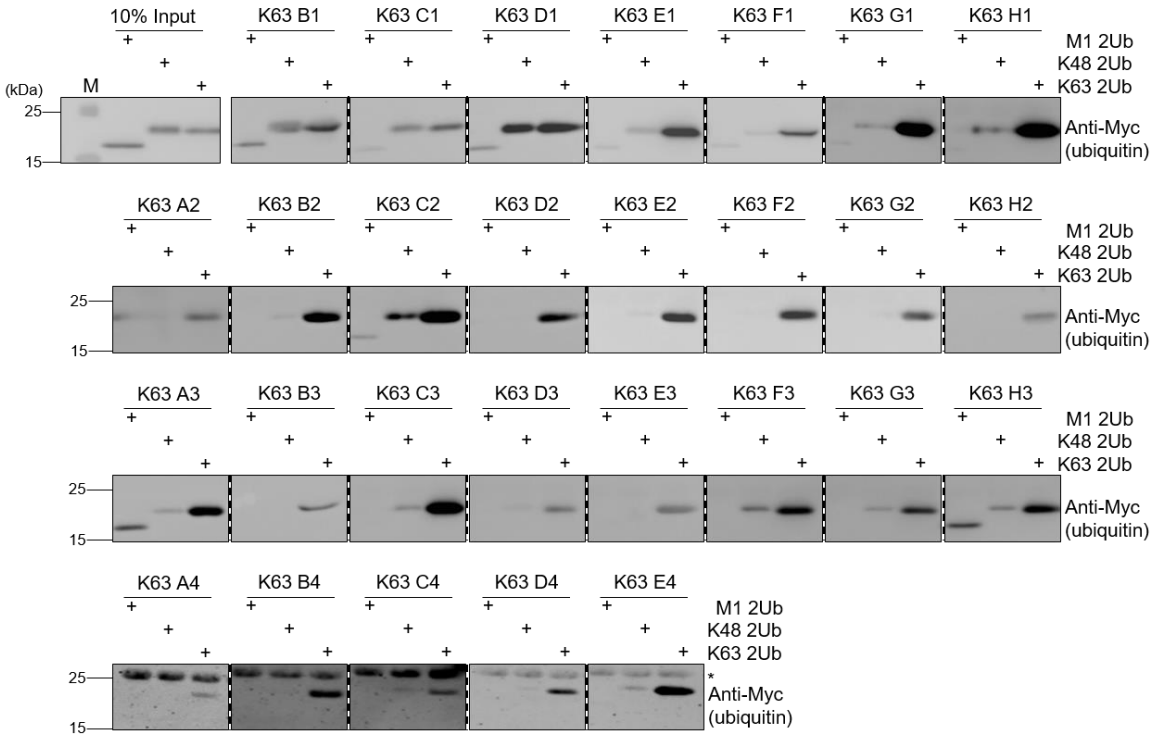

Figure 3.2: First screen of the second round resulted in 18 promising anti-K63 DARPin candidates. Pull-down results to validate selectivity of the indicated anti-K63 DARPins, in comparison to 10% of the input. Flag-pull-down with the Flag-tagged DARPins and Myc-tagged ubiquitin dimers of the indicated linkages was performed and analyzed by Western blotting against the Myc-tag of the ubiquitin dimers. * = signal of the light chain of M2 Flag-antibody from the beads used for pull-down, as last pull-downs were detected with a different Myc-antibody. Full blots and loading control are enclosed in Appendix Figure 6.1.

The result of the dimer pull-down experiment indicated that out of the 28 tested DARPins, which were newly raised against the K63-linked ubiquitin dimer, 18 DARPins (namely F1, G1, H1, A2, B2, D2, E2, F2, G2, H2, B3, C3, D3, E3, A4, B4, D4, E4) exclusively or at least with a strong preference bound K63-linked ubiquitin dimers (Figure 3.2). These 18 DARPins were thus further validated in a second pull-down using longer ubiquitin chains (Figure 3.3).

Figure 3.3 illustrates that all 18 DARPins were capable of pulling down K63-linked ubiquitin chains, albeit starting from different oligomers and with varying binding strengths. Nevertheless, all of the tested DARPins also showed a pull-down of K48-linked ubiquitin chains and/or the linear hexaubiquitin control. It was later discovered that this was partly attributable to an interaction of the K48-linked chains with the used magnetic Flag beads, particularly in the higher molecular weight range. This was abolished by the introduction of a further wash step for subsequent pull-downs. Nevertheless, based on the results of this experiment, the six DARPins that exhibited the highest specificity for shorter ubiquitin chains (namely G1, H2, B3, C3, D3, and E3) were selected for further analysis. These DARPins were then compared to the three anti-K63 DARPins that were selected during the initial screening phase of my master's thesis (D2-old, F2-old, and G3-old) (Appendix Figure 6.2, G-I). From this comparison, a choice of the following five anti-K63 DARPins was made for further characterization: C3, D2-old (hereafter referred to as D2), E3, G1, and G3-old (hereafter referred to as G3).

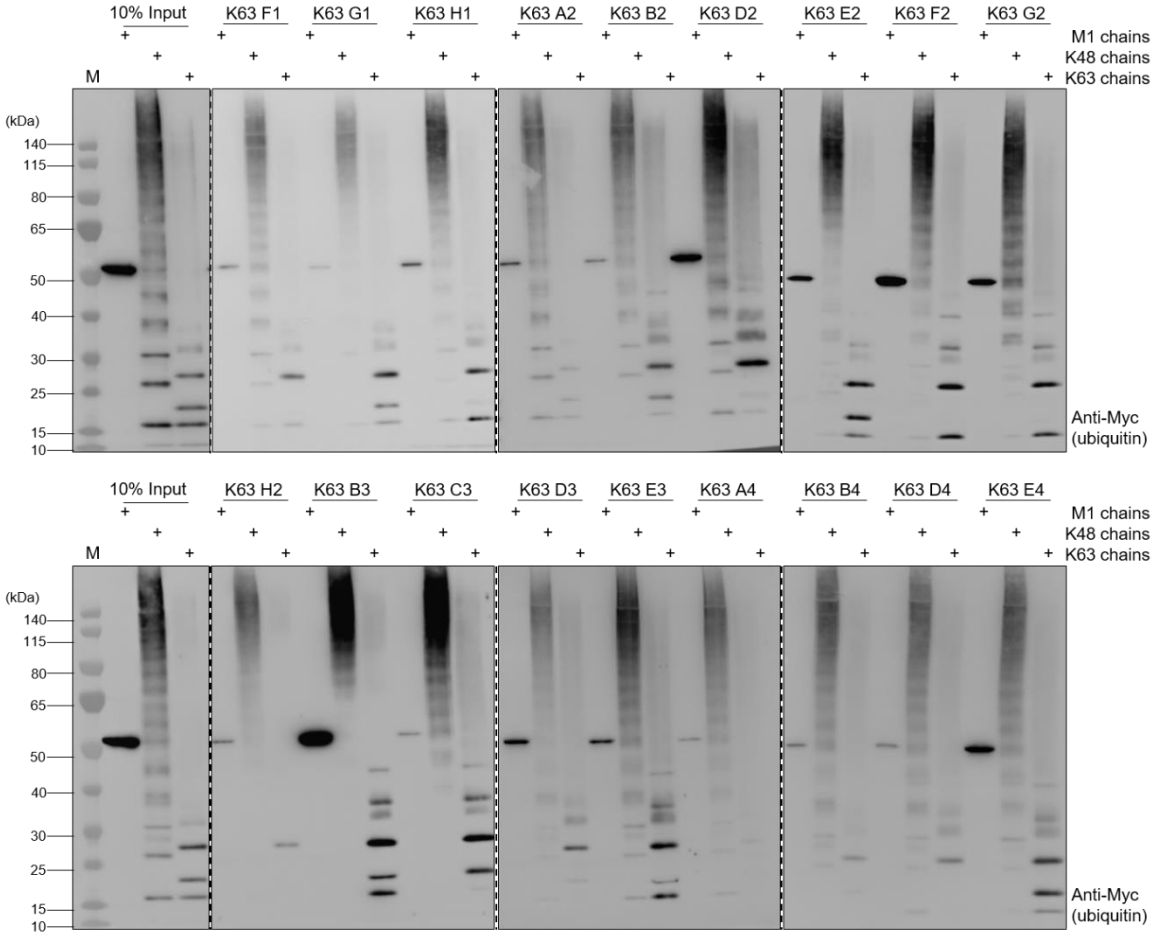

Figure 3.3: Validation of the second round of anti-K63 DARPins identified three new promising candidates. Pull-down results to validate selectivity of the indicated anti-K63 DARPins, in comparison to 10% of the input. Flag-pull-down with the Flag-tagged DARPins and Myc-tagged ubiquitin chains of the indicated linkages was performed and analyzed by Western blotting against the Myc-tag of the ubiquitin chains.

3.2.1.2 New screening completed selected anti-K48 DARPins

During my master's thesis screening,[479] three anti-K48 DARPins, namely K48 A1, K48 G2, and K48 E4, were identified to be specific for K48-linked ubiquitin dimers and chains (Appendix Figure 6.3A+B). Among them, the anti-K48 DARPin G2 seemed a promising candidate for a biosensor as it did not affect chain formation or degradation of K48-linked ubiquitin chains.[479]

However, pull-downs, performed to investigate the specificity of the anti-K48 DARPins *in cellulo*, showed no pull-down of any ubiquitin conjugate by G2, but certainly of K48 A1 and E4 (Figure 3.4A and Appendix Figure 6.4). This raised the question of whether the investigated interaction with K48-linked ubiquitin chains *in vitro* was due to precipitation of the K48-linked ubiquitin chains on the beads, which was observed in the initial pull-downs as mentioned before. For clarification, new pull-downs were conducted using ubiquitin dimers and tetramers (Figure 3.4B), as well as freshly synthesized free ubiquitin chains (Appendix Figure 6.3C) linked via K48 and K63. To rule out precipitation, the negative control DARPin (E3_5) was run alongside and the pull-down results were always compared to those of anti-K48 DARPin A1.

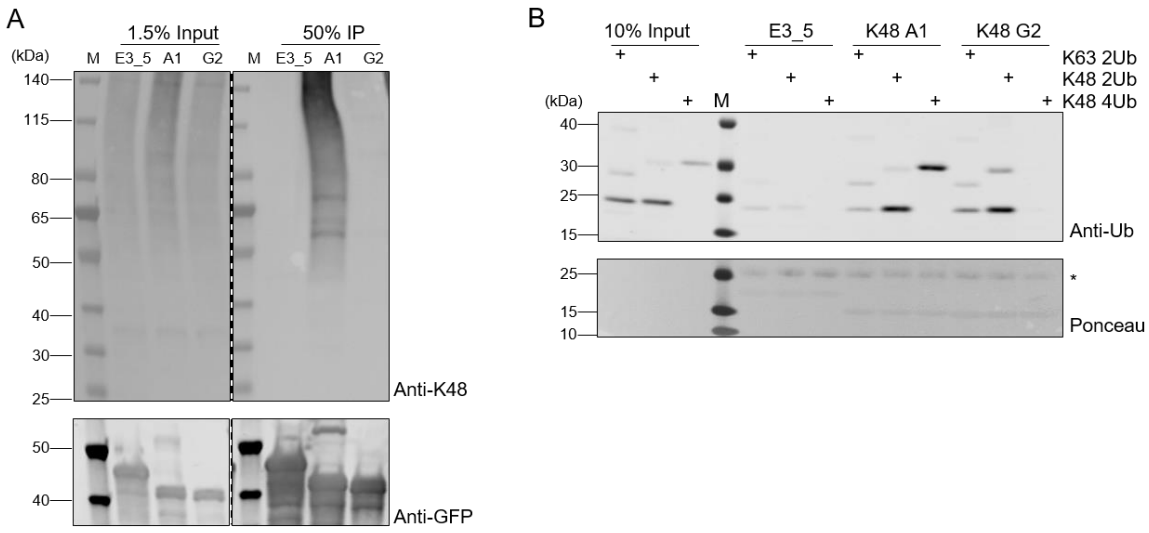

Figure 3.4: Anti-K48 DARPin G2 does not interact with K48-linked ubiquitin polymers longer than dimers. Pull-down results to test the binding of the anti-K48 DARPin G2 toward ubiquitin conjugates in cell extract (A) or dimers or tetramers (B) in comparison to the control DARPin E3_5 and the anti-K48 DARPin A1. (A) Pull-down result of the GFP-tagged DARPins expressed in HeLa cells and pulled-down using the GFP-Trap, analyzed by Western blotting with the indicated antibodies. 1.5% of the input and 50% of the pull-down were loaded on each gel. Conducted by Philipp Elleringmann.[482] (B) Flag-pull-down with the Flag-tagged DARPins and the indicated ubiquitin polymer of the indicated linkages was performed and analyzed by Western blotting against ubiquitin. 10% of the input and 100% of the pull-downs were loaded. Equal loading of the DARPins was confirmed by Ponceau staining. * = signal of light chain of M2 Flag-antibody from the beads used in the pull-down.

While A1 showed a strong pull-down of every ubiquitin polymer linked via K48, G2 only interacted with the K48-linked ubiquitin dimer but not with the tetramer (Figure 3.4B). It exhibited only a weak interaction with longer free ubiquitin chains (Appendix Figure 6.3C) and no interaction with K48-linked ubiquitin conjugates on a substrate (in this case GFP, Appendix Figure 6.3D). These properties may be explained by the different conformations that K48-linked ubiquitin chains can adopt. Already the K48-linked ubiquitin dimer can adopt two distinct conformations: an open, more linear one and a more closed one due to trans-ubiquitin interactions between the hydrophobic patches.[9, 483] An even tighter globular structure has been described for the ubiquitin tetramer as an ”asymmetric dimer of ubiquitin dimers”[484], which buries the hydrophobic surface in the middle of the tetramer. This structure may inhibit binding by covering the G2 binding site. If the ubiquitin chain is coupled to a substrate, it may have a similar effect and hinder the binding of G2. This could explain why free ubiquitin chains are still bound to some extent (Appendix Figure 6.3C), but this affinity is lost for tetramers or when K48-linked ubiquitin chains are conjugated to a substrate (Figure 3.4, Appendix Figure 6.3D). However, overall, these findings showed that G2 is not suitable for use as an *in vivo* sensor and is therefore excluded from further characterization.

After eliminating G2, all previously purified anti-K48 DARPins were screened again to identify the five most promising candidates for a K48-specific *in vivo* sensor. The previously selected anti-K48 DARPins A1 and E4 showed a rather strong inhibitory effect on K48-linked ubiquitin chain formation *in vitro*, thus it was screened for less inhibitory candidates. The inhibitory effect of all anti-K48 DARPins on the enzymatic assembly of K48-linked ubiquitin chains was investigated in a FRET-based assay.

Therefore, ubiquitin was fused with either YFP or CFP to enable the detection of fluorescence energy transfer between the two moieties when assembled into ubiquitin chains. The donor (CFP) emits fluorescence energy at ~450 nm, which is transferred to the acceptor (YFP) resulting in a detectable signal at ~530 nm.[485–488] The screen showed that the effects of the anti-K48 DARPins vary widely, with C3, A4 and H3 being the least inhibitory after the eliminated G2 (Figure 3.5A+B). On the other hand, H2, D1 and D2 exhibited the strongest effect on chain formation, stronger than A1. The anti-K48 DARPin E4 showed an intermediate effect. The six least inhibitory candidates were evaluated in a second FRET-assay against A1 and E4 (Appendix 6.5A+B) and tested for their selectivity for K48-linked tetrameric polyubiquitin (Appendix 6.5C). In contrast to all other candidates tested, A4 did not show any pull-down of K48-linked tetraubiquitin. Therefore, it was excluded.

The remaining DARPins were tested for their affinity towards longer ubiquitin chains linked via K48 and K63 (Figure 3.5C). Based on this comparison, the anti-K48 DARPins C3, H1 and H3 seemed to be the most specific ones and were chosen for further characterization together with A1 and E4.

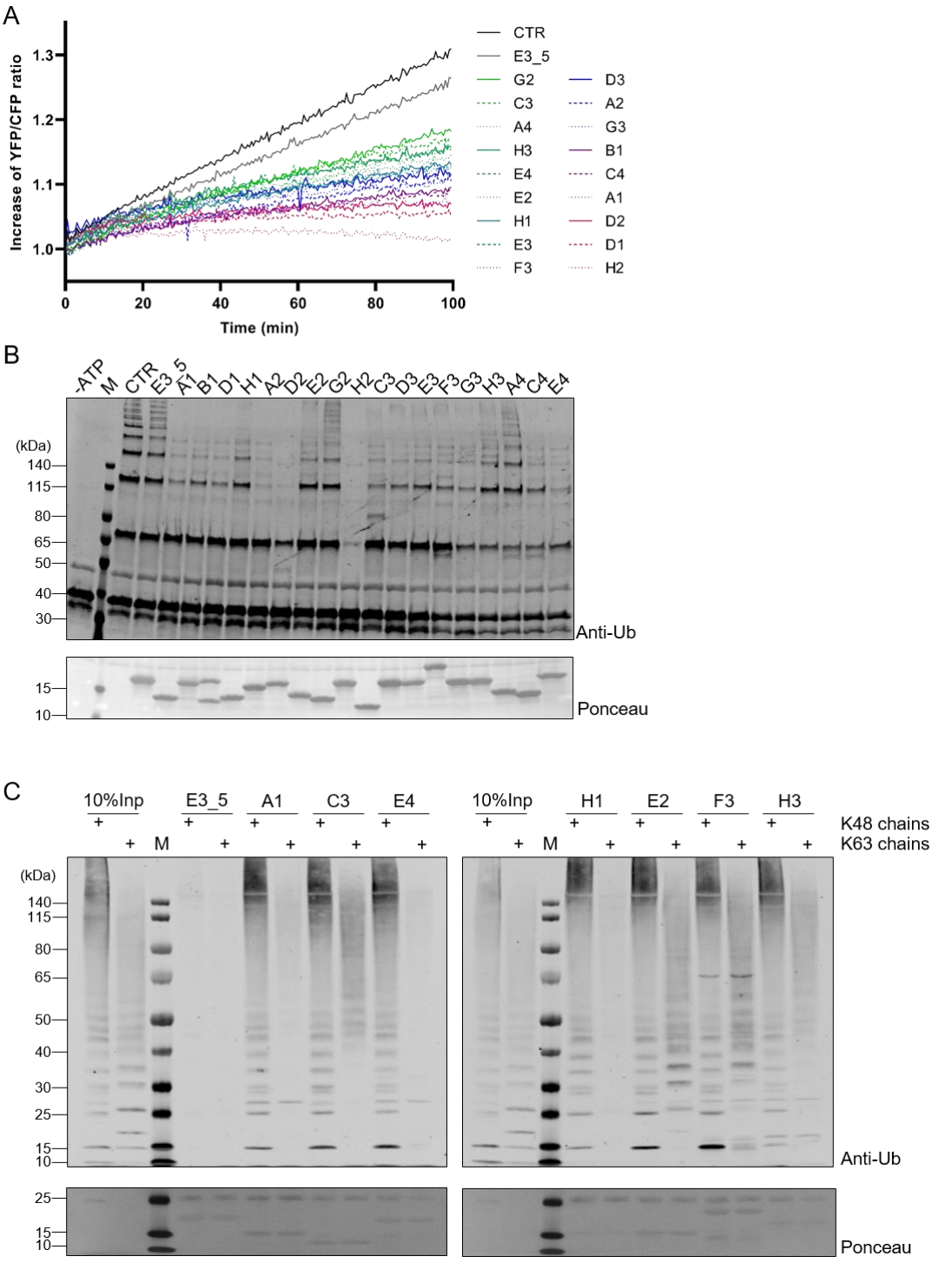

Figure 3.5: New screen identified three new, less inhibitory anti-K48 DARPin candidates. (A, B) Graph (A) and respective Western blot (B) showing the increase of the YFP/CFP-ratio over time as a read-out of the ubiquitin chain formation with YFP- and CFP-tagged ubiquitin in the presence of the indicated anti-K48 DARPin in two-fold excess. Western blots show the endpoint of this ubiquitin conjugation assay (C) Flag-pull-down results to test the affinity of the indicated anti-K48 DARPin (Flag-tagged) toward specifically linked *in vitro* synthesized free ubiquitin chains in comparison to the control DARPin E3_5. The pull-down was analyzed by Western blotting against ubiquitin. 10% of the input and 100% of the pull-down were loaded. Equal loading of the DARPins was confirmed by Ponceau staining.

3.2.2 *In vitro* characterization of DARPins

The initial screenings identified five DARPins per linkage that exhibited high affinity and specificity towards K48- or K63-linked ubiquitin dimers and chains, respectively. These five candidates were subsequently further characterized and compared to the commercialized TUBE in regard to their specificity *in vitro* and *in vivo*. Additionally, their effect on chain conjugation and deconjugation was examined to estimate their inhibitory effects. Based on these experiments, the most suitable candidate for both linkages was identified as a suitable biosensor.

3.2.2.1 DARPins are more specific *in vitro* than the respective TUBE

The selectivity of the five anti-K48 DARPins, as well as the five best anti-K63 DARPins, for specifically linked ubiquitin dimers and chains was directly compared to that of the negative control DARPin E3_5 and the respective linkage-specific TUBE.

All five of the selected anti-K48 DARPins demonstrated a strong binding and selectivity to the K48-linked ubiquitin dimer. In contrast, the commercially available anti-K48 TUBE did not bind the dimer at all (Figure 3.6A). This lack of binding was also shown for the K48-linked triubiquitin (Figure 3.6B), and is a consequence of the design of the TUBE, which consists of four naturally occurring UBDs linked at a specific distance to bind to ubiquitin only when linked via K48. However, because each single UBD has a very weak affinity for the individual ubiquitin subunits, shorter polyubiquitins than tetramers are not sufficiently bound.[227] Thus, the identified DARPins demonstrated a significant advantage over the anti-K48 TUBE and could close the gap of binding and detecting these short K48-linked polymers for analysis. Additionally, two anti-K48 DARPins (A1 and E4) were identified that strongly bind to K48-linked ubiquitin chains but only weakly to K63-linked chains. These DARPins exhibit better selectivity than the anti-K48 TUBE, which pulled down a significant amount of K63-linked ubiquitin chains (Figure 3.6B).

The five selected anti-K63 DARPins, like the anti-K63 TUBE, exhibited strong affinity and selectivity for the K63-linked ubiquitin dimer (Figure 3.6C). The DARPins all displayed a slightly stronger selectivity for the *in vitro* synthesized K63-linked ubiquitin chains than the anti-K63 TUBE, which in contrast to the anti-K63 DARPins showed an interaction especially with longer ubiquitin chains linked via K48 (Figure 3.6D).

Overall, the identified anti-K48 and anti-K63 DARPins showed good selectivity for their respective ubiquitin dimers and chains *in vitro*. For both linkages DARPins were identified that showed a stronger selectivity than the respective TUBE for specifically linked ubiquitin chains. Additionally, the anti-K48 DARPins demonstrated the advantage of binding K48-linked ubiquitin dimers and trimers, which have so far remained undetected by the anti-K48 TUBE. The properties of these selective binders will be characterized in more depth subsequently.

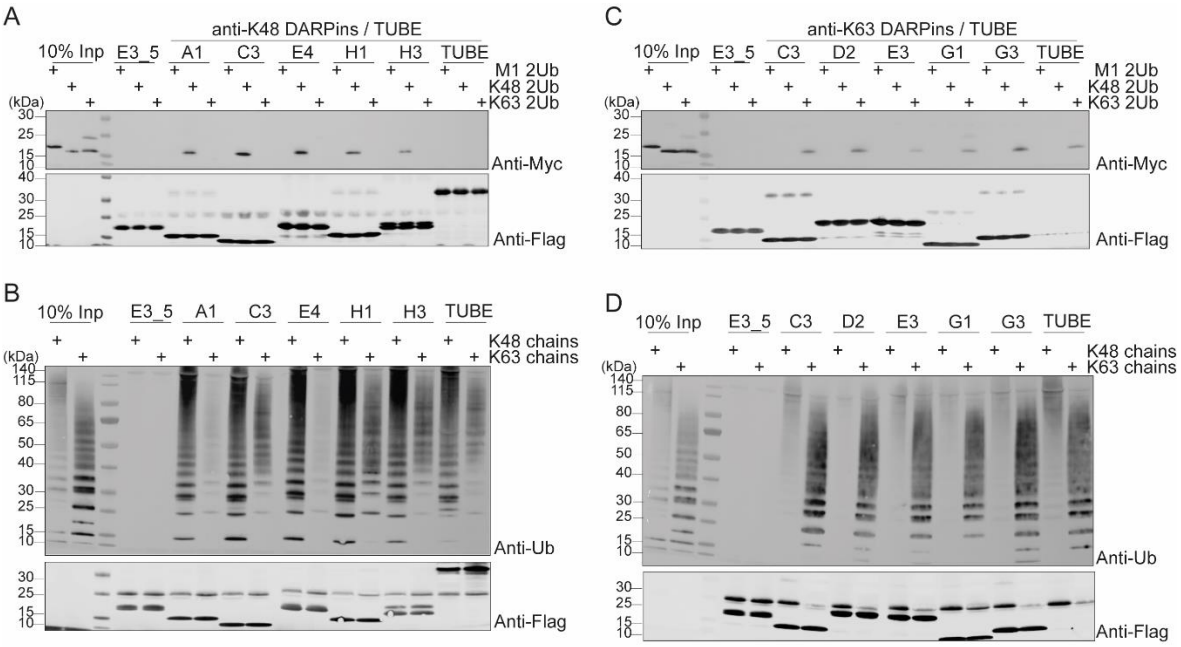

Figure 3.6: The five most promising DARPins show higher selectivity than the respective TUBE *in vitro*. The DARPins specifically bind the linkage they were selected for. (A, C). Flag-pull-down with the indicated Flag-tagged anti-K48 DARPins (A) or anti-K63 DARPins (C), the respective TUBE and specifically linked, Myc- tagged ubiquitin dimers (M1, K48 and K63) was performed and analyzed by Western blotting against the Myc-tag of the ubiquitin dimers and the Flag-tag of the DARPins. (B, D) Flag-pull-down with the indicated Flag-tagged anti-K48 DARPins (B) or anti-K63 DARPins (D), the respective TUBE and enzymatically synthesized K48- or K63-linked ubiquitin chains was performed and analyzed by Western blotting against ubiquitin and the Flag-tag of the DARPins. 10% Input (Inp) and 100% pull-down is loaded.

3.2.2.2 Linkage-selective DARPins as binding tools for ubiquitylated proteins from cell extract

The previous experiment demonstrated the specificity of the DARPins for enzymatically synthesized ubiquitin chains. The next step was to investigate whether the DARPins also exhibited selectivity in the non-exclusive system of a cell extract, thereby enabling the binding and isolation of proteins decorated with K48- or K63-linked polyubiquitin from cells. Therefore, pull-downs of whole cell extracts from mammalian (Figure 3.7) and yeast (Appendix Figure 6.8) were performed using purified DARPins. The results were analyzed using pan- and linkage-specific ubiquitin antibodies.

As shown in Figure 3.7A, all anti-K48 DARPins efficiently bound to ubiquitin chains from mammalian cell lysate. The K48-specific antibody demonstrated that the DARPin efficiently enriched for K48-linked ubiquitin chains. Furthermore, all tested DARPins exhibited a greater affinity to K48-ubiquitylated proteins compared to the anti-K48 TUBE, which only showed a strong pull-down signal in the high molecular weight range of K48-linked polyubiquitin.

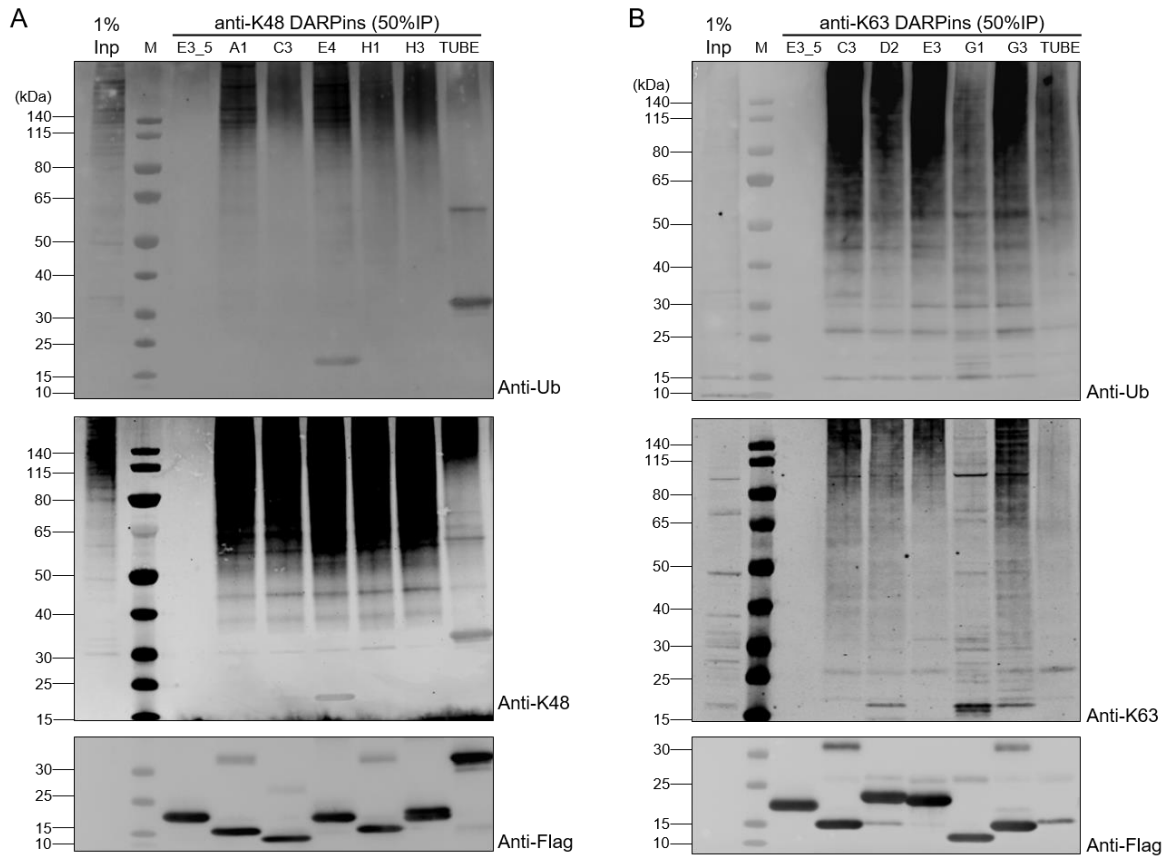

Figure 3.7: The DARPins keep their specificity in mammalian cell extract. (A, B) Flag-pull-down from HeLa cell extract (1 mg total protein) with the indicated Flag-tagged anti-K48 (A) or anti-K63 DARPins (B), the respective TUBE and the control DARPin E3_5. 1% Input and 50% of the pull-down were analyzed by Western blot with antibodies against ubiquitin, the specific ubiquitin linkage (K48 or K63) and the Flag-tag of the DARPins.

The anti-K63 TUBE performed slightly better than its K48 analog, as it bound a comparable amount of ubiquitin conjugates as the anti-K63 DARPin G1, yet still less than the other tested DARPin candidates (Figure 3.7B). The blot developed with the K63-linkage specific antibody revealed that all probes enriched for K63-linked ubiquitin chains. However, the signal for the TUBE was slightly weaker than that of the tested anti-K63 DARPins, which demonstrated a strong pull-down from the dimer to high molecular weight ubiquitin chains, indicating the high affinity of the anti-K63 DARPins.

The findings for both DARPin sets were reproducible in *S. cerevisiae* cell lysate, demonstrating that the DARPins can be used in versatile environments (compare Appendix Figure 6.8). Overall, the pull-downs show that our DARPins can detect and isolate proteins decorated with specifically linked ubiquitin chains from cells with better affinity and selectivity than the corresponding TUBE.

3.2.2.3 Inhibitory effect of the DARPin on ubiquitylation and cell survival

3.2.2.3.1 DARPins show inhibitory effect on ubiquitin chain (de-)conjugation

Since the DARPins shall be used *in vivo*, it is important to know whether and to which extent they influence and inhibit ubiquitin reactions, as this has implications for how the DARPins can be used and whether their expression levels need to be regulated. The last five candidates of the anti-K48 and anti-K63 DARPins were directly compared with the respective TUBE to investigate possible differences that might make certain DARPins more suitable for a certain application, e.g. as a non-disturbing sensor or as a molecular trap that enriches a certain signal. This comparison also served as a basis for the selection of the final DARPin, which will be used as a biosensor *in vivo*.

Enzymatic *in vitro* assays of the ubiquitylation and deubiquitylation reaction were used to provide important insights into whether the DARPin interaction inhibits the binding of other enzymes such as writers and erasers. K48-linked ubiquitin chains were formed with the linkage-specific E2 Ubc7 with the help of Cue1, while the K63-linked ubiquitin chains were formed with the linkage-specific E2 pair Ubc13/Mms2 and Pib1. The K48-specific DUB OTUB1 was used for the deconjugation of the K48-linked ubiquitin chains and the K63-specific DUB AMSH for the K63-linkage deconjugation. For better quantification, a FRET-based assay was used to monitor the enzymatic ubiquitin chain formation or deconjugation of YFP and CFP ubiquitin in the presence of the respective DARPin (1:1 ratio).

The addition of ATP lead to an increase of the FRET signal, indicating ubiquitin chain formation (Figure 3.8 A+C), whereas the addition of the respective linkage-specific DUB resulted in a decrease of the FRET signal (Figure 3.8 B+D), validating this system. The addition of all five anti-K48 DARPins reduced ubiquitin chain formation similarly to the addition of the anti-K48 TUBE (Figure 3.8A), with DARPin H3 showing the mildest effect and DARPin A1 showing the strongest effect. This data showed that all tested K48-specific binders, DARPins and the TUBE, block the E1-E3 interaction with ubiquitin to some extent. The enzymatic degradation of K48-linked ubiquitin chains by OTUB1 was also reduced in the presence of all anti-K48 DARPins and the corresponding TUBE (Figure 3.8B). However, while its inhibition rate of the chain formation reaction was comparable to that of the other DARPins, the inhibitory effect of DARPin H1 was greatly reduced compared to that of the other DARPins, suggesting a different binding mode of H1.

The five anti-K63 DARPins also all affected the conjugation (Figure 3.8C) and deconjugation (Figure 3.8D) of K63-linked ubiquitin chains. Especially for the conjugation reaction, the differences between the individual DARPins varied much more than for the anti-K48 DARPins. Anti-K63 DARPin G3 strongly inhibited ubiquitin conjugation and deconjugation, whereas DARPin E3 showed a relatively small effect on the conjugation reaction. However, a direct comparison of the results of the conjugation and deconjugation reactions must be taken with caution, since the mechanisms of the two reactions as well as the activity of the writers and erasers are different. This can be *inter alli* seen when comparing the measured raw values at the starting and endpoint of the reaction. The YFP/CFP ratio for the conjugation reaction increased for E3_5 from 1.51 to 5.98, for the deconjugation reaction it started in the same range at 5. 46 for the deconjugation reaction, but only decreased to 3.04 - showing that the cleavage by AMSH did not lead to a complete restoration of the individual ubiquitin moieties. This is supported by the corresponding Western blot, in which the samples are separated after the measurement (Appendix Figure 6.9). Therefore, this assay should mainly be used to compare the effects of DARPins between candidates and to the TUBE in the same reaction.

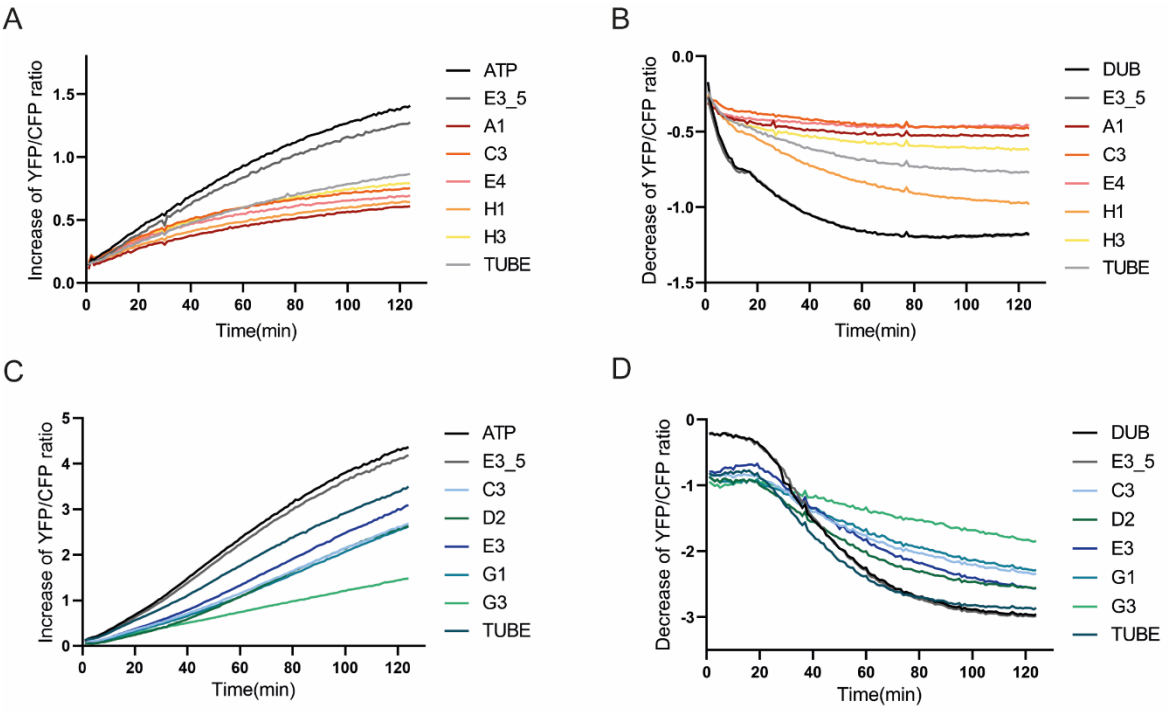

Figure 3.8: All DARPins affect ubiquitin chain (de-)conjugation *in vitro*. (A-D) Direct comparison of the inhibitory effect of all five anti-K48 (A, B) and anti-K63 (C, D) DARPins and the corresponding TUBE. Graph showing the change of the relative YFP/CFP-ratio (normalized to control without ATP/DUB) over time as readout of the enzymatic K48- (A, B) or K63-linked (C, D) ubiquitin chain formation (A, C) or deconjugation (B, D) in the presence of the anti-K48 DARPins (A, B) or anti-K63 DARPins (C, D) including the respective TUBE and the control DARPin E3_5 in the ratio 1:1 to ubiquitin, measured in triplicates.

The FRET experiments were also performed in the presence of DARPin excess (2-fold, 5-fold, data not shown) over ubiquitin, which showed an increased inhibitory effect, suggesting a concentration dependence for all DARPins

The measurements demonstrated that all DARPins can influence both the formation and degradation of ubiquitin chains. The inhibitory effects were comparable to those of the respective TUBEs. For *in vivo* experiments, particularly when longer processes are to be monitored, a less inhibitory candidate might be preferable. Nevertheless, as it was demonstrated for all DARPins that this effect is concentration-dependent, regulating the utilized concentration or expression level may also modulate this effect.

3.2.2.3.2 DARPins have no or very mild effect on cell survival in unperturbed conditions

The next step was to investigate whether the inhibitory effect observed in the *in vitro* ubiquitin chain reactions translate into a defect in cell growth and survival and how this affect the use of the DARPins *in vivo*. To investigate this, the DARPins were inducibly expressed in budding yeast (*S. cerevisiae*, Gal-promotor) and mammalian cells (RPE-1, CMV-promotor) and the effect of DARPin expression on cell survival was analyzed.

The expression of the anti-K48 DARPins in *S. cerevisiae* did not influence cell growth in unperturbed conditions, as shown in Figure 3.9A. Various sources of cell stress were tested, including ER stress (tunicamycin), DNA damage (MMS) and osmotic stress (NaCl and sorbitol). Since K48-linked ubiquitin chains have been implicated in the resolution of all these stresses,[489–495] it is not surprising that the expression of the anti-K48 DARPins, which reduce the conjugation of K48-linked ubiquitin chains, lead to reduced cell survival under these conditions (Figure 3.9A).

After long-term expression of the anti-K48 DARPins in mammalian cells (approximately 8 days), a mild effect was observed due to the expression of the DARPins A1 and E4, even under unperturbed conditions (Figure 3.9B). For anti-K48 DARPin A1, this effect is also a result of the expression conditions themselves, as the decrease was no longer significant when compared to the survival of the cell line expressing the negative control DARPin E3_5, while a significant effect remained for E4. Therefore, it is crucial to control the concentration of DARPins and to keep the expression time as short as possible when using them in *in vivo* experiments.

In contrast, none of the anti-K63 DARPins had a significant effect on cell growth in either yeast (Figure 3.9C) or mammalian cells (Figure 3.9D) under unperturbed conditions and when exposed to tunicamycin, MMS, NaCl or Sorbitol. Only the DNA damage caused by MMS resulted in a growth defect of DARPin-expressing cells. This stress also relies mostly on K63-linked ubiquitin chain formation.[127–129, 496, 497] Two anti-K63 DARPins, namely G1 and C3, showed a weaker effect than the others, making them the preferred candidates for an *in vivo* sensor.

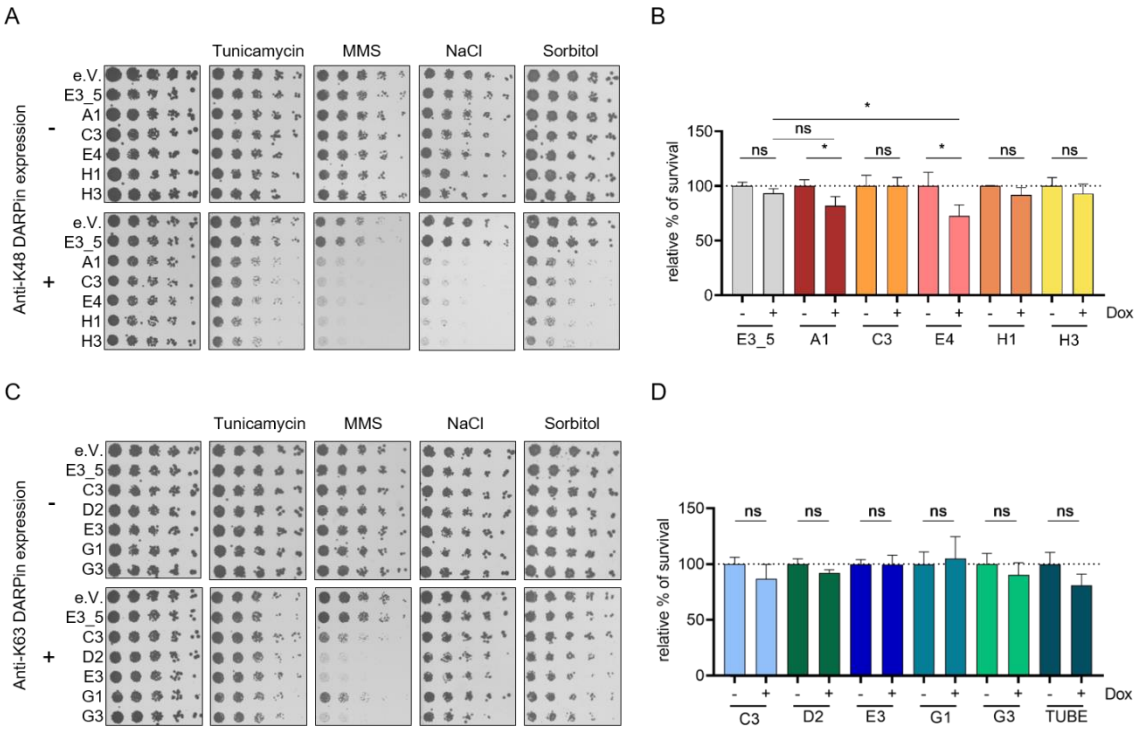

Figure 3.9: The DARPins show no or only mild effect on unperturbed cell growth. (A, C) Spot assays showing growth of *S. cerevisiae* cells in serial dilution with and without expression of anti-K48 (A) or anti-K63 DARPins (C) in unperturbed or stress conditions with indicated stressors (Dosage: Tunicamycin 0.2 µg/mL, MMS 0,005%, NaCl 0.75 M, Sorbitol 1 M). (B, D) Influence of anti-K48- (B) and anti-K63 DARPins (D) or K63-TUBE expression on survival of RPE1 cells. The survival was measured by the number of colonies in a colony formation assay after 8 days with or without DARPin expression induced by 2 ng/µL doxycycline. The height of the bars represents the mean of three replicates and shows cell survival relative to the respective uninduced samples, which was set to 100%. Significance levels were calculated using an unpaired t-test (ns, non-significant, *: $p<0.05$). E3_5= control DARPin.

3.2.3 The selected final DARPins were further characterized

Based on the results of the previous experiments, a candidate for each linkage was chosen that appeared to be the most promising for a selective biosensor.

The anti-K48 DARPins A1 and E4 have been demonstrated to be the most selective and strongest binders based on their pull-down results (Figure 3.6A+B and 3.7A), but they have also been shown to be the most inhibitory candidates (Figure 3.8A+B and Figure 3.9A+B). However, as it was demonstrated that the inhibitory effect can be regulated by the utilized concentration, the robust selectivity and binding affinity were given greater consideration. In the direct comparison of A1 and E4, A1 exhibited greater selectivity and a slightly milder inhibitory effect than E4. Therefore, A1 was chosen for further characterization.

The selection of the final anti-K63 DARPin was not primarily based on its selectivity, as this was comparable for all candidates (Figure 3.6D), but also on its inhibitory properties (Figure 3.9C+D). Thus, anti-K63 DARPin G1 was chosen, which exhibited the least inhibitory effect for further investigations.

3.2.3.1 Final candidates proved selectivity when confronted with all linkages

In this experiment, the selectivity of the final candidates was subjected to further validation. In the previous validation this had been investigated solely for M1, K48- and K63-linked ubiquitin dimers and chains. In this experiment now, the anti-K48 DARPin A1 and the anti-K63 DARPin G1 were tested against ubiquitin dimers of all linkage types.

The result demonstrated a high specificity of anti-K48 DARPin A1, with the K48-linked dimer being the sole target (Figure 3.10A). Anti-K63 DARPin G1 also demonstrated a high affinity for the K63-linked dimer, with a mild interaction observed for the K11-linked dimer and a marginal interaction for the K27-linked ubiquitin dimer (Figure 3.10B).

Figure 3.10: The final anti-K48 and anti-K63 DARPin show high selectivity *in vitro*. Flag-pull-downs with the Flag-tagged control DARPin E3_5, anti-K48 DARPin A1 (A) or anti-K63 DARPin G1 (B) and ubiquitin dimers with all eight possible linkages was performed and analyzed by anti-ubiquitin Western blotting. 10% Input (Inp) and 100% pull-down is loaded.

This results demonstrated the high specificity of both DARPins, even when confronted with all linkages found in mammalian cells. This makes them promising tools for the specific interaction with their respective linkage. The subsequent mass spectrometry analysis investigated how this specificity translates to a pull-down approach from whole cell extract.

3.2.3.2 Mass spectrometry analysis revealed high specificity of the DARPins exceeding the ones of the TUBEs

To obtain a more quantitative analysis of the selectivity of our final DARPins for their respective linkage, a mass spectrometry approach was used. The ubiquitin linkages can be identified through specific diGly signature peptides, which are generated for each chain linkage type by trypsin digestion (compare section 1.1.8.2).[107, 126] Quantitative analysis of each peptide then provides an overview of the linkage distribution. To enhance the detection of the linkage distribution in the input sample (crude Hela cell lysate), a GlyGly enrichment kit (PTMScan® Ubiquitin Remnant Motif (K-ε-GG) Kit, CST) that contains a specific antibody against the GlyGly motif was utilized.

The analysis revealed the detection of all seven ubiquitin chain types linked via a lysine residue in the HeLa cell extract (Figure 3.11). The measured distribution was as followed: 38.69% K48, 38.41% K63, 17.61% K11, 3.18% K29, 1.98% K6, 0.10% K33 and 0.02% K27. Previous studies have shown that the distribution of linkages in mammalian cells varies substantially among different cell lines, cell cycle stages and cell differentiations.[97] However, although the individual percentages vary, several studies have demonstrated that under normal growth conditions, K48 and K63 are the most abundant linkages in mammalian cell lines, followed by K11, while the other linkages are present in single-digit percentages.[96, 106, 498] This is also true for our measurement, validating our method. It is important to note that the distinct sequences of the different peptides for the different linkages result in significant differences in their ionization efficiency, which consequently affect their intensities in the resulting spectra.[499] Since no standard was used in our measurement, the measured values should be understood as relative rather than absolute values.

Compared to the input, the anti-K48 DARPin A1 strongly enriched the K48-linkage, pulling out approximately 25% of all K48 linkages present and increasing its proportion from 38% to 67% of the total pulled-down ubiquitin chains (Figure 3.11). The remaining interaction partners were linked via K63 (14%), K11 (14%), and K6 (4%). This may be due to unspecific binding of the DARPin or, partially, to branched chains, which have been shown to make up 5-20% of all linked polyubiquitin chains.[183, 184]

In comparison, the anti-K48 TUBE exhibited a much lower affinity in general, pulling down only 1.3% of the input and 0.26% of the K48-linked ubiquitin chains despite being used at the same molarity as the anti-K48 DARPin A1. The analysis revealed that only 7.6% of the pulled-down linkages were linked by K48, while over 40% were linked via K11, enriching this linkage by 2.3-fold. The relative abundance of the K63 linkage at 36% was comparable to that of the input. Overall, this demonstrates a failure of the anti-K48 TUBE to bind and isolate K48-linked polyubiquitin chains in our experimental setup. It needs further investigation to determine if the TUBE's non-functionality was due to the pull-down procedure.

The anti-K63 DARPin G1 pulled down 9.8% of the absolute amounts of K63-ubiquitylated conjugates and relatively enriched the linkage by 1.7-fold compared to the input (Figure 3.11). The analyzed peptides show that the DARPin mainly bound K63-linked ubiquitin chains (64.39%), but also pulled-down a proportion of K48-linkages. However, a large fraction of this 28% is likely due to branching, as it has been shown that approximately 20% of all K63-linked ubiquitin chains are branched with K48.[106]

In contrast to the anti-K48 TUBE, the anti-K63 TUBE demonstrated comparable ubiquitin-binding efficiency to that of the anti-K63 DARPin G1. However, it was found to be less selective than K63 G1, as it enriched K48-linked ubiquitin chains up to 46%, while K63-linked chains had a relative abundance of 43.7%.

Overall, the mass spectrometry measurement showed that our DARPins can efficiently isolate proteins decorated with the respective ubiquitin chains. Both DARPins exhibit high affinity and selectivity in cell extracts, surpassing the properties of the corresponding TUBE.

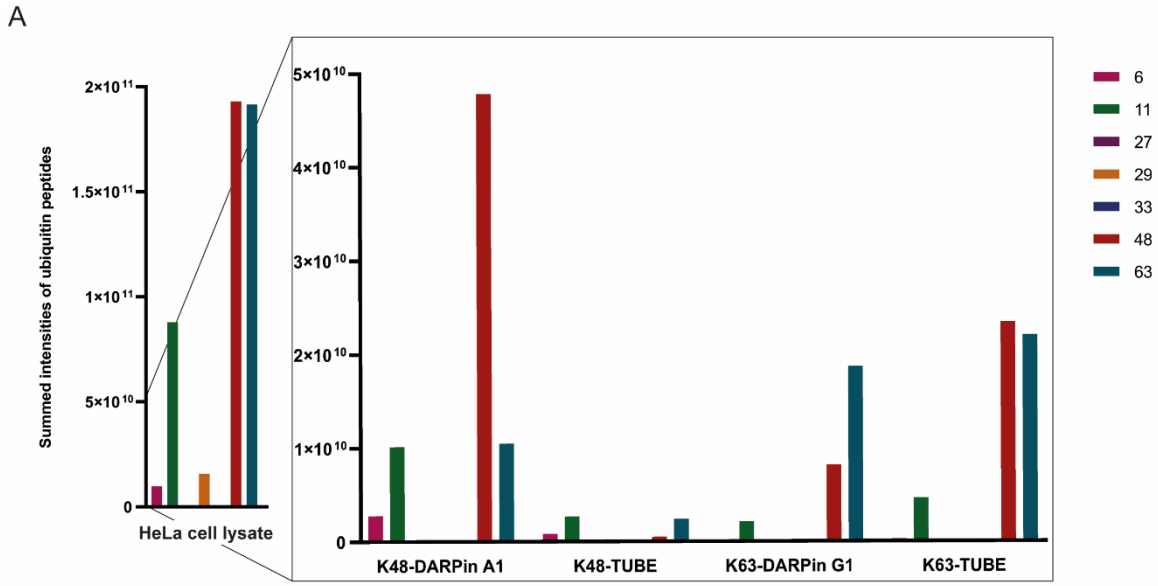

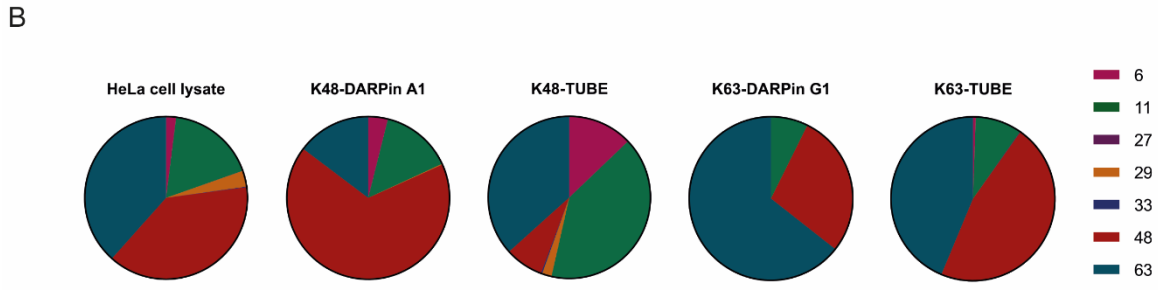

Linkage	HeLa cell lysate	K48-DARPin A1	K48-TUBE	K63-DARPin G1	K63-TUBE
6	1.98%	3.91%	12.85%	0%	0.56%
11	17.61%	14.22%	40.69%	7.35%	9.20%
27	0.02%	0%	0%	0%	0.11%
29	3.18%	0.16%	1.90%	0%	0%
33	0.10%	0%	0.25%	0%	0%
48	38.69%	67.01%	7.64%	28.26%	46.42%
63	38.41%	14.70%	36.67%	64.39%	43.72%

Figure 3.11: Mass spectrometry analysis demonstrates high selectivity of the final DARPins in HeLa cell extract. (A) Absolute numbers of summed intensities of ubiquitin peptides with GlyGly site corresponding to the respective ubiquitin linkage for the total HeLa cell lysate or the pull-downs by the anti-K48 DARPin A1, the anti-K48 TUBE, the anti-K63 DARPin G1 or the anti-K63 TUBE. (B) Pie chart and table of the relative amounts of the seven identified polyubiquitin linkages in whole HeLa cell lysate or the pull-downs by the indicated DARPin or TUBE.

3.2.3.3 DARPins show affinities in the nanomolar range

After demonstrating the ability of the DARPins to bind the specific ubiquitin linkage they were raised against, both *in vitro* and *in vivo*, the binding affinity was quantified using the surface plasmon resonance technology. To account for background binding to the chip surface, particularly by anti-K48 DARPin A1, and to address unstable capture, several different coupling and detection methods were tested. The optimal experimental setup was identified as capturing the biotinylated DARPin on the surface of a Biacore SA chip and using various ubiquitin conjugates as analytes. The interaction between the DARPin and increasing concentrations of these conjugates was quantified to determine the affinity of the DARPin towards the tested substrate.

The anti-K48 DARPin A1 bound to both tested K48-linked substrates with affinities of 51.9 nM (dimer) and 78.4 nM (tetramer) (Table 3.1, graphs see Appendix Figure 6.11). These results confirmed the findings of previous tests using a CAP chip, for which a slightly higher affinity of 45.6 nM of anti-K48 DARPin A1 against the K48-linked ubiquitin dimer was measured (Appendix Figure 6.11E). Therefore, the affinity for K48-linked ubiquitin conjugates is in the range of 50-70 nM with only a slight difference depending on the chain length. This value is comparable to the published affinity of 20 nM for the anti-K48 TUBE against K48-linked ubiquitin tetramers. However, no binding was detected up to a concentration of 1 µM when the affinity of the anti-K48 TUBE was measured against K48-linked ubiquitin dimers. These measurements are in alignment with the previously performed pull-downs (Figure 3.6B) and are attributed to the structure of the TUBEs, which only can reach its strong affinity when all four UBDs are bound.[227] Therefore, this demonstrated a clear advantage of the DARPin over the TUBEs in detecting K48-linked dimers and trimers.

Measurements of the affinity of anti-K48 DARPin A1 towards monoubiquitin did not reach saturation, with the highest measured concentration being 100 µM. Therefore, the indicated affinity was only estimated mathematically by the Biacore evaluation software to be approximately 13.2 mM, which is far outside the used concentration range of the measurement. This suggests a more than 15,000-fold preference of K48 A1 for K48-linked diubiquitin over monoubiquitin. The DARPin's low affinity for monoubiquitin is crucial for its *in vivo* use, as monoubiquitylated proteins make up 30-80% of the ubiquitin pool in mammalian cells.[96] Therefore, high discrimination is essential. The affinity of K48 A1 toward K63-linked diubiquitin was measured at 1480 nM, indicating a 29-fold preference for K48 over K63 dimers (Table 3.1).

Surprisingly, the affinity of the anti-K63 DARPin G1 for the K63-bound ubiquitin dimer was measured to be rather weak at 1.45 µM (Table 3.1). However, when the length of the oligomer was increased to a tetramer, the affinity increased drastically to 6.9 nM, which is as strong as the anti-K63 TUBE.[228] DARPin G1 exhibited a more than 6,000-fold preference over monoubiquitin and nearly 8,000-fold preference over K48-linked ubiquitin. Even when comparing at the dimer level, a 38-fold preference for K63 over K48 was still determined.

Overall, both DARPins showed nanomolar affinities to their respective ubiquitin linkages, which are comparable to or even higher than their corresponding TUBE. Their affinities are in the same range as linkage-specific ubiquitin antibodies[212, 500], and especially their low affinity to monoubiquitin makes them suitable candidates for *in vivo* usage.

Table 3.1: Equilibrium dissociation constants (K_D) for the DARPins interacting with the indicated ubiquitin conjugates. All values were measured by SPR in triplicates. *Values estimated as saturation was not reached. n.d = not determined.

DARPin	MonoUb (nM)	K48 2Ub (nM)	K63 2Ub (nM)	K48 4Ub (nM)	K63 4Ub (nM)
Anti-K48 A1	13,213,300 ±531500*	51.86 ± 7.56	1,480 ± 200	78.38 ±18.81	n.d.
Anti-K63 G1	45,900 ± 9,800	54,470 ± 12,340*	1,450 ± 320	n.d.	6.93 ± 1.14

3.2.3.4 Structural insights explain specificity of DARPins

To gain a better understanding of how DARPins achieve this high affinity, their observed linkage specificity and to identify their binding interfaces, we collaborated with the group of Prof. Yogesh Kulathu (University of Dundee, Scotland) to determine the crystal structure of anti-K48 DARPin A1 and anti-K63 DARPin G1 bound to their respective diubiquitin conjugate.

The crystal structure of the anti-K48 DARPin A1 in complex with K48-linked diubiquitin was solved at 2.45 Å. The structure revealed multiple interactions, which were clustered in three main binding sites (Figure 3.12A). Binding sites 1 and 3 interaced with the distal ubiquitin, while binding site 2 showed an interaction of Trp101 of the DARPin with both ubiquitin moieties. More specifically, it interacted with the Ile44 patch of the proximal ubiquitin and with the Ile36 patch, mainly Leu71 and Leu73 of the distal ubiquitin. Studies have shown that K48-linked ubiquitin chains can adopt two distinct confirmations: an open and a closed conformations.[501–504] A comparison to the crystal structures of these two conformations revealed that the K48-DARPins A1 captured a state more representing the closed conformation of the K48-linked ubiquitin dimer (Appendix Figure 6.14). Only in this closed conformation, which is achieved when ubiquitin is linked via Lys48, the two hydrophobic patches of the ubiquitin moieties are in such close proximity that loop 3 of anti-K48 DARPin A1 can interact with both simultaneously (site 2, Figure 3.12A). This explains the high selectivity of the anti-K48 DARPin A1.

The selectivity appeared to be primarily based on hydrophobic interactions and π-stacking through Trp residues. To investigate whether the interaction could be eliminated by mutating these residues, a pull-down was performed with WxxA mutants introduced in all three binding sites. For site 1 (Loop 1 with Ub^{dist}), the salt bridges formed by the Asp residues 34, 47 and 67 with the Arg42 and Glu49 of the distal ubiquitin seem to also play an important role, since the mutation of Trp36 and Trp38 at this binding site alone did not result in a loss of interaction (Figure 3.12B). Only when combined with the mutation of Trp112 of site 3 (DARPin α7 helix with Ub^{dist}), the interaction was abolished, while this mutation alone only led to a reduced affinity. Site 3 represented another hydrophobic interface based on Trp112 of the C-terminal region of the DARPin and the hydrophobic Ile44 patch residues on the distal ubiquitin, forming an additionally cation-π bond with His68 of Ub^{dist}.

The interaction of site 2 is driven by a hydrophobic core formed between DARPin residues centered on Trp101 and the hydrophobic patches of both ubiquitins. Mutations in site 2 (Loop2/3 with Ub^{dist}/Ub^{prox} interface) completely abolished the interaction in the pull-down assay, highlighting the importance of this interaction site for binding and specificity (Figure 3.12B).

The crystal structure of the anti-K63 DARPin G1 in complex with K63-linked diubiquitin was solved at 1.70 Å, but has not been fully refined yet and thus has to be regarded as preliminary data while further processing is ongoing. The crystal structure (Figure 3.13A) revealed diverse interactions, which can be clustered in four sites. Specificity appears to be again mainly achieved through tryptophan-mediated hydrophobic interactions. The structure also shows an interaction with the two Lys48 residues. For example at site 4 (DARPin α6 helix – Ub^{dist}), which is mainly based on scaffold residues, Glu95 interacts with Lys48 of the distal ubiquitin. The interaction between the two Ile44 patches of both ubiquitin moieties appears to mainly mediate the overall interaction and specificity. Specifically, the interaction of site 1 (Loop1 with Ub^{prox}) with Trp48 of the DARPin and Arg42 and the Ile44 patch on the proximal ubiquitin dictated the specificity. When mutated, the interaction with K63-linked ubiquitin dimers is retained, but a complete loss of specificity can be observed (Figure 3.13B, Appendix Figure 6.13). Mutations in site 2 and 3 seem to weaken or eliminate the interaction to the point where it cannot be detected in a pull-down experiment (Figure 3.13B). Site 2 (Loop3 with Ub^{prox}) interacts mainly with Phe45 and other hydrophobic residues of the proximal ubiquitin moiety. Site 3 (DARPin α5 helix – Ub^{dist}) is centered on Trp83, Trp91, and Trp92, interacting mainly with the Ile44 patch of the distal ubiquitin through hydrophobic interactions and a cation π-bond of Trp91 with His63 of ubiquitin.

Taken together, this indicates that the DARPins appear to interact with common interaction motifs of ubiquitin, specifically the Ile36 and Ile44 patches. These patches have defined distances and relative orientations that are specific to the chain linkage between the two moieties, resulting in high specificity and high-affinity recognition of the DARPins primarily through hydrophobic interactions. As these patches have also been shown to be crucial for ubiquitin chain formation and deconjugation[28, 505–508], this also explains the concentration-dependent inhibitory effect of the DARPins, which compete with the ubiquitin writers, erasers and readers for this binding site.

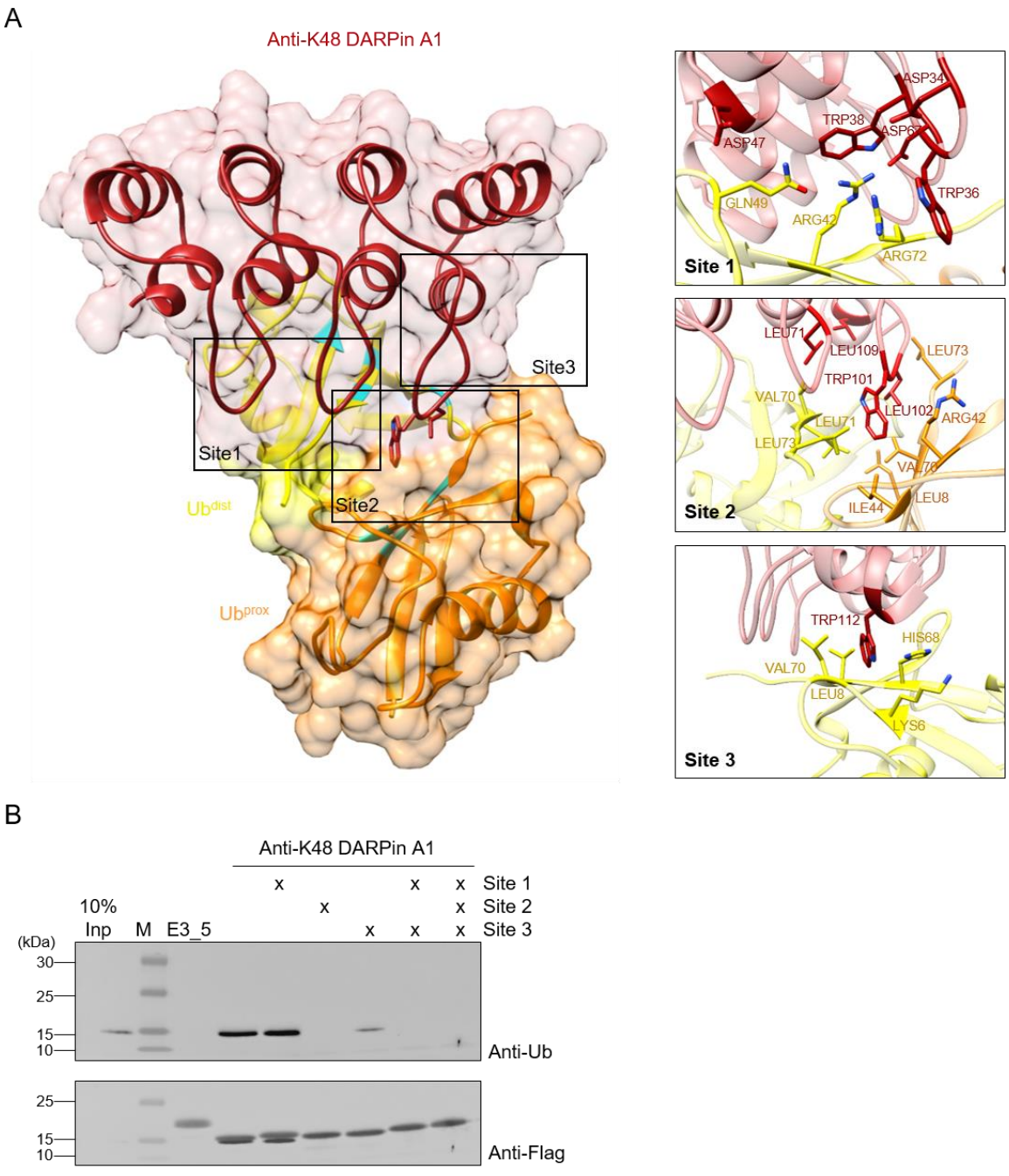

Figure 3.12: Crystal structure explained the high specificity of the anti-K48 DARPin A1. (A) Crystal structure of anti-K48 DARPin A1 (red) with K48-linked diubiquitin (distal ubiquitin in yellow, proximal in orange) at 2.45 Å. Ile44 patch marked in cyan. Close-up views showing the interaction sites with involved residues. Crystal structure by Lee Armstrong (University of Dundee, UK). (B) Flag pull-down using the Flag-tagged anti-K48 DARPin A1 wild-type and different mutants introduced at the indicated interaction sites. (site 1: W36A, W38A, site 2: W101A, L102A, site 3: W112A) and a K48-linked ubiquitin dimer. Analyzed by Western blotting against ubiquitin and the Flag-tag of the DARPins. 10% of input and 100% of pull-down loaded. For data collection statistics see Appendix Table 6.2.

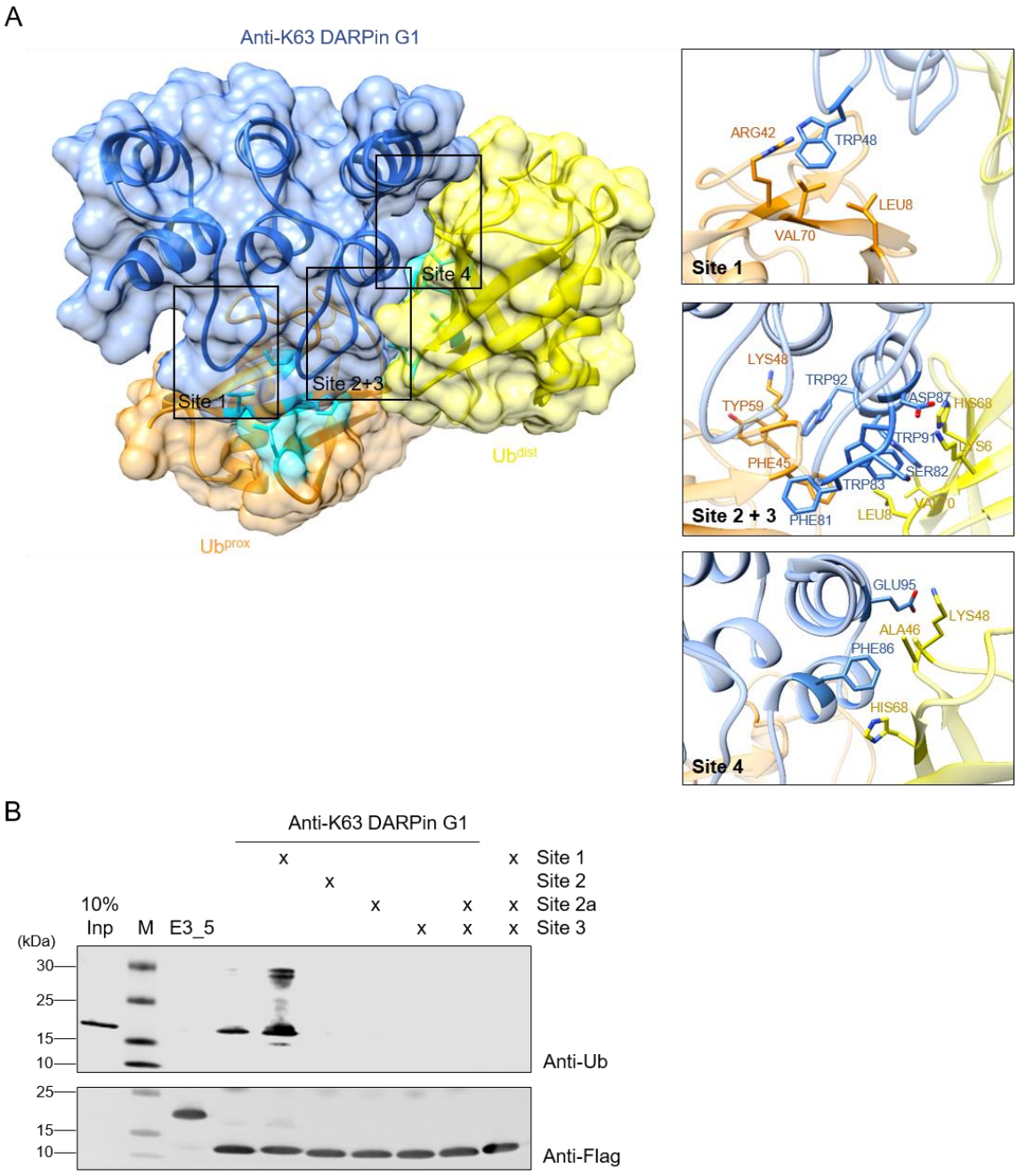

Figure 3.13: Crystal structure explained the high specificity of the anti-K63 DARPin G1. (A) Crystal structure of anti-K63 DARPin G1 (blue) with K63-linked diubiquitin (distal ubiquitin in yellow, proximal in orange) at 1.70 Å. Close-up views showing the interaction sites with involved residues. Crystal structure by Anna Perez (University of Dundee, UK). (B) Flag pull-down using the Flag-tagged anti-K63 DARPin G1 wild-type and different mutants introduced at the indicated interaction sites. (site 1: W48A, site 2: W83A, site 2a: F81A, S82A, W83A site 3: W91A W92A) and a K63-linked ubiquitin dimer. Analyzed by Western blotting against ubiquitin and the Flag-tag of the DARPins. 10% of input and 100% of pull-down loaded. For data collection statistics see Appendix Table 6.2.

3.2.3.5 DARPins have IC_{50} values in the micromolar area

Following this comprehensive *in vitro* characterization of the specificity and affinity, the inhibitory properties of the two final candidates were further studied, with a special focus on the concentration-dependency of this effect.

Therefore, FRET assay for both chain formation and deconjugation with increasing DARPin concentrations of anti-K48 DARPin A1 and anti-K63 DARPin G1 were performed. A concentration dependence was clearly confirmed in all four setups (Figure 3.14A-D).

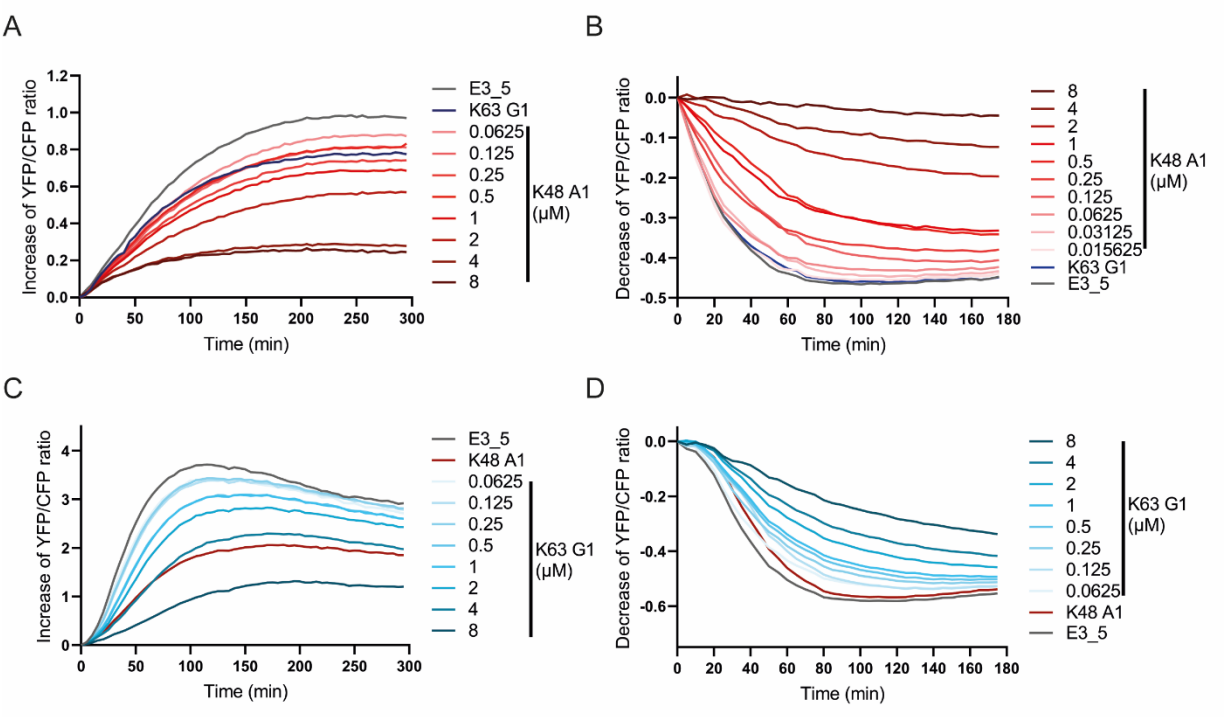

Figure 3.14: The inhibitory effect of both DARPins is concentration dependent. Graph showing the change of the relative YFP/CFP-ratio over time as readout of the enzymatic K48 (A, B) or K63-linked (C, D) ubiquitin chain formation (A, C) or deconjugation (B, D) in the presence of increasing concentrations of the corresponding anti-K48 DARPin A1 (A, B) or anti-K63 DARPin G1 (C, D). As controls the respective other DARPin and the control DARPin E3_5 in the highest concentration were measured along. Measured in triplicates

Using the residual activity of the enzymatic chain formation or deconjugation as a readout of the initial slope (first 60 min) of the measured FRET curves plotted against logarithmic DARPin concentration (Appendix Figure 6.17), the IC_{50} values for DARPin K48 A1 and K63 G1 on chain formation and cleavage of the specifically linked ubiquitin chain were calculated using Graph Pad Prism 8.3 and are summarized in the following Table 3.2.

Table 3.2: Calculated IC_{50} values for anti-K48 DARPin A1 and anti-K63 DARPin G1.

DARPin	IC_{50} on respective chain conjugation (µM)	IC_{50} on respective chain deconjugation (µM)
Anti-K48 DARPin A1	1.75	1.36
Anti-K63 DARPin G1	4.90	3.57

All IC_{50} values are in the single-digit µM range. For both DARPins the effect on the deconjugation reaction is stronger (indicated by a lower IC_{50}) compared to the conjugation reaction. When transferred to a cellular environment, where there is typically an equilibrium between chain conjugation and deconjugation, this would result in an enrichment of ubiquitin chains, which could be advantageous for the detection of ubiquitylation events. When examined for their effect on the opposite chain linkage, both DARPins did not affect chain deconjugation (Figure 3.14B+D) when added in 4-fold excess. However, they surprisingly reduced chain formation also of the respective other linked ubiquitin chain (Figure 3.14A+C). In particular, K48 A1 strongly reduced the formation of K63-linked ubiquitin chains. It remains to be investigated whether this is due to a basal affinity for K63-linked ubiquitin chains in this exclusive system or to a direct effect on the enzymes themselves.

The measurements and quantifications demonstrated that the DARPins exert an influence on both ubiquitin chain formation and degradation in a concentration-dependent manner. Consequently, a regulation of the utilized concentration or an expression level below the IC_{50} in cells can serve to mitigate this effect.

3.2.4 DARPins as *in vivo* sensors in yeast and mammalian cells

3.2.4.1 DARPins can be expressed and visualized in yeast and mammalian cells

As shown already in the *in vivo* inhibition screen (Figure 3.9), the anti-K48 DARPin A1 and anti-K63 DARPin G1 can be expressed in yeast and mammalian cells. Their effects on cell growth and survival under stress (Figure 3.9) and the pull-down results after expression (Appendix Figure 6.4), also show that they are functional in the cellular environment. Therefore the next step was to test the DARPins as biosensors to monitor linkage-specific ubiquitylation processes inside the cell. Thus they were tagged with GFP to enable visualization by microscopy.

Using these constructs, the expression pattern of stably integrated DARPins (induced with 0.5 ng/µL doxycycline) was first examined in unperturbed *S. cerevisiae* cells (Figure 3.15A). The expression of the two specific DARPins (K48 A1 and K63 G1), as well as the control DARPin E3_5 was detectable in yeast cells (Figure 3.15A). While E3_5 was rather homogeneously distributed, both specific DARPins showed a preferential nuclear localization. For the K48-specific DARPin this is explained by the fact that the K48-linked ubiquitin chains are mainly a degradation signal and the majority of proteasomes are found in the nucleus of dividing yeast cells.[509, 510] It is thus an indication that the DARPin A1 colocalizes with K48-ubiquitylated proteins.

To achieve more homogeneous distribution between the nucleus and the cytosol, the DARPins were tagged with two nuclear export signal (NES) tags. This short peptide targets proteins for the export from the nucleus to the cytoplasm by nuclear transport.[511] The tagging led to the desired more even distribution of the GFP-tagged DARPins inside the cell, but also weakened the overall expression (Figure 3.15A+B and Appendix Figure 6.18A). However, this low background may be beneficial in cases where a strong local increase of specifically linked ubiquitin chains is expected, so both the system without and with NES-tag may be valuable as sensors depending on the experiment.

For the first expression test in mammalian cells, a transient transfection of GFP-tagged DARPins (200 ng plasmid, constitutive promotor) in HeLa wild-type cells was conducted. The result 48 h after transfection showed a very heterogeneous population of cells: while some expressed the construct very strongly, the majority did not express the DARPins at all (Figure 3.15C).

Therefore, a cell line was generated in which the DARPins fused to YFP were stably integrated. For this purpose, it was switched from HeLa to RPE-1 cells, a cell line that is not derived from a tumor but from “normal” human retinal pigment epithelial immortalized by the human telomerase reverse transcriptase subunit (hTERT).[512, 513] Thus, this cell line has a near-diploid karyotype and has been used extensively to study the physiological functions of human genes and proteins in a more natural context than in tumor cell lines.[512] The integration was conducted by a master student working with me on this project: Philipp Elleringmann. It worked well and although the anti-K63 DARPin G1 was slightly less expressed (Appendix Figure 6.18B) the expression was nicely visible and homogenous between different cells. The anti-K48 DARPin A1 again showed a small preference for nuclear localization (Figure 3.15D), consistent with previous stainings using the K48 linkage-specific antibody,[514] while the anti-K63 DARPin G1 was evenly distributed inside the cell, also consistent with K63-linkage specific antibody staining.[515]

The expression tests proved that the DARPins can be transiently and stably expressed in yeast and mammalian cells, and are present in both the cytosol and nucleus, thus allowing detection of processes involving K48- or K63-linked ubiquitin chains in both compartments.

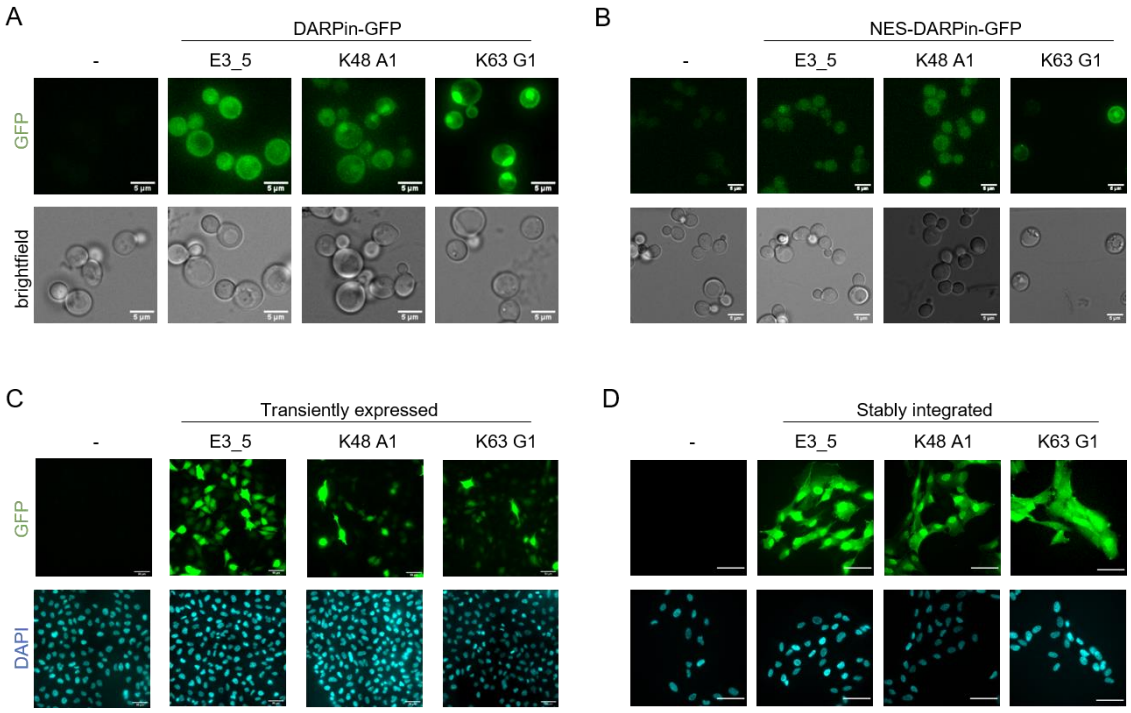

Figure 3.15: The DARPins can be expressed in yeast and mammalian cells. (A, B) Expression of GFP-tagged anti-K48 DARPin A1, anti-K63 DARPin G1 and E3_5 integrated in *S. cerevisiae* cells with (B) and without (A) NES-Tag. Expression was induced with 0.5 ng/µL doxycycline for 24 h and cells were visualized with the DeltaVision microscope. Scale bars = 5 µm. (C, D) Expression of GFP-tagged anti-K48 DARPin A1, anti-K63 DARPin G1 and E3_5 after transient transfection in HeLa cells (C) or stably integrated in RPE-1 cells (D). (C) HeLa cells were transfected with 200 ng of GFP-DARPin plasmid and fixed after 48 h with 4% PFA, stained with DAPI and imaged with the AF7000 microscope. Scale bars = 50 µm. (D) DARPin expression was induced with 2 ng/µL doxycycline and after 24 h fixed with 4% PFA, stained with DAPI and imaged with the AF7000 microscope. Scale bars = 10 µm. (D) Conducted by Philipp Elleringmann.[482] E3_5 = Negative control DARPin.

3.2.4.2 Colocalization with antibodies and the proteasome

The initial expression test showed a localization of the DARPins that looked comparable to that of the respective linkage-specific antibody. To validate this hypothesis and to provide a proof of principle that the DARPins can be used to visualize linkage-specific ubiquitin chains, cells expressing the YFP-tagged DARPins were co-stained with the corresponding antibody.[514, 515]

To induce a pattern, which allows a more direct comparison of the staining of the DARPins and respective antibodies and to investigate whether the DARPins can move dynamically together with their bound ubiquitin chains, half of the samples were heat-shocked (43°C, 2 h). This proteotoxic condition leads to diverse liquid- liquid phase separation (LLPS) processes and the formation of cytoplasmic protein aggregates containing ubiquitin conjugates.[516–520]

The colocalization of the anti-K48 DARPin A1 with the K48-specific antibody staining, especially in the heat shock-induced granules, was striking (Figure 3.16), while the control DARPin E3_5 did not colocalize with the aggregates. For the anti-K63 DARPin G1, fewer structures were stained by the K63-antibody, which is due to the fact that K63-linked ubiquitin chains are less pronounced in stress granules.[521] However, the few patterns that were formed showed a nice overlap with the staining of the YFP-tagged anti-K63 DARPin G1. In addition, G1 stained foci within the nuclei. These could be associated with DNA damage sites known to be highly K63-ubiquitylated.[522]

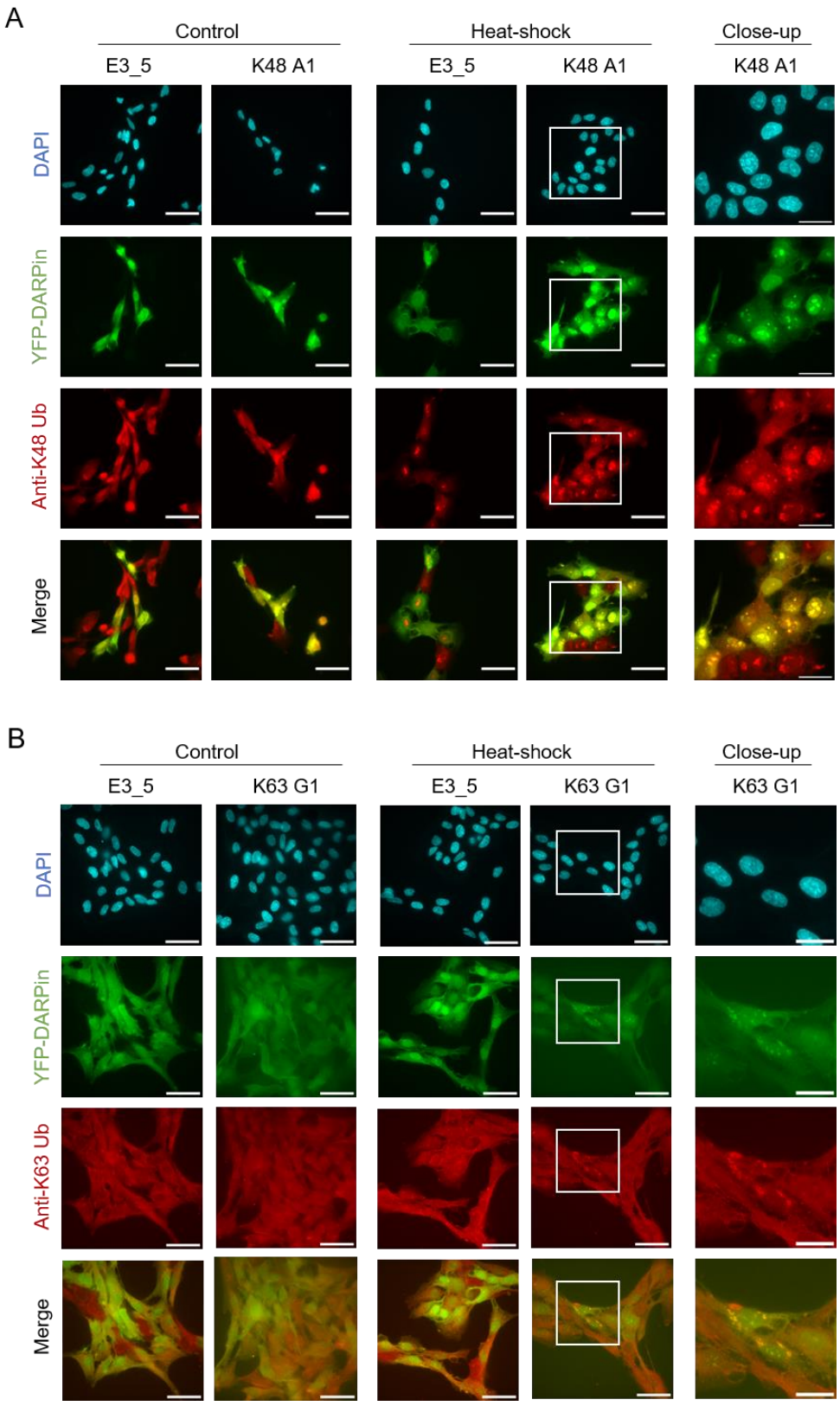

Figure 3.16: The DARPins colocalize with their respective antibody. (A, B) The colocalization between the signal of the linkage-specific ubiquitin antibody: anti-K48 (Apu2, A) or anti-K63 (HWA4C4, B) and the corresponding YFP-tagged anti-K48 DARPin A1 (A) or anti-K63 DARPin G1 (B) (green channel) was investigated. Stable integrated RPE-1 cells were used, expression was induced with 2 ng/µL doxycycline for 24 h. For the heat-shocked samples cells were stressed for 2 h at 43°C. They were fixed with PFA, stained with DAPI (blue) and the linkage-specific antibody (red) and imaged with the AF7000 microscope. Scale bars = 50 µm. Conducted by Philipp Elleringmann.[482]

For the anit-K48 DARPin A1, another colocalization experiment was performed in mammalian cells (Figure 3.17). As K48-linked ubiquitin chains are mainly understood as a signal for proteasomal degradation[31, 523–525], an overlapping signal with the proteasome staining is expected. Therefore, co-staining was performed with an antibody against PSMB5, a core protein of the 20S proteasome complex. Again, heat shock was used to induce proteotoxic stress and accumulation of proteasome-containing foci. Indeed, some but not all of these foci showed an overlap of both channels (Figure 3.17). This indicates that the presence of K48-linked ubiquitin chains only in some structures directly leads to proteasomal degradation.

The colocalization with antibodies showed that the DARPins can be used to visualize fixed and dynamic structures inside the cells, comparable to the respective linkage-specific antibodies. In contrast to antibodies, the small and simple structure of the DARPins allows them their expression inside the cell, thus enabling live-cell imaging.

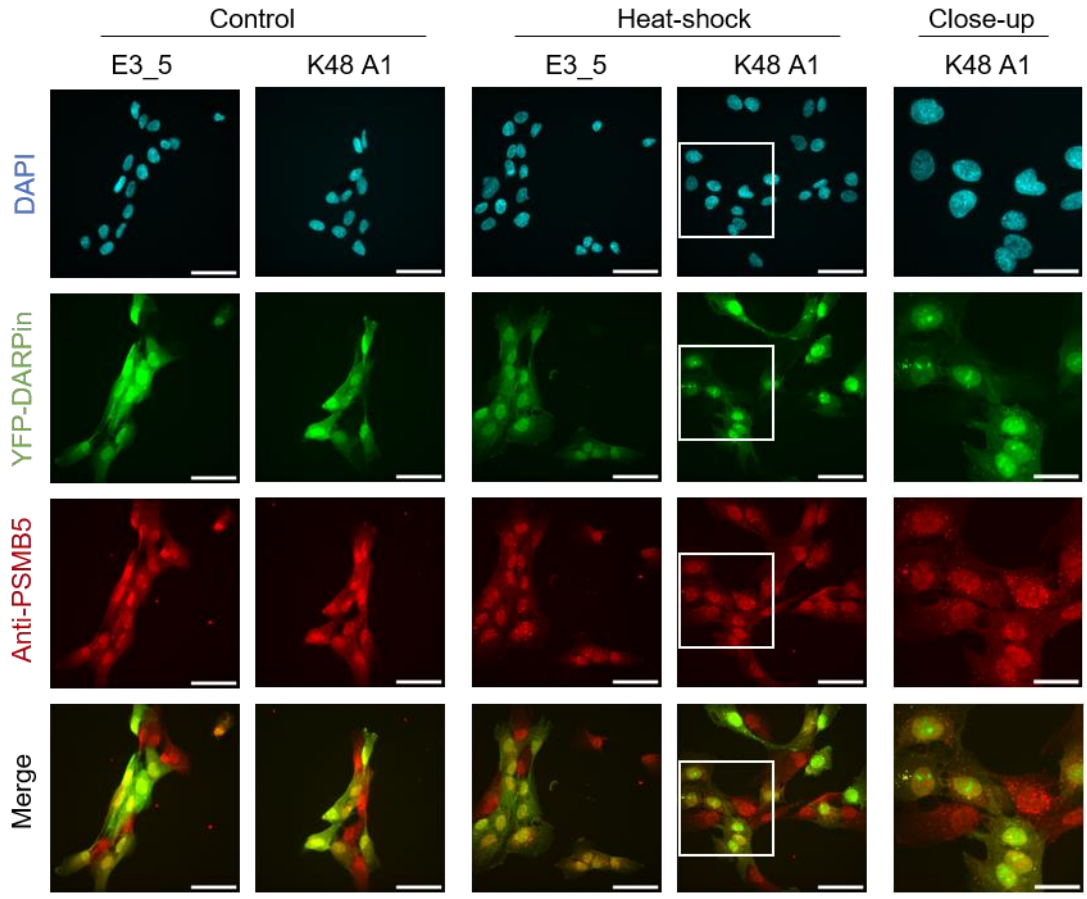

Figure 3.17: Anti-K48 DARPin A1 partially colocalizes with the proteasome. The colocalization between the signal of the proteasomal subunit PSMB5 and the YFP-tagged anti-K48 DARPin A1 (green channel) was investigated. Stable integrated RPE-1 cells were used, and expression was induced with 2 ng/µL doxycycline for 24 h. For the heat-shock samples, cells were stressed for 2 h at 43°C. They were fixed with PFA, stained with DAPI (blue) and the antibody against PSMB5 (red) and imaged with the AF7000 microscope. Scale bars = 50 µm. Conducted by Philipp Elleringmann.[482]

3.2.4.3 DARPins as tools for the detection of ubiquitylation in stress granules and aggresomes

The preceded experiment showed an association of the specific DARPins to heat-stress induced aggregates. It was assumed that these aggregates might be stress granules. Stress granules (SG) are membraneless ribonucleoprotein-based organelles that form in the cytoplasm of a cell upon exposure to various environmental stressors, such as heat shock, oxidative stress, viral infection, osmotic stress or UV irradiation.[495, 526–528] Throughout publications, various authors have linked the SG homeostasis with the ubiquitin system. Many reports show the presence of ubiquitin itself[516–518, 520, 529] as well as many enzymes of the ubiquitin system in SGs, including DUBs, 26S proteasome and p97.[517, 521, 530–532] Tolay and Buchberger investigated which linkage types are involved and showed that SGs induced by different stressors have different involvement of the ubiquitin system in total abundance and enzymes required. In the stress granules with the highest ubiquitin content (induced by H_2O_2, arsenite and heat shock) mainly K48-linked ubiquitin chains, but also K63-linked ubiquitin chains were detected using linkage-specific antibodies.[521] Thus this system was used to test the specificity of our linkage-specific DARPins by investigating if this data was reproducible with the DARPins. Therefore, another colocalization experiment was performed with an antibody against the SG-marker G3BP1 and the linkage-specific DARPins, testing different inducers of SG formation.

The RPE-1 cells with integrated YFP-tagged DARPins were treated with four different sources of stress (heat-stress in two variations, MG-132, arsenite and sorbitol). Similar to the previous experiments (Figure 3.16 and 3.17), heat stress induced DARPin foci that colocalized with the signal of the K48-linkage specific antibody. However, no foci were detected with the G3BP1 antibody. The same was true for cells treated with the proteasome inhibitor MG-132. After sorbitol treatment, no foci formation was observed in any of the channels. The only stress that induced foci containing the stress granules marker G3BP1 was arsenite, but there was no colocalization of the DARPins or the anti-K48 antibody to these granules detectable (Figure 3.18A).

Different conditions of expression, treatment or detection (different antibodies) were tested, but in most cases very few foci containing G3BP1 were detectable. This is in contrast to the published data of Tolay and Buchberger, who found that depending on the stressor, 45-100% of the cells contained stress granules.[521] The biggest difference to their set-up was the cell line - so different cell lines were investigated on their stress granules formation upon heat stress (Appendix Figure 6.20A). Indeed, it was observed that while HeLa and U2OS cells formed nice foci containing G3BP1, which colocalized with the signal of the K48-antibody, no stress granule formation was detectable in RPE-1 cells. This discrepancy could be attributed to the nature of the cells. Both HeLa and U2OS cells are derived from cancerous cells and display aneuploidy, which leads to various types of stress.[533] This could render the already stressed cell more susceptible to a robust response to certain stress conditions, while the more "healthy" RPE-1 cells may be better equipped to cope with them.

Therefore, with the help of Nazife Tolay, first author of the previously cited paper, the DARPins K48 A1 and K63 G1 were stably integrated into HeLa cells (for expression level compare Appendix Figure 6.20B) and the colocalization experiment upon heat stress was repeated.

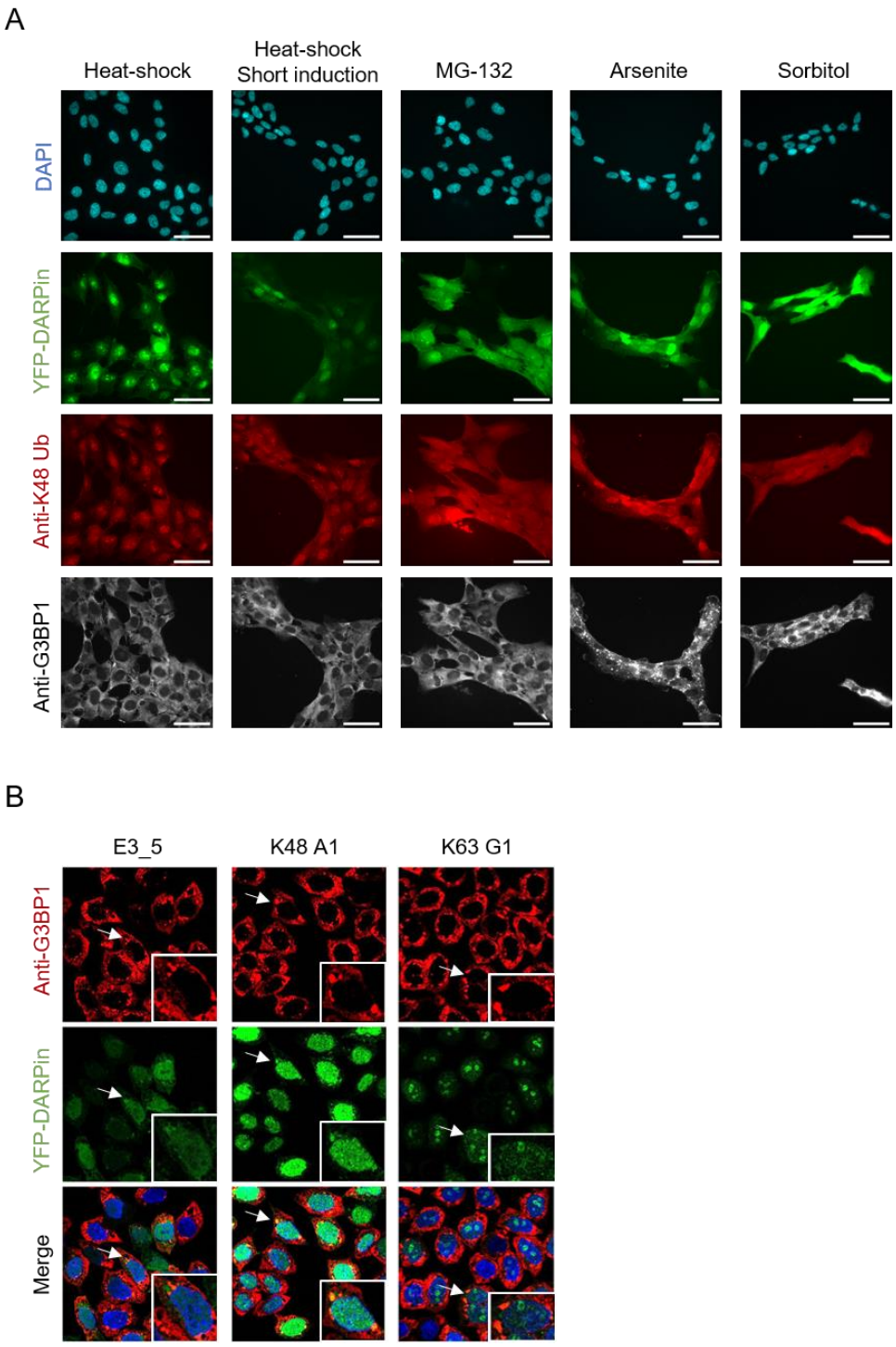

Figure 3.18: DARPin colocalize with stress granules in HeLa cells. (A) The colocalization of the YFP-tagged anti-K48 DARPin A1, the staining of the K48-antibody and the staining of G3BP1 as stress granules marker was investigated after cells were treated with different stressors. Expression of the DARPins in RPE-1 cells was induced with 2 ng/µL doxycycline for 24 h (2 h for the short induction sample). Cells were then either heat shocked for 2 h at 43°C, treated with 10 µM MG-132 for 3 h, 0.5 mM Sodiumarsenite for 30 min or with 0.4 M Sorbitol prior to fixation with 4% PFA. They were stained with DAPI (blue) and antibodies against K48-linked ubiquitin (Apu2, red) and G3BP1 (grey) and imaged with the AF7000 microscope. Scale bars = 50 µm. Conducted by Philipp Elleringmann.[482] (B) The colocalization of the YFP-tagged DARPins E3_5, K48 A1 or K63 G1 and the staining of G3BP1 as stress granules marker was investigated after cells were subjected to heat-stress (43°C, 2 h). Expression of the DARPins in HeLa cells was induced with 1 µg/mL tetracycline for 24 h. They were fixed with PFA and stained with DAPI (blue) and the G3BP1-antibody (red) and imaged by confocal immunofluorescence microscopy. Representative DARPin-positive SGs are magnified in the inset. Scale bars = 10 µm. Conducted by Nazife Tolay.

In this cell line, the stress granule formation upon heat stress was detectable based on the G3BP1 foci surrounding the nucleus (Figure 3.18B). The anti-K48 DARPin A1 partially localized to these granules, confirming the involvement of K48-linked ubiquitin chains. The anti-K63 DARPin signal only weakly overlapped with the stress granule staining (Figure 3.18B). The fact that K63-linked ubiquitin chains are found to a lesser extent in heat shock-induced stress granules is consistent with published data, but whether our DARPin G1 also localizes to nearly 10% of stress granules as shown with the K63-linkage specific antibody[521] is questionable and further experiments are needed to allow quantification. Another observation from this experiment by Nazife was again the G1-positive-foci in the nucleus, which could indicate DNA damage sites. Thus, colocalization experiments with associated markers should be performed for clarification.

After the linkage-specific ubiquitin involvement in stress granules formation was analyzed in mammalian cells, the same should be investigated in *S. cerevisiae*. It is known that in *S. cerevisiae* prolonged stress, such as nutrient limitation, results in transient nonproliferation, which is termed quiescence. In quiescence, proteasomes are transported from the nucleus to the cytoplasm and sequestered into cytoplasmic storage granules *inter alli* stress granules to prevent autophagic degradation.[534, 535] Although the requirement of enzymes of the ubiquitin system as the DUB Ubp3 and VCP have been shown in yeast, the ubiquitin linkages involved remain unknown.[536, 537] Here the DARPins could be a helpful tool to gain a deeper insight into the prevalence and relevance of K48- and K63-linked ubiquitin chains in the formation and resolution of stress granules. For this purpose, the stress granules marker Pab1 was tagged endogenously with mCherry and the induction of stress granules was tested with different stressors (Figure 3.19A). Various published methods were tested to induce quiescence and single foci were detected when the cells were grown for two days without dilution in SC-complete or for additional stress in SC-minimal medium as well as after osmotic stress (sorbitol) and starvation (without glucose).

For the first colocalization experiments, a set-up was used in which the cells were starved by growth for two days in SC-minimal medium (Figure 3.19). After this treatment, however, the number of cells showing stress granules was very low. In addition, because not all cells expressed the respective DARPin, very few cells were found that had both stress granule foci and DARPin expression. Nevertheless, for the anti-K48 DARPin A1, an overlap of the signal of both A1 and the stress granule marker Pab1 was seen in some of these cells (Figure 3.19B, close-up).

This was promising, but the low abundance of stress granules made the detection of colocalization very challenging. In literature, it has been suggested that after starvation, approximately 21% of yeast cells show stress granule foci of Pab1-GFP.[538] Since this could not be reproduced with Pab1-mCherry in our hands, the fluorophores were switched and Pab1 was tagged with GFP while the DARPins were tagged with mRuby. Glucose starvation for 2 h was used to induce stress granules, and although more cells showed stress granule formation, colocalization with the anti-K48 DARPin A1 was still rare (Figure 3.19C). The anti-K63 DARPin G1, on the other hand, did not appear to localize to stress granules (Figure 3.19C), suggesting that K63-linked ubiquitin chains are not as abundant in yeast stress granules upon starvation. Due to weak colocalization and high background signal, quantification was not possible. This has led to the switch back to the larger and easier to visualize mammalian cells for the subsequent analysis.

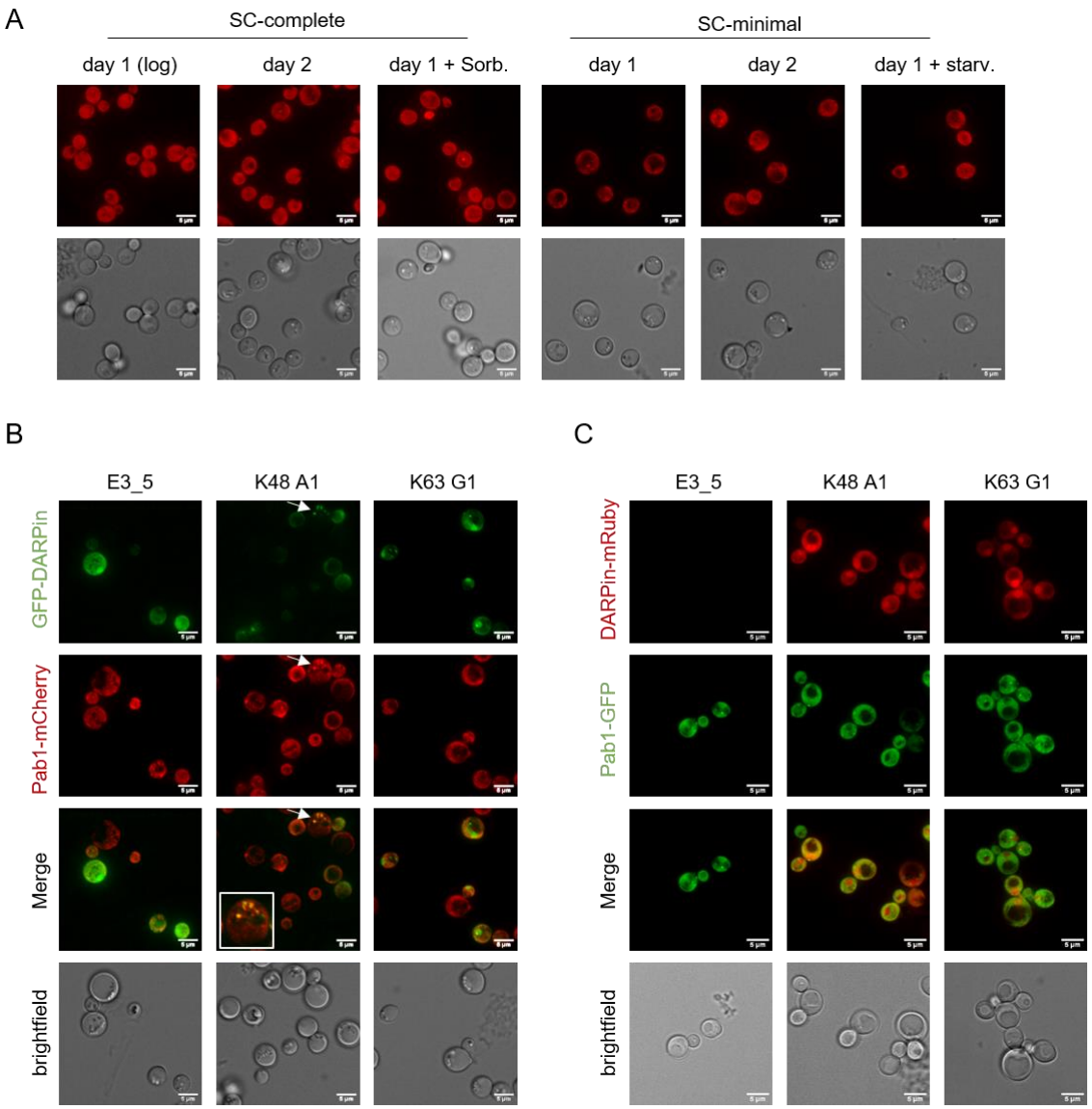

Figure 3.19: Rare induction of stress granules complicated DARPin colocalization experiments in *S. cerevisiae*. (A) DF5 cells expressing endogenous Pab1-mCherry (red) were grown under different conditions and imaged with the DeltaVision microscope. Cells were grown in SC-complete or SC-minimal medium for the indicated amount of time. For the sorbitol sample 1% sorbitol and 1% glucose was used instead of 2% glucose as carbon source and for the starvation sample, cells were starved and grown in medium lacking glucose for 2.5h. (B+C) The colocalization of the GFP (B) or mRuby-tagged (C) DARPins E3_5, K48 A1 or K63 G1 and Pab1 as stress granules marker tagged with mCherry (B) or GFP (C) was investigated after cells were starved (without glucose) for 2 h. Cells were imaged without fixation with the DeltaVision microscope. Scale bars = 5 µM.

As shown, some of the foci formed by the DARPins (and also detected by the K48-specific antibody) upon heat stress are due to the accumulation of specifically linked ubiquitin chains in stress granules in mammalian cells. However, there were a large number of foci formed upon heat stress that did not colocalize with the stress granule marker, so it was asked whether this could be due to other phase separation processes induced by the elevated temperature. It was shown that heat shock can also induce the formation of aggresomes, which consist mainly of polyubiquitylated proteins. These often misfolded cytotoxic proteins are accumulated and initiate the switch from the UPS to autophagy.[539–541]

The simplest way to induce aggresome formation is through proteasome inhibition.[542, 543] Therefore, Hela cells expressing the specific DARPins were treated with 1 µM bortezomib for 18 h. The first experiment (Figure 3.20A) showed a clear formation of ubiquitin positive foci around the nucleus. This almost completely overlapped with the foci formed by the anti-K48 DARPin A1. The extra-nuclear foci formed by the anti-K63 DARPin G1 also colocalized with the ubiquitin signal, while additional foci were visible within the nucleus. The sample with the negative control DARPin E3_5 did not show any foci formation, indicating that the foci are specific to the accumulation of specific ubiquitin chains in the phase-separated structures.

To confirm that these are indeed aggresomes, the experiment was repeated, including staining with thioflavin-S, which stains protein aggregation and thus aggresomes.[544] Indeed, the signal of all three channels overlapped strongly for K48 A1, partially with K63 G1 and not with E3_5 (Figure 3.20B). This is consistent with the expected linkages found in these aggresomes. As they contain mainly degradation-prone proteins, they will be heavily decorated with K48-linked ubiquitin chains, but the presence and involvement of K63-linked ubiquitin chains has also been shown.[545–548]

Overall, it was shown that the DARPins can visualize an accumulation of specifically linked ubiquitin chains in different cellular structures, also in response to specific stressors. For the classification of these structures, colocalization with an appropriate marker can be performed. Since DARPins, unlike antibodies, can be used in live-cell microscopy, they enable future studies of the dynamics of these phase-separated structures.

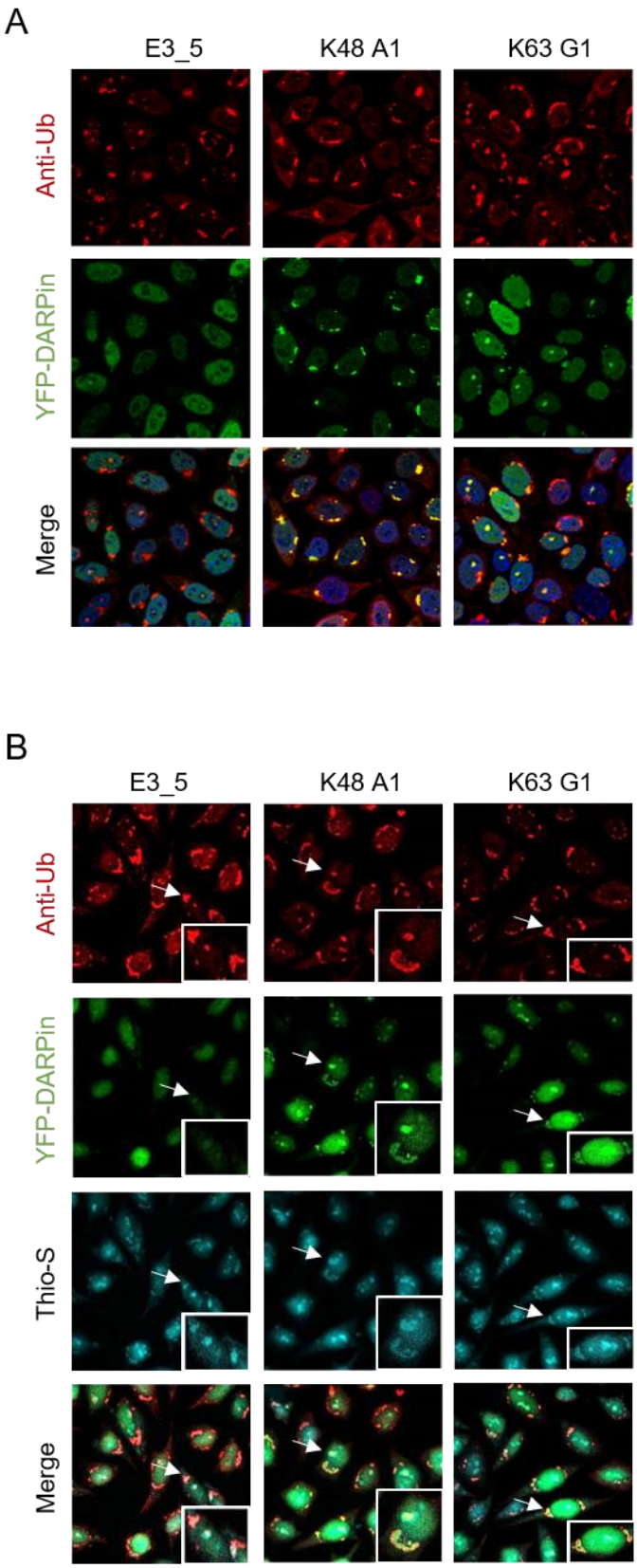

Figure 3.20: Both DARPins colocalize with aggresomes. (A, B) The colocalization of the YFP-tagged DARPins E3_5, K48 A1 or K63 G1 (green) and the ubiquitin staining was investigated after cells were treated with 1 µM bortezomib for 18 h. Expression of the DARPins in HeLa cells was induced with 1 µg/mL tetracycline for 24 h. They were fixed with PFA and stained with DAPI (A, blue) or thioflavin-S (B, blue) and the antibody against ubiquitin (red) and imaged by confocal immunofluorescence microscopy. Representative DARPin-positive aggresomes are magnified in the inset. Scale bars = 10 µm. Conducted by Nazife Tolay.

3.2.4.4 DARPins can track ubiquitin-dependent processes at DNA damage sites

The advantage of DARPins over classical antibodies is the possible application of them in live-cell imaging. This was further explored. It is hypothesized that expression of the YFP-labeled specific DARPins will allow tracking of specific ubiquitin chain formation and deconjugation in response to a particular cell state or stress.

To study this, the cellular response to DNA damage was investigated using live-cell imaging. For this purpose, the so-called laser track system was used, in which laser-mediated microirradiation is used to induce highly localized damage to DNA in the nucleus on a submicrometer scale. The laser source is integrated into a confocal microscope equipped with an environmentally controlled microscope stage that allows time course analysis. The use of fluorescently labeled DNA repair proteins, or in our case the DARPins, as probes against K48- and K63-ubiquitylation events, allows the recording of the cellular response in real time. This, together with the high spatial precision of the damage inflicted, makes laser microirradiation a key method to gain insight into the complex spatio-temporal dynamics of DNA damage and repair.[549–552]

Different lasers can be used to induce damage; in our set-up an ultraviolet A (UVA) laser (355 nm) was used and the *in vivo* response was monitored by taking microscopy images of the GFP-channel every 15 s for 30 min (representative images and time points are shown in Figure 3.21, overview images in Appendix Figure 6.21). In all samples, laser irradiation caused photobleaching of the nuclear pool of YFP-tagged DARPins, but the YFP signal recovered to initial intensities within 5 min, showing the mobility of the DARPins within the cell. Beyond this recovery, no further effect or accumulation of the control DARPin E3_5 was observed over the course of 30 minutes, proving the low background of the system. In the cells expressing the anti-K48 DARPin A1, an accumulation of YFP-signal at the DNA damage site was detected by eye after approximately 2.5 min. Due to their degradative nature, K48-linked ubiquitin chains are subject to rapid turnover. Therefore, it has been challenging to visualize them and study their contribution to certain pathways, such as DNA damage signaling in the past.[494, 523] However, using new methods several groups have identified different roles for K48-linked ubiquitin chains in DDR signaling, including removal of Ku80 or recruitment of p97 to damage sites.[492–494] The anti-K48 DARPin A1 nicely illustrates these implications of K48-linked ubiquitin chains by their strong accumulation at DNA damage sites. Due to its strong binding and signal, the DARPin thereby proved to be a valuable tool for visualizing also transient effects of K48-linked ubiquitin chains. The K48 A1 signal at DNA damage sites increased up to about 20 minutes and then remained constant for the remaining 10 minutes, being in agreement with a previously performed laser track experiment using the linkage-specific K48 antibody at 5 min and 1 h after microirradiation.[494]

The anti-K63 DARPin G1 signal became visible at the DNA damage site slightly earlier, at about 1 minute. The signal intensity increased up to 20 minutes, then remained stable until the end of the tracking. Many studies have shown the involvement of K63-linked ubiquitin chains in various DNA damage signaling pathways, ranging from the pathway selection itself, over DNA damage bypass, to NER and DSB repair (HR and NEHJ).[127–129, 496, 497, 522, 553–555] Therefore this early and strong recruitment of the anti-K63 DARPin G1 was not surprising, even though its expression was lower than that of the anti-K48 DARPin A1 (Appendix Figure 6.21A).

The results are also in agreement with the previously conducted laser tracks by Feng and Chen, who stained with the K63-linkage-specific antibody 5 min and 4 h after damage and saw a strong K63 signal at the damage site for both time points.[494]

Additionally, it was observed that in most cells expressing anti-K63 DARPin G1, bright foci appeared outside the nucleus immediately after laser irradiation and were rapidly resolved within the first 5 min of live-cell imaging. Whether these are indicative of stress granules, aggresomes, or the demonstrated role of K63-linked ubiquitin chains in intracellular trafficking[130] needs to be further investigated.

Overall, this experiment nicely illustrated the usability of both specific DARPins as probes to visualize and track specifically linked ubiquitylation processes in time and space by live-cell imaging.

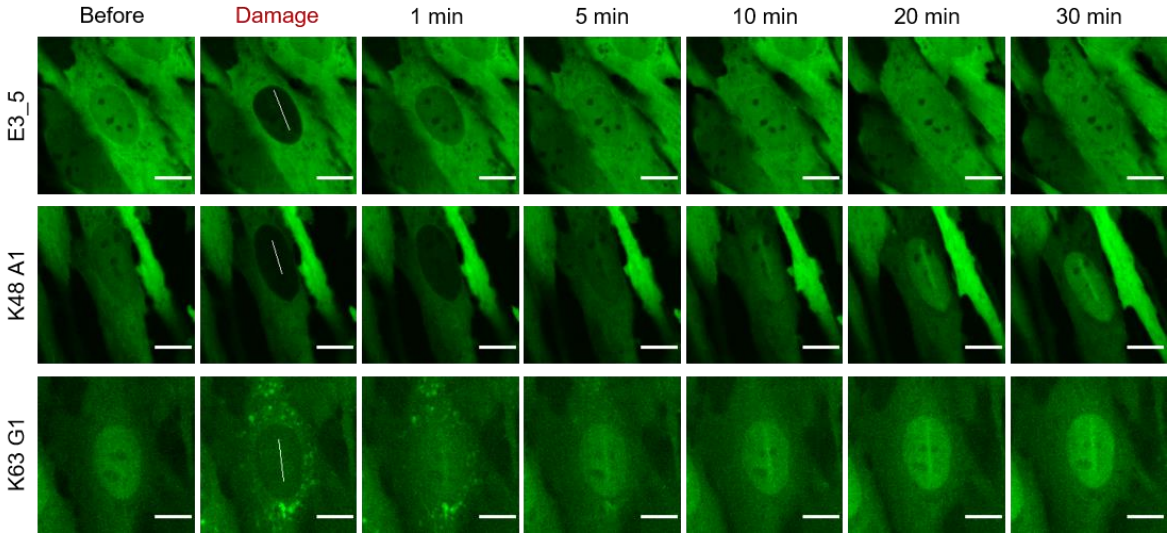

Figure 3.21: DARPins can be used to monitor ubiquitylation processes upon DNA damage. Representative image showing the accumulation of YFP-tagged E3_5, K48 A1 or K63 G1 DARPin respectively at sites of laser-induced DNA damage in RPE-1 cells. Expression of DARPins was induced with 2 ng/µL doxycycline for 24h. The white line indicates the laser path of the 355 nm laser (50% laser power) and thereby represents the site of damage inside the living cell. Scale bar = 10 µM.

3.2.5 Development of a sensor for K48-K63-branched ubiquitin chains

After the specific binding of the DARPins to their respective linkage and their applicability *in vitro* and *in vivo* was demonstrated, both the anti-K48 A1 and the anti-K63 DARPin G1 were combined to create a tool for studying K48-K63-branched ubiquitin chains, which have not been well characterized yet despite their high abundance.[96]

Therefore, a bimolecular K48-K63-branched chain sensor was developed by combining the two linkage-specific DARPins. As detection method a bimolecular fluorescence complementation (BiFC) approach was used, which relies on the refolding of a splitted fluorescence protein upon close proximity of the two halfs. Therefore, this biosensor was generated by fusing the anti-K48 DARPin A1 or the anti-K63 DARPin G1 respectively to the N-terminal (aa1-154) and C-terminal (aa155-238) residues of the mVenus fluorescent protein, a modified version of the yellow fluorescent protein (YFP). The linkage-specific DARPins can recognize and bind to their respective linkages within the K48-K63-branched ubiquitin chain. Simultaneous binding to K48-K63-branched ubiquitin chains brings the non-fluorescent Venus fragments into close proximity, allowing reconstitution of the native fluorescence complex and thus leading to emission of a bright fluorescence signal.[234, 556–559] This fluorescent signal can be detected and quantified by fluorescence microscopy or fluorescence spectroscopy, allowing detection and characterization of branched ubiquitin chains *in vitro* and *in vivo*.

The nYFP-labeled anti-K48 DARPin A1 and its counterpart cYFP-labeled anti-K63 DARPin G1 were cloned and purified by Julia Reidel, a former bachelor student. She also performed the primary screening and *in vitro* assays. To minimize false positive results due to non-specific self-association of the Venus fragments, the concentration threshold for this spontaneous reassociation was investigated by measuring the fluorescence signal of samples containing increasing amounts of nYFP-K48-A1 and cYFP-K63-G1 DARPin using the Tecan microplate reader (Appendix Figure 6.22A). The following *in vitro* studies were then performed with a concentration below this threshold (0.25 µM) for both DARPin components to investigate the specificity of the DARPin based K48-K63-branched chain probe without background signal.[560]

3.2.5.1 The K48-K63-branched chain sensor can detect branched polyubiquitin and monitor their synthesis *in vitro*

First, the ability of the designed biosensor to specifically detect K48-K63-branched ubiquitin trimers *in vitro* was investigated. For this purpose, 0.25 µM of both parts, the nYFP-tagged DARPin K48 A1 and the cYFP-tagged DARPin K63 G1, were mixed without anything (negative control=NC), with 1 µM of a homotypic dimer linked by K48 or K63, the mixture of both dimers or the K48-K63-branched triubiquitin. Samples were incubated for 3 h at room temperature to allow binding, reassociation, and maturation of the probe, and then the fluorescence signal was measured as relative fluorescence units (RFU) (Figure 3.22A). The negative control gave the lowest fluorescence signal, proving very little spontaneous reassociation of the YFP-halfs at the used concentration. When incubated with specifically K48- or K63-linked ubiquitin dimers or the mixture, a slight increase in fluorescence is measured. This may be due to a small crowding effect or unspecific binding of one DARPin to the opposite ubiquitin dimer. However, a significant increase was only observed when the two BiFC-DARPins were incubated with the K48-K63-branched ubiquitin trimer, demonstrating the specificity of this probe for the heterotypically linked ubiquitin conjugate. Western blot analysis (Figure 3.22B) of the samples after the measurement showed that all ubiquitin constructs and DARPins were used at comparable concentrations, proving that the increase in fluorescence was due to the simultaneous binding of both specific DARPins to the K48-K63-branched ubiquitin trimer, which allowed reconstitution of the Venus fluorophore.

In another BiFC assay, it was investigated whether the designed biosensor can not only detect clean K48-K63-branched ubiquitin conjugates but also serve as a tool to monitor their synthesis. For this purpose, K63-linked ubiquitin chains were formed enzymatically prior to the measurement, then UBE2K (section 1.1.4.2) was added together with the K63R mutant of ubiquitin to induce branching vie K48. The fluorescence signal generated during chain formation was measured for 5 h (Figure 3.22C). At the same time, to determine the specificity of the sensor system, another sample was measured in which a K63-linked ubiquitin chain out of K48R ubiquitin mutants was prepared beforehand and a K48-linked ubiquitin chain build of K63R ubiquitin mutants was enzymatically formed during the measurement by the K48-specific enzymes Ubc7 and Cue1. Since both chains consist of the mutants excluding branching by the other linkage, a mixture of homotypic chains was formed, to which only one part of the sensor should bind. In addition, a negative control consisting only of the DARPins as well as samples in which clean homotypic K48- or K63-linked ubiquitin chains were enzymatically formed, were measured simultaneously. The detailed composition of all samples is listed in Table 2.10.

The obtained fluorescence curves are depicted in Figure 3.22C. The measured fluorescence intensities of all samples containing only homotypic chains were significantly lower than those of the sample in which K48-K63-branched ubiquitin chain were synthesized. The curve of this sample had a sigmoidal shape: it showed an almost linear increase in the beginning, then the increase became less steep until the curve asymptotically approached an RFU value of about 60,000 - more than 3 times higher than the end points of the homotypic chains. The corresponding ubiquitin blot (Figure 3.22D) showed successful ubiquitin chain formation for all samples. To demonstrate the formation of the specific ubiquitin chains in the respective sample, an UbiCrest assay was employed. In this assay, the K63-linkage-specific DUB AMSH and K48-specific OTUB1 were added to each sample. A decreased signal after digestion indicated the presence of the specific linkage. The UbiCrest assay (Appendix Figure 6.22B) demonstrated by the distinct digestion patterns that the desired ubiquitin chain linkages were formed in each sample.

The measurements proves that the bimolecular DARPin probe specifically detects K48-K63-branched polyubiquitin. It can distinguish between the mixture of homotypic chains and the branched form and can monitor their synthesis *in vitro*. Since there is only one fluorescence signal emitted when branched chains are formed, this tool allows easy measurement and can be very valuable to analyze whether a certain protein is decorated with a K48-K63-linked branch chain or whether an E2 or E3 is able to form branched chains on a substrate.

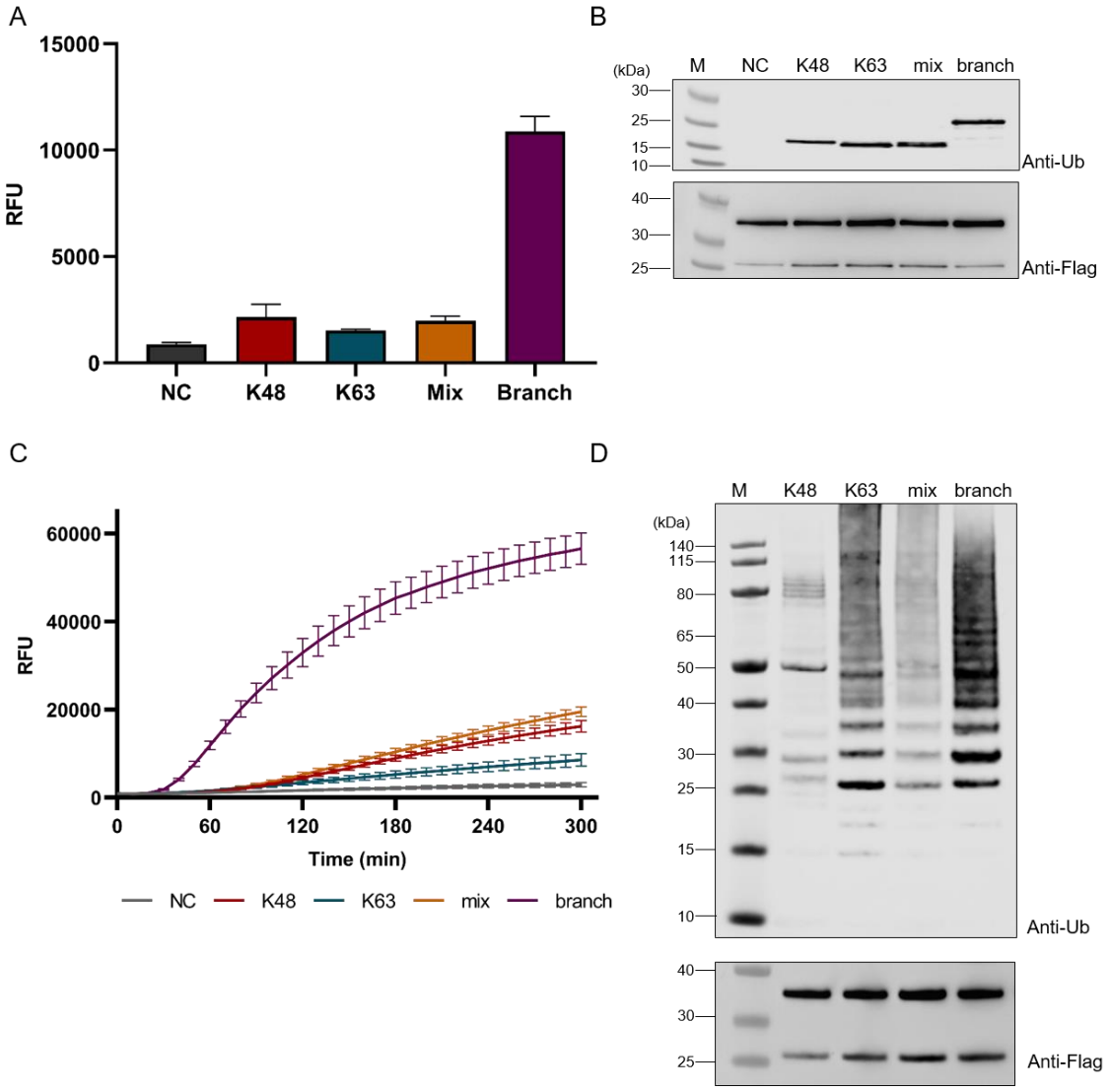

Figure 3.22: The K48-K63-branched chain sensor specifically detects branched ubiquitylation *in vitro*. (A, C) The specificity of the BiFC probes was tested in the context of specifically linked ubiquitin dimers and trimers (A) or ubiquitin chain synthesis (C). 0.25 µM of the nYFP-tagged DARPin K48 A1 and the cYFP-tagged DARPin K63 G1 each were mixed with 1 µM of differently linked ubiquitin constructs (A) or an enzymatic chain reaction forming specifically linked or branched ubiquitin chains (C). The samples of the dimer/trimer measurement (A) were first incubated for 3 h at room temperature before measuring the fluorescence signal, while the fluorescence emissions (EX/EM = 485 nm/ 530 nm) of the samples with the chain reaction (C) was continuously measured every 10 min for 5 h during its incubation at 37°C using the Tecan Spark. The measurements were performed in triplicates, and the results were expressed as mean ± SD in the respective graphs. (B, D) Western blot image of samples taken after the measurement. For each sample, 10 µL (B) or 15 µL (D) were loaded and to confirm equal concentrations. Analysis was done by Western blot against ubiquitin and the Flag-tag of the DARPins. Abbreviations: NC = negative control, EX = excitation wavelength, EM = emission wavelength, SD = standard deviation, RFU= relative fluorescence units.

3.2.5.2 The K48-K63-branched chain sensor was tested *in vivo*

After demonstrating specificity *in vitro*, the K48-K63-branched chain probe was also tested for recognition of K48-K63-branched ubiquitin chains *in vivo*. As demonstrated previously (Figure 3.21) and in agreement with several publications, DNA damage sites are highly ubiquitylated in a K48- or K63-linked manner.[492, 493, 522, 561, 562] Additionally, a recently preprint published on bioRxiv by Lange *et al*. using a branched-chain nanobody showed that branched chains are also found at sites of DNA damage.[220] To investigate whether our BiFC-based K48-K63-branched chain sensor can reproduce these findings, another laser track experiments was performed after expression of the bimolecular probe (nYFP-tagged anit-K48-DARPin A1 and cYFP-tagged anit-K63-DARPin G1) or a negative control in which one part of the bimolecular sensor, here the anti-K48 DARPin A1, was exchanged with the control DARPin E3_5.

In general, the fluorescence signal inside the cells was very low due to the BiFC nature of the probes, so the contrast had to be greatly increased. The laser induced a slight photobleaching, showing that some mature YFP is present in the cell, partly due to spontaneous reassociation, as some signal is also visible in the negative control, but otherwise suggesting the detection of branched chain inside the cell (Figure 3.23). The induced DNA damage along the laser tracks did not cause any change in the fluorescence signal in the negative control sample. In the samples expressing the K48-K63-branched chain probe, some foci formation was observed. However, these were not only present at the sites of DNA damage, but also in the cytosol. A possible explanation could be that the high intensity laser leads to the formation of cytoplasmic aggregates containing branched ubiquitin chains. This will be further investigated by colocalization experiments with respective markers. The foci formed in the nucleus were in the area of the induced DNA damage, but did not completely label it. In other cells, the effect was even weaker (see Appendix Figure 6.23), and only single foci appeared briefly in the course of the live-cell imaging.

In general, this experiment showed that, at least in this setup, the probe did not efficiently detect perhaps very transient branched ubiquitin chains at the DNA damage site. This could be due to the nature of the BiFC, which requires long maturation (about 40 min) before emitting a fluorescence signal, but it could also show that, in contrast to Lange *et al*'s findings, only homotypic but not branched chains are formed in UVA-induced DNA damage.[220] Therefore, further studies need to be performed, maybe also testing a different probe set-up, e.g. based on FRET instead of BiFC detection.

However, this experiment also showed that the K48-K63-branched chain sensor stained foci inside the cell during the time course, suggesting the formation and detection of branched chains. These foci should be examined more closely and further colocalization experiments of the branched ubiquitin chain sensor and e.g. stress granule markers could shed light on the nature of these foci. The probes could then be a valuable tool to further investigate which stressors induce the formation of branched ubiquitin chains in these foci.

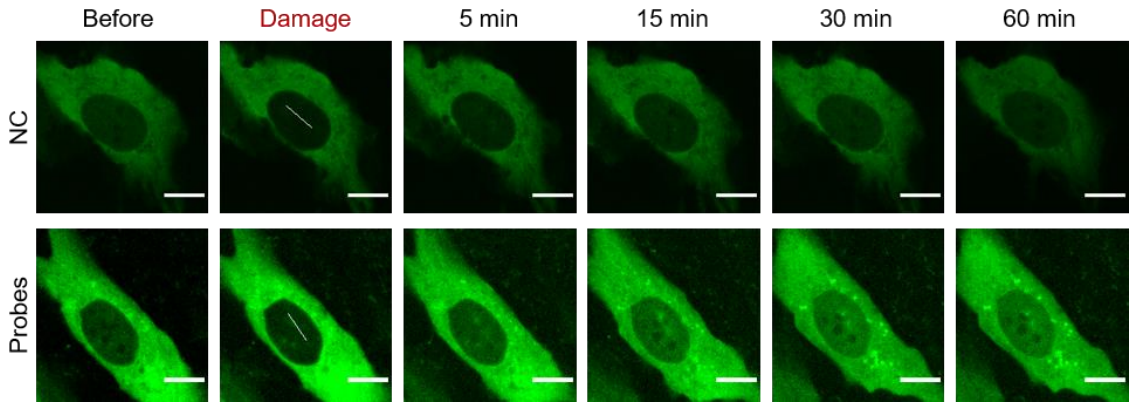

Figure 3.23: The K48-K63-branched chain sensor did not efficiently monitor branched ubiquitylation upon DNA damage. Representative image showing the accumulation of the negative control (nYFP-tagged K48 A1 + c-YFP-tagged E3_5) or K48-K63-branched chain probe (nYFP-tagged K48 A1+and cYFP-tagged K63 G1) respectively at sites of laser-induced DNA damage in RPE-1 cells. Expression of DARPins was induced with 2 ng/µL doxycycline for 24 h. The white line indicates the laser path of the 355 nm laser (50% laser power) and thereby represents the site of DNA damage inside the living cell. Scale bar = 10 µM.

3.3 Discussion

The aim of this project was to create independent affinity probes for the recognition, inhibition, and tracking of linkage-specific ubiquitin signaling using DARPins. These DARPins were raised against dimers of the two most extensively studied ubiquitin linkages, K48 and K63 in collaboration with the Plückthun group in Zürich. In the initial stages of this project, 80 DARPins, received from Zürich, were screened to identify candidates that specifically interacted with the desired linkage. The screening approach consisted of two pull-down steps and identified five specific candidates for both the anti-K48 DARPins and the anti-K63 DARPins (Section 3.2.1).

The following paragraphs will discuss the properties of the anti-K48 and anti-K63 DARPins, particularly their specificity and affinity. Special focus will be given to anti-K48 DARPin A1 and anti-K63 DARPin G1, as these were chosen for usage *in vivo* and thus have been characterized in more detail. Structural insights allow for a correlation between their properties and the binding sites of the DARPins to the respective ubiquitin dimers. The possibility of interference of the DARPins with the endogenous ubiquitin signaling due to their inhibitory effects will be discussed. Potential applications of the characterized DARPins *in vitro* and *in vivo* will be presented, and a comparison with the commercially available tools, particularly the TUBEs, will be provided. Finally, the limitations of the anti-K48 and anti-K63 DARPin system and future perspectives will be outlined.

3.3.1 Properties of the anti-K48 and anti-K63 DARPins

All five selected candidate DARPins for both the K48- and K63-linkage demonstrated high selectivity for the intended ubiquitin linkage in pull-downs *in vitro* (Figure 3.6) and from cell extract (Figure 3.7). The pull-down assays for the anti-K48 DARPins revealed DARPins A1 and E4 as the strongest and most specific binders (Figure 3.6B and 3.7A). Given that anti-K48 DARPin A1 exhibited a slightly reduced inhibitory effect (Figure 3.9A+B), it was selected as candidate for the *in vivo* sensor. For anti-K63 DARPin G1 in addition to its high specificity (Figure 3.6C+D), the mild effect on cell growth after expression (Figure 3.9C+D) was also decisive for its choice as *in vivo* sensor.

3.3.1.1 Properties of anti-K48 DARPin A1

The anti-K48 DARPin A1 has an affinity of 50-80 nM towards its target ubiquitin chains. Thereby, it showed a slightly higher affinity towards K48-linked dimers than tetramers (Table 3.1). This may be attributed to the closed structure of K48-linked ubiquitin chains. In a tetrameric form, the structure is even more compact (Figure 1.8), with the hydrophobic patches being buried. As these patches were shown by the crystal structure (Figure 3.12) to be crucial for interaction, this impedes A1 binding. Nevertheless, the impact was not particularly pronounced, likely due to the oscillation between open and closed forms, as demonstrated for K48-linked chains (Figure 1.8).[483, 484]

The 29-fold preference for K48-linked dimers over K63 and approximately 15,000-fold over monoubiquitin, as measured via SPR (Table 3.1), reflected the high selectivity of A1 observed in the pull-downs *in vitro*, even when confronted with all possible ubiquitin linkages (see Figure 3.10A).

The measured affinities are comparable to those of the corresponding linkage-specific antibody and TUBE, as well as the newly identified high-affinity UBD that interacts with monoubiquitin, with an affinity of 5 nM.[212, 226, 563] The affimers against K6 and K33 have been shown to exhibit stronger affinities in the range of 20-50 pM.[160] However, since the K48-linkage is the most prevalent in mammalian cells, the required affinity of a specific probe is lower compared to noncanonical linkages that are less prevalent. The total concentration of ubiquitin in mammalian cells has been shown to be as high as 85 µM, of which 10-20% of this are present in ubiquitin chains. Of these chains, 50-80% are linked via K48.[96, 106] Therefore, the concentration of K48-linked ubiquitin chains can be estimated to be in the single-digit micromolar range, which is approximately 100-times higher than the affinity of our probe, making it suitable for efficient binding *in vivo*.

This was demonstrated by the strong enrichment of K48-linked polyubiquitin conjugates from cell extract, quantified by mass spectrometry (see Figure 3.11). Two-thirds of the pull-down signal from the anti-K48 DARPin was attributed to K48-linked ubiquitin chains. The remaining third was split between K63, K11, and K6-linked ubiquitin conjugates (Figure 3.11B). This is consistent with previous findings from immunoprecipitation experiments in mammalian cell lines. Valkevich *et al.* found that when using the K48-linkage specific antibody, the immunoprecipitation of high-molecular weight K48-linked ubiquitin conjugates also typically contains K6, K11, and K63-linked conjugates.[190] The high abundance of K63-linked ubiquitin chains may be mainly attributed to the high prevalence of K48-K63-branched ubiquitin chains.[106] As K6-K48- and K11-K48-branched chains have also been identified, this could also provide a possible explanation for their co-precipitation.[187, 192] Another reason could be that, for both of these linkages (K6 and K11), it has been shown that they can adopt a closed conformation.[112] Therefore, the anti-K48 DARPin A1 may have a slight affinity towards these linkages, which was not shown at the dimer level but could be pronounced with longer chains. To investigate this further, the affinity of A1 towards the K11 and K6-linked ubiquitin tetramer could be analyzed by a pull-down approach or even quantified by SPR. However, as this co-immunoprecipitation has also been shown with the K48-linkage specific antibody,[190] and the anti-K48 TUBE even showed far more non-specific binding of these linkages (Figure 3.11), it is more likely that these interactions are mainly attributed to the ubiquitin code itself.

3.3.1.2 Properties of anti-K63 DARPin G1

The anti-K63 DARPin G1 demonstrated an even stronger affinity than the anti-K48 DARPin A1 (Table 3.1) towards the K63-linked tetraubiquitin, with an affinity of 6.9 nM. Consequently, this DARPin also exhibits a similar affinity to that of its respective antibody and TUBE,[75, 212, 227] suggesting that it may also be a promising binder also *in vivo*. G1 exhibited a significant difference in affinities towards K63-linked ubiquitin dimers and tetramers (Table 3.1). This difference in affinities is also evident in the pull-down of the K63-linked ubiquitin chains (Figure 3.6D), where G1 only showed strong binding from tetramers onwards. The reason for this is most likely not the structure of the K63-linked ubiquitin chains, but is caused by the probe itself. In size exclusion runs, G1 has been found to run dimeric (Appendix Figure 6.7). Therefore, the dimeric construct probably can only develop its full affinity when it interacts with K63-linked polyubiquitin constructs longer then tetramers.

At this tetrameric level, G1 exhibited a preference for K63-linked ubiquitin tetramers that was nearly 8,000-fold greater than its preference for K48-linked tetramers (Table 3.1). Moreover, G1 demonstrated a preference for K63 over monoubiquitin that exceeded 6,000-fold. As monoubiquitylated substrates and free ubiquitin constitutes over 80% of the ubiquitin pool,[96] the differentiation between these forms and the desired linkage is crucial for its *in vivo* usage.

Upon examination of binding to all possible ubiquitin dimers, G1 demonstrated the strongest interaction with the K63-linked ubiquitin dimer, while also exhibiting weak binding to dimers linked via K11 and K27 (Figure 3.10B). Given that K27-linked ubiquitin chains are considerably less abundant in mammalian cells, this should not present significant selectivity issues *in vivo*.[96, 97, 106] This was also demonstrated by the mass spectrometry quantification, in which this interaction was not detected (Figure 3.11). In contrast, the slight interaction with K11, as well as K48-linked substrates, was detected by the MS analysis. The results of the mass spectrometry analysis indicate that the preference of G1 for K63- over the K48-linkage can be calculated with a 2.3-fold preference, which is considerably below the measured preferences *in vitro*. It is therefore postulated that a significant proportion of the K48-linked ubiquitin chains precipitated as a consequence of the presence of K48-K63-branched chains, given that approximately 20% of all K63-linked ubiquitin chains are branched with K48.[106] This is also in alignment with previous research, which demonstrated that polyubiquitylated conjugated precipitated from cell extract can be modified by a mixtures of K48, K63, and K11 linkages.[126] Therefore, the K11 and K48 linkages observed in the G1 pull-down sample are likely to be predominantly derived from the ubiquitin landscape within the cell, and do not negate the selectivity of our anti-K63 DARPin, which demonstrated overall a high degree of selectivity.

3.3.1.3 Structural insights explain properties of the DARPins

The basis for the high affinity and specificity of the DARPins was revealed by the crystal structures of the anti-K48 DARPin A1 and the anti-K63 DARPin G1 with their respective ubiquitin dimers (Figure 3.12+3.13). The results demonstrated the presence of multiple interaction sites for both DARPins, with both DARPins exhibiting a strong interaction with the Il44 patches of the two ubiquitin moieties.

In case of the anti-K48 DARPin A1, this interaction is centered on loop 3 of the DARPin, particularly on Trp101 and Leu102. This was demonstrated by the mutation of these residues, which resulted in a complete abolishment of interaction, highlighting its significance not only for selectivity but also for binding (Figure 3.12B). These residues were shown to interact with both Ile44 patches, which are positioned in close proximity only if the ubiquitin dimer is linked via K48 and adopts the closed conformation that is characteristic for this linkage type. Structural alignments of both conformational states of the K48-linkage (Appendix Figure 6.14) validated that the K48-linked ubiquitin dimer bound to the anti-K48 DARPin A1 adopts a conformation related to the closed conformation.

For the anti-K63 DARPin G1, specificity was found to primarily determined by interaction site 1. A mutation of Trp48 in this region demonstrated an enhanced binding (Figure 3.13B), but a loss of its specificity (Appendix Figure 6.13B). Mutations in the other interaction sites of anti-K63 DARPin G1 result in a loss of binding affinity. Therefore, these sites appear to mediate binding to ubiquitin in general (Figure 3.13B and Appendix Figure 6.13B), resulting in the measured high affinity. The loss of interaction observed following the mutation of predominantly Trp residues in both structures indicates that the interactions are primarily based on hydrophobic interactions. This is in consistent with the fact that the majority of ubiquitin recognitions are mediated through its hydrophobic surface patches.[9, 11, 15] Furthermore, this also explains the strong affinity found for both DARPins, as hydrophobic interactions have been shown to often contribute the most to the stability of a protein interaction due to the large surface areas involved and the significant entropic benefits.[564, 565] When combined with salt bridges for stabilization, as it is especially found for the anti-K63 DARPin G1, this results in the strong affinity in the low nanomolar range.

The two crystal structures revealed that the majority of interactions were mediated by loop residues of the DARPins (Figure 3.12 and 3.13), with the last loop in particular containing two out of three identified interaction sites for both DARPins. One site, for G1, the one determining specificity, was located in the first loop. The majority of residues identified important for interaction are situated in positions that were randomized in the library used for the DARPin selection process (Figure 1.11 and Appendix Figure 6.6). For the anti-K48 DARPin A1, only two out of the ten identified interactions were mediated by non-randomized framework residues. This is consistent with the literature, which states that approximately 75% of interactions are mediated by these residues.[256] A sequence alignment for all five chosen anti-K48 and anti-K63 DARPins (see Appendix Figure 6.6A) revealed that their randomizable residues are mainly composed of hydrophobic residues, indicating that also their specific binding to ubiquitin is mainly based on hydrophobic interactions. Especially, within the last loop and the C-Cap, which was shown to mediate the main interaction for both DARPins, a high degree of conservation of hydrophobic residues was observed among all 10 selective DARPins. The sequences of the anti-K63 DARPins revealed the presence of more charged residues (Appendix Figure 6.6C), suggesting the formation of additional salt bridges.

This comparison demonstrated that, despite having used a completely unbiased approach, hydrophobic interactions utilizing the same patches as those utilized by natural occurring UBDs provide the most specific interactions with ubiquitin. This suggests that it is difficult to develop a specific probe that is independent of these features and, consequently will not interact with the same patches also used by its natural writers, readers, and erasers.

3.3.2 Interference of the DARPins with ubiquitin signaling

As the DARPins were employed *in vivo*, it was important to investigate their impact on ubiquitin chain conjugation and deconjugation in order to estimate its effect on ubiquitin signaling and to potentially adjust experimental conditions to prevent the distortion of *in vivo* processes. The FRET-based assays to study the effect of the DARPins on ubiquitin conjugation and deconjugation revealed that all DARPins that also bound ubiquitin chains- i.e. excluding anti-K48 DARPins G2 and A4 - exhibited some inhibitory effect of ubiquitin chain conjugation and deconjugation. This indicated that they all appear to impede the binding of the conjugation and deconjugation machinery to some extent (Figure 3.5A and 3.8A+B).

There are two possible explanations for this. All the writers used in this study have been shown to interact with the Ile44 patch (Figure 1.5).[28, 40, 41, 45] As demonstrated by the crystal structures of anti-K48 DARPin A1 and anti-K63-DARPin G1, and proposed for all the other DARPins based on the sequence alignment, this patch on both the distal and proximal ubiquitin is also crucial for the interaction of the DARPins. Consequently, an allosteric competition for this patch is expected.

The second effect that is likely contributing to the inhibitory effect is steric hindrance, whereby not necessarily the direct binding site but the whole positioning and excess of the enzyme to ubiquitin is blocked by the DARPin. To further investigate this, the structures of the linkage-specific E2s and DUBs used in the FRET assays were overlaid with those of the DARPins in complex with the respective diubiquitin (Appendix Figures 6.15 and 6.16). For the K63-specific ubiquitin system, the crystal structure of Ubc13 and Mms2 in complex with the distal ubiquitin (PDB: 2GMI) was utilized and revealed that anti-K63 DARPin G1 and Mms2 exhibit a high degree of overlap and utilize similar binding sites including the Ile44patch on the proximal ubiquitin, thereby blocking excess for the respective other protein (Appendix Figure 6.16A). This observation explains the inhibitory effect monitored for G1 on chain conjugation (Figure 3.8C). In the case of the K48-specific system, no crystal structure of Ubc7 in complex with ubiquitin is available. Therefore, ColabFold was queried with the sequences of Ubc7 (PDB: 2UCZ) and ubiquitin (PDB: 1UBQ) and the interaction was predicted with AlphaFold2-Multimere.[566, 567] The models exhibit minimal predicted alignment error (pAE) throughout, with a minor exception in a local region around position 100 (Appendix Figure 6.15C). This suggests correct packaging of both proteins in complex, and therefore the interaction predicted by the AlphaFold modeling can be considered accurate. The model proposed that Ubc7 exhibited a strong interaction with the Ile44 patch. Furthermore, the overlay with the crystal structure of anti-K48 DARPin A1 demonstrated that the interaction sites, particularly those on the distal ubiquitin, were in competition. Overall the position of the anti-K48 DARPin A1 and Ubc7 were nearly identical, indicating a high steric hindrance and explaining the strong inhibitory effect overserved (Appendix Figure 6.15A and Figure 3.8A).

It is likely that steric hindrance is also the primary reason why the DARPins also block deconjugation to some extent as for example, AMSH was shown to not rely on Ile44 interaction but more strongly uses the Ile36 patch, thereby reducing the possibility of an allosteric inhibition. The overlay of the anti- K48 DARPin A1 with its respective DUB OTUB1 in complex with diubiquitin demonstrated a notable overlap, particularly of the C-terminal region of A1, which sterically hinders simultaneous binding of OTUB1 (Appendix Figure 6.15B).

In the case of the anti-K63 DARPin G1, the overlay was less definitive, due to the differing orientations of the K63-linked ubiquitin dimers in the two crystal structures used for the overlay. Consequently, the proximal ubiquitins are positioned differently, making a direct comparison difficult. However, it is notable that the last loop of the DARPin G1 and AMSH appear to sterically block each other (Appendix Figure 6.16B). A comparison of the overlays of the E2 and the DUB for both DARPins reveals that the region of interaction and positioning is more similar for the DARPins and E2s than for the DUB. This may explain the stronger inhibition of the conjugation reaction than the deconjugation.

Nevertheless, despite the crystal structures demonstrating robust allosteric and steric inhibition, both ubiquitin chain conjugation and deconjugation were reduced, but by far not completely abolished, even though the DARPins were pre-incubated with the samples. One explanation for this observation is a low dissociation time (k_{off}) of the DARPins, which allows for a rapid exchange between binding partners. This low k_{off} of anti-K48 DARPin A1 was demonstrated using the CAP-chip approach on the SPR (Appendix Figure 6.11E). For the anti-K63 DARPins G1 only the affinity itself has been measured so far. To gain further insights into the dynamics of the interaction, it would thus be beneficial to measure the association and dissociation times. Given the dynamic nature of the system, a concentration-dependent effect is expected, which was demonstrated for both DARPin variants and both reactions (Figure 3.14). The FRET-based assays enabled the determination of IC_{50} values, which were calculated in the micromolar range for both DARPins and both reactions. These IC_{50} values are in the range of the K_D values of E1, which was shown to be approximately 10 µM,[568] while for Mms2 and Cue1 affinities of approximately 100 µM have been determined.[69, 569] Additionally, the affinities of DUBs were also found in a similar range,[226, 570, 571] indicating a competitive relationship between the DARPins and the writers or erasers of ubiquitin chains. Consequently, to ensure ubiquitin chain signaling *in vivo*, the DARPin concentrations should be maintained below these values to enable binding of E1 and DUBs. As the measured K_Ds of both DARPins are 20-fold for anti-K48 DARPin A1 or even 500-fold for anti-K63 DARPin G1 lower than their IC_{50} values, a concentration between these two values ensures a good affinity combined with a still low inhibitory effect.

The IC_{50} values showed that the effect of both DARPins on the deconjugation reaction was more pronounced than on the conjugation reaction. This suggests that the DARPins may function as molecular traps, stabilizing specifically linked ubiquitin chains in the cellular environment by shielding them from deconjugation while allowing conjugation to occur more efficiently. This could be advantageous for the detection of rare ubiquitylation events. Nevertheless, given that there are additional writers and erasers of this specific linkage or of ubiquitin chains in general, including unspecific DUBs, further studies, such as the repetition of the inhibition analysis with these other writers and erasers, are needed to clarify this conclusively. One initial indication of this molecular trap property is that, following the expression of anti-K48 DARPin A1, an accumulation of ubiquitin chains was observed in yeast cells, and to a lesser extent in mammalian cells, in comparison to cells expressing the negative control DARPin E3_5 (Appendix Figure 6.4).

This demonstrated that the inhibitory effect also translates to the cell environment, if this also has effects on the whole cell and thus cell survival was investigated for yeast and mammalian cells with spot and colony formation assay, respectively.

In budding yeast, the inhibitory effect was comparable in strength for all anti-K48 DARPins and only detectable following stress (Figure 3.9A), whereas in mammalian cells, an effect for the most strongest binders, A1 and E4, was also observed under unperturbed conditions (Figure 3.9B). Given that no significant effect was observed when comparing the effect of expression of A1 and E3_5, it can be concluded that a significant portion of the effect of A1 in unperturbed mammalian cells can be attributed to general expression conditions (Figure 3.9A+B). Consequently, A1 was preferred over E4. The anti-K48 DARPins C3, H1, and H3 demonstrated no significant effect, even when compared to their uninduced conditions. Therefore, they may be beneficial for approaches that monitor the dynamic of chain formation over an extended period and can accommodate for their reduced selectivity. The expression of any anti-K63 DARPin did not result in an observable growth defects in unperturbed yeast or mammalian cells. Only under conditions of DNA damage an inhibitory effect was observed for some DARPins. A comparison of the effects of the anti-K63 DARPins in all these *in vivo* assays revealed that cells expressing anti-K63 DARPin G1 exhibited the least sensitivity (Figure 3.9C).

Overall, the experiments demonstrated that all specific DARPins can impede ubiquitin chain conjugation and deconjugation due to allosteric and steric hindrance. This can influence ubiquitin levels or cell growth, particularly when used under stress conditions or for an extended period. However, as this inhibitory effect is concentration-dependent, a system that allows for the control of expression levels to a range below the IC_{50} values can diminish this effect. Consequently, inducible systems for yeast and mammalian cells were developed. In theory, the expression level of the DARPins in the doxycycline-inducible mammalian cell lines with the Tet-ON system can be controlled by titrating the added doxycycline. However, laboratory experiments conducted during Philipp Elleringmann's master's thesis demonstrated that as little as 1 ng/mL of doxycycline was sufficient to induce expression.[482] This induction did not significantly change with increasing concentrations up to 2 µg/mL doxycycline. Consequently, the RPE1 cells with integrated DARPins exhibited characteristics more like an on-off system than a titratable system in our hands. Therefore, we chose to maintain low levels of DARPins by keeping the expression duration as brief as feasible, rather than modifying the expression concentration. This approach proved effective in the experiments conducted in this study. However, in the long term, other expression systems, such as the ecdysone or glucocorticoid-inducible system, could be tested to determine if they offer superior titratability and thus finer DARPin expression regulation.[572–574]

3.3.3 The DARPins are versatile tools

The function-topology relationship of linkage-specific ubiquitin signaling is still not completely understood. A main portion of linkage-specific ubiquitin analysis continues to rely on *in vitro* techniques, such as mass spectrometry approaches. However, the majority of proteomics data only provide a steady-state snapshot of the ubiquitylation status, but lacks information regarding relative abundance or the dynamic of a process.[21] In recent years, more and more linkage-specific tools have been developed, including linkage-specific antibodies, nanobodies, affimeres, TUBEs, and other UBD based tools.[75, 160, 212, 219, 220, 227, 228, 233, 237] With the exception of the antibodies, these linkage-specific tools can also be used *in vivo*, which has led to valuable insights into the prevalence and importance of certain ubiquitin linkages.

However, for the two most studied linkages, K48 and K63, an independent tool was still lacking that could be used *in vitro*, but especially *in vivo* as a biosensor for monitoring the diverse processes these linkages were associated with. This gap was sought to be filled by the here characterized anti-K48 and anti-K63 DARPins. The following sections describe the versatile applications of the DARPins *in vitro* and *in vivo* and the following chapter will present a comparison with the existing technologies, with a particular focus on the anti-K48 and anti-K63 TUBEs.

3.3.3.1 *In vitro* applications of the DARPins

In vitro, the primary application of the five characterized anti-K48 and anti-K63 DARPins is to specifically pull-down polyubiquitin chains linked via K48 or K63, respectively. This includes purified or enzymatically created ubiquitin chains (Figure 3.6), as well as ubiquitylated conjugates from cell lysate from different species (Figure 3.7 and Appendix Figure 6.8). Moreover, it has been demonstrated that purified DARPins (Figure 3.7) as well as DARPins expressed within the cell (Appendix Figure 6.4) can be utilized. As the characterized DARPins exhibited varying affinities, selectivities, and inhibitory effects, this diverse array of DARPins offers a valuable tool set for users which can be used depending on the desired application. For instance, as previously outlined, anti-K48 DARPin A1, and E4 to a lesser extent, was demonstrated to enrich K48-linked ubiquitin chains, thereby enabling the stabilization of the otherwise transient K48-linked ubiquitin signal. This may facilitate the identification of rare ubiquitylation events.

The pull-down can be analyzed using Western blotting or, for a more quantitative approach, mass spectrometry. As pull-downs using the DARPins already efficiently enriches the specifically linked ubiquitin signal, the tedious and expensive GlyGly-enrichment step can be omitted. The DARPins enables the isolation of a large fraction of K48- or K63-linked ubiquitin chains from cell extracts (Figure 3.11). In this work, we just studied the distribution of linkages to investigate the specificity of our probes. However, this methodology can also be utilized to examine the biological relevance of linkage-specific ubiquitylation of certain proteins in a specific context, such as exposure to a particular stressor. Furthermore, this approach can be employed to identify substrates of specific writers or erasers by comparing a wild-type strain with a knock-out/down strain. Additionally, it can be utilized to identify the interactome of a specifically ubiquitylated protein. For all of these approaches, the protocol used here provides a solid foundation but may need to be adapted in certain instances.

Additionally, it was investigated whether the DARPins could be used as conventional antibodies for the detection of linkage-specific ubiquitin chains on a Western blot. To achieve this, biotinylated DARPins were created and incubated with a blot containing varying amounts of purified ubiquitin dimers linked via M1, K48 or K63 (Appendix Figure 6.19). No K48-linked ubiquitin dimer was detected with the biotinylated anti-K48 DARPin A1, even at the highest concentration tested (1 µg). However, this was also the case with the K48-linkage-specific antibody, which has a claimed detection limit of 300 ng,[575] highlighting the need for a new, reliable K48-linkage specific detection probe. Only the general ubiquitin antibody P4D1 was able to detect the ubiquitin signal, but as previously published, it demonstrated a stronger affinity to K63-linked chains compared to K48-linked chains.[481] The lack of interaction between the anti-K48 DARPin and the K48-linked ubiquitin dimer may be attributed to the denaturing process during Western blotting, which disrupts the folding of ubiquitin chains. As the anti-K48 DARPin A1 was demonstrated to recognize the fold of the K48-linked dimer, rather than the linkage itself (Figure 3.12), it is possible that this denaturation results in the DARPin losing its interaction site and thus its affinity. Whether this hypothesis is accurate, has to be further evaluated. Conversely, technical issues may also have contributed to this outcome. Thus, it could be beneficial to test optimized blotting conditions for ubiquitin or to test a DARPin directly coupled to a fluorophore or HRP.[576]

3.3.3.2 DARPins as tools for monitoring proteostasis

To employ the DARPins as biosensors *in vivo*, inducible expression systems were created in yeast and mammalian cells (Figure 3.15). To assess the specificity of our probes *in vivo*, colocalization experiments were conducted using the anti-K48 DARPin A1 and anti-K63 DARPin G1 and the respective linkage-specific antibody. The observed signal patterns for the linkage-specific antibodies and the respective DARPins in cells subjected to heat stress were found to be congruent, thereby demonstrating the specificity of our probes (Figure 3.16).

As K48-linked ubiquitin chains primarily function in proteasomal signaling,[116, 117] the colocalization of the anti-K48 DARPin A1 with an antibody against a proteasomal subunit (PSMB5) was investigated under proteotoxic stress induced by heat stress. Both channels demonstrated foci formation, with some overlap between the signal of the anti-K48 DARPin A1 and proteasome foci (Figure 3.17). However, a considerable proportion of these foci lacked colocalization, indicating that upon heat stress, distinct structures are formed in which K48-linked ubiquitin chains are present, but not proteasomes, and *vice versa*. This observation may be attributed to the kind of foci, as various different proteasomal foci have been found to be induced upon heat stress, which are localized and composed differently. The levels and types of ubiquitin also vary between different kinds of stress-induced granules, as well as within a single family of stress-induced granules.[510, 521] Conversely, it has been demonstrated that p62 foci, which are frequently formed in the nucleus in response to heat stress and are often associated with ubiquitin, which is linked via K48, but only with orphan proteasomal subunits, including PSME1-3, rather than the PSMB5 used in this study.[510, 577, 578] Thus, the nuclear foci observed with the anti-K48 DARPin A1 antibody but not with the PDMB5 antibody (Figure 3.17) could reflect these p62 granules. Overall, there is a wide variety of granules with different compositions formed upon heat stress. This is reflected in the detection of different granules by different antibodies, and, in this case, the specific anti-K48 DARPin A1, explaining the only partially overlapping signal. Nevertheless, the colocalization of proteasomal subunits and K48-linked ubiquitin chains suggests the involvement of proteasomal degradation in some granules.

Further studies on temporal dynamics and colocalization experiments with different granule markers could provide more insight into the diverse nature of granules and their ubiquitin involvement. One type of granules for which an involvement of K48-linked ubiquitin chains was already quantified are stress granules.[521] Therefore, we sought to utilize this system to test the specificity of our DARPins and aimed on further expanding the biological understanding of these structures by studying the dynamics and timely impact on K48- and K63-linked ubiquitin chains in greater detail.

Despite the use of various stressors, treatment, and detection methods, no or only infrequent foci of the stress granule marker G3BP1 were observed in the RPE-1 cell lines (Figure 3.18A). A direct comparison revealed that this phenomenon was attributable to the cell line and potentially related to its nature, as it was not derived from cancerous cells (Appendix Figure 6.20A). In collaboration with Nazife Tolay (Buchberger lab, University of Würzburg), the experiment was repeated using DARPin-expressing HeLa cells. This resulted in a partial colocalization, particularly for the anti-K48 DARPin A1 (Figure 3.18B), which demonstrated the utility of the DARPins for this purpose. The degree of overlap was not quantified, but appeared to be less than the 10% level observed with the linkage-specific antibody.[521] It can be postulated that this discrepancy may be attributed to the inhibitory effect of the DARPins or a possible interference with aggregation, given that the DARPins were present before and during stress granule formation, in contrast to the antibody, which was only added after fixation. Nevertheless, a direct comparison and quantification would be necessary to allow for more precise conclusions. Should the inhibitory hypothesis be validated, a shorter expression time of the DARPins should be evaluated. Once these questions have been resolved, it would be possible to monitor the dynamics of linkage-specific ubiquitin chains during the stress granule build-up and resolution using the DARPins. This would advance the understanding gained from antibody detection in fixed cells. In order to achieve this, a new HeLa cell line containing a mCherry-tagged G3BP1, which was created by Philipp Schönberger in our laboratory, will be combined with the inducible DARPin system to enable live-cell imaging. This approach could prove useful for visualizing the role of specifically linked ubiquitin chains in the process of stress granule formation and deconjugation, as well as for differentiating the roles of different linkages in this process.

As only a portion of the heat-stress-induced foci in mammalian cells stained with the DARPins appeared to originate from stress granules, colocalization with another LLPS compartment was investigated: aggresomes. Aggresomes are perinuclear inclusion bodies that are formed in response to the accumulation of misfolded or aggregated proteins. They have been associated with the switch from the ubiquitin-proteasome system (UPS) to autophagy and were shown to contain a high amount of ubiquitylated proteins, linked via K48, but also contain K63-linked ubiquitin chains.[539–541, 545–548] Colocalization experiments revealed a notable overlap of the aggresomal signal from thioflavin S, ubiquitin, and the linkage-specific DARPins. Anti-K48 DARPin A1 exhibited nearly a complete colocalization with aggresomes, whereas anti-K63 DARPin G1 demonstrated partial colocalization with thioflavin S-positive sites, consistent with the lower prevalence of K63-linked ubiquitin chains in aggresomes.

The colocalization of the DARPins with specific stress granule markers was also tested for *S. cerevisiae*, for which even less is known than about stress granule composition in mammalian cells. A variety of stressors and detection methods were employed, yet the formation of rare foci and the colocalization with the fluorophore-tagged DARPins were observed with great infrequency (Figure 3.19).

The presence of a strong background signal further complicated the quantification process, indicating that the DARPins are not optimal for detecting rear colocalization events that result only in a weak accumulation of ubiquitin chains in smaller species like yeast due to the lack of resolution.

A notable observation that was made in all these experiments was that upon induction of LLPS both by heat stress and proteasome inhibition, the anti-K63 DARPin G1 stained foci in the nucleus. The foci exhibited partial overlap with the signal of ubiquitin, weak overlap with the K63-linkage-specific antibody, and no overlap with the staining of stress granules or aggresomes (Figure 3.16B, 3.18, and 3.20). As the K63-specific antibody has been shown to give a relatively weak signal in our hands, also in processes in which K63-linked ubiquitin chains have been observed previously, this might suggest that the anti-K63 DARPin G1 may be more sensitive at detecting processes within the nucleus than the antibody. However, further colocalization experiments with different markers are necessary to elucidate the nature of these foci and to exclude the possibility that they are aggregates of the DARPin itself. It is conceivable that the K63-linked ubiquitin chains may mark DNA damage sites, which are highly K63-ubiquitylated, or may indicate sites of transcription regulation or other nuclear stress granules, with which K63-linked ubiquitin chains have been associated.[522, 546, 579, 580]

The colocalization experiments conducted so far have demonstrated that the linkage-specific DARPins can be employed in the detection of ubiquitin chains in LLPS compartments formed upon cell stress in mammalian cells. They have a comparable detection specificity to that of the linkage-specific antibodies and thus can be utilized to gain further insight into the diverse composition of the various forms of LLPS.

Furthermore, the DARPins are suitable for live-cell imaging. Thus, colocalization experiment with a flourophore-tagged marker of the investigated membrane-less compartments allows monitoring of the dynamics of specifically linked ubiquitin chains in these departments. This is currently not possible in real time. This would simplify the investigation of these processes and could help to answer questions regarding a possible function of the specifically linked ubiquitin chains inside this foci. It is still not fully understood whether these ubiquitin conjugates are just carried along by proteins aggregating in these compartments or whether these are mainly active sites of ubiquitylation and deconjugation. Ubiquitylation could either promote aggregation or lead to the resolution of these structures. The literature contains evidence of different functions for ubiquitin chains in LLPSs, and it is therefore unlikely that K48- or K63-linked chains will have a single function in all these structures.[510, 521, 546, 581–584] It is more probable that they will have multiple functions that will differ between different LLPSs. To distinguish and further investigate the functions of K48- and K63-linked ubiquitin chains, the linkage-specific DARPins could thus be a valuable tool.

3.3.3.3 DARPins as tools for studying DNA damage response

To investigate the usability of the linkage-specific DARPins as live-cell probes, microirradiation was employed to introduce spatially and temporally defined DNA damage sites. Both DARPins exhibited strong colocalization at the induced focal sites, which reflected the known involvement of their respective ubiquitin chains in DNA damage (Figure 3.21).[127–129, 492, 493, 496, 497, 522, 553–555]

This demonstrated the usability of the linkage-specific DARPins as biosensors *in vivo*, even in a complex spatio-temporal dynamic setting such as DNA damage and repair. The experiment also demonstrated the mobility of the DARPin probes, as evidenced by the replenishment of the nuclear pool following photobleaching. This proves that the DARPins are capable of freely moving between the cytosol and the nucleus, thus allowing for the visualization of processes in both compartments.

The results are in agreement with previously conducted studies that have investigated the recruitment of K48- and K63-linked ubiquitin chains to laser tracks by immunostaining at different time points after damage with linkage-specific antibodies. [492–494] A study by Feng and Chen found a strong accumulation of both antibodies to the laser stripes 5 minutes after damage,[494] which is consistent with our data (Figure 3.21). As a signal by the linkage-specific DARPins for both ubiquitin chain types also began to emerge within less than five minutes, it can be concluded that the DARPins did not significantly inhibit or decelerate chain formation at damage sites. It was demonstrated that K48-linked ubiquitylation at damage sites peaks at 15-30 min and subsequently decreases sharply within the next hour, with complete disappearance after 1-2 h. In contrast, K63-linked ubiquitylation was shown to peak 1 h after damage induction and persisted for at least 4 h. [492–494] Therefore, a time course exceeding the 30-minute duration should be considered to permit direct comparison and investigate the extent to which the inhibitory effect observed for the DARPins *in vitro* translates to this process, and whether it affects the resolution of the ubiquitin signaling. Depending on these results, live-cell imaging using the DARPins could elucidate the temporal involvement of K48- and K63-linked ubiquitin chains in damage resolution.

By employing UBD-based probes another recent study by Qin *et al.* observed differing dynamics in ubiquitin chain recruitment to DNA damage sites. The study observed that K48-linked ubiquitin chains appeared to be recruited to DNA damage sites at a faster rate (half-time ~17 s) than K63-linked chains (half-time ~30 s). Furthermore, they observed a decrease in the K48-linked ubiquitin signal after 30 min. This could be interpreted as a first hint that our anti-K48 DARPin A1 protects K48-linked ubiquitin chains against DUB cleavage to a certain extent as shown *in vitro* (compare Figure 3.8, Table 3.2), thus prolonging the signal. However, another reason for the different observations could be the different set-ups, especially regarding that their study utilized a distinct laser wavelength of 561 nm, which has been demonstrated to induce oxidative DNA damage, predominantly leading to single-strand breaks and initiating BER. In contrast, the laser utilized in our set-up with a wavelength of 355 nm primarily induces photodamage, which is primarily repaired by NER.[549, 585–588] Thus, the disparate ubiquitylation dynamics observed could be a result of studying different DNA damage pathways. Therefore, it would be of interest to compare the dynamics at DNA damage sites introduced by different wavelengths, site by site, with the antibodies and the DARPins.

It can be summarized that the timely involvement as well as the functions of K48-and K63-linked ubiquitin chains in different DDR pathways are not fully understood yet. As the linkage-specific DARPins have been demonstrated to detect specifically linked ubiquitin chains *in vivo* in time and space, they could prove to be a valuable tool for further investigations. Nevertheless, the applicability of the DARPins in live-cell imaging for the monitoring of the recruitment and resolution of K48- or K63-linked polyubiquitin chains is not limited to laser tracks. Rather, it can also be applied to stress granules, aggresomes, and essentially any spatially distinguishable structure. Moreover, the DARPins can be employed in live-cell imaging to investigate non-separated processes by monitoring colocalization with an appropriate marker protein, thus helping to decipher the ubiquitin code in many different contexts.

3.3.3.4 Applications of the K48-K63-branched chain sensor

Although studies have shown that branched ubiquitin chains make up 5-20% of polymeric ubiquitin chains in mammalian cells,[106] the physiological roles of branched ubiquitin chains have long been poorly understood due to a lack of appropriate tools and methodologies.[184, 187, 188] A linkage-specific antibody is available for K11-K48-branched ubiquitin chains, which has enabled their specific detection and yielded significant insights.[186] However, for other branched chains, detection still primarily relies on sophisticated mass spectrometry approaches, which also encounter limitations at certain branching points (see section 1.1.8.2). Alternatively, linkage-specific antibodies, TUBEs, or the expression of ubiquitin mutants in cells can be employed. Consequently, the development of a K48-K63-branched ubiquitin sensor could potentially provide valuable insights into this linkage. A recently published preprint by Lange *et al*. presented a new detection tool for branched chains in the form of a K48-K63-branch-specific nanobody. The nanobody exhibits picomolar affinity and has been shown to directly interact with the branching point of the branched chain, i.e. the ubiquitin moiety, which is linked to two ubiquitins.

We chose a different design approach and combined the anti-K48 and anti-K63 DARPin A1 and G1, each recognizing one branch of the branched ubiquitin chains. This resulted in the creation of a bimolecular K48-K63-branched ubiquitin chains sensor. In addition, the detection system differs. While the nanobody was equipped with a detector element (i.e., a fluorescent dye) that consistently produces a measurable signal, a BiFC approach was employed for our probe, which only emits a signal upon target recognition. Therefore each DARPin fused to a part of mVenus and the system was first evaluated with *in vitro* experiments. These demonstrated that the branched-chain probe can bind branched K48-K63-linked polyubiquitin, both pre-made as well as monitoring their synthesis, with high affinity and selectivity. Thereby it exhibiting minimal background binding to homogeneous chains or a mixture of both K48- and K63-linked ubiquitin chains (Figure 3.22). It is important to note that due to the long maturation time of the complemented fluorophore, the signal was observed to be delayed. Even for the purified dimers and trimers, an increase in signal was visible for up to three hours (data not shown). Consequently, the samples were incubated for three hours prior to measurement, in accordance with previous BiFC experiments.[233] A control that has not yet been included is a heterogenous K48-K63-mixed ubiquitin chain. As this also allows avidity binding of both DARPins, it is thought to also deliver a signal. However, this signal may be reduced in comparison to branched ubiquitin chains, as in these the local ubiquitin concentration is higher and it potentially provides more possible binding sites for the two DARPins, which brings them close enough to allow refolding.[188] However, it is important to mention that it has not yet been conclusively clarified whether mixed or branched chains result in disparate outcomes for proteins inside cells. Therefore, further investigations are required to elucidate the biological differences between these chains. Thus far, the distinct architecture that results in a positive BiFC signal by the presented probe can be validated through a subsequent step involving UbiCrest (Appendix Figure 6.22B) or MS analysis.

To the best of my knowledge, the developed bimolecular K48-K63-branched chain sensor represents the first tool utilized for the detection of K48-K63-branched ubiquitin chains *in vitro*. It is anticipated that this tool will prove beneficial for the study of protein decorated with a K48-K63-linked branched chain. The spectrometry assay can also be used to assess the ability of an E2 or E3 to form K48-K63-branched chains. The BiFC assay offers a low background approach with an easy readout, making it suitable for high-throughput screening of different E2/E3s for this function. This approach could facilitate the identification of candidates that possess this function in various pathways, as despite the high prevalence of these chains, few writers of this code have been identified to date.

The K48-K63-branched chain nanobody was employed in pull-down approaches to isolate K48-K63-branched ubiquitin chains from cell lysates.[220] A pull-down approach was also evaluated for our set-up. However, even though stated differently in the manual,[589] the Chromotek GFP-Trap also bound the fragmented mVenus halfs, thus enriching not only branched chains but also homogeneous K48- or K63-linked chains (Appendix Figure 6.19B). Therefore this approach was no longer pursued

The K48-K63-branched nanobody was employed as a biosensor *in vivo* to visualize the involvement of K48-K63-branched ubiquitin chains at DNA damage sites induced by microradiation (355 nm). The authors to detected a rapid recruitment (less than 2 min) of the nanobody to sites of DNA damage.[220] Therefore, a microirradiation assay was used for testing our K48-K63-branched sensor on DARPin basis *in vivo*. In contrast to the findings of Lange *et al.*, no localization of the probe to damage sites was visible over the course of 60 min (Figure 3.22). Only a few bright, predominantly cytoplasmic foci were observed. These could be aggregates, such as aggresomes or stress granules, induced by the stress caused by the laser. To elucidate the origin of these foci, colocalization experiments with respective markers would be beneficial and could provide new insights into the biological function of K48-K63-branched ubiquitin chains, which so far have not been found to be directly involved in these types of aggregates. As a first attempt, colocalization with mCherry-tagged G3B1 will be tested.

Our findings could suggest that in contrast to Lange *et al*'s findings, only homotypic but not branched chains are formed in UVA-induced DNA damage.[220] However, a more likely reason for the lack of detection at DNA damage sites could be the delayed emission of a flourescence signal of the probes, as the reassociated mVenus has to mature first, which requires about 40 min.[590] In contrast, the branched ubiquitin chain signal may be very transient, as it has been shown that K48-K63-branched ubiquitin chains are associated with proteasomal degradation.[195] This transient nature of the branched chains was also underscored by Lange *et al.*, who could only capture the branched chains in pull-downs after p97 inhibition and who observed that the nanobody signal at laser stripes already declined after 10 minutes.[220] Although it has been demonstrated that for some BiFC approaches a signal was also detectable within minutes,[233] it is possible that its full strength has not yet been reached due to the incomplete maturation of the signal, which makes it challenging to detect. If the formation of the BiFC complexes is reversible, as has been shown under certain conditions *in vivo*,[591] the signal may therefore never be detectable as the half-live of the ubiquitin chain could be shorter than the maturation time of mVenus. Even if the reassociation of the Venus fragments is irreversible, as has been shown *in vitro* due to the enormous stabilization of the BiFC complex[557, 558], the probe may still lose its binding scaffold through proteasomal degradation and thus no longer accumulate at one site. An indication for this could be the overall increasing fluorescence intensity in the nucleus. However, further studies are needed to evaluate this hypothesis.

Should the BiFC approach, particularly due to its long maturation period, prove unsuccessful in detecting signals at DNA damage sites or at other known pathways with which K48-K63-branched chains have been associated, a different probe setup could be tested. One possibility would be to switch the system from a detection method based on BiFC to a FRET-based approach. Förster resonance energy transfer (FRET) is a widely employed method for the detection and localization of protein-protein interaction sites *in vivo*.[592] It could be readily adapted to our K48-K63-branched chain sensor, as the DARPin could be tagged with one FRET fluorophore each, thus only the mechanism of fluorescent signal generation would differ from the BiFC approach. In contrast to the BiFC analysis, there is no discernible delay between the molecular detection step and the emission of the fluorescent signal. Together with the reversible nature of the fluorophore interaction, this allows for the instantaneous real-time monitoring of changes in protein interactions or in our set-up the monitoring of K48-K63-branched chain formation and deconjugation, provided that the DARPins do not shield deconjugation.[234, 590, 592, 593] The FRET approach might even allow further insights into the chain architecture of branched chains, such as the order in which the chains were built. As a single fluorophore could detect the homologous chains, and an occurring FRET signal would then indicate the conjugation of the other linkage on top of this already existing chain. The extent to which this detection could be differentiated *in vivo* remains to be determined.

However, the FRET approach also has some disadvantages in comparison to BiFC. The primary reason for selecting the BiFC approach in the first place was the low background signal, which would be significantly higher for a FRET-based approach as upon excitation the donor fluorophore produces a high amount of fluorescence itself. Thus, appropriate controls must be implemented to quantify the change in fluorescence intensity in the presence versus the absence of energy transfer between fluorophores. This property renders it challenging to detect weak interactions. In contrast, the formation of highly stable BiFC complexes can trap weak protein interactions, thus making them detectable. Furthermore, the FRET system necessitates the use of two fluorophores, which limits the available channels for colocalization experiments of the branched chains with a specific target. This limitation can be circumvented by employing the BiFC approach. Consequently, depending on the anticipated longevity of K48-K63-branched ubiquitin chains and the necessity for colocalization experiments, the FRET system or the BiFC approach may be advantageous and should be tested.[234, 593]

It can be concluded that the developed K48-K63-branched chain sensor based on a BiFC system is not optimal for visualizing transient events such as the build-up and resolution of K48-K63-branched ubiquitin chains in DNA damage seems to be. However, as non-proteolytic functions of K48-K63-branched ubiquitin chains have also been shown,[106] the signal must not be this transient in all pathways. Consequently, other processes, such as granular formation, will be investigated as this could also explain the foci formed during the microirradiation experiments. Furthermore, inhibiting or delaying the degradation of branched ubiquitin chains by inhibiting p97 or their respective DUB could enable detection. Another approach would be to fuse the linkage-specific DARPins with FRET pairs, which would allow for real-time monitoring and maybe even insights into the chain architecture. For now, the principal advantage of the developed BiFC-based K48-K63-branched ubiquitin chain sensor lies in its capacity to readily identify branched chain conjugates *in vitro*, thereby enabling high-throughput screening of new writers, erasers, and substrates without the confounding influence of a significant background signal.

3.3.4 Comparison of the DARPins to other available tools

The first tools developed for the specific detection of K48- or K63-linked ubiquitin chains were the linkage-specific antibodies. The K48-linked antibody Apu2 was shown to have an affinity of 1.2 nM, while the anti-K63 antibody presented in the same paper (Apu3) has a K_D of 6 nM.[212] However it has to be mentioned, that this is not the clone used in this study (HWA4C4), for which no K_D is specified. The anti-K63 DARPin G1 has a similar affinity to the published K_D, while the anti-K48 DARPin A1 is slightly weaker, but still within the same range (Table 3.1). Therefore, no significant difference is anticipated, particularly in *in vivo* settings, as their affinity is still considerably lower than the concentration found within the cell. This was also demonstrated by the conducted colocalization stainings, which revealed nearly congruent signals produced by the DARPins and their respective antibodies (Figure 3.16). One advantage of the antibodies over the DARPins is their usability for the detection of linkage-specific ubiquitin conjugates on Western blots,[212] a task for which our DARPins so far have proven unsuccessful. Moreover, they have proven to be highly useful for ELISA and immunoprecipitation assays, although the K63-linked antibody occasionally exhibits a lack of selectivity (as evidenced by internal experiments). However, their use *in vivo* is severely limited, as they cannot be easily expressed in most cells, due to their large and complex structure, which includes a complex maturation process.[168] Consequently, the primary rationale for the development of DARPins and their principal advantage over linkage-specific antibodies is their capacity to serve as a biosensor within the cell.

Tools that potentially also could be used as biosensors are the recently presented K48- and K63-linkage-specific nanobodies. However, they are currently only available as purified proteins,[594, 595] and the only published work to date is a protocol for using them for enrichment of specifically linked ubiquitin conjugates from cell extract for subsequent mass spectrometry analysis.[219] As the linkage-specific DARPins also demonstrated great properties in this approach (Figure 3.11), a direct comparison of the specificity of the nanobodies to the DARPins would be of interest.

Another approach, which was employed for live-cell imaging of specifically K48-linked ubiquitin chains is ubiquitination-induced fluorescence complementation (UiFC).[233] This approach is based on a BiFC assay in which each mVenus half is fused to three tandem UIMs. This design renders it particularly prone to the detection of longer K48-linked ubiquitin chains, in contrast to the anti-K48 DARPin A1, which efficiently binds already K48-linked ubiquitin dimers (Figure 3.6A). It was demonstrated that the UiFC has a preference for K48 over K63-linked ubiquitin chains *in vitro* and *in vivo*, although this was not quantified. Additionally, interactions with K11-linked ubiquitin chains were observed *in vitro*.[233] A quantification of this preference would be necessary for a direct comparison to the selectivity of the anti-K48 DARPin A1. A further disadvantage of the system lies in the nature of the detection system. As previously discussed, the BiFC may exhibit a delayed signal emission, potentially rendering it more challenging to capture transient signals than with fluorophore-tagged DARPins. As of cause also the other above discussed advantages and disadvantages of the BiFC approach apply, a direct comparison for the detection of K48-linked ubiquitin chains for example at DNA damage sites would be interesting.

Besides these tools so far the TUBEs remain the gold standard in the detection and enrichment of K48- and K63-linked ubiquitin chains. Therefore, a more comprehensive comparison of the DARPin to their respective TUBEs will be conducted in the subsequent paragraphs.

3.3.4.1 Comparison of the anti-K63 DARPin G1 to the TUBE

The basis for the TUBEs was developed by Sims *et al*. in 2012, although they were not yet called TUBEs yet, but tUIMs. They developed two variants of specifically linked UIMs showing a K63-linkage specificity, which they subsequently characterized *in vivo*. The Vx3 variant is based on three UIMs of VPS27 and Rx3(A7) is derived from the UIMs of RAP80.[228] The specific UIMs on which the commercially available anti-K63 TUBEs are based are not entirely clear, as they merely state that they have further developed the tUIMs of Sims *et al* into the anti-K63 TUBE. As for the anti-K48 TUBE, only the manual, the webpage, and a poster, but no publication are available for this reagent,[229, 596, 597] the comparison, especially for *in vivo* usage, will be based on the published data by Sims *et al*.

The manual states that the anti-K63 TUBE binds K63-linked ubiquitin chains with a low nanomolar range, exhibiting a 1,000- to 10,000-fold preference over other linkages.[229] These parameters align well with the characteristics measured for the Rx3 construct (K_D = 5 nM), suggesting that this is the basis for the anti-K63 TUBE.[228] Therefore, the K_D of the anti-K63 DARPin G1, which was found to be 7 nM, is comparable to the affinity of the anti-K63 TUBE. Additionally, the preference of the anti-K63 DARPin G1 was found to be within the same range, with a 6,000-fold preference over monoubiquitin and an 8,000-fold preference over K48-linked ubiquitin dimers (Table 3.1). A direct comparison of how these values translate to pull-down approaches revealed that while the affinity of the TUBE and G1 was indeed comparable, the anti-K63 TUBE appeared to be less selective, pulling down more K48-linked ubiquitin chains (Figure 3.6D). This difference became more obvious in the quantification by MS (Figure 3.11), in which, despite the high postulated preference, the anti-K63 TUBE pulled down a large amount of K48-linked ubiquitin chains, significantly more than the anti-K63 DARPin G1. It is important to note that the anti-K63 TUBE concentration utilized in the pull-down (0.5 µM) was at the upper limit of the recommended concentrations for pull-downs by the manual.[229] As the authors emphasized the potential for off-target binding to become increasingly prevalent at concentrations above the dissociation constant, a further reduction in the concentration of the anti-K63 TUBE may restore its selectivity. However, it is necessary to ascertain whether a reduction in TUBE concentration would also result in a reduction of the quantity of enriched K63-linked ubiquitin conjugates.

Sims *et al*. demonstrated the usability of Vx3 and the Rx3(A7) for colocalization experiments and as biosensors *in vivo*. However, they also identified a pronounced inhibitory effect following the expression of both tUIMs, resulting *inter alli* in a delayed foci resolution at DNA damage sites. It was demonstrated that GFP-Rx3 *in vivo* began inhibiting K63-linkage-specific processes as soon as its expression via GFP-signal was detectable, and at higher concentrations, Rx3 expression was demonstrated to inhibit general ubiquitin-dependent processes.[228] To establish an upper limits for the expression of Rx3, an IC_{50} value was evaluated using a cell-based assay.[228] This IC_{50} was estimated to range between 1-10 µM, which is the same range as both IC_{50} values determined *in vitro* for anti-K63 DARPin G1 (Table 3.1). However, it should be noted that IC_{50} values are highly specific to the assay and conditions under which they were calculated, as well as the target for which they were determined.[598] Consequently, it is not straightforward to compare IC_{50} values from different studies. Nevertheless, the same range could indicate comparable inhibition modes and similar effects in the cellular environment. The expression of Rx3 for 20 h led to a doubling of K63-linked conjugated ubiquitin in cell extracts.[228]

As we were kindly provided with the Rx3 construct by the Cohen lab (Harvard University, Cambridge), we were able to compare this phenotype directly with the effect of the anti-K63 DARPins. We observed a pronounced enrichment of K63-linked ubiquitin chains for Rx3 and the anti-K63 DARPin G3 and E3, but not G1 (Appendix Figure 6.4), suggesting a milder inhibitory effect of G1.

Overall, it can be stated that the anti-K63 DARPin G1 and the anti-K63 TUBE appear to exhibit similar properties with regard to their binding mode and affinity. However, the anti-K63 DARPin G1 demonstrated greater specificity for K63-linkages in a cellular environment. Moreover, for Rx3 a strong inhibitory effect was demonstrated *in vivo*, which could not be diminished even with low expression levels. Thus, the less inhibitory G1 may be a suitable alternative for monitoring dynamic processes. Additionally, the commercially available TUBE is only sold as purified protein, but is not available as a plasmid. Therefore, *in vivo* analysis are only possible after Rx3 plasmid inquiry from the Cohen lab. However, as there is no definitive evidence that the published Rx3 is identical to the TUBE, it is unclear how well *in vitro* and *in vivo* properties can be related. Consequently, in order to have a more universally applicable tool, the well-characterized anti-K63 DARPin G1 may be a preferable option for a wide range of applications.

3.3.4.2 Comparison of the anti-K48 DARPin A1 to the TUBE

As there is no publication regarding the anti-K48 TUBE, the only available source of information is the respective manual and the webpage.[563, 599] However, the data underlying the claims made in the manual are not publicly available. The only experiment for which data is shown is a pull-down of tetraubiquitin of all linkages except K27, which shows a binding of only the K48-linked tetramer.[599] The interaction with K48-linked tetraubiquitin could be reproduced, but no interaction was found with K48-linked ubiquitin dimers or trimers in pull-downs or by affinity measurements (Figure 3.6A+B, Appendix Figure 6.11F). This is due to the design of the K48-linked TUBE, which consists of four naturally occurring UBDs.[599] In order for the TUBE to achieve a high affinity to the K48-linked ubiquitin chains, they must consist of at least four moieties, as this allows for all four UBDs to bind simultaneously. However, recent years have seen the overturning of the long-held dogma that a K48-linked tetramer is always necessary for proteasomal degradation. It has been demonstrated that shorter K48-linked ubiquitin chains also have a function in cells and can efficiently trigger proteasomal degradation, especially when multiple ubiquitin sites are present or they are branched with K11.[120, 166, 600] This information is lost when using the anti-K48 TUBE. Therefore, the anti-K48 DARPin A1, which binds efficiently starting at the dimer level, may be a valuable tool in elucidating the roles of shorter K48-linked ubiquitin substrates.

The manual claims that the anti-K48, as demonstrated for the other TUBEs, protects K48-linked ubiquitin signals from proteasomal degradation, thereby stabilizing and enriching modified proteins. The FRET-based investigation of the effects of the TUBE and the anti-K48 DARPins revealed that the inhibitory properties of the anti-K48 DARPins were very similar for conjugation and deconjugation (Figure 3.8A+B), thus a similar property was proposed for the DARPins. This was supported by the accumulation of K48-linked ubiquitin chains upon the expression of the anti-K48 DARPins A1 in mammalian and yeast cells (Appendix Figure 6.4).

The manual states an affinity of approximately 20 nM for the anti-K48 TUBE towards K48-linked tetraubiquitin, which is within the same range as the affinity measured for the anti-K48 DARPin A1 (78 nM for K48-linked tetraubiquitin). It claims to have a at least 100-fold preference for K48 over all other linkages on a tetramer level.[563] This would be stronger than the approximately 30-fold preference, measured for A1 for the K48- over the K63-linkage. However, this higher affinity and selectivity was not reflected in any of the conducted analyses in this work. In the initial pull-downs of K48- or K63-linked ubiquitin chains, the anti-K48 TUBE demonstrated a stronger binding to long K63-linked ubiquitin chains than the anti-K48 DARPin A1 (Figure 3.6B). Additionally, a significantly lower quantity of K48-linked ubiquitin chains was isolated from mammalian cell lysates (Figure 3.7) and yeast cell extract (Appendix Figure 6.8), for which barely a discernible signal was observed in the anti-K48 blot. This overall lower amount of pull-down was also reflected in the mass spectrometry analysis (Figure 3.11A), which revealed that only 1.3% of all ubiquitylated conjugates were isolated by the TUBE (0.261% of all K48-linked ubiquitin substrates), while DARPin A1 bound about 10-fold more in general and 95-fold more of the K48-ubiquitylated substrates. This could indicate that the TUBE has a lower affinity than previously assumed or that a significant proportion of substrates are modified with K48-linked ubiquitin dimers or trimers, potentially including branched chains. These substrates would not be covered by the TUBE, but only by the DARPin and could therefore explain part of the discrepancy.

Also when checking the linkage distribution in the sample pulled-down by the TUBE, it did not demonstrate the stated specificity. In contrast, the anti-K48 TUBE exhibited strong enrichment for K11, but not for K48-ubiquitylated substrates (Figure 3.11B). Thus, in our hands, the anti-K48 TUBE failed to fulfill its intended purpose. However, it cannot be ruled out that the TUBE was not correctly folded or otherwise not functional in the used setup, despite the buffer and other conditions being adapted from the manual. Nevertheless, as the anti-K48 TUBE also failed to meet the expectations from the manual in previous pull-down experiments, the anti-K48 DARPin A1 represents a viable alternative, as it seems to have a higher affinity and specificity at least in the conditions used for our experiments, which represent standard conditions for pull-down approaches.

Another significant advantage of the anti-K48 DARPin A1 over the anti-K48 TUBE is its capacity to be expressed in cells, thereby enabling live-cell imaging. As the anti-K48 TUBE is commercially available only as a purified protein, it cannot be employed in such experiments, thereby limiting its utility to approaches for which also the linkage-specific antibody can be used.

3.3.5 Limitations

This study has demonstrated that DARPins are highly stable and selective tools, capable of differentiating between small differences such as linkages. The created and characterized anti-K48 and anti-K63 DARPins were found to be suitable for use in a wide range of applications, both *in vitro* and *in vivo*. One exception was immunoblotting, for which initial attempts to use DARPins to detect linkage-specific signals on blots were unsuccessful. However, further optimization of the blotting procedure and the use of a more sensitive detection method could still be tested.

It was sought to develop an independent biosensor that would not be based on natural occurring UBDs and thus not interact with the same interaction sites as natural UBDs, to ensure that the biosensor does not interfere with ubiquitin signaling. However, both the anti-K48 DARPin A1 and the anti-K63 DARPin G1 gained their high specificity and affinity through the interaction with the Ile44 patches of both ubiquitin moieties. Consequently, despite the unbiased approach employed, it was not possible to develop a specific tool that was independent of these binding sites and could thus allow simultaneous binding of writers, readers, and erasers to the specific ubiquitin chain.

Therefore, an effect on chain conjugation and deconjugation was observed for all the specific DARPins (Figure 3.8), which for some also translated into a mild cytotoxicity, particularly under stress conditions (Figure 3.9). However, as the inhibitory effect was shown to be concentration dependent, it can be diminished by regulating expression levels and times. It is therefore advisable to refrain from transfection of the DARPins, particularly in the case of prolonged use exceeding 24 h. Instead, the use of inducible expression systems is recommended. Using this system, it was demonstrated that both linkage-specific DARPins allow ubiquitin chains to be formed and are capable of monitoring the accumulation of their target ubiquitin chains *in vivo*. Consequently, they can be utilized as biosensors to monitor the ubiquitylation reaction in response to a specific stressor. Particularly for the anti-K48 DARPin A1, further research is necessary to ascertain whether it also allows ubiquitin deconjugation *in vivo* and, thus, could also monitor the resolution of ubiquitin signaling. Should a robust inhibitory effect be identified, mutational studies could be conducted to weaken the interaction while maintaining specificity. One such mutation, could potentially be W112A at site 3 (Figure 3.12). Therefore, this mutant should be tested for its ability to allow more binding of the respective DUBs.

Both DARPins were combined to create a K48-K63-branched ubiquitin chain sensor based on a BiFC approach. This approach has been demonstrated to be highly sensitive *in vitro*, but has not yet been demonstrated to be capable of detecting branched chains *in vivo*. This may be due to the delay associated with fluorophore maturation. Thus, alternative scenarios or detection methods, such as FRET, should be tested. However, the recent development of a K48-K63-specific nanobody has presented a highly specific and high-affinity binder for *in vivo* use.[220] Consequently, the application of the K48-K63-branched ubiquitin chain sensor shall be focused on the *in vitro* aspects or can be employed as an additional tool, for instance, to enable the simultaneous monitoring of homogeneous and heterogeneous ubiquitin chains by FRET or to provide a reduced background for low abundant signals.

Also the K48- and K63-specific nanobodies that were developed last year have the potential to be used in similar applications, including *in vivo* applications, as the linkage-specific DARPins. Nevertheless, as to date, no such application has been published, our well-characterized DARPins have a head start in this respect.

3.3.6 Future perspective

This work demonstrated the development and characterization of K48- and K63-linkage-specific DARPins. They have been extensively characterized *in vitro* regarding their specificity, affinity, and inhibitory effects. To further enhance and refine the *in vitro* characterization of their specificity, the affinities of the linkage-specific DARPins A1 and G1 could be measured for differently linked tetraubiquitin, such as M1 or K11. Of particular interest would be K11 as both final DARPins enriched substrates linked via this linkage from cell extracts. The affinity measurement could help elucidate whether this is due to unspecific binding or if the K11-linkage is enriched as part of branched ubiquitin chains.

The structural insights gained from the crystal structures have allowed a more profound comprehension of the specific and high-affinity interactions between the DARPins and their respective ubiquitin dimers. This knowledge can be utilized to modify the properties of the DARPins. For instance, a less potent and thus potentially less inhibitory K48-specific binder could be generated by the W112A mutation in anti-K48 DARPin A1, or a non-specific ubiquitin binder with high affinity could be created by the W48A mutation in anti-K63 DARPin G1. Both of these DARPins could be beneficial for certain approaches and would further expand the toolbox for detecting linkage-specific and general ubiquitin signaling.

This work demonstrated the usability of the anti-K48 DARPin A1 and the anti-K63 DARPin G1 for the detection of several structures and processes *in vivo*. To gain a deeper insight into the dynamics and the involvement of linkage-specific ubiquitylation in the formation and resolution of stress-induced LLPS compartments, such as stress granules or aggresomes, live-cell imaging in cells expressing fluorophore-tagged marker proteins will be conducted. The laser tracks will be repeated with a longer time course in order to allow for the tracking of the resolution of damage-induced foci, provided that the linkage-specific DARPins do not inhibit deconjugation. Should this occur, the expression system should be adapted to result in a less strong expression. This could be achieved by testing other titratable expression systems or by inducing the expression for a shorter time. An alternative approach would be to sort for a low-expressing clone via FACS. It was demonstrated that the inhibitory effect was concentration dependent, thus a lower expression would allow for better interaction with DUBs and thus allow resolution of the signal.

The combination of the anti-K48 and anti-K63 DARPin yielded a K48-K63-branched ubiquitin chain sensor, which was demonstrated to be highly selective *in vitro*. However, its efficacy *in vivo* has not yet been convincingly demonstrated, likely due to the transient nature of the branched chain signal at DNA damage sites, which did not align with the slow detection system of the BiFC-based probe. Other approaches that are expected to yield a more stable signal will be tested, such as colocalization experiments with stress granules and aggresomes. Alternatively, a switch to a FRET-based detection could be considered. While the BiFC allows the monitoring of K48-K63-branched chains in general, a trimeric system, for which GFP was shown to be split into three parts that can refold upon close proximity, could allow even more specifically to detect K48-K63-branched chains only associated with certain processes.[601] For instance, the involvement of branched chains in DNA damage bypass could be investigated and compared using this system. This can be achieved by tagging one-third of GFP to PCNA, one to the anti-K48 DARPin, and one to the anti-K63 DARPin. This approach would not only permit the monitoring of the formation and deconjugation of K48-K63-branched chains during this specific process, but would also allow for the clarification of the factors involved, for example by inhibiting p97 or certain DUBs that have been proposed to be involved.[220]

In conclusion, the presented DARPins are well-characterized high-affinity probes that can be used for the specific detection of K48- and K63-linked ubiquitin chains *in vitro* and *in vivo*. These probes enable the recognition and tracking of linkage-specific ubiquitin chains in cells, and due to their protective effect, in particular, anti-K48 DARPin A1 was also demonstrated to enrich this signal upon expression. A combination of these two linkage-specific DARPins generated a K48-K63-branched chain tool which exhibited high selectivity *in vitro*. While further optimization is required for the *in vivo* approach, the results demonstrate that the DARPins represent a valuable foundation for the development of a versatile toolbox for the study of linkage-specific ubiquitin signals, both for homogenous and heterogeneous ubiquitin chains. The concept is universal and DARPins against other linkages could be generated and characterized according to the here presented procedure. Furthermore, a combination of these DARPins could be employed to study all types of branched ubiquitin chains, which remain poorly understood so far. Moreover, the DARPins could be combined also with other linkage-specific probes such as nanobodies or affimers. For instance, a K6-K48-branched ubiquitin chain sensor could be based on the K6-specific affimer and the anti-K48 DARPin. Collectively, this could result in a comprehensive and versatile toolbox for studying all linkage-specific signals in homolytic and in branched or mixed chains, both *in vitro* and *in vivo*. Thus providing a decisive contribution to the ultimate resolution of the ubiquitin code.

4 Results and Discussion II

Mechanistic analysis of the function of polyubiquitin chains in Exo1 recruitment for DNA damage bypass

4.1 Background and aim of this project

Avoiding genome instability and potential carcinogenesis through complete and precise duplication of its genome is one of the essential requirements of proliferating cells. Because the single-stranded DNA (ssDNA) produced during replication is particularly fragile, the process of DNA replication must be carefully controlled, especially in the presence of damage, as lesions in the template DNA lead to polymerase arrest. In this scenario, the cell relies on two DNA damage bypass mechanisms to efficiently overcome the arrest.[602, 603] The first, called translation synthesis (TLS), is an error-prone mechanism that uses specialized DNA polymerases to synthesize directly over the lesion. The second, called template switching (TS), is more error-free and uses a recombination-like mechanism that involves transient use of the undamaged sister chromatid.[343] In eukaryotes, damage bypass and the pathway choice are controlled by ubiquitylation of the DNA sliding clamp, proliferating cell nuclear antigen (PCNA). Monoubiquitylation of PCNA promotes recruitment of damage-tolerant DNA polymerases and thus TLS, whereas extension of monoubiquitin to a K63-linked polyubiquitin chain on PCNA promotes TS.[361]

While the activation of damage-tolerant DNA polymerases by monoubiquitylated PCNA is well characterized, the mechanism by which polyubiquitylated PCNA activates TS is still poorly understood. For certain proteins, including Mgs1/WRNIP1 or ZRANB3, a preferential interaction with polyubiquitylated PCNA has been reported; however, their role in the pathway is still uncertain.[352, 394–396] In addition, several other factors have been reported to (in)directly contribute to TS, including the 9-1-1 checkpoint clamp, the replicative polymerase δ, the Shu complex or the endonuclease Exo1.[388, 389, 392, 453] However, their relevance as key mediators of TS need to be characterized.

In recent years, evidence has accumulated that the process of DNA damage bypass can occur in a post-replicative manner and that template switching at these post-replicative gaps is prepared by Exo1 widening the daughter-strand gaps to allow recombination factors to assemble.[387–389, 399, 400, 404] This was supported by recent findings from our group showing that deletion of *EXO1* reduces the damage-dependent accumulation of single-stranded regions within tracts of newly replicated DNA and that this daughter-strand gap expansion promotes TS. In addition, it was further shown, that the daughter-strand expansion by Exo1 is facilitated to induce checkpoint signaling and that in this process, the checkpoint kinase Rad53 is activated and inhibits further Exo1 activity via a negative feedback loop to prevent gap erosion and associated genome instability. So overall, it has been proposed that Exo1, in cooperation with Pif1, can facilitate the topological transactions at daughter-strand gaps associated with the TS pathway of DNA damage bypass.[390, 453]

Unpublished data from a former postdoc in our group and first author of these studies, Nestor García-Rodríguez, showed in yeast two-hybrid (Y2H) screens and by crude pull-down assays with GST-Exo1 containing cell lysate that Exo1 not only interacted with yeast PCNA Pol30, but appeared to interact preferentially with its polyubiquitylated form (Figure 4.1).

This led to the hypothesis that Exo1 directly binds polyubiquitylated PCNA and is thus the key mediator explaining how K63-polyubiquitylated PCNA promotes TS.

The objective of this project was to investigate this hypothesis and, therefore, to characterize if there is a direct interaction between Exo1 and polyubiquitylated PCNA in *S. cerevisiae*. Additionally, the specificity of Exo1 for K63-linked polyubiquitylated PCNA is investigated. In particular, this research aimed to biochemically identify and study the specific motifs and binding sites of Exo1 with PCNA and ubiquitin, as well as to elucidate the biological relevance of these interactions within the context of TS.

The direct interaction was to be investigated in pull-down approaches. Therefore, the first step was to express and purify Exo1 in sufficient amounts and purity. Different expression (*E.coli*, yeast, Sf9 cells) and purification systems (e.g. affinity chromatography, SEC, ion exchange) were tested to obtain purified Exo1 in sufficient amounts. As this could not be achieved for the full-length constructs, truncations were screened using the yeast two-hybrid system and the minimal Exo1 fragment that still showed the interaction with polyubiquitylated PCNA was identified. After optimization of the purification and pull-down conditions, pull-down experiments with this fragment revealed direct interactions of Exo1 with PCNA, ubiquitin and ubiquitylated PCNA. Additionally, the comparison of the pull-down results for PCNA, mono- and polyubiquitylated PCNA, as well as free ubiquitin chains of different linkages, provided information on the affinity and specificity of Exo1 for the respective binding partners. Sequence analysis, *in vitro* and *in vivo* interaction assays, and mutational studies were used to identify and verify a PCNA interaction motif (PIP) and a potential UBD. The biological relevance of the interaction between Exo1 and polyubiquitylated PCNA and thus the impact of the mutations was studied by genetic assays under damage conditions.

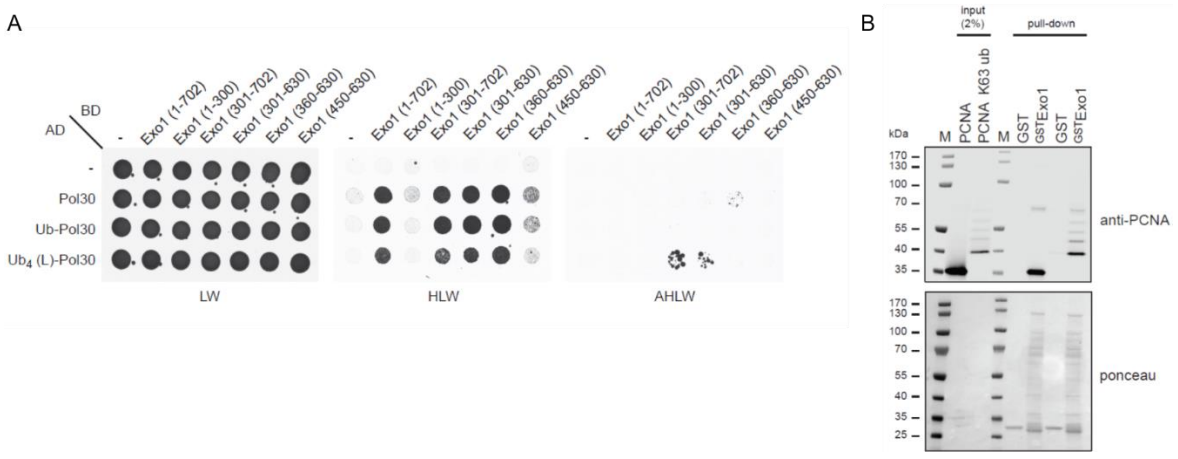

Figure 4.1: Exo1 interacts with unmodified and ubiquitylated PCNA. (A) Yeast two-hybrid screen showing the interaction of different Exo1 constructs (BD) with differently ubiquitylated Pol30 (AD), spotted on plates lacking leucine (L), tryptophan (W), histidine (H) and adenine (A) as indicated. The yeast were grown for 4 days. (B) Western blot of the crude pull-down of PCNA or ubiquitylated PCNA by GST-tagged Exo1 containing cell lysate. 100% of the pull-down and 2% of input were loaded and detected by PCNA antibody. Loading control with Ponceau. Conducted by Nestor García-Rodríguez.

4.2 Results

4.2.1 Identification of purification strategies for Exo1

To investigate a direct interaction between Exo1 and (ubiquitylated) PCNA using pull-down assays, the first step was to purify Exo1. Therefore, various constructs from different expression systems, ranging from *E.coli* over yeast to insect cells (Sf9), were tested. In addition, different tags were investigated for purification and solubilization of the protein. Table 4.1 summarizes the constructs that were tested, along with their expression systems and purification methods, as well as the observations and problems encountered.

Table 4.1: Overview of tested Exo1 constructs with expression system, purification method and encountered problems. *Tested by Nestor García-Rodríguez.

Construct	Expression system	Purification	Observation/Problems
His6-TEV-Exo1*	*E.coli*	IMAC	Protein not soluble
His-Exo1*	*Sf9*	IMAC, SEC	Little Solubility
MBP-TEV2-Exo1-His6	*E.coli*	IMAC, HisTrap, Amylose beads	MBP helps solubilize Exo1 Weak binding to Ni beads
MBP-TEV2-Exo1 (301-702)-His6	*E.coli*	IMAC, Amylose beads	Good purification but aggregates
MBP-TEV2-Exo1 (1-300)-His6	*E.coli*	IMAC, Amylose beads	Good purification but aggregates
His6-MBP-TEV2-Exo1	*E.coli*	IMAC, Amylose beads	Better binding to Ni-beads, also aggregation
His-Exo1*	Yeast	-	Low expression
His-MBP-Exo1*	Yeast	IMAC	Low expression, 50% soluble
GST-Exo1	*E.coli*	GSH-beads, SEC	Cleavage products
His6-SMT3-Exo1	*E.coli*	IMAC	Cleavage products
GST-Exo1 (D173A)	*E.coli*	GSH-beads, SEC	Cleavage products
SMT3-Exo1-Avi-His6	*E.coli*	IMAC	Weak expression, cleavage
His6-SMT3-Flag-Exo1	*E.coli*	IMAC	Strong cleavage products
His-Exo1 (D173A)	Sf9	IMAC, SEC	Little Solubility
GST-Exo1 (301-702)	*E.coli*	GSH-beads, SEC	Cleavage, unstable, promising for direct PD
GST-Exo1	Sf9	GSH-beads, SEC	Weak expression, good solubility, weak binding, cleavage
GST-Exo1 (D173A)	Sf9	GSH-beads, SEC	Weak expression, good solubility, weak binding, cleavage
GST-Exo1 (301-702)	Sf9	GSH-beads, SEC	Weak expression, good solubility, weak binding, cleavage

Continued on next page

Exo1-Flag-His6	Sf9	HisTrap, Flag-beads	Lower expression as Exo1-Flag
Exo1-Flag[471]	Sf9	Flag-beads, SEC, HiTrap	Lost at SEC, aggregation on Flag-beads?
Exo1 (D173A) -Flag	Sf9	Flag-beads, SEC	Lost at SEC, aggregation on Flag-beads?
Exo1-His-Flag [604]	Yeast	HisTrap, Flag-beads	Lost lots during purification, small yield
Exo1 (301-702)-Flag	Sf9	Flag-beads, HiTrap	Most promising construct, low yield (2.4 mg/L), clean, stability problem

In addition to the wild-type construct, the catalytic dead mutant D173A mutant, which has been shown to disrupt the nuclease activity[470, 605, 606] was used in different constructs. Thus it was hoped that overexpression of this Exo1 mutant would be better tolerated by the cells. However, no difference in expression was observed and the constructs encountered the same problems as their wild-type counterparts.

In general, Exo1 constructs with only a His-tag exhibited low solubility. This was improved by the addition of a MBP-tag. However, this resulted in strong aggregation, as observed in SEC runs performed with these constructs. Both GST and SMT3-tags were cleaved during the purification process. Furthermore, when the GST-tagged construct was expressed in Sf9 cells, it exhibited weak binding to GSH-beads. This was attributed to the endogenous high affinity GSH binding of the insect cells.[607] Overall, the most promising results were achieved with the Flag-tagged constructs from insect cells. This is in line with the two published constructs that were purified by other groups and were both Flag-tagged.[471, 604] One of these was purified from yeast and the other one from insect cells

In addition to the full-length constructs, a N-terminal (1-300) and a C-terminal (301-702) fragments of Exo1 were also tested for purification. The C-terminal fragment, which Nestor identified as having the being the strongest interaction with polyubiquitylated PCNA in the yeast two-hybrid screen (Figure 4.1), was tagged with a Flag-tag and expressed in Sf9 cells. This construct gave the purest protein and the highest yield of all the constructs tested. However, the purified protein was unstable when stored at -80°C. Therefore, most of the pull-down assays were performed with Exo1 constructs that were directly coupled to the Flag-beads without further purification by HiTrap.

4.2.2 Investigation of a direct interaction of Exo1 with (ubiquitylated) PCNA

The first pull-down was performed using the procedure previously employed by Nestor García-Rodríguez (Figure 4.1B). Therefore, GST-tagged Exo1 constructs were directly coupled from *E. coli* cell lysate to GSH-beads. The pull-down efficiency was compared for the wild-type, the nuclease dead mutant (D173A) and the C-terminal fragment (301-702). The result showed that the interaction of all constructs was stronger than the pull-down of free GST, which was used as a negative control (Figure 4.2A). When comparing the different constructs, it is evident that the C-terminal fragment gave the strongest pull-down signal.

The main reason for this seems to be the increased stability of the construct, as shown by Ponceau staining (Figure 4.2A). The full length constructs only showed a weak band at the expected size (around 106 kDa), but in contrast a strong band for free GST was visible in their lanes, indicating that most of the Exo1 construct was cleaved and lost during the washing steps. The C-terminal fragment showed a significant reduction in the free GST signal and the intensity of the intact Exo1 band at around 70 kDa was almost as strong as the free GST used as a negative control. Furthermore, the GSH beads bound fewer total impurities, resulting in a cleaner result, thus making the C-terminal construct the preferred one for further studies.

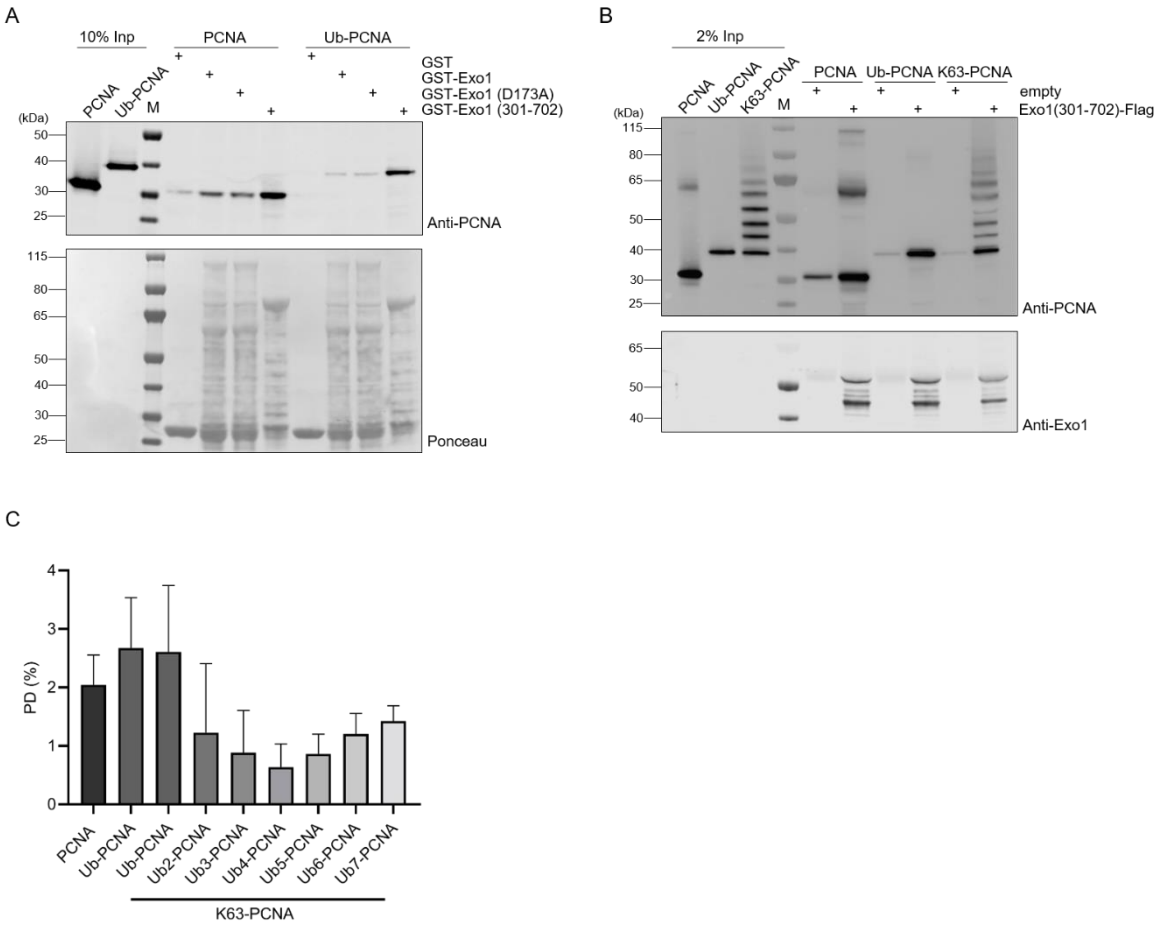

Figure 4.2: The interaction of Exo1 with PCNA and its ubiquitylated forms is direct. (A) Western blot of crude pull-down of PCNA and Ub-PCNA by the indicated GST-tagged Exo1 construct. GST-Exo1 construct expressing cell lysate was incubated with GSH beads, washed and then incubated directly with PCNA or Ub-PCNA. Free GST was used as a negative control. 100% of the pull-down and 2% of the input were loaded and detected with the PCNA antibody. Ponceau as loading control. (B) The Flag-tagged Exo1 construct (301-702) was coupled directly from Sf9 cell extract to Flag-beads and the interaction with PCNA, monoubiquitylated PCNA (Ub-PCNA) and K63-linked polyubiquitylated PCNA (K63-PCNA) was tested by pull-down and analyzed by Western blotting against PCNA. Pure Sf9 lysate was used as negative control (empty). 100% of the pull-down and 2% of the input were loaded. The loading of Exo1 was analyzed using the anti-Exo1 antibody. (C) Quantification of the pull-down signal of each band on the Western blot. The signal of the negative control (empty) was subtracted and the intensity is shown as a percentage of the input. Measured and analyzed by quantifying the band intensity of three independent Western blots from pull-downs performed analogously to C, using the anti-PCNA antibody, the Licore detector, and Image Studio software.

The results of the purification tests (Section 4.2.1) and the first pull-downs (Figure 4.2A) indicate that the most clean and stable product was obtained by expressing the C-terminal construct in Sf9 cells. Consequently, Flag-tagged Exo1 301-702 expressed in Sf9 cells was used for subsequent experiments. To ensure stability, the protein was extracted from the Sf9 cell lysate using Flag-beads, washed, and then used directly in pull-downs with PCNA, monoubiquitylated PCNA, and enzymatically linked K63-polyubiquitylated PCNA. The C-terminal Exo1 construct showed a significantly stronger interaction with all three PCNA constructs compared to the control, for which Flag-beads were incubated with wild-type Sf9 lysate (Figure 4.2B). The pull-down efficacy was quantified based on the respective band intensity using Image studio software and presented as a percentage of the input signal after subtracting the background (Figure 4.2C). The results indicate a stronger affinity for ubiquitylated PCNA than for unmodified PCNA. Then the interaction initially decreased as the length of the ubiquitin chains increased. However, with longer ubiquitin chains, the affinity increased again. Therefore, the tetraubiquitin modified PCNA exhibited the weakest interaction, while the longest tested ubiquitin chain, comprising seven moieties, demonstrated the strongest pull-down signal of all polyubiquitylated species. However, this pull-down was still weaker than with the monoubiqutylated substrate. Thus this experiment could not reproduce the preference for polyubiquitylated over monoubiquitylated PCNA observed in the Y2H.

The observation that more ubiquitylated PCNA was bound than unmodified PCNA, in conjunction with the Y2H screen, indicated the potential presence of a UBD in Exo1, in addition to a PCNA interaction motif. The presence of both motives will be examined in more detail during the course of this study. First a minimal Exo1 fragment that still interacts with ubiquitylated PCNA was sought to be identified for better handeling.

4.2.3 Identification of minimal Exo1 fragment

To identify the minimal fragment of Exo1 for interaction with polyubiquitylated PCNA and to address the stability issues of the C-terminal fragment of Exo1, a yeast two-hybrid screen with different truncations, schematically shown in Figure 4.3A, was conducted. The Y2H experiment demonstrated that the shortest truncation, which still exhibited a strong interaction with polyubiquitylated PCNA, by growth on the AHLW plate, was the fragment ranging from 301-402 (Figure 4.3B). It is worth noting, that this fragment lacks any previously identified interaction sites as well as the nuclease activity domain.

The fragment 301-360 exhibited a significant loss of interaction, as it did not show any growth with the Pol30 or Ub-Pol30 construct (Figure 4.3B). However, it showed some growth on the HLW-plate with the Ub4(linker)-Pol30 construct, which makes this region an interesting area to search for a potential ubiquitin binding domain.

In contrast, the loss of interaction with Pol30 and Ub-Pol30 by this truncation suggests that a possible PIP box is outside of this region. As fragment 301-402 showed strong interaction with polyubiquitylated PCNA, it indicates that both motifs are present in it. Therefore, it is assumed that the PIP interaction motif is located in the 360-402 region. Consequently, the presence of both motifs in these predicted respective regions would validate the strong interaction of 301-402 and make it the optimal minimal fragment.

The structure of the minimal fragment 301-402 is highlighted in red in the Alphafold predicted structure of Exo1 (Figure 4.3C). The fragment comprises of three α-helices connected by disordered regions. These structures are of great interest for further investigation and mutational studies, as the most common PIP motifs have been shown to adopt α-helical conformation.[608–611] Additionally, many UBDs (section 1.1.5) have been reported to consist of single or multiple α-helices.[15]

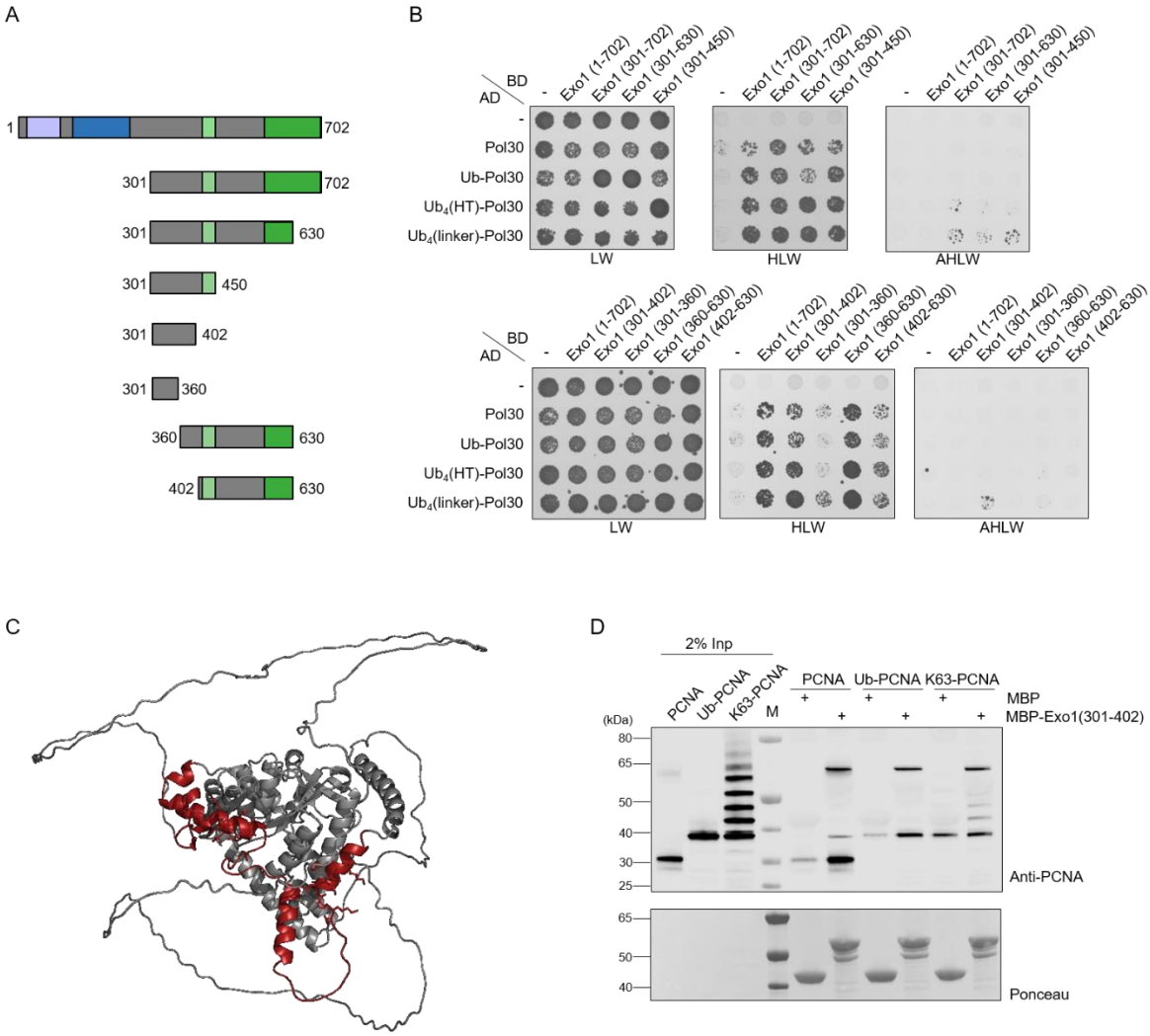

Figure 4.3: A minimal Exo1 fragment was identified, which interacts with ubiquitylated PCNA. (A) Schematic representation of the Exo1 protein and its fragments used in the Y2H assay (B). Purple = N-terminal nuclease domain, blue= Internal nuclease domain, lime = Mlh1 binding domain, green = Msh2 binding domain. (B) Yeast two-hybrid screen investigating the interaction of these different Exo1 truncations (BD) with differentially ubiquitylated Pol30 (AD), spotted on plates lacking leucine (L), tryptophan (W), histidine (H) and adenine (A) as indicated and grown for 4 days. (C) AlphaFold-predicted structure of yeast Exo1. The minimal fragment 301-402 is highlighted in red. (D) Amylose bead pull-down with purified MBP-tagged minimal Exo1 fragment (301-402) or MBP as negative control and PCNA, mono- or polyubiquitylated PCNA was performed and analyzed by Western blotting against PCNA. Ponceau for equal loading control of MBP and MBP-tagged Exo1 (301-402).

The minimal fragment was tagged with MBP or GST and purified successfully, yielding sufficient amounts for the interaction assays. The purified proteins were used to confirm the interaction with PCNA and its ubiquitylated forms, which have been previously demonstrated with the entire C-terminal fragment from Sf9 cells (section 4.2.2). MBP served as a negative control, and the pull-down was conducted with amylose beads. The results confirmed the interaction and demonstrated the effectiveness of the purification process. The construct was shown to interact with unmodified, mono- and polyubiquitylated PCNA, making it a suitable construct for identifying interaction motifs and verifying them through mutational studies (Figure 4.3D).

4.2.4 A PIP-box in Exo1 was identified and validated by mutagenesis

Since the pull-downs and Y2H suggested a direct interaction with PCNA, sequence alignment and mutational studies were conducted to identify and characterize a possible PIP-box.

Within the Exo1 sequence, Nestor García-Rodríguez identified four motifs (Figure 4.4A) that are similar to the canonical PIP-box motif QxxΨxxϑϑ, where Ψ represents an aliphatic hydrophobic residue (L, M, I, V) and ϑ represents an aromatic amino acid (often Y or F).[612] To investigate their influence, Exo1 constructs were cloned with mutations at the canonical residues in all four motifs (marked in red, Figure 4.4A). These were tested in a Y2H screen, indicating the involvement of the potential PIP boxes 1 and 2, as the interaction is lost for mutants in both regions (Figure 4.4A). Since these two sequences are located in the region of the identified minimal fragment, this is consistent with the performed truncation screen.

To validate this observation further, C-terminal Exo1 fragments containing the mutations of these two possible PIP-boxes were purified and their interaction with PCNA was examined in a pull-down assay. A clear loss of interaction was observed only when the potential PIP-box 2 was mutated, but not PIP1 (Figure 4.4B). The same PIP2 mutation was introduced in the MBP-tagged minimal fragment MBP-Exo1 (301-402) and the loss of interaction with PCNA was confirmed (Figure 4.4C). It was investigated whether the interaction is mediated predominantly by one of the residues or if the mutation of all three residues is necessary (Appendix Figure 6.24A). Two mutants were created: one with an alanine mutation introduced only at I391 and one where the conserved two phenylalanine residues (F394 and F395) were mutated. Interaction analysis showed that both mutations resulted in an equal reduction of the interaction with PCNA as the combined mutation, demonstrating the significance of the entire motif.

Further investigation of the interaction loss of the potential PIP-box 1 observed in the Y2H revealed an expression defect in all constructs containing the PIP1 mutation, as evidenced by the expression levels of 9Myc-tagged Exo1 constructs (Appendix Figure 6.24B). Thus the observed effect in the Y2H is due to an expression defect and not a loss of interaction *per se*. In contrast, constructs with the PIP2 mutation showed comparable expression to the wild-type (Appendix Figure 6.24B).

It was further investigated whether the mutation of the identified PIP-box also abolished the interaction with polyubiquitylated PCNA. The pull-down of the wild-type and PIP2 mutant GST-tagged minimal Exo1 fragment showed a clear decrease, but not a complete loss of interaction with polyubiquitylated PCNA. This suggested the presence of another interaction site, most likely a UBD, within the minimal fragment (Figure 4.4D).

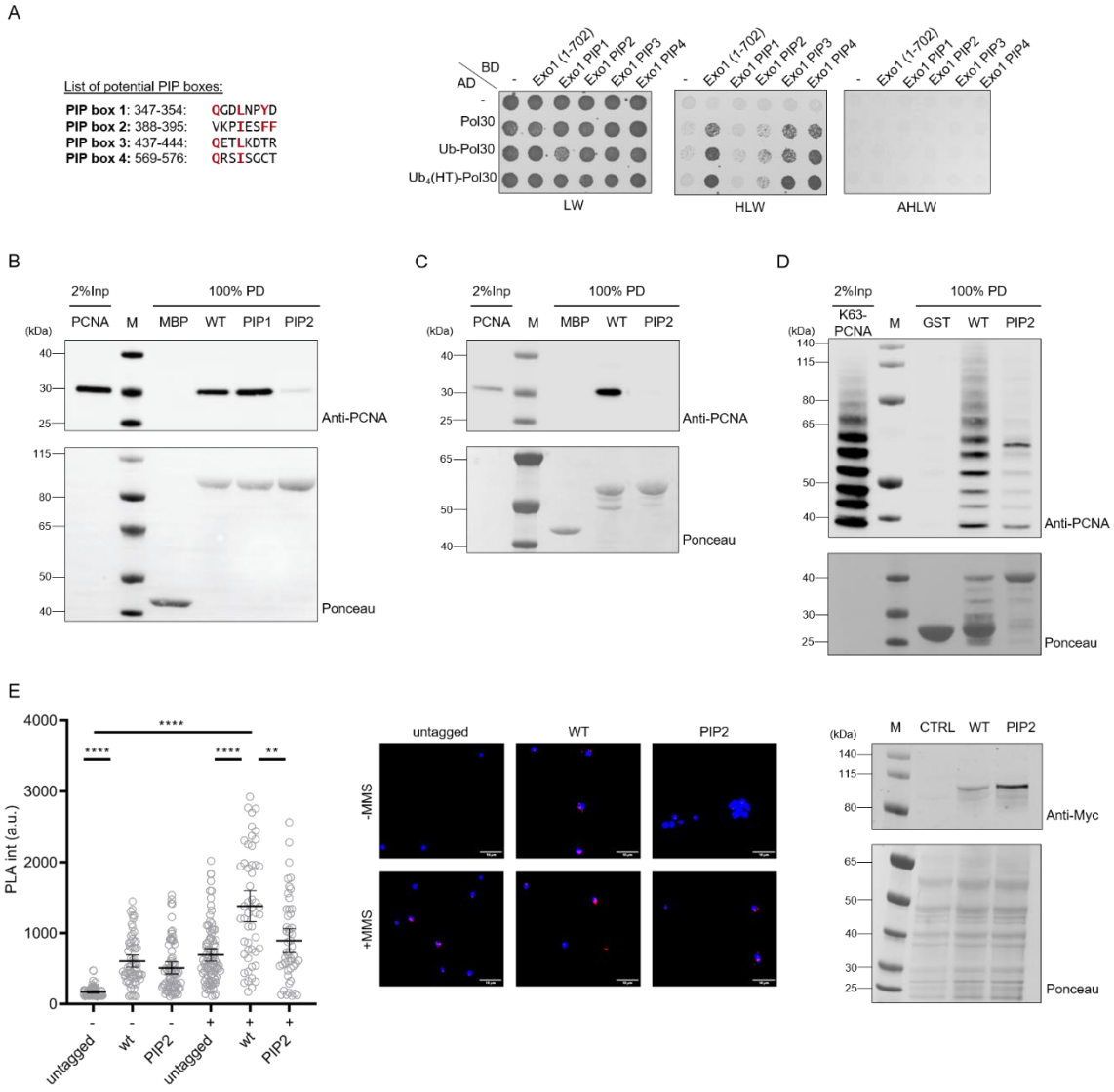

Figure 4.4: Mutation of PIP2 leads to a loss of interaction with PCNA *in vitro* and *in vivo*. (A) List of potential PIP boxes and yeast two-hybrid screen examining the interaction of the mutant of these potential PIP boxes (residues mutated to alanine in red) of Exo1 (BD) with differentially ubiquitylated Pol30 (AD), spotted on plates lacking leucine (L), tryptophan (W), histidine (H) and adenine (A) as indicated and grown for 4 days. (B-D) Pull-downs to investigate the interaction of wild-type (WT) or PIP mutants of Exo1 with PCNA (B, C) or K63-polyubiquitylated PCNA (D). Amylose or GSH-bead pull-downs were performed with purified MBP- (B, C) or GST-tagged (D) C-terminal (301-702, B) or minimal fragment of Exo1 (301-402, C,D) and analyzed by Western blotting against PCNA. Free MBP or GST was used as negative control. Ponceau was used for validating equal loading. (B) Performed by Nestor García-Rodríguez. (E) PLA assay to study the interaction of PCNA (anti-Pol30 antibody) with Myc-tagged Exo1 (Myc antibody) wild-type (WT) and PIP mutant (PIP2). A strain with untagged Exo1 (CTRL) was used as a negative control. Left: Dot plots of PLA signal intensities with means ± 95% confidence intervals. Significance levels were calculated using the two-tailed Mann–Whitney test (ns: not significant, ****:$p < 0.0001$, **: $p < 0.01$) Middle: Representative images, DAPI (blue), PLA (magenta), scale bar = 10 μm. Right: Western blot to monitor 9Myc-Exo1 expression levels of the strains used. Ponceau for loading control.

To confirm this interaction between Exo1 and ubiquitylated PCNA *in vivo* in the context of DNA damage, a PLA assay was performed. The experiment also examined whether this interaction is lost or diminished by mutation of the identified PIP-box. Both the Exo1 wild-type and PIP mutant were tagged with a 9Myc-tag and one antibody against this tag was used, while the other used antibody was against PCNA. A strain with an untagged Exo1 was utilized as a negative control.

The samples were divided into two halves. One half was treated with 0.02% MMS for 90 minutes, while the other half remained untreated, to see if the interaction is enhanced upon DNA damage, as PCNA is known to be polyubiquitylated in this context. The PLA signal for the 9Myc-tagged Exo1 wild-type showed a significant increase compared to the untagged control in both treated and untreated conditions (Figure 4.4E). These demonstrated the assay's capability to detect and quantify the interaction between PCNA and Exo1 *in vivo*. Additionally, the signal significantly increased after MMS treatment, providing strong evidence of a damage-dependent interaction. The PIP mutation significantly reduced interaction after DNA damage, despite the construct being more expressed, as shown by the Western blot (Figure 4.4E). This reduction suggested the involvement of the PIP motif in mediating interaction between Exo1 and PCNA in the context of DNA damage, in alignment with the pull-down experiments.

Although this result is very promising, it is important to note that the experiment was conducted only once and technical complications prevented its reproduction. To improve the PLA process, further optimizations should be performed, and a positive control (two PCNA antibodies) should be included.

Overall, a motif resembling a non-canonical PIP-box was identified, which, when mutated, led to a loss of interaction between Exo1 and PCNA *in vitro*. The PLA assay confirmed the interaction and the mediation by the identified PIP-box within the cell. It also demonstrated a DNA damage dependency of this interaction. Although further optimization and repetitions of this assay are necessary to conclusively demonstrate the relevance of this identified PIP motif *in vivo*, the results obtained so far provide strong evidence for its potential significance.

4.2.5 Pull-downs suggested a K63-linkage specificity of Exo1

Based on the observation of increased interaction of Exo1 and PCNA in the presence of DNA damage in the PLA assay and the stronger signal with polyubiquitylated PCNA in the Y2H assay, it has been hypothesized that Exo1 may recognize the K63-linked polyubiquitylated PCNA to induce TS after DNA damage during replication. To test this hypothesis, the linkage preference of Exo1 was investigated.

In the first experiment, Flag-Exo1 was directly coupled from Sf9 cell lysate and a pull-down was performed with enzymatically formed K48- and K63-linked ubiquitin chains, as well as an M1-linked hexaubiquitin (Figure 4.5A). The results showed the strongest increase in pull-down signal, compared to the empty bead control, for high molecular weight K63-linked ubiquitin chains, whereas no interaction was observed with the M1-linked hexamer. The high background signal resulted mainly from the aggregation of K48-linked ubiquitin chains on the Flag beads, as previously shown for the first DARPin pull-downs (section 3.2.1.1), made it challenging to provide a conclusive statement regarding the affinity of Exo1 towards this linkage.

To obtain more reliable results, pull-downs using the purified MBP-tagged minimal fragment of Exo1 (301-402) and M1, K48, or K63-linked ubiquitin dimers (Figure 4.5B) and tetramers (Figure 4.5C) were performed. In both pull-down set-ups a stronger interaction with K63-linked polyubiquitin was overserved in comparison to the other linkages, indicating that Exo1 has a preference for K63-linked polyubiquitin. Due to the generally weak affinity of Exo1 to ubiquitin all blots showed some background signals. Based on a comparison with the loaded input, less than 1% of the ubiquitin species were bound. This is not surprising as the affinity of naturally occurring UBDs to ubiquitin is typically weak, with K_D values in the high micromolar range, and have proven to be very transient, making them hard to capture in pull-downs.[71–74] The strongest increase in signal over the background was observed for the ubiquitin constructs linked via K63, especially for the K63-linked trimer, which resulted from incomplete K63R mutation of the ubiquitin mutant used for the dimer formation. Although only a fraction of the trimer was present in the input (Figure 4.5B), mainly containing the K63-linked dimer, the signals received in the pull-down were equally strong. This indicates a stronger interaction of Exo1 with longer polyubiquitin, which is consistent with the previous pull-down (Figure 4.5A) and with the quantifications of the single bands of the polyubiquitylated PCNA pull-downs, which also showed an increase in affinity with an increase in chain length (Figure 4.2C).

Overall, the performed pull-downs suggest a slight preference of Exo1 for K63-linked ubiquitin chains, which increases with chain length. Beyond the question of linkage selectivity, the pull-downs demonstrated binding of free ubiquitin chains without any PCNA substrate. This strongly suggests the existence of at least one UBD in Exo1. The following paragraph aims to identify and characterize this motif.

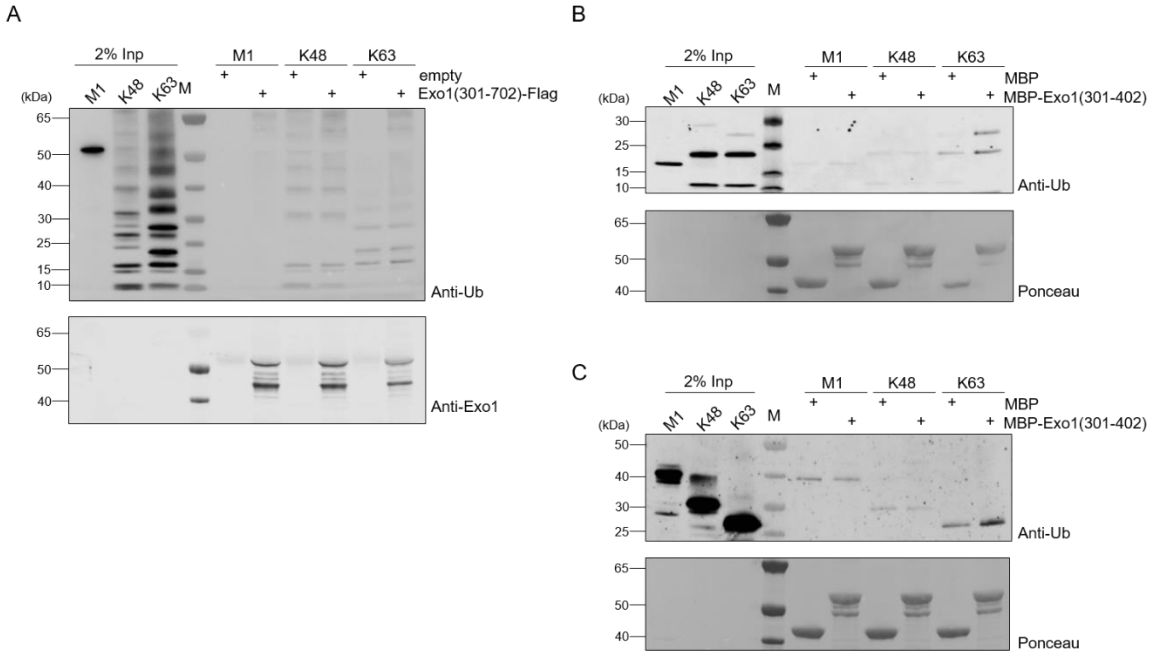

Figure 4.5: Exo1 shows a slight preference for K63-linked ubiquitin conjugates. (A) Pull-down result of the Flag-tagged Exo1 construct (301-702) coupled directly from Sf9 cell extract to Flag-beads with specifically linked ubiquitin chains (M1, K48 or K63-linked). Analyzed by Western blotting against ubiquitin. Pure Sf9 lysate was used as a negative control (empty). The loading of Exo1 was analyzed with anti-Exo1 antibody. (B, C) Amylose bead pull-down with purified MBP-tagged Exo1 (301-402) or MBP as a negative control and specifically linked ubiquitin dimers (B) and tetramers (C) (M1, K48 or K63-linked) was performed and analyzed by Western blotting against ubiquitin. Ponceau for equal loading control of MBP and MBP-tagged Exo1 (301-402). 100% of the pull-down and 2% of the input were loaded.

4.2.6 A potential UBD was identified and tested

The results of the Y2H experiments using different truncations (Figure 4.3B) indicate that a potential ubiquitin binding domain of Exo1 may be located in the region of aa301-360. To confirm this, the minimal fragment ranging from 301-402 was split at amino acid 360 into two parts (as shown in Figure 4.6A) and both fragments were tested in a pull-down assay with K63-linked tetraubiquitin (Figure 4.6B). The result confirmed the observation made in the Y2H experiment, demonstrating that only the fragment from 301-360 interacted with ubiquitin chains.

Kay Hofman from the Institute of Genetics at the University of Cologne helped identify a possible UBD in this region, ranging from aa337–346, using sequence alignment and AlphaFold modeling. This region showed weak similarity to a MIU/IUIM UBD, which has similar binding properties as UIM domains. The MIU/IUIM UBDs were found to bind specifically K63- and K48-linked ubiquitin chains and contain a critical alanine.[613–615]. In Exo1, this was predicted to be potentially A346.

Different mutants in this potential UBD region (aa337-346, highlighted in blue in Figure 4.6A) specifically at the identified alanine were introduced in the MBP-Exo1 (302-402) fragment. Pull-down experiments with this mutants and PCNA confirmed that the binding to PCNA was preserved (Appendix Figure 6.24), showing the correct folding of these mutants. The first tested mutation was the mutation of the I345 A346 motif to SG, and the impact on ubiquitin binding was investigated. The mutation did not affect the interaction with K63-linked tetraubiquitin (Figure 4.6C). In addition, a conserved histidine at position 342 was mutated to alanine (UBD2) and tested again in a pull-down with K63-linked tetraubiquitin (Figure 4.6D), but no reduction of interaction was observed. The mutations of alanine to larger and charged residues, such as aspartic acid, phenylalanine, or arginine (Figure 4.6E), were also unsuccessful in decreasing the interaction with tetraubiquitin. In contrast, the A346F mutation seemed to even slightly enhance the interaction, but this observation was not investigated further due to the possibility of a slightly higher concentration compared to the wild-type construct. As a final attempt, the entire identified sequence was deleted from the fragment (Δ8), and the pull-down was repeated (Figure 4.6F). However, there was no decrease in the interaction between the Exo1 fragment and K63-linked tetraubiquitin observed. Also initial *in vivo* interaction studies using a yeast two-hybrid assay, comparing the wild-type and the UBD mutation in different constructs, showed no decrease in interaction upon mutation (Appendix Figure 6.25A).

Overall, the results indicate that the prediction is incorrect and that there is no ubiquitin binding domain (UBD) in this region. If one continues to assume that the UBD is located in the minimal fragment, this leaves approximately 50 amino acids that could potentially harbor an UBD. It is possible that the UBD in Exo1 is of a different nature than the previously identified ones and thus did not appear in the alignments and modeling. To investigate further, a random mutagenesis PCR could be used to determine if mutants introduced in this region lead to a reduced interaction with K63-linked ubiquitin.

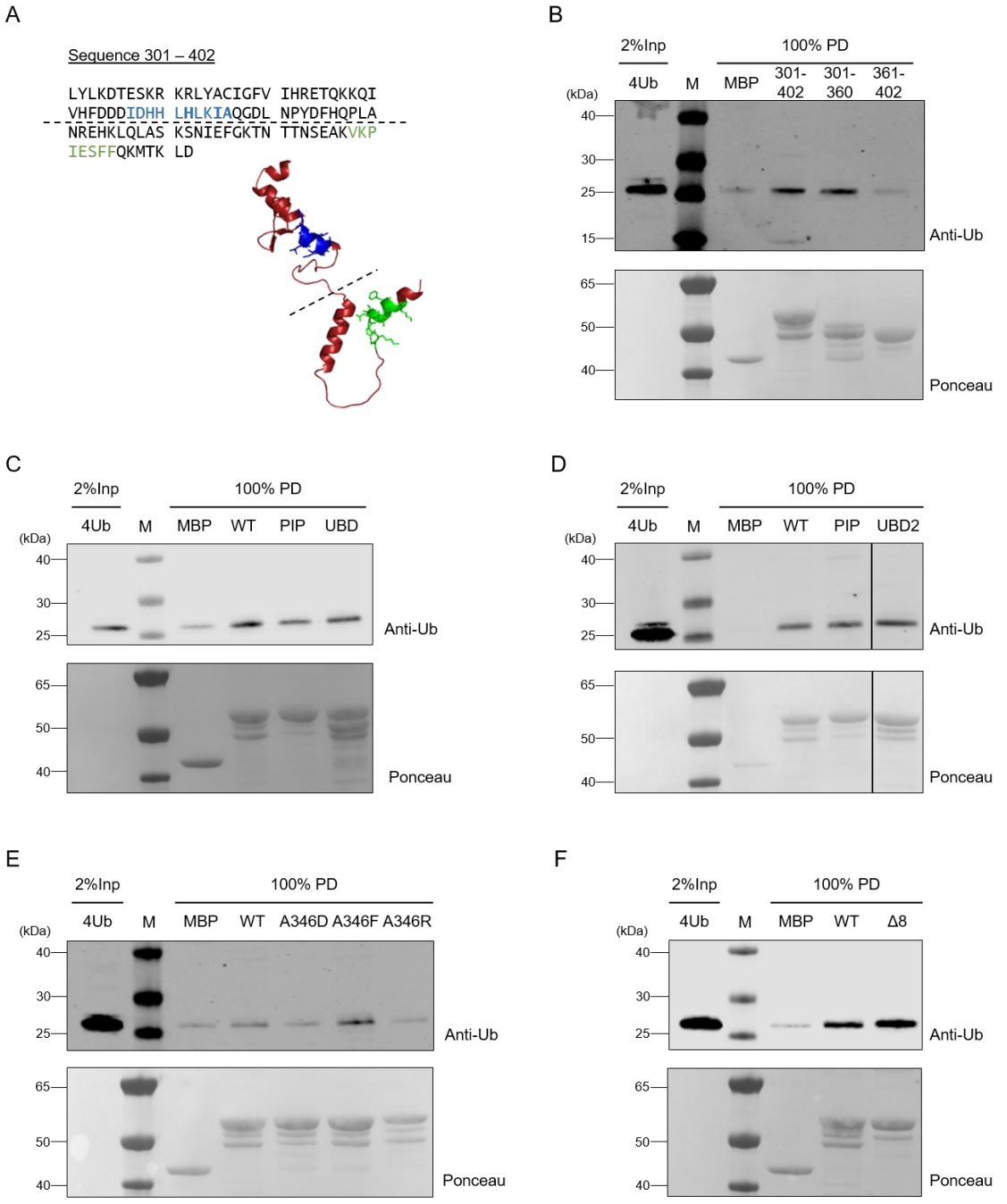

Figure 4.6: Different mutations and deletions could not verify the proposed UBD. (A) Sequence overview of the minimal Exo1 fragment. Highlighted in green is the identified PIP-box, in blue the potential UBD. The dashed line indicates the splitting site for the pull-down in (B) (B-F) Pull-downs to investigate the interaction of wild-type (WT) and indicated truncation (A), UBD mutants (C-E) or deletion (F) of Exo1 with K63-linked tetraubiquitin. Amylose pull-downs were performed with purified MBP-tagged minimal fragment of Exo1 (301-402) and analyzed by Western blot against ubiquitin. Free MBP was used as negative control. Ponceau was used for validating equal loading. UBD= I345S and A346G, UBD2= H342A and Δ8 represents the deletion of aa339-346.

4.2.7 Investigation of the biological relevance of Exo1 domains for TS

The PLA assay showed that Exo1 interacts with PCNA predominantly after DNA damage. To determine the biological relevance of this interaction and the contribution of the domains to the repair pathways, two genetic assays were conducted. It is hypothesized that Exo1 interacts with K63-polyubiquitylated PCNA and that this interaction is important for the initiation of the template-switching (TS) pathway; thus, two genetic assays were performed that have been described for the investigation of TS factors.[388, 400, 616] The *EXO1* knock-out has been shown to rescue the sensitivity effect in both assays.[388, 390] Therefore, the effect of the PIP-box and assumed UBD mutant were tested to investigate if the interaction between PCNA and Exo1, mediated by these sites, is essential for this effect.

As a first genetic assay, it was investigated whether the Exo1 mutants suppress the MMS sensitivity of the smc6-56 mutant strain (Figure 4.7A). The sensitivity of this strain is due to a defect in resolving recombination intermediates created during TS. If a mutation causes a defect in TS early on, these structures are not formed, and the sensitivity can be rescued. This was observed in the case of the knock-out of *EXO1*, which reproduced its role in this pathway as previously shown.[390] The mutation in the PIP-box had no effect in this assay, but the mutation of the potential UBD partially rescued the phenotype (Figure 4.7A).

The same effect of the two mutants was also observed in the second genetic assay tested (Figure 4.7B). This assay is based on the cold-sensitivity conferred by the deletion of the non-essential polymerase subunit Pol32. It is known that cold sensitivity of *pol32* mutant can be rescued by TS mutants. The previously reported rescue of *pol32* mutant was observed upon deletion of *EXO1*.[388] Similar to the previous assay, the PIP-box mutation did not improve the phenotype, while mutations in the potential UBD showed a rescue effect (Figure 4.7B).

There are several potential explanations for these observations. The lack of rescue resulting from the PIP-box mutation may be due to the existence of another interaction site that mediates the interaction of polyubiquitylated PCNA and Exo1, possibly through one or multiple UBDs. It is possible that then even in the absence of the PCNA interaction, these UBDs are sufficiently strong to mediate the interaction and thus initiate TS. However, it could also be that the direct interaction with PCNA is not needed for TS.

The most probable explanation for the rescue observed in the UBD mutant, despite its not proven function *in vitro*, is that it results in the expression of a non-functional protein. Unfortunately, the Exo1 antibody is not sufficiently strong to detect expression levels in the yeast strains used for the spot assay. Therefore, strains with a 9Myc-tag were cloned for all mutants of interest in order to repeat the experiment. When comparing the expression levels of 9Myc-Exo1 in these strains, it became evident that the UBD mutant indeed was less prevalent than the wild-type or PIP2 Exo1 construct (Appendix Figure 2.25C), supporting the hypothesis that the mutation of UBD influences the expression or stability level of Exo1. However, as the wild-type *exo1* strain in this experimental set-up did not demonstrate any sensitivity to MMS, in contrast to the PIP2 mutant (Appendix Figure 2.25B), new clones will be screened to ensure a similar expression level and functional Exo1 proteins before repeating the genetic assays.

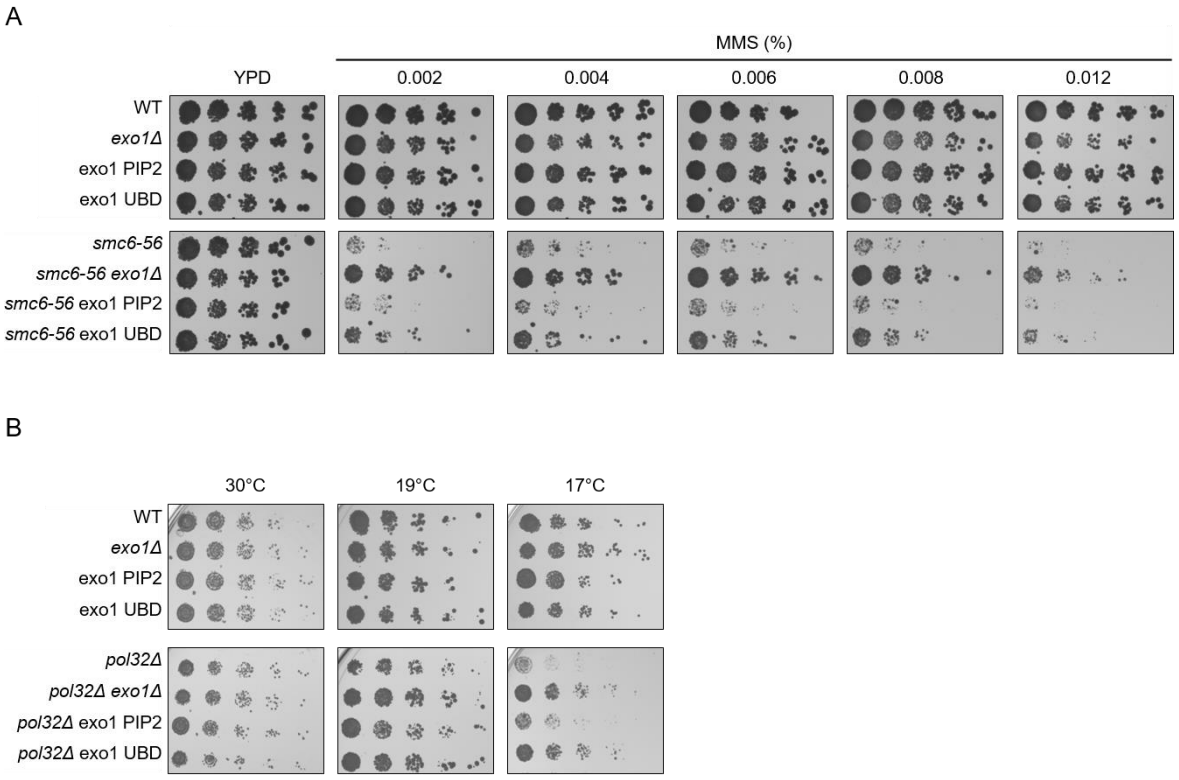

Figure 4.7: Mutation of UBD, but not the PIP-box of Exo1 affect TS. (A) Effect of MMS damage on a wild-type or MMS sensitive smc6-56 strain in which *Exo1* is deleted, expressed as wild-type or the indicated PIP2 or UBD (I345S & A346G) mutant. Serial dilutions of relevant strains were spotted onto plates containing the indicated concentrations of MMS (B) Temperature effect on a wild-type and cold-sensitive *pol32Δ* strain in which *EXO1* is deleted, expressed as wild-type or the indicated mutant. Serial dilutions of relevant strains were spotted onto YPD plates and incubated at the indicated temperatures for three days.

4.3 Discussion

4.3.1 Purification problems and strategies

As reported in section 4.2.1, full-length Exo1 is difficult to purify and the created constructs have exhibited various issues, including solubility, stability, and aggregation problems. This is in alignment with previous reports of difficulties in isolating full-length yeast and human Exo1 using bacterial and yeast overexpression systems.[407, 408, 427, 470, 617, 618] Stability issues have been reported directly or indirectly through elaborate purification procedures, for example, in the 16-hour purification from Bowen *et al*.[604] Degradation products have been observed such as a 42 kDa band, which may refer to the nuclease domain of Exo1.[427] For the purification products from Sf9 cells less degradation products were observed, but a significant loss of Exo1 during column chromatography as well as mutations that were not purifiable (like the D78A and D173A double mutant) have been reported.[470, 619] For the few successful attempts to purify full-length Exo1 from yeast or Sf9 cells, the reported yields were quite low (e.g. 9% or 100-500 µg/L from yeast).[427, 471, 604]

As evidenced by the superior purification of the 301-702 fragment, the purification difficulties may be mainly attributed to the N-terminal nuclease domain as the nuclease activity in excess can be toxic to the cell. However, we and others have observed no difference in purification efficiency between the wild-type and nuclease-dead (D173A) mutant.[470, 620] It was demonstrated that the D173A mutation retains residual nuclease activity, weak DNA nicking activity, and most importantly, the same DNA binding capability. Multiple other residues have been shown to contribute to Exo1s nuclease activity by positioning the DNA (H36, K85, R92, K121), coordinating the Mg^{2+} ion (D78, D171) and by binding to DNA (K185, G236).[410, 620] Therefore, additional mutations in this site may reduce interaction with DNA, which potentially causes toxicity during overexpression or precipitation during the purification procedure. Furthermore, the sequence of the N-terminal domain may be generally challenging for lower eukaryotes or bacteria to express and fold correctly, thus leading to the observed expression and purification issues. This is supported by Yan *et al.'s* recent observation that expression of the full-length protein in *E. coli* was enabled after codon optimization of the first 348 amino acids.[621]

Overall, purifying full-length Exo1 remains a challenging task, likely due to the structure and function of its N-terminal nuclease domain. Therefore, if the goal is to study protein-protein interactions primarily mediated via the C-terminus, it is preferable to purify C-terminal fragments of Exo1, such as the C-terminal (301-702) or minimal fragment (301-402) used in this work, as this results in clean proteins that can be expressed in *E.coli*.

4.3.2 Exo1 as a specific reader for polyubiquitylated PCNA

The overall aim of this project was to address one of the most puzzling question regarding the template switching pathway: to identify the specific reader of K63-linked polyubiquitin chains on PCNA. The requirements for such a factor a directly interaction with PCNA and ubiquitin. It is thereby expected to show a stronger affinity for polyubiquitylated PCNA than for monoubiquitylated or unmodified PCNA and a linkage preference for K63-linked polyubiquitin chains.

The pull-down assays demonstrated that the interaction observed in the initial yeast two-hybrid (Figure 4.1) assay is indeed direct, with Exo1 binding to PCNA, ubiquitylated PCNA, and free ubiquitin chains (Figure 4.2, 4.3, 4.4 and 4.6). Truncation studies and sequence analysis revealed potential motifs for the interaction with PCNA and ubiquitin.

4.3.2.1 Identification and validation of a non-canonical PIP-box in Exo1

The PCNA interaction motif identified in the region of aa388-395 of Exo1, designated PIP2, was found to mediate the direct interaction between Exo1 and PCNA. This was demonstrated by the loss of interaction observed in yeast two-hybrid (Figure 4.4A) and pull-downs (Figure 4.4B-D) after mutation of the conserved PIP-box residues in this sequence. The motif's location (aa388-395) aligned with the prediction based on the previous Y2H screens using different Exo1 truncations (Figure 4.3A). The initial *in vivo* PLA experiments also indicated a significantly reduced interaction between the Exo1-PIP-box mutant and PCNA during DNA damage. However, it is essential to exercise caution when interpreting these results since the experiment has not been repeated due to technical difficulties.

Structurally, the PIP-box is located inside an α-helix, as is the case for most other canonical and non-canonical PIP-boxes. The identified PIP-box sequence (VKPIESFF) belongs to the group of non-canonical PIP-boxes, which are defined by the absence of a glutamine at position 1.[612, 622] In these PIP-boxes, the residues at the last two positions are crucial for their interaction. In the identified PIP-box of Exo1, these are two phenylalanines. The FF-motif is a common feature found in both canonical and non-canonical PIP-boxes, leading to affinities with K_Ds ranging from low nanomolar to low micromolar values. The motif is found also in various proteins, including the endonuclease FEN1, polymerases, ligases, and PCNA-interactors such as RFC.[611]

A sequence alignment of *S. cerevisiae* Exo1 with other yeast species revealed that the FF-motif is highly conserved (Appendix Figure 6.26A), making the presence of the same PIP-box in these species very likely. In higher eukaryotes, this motif is replaced by an IW. As also no additional residues of the PIP-box consensus sequence were found in this area, a PIP-box in this region is unlikely for these species. However, another PIP-box has been described in human EXO1, located in the C-terminus from aa788-795. This PIP-box (QIKLNELW) is a canonical PIP-box and is conserved in other higher eukaryotes, such as mouse, Xenopus, and Zebrafish. Mechanistically, it has been shown that this PIP-box is crucial for the recruitment of hEXO1 to DNA replication foci, and that the interaction with PCNA increases the processivity of EXO1 in DNA resection.[418, 623]

4.3.2.2 Investigations of the potential UBD

Despite various tested mutations and the deletion of the entire region of the predicted UBD, the direct interaction observed in pull-down approaches was not significantly reduced (Figure 4.6). In the Y2H assay, the mutation in the potential UBD of Exo1 did also not decrease the interaction with the tested PCNA constructs. There might even be a slight increase in interaction observable for the C-terminal Exo1 construct (301-702) upon mutation of the UBD (Appendix Figure 6.25A).

In contrast, the conducted genetic assay demonstrated a rescue effect for the Exo1 constructs with mutations in the UBD region in both tested assays (Figure 4.7). This would indicate a relevance of this domain for the template switching pathway. However, as no effect on the interactions was found *in vitro*, it is more likely that the mutation causes the Exo1 protein to be less expressed or less stable in cells. This is supported by the lower prevalence of the 9-Myc tagged UBD construct (Appendix Figure 6.25C). Therefore, the effect on expression and stability needs to be conclusively clarified before interpreting these genetic assays further.

Further investigations are necessary to address the open question regarding a potential UBD in Exo1. To identify a new sequence that potentially mediates the interaction of Exo1 with ubiquitin, a random mutagenesis PCR for the remaining amino acids of the identified fragment (aa301-360) could be performed. The products can be screened for reduced interaction with K63-linked ubiquitin. As pull-downs in this set-up were shown to be sensitive to small experimental changes and often have a strong background, the reduction of binding caused by a certain mutation should always be complemented with another mode of interaction study to ensure reliable results. This could be achieved through the already used *in vivo* methods, such as Y2H or PLA, or through the use of alternative binding assays, such as surface plasmon resonance (SPR), fluorescence polarization, or thermophoresis. These approaches are often more laborious than pull-down approaches, but they permit more quantitative characterization of the binding of specific Exo1 mutants with ubiquitin. Hit candidates can then be further verified in genetic assays to investigate their biological relevance for the initiation of TS, both singly and in combination with the identified PIP-box.

4.3.2.3 Preference of Exo1 towards K63-linked ubiquitin constructs

For Exo1 to specifically initiate TS, it has to specifically interact with K63-linked polyubiquitylated PCNA, as for example K48-linked ubiquitin chains on PCNA have been shown to not lead to TS but to proteasomal degradation of PCNA.[466]

Therefore, we tested the interaction with differently linked ubiquitin polymers (Figure 4.5). The results hint towards a preference of Exo1 for binding K63-linked polyubiquitin. However, caution must be exercised in interpreting these results due to the high background binding shown in the blots. It was also tested whether there is a preferential binding for differently linked ubiquitin chains on PCNA (data not shown), but no preference was observed. This lack of preference could be due to the strong interaction of the PIP-box with PCNA in general, as PIP-boxes typically have a higher K_D than UBDs.[73, 74, 611] Thus this experiment should be repeated using the Exo1 PIP mutant.

In general, it remains unclear how linkage specificity for Exo1 is achieved. Proteins either achieve their ubiquitin linkage specificity through domains that specifically recognize the linker region or through linkage-specific avidity.[15, 72] For the latter, more than one ubiquitin-binding domain (UBD) would need to be present. The presence of at least two UBDs in Exo1 is questionable in our identified truncation (301-360), as only around 50 aa are left for a potential UBD sequence after excluding the eight extensively tested amino acids. Most UBDs have secondary structures, often α-helices. Based on the AlphaFold prediction of the fragment aa301-360 (Figure 4.6A), this further limits the region to approximately 35-40 amino acids. As one ubiquitin-binding domain (UBD) normally consists of 20-150 amino acids, the presence of two UBDs in this region seems unlikely.[70] Thus, Exo1 would need to mutimerize for linkage-specific avidity or the UBD in Exo1 must directly recognized the K63-linkage itself. It is possible that this UBD is of a different nature than the previously identified ones, thus it did not appear in the alignments and modeling.

Further investigations are necessary to address the open questions regarding a potential UBD in Exo1 and how this potentially achieves linkage-specificity.

4.3.2.4 Selectivity and avidity effect of Exo1

A direct interaction of Exo1 with pure PCNA as well as with pure K63-linked tetraubiquitin was demonstrated, indicating the presence of two interaction motifs, a PIP-box and at least one UBD (Figure 4.4 and 4.6). The PIP-box was identified and characterized, demonstrating a clear affinity of Exo1 to PCNA. Despite the lack of a concrete domain that could be identified for the ubiquitin binding, the pull-downs demonstrated also a direct affinity of Exo1 to polyubiquitin. Consequently, a fragment encompassing both of these interaction sites, as is the case for every fragment larger than the minimal fragment, would be expected to exhibit an avidity effect.

The avidity principle is employed in numerous proteins within the cell, often also readers of the ubiquitin code, for which frequently a UBD is combined with another UBD or a substrate-specific binding domain. The combination of cooperative interactions, which individually possess relatively low affinity, can result in high affinity and selectivity through avidity effects.[624] This avidity effect is the primary underlying principle of TUBEs. As a single UBD typically exhibits only a very low affinity in the high micromolar range, the TUBEs combine three or four of them to achieve their nanomolar affinities.[227, 228] Additionally, this principle was employed in the design of probes that specifically bind ubiquitylated PCNA, while only exhibit a low affinity for unmodified PCNA, by combining a PIP-box and at least one UBD. This lead to a preference for ubiquitylated over unmodified PCNA of least 130-fold due to the avidity of the PIP-box and UBDs of the biosensor.[625] A specific reader of ubiquitylated PCNA is therefore expected to be based on the same concept and utilize avidity to differentiate the ubiquitylation status of PCNA.

A comparison of the interaction of Exo1 with PCNA and monoubiquitylated PCNA revealed a stronger interaction of the C-terminal fragment of Exo1 (Figure 4.2) with monoubiquitylated PCNA, indicating an avidity effect. This effect was less pronounced in pull-downs using the minimal fragment (Figure 4.3) and in Y2H screens (Figure 4.1 and 4.3). However, the construct containing the mutation of the PIP-box demonstrated a markedly reduced interaction compared to the wild-type (Figure 4.4), yet retained the capacity to bind ubiquitylated PCNA to a sufficient extent. This suggests that there is some affinity remaining, which is enhanced by the PIP-box, indicating again the presence of an avidity effect.

To further elucidate this phenomenon, more quantitative measurements, such as surface plasmon resonance (SPR), fluorescence polarization, or thermophoresis, shall be employed. Comparative analysis of the affinities of Exo1 truncations that interact with PCNA and/or ubiquitin, as well as the measurement of respective mutants of the motifs, such as the PIP-box, may provide insight into the existence of an avidity effect of the at least two binding domains.

If Exo1 contains a further UBD that mediates the K63-linkage specificity, the avidity effect should be even more pronounced for K63-polyubiquitylated PCNA. This was strongly indicated by the Y2H assays, which demonstrated enhanced growth of strains containing polyubiquitylated PCNA relative to the unmodified form of PCNA (Figure 4.1 and 4.3). However, this effect could not be reproduced in pull-down assays *in vitro*, as Exo1 demonstrated a weaker interaction with ubiquitin chains on PCNA (Figure 4.2). The reasons for this discrepancy and the differences between the two assays (Y2H and pull-down) will be further elaborated in the following paragraph.

4.3.3 The discrepancy between the Y2H and PD assays

The yeast two-hybrid (Y2H) assay is a widely used approach for investigating protein-protein interactions, offering straightforward, reliable, and expedient studies with fundamental laboratory equipment. Nevertheless, it is essential to acknowledge the limitations of this method. Primarily, it does not permit for adjustments to account for differences in the expression levels of the studied proteins. Additionally, it lacks information about the kinetics of the interaction and its limited signal resolution makes it only semi-quantitative. In particular, generally weak interaction or minor alterations in the K_D of a few-fold magnitude cannot be discerned.[626, 627] For instance, the propably quite weak interaction between Exo1 and ubiquitin chains in the absence of PCNA was not observed in the Y2H assay (data not shown).

It is also important to note that a yeast two-hybrid system does not always demonstrate direct interaction, but rather close proximity. Therefore, it is possible that another protein may act as an adapter between the two candidates, in our case Exo1 and the PCNA constructs. Consequently, the direct interaction was investigated by pull-down assays, which also appear to be somewhat more sensitive, as they were able to capture the interaction with free ubiquitin polymers (Figure 4.6). When comparing the results of these two assays used in this study for investigating the interaction of Exo1 and polyubiquitylated PCNA, it is essential to consider another major differences in their set-up: the different topologies of the used PCNA constructs.

The ubiquitylation of PCNA is a highly specific topological system. However, it has been shown that the site of ubiquitin attachment is not critical for downstream signaling. An N-terminal fusion of ubiquitin to PCNA, as employed in both approaches, was demonstrated to possess enough conformational flexibility to trigger TLS.[628–630] Similarly, the position of the first ubiquitin is not critical for efficiently triggering TS as it has been demonstrated that a K63-linked ubiquitin chain positioned at the N-terminus and not at the natural K164, can efficiently trigger TS, thus mimicking polyubiquitylation on PCNA inside the cell.[631]

For the pull-down approaches, exactly this build-up was used as a N-terminal fusion of ubiquitin to PCNA (Ub-PCNA) was enzymatically, K63-specific ubiquitylated. In the Y2H assays, two different constructs were tested. Both were based on linear fusions of four ubiquitin moieties to PCNA. One was fused directly head-to tail (HT), while the other incorporated a small linker (VQIQ) between the single ubiquitin moieties. In literature, it was observed that the head-to-tail fusion did not allow any significant DNA damage rescue, while the linker fusion suppressed the damage sensitivity of *rad18Δ* cells to some degree. Although it was demonstrated that this may be predominantly due to TLS and not TS, it demonstrates that the linker allows the recognition and binding of factors that recognize monoubiquitylation, while the head-to-tail fusion sterically hinders this interaction.[632] This could also explain why the conducted Y2H screen showed an interaction of Exo1 with the linker version, but not the head-to-tail fusion (Figure 4.1 and 4.3).

However, it is surprising that, even though no additional rescue effect of this linear fusion constructs to monoubiquitylated PCNA was found *in vivo*, Exo1 appears to interact with them preferentially over monoubiquitylated PCNA in the Y2H (Figure 4.1 and 4.3), which has led us to hypothesize that Exo1 may be a preferential reader of polyubiquitylated PCNA. This hypothesize is based on the previous successful identification of Mgs1 as interactor of polyubiquitylated PCNA, which was also first identified with this Y2H method. Mgs1 retained this preference for K63-linked polyubiquitin chains on PCNA, thereby validating this method as a first interaction screen.[396] This appears to differ for Exo1, as it did not retain its preference for polyubiquitylated PCNA in the performed pull-downs with K63-linked ubiquitin chains on PCNA (Figure 4.2). To investigate if this discrepancy is indeed due to the different topology of the ubiquitin chains on PCNA used, it would be worth to conduct a pulldown directly comparing the interaction of Exo1 with the enzymatically formed K63-linked ubiquitin chains versus its interaction with the ubiquitin fusions on PCNA.

An even more natural orientation would be provided by the split-Ub PCNA system. In this system, PCNA was split between amino acids 163 and 164, and the second fragment was then attached with ubiquitin at the N-terminus. The resulting fusion protein resembles PCNA ubiquitylated at K164 and has been shown to form stable trimers and support TS.[633] However, experiments conducted in our laboratory have revealed that this split Ub-PCNA is not well enzymatically polyubiquitylated *in vitro*. Therefore, a fusion approach involving the coupling of purified, enzymatically synthesized K63-linked ubiquitin chains to the split PCNA may be necessary. This method was previously employed by Yakoub *et al.*, in which a K63-linked triubiquitin was prepared with a G76C mutation in the proximal ubiquitin, which could then be coupled to a K164 mutation in PCNA.[625] This approach may yield the most reliable construct, as it most closely resembles the natural K63-linked polyubiquitylated PCNA.

In summary, the discrepancy in the observed preference of Exo1 for polyubiquitylated PCNA between the pull-down and Y2H approaches is possibly attributed to the experimental set-up. Either due to the involvement of another factor in the Y2H approach or due to the different topologies of the PCNA constructs used, which might sterically hinder the binding of the UBD motif of Exo1 to the polyubiquitylated form. To further investigate this discrepancy, a direct comparison of both PCNA constructs will be conducted. Additionally, as both differ from the naturally occurring ubiquitylation on residue K164, it should be considered to use an even more natural representative construct.

In general, the pull-down approach with enzymatically synthesized K63-polyubiquitylated PCNA seems to be a more sensitive method for investigating direct interactions compared to the Y2H. Although the pull-down method is a reliable approach for investigating direct interactions with PCNA or ubiquitylated PCNA, especially when utilizing the more natural split-Ub-PCNA construct, these *in vitro* approaches do not fully reflect the actual *in vivo* setup, where PCNA is loaded on DNA and accompanied by various additional factors. Consequently, further *in vivo* studies were conducted to investigate the biological relevance of the observed interaction between Exo1 and PCNA in a biological context.

4.3.4 Biological relevance of the domains

An initial analysis for evaluating the interaction *in vivo* was conducted using a PLA, which showed a statistically significant increase in the interaction between PCNA and wild-type Exo1 upon DNA damage (Figure 4.4E). This suggests an increased interaction with polyubiquitylated PCNA compared to unmodified PCNA, as DNA damage leads to polyubiquitylation of PCNA. To investigate the difference between mono- and polyubiquitylated PCNA further, the PLA should be repeated using a wild-type and an *ubc13Δ* strain upon damage. One other possibility is to use the tailor-made E3s developed in our lab, which can specifically ubiquitylate PCNA.[466] In this case, the interaction of Exo1 with PCNA could be compared in a *rad5Δ* background with and without PIP-E3(63). The PIP-E3 system would also enable further investigation into the linkage-dependency of this interaction. The recently published Ubiquiton technique, could provide even clearer insight as it allows for the creation of polyubiquitin chains on PCNA in the absence of DNA damage.[634] In all of these scenarios, the interaction between ubiquitylated PCNA and Exo1 shall be monitored to gain deeper insights into what mediates this interaction and whether a preferential binding to a certain ubiquitylation status and chain type of PCNA can be demonstrated.

The PLA also demonstrated that the PIP-box in Exo1 was necessary for the damage-induced interaction of Exo1 and PCNA (Figure 4.4E). Thus, it was very surprising that no biological effect on TS was observed by the PIP2 mutation in the conducted genetic assays (Figure 4.7). This could suggests that the discovered PIP-box may not be relevant in this context, but possibly only in other pathways where both Exo1 and PCNA are present, such as mismatch repair. However, this would contradicts the observations from human cells, in which the interaction between EXO1 and PCNA was found to be particularly crucial at DNA replication foci, while for DSBs and MMR, an interaction with hMlh1 was deemed more important.[623]

It is also possible that technical factors, such as varying expression levels or inadequate damage, could explain this discrepancy. Therefore, it is necessary to repeat the genetic assays with smaller dosage steps and while monitoring the expression levels using tagged Exo1 constructs. Therefore different orientations and tags shall be tested, as the 9Myc-tagged Exo1 wild-type construct lost its sensitivity in the *smc6-56* assays. Additionally, it is possible that another domain, such as a UBD, may also mediate the interaction. In the absence of PIP-binding, the remaining binding affinity may be sufficient *in vivo* to suppress the phenotype. This would be consistent with the results of the pull-down of K63-linked polyubiquitylated PCNA by the Exo1 PIP-box mutant or the PLA result of the PIP-mutant, as for both a reduced but still significant interaction was observed (Figure 4.4D+E).

To verify this hypothesis, an Exo1 construct with a deletion of the entire minimal fragment sequence, could be cloned. As this sequence was shown to contain the PIP-box and was necessary for the interaction with ubiquitin it would be expected that such a construct would lead to a complete loss of interaction with polyubiquitylated PCNA. This could be determined via pull-down approaches and then it could be checked if this construct now causes damage sensitivity and impairment of TS while preserving other functions of Exo1 in genetic assays. Furthermore, the effect of wild-type vs PIP and possible UBD mutant could be examined with other biological indicators of DNA damage bypass, such as the recruitment of Exo1 wild-type and PIP-box mutation to locations of DNA damage bypass. This can be observed by co-localizing with other established transcription and replication factors, such as RPA, following MMS treatment. 2D-gel analysis or electron microscopy could also be employed to directly visualize the formation of the Holliday junctions between sister chromatids as the X-shaped structure formed during TS.[365, 382, 384, 387] In all of this the implications of mutations like the PIP-box, but also of different truncations, can be investigated and would allow further insights into its biological relevance.

Overall, the PLA demonstrated that the close proximity of Exo1 and PCNA is induced by DNA damage and also indicated that the PIP-box is relevant for this interaction. However, the latter finding could not be reproduced by the genetic assay employed. As both assays encountered technical difficulties, these must first be resolved in order to facilitate a direct comparison and verify the biological relevance of the identified PIP-box in the context of TS. Furthermore, other pathways in which both Exo1 and PCNA participation has been demonstrated shall be investigated to determine if a direct interaction mediated via the identified PIP-box is necessary for these pathways. Additional analysis in the absence of factors that initiate TS, such as a *ubc13Δ* background or the targeted inducible K63-ubiquitylation of PCNA using the tailor-made PIP-E3(63) or Ubiquiton system, will permit further investigation into the preferential binding of Exo1 toward polyubiquitylated PCNA.

4.3.5 Further perspectives

This research project aimed to address the question whether Exo1 binds K63-polyubiquitylated PCNA and thus to identify the specific interaction motifs of Exo1 with PCNA and ubiquitin. A non-canonical PIP-box was identified and validated *in vitro*. To assess the biological functions of this motif *in vivo*, further experiments are required. Genetic assays or PLA should be used to determine the involvement of this motif in template switching, as well as its effects in the various other pathways in which Exo1 and PCNA have been shown to be involved. This investigation will shed light on the implications of the direct interaction of Exo1 and PCNA mediated by the identified PIP-box. Further investigations are necessary to resolve the question of whether the structure of Exo1 contains a UBD and the implications of this. To identify the binding mode of both domains, a crystallographic or NMR approach with the purified Exo1 fragment 301-402 and K63-polyubiquitylated PCNA can be considered.

A series of experiments was conducted to investigate the preferential interaction of Exo1 with K63-linked polyubiquitylated PCNA, which would be expected for a specific reader of this signal and thus a key mediator of TS. However, the results are not yet definitive, and further experiments are necessary to determine the specificity of Exo1 towards polyubiquitin versus monoubiquitin modification on PCNA. *In vitro*, more quantitative methods, such as SPR or fluorescence polarization, shall be employed to study the affinity of Exo1 toward different PCNA constructs in greater detail. *In vivo*, the PLA method must be optimized in order to enable further exploitation. It is recommended that the interaction of Exo1 and PCNA shall also be explored via PLA in an *ubc13Δ* or *rad5Δ* background to determine if this interaction is specific for the template switching pathway. An alternative approach would be to employ targeted ubiquitylation via the PIP-E3 or Ubiquiton system to assess whether this leads to the specific interaction between Exo1 and PCNA. By testing the K63-linkage-specific PIP-E3 or Ubiquitin system alongside other linkage-specific systems, such as the K48-specific PIP-E3 or Ubiquitin, this might also help to elucidate the potential linkage-specificity of Exo1.

Furthermore, a mass spectrometry approach could be employed to unbiasedly identify binding partners of K63-polyubiquitylated PCNA. For instance, a pull-down of PCNA after SILAC could be conducted using an unmodified PCNA condition, a conditions with monoubiquitylated PCNA and one with K63-linked polyubiquitylated PCNA for example induced by the PIP-E3(63) in a *rad5* knock-out background. This approach would help to identify specific interactors for each condition, with particular interest on those that interact specifically with polyubiquitylated PCNA. Another method that could provide valuable insight into the interactome of K63-linked polyubiquitylated PCNA is a method that is currently being developed in our laboratory. This approach is based on a split-TURBO ID, which is only activated upon the formation of a specifically linked ubiquitin chain. It biotinylates all proteins in close proximity to this specific ubiquitin chain (writers, readers, and potentially erasers), thereby creating a fingerprint of this specific linkage. The use of the K63-specific system in conjunction with a condition in which PCNA is specifically ubiquitylated with K63-linked ubiquitin chains will result in the formation of a biotinylated fingerprint induced by the K63-linked chain formation. A comparison of this biotinylated proteome to the biotinylated proteome of a condition in which PCNA is not polyubiquitylated may reveal specific readers of the K63-linked ubiquitin chains on PCNA. The identification of Exo1 as a target in one of these mass spectrometry (MS) approaches would demonstrate its preferential interaction with K63-linked polyubiquitylated PCNA and provide substantial support for the hypothesis of its function in initiating TS.

It has been demonstrated that Exo1 functions in general in TS, as has its epistasis with other TS factors. It is proposed that Exo1 facilitates strand invasion by gap expansion and is recruited to the DNA damage bypass site via 9-1-1.[388, 390, 439] The interaction with 9-1-1 has been demonstrated through a Y2H and an epistatic effect in TS.[388, 635] Thus, this interaction could also occur later in the pathway and does not necessarily exclude recruitment of Exo1 via polyubiquitylated PCNA. It has been demonstrated that Exo1 primarily functions as a 5'-3' exonuclease, thereby moving away from PCNA as illustrated in the current model (Figure 1.15). However, it has not yet been demonstrated whether the gap is present in an extended form as depicted in the model. It can therefore be postulated that the gap may loop back, thus bringing the 5' end and the polyubiquitylated PCNA into closer proximity. This would be a possibility to ensure that the recruitment of Exo1 via polyubiquitylated PCNA and the function of Exo1 at the 5' end do not exclude each other. For human EXO1 it was demonstrated that the interaction of EXO1 with PCNA enhances the processivity of EXO1 in DNA resection.[418, 623] It would be of interest to determine whether this also applies to yeast Exo1. Therefore, the DNA damage gap size shall be compared in a wild-type and PIP-box mutant of Exo1 by utilizing fiber assays or monitoring RPA content at DNA damage sites.

There are still many unresolved questions regarding the process of template switching, and further research is needed to identify possible additional factors. The discovery of the PIP-box and a potential interaction of Exo1 with polyubiquitylated PCNA may require adjustments to the positioning of Exo1 in the current model or the overall model. Therefore, additional research is required to clarify this interaction and its relevance in the DNA damage bypass. This will help resolving the open questions in the template switching and ultimately help to create a complete model for this pathway.

5 References

[1] K. W. Barber, J. Rinehart, The ABCs of PTMs. *Nat. Chem. Biol.* 14, 188–192 (2018).

[2] G. A. Khoury, R. C. Baliban, C. A. Floudas, Proteome-wide post-translational modification statistics: frequency analysis and curation of the swiss-prot database. *Sci. Rep.* 1, 90 (2011).

[3] J. M. Berg, J. L. Tymoczko, L. Stryer, G. J. Gatto, *Biochemie* (Springer Spektrum, Berlin, 7. Auflage., 2013; http://dx.doi.org/10.1007/978-3-8274-2989-6).

[4] M. Mann, O. N. Jensen, *Nature Biotechnology*, in press.

[5] I. L. Goldknopf, M. F. French, R. Musso, H. Busch, Presence of protein A24 in rat liver nucleosomes. *Proceedings of the National Academy of Sciences of the United States of America*. 74, 5492--5495 (1977).

[6] R. B. Damgaard, The ubiquitin system: from cell signalling to disease biology and new therapeutic opportunities. *Cell Death Differ.* 28, 423–426 (2021).

[7] A. Zuin, M. Isasa, B. Crosas, Ubiquitin Signaling: Extreme Conservation as a Source of Diversity. *Cells*. 3, 690–701 (2014).

[8] J. W. Yewdell, Not such a dismal science: the economics of protein synthesis, folding, degradation and antigen processing. *Trends Cell Biol.* 11, 294–297 (2001).

[9] D. Komander, M. Rape, The ubiquitin code. *Annu Rev Biochem*. 81, 203--229 (2012).

[10] S. Vijay-Kumar, C. E. Bugg, W. J. Cook, Structure of ubiquitin refined at 1.8 A resolution. *Journal of molecular biology*. 194, 531--544 (1987).

[11] C. Alfano, S. Faggiano, A. Pastore, The Ball and Chain of Polyubiquitin Structures. *Trends Biochem Sci*. 41, 371--385 (2016).

[12] Y. Kimura, K. Tanaka, Regulatory mechanisms involved in the control of ubiquitin homeostasis. *J. Biochem.* 147, 793–798 (2010).

[13] C. P. Grou, M. P. Pinto, A. V. Mendes, P. Domingues, J. E. Azevedo, The de novo synthesis of ubiquitin: identification of deubiquitinases acting on ubiquitin precursors. *Sci. Rep.* 5, 12836 (2015).

[14] R. E. Lenkinski, D. M. Chen, J. D. Glickson, G. Goldstein, Nuclear magnetic resonance studies of the denaturation of ubiquitin. *Biochim. Biophys. Acta (BBA) - Protein Struct.* 494, 126–130 (1977).

[15] I. Dikic, S. Wakatsuki, K. J. Walters, Ubiquitin-binding domains - from structures to functions. *Nat Rev Mol Cell Bio*. 10, 659--671 (2009).

[16] K. E. Sloper-Mould, J. C. Jemc, C. M. Pickart, L. Hicke, Distinct functional surface regions on ubiquitin. *J Biol Chem*. 276, 30483--30489 (2001).

[17] S. Rahighi, F. Ikeda, M. Kawasaki, M. Akutsu, N. Suzuki, R. Kato, T. Kensche, T. Uejima, S. Bloor, D. Komander, F. Randow, S. Wakatsuki, I. Dikic, Specific recognition of linear ubiquitin chains by NEMO is important for NF-kappaB activation. *Cell*. 136, 1098--1109 (2009).

[18] L. Jin, A. Williamson, S. Banerjee, I. Philipp, M. Rape, Mechanism of ubiquitin-chain formation by the human anaphase-promoting complex. *Cell*. 133, 653--665 (2008).

[19] J. M. Winget, T. Mayor, The Diversity of Ubiquitin Recognition: Hot Spots and Varied Specificity. *Mol. Cell*. 38, 627–635 (2010).

[20] A. J. McClellan, S. H. Laugesen, L. Ellgaard, Cellular functions and molecular mechanisms of non-lysine ubiquitination. *Open Biol.* 9, 190147 (2019).

[21] K. N. Swatek, D. Komander, Ubiquitin modifications. *Cell Res*. 26, 399--422 (2016).

[22] R. Yau, M. Rape, The increasing complexity of the ubiquitin code. *Nat. Cell Biol.* 18, 579–586 (2016).

[23] M. D. Stewart, T. Ritterhoff, R. E. Klevit, P. S. Brzovic, E2 enzymes: more than just middle men. *Cell Res.* 26, 423–440 (2016).

[24] N. Zheng, N. Shabek, Ubiquitin Ligases: Structure, Function, and Regulation. *Annu. Rev. Biochem.* 86, 1–29 (2015).

[25] K. F. Witting, M. P. C. Mulder, H. Ovaa, Advancing our Understanding of Ubiquitination Using the Ub-Toolkit. *J Mol Biol*. 429, 3388--3394 (2017).

[26] Y. Ye, M. Rape, Building ubiquitin chains: E2 enzymes at work. *Nat Rev Mol Cell Bio*. 10, 755--764 (2009).

[27] D. Finley, H. D. Ulrich, T. Sommer, P. Kaiser, The ubiquitin-proteasome system of Saccharomyces cerevisiae. *Genetics*. 192, 319--360 (2012).

[28] I. Lee, H. Schindelin, Structural insights into E1-catalyzed ubiquitin activation and transfer to conjugating enzymes. *Cell*. 134, 268--278 (2008).

[29] M. W. Lake, M. M. Wuebbens, K. V. Rajagopalan, H. Schindelin, Mechanism of ubiquitin activation revealed by the structure of a bacterial MoeB-MoaD complex. *Nature*. 414, 325--329 (2001).

[30] C. M. Pickart, MECHANISMS UNDERLYING UBIQUITINATION. *Biochemistry*. 70, 503–533 (2001).

[31] A. Hershko, A. Ciechanover, The ubiquitin system. *Annu Rev Biochem*. 67, 425--479 (1998).

[32] A. L. Haas, J. V. Warms, A. Hershko, I. A. Rose, Ubiquitin-activating enzyme. Mechanism and role in protein-ubiquitin conjugation. *J. Biol. Chem.* 257, 2543–8 (1982).

[33] S. Jentsch, The ubiquitin-conjugation system. *Annual review of genetics*. 26, 179--207 (1992).

[34] S. J. L. van Wijk, H. T. M. Timmers, The family of ubiquitin-conjugating enzymes (E2s): deciding between life and death of proteins. *FASEB J.* 24, 981–993 (2010).

[35] Z. M. Eletr, D. T. Huang, D. M. Duda, B. A. Schulman, B. Kuhlman, E2 conjugating enzymes must disengage from their E1 enzymes before E3-dependent ubiquitin and ubiquitin-like transfer. *Nat. Struct. Mol. Biol.* 12, 933–934 (2005).

[36] M. D. Petroski, R. J. Deshaies, Mechanism of lysine 48-linked ubiquitin-chain synthesis by the cullin-RING ubiquitin-ligase complex SCF-Cdc34. *Cell*. 123, 1107--1120 (2005).

[37] M. Windheim, M. Peggie, P. Cohen, Two different classes of E2 ubiquitin-conjugating enzymes are required for the mono-ubiquitination of proteins and elongation by polyubiquitin chains with a specific topology. *Biochem J*. 409, 723--729 (2008).

[38] Y. David, T. Ziv, A. Admon, A. Navon, The E2 ubiquitin-conjugating enzymes direct polyubiquitination to preferred lysines. *J Biol Chem*. 285, 8595--8604 (2010).

[39] A. J. Middleton, C. L. Day, The molecular basis of lysine 48 ubiquitin chain synthesis by Ube2K. *Sci Rep-uk*. 5, 16793 (2015).

[40] A. P. VanDemark, R. M. Hofmann, C. Tsui, C. M. Pickart, C. Wolberger, Molecular Insights into Polyubiquitin Chain Assembly Crystal Structure of the Mms2/Ubc13 Heterodimer. *Cell*. 105, 711–720 (2001).

[41] S. McKenna, L. Spyracopoulos, T. Moraes, L. Pastushok, C. Ptak, W. Xiao, M. J. Ellison, Noncovalent interaction between ubiquitin and the human DNA repair protein Mms2 is required for Ubc13-mediated polyubiquitination. *J Biol Chem*. 276, 40120--40126 (2001).

[42] L. Deng, C. Wang, E. Spencer, L. Yang, A. Braun, J. You, C. Slaughter, C. Pickart, Z. J. Chen, Activation of the IkappaB kinase complex by TRAF6 requires a dimeric ubiquitin-conjugating enzyme complex and a unique polyubiquitin chain. *Cell*. 103, 351--361 (2000).

[43] T. F. Moraes, R. A. Edwards, S. McKenna, L. Pastushok, W. Xiao, J. MarkN. Glover, M. J. Ellison, *Nature Structural Biology*, in press.

[44] Y.-S. Choi, Y.-J. Lee, S.-Y. Lee, L. Shi, J.-H. Ha, H.-K. Cheong, C. Cheong, R. E. Cohen, K.-S. Ryu, Differential Ubiquitin Binding by the Acidic Loops of Ube2g1 and Ube2r1 Enzymes Distinguishes Their Lys-48-ubiquitylation Activities*. *J. Biol. Chem.* 290, 2251–2263 (2015).

[45] W. J. Cook, P. D. Martin, B. F. P. Edwards, R. K. Yamazaki, V. Chau, Crystal Structure of a Class I Ubiquitin Conjugating Enzyme (Ubc7) from Saccharomyces cerevisiae at 2.9 Å Resolution † , ‡. *Biochemistry*. 36, 1621–1627 (1997).

[46] R. Swanson, M. Locher, M. Hochstrasser, A conserved ubiquitin ligase of the nuclear envelope/endoplasmic reticulum that functions in both ER-associated and Matα2 repressor degradation. *Genes Dev.* 15, 2660–2674 (2001).

[47] J.-G. Lee, H.-S. Youn, J. Y. Kang, S.-Y. Park, A. Kidera, Y. J. Yoo, S. H. Eom, Crystal structure of the Ube2K/E2-25K and K48-linked di-ubiquitin complex provides structural insight into the mechanism of K48-specific ubiquitin chain synthesis. *Biochem. Biophys. Res. Commun.* 506, 102–107 (2018).

[48] L. Pluska, E. Jarosch, H. Zauber, A. Kniss, A. Waltho, K. Bagola, M. von Delbruck, F. Lohr, B. A. Schulman, M. Selbach, V. Dotsch, T. Sommer, The UBA domain of conjugating enzyme Ubc1/Ube2K facilitates assembly of K48/K63-branched ubiquitin chains. *Embo J*. 40, e106094 (2021).

[49] Z. Chen, C. M. Pickart, A 25-kilodalton ubiquitin carrier protein (E2) catalyzes multi-ubiquitin chain synthesis via lysine 48 of ubiquitin. *The Journal of biological chemistry*. 265, 21835--21842 (1990).

[50] Q. Yang, J. Zhao, D. Chen, Y. Wang, E3 ubiquitin ligases: styles, structures and functions. *Mol. Biomed.* 2, 23 (2021).

[51] R. J. Deshaies, C. A. P. Joazeiro, RING domain E3 ubiquitin ligases. *Annu Rev Biochem.* 78, 399--434 (2009).

[52] C. D. Lima, B. A. Schulman, Structural biology: A protein engagement RING. *Nature*. 489, 43--44 (2012).

[53] B. Sharma, J. Taganna, Genome-wide analysis of the U-box E3 ubiquitin ligase enzyme gene family in tomato. *Sci. Rep.* 10, 9581 (2020).

[54] M. D. Ohi, C. W. V. Kooi, J. A. Rosenberg, W. J. Chazin, K. L. Gould, Structural insights into the U-box, a domain associated with multi-ubiquitination. *Nat Struct Mol Biol*. 10, 250--255 (2003).

[55] R. K. Singh, M. Gonzalez, M.-H. M. Kabbaj, A. Gunjan, Novel E3 ubiquitin ligases that regulate histone protein levels in the budding yeast Saccharomyces cerevisiae. *Plos One*. 7, e36295 (2012).

[56] H. C. Kim, J. M. Huibregtse, Polyubiquitination by HECT E3s and the determinants of chain type specificity. *Mol Cell Biol*. 29, 3307--3318 (2009).

[57] Z. M. Eletr, B. Kuhlman, Sequence determinants of E2-E6AP binding affinity and specificity. *J Mol Biol*. 369, 419--428 (2007).

[58] L. K. Ries, B. Sander, K. K. Deol, M.-A. Letzelter, E. R. Strieter, S. Lorenz, Analysis of ubiquitin recognition by the HECT ligase E6AP provides insight into its linkage specificity. *J Biol Chem* (2019), doi:10.1074/jbc.ra118.007014.

[59] J. M. Huibregtse, M. Scheffner, S. Beaudenon, P. M. Howley, A family of proteins structurally and functionally related to the E6-AP ubiquitin-protein ligase. *Proc. Natl. Acad. Sci.* 92, 2563–2567 (1995).

[60] D. M. Wenzel, A. Lissounov, P. S. Brzovic, R. E. Klevit, UBCH7 reactivity profile reveals parkin and HHARI to be RING/HECT hybrids. *Nature*. 474, 105--108 (2011).

[61] B. Gerlach, S. M. Cordier, A. C. Schmukle, C. H. Emmerich, E. Rieser, T. L. Haas, A. I. Webb, J. A. Rickard, H. Anderton, W. W.-L. Wong, U. Nachbur, L. Gangoda, U. Warnken, A. W. Purcell, J. Silke, H. Walczak, Linear ubiquitination prevents inflammation and regulates immune signalling. *Nature*. 471, 591--596 (2011).

[62] D. M. Wenzel, R. E. Klevit, Following Ariadne's thread: a new perspective on RBR ubiquitin ligases. *BMC Biol.* 10, 24 (2012).

[63] C. G. Burd, S. D. Emr, Phosphatidylinositol(3)-phosphate signaling mediated by specific binding to RING FYVE domains. *Molecular cell*. 2, 157--162 (1998).

[64] C. Renz, V. Albanèse, V. Tröster, T. K. Albert, O. Santt, S. C. Jacobs, A. Khmelinskii, S. Léon, H. D. Ulrich, Ubc13–Mms2 cooperates with a family of RING E3 proteins in budding yeast membrane protein sorting. *J Cell Sci*. 133, jcs244566 (2020).

[65] M. B. Metzger, Y.-H. Liang, R. Das, J. Mariano, S. Li, J. Li, Z. Kostova, R. A. Byrd, X. Ji, A. M. Weissman, A structurally unique E2-binding domain activates ubiquitination by the ERAD E2, Ubc7p, through multiple mechanisms. *Mol Cell*. 50, 516--527 (2013).

[66] T. Biederer, C. Volkwein, T. Sommer, Role of Cue1p in Ubiquitination and Degradation at the ER Surface. *Science*. 278, 1806–1809 (1997).

[67] N. W. Bays, R. G. Gardner, L. P. Seelig, C. A. Joazeiro, R. Y. Hampton, Hrd1p/Der3p is a membrane-anchored ubiquitin ligase required for ER-associated degradation. *Nat Cell Biol*. 3, 24--29 (2001).

[68] K. Bagola, M. von Delbruck, G. Dittmar, M. Scheffner, I. Ziv, M. H. Glickman, A. Ciechanover, T. Sommer, Ubiquitin binding by a CUE domain regulates ubiquitin chain formation by ERAD E3 ligases. *Mol Cell*. 50, 528--539 (2013).

[69] M. von Delbruck, A. Kniss, V. V. Rogov, L. Pluska, K. Bagola, F. Lohr, P. Guntert, T. Sommer, V. Dotsch, The CUE Domain of Cue1 Aligns Growing Ubiquitin Chains with Ubc7 for Rapid Elongation. *Mol Cell*. 62, 918--928 (2016).

[70] L. Hicke, H. L. Schubert, C. P. Hill, Ubiquitin-binding domains. *Nat Rev Mol Cell Bio*. 6, 610--621 (2005).

[71] K. Husnjak, I. Dikic, Ubiquitin-binding proteins: decoders of ubiquitin-mediated cellular functions. *Annu Rev Biochem.* 81, 291--322 (2012).

[72] R. S. Kang, C. M. Daniels, S. A. Francis, S. C. Shih, W. J. Salerno, L. Hicke, I. Radhakrishnan, Solution Structure of a CUE-Ubiquitin Complex Reveals a Conserved Mode of Ubiquitin Binding. *Cell*. 113, 621–630 (2003).

[73] R. D. Fisher, B. Wang, S. L. Alam, D. S. Higginson, H. Robinson, W. I. Sundquist, C. P. Hill, Structure and ubiquitin binding of the ubiquitin-interacting motif. *J Biol Chem*. 278, 28976--28984 (2003).

[74] S. L. Alam, J. Sun, M. Payne, B. D. Welch, B. K. Blake, D. R. Davis, H. H. Meyer, S. D. Emr, W. I. Sundquist, Ubiquitin interactions of NZF zinc fingers. *EMBO J.* 23, 1411–1421 (2004).

[75] J. J. Sims, R. E. Cohen, Linkage-specific avidity defines the lysine 63-linked polyubiquitin-binding preference of rap80. *Mol Cell*. 33, 775--783 (2009).

[76] M. J. Clague, S. Urbe, D. Komander, Breaking the chains: deubiquitylating enzyme specificity begets function. *Nat Rev Mol Cell Bio* (2019), doi:10.1038/s41580-019-0099-1.

[77] N. A. Snyder, G. M. Silva, Deubiquitinating enzymes (DUBs): Regulation, homeostasis, and oxidative stress response. *J. Biol. Chem.* 297, 101077 (2021).

[78] Y. Li, D. Reverter, Molecular Mechanisms of DUBs Regulation in Signaling and Disease. *Int. J. Mol. Sci.* 22, 986 (2021).

[79] T. E. T. Mevissen, D. Komander, Mechanisms of Deubiquitinase Specificity and Regulation. *Annu Rev Biochem*. 86, 159--192 (2017).

[80] A. Y. Amerik, M. Hochstrasser, Mechanism and function of deubiquitinating enzymes. *Biochim. Biophys. Acta (BBA) - Mol. Cell Res.* 1695, 189–207 (2004).

[81] X. I. Ambroggio, D. C. Rees, R. J. Deshaies, JAMM: A Metalloprotease-Like Zinc Site in the Proteasome and Signalosome. *PLoS Biol.* 2, e2 (2004).

[82] R. K. Shrestha, J. A. Ronau, C. W. Davies, R. G. Guenette, E. R. Strieter, L. N. Paul, C. Das, Insights into the Mechanism of Deubiquitination by JAMM Deubiquitinases from Cocrystal Structures of the Enzyme with the Substrate and Product. *Biochemistry*. 53, 3199–3217 (2014).

[83] I. Dikic, Proteasomal and Autophagy Degradation Systems. *Annu. Rev. Biochem.* 86, 1–32 (2016).

[84] C. M. Pickart, I. A. Rose, Ubiquitin carboxyl-terminal hydrolase acts on ubiquitin carboxyl-terminal amides. *J. Biol. Chem.* 260, 7903–7910 (1985).

[85] D. D. Sahtoe, T. K. Sixma, Layers of DUB regulation. *Trends Biochem. Sci.* 40, 456–467 (2015).

[86] F. E. Reyes-Turcu, J. R. Shanks, D. Komander, K. D. Wilkinson, Recognition of polyubiquitin isoforms by the multiple ubiquitin binding modules of isopeptidase T. *J Biol Chem*. 283, 19581--19592 (2008).

[87] M. K. Hospenthal, T. E. T. Mevissen, D. Komander, Deubiquitinase-based analysis of ubiquitin chain architecture using Ubiquitin Chain Restriction (UbiCRest). *Nat. Protoc.* 10, 349–361 (2015).

[88] L. Kategaya, P. D. Lello, L. Rouge, R. Pastor, K. R. Clark, J. Drummond, T. Kleinheinz, E. Lin, J.-P. Upton, S. Prakash, J. Heideker, M. McCleland, M. S. Ritorto, D. R. Alessi, M. Trost, T. W. Bainbridge, M. C. M. Kwok, T. P. Ma, Z. Stiffler, B. Brasher, Y. Tang, P. Jaishankar, B. R. Hearn, A. R. Renslo, M. R. Arkin, F. Cohen, K. Yu, F. Peale, F. Gnad, M. T. Chang, C. Klijn, E. Blackwood, S. E. Martin, W. F. Forrest, J. A. Ernst, C. Ndubaku, X. Wang, M. H. Beresini, V. Tsui, C. Schwerdtfeger, R. A. Blake, J. Murray, T. Maurer, I. E. Wertz, USP7 small-molecule inhibitors interfere with ubiquitin binding. *Nature*. 550, 534--538 (2017).

[89] M. S. Ritorto, R. Ewan, A. B. Perez-Oliva, A. Knebel, S. J. Buhrlage, M. Wightman, S. M. Kelly, N. T. Wood, S. Virdee, N. S. Gray, N. A. Morrice, D. R. Alessi, M. Trost, *Nature Communications*, in press.

[90] J. McCullough, M. J. Clague, S. Urbe, AMSH is an endosome-associated ubiquitin isopeptidase. *J Cell Biology*. 166, 487--492 (2004).

[91] Y. Sato, A. Yoshikawa, A. Yamagata, H. Mimura, M. Yamashita, K. Ookata, O. Nureki, K. Iwai, M. Komada, S. Fukai, Structural basis for specific cleavage of Lys 63-linked polyubiquitin chains. *Nature*. 455, 358--362 (2008).

[92] M. Hologne, F.-X. Cantrelle, G. Riviere, F. Guilliere, X. Trivelli, O. Walker, NMR Reveals the Interplay among the AMSH SH3 Binding Motif, STAM2, and Lys63-Linked Diubiquitin. *J Mol Biol*. 428, 4544--4558 (2016).

[93] M. J. Edelmann, A. Iphofer, M. Akutsu, M. Altun, K. D. Gleria, H. B. Kramer, E. Fiebiger, S. Dhe-Paganon, B. M. Kessler, Structural basis and specificity of human otubain 1-mediated deubiquitination. *Biochem J*. 418, 379--390 (2009).

[94] N. Frias-Staheli, N. V. Giannakopoulos, M. Kikkert, S. L. Taylor, A. Bridgen, J. Paragas, J. A. Richt, R. R. Rowland, C. S. Schmaljohn, D. J. Lenschow, E. J. Snijder, A. Garcia-Sastre, H. W. Virgin, Ovarian tumor domain-containing viral proteases evade ubiquitin- and ISG15-dependent innate immune responses. *Cell Host Microbe*. 2, 404--416 (2007).

[95] S. Nakada, I. Tai, S. Panier, A. Al-Hakim, S.-I. Iemura, Y.-C. Juang, L. O'Donnell, A. Kumakubo, M. Munro, F. Sicheri, A.-C. Gingras, T. Natsume, T. Suda, D. Durocher, Non-canonical inhibition of DNA damage-dependent ubiquitination by OTUB1. *Nature*. 466, 941--946 (2010).

[96] S. E. Kaiser, B. E. Riley, T. A. Shaler, R. S. Trevino, C. H. Becker, H. Schulman, R. R. Kopito, Protein standard absolute quantification (PSAQ) method for the measurement of cellular ubiquitin pools. *Nat Methods*. 8, 691--696 (2011).

[97] M. J. Clague, C. Heride, S. Urbe, The demographics of the ubiquitin system. *Trends Cell Biol*. 25, 417--426 (2015).

[98] R. L. Seale, Rapid turnover of the histone-ubiquitin conjugate, protein A24. *Nucleic Acids Res.* 9, 3151–3158 (1981).

[99] M. R. Northam, K. M. Trujillo, Histone H2B mono-ubiquitylation maintains genomic integrity at stalled replication forks. *Nucleic Acids Res*. 44, 9245--9255 (2016).

[100] A. Gallego-Sanchez, S. Andres, F. Conde, P. A. San-Segundo, A. Bueno, Reversal of PCNA ubiquitylation by Ubp10 in Saccharomyces cerevisiae. *Plos Genet*. 8, e1002826 (2012).

[101] P. Stelter, H. D. Ulrich, Control of spontaneous and damage-induced mutagenesis by SUMO and ubiquitin conjugation. *Nature*. 425, 188--191 (2003).

[102] D. K. Stringer, R. C. Piper, A single ubiquitin is sufficient for cargo protein entry into MVBs in the absence of ESCRT ubiquitination. *J Cell Biology*. 192, 229--242 (2011).

[103] D. Hoeller, N. Crosetto, B. Blagoev, C. Raiborg, R. Tikkanen, S. Wagner, K. Kowanetz, R. Breitling, M. Mann, H. Stenmark, I. Dikic, Regulation of ubiquitin-binding proteins by monoubiquitination. *Nat Cell Biol*. 8, 163--169 (2006).

[104] Y. Mosesson, K. Shtiegman, M. Katz, Y. Zwang, G. Vereb, J. Szollosi, Y. Yarden, Endocytosis of receptor tyrosine kinases is driven by monoubiquitylation, not polyubiquitylation. *J Biol Chem*. 278, 21323--21326 (2003).

[105] I. Ziv, Y. Matiuhin, D. S. Kirkpatrick, Z. Erpapazoglou, S. Leon, M. Pantazopoulou, W. Kim, S. P. Gygi, R. Haguenauer-Tsapis, N. Reis, M. H. Glickman, O. Kleifeld, *Mol Cell Proteomics*, in press, doi:10.1074/mcp.m111.009753.

[106] F. Ohtake, Y. Saeki, S. Ishido, J. Kanno, K. Tanaka, The K48-K63 Branched Ubiquitin Chain Regulates NF-κB Signaling. *Mol Cell*. 64, 251–266 (2016).

[107] J. Peng, D. Schwartz, J. E. Elias, C. C. Thoreen, D. Cheng, G. Marsischky, J. Roelofs, D. Finley, S. P. Gygi, A proteomics approach to understanding protein ubiquitination. *Nat. Biotechnol.* 21, 921–926 (2003).

[108] P. Xu, D. M. Duong, N. T. Seyfried, D. Cheng, Y. Xie, J. Robert, J. Rush, M. Hochstrasser, D. Finley, J. Peng, Quantitative proteomics reveals the function of unconventional ubiquitin chains in proteasomal degradation. *Cell*. 137, 133--145 (2009).

[109] Y. Ryabov, D. Fushman, Interdomain mobility in di-ubiquitin revealed by NMR. *Proteins Struct Funct Bioinform*. 63, 787--796 (2006).

[110] R. Varadan, O. Walker, C. Pickart, D. Fushman, Structural properties of polyubiquitin chains in solution. *Journal of molecular biology*. 324, 637--647 (2002).

[111] O. F. Lange, N.-A. Lakomek, C. Fares, G. F. Schroder, K. F. A. Walter, S. Becker, J. Meiler, H. Grubmuller, C. Griesinger, B. L. de Groot, Recognition dynamics up to microseconds revealed from an RDC-derived ubiquitin ensemble in solution. *Science*. 320, 1471--1475 (2008).

[112] D. Fushman, O. Walker, Exploring the Linkage Dependence of Polyubiquitin Conformations Using Molecular Modeling. *J. Mol. Biol.* 395, 803–814 (2010).

[113] R. Varadan, M. Assfalg, A. Haririnia, S. Raasi, C. Pickart, D. Fushman, Solution conformation of Lys63-linked di-ubiquitin chain provides clues to functional diversity of polyubiquitin signaling. *J Biol Chem.* 279, 7055--7063 (2004).

[114] A. Hershko, E. Leshinsky, D. Ganoth, H. Heller, ATP-dependent degradation of ubiquitin-protein conjugates. *Proc. Natl. Acad. Sci.* 81, 1619–1623 (1984).

[115] A. Ciehanover, Y. Hod, A. Hershko, A heat-stable polypeptide component of an ATP-dependent proteolytic system from reticulocytes. *Biochem. Biophys. Res. Commun.* 81, 1100–1105 (1978).

[116] A. Hershko, A. Ciechanover, H. Heller, A. L. Haas, I. A. Rose, Proposed role of ATP in protein breakdown: conjugation of protein with multiple chains of the polypeptide of ATP-dependent proteolysis. *Proc. Natl. Acad. Sci.* 77, 1783–1786 (1980).

[117] A. Varshavsky, The early history of the ubiquitin field. *Protein Sci.* 15, 647–654 (2006).

[118] D. Finley, S. Sadis, B. P. Monia, P. Boucher, D. J. Ecker, S. T. Crooke, V. Chau, Inhibition of proteolysis and cell cycle progression in a multiubiquitination-deficient yeast mutant. *Molecular and cellular biology*. 14, 5501--5509 (1994).

[119] J. S. Thrower, L. Hoffman, M. Rechsteiner, C. M. Pickart, Recognition of the polyubiquitin proteolytic signal. *Embo J*. 19, 94--102 (2000).

[120] Y. Lu, B. Lee, R. W. King, D. Finley, M. W. Kirschner, Substrate degradation by the proteasome: a single-molecule kinetic analysis. *Science*. 348, 1250834 (2015).

[121] T. Tasaki, S. M. Sriram, K. S. Park, Y. T. Kwon, The N-end rule pathway. *Annu Rev Biochem*. 81, 261--289 (2012).

[122] A. Klotzbucher, E. Stewart, D. Harrison, T. Hunt, The “destruction box” of cyclin A allows B-type cyclins to be ubiquitinated, but not efficiently destroyed. *The EMBO journal*. 15, 3053--3064 (1996).

[123] K. Flick, S. Raasi, H. Zhang, J. L. Yen, P. Kaiser, *Nature cell biology*, in press.

[124] K. Flick, I. Ouni, J. A. Wohlschlegel, C. Capati, W. H. McDonald, J. R. Yates, P. Kaiser, Proteolysis-independent regulation of the transcription factor Met4 by a single Lys 48-linked ubiquitin chain. *Nat Cell Biol*. 6, 634--641 (2004).

[125] P. Tonzi, Y. Yin, C. W. T. Lee, E. Rothenberg, T. T. Huang, Translesion polymerase kappa-dependent DNA synthesis underlies replication fork recovery. *Elife*. 7, e41426 (2018).

[126] L. Phu, A. Izrael-Tomasevic, M. L. Matsumoto, D. Bustos, J. N. Dynek, A. V. Fedorova, C. E. Bakalarski, D. Arnott, K. Deshayes, V. M. Dixit, R. F. Kelley, D. Vucic, D. S. Kirkpatrick, *Mol Cell Proteomics*, in press, doi:10.1074/mcp.m110.003756.

[127] A. Al-Hakim, C. Escribano-Diaz, M.-C. Landry, L. O’Donnell, S. Panier, R. K. Szilard, D. Durocher, The ubiquitous role of ubiquitin in the DNA damage response. *Dna Repair*. 9, 1229--1240 (2010).

[128] G. Smeenk, N. Mailand, Writers, Readers, and Erasers of Histone Ubiquitylation in DNA Double-Strand Break Repair. *Frontiers Genetics*. 7, 122 (2016).

[129] P. Schwertman, S. Bekker-Jensen, N. Mailand, Regulation of DNA double-strand break repair by ubiquitin and ubiquitin-like modifiers. *Nat. Rev. Mol. Cell Biol*. 17, 379–394 (2016).

[130] Z. Erpapazoglou, O. Walker, R. Haguenauer-Tsapis, Versatile roles of k63-linked ubiquitin chains in trafficking. *Cells*. 3, 1027--1088 (2014).

[131] E. Lauwers, C. Jacob, B. André, K63-linked ubiquitin chains as a specific signal for protein sorting into the multivesicular body pathway. *J. Cell Biol.* 185, 493–502 (2009).

[132] Z. Erpapazoglou, M. Dhaoui, M. Pantazopoulou, F. Giordano, M. Mari, S. Léon, G. Raposo, F. Reggiori, R. Haguenauer-Tsapis, A dual role for K63-linked ubiquitin chains in multivesicular body biogenesis and cargo sorting. *Mol. Biol. Cell*. 23, 2170–2183 (2012).

[133] F. Huang, X. Zeng, W. Kim, M. Balasubramani, A. Fortian, S. P. Gygi, N. A. Yates, A. Sorkin, Lysine 63-linked polyubiquitination is required for EGF receptor degradation. *Proc. Natl. Acad. Sci.* 110, 15722–15727 (2013).

[134] P. S. Manzanillo, J. S. Ayres, R. O. Watson, A. C. Collins, G. Souza, C. S. Rae, D. S. Schneider, K. Nakamura, M. U. Shiloh, J. S. Cox, The ubiquitin ligase parkin mediates resistance to intracellular pathogens. *Nature*. 501, 512–516 (2013).

[135] C. Wang, L. Deng, M. Hong, G. R. Akkaraju, J. Inoue, Z. J. Chen, TAK1 is a ubiquitin-dependent kinase of MKK and IKK. *Nature*. 412, 346--351 (2001).

[136] H. Wajant, P. Scheurich, TNFR1-induced activation of the classical NF-κB pathway. *FEBS J.* 278, 862–876 (2011).

[137] M. Tracz, W. Bialek, Beyond K48 and K63: non-canonical protein ubiquitination. *Cell Mol Biol Lett*. 26, 1 (2021).

[138] K. Rittinger, F. Ikeda, Linear ubiquitin chains: enzymes, mechanisms and biology. *Open Biol*. 7 (2017), doi:10.1098/rsob.170026.

[139] H. Tsuchiya, F. Ohtake, N. Arai, A. Kaiho, S. Yasuda, K. Tanaka, Y. Saeki, In Vivo Ubiquitin Linkage-type Analysis Reveals that the Cdc48-Rad23/Dsk2 Axis Contributes to K48-Linked Chain Specificity of the Proteasome. *Mol Cell*. 66, 488-502.e7 (2017).

[140] T. Kirisako, K. Kamei, S. Murata, M. Kato, H. Fukumoto, M. Kanie, S. Sano, F. Tokunaga, K. Tanaka, K. Iwai, A ubiquitin ligase complex assembles linear polyubiquitin chains. *Embo J*. 25, 4877--4887 (2006).

[141] J. J. Smit, D. Monteferrario, S. M. Noordermeer, W. J. van Dijk, B. A. van der Reijden, T. K. Sixma, The E3 ligase HOIP specifies linear ubiquitin chain assembly through its RING-IBR-RING domain and the unique LDD extension. *EMBO J.* 31, 3833–3844 (2012).

[142] I. R. Kelsall, J. Zhang, A. Knebel, J. S. C. Arthur, P. Cohen, The E3 ligase HOIL-1 catalyses ester bond formation between ubiquitin and components of the Myddosome in mammalian cells. *Proc. Natl. Acad. Sci.* 116, 13293–13298 (2019).

[143] F. Ikeda, Y. L. Deribe, S. S. Skånland, B. Stieglitz, C. Grabbe, M. Franz-Wachtel, S. J. L. van Wijk, P. Goswami, V. Nagy, J. Terzic, F. Tokunaga, A. Androulidaki, T. Nakagawa, M. Pasparakis, K. Iwai, J. P. Sundberg, L. Schaefer, K. Rittinger, B. Macek, I. Dikic, SHARPIN forms a linear ubiquitin ligase complex regulating NF-κB activity and apoptosis. *Nature*. 471, 637–641 (2011).

[144] C. H. Emmerich, A. Ordureau, S. Strickson, J. S. C. Arthur, P. G. A. Pedrioli, D. Komander, P. Cohen, Activation of the canonical IKK complex by K63/M1-linked hybrid ubiquitin chains. *Proc National Acad Sci*. 110, 15247--15252 (2013).

[145] M. Hrdinka, M. Gyrd-Hansen, The Met1-Linked Ubiquitin Machinery: Emerging Themes of (De)regulation. *Mol Cell*. 68, 265--280 (2017).

[146] B. K. Fiil, M. Gyrd-Hansen, Met1-linked ubiquitination in immune signalling. *FEBS J*. 281, 4337–4350 (2014).

[147] Y. Sasaki, S. Sano, M. Nakahara, S. Murata, K. Kometani, Y. Aiba, S. Sakamoto, Y. Watanabe, K. Tanaka, T. Kurosaki, K. Iwai, Defective immune responses in mice lacking LUBAC-mediated linear ubiquitination in B cells. *EMBO J.* 32, 2463–2476 (2013).

[148] E. M. van Well, V. Bader, M. Patra, A. Sanchez-Vicente, J. Meschede, N. Furthmann, C. Schnack, A. Blusch, J. Longworth, E. Petrasch-Parwez, K. Mori, T. Arzberger, D. Trumbach, L. Angersbach, C. Showkat, D. A. Sehr, L. A. Berlemann, P. Goldmann, A. M. Clement, C. Behl, A. C. Woerner, C. Saft, W. Wurst, C. Haass, G. Ellrichmann, R. Gold, G. Dittmar, M. S. Hipp, F. U. Hartl, J. Tatzelt, K. F. Winklhofer, A protein quality control pathway regulated by linear ubiquitination. *Embo J* (2019), doi:10.15252/embj.2018100730.

[149] Z. Wu, L. A. Berlemann, V. Bader, D. A. Sehr, E. Dawin, A. Covallero, J. Meschede, L. Angersbach, C. Showkat, J. B. Michaelis, C. Münch, B. Rieger, D. Namgaladze, M. G. Herrera, F. C. Fiesel, W. Springer, M. Mendes, J. Stepien, K. Barkovits, K. Marcus, A. Sickmann, G. Dittmar, K. B. Busch, D. Riedel, M. Brini, J. Tatzelt, T. Cali, K. F. Winklhofer, LUBAC assembles a ubiquitin signaling platform at mitochondria for signal amplification and transport of NF-κB to the nucleus. *Embo J*, e112006 (2022).

[150] T. M. Durcan, M. Y. Tang, J. R. Pérusse, E. A. Dashti, M. A. Aguileta, G. McLelland, P. Gros, T. A. Shaler, D. Faubert, B. Coulombe, E. A. Fon, USP8 regulates mitophagy by removing K6-linked ubiquitin conjugates from parkin. *EMBO J.* 33, 2473–2491 (2014).

[151] A. Ordureau, J.-M. Heo, D. M. Duda, J. A. Paulo, J. L. Olszewski, D. Yanishevski, J. Rinehart, B. A. Schulman, J. W. Harper, Defining roles of PARKIN and ubiquitin phosphorylation by PINK1 in mitochondrial quality control using a ubiquitin replacement strategy. *Proc National Acad Sci*. 112, 6637--6642 (2015).

[152] A. Ordureau, S. A. Sarraf, D. M. Duda, J.-M. Heo, M. P. Jedrychowski, V. O. Sviderskiy, J. L. Olszewski, J. T. Koerber, T. Xie, S. A. Beausoleil, J. A. Wells, S. P. Gygi, B. A. Schulman, J. W. Harper, Quantitative Proteomics Reveal a Feedforward Mechanism for Mitochondrial PARKIN Translocation and Ubiquitin Chain Synthesis. *Mol. Cell*. 56, 360–375 (2014).

[153] B. Bingol, J. S. Tea, L. Phu, M. Reichelt, C. E. Bakalarski, Q. Song, O. Foreman, D. S. Kirkpatrick, M. Sheng, *Nature*, in press.

[154] C. N. Cunningham, J. M. Baughman, L. Phu, J. S. Tea, C. Yu, M. Coons, D. S. Kirkpatrick, B. Bingol, J. E. Corn, USP30 and parkin homeostatically regulate atypical ubiquitin chains on mitochondria. *Nat. Cell Biol.* 17, 160–169 (2015).

[155] A. E. H. Elia, A. P. Boardman, D. C. Wang, E. L. Huttlin, R. A. Everley, N. Dephoure, C. Zhou, I. Koren, S. P. Gygi, S. J. Elledge, Quantitative Proteomic Atlas of Ubiquitination and Acetylation in the DNA Damage Response. *Mol Cell*. 59, 867--881 (2015).

[156] J. R. Morris, E. Solomon, BRCA1: BARD1 induces the formation of conjugated ubiquitin structures, dependent on K6 of ubiquitin, in cells during DNA replication and repair. *Hum Mol Genet*. 13, 807--817 (2004).

[157] F. Wu-Baer, K. Lagrazon, W. Yuan, R. Baer, The BRCA1/BARD1 Heterodimer Assembles Polyubiquitin Chains through an Unconventional Linkage Involving Lysine Residue K6 of Ubiquitin*. *J. Biol. Chem.* 278, 34743–34746 (2003).

[158] J. B. Heidelberger, A. Voigt, M. E. Borisova, G. Petrosino, S. Ruf, S. A. Wagner, P. Beli, Proteomic profiling of VCP substrates links VCP to K6-linked ubiquitylation and c-Myc function. *EMBO Rep.* 19 (2018), doi:10.15252/embr.201744754.

[159] K. B. Cassidy, S. Bang, M. Kurokawa, S. A. Gerber, Direct regulation of Chk1 protein stability by E3 ubiquitin ligase HUWE1. *FEBS J.* 287, 1985–1999 (2020).

[160] M. A. Michel, K. N. Swatek, M. K. Hospenthal, D. Komander, Ubiquitin Linkage-Specific Affimers Reveal Insights into K6-Linked Ubiquitin Signaling. *Mol Cell*. 68, 233-246.e5 (2017).

[161] Y. Yuan, Y. Miao, L. Qian, Y. Zhang, C. Liu, J. Liu, Y. Zuo, Q. Feng, T. Guo, L. Zhang, X. Chen, L. Jin, F. Huang, H. Zhang, W. Zhang, W. Li, G. Xu, H. Zheng, Targeting UBE4A Revives Viperin Protein in Epithelium to Enhance Host Antiviral Defense. *Mol. Cell*. 77, 734-747.e7 (2020).

[162] A. S. Rahmanto, C. J. Blum, C. Scalera, J. B. Heidelberger, M. Mesitov, D. Horn-Ghetko, J. F. Gräf, I. Mikicic, R. Hobrecht, A. Orekhova, M. Ostermaier, S. Ebersberger, M. M. Möckel, N. Krapoth, N. D. S. Fernandes, A. Mizi, Y. Zhu, J.-X. Chen, C. Choudhary, A. Papantonis, H. D. Ulrich, B. A. Schulman, J. König, P. Beli, K6-linked ubiquitylation marks formaldehyde-induced RNA-protein crosslinks for resolution. *Mol. Cell*. 83, 4272-4289.e10 (2023).

[163] D. Srivastava, O. Chakrabarti, Mahogunin-mediated α-tubulin ubiquitination via noncanonical K6 linkage regulates microtubule stability and mitotic spindle orientation. *Cell Death Dis.* 5, e1064–e1064 (2014).

[164] R. Mukherjee, P. Majumder, O. Chakrabarti, MGRN1-mediated ubiquitination of α-tubulin regulates microtubule dynamics and intracellular transport. *Traffic*. 18, 791–807 (2017).

[165] M. L. Matsumoto, K. E. Wickliffe, K. C. Dong, C. Yu, I. Bosanac, D. Bustos, L. Phu, D. S. Kirkpatrick, S. G. Hymowitz, M. Rape, R. F. Kelley, V. M. Dixit, K11-linked polyubiquitination in cell cycle control revealed by a K11 linkage-specific antibody. *Mol Cell*. 39, 477--484 (2010).

[166] H.-J. Meyer, M. Rape, Enhanced protein degradation by branched ubiquitin chains. *Cell*. 157, 910--921 (2014).

[167] G. L. Grice, I. T. Lobb, M. P. Weekes, S. P. Gygi, R. Antrobus, J. A. Nathan, The Proteasome Distinguishes between Heterotypic and Homotypic Lysine-11-Linked Polyubiquitin Chains. *Cell Rep.* 12, 545–553 (2015).

[168] J. N. Dynek, T. Goncharov, E. C. Dueber, A. V. Fedorova, A. Izrael-Tomasevic, L. Phu, E. Helgason, W. J. Fairbrother, K. Deshayes, D. S. Kirkpatrick, D. Vucic, c-IAP1 and UbcH5 promote K11-linked polyubiquitination of RIP1 in TNF signalling. *Embo J*. 29, 4198--4209 (2010).

[169] A. Paul, B. Wang, RNF8- and Ube2S-Dependent Ubiquitin Lysine 11-Linkage Modification in Response to DNA Damage. *Mol. Cell*. 66, 458-472.e5 (2017).

[170] C.-Q. Lei, X. Wu, X. Zhong, L. Jiang, B. Zhong, H.-B. Shu, USP19 Inhibits TNF-α– and IL-1β–Triggered NF-κB Activation by Deubiquitinating TAK1. *J. Immunol.* 203, 259–268 (2019).

[171] Q. Wang, X. Liu, Y. Cui, Y. Tang, W. Chen, S. Li, H. Yu, Y. Pan, C. Wang, The E3 ubiquitin ligase AMFR and INSIG1 bridge the activation of TBK1 kinase by modifying the adaptor STING. *Immunity*. 41, 919--933 (2014).

[172] M. Gatti, S. Pinato, A. Maiolica, F. Rocchio, M. G. Prato, R. Aebersold, L. Penengo, RNF168 promotes noncanonical K27 ubiquitination to signal DNA damage. *Cell Reports*. 10, 226--238 (2015).

[173] E. S. Johnson, P. C. Ma, I. M. Ota, A. Varshavsky, A proteolytic pathway that recognizes ubiquitin as a degradation signal. *The Journal of biological chemistry*. 270, 17442--17456 (1995).

[174] M. Koegl, T. Hoppe, S. Schlenker, H. D. Ulrich, T. U. Mayer, S. Jentsch, A Novel Ubiquitination Factor, E4, Is Involved in Multiubiquitin Chain Assembly. *Cell*. 96, 635–644 (1999).

[175] C. Liu, W. Liu, Y. Ye, W. Li, Ufd2p synthesizes branched ubiquitin chains to promote the degradation of substrates modified with atypical chains. *Nat. Commun.* 8, 14274 (2017).

[176] B. Huang, S.-H. Baek, *Mol. Pharmacol.*, in press, doi:10.1124/mol.116.106716.

[177] S. Zucchelli, M. Codrich, F. Marcuzzi, M. Pinto, S. Vilotti, M. Biagioli, I. Ferrer, S. Gustincich, TRAF6 promotes atypical ubiquitination of mutant DJ-1 and alpha-synuclein and is localized to Lewy bodies in sporadic Parkinson's disease brains. *Hum. Mol. Genet.* 19, 3759–3770 (2010).

[178] C. Fei, Z. Li, C. Li, Y. Chen, Z. Chen, X. He, L. Mao, X. Wang, R. Zeng, L. Li, Smurf1-mediated Lys29-linked nonproteolytic polyubiquitination of axin negatively regulates Wnt/\textgreekb-catenin signaling. *Mol Cell Biol*. 33, 4095--4105 (2013).

[179] W.-C. Yuan, Y.-R. Lee, S.-Y. Lin, L.-Y. Chang, Y. P. Tan, C.-C. Hung, J.-C. Kuo, C.-H. Liu, M.-Y. Lin, M. Xu, Z. J. Chen, R.-H. Chen, K33-Linked Polyubiquitination of Coronin 7 by Cul3-KLHL20 Ubiquitin E3 Ligase Regulates Protein Trafficking. *Mol Cell*. 54, 586--600 (2014).

[180] A. K. Al-Hakim, A. Zagorska, L. Chapman, M. Deak, M. Peggie, D. R. Alessi, Control of AMPK-related kinases by USP9X and atypical Lys(29)/Lys(33)-linked polyubiquitin chains. *Biochem J*. 411, 249--260 (2008).

[181] H. Huang, M.-S. Jeon, L. Liao, C. Yang, C. Elly, J. R. Yates, Y.-C. Liu, K33-linked polyubiquitination of T cell receptor-zeta regulates proteolysis-independent T cell signaling. *Immunity*. 33, 60--70 (2010).

[182] X. Liu, B. Xu, J. Yang, L. He, Z. Zhang, X. Cheng, H. Yu, X. Liu, T. Jin, Y. Peng, Y. Huang, L. Xia, Y. Wang, J. Wu, X. Wu, S. Liu, L. Shan, X. Yang, L. Sun, J. Liang, Y. Zhang, Y. Shang, UHRF2 commissions the completion of DNA demethylation through allosteric activation by 5hmC and K33-linked ubiquitination of XRCC1. *Mol. Cell*. 81, 2960-2974.e7 (2021).

[183] K. N. Swatek, J. L. Usher, A. F. Kueck, C. Gladkova, T. E. T. Mevissen, J. N. Pruneda, T. Skern, D. Komander, Insights into ubiquitin chain architecture using Ub-clipping. *Nature*. 572, 533–537 (2019).

[184] S. O. Crowe, A. S. J. B. Rana, K. K. Deol, Y. Ge, E. R. Strieter, Ubiquitin Chain Enrichment Middle-Down Mass Spectrometry Enables Characterization of Branched Ubiquitin Chains in Cellulo. *Anal. Chem.* 89, 4428–4434 (2017).

[185] Y. A. Kristariyanto, S. A. A. Rehman, D. G. Campbell, N. A. Morrice, C. Johnson, R. Toth, Y. Kulathu, K29-selective ubiquitin binding domain reveals structural basis of specificity and heterotypic nature of k29 polyubiquitin. *Mol Cell*. 58, 83--94 (2015).

[186] R. G. Yau, K. Doerner, E. R. Castellanos, D. L. Haakonsen, A. Werner, N. Wang, X. W. Yang, N. Martinez-Martin, M. L. Matsumoto, V. M. Dixit, M. Rape, Assembly and Function of Heterotypic Ubiquitin Chains in Cell-Cycle and Protein Quality Control. *Cell*. 171, 918-933.e20 (2017).

[187] M. E. French, C. F. Koehler, T. Hunter, Emerging functions of branched ubiquitin chains. *Cell Discov.* 7, 6 (2021).

[188] A. Waltho, T. Sommer, The Ubiquitin Code. *Methods Mol Biology*. 2602, 19–38 (2022).

[189] M. K. Hospenthal, S. M. V. Freund, D. Komander, Assembly, analysis and architecture of atypical ubiquitin chains. *Nat Struct Mol Biol*. 20, 555–565 (2013).

[190] E. M. Valkevich, N. A. Sanchez, Y. Ge, E. R. Strieter, Middle-Down Mass Spectrometry Enables Characterization of Branched Ubiquitin Chains. *Biochemistry*. 53, 4979–4989 (2014).

[191] R. T. VanderLinden, C. W. Hemmis, B. Schmitt, A. Ndoja, F. G. Whitby, H. Robinson, R. E. Cohen, T. Yao, C. P. Hill, Structural Basis for the Activation and Inhibition of the UCH37 Deubiquitylase. *Mol. Cell*. 57, 901–911 (2015).

[192] Y.-S. Wang, K.-P. Wu, H.-K. Jiang, P. Kurkute, R.-H. Chen, Branched Ubiquitination: Detection Methods, Biological Functions and Chemical Synthesis. *Molecules*. 25, 5200 (2020).

[193] D. L. Haakonsen, M. Rape, Branching Out: Improved Signaling by Heterotypic Ubiquitin Chains. *Trends Cell Biol.* 29, 704–716 (2019).

[194] S. Rahighi, I. Dikic, Selectivity of the ubiquitin-binding modules. *FEBS Lett.* 586, 2705–2710 (2012).

[195] F. Ohtake, H. Tsuchiya, Y. Saeki, K. Tanaka, K63 ubiquitylation triggers proteasomal degradation by seeding branched ubiquitin chains. *Proc. Natl. Acad. Sci.* 115, E1401–E1408 (2018).

[196] A. J. Boughton, S. Krueger, D. Fushman, Branching via K11 and K48 Bestows Ubiquitin Chains with a Unique Interdomain Interface and Enhanced Affinity for Proteasomal Subunit Rpn1. *Structure*. 28, 29-43.e6 (2020).

[197] S. Kolla, M. Ye, K. G. Mark, M. Rapé, Assembly and function of branched ubiquitin chains. *Trends Biochem Sci* (2022), doi:10.1016/j.tibs.2022.04.003.

[198] M. M. Olszewski, C. Williams, K. C. Dong, A. Martin, The Cdc48 unfoldase prepares well-folded protein substrates for degradation by the 26S proteasome. *Commun. Biol.* 2, 29 (2019).

[199] J. H. Hong, D. Ng, T. Srikumar, B. Raught, The use of ubiquitin lysine mutants to characterize E2–E3 linkage specificity: Mass spectrometry offers a cautionary “tail.” *PROTEOMICS*. 15, 2910–2915 (2015).

[200] A. Ordureau, C. Munch, J. W. Harper, Quantifying ubiquitin signaling. *Mol Cell*. 58, 660--676 (2015).

[201] D. L. Swaney, P. Beltrao, L. Starita, A. Guo, J. Rush, S. Fields, N. J. Krogan, J. Villen, Global analysis of phosphorylation and ubiquitylation cross-talk in protein degradation. *Nat Methods*. 10, 676--682 (2013).

[202] G. Xu, J. S. Paige, S. R. Jaffrey, Global analysis of lysine ubiquitination by ubiquitin remnant immunoaffinity profiling. *Nat Biotechnol*. 28, 868--873 (2010).

[203] G. Xu, S. R. Jaffrey, Proteomic identification of protein ubiquitination events. *Biotechnology genetic engineering reviews*. 29, 73--109 (2013).

[204] N. J. Denis, J. Vasilescu, J.-P. Lambert, J. C. Smith, D. Figeys, Tryptic digestion of ubiquitin standards reveals an improved strategy for identifying ubiquitinated proteins by mass spectrometry. *Proteomics*. 7, 868--874 (2007).

[205] W. Kim, E. J. Bennett, E. L. Huttlin, A. Guo, J. Li, A. Possemato, M. E. Sowa, R. Rad, J. Rush, M. J. Comb, J. W. Harper, S. P. Gygi, Systematic and quantitative assessment of the ubiquitin-modified proteome. *Mol Cell*. 44, 325--340 (2011).

[206] S. A. Wagner, P. Beli, B. T. Weinert, M. L. Nielsen, J. Cox, M. Mann, C. Choudhary, *Mol. Cell. Proteom.*, in press, doi:10.1074/mcp.m111.013284.

[207] J. Cox, M. Mann, Quantitative, high-resolution proteomics for data-driven systems biology. *Annu Rev Biochem*. 80, 273--299 (2011).

[208] A. Thompson, J. Schafer, K. Kuhn, S. Kienle, J. Schwarz, G. Schmidt, T. Neumann, R. Johnstone, A. K. A. Mohammed, C. Hamon, Tandem mass tags: a novel quantification strategy for comparative analysis of complex protein mixtures by MS/MS. *Analytical chemistry*. 75, 1895--1904 (2003).

[209] S.-E. Ong, B. Blagoev, I. Kratchmarova, D. B. Kristensen, H. Steen, A. Pandey, M. Mann, Stable isotope labeling by amino acids in cell culture, SILAC, as a simple and accurate approach to expression proteomics. *Molecular cellular proteomics : MCP*. 1, 376--386 (2002).

[210] I. Sahu, H. Zhu, S. J. Buhrlage, J. A. Marto, Proteomic approaches to study ubiquitinomics. *Biochim. Biophys. Acta (BBA) - Gene Regul. Mech.* 1866, 194940 (2023).

[211] D. S. Kirkpatrick, S. A. Gerber, S. P. Gygi, The absolute quantification strategy: a general procedure for the quantification of proteins and post-translational modifications. *Methods*. 35, 265--273 (2005).

[212] K. Newton, M. L. Matsumoto, I. E. Wertz, D. S. Kirkpatrick, J. R. Lill, J. Tan, D. Dugger, N. Gordon, S. S. Sidhu, F. A. Fellouse, L. Komuves, D. M. French, R. E. Ferrando, C. Lam, D. Compaan, C. Yu, I. Bosanac, S. G. Hymowitz, R. F. Kelley, V. M. Dixit, Ubiquitin chain editing revealed by polyubiquitin linkage-specific antibodies. *Cell*. 134, 668--678 (2008).

[213] M. L. Matsumoto, K. C. Dong, C. Yu, L. Phu, X. Gao, R. N. Hannoush, S. G. Hymowitz, D. S. Kirkpatrick, V. M. Dixit, R. F. Kelley, Engineering and structural characterization of a linear polyubiquitin-specific antibody. *J Mol Biol*. 418, 134--144 (2012).

[214] Y. Yu, Q. Zheng, S. K. Erramilli, M. Pan, S. Park, Y. Xie, J. Li, J. Fei, A. A. Kossiakoff, L. Liu, M. Zhao, K29-linked ubiquitin signaling regulates proteotoxic stress response and cell cycle. *Nat. Chem. Biol.* 17, 896–905 (2021).

[215] M. P. Wandel, C. Pathe, E. I. Werner, C. J. Ellison, K. B. Boyle, A. von der Malsburg, J. Rohde, F. Randow, GBPs Inhibit Motility of Shigella flexneri but Are Targeted for Degradation by the Bacterial Ubiquitin Ligase IpaH9.8. *Cell Host Microbe*. 22, 507-518.e5 (2017).

[216] T. Scientific, Ed., Ub-K6 Polyclonal Antibody, (available at https://www.thermofisher.com/order/genome-database/dataSheetPdf?producttype=antibody&;productsubtype=antibody_primary&productId=PA5-120610&version=10).

[217] T. F. Scientific, Ed., Ub-K33 Polyclonal Antibody, (available at https://www.thermofisher.com/order/genome-database/dataSheetPdf?producttype=antibody&;productsubtype=antibody_primary&productId=PA5-120623&version=10).

[218] U. Rothbauer, K. Zolghadr, S. Tillib, D. Nowak, L. Schermelleh, A. Gahl, N. Backmann, K. Conrath, S. Muyldermans, M. C. Cardoso, H. Leonhardt, Targeting and tracing antigens in live cells with fluorescent nanobodies. *Nat. Methods*. 3, 887–889 (2006).

[219] M. Gonzalez-Santamarta, L. Ceccato, A. S. Carvalho, J.-C. Rain, R. Matthiesen, M. S. Rodriguez, The Ubiquitin Code. *Methods Mol Biology*. 2602, 125–136 (2022).

[220] S. M. Lange, M. R. McFarland, F. Lamoliatte, D. Kwasna, L. Shen, I. Wallace, I. Cole, L. A. Armstrong, A. Knebel, C. Johnson, V. D. Cesare, Y. Kulathu, Comprehensive approach to study branched ubiquitin chains reveals roles for K48-K63 branches in VCP/p97-related processes (2023), doi:10.1101/2023.01.10.523363.

[221] C. Tiede, R. Bedford, S. J. Heseltine, G. Smith, I. Wijetunga, R. Ross, D. AlQallaf, A. P. Roberts, A. Balls, A. Curd, R. E. Hughes, H. Martin, S. R. Needham, L. C. Zanetti-Domingues, Y. Sadigh, T. P. Peacock, A. A. Tang, N. Gibson, H. Kyle, G. W. Platt, N. Ingram, T. Taylor, L. P. Coletta, I. Manfield, M. Knowles, S. Bell, F. Esteves, A. Maqbool, R. K. Prasad, M. Drinkhill, R. S. Bon, V. Patel, S. A. Goodchild, M. Martin-Fernandez, R. J. Owens, J. E. Nettleship, M. E. Webb, M. Harrison, J. D. Lippiat, S. Ponnambalam, M. Peckham, A. Smith, P. K. Ferrigno, M. Johnson, M. J. McPherson, D. C. Tomlinson, Affimer proteins are versatile and renewable affinity reagents. *Elife*. 6 (2017), doi:10.7554/elife.24903.

[222] Avacta, Ed., Product data sheet Affimer (36-28) to diUbiquitin K48-linkage (available at https://www.avacta.com/products/anti-diubiquitin-k48-linkage-affimer-36-28).

[223] R. Layfield, D. Tooth, M. Landon, S. Dawson, J. Mayer, A. Alban, Purification of poly-ubiquitinated proteins by S5a-affinity chromatography. *Proteomics* (2001).

[224] R. Hjerpe, M. S. Rodriguez, Efficient approaches for characterizing ubiquitinated proteins. *Biochem Soc T*. 36, 823--827 (2008).

[225] M. Mattern, J. Sutherland, K. Kadimisetty, R. Barrio, M. S. Rodriguez, Using Ubiquitin Binders to Decipher the Ubiquitin Code. *Trends Biochem Sci*. 44, 599–615 (2019).

[226] M. Zhang, J. M. Berk, A. B. Mehrtash, J. Kanyo, M. Hochstrasser, A versatile new tool derived from a bacterial deubiquitylase to detect and purify ubiquitylated substrates and their interacting proteins. *PLoS Biol.* 20, e3001501 (2022).

[227] R. Hjerpe, F. Aillet, F. Lopitz-Otsoa, V. Lang, P. England, M. S. Rodriguez, Efficient protection and isolation of ubiquitylated proteins using tandem ubiquitin-binding entities. *Embo Rep*. 10, 1250--1258 (2009).

[228] J. J. Sims, F. Scavone, E. M. Cooper, L. A. Kane, R. J. Youle, J. D. Boeke, R. E. Cohen, Polyubiquitin-sensor proteins reveal localization and linkage-type dependence of cellular ubiquitin signaling. *Nat Methods*. 9, 303--309 (2012).

[229] L. Inc., Ed., Manual FLAG K63-TUBEs: Catalog Number: UM604 (2011) (available at https://lifesensors.com/wp-content/uploads/2017/02/Flag-K63TUBE-Manual_061913.pdf).

[230] L. Inc., Ed., Manual K48 TUBE HF (High Fidelity), His6: Catalog Number: UM207 (2018) (available at https://lifesensors.com/wp-content/uploads/2019/08/UM207_K48TUBE-HF-His-Manual-2018.pdf).

[231] LifeSensors, Ed., Anti-M1 TUBE, Biotin, (available at https://lifesensors.com/product/detection-of-polyubiquitin-protein-um306-m1-tube/).

[232] S. J. L. van Wijk, E. Fiskin, M. Putyrski, F. Pampaloni, J. Hou, P. Wild, T. Kensche, H. E. Grecco, P. Bastiaens, I. Dikic, Fluorescence-Based Sensors to Monitor Localization and Functions of Linear and K63-Linked Ubiquitin Chains in Cells. *Mol Cell*. 47, 797–809 (2012).

[233] Z. Chen, Y. Zhong, Y. Wang, S. Xu, Z. Liu, I. V. Baskakov, M. J. Monteiro, M. Karbowski, Y. Shen, S. Fang, Ubiquitination-Induced Fluorescence Complementation (UiFC) for Detection of K48 Ubiquitin Chains In Vitro and in Live Cells. *Plos One*. 8, e73482 (2013).

[234] T. K. Kerppola, Bimolecular Fluorescence Complementation (BiFC) Analysis as a Probe of Protein Interactions in Living Cells. *Biophysics*. 37, 465–487 (2008).

[235] M. J. Pinto, J. R. Pedro, R. O. Costa, R. D. Almeida, Visualizing K48 Ubiquitination during Presynaptic Formation By Ubiquitination-Induced Fluorescence Complementation (UiFC). *Front. Mol. Neurosci.* 9, 43 (2016).

[236] S. J. van Wijk, S. Fulda, I. Dikic, M. Heilemann, Visualizing ubiquitination in mammalian cells. *Embo Rep*. 20 (2019), doi:10.15252/embr.201846520.

[237] W. Qin, C. Steinek, K. Kolobynina, I. Forné, A. Imhof, M. C. Cardoso, H. Leonhardt, Probing protein ubiquitination in live cells. *Nucleic Acids Res* (2022), doi:10.1093/nar/gkac805.

[238] J. Helma, M. C. Cardoso, S. Muyldermans, H. Leonhardt, Nanobodies and recombinant binders in cell biology. *J Cell Biol*. 209, 633--644 (2015).

[239] Y. L. Boersma, Protein Scaffolds, Design, Synthesis, and Applications. *Methods Mol. Biol.* 1798, 307–327 (2018).

[240] A. P. Caputi, P. Navarra, Beyond antibodies: ankyrins and DARPins. From basic research to drug approval. *Curr. Opin. Pharmacol.* 51, 93–101 (2020).

[241] A. Pluckthun, Designed ankyrin repeat proteins (DARPins): binding proteins for research, diagnostics, and therapy. *Annu Rev Pharmacol*. 55, 489--511 (2015).

[242] M. A. Andrade, C. Perez-Iratxeta, C. P. Ponting, Protein Repeats: Structures, Functions, and Evolution. *J. Struct. Biol.* 134, 117–131 (2001).

[243] Z. Pancer, M. D. Cooper, THE EVOLUTION OF ADAPTIVE IMMUNITY. *Immunology*. 24, 497–518 (2006).

[244] L. K. Mosavi, T. J. Cammett, D. C. Desrosiers, Z.-Y. Peng, The ankyrin repeat as molecular architecture for protein recognition. *Protein Sci*. 13, 1435--1448 (2004).

[245] P. Michaely, D. R. Tomchick, M. Machius, R. G. W. Anderson, Crystal structure of a 12 ANK repeat stack from human ankyrinR. *EMBO J.* 21, 6387–6396 (2002).

[246] J. Li, A. Mahajan, M.-D. Tsai, Ankyrin repeat: a unique motif mediating protein-protein interactions. *Biochemistry-us*. 45, 15168--15178 (2006).

[247] B. Kobe, A. V. Kajava, When protein folding is simplified to protein coiling: the continuum of solenoid protein structures. *Trends Biochem. Sci.* 25, 509–515 (2000).

[248] T. Brunette, F. Parmeggiani, P.-S. Huang, G. Bhabha, D. C. Ekiert, S. E. Tsutakawa, G. L. Hura, J. A. Tainer, D. Baker, Exploring the repeat protein universe through computational protein design. *Nature*. 528, 580–584 (2015).

[249] T. Z. Grove, A. L. Cortajarena, L. Regan, Ligand binding by repeat proteins: natural and designed. *Curr. Opin. Struct. Biol.* 18, 507–515 (2008).

[250] R. G. Walker, A. T. Willingham, C. S. Zuker, A Drosophila mechanosensory transduction channel. *Science (New York, N.Y.)*. 287, 2229--2234 (2000).

[251] C. Reichen, C. Madhurantakam, A. Plückthun, P. R. E. Mittl, Crystal structures of designed armadillo repeat proteins: Implications of construct design and crystallization conditions on overall structure. *Protein Sci.* 23, 1572–1583 (2014).

[252] M. Valerio-Lepiniec, A. Urvoas, A. Chevrel, A. Guellouz, Y. Ferrandez, A. Mesneau, I. L. de la Sierra-Gallay, M. Aumont-Nicaise, M. Desmadril, H. van Tilbeurgh, P. Minard, The αRep artificial repeat protein scaffold: a new tool for crystallization and live cell applications. *Biochem. Soc. Trans.* 43, 819–824 (2015).

[253] H. K. Binz, P. Amstutz, A. Kohl, M. T. Stumpp, C. Briand, P. Forrer, M. G. Grutter, A. Pluckthun, High-affinity binders selected from designed ankyrin repeat protein libraries. *Nat Biotechnol*. 22, 575--582 (2004).

[254] K. W. Tripp, D. Barrick, The Tolerance of a Modular Protein to Duplication and Deletion of Internal Repeats. *J. Mol. Biol.* 344, 169–178 (2004).

[255] G. Interlandi, S. K. Wetzel, G. Settanni, A. Pluckthun, A. Caflisch, Characterization and further stabilization of designed ankyrin repeat proteins by combining molecular dynamics simulations and experiments. *J Mol Biol*. 375, 837--854 (2008).

[256] R. N. Gilbreth, S. Koide, Structural insights for engineering binding proteins based on non-antibody scaffolds. *Curr. Opin. Struct. Biol.* 22, 413–420 (2012).

[257] M. T. Stumpp, H. K. Binz, P. Amstutz, DARPins: A new generation of protein therapeutics. *Drug Discov. Today*. 13, 695–701 (2008).

[258] A. Kohl, H. K. Binz, P. Forrer, M. T. Stumpp, A. Plückthun, M. G. Grütter, Designed to be stable: Crystal structure of a consensus ankyrin repeat protein. *Proc. Natl. Acad. Sci.* 100, 1700–1705 (2003).

[259] H. K. Binz, T. R. Bakker, D. J. Phillips, A. Cornelius, C. Zitt, T. Göttler, G. Sigrist, U. Fiedler, S. Ekawardhani, I. Dolado, J. A. Saliba, G. Tresch, K. Proba, M. T. Stumpp, Design and characterization of MP0250, a tri-specific anti-HGF/anti-VEGF DARPin® drug candidate. *mAbs*. 9, 1262–1269 (2017).

[260] H. K. Binz, M. T. Stumpp, P. Forrer, P. Amstutz, A. Plückthun, Designing Repeat Proteins: Well-expressed, Soluble and Stable Proteins from Combinatorial Libraries of Consensus Ankyrin Repeat Proteins. *J. Mol. Biol.* 332, 489–503 (2003).

[261] G. Houlihan, P. Gatti-Lafranconi, M. Kaltenbach, D. Lowe, F. Hollfelder, An experimental framework for improved selection of binding proteins using SNAP display. *J. Immunol. Methods*. 405, 47–56 (2014).

[262] D. Steiner, P. Forrer, A. Pluckthun, Efficient selection of DARPins with sub-nanomolar affinities using SRP phage display. *J Mol Biol*. 382, 1211--1227 (2008).

[263] M. Schütz, A. Batyuk, C. Klenk, L. Kummer, S. de Picciotto, B. Gülbakan, Y. Wu, G. A. Newby, F. Zosel, J. Schöppe, E. Sedlák, P. R. E. Mittl, R. Zenobi, K. D. Wittrup, A. Plückthun, Generation of Fluorogen-Activating Designed Ankyrin Repeat Proteins (FADAs) as Versatile Sensor Tools. *J. Mol. Biol.* 428, 1272–1289 (2016).

[264] J. Hanes, A. Plückthun, In vitro selection and evolution of functional proteins by using ribosome display. *Proc. Natl. Acad. Sci.* 94, 4937–4942 (1997).

[265] B. Dreier, A. Pluckthun, Ribosome display: a technology for selecting and evolving proteins from large libraries. *Methods in molecular biology (Clifton, N.J.)*. 687, 283--306 (2011).

[266] R. Tamaskovic, M. Simon, N. Stefan, M. Schwill, A. Pluckthun, Designed ankyrin repeat proteins (DARPins) from research to therapy. *Methods Enzymol*. 503, 101--134 (2012).

[267] P. Forrer, H. K. Binz, M. T. Stumpp, A. Pluckthun, Consensus design of repeat proteins. *Chembiochem*. 5, 183--189 (2004).

[268] M. A. Seeger, A. Mittal, S. Velamakanni, M. Hohl, S. Schauer, I. Salaa, M. G. Grutter, H. W. van Veen, Tuning the drug efflux activity of an ABC transporter in vivo by in vitro selected DARPin binders. *Plos One*. 7, e37845 (2012).

[269] J. Hanes, C. Schaffitzel, A. Knappik, A. Pluckthun, Picomolar affinity antibodies from a fully synthetic naive library selected and evolved by ribosome display. *Nat Biotechnol*. 18, 1287--1292 (2000).

[270] P. Amstutz, H. K. Binz, P. Parizek, M. T. Stumpp, A. Kohl, M. G. Grutter, P. Forrer, A. Pluckthun, Intracellular kinase inhibitors selected from combinatorial libraries of designed ankyrin repeat proteins. *J Biol Chem*. 280, 24715--24722 (2005).

[271] P. Amstutz, H. Koch, H. K. Binz, S. A. Deuber, A. Plückthun, Rapid selection of specific MAP kinase-binders from designed ankyrin repeat protein libraries. *Protein Eng. Des. Sel.* 19, 219–229 (2006).

[272] P. Parizek, L. Kummer, P. Rube, A. Prinz, F. W. Herberg, A. Plückthun, Designed Ankyrin Repeat Proteins (DARPins) as Novel Isoform-Specific Intracellular Inhibitors of c-Jun N-Terminal Kinases. *ACS Chem. Biol.* 7, 1356–1366 (2012).

[273] L. Kummer, P. Parizek, P. Rube, B. Millgramm, A. Prinz, P. R. E. Mittl, M. Kaufholz, B. Zimmermann, F. W. Herberg, A. Pluckthun, Structural and functional analysis of phosphorylation-specific binders of the kinase ERK from designed ankyrin repeat protein libraries. *Proc National Acad Sci*. 109, E2248-57 (2012).

[274] P. Milovnik, D. Ferrari, C. A. Sarkar, A. Pluckthun, Selection and characterization of DARPins specific for the neurotensin receptor 1. *Protein Eng Des Sel*. 22, 357--366 (2009).

[275] C. Jost, A. Plückthun, Engineered proteins with desired specificity: DARPins, other alternative scaffolds and bispecific IgGs. *Curr. Opin. Struct. Biol.* 27, 102–112 (2014).

[276] M. A. Bukowska, M. G. Grutter, New concepts and aids to facilitate crystallization. *Curr Opin Struc Biol*. 23, 409--416 (2013).

[277] M. A. Seeger, R. Zbinden, A. Flütsch, P. G. M. Gutte, S. Engeler, H. Roschitzki-Voser, M. G. Grütter, Design, construction, and characterization of a second-generation DARPin library with reduced hydrophobicity. *Protein Sci*. 22, 1239–1257 (2013).

[278] S. Koide, S. S. Sidhu, The Importance of Being Tyrosine: Lessons in Molecular Recognition from Minimalist Synthetic Binding Proteins. *ACS Chem. Biol.* 4, 325–334 (2009).

[279] A. Batyuk, Y. Wu, A. Honegger, M. M. Heberling, A. Plückthun, DARPin-Based Crystallization Chaperones Exploit Molecular Geometry as a Screening Dimension in Protein Crystallography. *J. Mol. Biol.* 428, 1574–1588 (2016).

[280] E. Brient-Litzler, A. Plückthun, H. Bedouelle, Knowledge-based design of reagentless fluorescent biosensors from a designed ankyrin repeat protein. *Protein Eng., Des. Sel.* 23, 229–241 (2010).

[281] L. Kummer, C.-W. Hsu, O. Dagliyan, C. MacNevin, M. Kaufholz, B. Zimmermann, N. V. Dokholyan, K. M. Hahn, A. Plückthun, Knowledge-Based Design of a Biosensor to Quantify Localized ERK Activation in Living Cells. *Chem. Biol.* 20, 847–856 (2013).

[282] J.-P. Theurillat, B. Dreier, G. Nagy-Davidescu, B. Seifert, S. Behnke, U. Zurrer-Hardi, F. Ingold, A. Pluckthun, H. Moch, Designed ankyrin repeat proteins: a novel tool for testing epidermal growth factor receptor 2 expression in breast cancer. *Modern Pathol*. 23, 1289--1297 (2010).

[283] R. Goldstein, J. Sosabowski, M. Livanos, J. Leyton, K. Vigor, G. Bhavsar, G. Nagy-Davidescu, M. Rashid, E. Miranda, J. Yeung, B. Tolner, A. Plückthun, S. Mather, T. Meyer, K. Chester, Development of the designed ankyrin repeat protein (DARPin) G3 for HER2 molecular imaging. *Eur. J. Nucl. Med. Mol. Imaging*. 42, 288–301 (2015).

[284] A. Eggel, G. Baravalle, G. Hobi, B. Kim, P. Buschor, P. Forrer, J.-S. Shin, M. Vogel, B. M. Stadler, C. A. Dahinden, T. S. Jardetzky, Accelerated dissociation of IgE-FcεRI complexes by disruptive inhibitors actively desensitizes allergic effector cells. *J. Allergy Clin. Immunol.* 133, 1709-1719.e8 (2014).

[285] M. J. Baumann, A. Eggel, P. Amstutz, B. M. Stadler, M. Vogel, DARPins against a functional IgE epitope. *Immunol. Lett.* 133, 78–84 (2010).

[286] Y. L. Boersma, G. Chao, D. Steiner, K. D. Wittrup, A. Plückthun, Bispecific Designed Ankyrin Repeat Proteins (DARPins) Targeting Epidermal Growth Factor Receptor Inhibit A431 Cell Proliferation and Receptor Recycling*. *J. Biol. Chem.* 286, 41273–41285 (2011).

[287] C. Jost, J. Schilling, R. Tamaskovic, M. Schwill, A. Honegger, A. Pluckthun, Structural basis for eliciting a cytotoxic effect in HER2-overexpressing cancer cells via binding to the extracellular domain of HER2. *Structure*. 21, 1979--1991 (2013).

[288] R. Tamaskovic, M. Schwill, G. Nagy-Davidescu, C. Jost, D. C. Schaefer, W. P. R. Verdurmen, J. V. Schaefer, A. Honegger, A. Plückthun, Intermolecular biparatopic trapping of ErbB2 prevents compensatory activation of PI3K/AKT via RAS–p110 crosstalk. *Nat. Commun.* 7, 11672 (2016).

[289] J. Winkler, P. Martin-Killias, A. Plückthun, U. Zangemeister-Wittke, EpCAM-targeted delivery of nanocomplexed siRNA to tumor cells with designed ankyrin repeat proteins. *Mol. Cancer Ther.* 8, 2674–2683 (2009).

[290] B. Dreier, G. Mikheeva, N. Belousova, P. Parizek, E. Boczek, I. Jelesarov, P. Forrer, A. Pluckthun, V. Krasnykh, Her2-specific multivalent adapters confer designed tropism to adenovirus for gene targeting. *J Mol Biol*. 405, 410--426 (2011).

[291] B. Dreier, A. Honegger, C. Hess, G. Nagy-Davidescu, P. R. E. Mittl, M. G. Grütter, N. Belousova, G. Mikheeva, V. Krasnykh, A. Plückthun, Development of a generic adenovirus delivery system based on structure-guided design of bispecific trimeric DARPin adapters. *Proc. Natl. Acad. Sci.* 110, E869–E877 (2013).

[292] M. T. Stumpp, K. M. Dawson, H. K. Binz, Beyond Antibodies: The DARPin® Drug Platform. *BioDrugs*. 34, 423–433 (2020).

[293] D. Callanan, D. Kunimoto, R. K. Maturi, S. S. Patel, G. Staurenghi, S. Wolf, J. K. Cheetham, T. C. Hohman, K. Kim, F. J. López, S. Schneider, J. Arnold, R. Avery, M. Bennett, B. Berger, B. Blodi, D. Boyer, D. Brown, D. Callanan, K. Csaky, F. Devin, D. W. Faber, S. Fraser-Bell, J. R. Ferencz, C. Framme, D. Gaucher, M. Gillies, M. Goldstein, R. Guymer, J. Heier, F. Holz, R. N. Khurana, G. Kokame, J.-F. Korobelnik, D. Kunimoto, P. Lanzetta, C. P. Lohmann, R. Maturi, S. Mohand-Said, G. Papastergiou, S. Patel, D. Pauleikhoff, A. Pollack, C. Pruente, S. Rose, I. Rosenblatt, U. Schmidt-Erfurth, A. Sharma, L. Singerman, E. Souied, G. Staurenghi, P. Tornambe, C. Wykoff, M. Zinkernagel, Double-Masked, Randomized, Phase 2 Evaluation of Abicipar Pegol (an Anti-VEGF DARPin Therapeutic) in Neovascular Age-Related Macular Degeneration. *J. Ocul. Pharmacol. Ther.* 34, 700–709 (2018).

[294] P. A. Campochiaro, R. Channa, B. B. Berger, J. S. Heier, D. M. Brown, U. Fiedler, J. Hepp, M. T. Stumpp, Treatment of Diabetic Macular Edema With a Designed Ankyrin Repeat Protein That Binds Vascular Endothelial Growth Factor: A Phase I/II Study. *Am. J. Ophthalmol.* 155, 697-704.e2 (2013).

[295] D. Kunimoto, Y. H. Yoon, C. C. Wykoff, A. Chang, R. N. Khurana, R. K. Maturi, H. Agostini, E. Souied, D. R. Chow, A. J. Lotery, M. Ohji, F. Bandello, R. Belfort, X.-Y. Li, J. Jiao, G. Le, W. Schmidt, Y. Hashad, C. and S. S. Groups, Efficacy and Safety of Abicipar in Neovascular Age-Related Macular Degeneration 52-Week Results of Phase 3 Randomized Controlled Study. *Ophthalmology*. 127, 1331–1344 (2020).

[296] A. Stahl, M. T. Stumpp, A. Schlegel, S. Ekawardhani, C. Lehrling, G. Martin, M. Gulotti-Georgieva, D. Villemagne, P. Forrer, H. T. Agostini, H. K. Binz, Highly potent VEGF-A-antagonistic DARPins as anti-angiogenic agents for topical and intravitreal applications. *Angiogenesis*. 16, 101–111 (2013).

[297] E. H. Souied, F. Devin, M. Mauget-Faÿsse, P. Kolář, U. Wolf-Schnurrbusch, C. Framme, D. Gaucher, G. Querques, M. T. Stumpp, S. Wolf, M. S. Group, Treatment of Exudative Age-Related Macular Degeneration with a Designed Ankyrin Repeat Protein that Binds Vascular Endothelial Growth Factor: a Phase I/II Study. *Am. J. Ophthalmol.* 158, 724-732.e2 (2014).

[298] S. Wolf, E. H. Souied, M. Mauget-Faysse, F. Devin, M. Patel, U. E. Wolf-SChnurrbursch, M. Stumpp, Phase I Mp0112 Wet AMD Study: Results Of A Single Escalating Dose Study With DARPinircledR MP0112 In Wet AMD. *Investigative Ophthalmology Visual Science* (2011).

[299] R. M. Hussain, T. A. Ciulla, Emerging vascular endothelial growth factor antagonists to treat neovascular age-related macular degeneration. *Expert Opin. Emerg. Drugs*. 22, 235–246 (2017).

[300] A. Mullard, FDA rejects first DARPin. *Nat. Rev. Drug Discov.* 19, 501–501 (2020).

[301] Molecular Partners to Regain Global Rights to Abicipar | Molecular Partners, (available at https://investors.molecularpartners.com/news-releases/news-release-details/molecular-partners-regain-global-rights-abicipar/).

[302] U. Fiedler, S. Ekawardhani, A. Cornelius, P. Gilboy, T. R. Bakker, I. Dolado, M. T. Stumpp, K. M. Dawson, MP0250, a VEGF and HGF neutralizing DARPin® molecule shows high anti-tumor efficacy in mouse xenograft and patient-derived tumor models. *Oncotarget*. 8, 98371–98383 (2017).

[303] A. Azaro, J. Rodon, M. R. Middleton, R. D. Baird, R. Herrmann, U. Fiedler, J. Haunschild, M. Häuptle, F. J. Hermann, S. Schreiner, A. Harstrick, K. M. Dawson, A. G. Omlin, First-in-class phase I study evaluating MP0250, a VEGF and HGF neutralizing DARPIN molecule, in patients with advanced solid tumors. *J. Clin. Oncol.* 36, 2520–2520 (2018).

[304] L. Rao, K. D. Veirman, D. Giannico, I. Saltarella, V. Desantis, M. A. Frassanito, A. G. Solimando, D. Ribatti, M. Prete, A. Harstrick, U. Fiedler, H. D. Raeve, V. Racanelli, K. Vanderkerken, A. Vacca, Targeting angiogenesis in multiple myeloma by the VEGF and HGF blocking DARPin® protein MP0250: a preclinical study. *Oncotarget*. 9, 13366–13381 (2018).

[305] Pipeline - Molecular Partners, (available at https://www.molecularpartners.com/pipeline/).

[306] A.-3/TICO S. Group*, C. Barkauskas, E. Mylonakis *et al.*, Efficacy and Safety of Ensovibep for Adults Hospitalized With COVID-19. *Ann. Intern. Med.* 175, M22-1503 (2022).

[307] N. Chatterjee, G. C. Walker, Mechanisms of DNA damage, repair, and mutagenesis. *Environ. Mol. Mutagen.* 58, 235–263 (2017).

[308] A. Carusillo, C. Mussolino, DNA Damage: From Threat to Treatment. *Cells*. 9, 1665 (2020).

[309] J. H. J. Hoeijmakers, DNA Damage, Aging, and Cancer. *N. Engl. J. Med.* 361, 1475–1485 (2009).

[310] T. LINDAHL, D. E. BARNES, Repair of Endogenous DNA Damage. *Cold Spring Harb. Symp. Quant. Biol.* 65, 127–134 (2000).

[311] T. A. Kunkel, Evolving Views of DNA Replication (In)Fidelity. *Cold Spring Harb. Symp. Quant. Biol.* 74, 91–101 (2009).

[312] L. A. Pray, DNA Replication and Causes of Mutation. *Nature Education* (2008)

[313] J. Nakamura, V. E. Walker, P. B. Upton, S. Y. Chiang, Y. W. Kow, J. A. Swenberg, Highly sensitive apurinic/apyrimidinic site assay can detect spontaneous and chemically induced depurination under physiological conditions. *Cancer Res.* 58, 222–5 (1998).

[314] O. D. Schärer, Chemistry and Biology of DNA Repair. *Angew. Chem. Int. Ed.* 42, 2946–2974 (2003).

[315] F. Henkler, K. Stolpmann, A. Luch, Molecular, Clinical and Environmental Toxicology, Volume 3: Environmental Toxicology. *Exp. Suppl.* 101, 107–131 (2012).

[316] A. J. Deans, S. C. West, DNA interstrand crosslink repair and cancer. *Nat. Rev. Cancer*. 11, 467–480 (2011).

[317] L. Cui, D. Bikard, Consequences of Cas9 cleavage in the chromosome of Escherichia coli. *Nucleic Acids Res.* 44, 4243–4251 (2016).

[318] M. E. Arana, T. A. Kunkel, Mutator phenotypes due to DNA replication infidelity. *Semin. Cancer Biol.* 20, 304–311 (2010).

[319] D. A. Erie, K. R. Weninger, Single molecule studies of DNA mismatch repair. *DNA Repair*. 20, 71–81 (2014).

[320] T.-H. Lee, T.-H. Kang, DNA Oxidation and Excision Repair Pathways. *Int. J. Mol. Sci.* 20, 6092 (2019).

[321] H. E. Krokan, M. Bjørås, Base Excision Repair. *Cold Spring Harb. Perspect. Biol.* 5, a012583 (2013).

[322] D. Lopez-Martinez, C.-C. Liang, M. A. Cohn, Cellular response to DNA interstrand crosslinks: the Fanconi anemia pathway. *Cell. Mol. Life Sci.* 73, 3097–3114 (2016).

[323] H. Walden, A. J. Deans, The Fanconi Anemia DNA Repair Pathway: Structural and Functional Insights into a Complex Disorder. *Annu. Rev. Biophys.* 43, 257–278 (2014).

[324] A. N. Blackford, S. P. Jackson, ATM, ATR, and DNA-PK: The Trinity at the Heart of the DNA Damage Response. *Mol. Cell*. 66, 801–817 (2017).

[325] K. A. Coleman, R. A. Greenberg, The BRCA1-RAP80 Complex Regulates DNA Repair Mechanism Utilization by Restricting End Resection*. *J. Biol. Chem.* 286, 13669–13680 (2011).

[326] C. Doil, N. Mailand, S. Bekker-Jensen, P. Menard, D. H. Larsen, R. Pepperkok, J. Ellenberg, S. Panier, D. Durocher, J. Bartek, J. Lukas, C. Lukas, RNF168 Binds and Amplifies Ubiquitin Conjugates on Damaged Chromosomes to Allow Accumulation of Repair Proteins. *Cell*. 136, 435–446 (2009).

[327] J. M. Daley, P. Sung, 53BP1, BRCA1, and the Choice between Recombination and End Joining at DNA Double-Strand Breaks. *Mol. Cell. Biol.* 34, 1380–1388 (2014).

[328] T. G. W. Graham, J. C. Walter, J. J. Loparo, Two-Stage Synapsis of DNA Ends during Non-homologous End Joining. *Mol. Cell*. 61, 850–858 (2016).

[329] H. H. Y. Chang, N. R. Pannunzio, N. Adachi, M. R. Lieber, Non-homologous DNA end joining and alternative pathways to double-strand break repair. *Nat. Rev. Mol. Cell Biol.* 18, 495–506 (2017).

[330] P. Ahnesorg, P. Smith, S. P. Jackson, XLF Interacts with the XRCC4-DNA Ligase IV Complex to Promote DNA Nonhomologous End-Joining. *Cell*. 124, 301–313 (2006).

[331] I. Brouwer, G. Sitters, A. Candelli, S. J. Heerema, I. Heller, A. J. M. de, H. Zhang, D. Normanno, M. Modesti, E. J. G. Peterman, G. J. L. Wuite, Sliding sleeves of XRCC4–XLF bridge DNA and connect fragments of broken DNA. *Nature*. 535, 566–569 (2016).

[332] T. M. Gottlieb, S. P. Jackson, The DNA-dependent protein kinase: Requirement for DNA ends and association with Ku antigen. *Cell*. 72, 131–142 (1993).

[333] T. Ochi, A. N. Blackford, J. Coates, S. Jhujh, S. Mehmood, N. Tamura, J. Travers, Q. Wu, V. M. Draviam, C. V. Robinson, T. L. Blundell, S. P. Jackson, PAXX, a paralog of XRCC4 and XLF, interacts with Ku to promote DNA double-strand break repair. *Science*. 347, 185–188 (2015).

[334] R. Scully, A. Panday, R. Elango, N. A. Willis, DNA double-strand break repair-pathway choice in somatic mammalian cells. *Nat. Rev. Mol. Cell Biol.* 20, 698–714 (2019).

[335] T. Liu, J. Huang, DNA End Resection: Facts and Mechanisms. *Genom., Proteom. Bioinform.* 14, 126–130 (2016).

[336] L. Postow, H. Funabiki, An SCF complex containing Fbxl12 mediates DNA damage-induced Ku80 ubiquitylation. *Cell Cycle*. 12, 587–595 (2013).

[337] J. van den Boom, M. Wolf, L. Weimann, N. Schulze, F. Li, F. Kaschani, A. Riemer, C. Zierhut, M. Kaiser, G. Iliakis, H. Funabiki, H. Meyer, VCP/p97 Extracts Sterically Trapped Ku70/80 Rings from DNA in Double-Strand Break Repair. *Mol. Cell*. 64, 189–198 (2016).

[338] W. Zhao, J. B. Steinfeld, F. Liang, X. Chen, D. G. Maranon, C. J. Ma, Y. Kwon, T. Rao, W. Wang, C. Sheng, X. Song, Y. Deng, J. Jimenez-Sainz, L. Lu, R. B. Jensen, Y. Xiong, G. M. Kupfer, C. Wiese, E. C. Greene, P. Sung, BRCA1–BARD1 promotes RAD51-mediated homologous DNA pairing. *Nature*. 550, 360–365 (2017).

[339] T. van der Heijden, M. Modesti, S. Hage, R. Kanaar, C. Wyman, C. Dekker, Homologous Recombination in Real Time: DNA Strand Exchange by RecA. *Mol. Cell*. 30, 530–538 (2008).

[340] S. Wu, J. Zhou, K. Zhang, H. Chen, M. Luo, Y. Lu, Y. Sun, Y. Chen, Molecular Mechanisms of PALB2 Function and Its Role in Breast Cancer Management. *Front. Oncol.* 10, 301 (2020).

[341] A. A. Sartori, C. Lukas, J. Coates, M. Mistrik, S. Fu, J. Bartek, R. Baer, J. Lukas, S. P. Jackson, Human CtIP promotes DNA end resection. *Nature*. 450, 509–514 (2007).

[342] M. K. Zeman, K. A. Cimprich, Causes and consequences of replication stress. *Nat. Cell Biol.* 16, 2–9 (2014).

[343] S. Boiteux, S. Jinks-Robertson, DNA repair mechanisms and the bypass of DNA damage in Saccharomyces cerevisiae. *Genetics*. 193, 1025--1064 (2013).

[344] C. Lawrence, The RAD6 DNA repair pathway in Saccharomyces cerevisiae: What does it do, and how does it do it? *BioEssays*. 16, 253–258 (1994).

[345] C. Hoege, B. Pfander, G.-L. Moldovan, G. Pyrowolakis, S. Jentsch, RAD6-dependent DNA repair is linked to modification of PCNA by ubiquitin and SUMO. *Nature*. 419, 135–141 (2002).

[346] G.-L. Moldovan, B. Pfander, S. Jentsch, PCNA, the Maestro of the Replication Fork. *Cell*. 129, 665–679 (2007).

[347] J. Spence, S. Sadis, A. L. Haas, D. Finley, A ubiquitin mutant with specific defects in DNA repair and multiubiquitination. *Molecular and cellular biology*. 15, 1265--1273 (1995).

[348] I. Unk, I. Hajdú, K. Fátyol, J. Hurwitz, J.-H. Yoon, L. Prakash, S. Prakash, L. Haracska, Human HLTF functions as a ubiquitin ligase for proliferating cell nuclear antigen polyubiquitination. *Proc. Natl. Acad. Sci.* 105, 3768–3773 (2008).

[349] I. Unk, I. Hajdú, K. Fátyol, B. Szakál, A. Blastyák, V. Bermudez, J. Hurwitz, L. Prakash, S. Prakash, L. Haracska, Human SHPRH is a ubiquitin ligase for Mms2–Ubc13-dependent polyubiquitylation of proliferating cell nuclear antigen. *Proc. Natl. Acad. Sci.* 103, 18107–18112 (2006).

[350] R. Kanao, H. Kawai, T. Taniguchi, M. Takata, C. Masutani, RFWD3 and translesion DNA polymerases contribute to PCNA modification–dependent DNA damage tolerance. *Life Sci. Alliance*. 5, e202201584 (2022).

[351] R. K. Chiu, J. Brun, C. Ramaekers, J. Theys, L. Weng, P. Lambin, D. A. Gray, B. G. Wouters, Lysine 63-Polyubiquitination Guards against Translesion Synthesis–Induced Mutations. *PLoS Genet.* 2, e116 (2006).

[352] A. Ciccia, A. V. Nimonkar, Y. Hu, I. Hajdu, Y. J. Achar, L. Izhar, S. A. Petit, B. Adamson, J. C. Yoon, S. C. Kowalczykowski, D. M. Livingston, L. Haracska, S. J. Elledge, Polyubiquitinated PCNA Recruits the ZRANB3 Translocase to Maintain Genomic Integrity after Replication Stress. *Mol. Cell*. 47, 396–409 (2012).

[353] T. Thakar, W. Leung, C. M. Nicolae, K. E. Clements, B. Shen, A.-K. Bielinsky, G.-L. Moldovan, Ubiquitinated-PCNA protects replication forks from DNA2-mediated degradation by regulating Okazaki fragment maturation and chromatin assembly. *Nat Commun*. 11, 2147 (2020).

[354] J. McIntyre, R. Woodgate, Regulation of translesion DNA synthesis: Posttranslational modification of lysine residues in key proteins. *DNA Repair*. 29, 166–179 (2015).

[355] L. J. Simpson, A. Ross, D. Szüts, C. A. Alviani, V. H. Oestergaard, K. J. Patel, J. E. Sale, RAD18-independent ubiquitination of proliferating-cell nuclear antigen in the avian cell line DT40. *EMBO Rep.* 7, 927–932 (2006).

[356] S. Zhang, J. Chea, X. Meng, Y. Zhou, E. Y. C. Lee, M. Y. W. T. Lee, PCNA is ubiquitinated by RNF8. *Cell Cycle*. 7, 3399–3404 (2008).

[357] K. Terai, T. Abbas, A. A. Jazaeri, A. Dutta, CRL4Cdt2 E3 Ubiquitin Ligase Monoubiquitinates PCNA to Promote Translesion DNA Synthesis. *Mol. Cell*. 37, 143–149 (2010).

[358] K. E. Coleman, Y. Yin, S. K. L. Lui, S. Keegan, D. Fenyo, D. J. Smith, E. Rothenberg, T. T. Huang, USP1-trapping lesions as a source of DNA replication stress and genomic instability. *Nat Commun.* 13, 1740 (2022).

[359] J. L. Parker, A. Bucceri, A. A. Davies, K. Heidrich, H. Windecker, H. D. Ulrich, SUMO modification of PCNA is controlled by DNA. *Embo J.* 27, 2422–2431 (2008).

[360] H. Windecker, H. D. Ulrich, Architecture and Assembly of Poly-SUMO Chains on PCNA in Saccharomyces cerevisiae. *J. Mol. Biol.* 376, 221–231 (2008).

[361] N. Garcia-Rodriguez, R. P. Wong, H. D. Ulrich, Functions of Ubiquitin and SUMO in DNA Replication and Replication Stress. *Frontiers Genetics*. 7, 87 (2016).

[362] J. L. Parker, H. D. Ulrich, A SUMO-interacting motif activates budding yeast ubiquitin ligase Rad18 towards SUMO-modified PCNA. *Nucleic Acids Res.* 40, 11380–11388 (2012).

[363] B. Pfander, G.-L. Moldovan, M. Sacher, C. Hoege, S. Jentsch, SUMO-modified PCNA recruits Srs2 to prevent recombination during S phase. *Nature*. 436, 428–433 (2005).

[364] E. Papouli, S. Chen, A. A. Davies, D. Huttner, L. Krejci, P. Sung, H. D. Ulrich, Crosstalk between SUMO and Ubiquitin on PCNA Is Mediated by Recruitment of the Helicase Srs2p. *Mol. Cell*. 19, 123–133 (2005).

[365] D. Branzei, B. Szakal, DNA damage tolerance by recombination: Molecular pathways and DNA structures. *DNA Repair*. 44, 68–75 (2016).

[366] L. S. Waters, B. K. Minesinger, M. E. Wiltrout, S. D'Souza, R. V. Woodruff, G. C. Walker, Eukaryotic Translesion Polymerases and Their Roles and Regulation in DNA Damage Tolerance. *Microbiol. Mol. Biol. Rev.* 73, 134–154 (2009).

[367] M. Bienko, C. M. Green, N. Crosetto, F. Rudolf, G. Zapart, B. Coull, P. Kannouche, G. Wider, M. Peter, A. R. Lehmann, K. Hofmann, I. Dikic, Ubiquitin-binding domains in Y-family polymerases regulate translesion synthesis. *Science*. 310, 1821--1824 (2005).

[368] N. Acharya, J.-H. Yoon, J. Hurwitz, L. Prakash, S. Prakash, DNA polymerase η lacking the ubiquitin-binding domain promotes replicative lesion bypass in humans cells. *Proc. Natl. Acad. Sci.* 107, 10401–10405 (2010).

[369] J. E. Sale, Translesion DNA Synthesis and Mutagenesis in Eukaryotes. *Cold Spring Harb. Perspect. Biol.* 5, a012708 (2013).

[370] V. Pagès, R. P. Fuchs, How DNA lesions are turned into mutations within cells? *Oncogene*. 21, 8957–8966 (2002).

[371] L. S. Waters, G. C. Walker, The critical mutagenic translesion DNA polymerase Rev1 is highly expressed during G2/M phase rather than S phase. *Proc. Natl. Acad. Sci.* 103, 8971–8976 (2006).

[372] A. Hendel, O. Ziv, Q. Gueranger, N. Geacintov, Z. Livneh, Reduced efficiency and increased mutagenicity of translesion DNA synthesis across a TT cyclobutane pyrimidine dimer, but not a TT 6-4 photoproduct, in human cells lacking DNA polymerase η. *DNA Repair*. 7, 1636–1646 (2008).

[373] A. Yamada, C. Masutani, S. Iwai, F. Hanaoka, Complementation of defective translesion synthesis and UV light sensitivity in xeroderma pigmentosum variant cells by human and mouse DNA polymerase η. *Nucleic Acids Res.* 28, 2473–2480 (2000).

[374] D. M. Korzhnev, M. K. Hadden, Targeting the Translesion Synthesis Pathway for the Development of Anti-Cancer Chemotherapeutics. *J. Med. Chem.* 59, 9321–9336 (2016).

[375] S. Shachar, O. Ziv, S. Avkin, S. Adar, J. Wittschieben, T. Reißner, S. Chaney, E. C. Friedberg, Z. Wang, T. Carell, N. Geacintov, Z. Livneh, Two-polymerase mechanisms dictate error-free and error-prone translesion DNA synthesis in mammals. *EMBO J.* 28, 383–393 (2009).

[376] Y. Masuda, F. Hanaoka, C. Masutani, DNA Replication, Recombination, and Repair, Molecular Mechanisms and Pathology, 249–304 (2016).

[377] J. Wojtaszek, C.-J. Lee, S. D'Souza, B. Minesinger, H. Kim, A. D. D'Andrea, G. C. Walker, P. Zhou, Structural Basis of Rev1-mediated Assembly of a Quaternary Vertebrate Translesion Polymerase Complex Consisting of Rev1, Heterodimeric Polymerase (Pol) ζ, and Pol κ*. *J. Biol. Chem.* 287, 33836–33846 (2012).

[378] S. K. Martin, R. D. Wood, DNA polymerase ζ in DNA replication and repair. *Nucleic Acids Res.* 47, 8348–8361 (2019).

[379] M. Bienko, C. M. Green, S. Sabbioneda, N. Crosetto, I. Matic, R. G. Hibbert, T. Begovic, A. Niimi, M. Mann, A. R. Lehmann, I. Dikic, Regulation of Translesion Synthesis DNA Polymerase η by Monoubiquitination. *Mol. Cell.* 37, 396–407 (2010).

[380] E. J. Davis, C. Lachaud, P. Appleton, T. J. Macartney, I. Näthke, J. Rouse, DVC1 (C1orf124) recruits the p97 protein segregase to sites of DNA damage. *Nat. Struct. Mol. Biol.* 19, 1093–1100 (2012).

[381] J. M. Park, S. W. Yang, K. R. Yu, S. H. Ka, S. W. Lee, J. H. Seol, Y. J. Jeon, C. H. Chung, Modification of PCNA by ISG15 Plays a Crucial Role in Termination of Error-Prone Translesion DNA Synthesis. *Mol. Cell.* 54, 626–638 (2014).

[382] N. P. Higgins, K. Kato, B. Strauss, A model for replication repair in mammalian cells. *J. Mol. Biol.* 101, 417–425 (1976).

[383] H. Zhang, C. W. Lawrence, The error-free component of the RAD6/RAD18 DNA damage tolerance pathway of budding yeast employs sister-strand recombination. *Proc. Natl. Acad. Sci.* 102, 15954–15959 (2005).

[384] G. Liberi, G. Maffioletti, C. Lucca, I. Chiolo, A. Baryshnikova, C. Cotta-Ramusino, M. Lopes, A. Pellicioli, J. E. Haber, M. Foiani, Rad51-dependent DNA structures accumulate at damaged replication forks in sgs1 mutants defective in the yeast ortholog of BLM RecQ helicase. *Genes Dev.* 19, 339–350 (2005).

[385] D. Branzei, F. Vanoli, M. Foiani, SUMOylation regulates Rad18-mediated template switch. *Nature*. 456, 915–920 (2008).

[386] E. C. Minca, D. Kowalski, Multiple Rad5 Activities Mediate Sister Chromatid Recombination to Bypass DNA Damage at Stalled Replication Forks. *Mol. Cell*. 38, 649–661 (2010).

[387] M. Giannattasio, K. Zwicky, C. Follonier, M. Foiani, M. Lopes, D. Branzei, Visualization of recombination-mediated damage bypass by template switching. *Nat. Struct. Mol. Biol.* 21, 884–892 (2014).

[388] G. I. Karras, M. Fumasoni, G. Sienski, F. Vanoli, D. Branzei, S. Jentsch, Noncanonical role of the 9-1-1 clamp in the error-free DNA damage tolerance pathway. *Mol Cell*. 49, 536--546 (2013).

[389] F. Vanoli, M. Fumasoni, B. Szakal, L. Maloisel, D. Branzei, Replication and recombination factors contributing to recombination-dependent bypass of DNA lesions by template switch. *Plos Genet*. 6, e1001205 (2010).

[390] N. Garcia-Rodriguez, R. P. Wong, H. D. Ulrich, The helicase Pif1 functions in the template switching pathway of DNA damage bypass. *Nucleic Acids Res*. 46, 8347--8356 (2018).

[391] O. Buzovetsky, Y. Kwon, N. T. Pham, C. Kim, G. Ira, P. Sung, Y. Xiong, Role of the Pif1-PCNA Complex in Pol δ-Dependent Strand Displacement DNA Synthesis and Break-Induced Replication. *Cell Rep.* 21, 1707–1714 (2017).

[392] L. G. Ball, K. Zhang, J. A. Cobb, C. Boone, W. Xiao, The yeast Shu complex couples error-free post-replication repair to homologous recombination. *Mol Microbiol*. 73, 89--102 (2009).

[393] H. D. Ulrich, H. Walden, Ubiquitin signalling in DNA replication and repair. *Nat. Rev. Mol. Cell Biol.* 11, 479–489 (2010).

[394] J. Yuan, G. Ghosal, J. Chen, The HARP-like Domain-Containing Protein AH2/ZRANB3 Binds to PCNA and Participates in Cellular Response to Replication Stress. *Mol. Cell*. 47, 410–421 (2012).

[395] N. Crosetto, M. Bienko, R. G. Hibbert, T. Perica, C. Ambrogio, T. Kensche, K. Hofmann, T. K. Sixma, I. Dikic, Human Wrnip1 Is Localized in Replication Factories in a Ubiquitin-binding Zinc Finger-dependent Manner*. *J. Biol. Chem.* 283, 35173–35185 (2008).

[396] I. Saugar, J. L. Parker, S. Zhao, H. D. Ulrich, The genome maintenance factor Mgs1 is targeted to sites of replication stress by ubiquitylated PCNA. *Nucleic Acids Res*. 40, 245–257 (2012).

[397] R. P. Wong, K. Petriukov, H. D. Ulrich, Daughter-strand gaps in DNA replication – substrates of lesion processing and initiators of distress signalling. *Dna Repair*, 103163 (2021).

[398] V. Gonzalez-Huici, B. Szakal, M. Urulangodi, I. Psakhye, F. Castellucci, D. Menolfi, E. Rajakumara, M. Fumasoni, R. Bermejo, S. Jentsch, D. Branzei, DNA bending facilitates the error-free DNA damage tolerance pathway and upholds genome integrity. *EMBO J.* 33, 327–340 (2014).

[399] Y. Daigaku, A. A. Davies, H. D. Ulrich, Ubiquitin-dependent DNA damage bypass is separable from genome replication. *Nature*. 465, 951--955 (2010).

[400] G. I. Karras, S. Jentsch, The RAD6 DNA damage tolerance pathway operates uncoupled from the replication fork and is functional beyond S phase. *Cell*. 141, 255--267 (2010).

[401] M. Lopes, M. Foiani, J. M. Sogo, Multiple Mechanisms Control Chromosome Integrity after Replication Fork Uncoupling and Restart at Irreparable UV Lesions. *Mol. Cell*. 21, 15–27 (2006).

[402] S. Mourón, S. Rodriguez-Acebes, M. I. Martínez-Jiménez, S. García-Gómez, S. Chocrón, L. Blanco, J. Méndez, Repriming of DNA synthesis at stalled replication forks by human PrimPol. *Nat. Struct. Mol. Biol*. 20, 1383–1389 (2013).

[403] M. Fumasoni, K. Zwicky, F. Vanoli, M. Lopes, D. Branzei, Error-free DNA damage tolerance and sister chromatid proximity during DNA replication rely on the Pol\textgreeka/Primase/Ctf4 Complex. *Mol Cell*. 57, 812--823 (2015).

[404] R. P. Wong, N. Garcia-Rodriguez, N. Zilio, M. Hanulova, H. D. Ulrich, Processing of DNA Polymerase-Blocking Lesions during Genome Replication Is Spatially and Temporally Segregated from Replication Forks. *Mol Cell*. 77, 3-16.e4 (2020).

[405] P. T. Tran, N. Erdeniz, L. S. Symington, R. M. Liskay, EXO1-A multi-tasking eukaryotic nuclease. *Dna Repair*. 3, 1549--1559 (2004).

[406] M. R. Lieber, The FEN-1 family of structure-specific nucleases in eukaryotic dna replication, recombination and repair. *BioEssays*. 19, 233–240 (1997).

[407] P. Szankasi, G. R. Smith, A DNA exonuclease induced during meiosis of Schizosaccharomyces pombe. *Journal of Biological Chemistry*. 267, 3014--3023 (1992).

[408] J. Qiu, Y. Qian, V. Chen, M. X. Guan, B. Shen, Human exonuclease 1 functionally complements its yeast homologues in DNA recombination, RNA primer removal, and mutation avoidance. *J Biol Chem*. 274, 17893--17900 (1999).

[409] E. M. Goellner, C. D. Putnam, R. D. Kolodner, Exonuclease 1-dependent and independent mismatch repair. *DNA Repair*. 32, 24–32 (2015).

[410] J. Orans, E. A. McSweeney, R. R. Iyer, M. A. Hast, H. W. Hellinga, P. Modrich, L. S. Beese, Structures of human exonuclease 1 DNA complexes suggest a unified mechanism for nuclease family. *Cell*. 145, 212--223 (2011).

[411] P. T. Tran, J. A. Simon, R. M. Liskay, Interactions of Exo1p with components of MutLalpha in Saccharomyces cerevisiae. *Proc National Acad Sci*. 98, 9760--9765 (2001).

[412] C. Dherin, E. Gueneau, M. Francin, M. Nunez, S. Miron, S. E. Liberti, L. J. Rasmussen, S. Zinn-Justin, B. Gilquin, J.-B. Charbonnier, S. Boiteux, Characterization of a Highly Conserved Binding Site of Mlh1 Required for Exonuclease I-Dependent Mismatch Repair. *Mol. Cell. Biol.* 29, 907–918 (2009).

[413] E. Gueneau, C. Dherin, P. Legrand, C. Tellier-Lebegue, B. Gilquin, P. Bonnesoeur, F. Londino, C. Quemener, M.-H. L. Du, J. A. Márquez, M. Moutiez, M. Gondry, S. Boiteux, J.-B. Charbonnier, Structure of the MutLα C-terminal domain reveals how Mlh1 contributes to Pms1 endonuclease site. *Nat. Struct. Mol. Biol.* 20, 461–468 (2013).

[414] D. X. Tishkoff, A. L. Boerger, P. Bertrand, N. Filosi, G. M. Gaida, M. F. Kane, R. D. Kolodner, Identification and characterization of Saccharomyces cerevisiae EXO1, a gene encoding an exonuclease that interacts with MSH2. *Proc National Acad Sci*. 94, 7487--7492 (1997).

[415] E. M. Goellner, C. D. Putnam, W. J. Graham, C. M. Rahal, B.-Z. Li, R. D. Kolodner, Identification of Exo1-Msh2 interaction motifs in DNA mismatch repair and new Msh2-binding partners. *Nat. Struct. Mol. Biol.* 25, 650–659 (2018).

[416] F. Zhang, J. Shi, S.-H. Chen, C. Bian, X. Yu, The PIN domain of EXO1 recognizes poly(ADP-ribose) in DNA damage response. *Nucleic Acids Res.* 43, 10782–10794 (2015).

[417] A. Cheruiyot, S. C. Paudyal, I.-K. Kim, M. Sparks, T. Ellenberger, H. Piwnica-Worms, Z. You, Poly(ADP-ribose)-binding promotes Exo1 damage recruitment and suppresses its nuclease activities. *DNA Repair*. 35, 106–115 (2015).

[418] X. Chen, S. C. Paudyal, R.-I. Chin, Z. You, PCNA promotes processive DNA end resection by Exo1. *Nucleic Acids Res*. 41, 9325–9338 (2013).

[419] A. H. Y. Tong, G. Lesage, G. D. Bader, H. Ding, H. Xu, X. Xin, J. Young, G. F. Berriz, R. L. Brost, M. Chang, Y. Chen, X. Cheng, G. Chua, H. Friesen, D. S. Goldberg, J. Haynes, C. Humphries, G. He, S. Hussein, L. Ke, N. Krogan, Z. Li, J. N. Levinson, H. Lu, P. Menard, C. Munyana, A. B. Parsons, O. Ryan, R. Tonikian, T. Roberts, A.-M. Sdicu, J. Shapiro, B. Sheikh, B. Suter, S. L. Wong, L. V. Zhang, H. Zhu, C. G. Burd, S. Munro, C. Sander, J. Rine, J. Greenblatt, M. Peter, A. Bretscher, G. Bell, F. P. Roth, G. W. Brown, B. Andrews, H. Bussey, C. Boone, Global mapping of the yeast genetic interaction network. *Science*. 303, 808--813 (2004).

[420] J. Ma, J. Jin, H. Lu, J. Zhang, Y. Li, X. Cai, Exonuclease 1 is a Potential Diagnostic and Prognostic Biomarker in Hepatocellular Carcinoma. *Front. Mol. Biosci.* 9, 889414 (2022).

[421] C. Zhou, M. Feng, X. Chen, Y. Gao, L. Chen, L. Li, D. Li, Y. Cao, Exonuclease 1 (EXO1) is a Potential Prognostic Biomarker and Correlates with Immune Infiltrates in Lung Adenocarcinoma. *Oncotargets Ther*. Volume 14, 1033–1048 (2021).

[422] E. P. Mimitou, L. S. Symington, Sae2, Exo1 and Sgs1 collaborate in DNA double-strand break processing. *Nature*. 455, 770–774 (2008).

[423] E. P. Mimitou, L. S. Symington, DNA end resection—Unraveling the tail. *DNA Repair*. 10, 344–348 (2011).

[424] Z. Zhu, W.-H. Chung, E. Y. Shim, S. E. Lee, G. Ira, Sgs1 Helicase and Two Nucleases Dna2 and Exo1 Resect DNA Double-Strand Break Ends. *Cell*. 134, 981–994 (2008).

[425] S. Gravel, J. R. Chapman, C. Magill, S. P. Jackson, DNA helicases Sgs1 and BLM promote DNA double-strand break resection. *Genes Dev.* 22, 2767–2772 (2008).

[426] R. E. Keelagher, V. E. Cotton, A. S. H. Goldman, R. H. Borts, Separable roles for Exonuclease I in meiotic DNA double-strand break repair. *DNA Repair*. 10, 126–137 (2011).

[427] P. Fiorentini, K. N. Huang, D. X. Tishkoff, R. D. Kolodner, L. S. Symington, Exonuclease I of Saccharomyces cerevisiae functions in mitotic recombination in vivo and in vitro. *Mol Cell Biol*. 17, 2764--2773 (1997).

[428] D. T. Kirkpatrick, J. R. Ferguson, T. D. Petes, L. S. Symington, Decreased meiotic intergenic recombination and increased meiosis I nondisjunction in exo1 mutants of Saccharomyces cerevisiae. *Genetics*. 156, 1549--1557 (2000).

[429] H. Tsubouchi, H. Ogawa, Exo1 roles for repair of DNA double-strand breaks and meiotic crossing over in Saccharomyces cerevisiae. *Mol Biol Cell*. 11, 2221--2233 (2000).

[430] K. A. Khazanehdari, R. H. Borts, EXO1 and MSH4 differentially affect crossing-over and segregation. *Chromosoma*. 109, 94–102 (2000).

[431] P. Szankasi, G. R. Smith, A role for exonuclease I from S. pombe in mutation avoidance and mismatch correction. *Science*. 267, 1166--1169 (1995).

[432] P. Szankasi, G. R. Smith, A DNA exonuclease induced during meiosis of Schizosaccharomyces pombe. *J. Biol. Chem.* 267, 3014–3023 (1992).

[433] S. Schaetzlein, R. Chahwan, E. Avdievich, S. Roa, K. Wei, R. L. Eoff, R. S. Sellers, A. B. Clark, T. A. Kunkel, M. D. Scharff, W. Edelmann, Mammalian Exo1 encodes both structural and catalytic functions that play distinct roles in essential biological processes. *Proc. Natl. Acad. Sci.* 110, E2470–E2479 (2013).

[434] K. Wei, A. B. Clark, E. Wong, M. F. Kane, D. J. Mazur, T. Parris, N. K. Kolas, R. Russell, H. Hou, B. Kneitz, G. Yang, T. A. Kunkel, R. D. Kolodner, P. E. Cohen, W. Edelmann, Inactivation of Exonuclease 1 in mice results in DNA mismatch repair defects, increased cancer susceptibility, and male and female sterility. *Genes Dev.* 17, 603–614 (2003).

[435] N. S. Amin, M. N. Nguyen, S. Oh, R. D. Kolodner, exo1-Dependent mutator mutations: model system for studying functional interactions in mismatch repair. *Mol Cell Biol*. 21, 5142--5155 (2001).

[436] L. Y. Kadyrova, B. K. Dahal, V. Gujar, J. M. Daley, P. Sung, F. A. Kadyrov, The nuclease activity of DNA2 promotes exonuclease 1–independent mismatch repair. *J Biol Chem*. 298, 101831 (2022).

[437] F. A. Calil, B.-Z. Li, K. A. Torres, K. Nguyen, N. Bowen, C. D. Putnam, R. D. Kolodner, Rad27 and Exo1 function in different excision pathways for mismatch repair in Saccharomyces cerevisiae. *Nat Commun*. 12, 5568 (2021).

[438] H. Hombauer, C. S. Campbell, C. E. Smith, A. Desai, R. D. Kolodner, Visualization of Eukaryotic DNA Mismatch Repair Reveals Distinct Recognition and Repair Intermediates. *Cell*. 147, 1040–1053 (2011).

[439] P. T. Tran, J. P. Fey, N. Erdeniz, L. Gellon, S. Boiteux, R. M. Liskay, A mutation in EXO1 defines separable roles in DNA mismatch repair and post-replication repair. *DNA Repair*. 6, 1572–1583 (2007).

[440] X. Sun, D. Thrower, J. Qiu, P. Wu, L. Zheng, M. Zhou, J. Bachant, D. M. Wilson, B. Shen, Complementary functions of the Saccharomyces cerevisiae Rad2 family nucleases in Okazaki fragment maturation, mutation avoidance, and chromosome stability. *DNA Repair*. 2, 925–940 (2003).

[441] G. Keijzers, D. Liu, L. J. Rasmussen, Exonuclease 1 and its versatile roles in DNA repair. *Crit. Rev. Biochem. Mol. Biol.* 51, 440–451 (2016).

[442] J. Qiu, M. X. Guan, A. M. Bailis, B. Shen, Saccharomyces cerevisiae exonuclease-1 plays a role in UV resistance that is distinct from nucleotide excision repair. *Nucleic Acids Res*. 26, 3077--3083 (1998).

[443] L. Maringele, D. Lydall, EXO1-dependent single-stranded DNA at telomeres activates subsets of DNA damage and spindle checkpoint pathways in budding yeast yku70Δ mutants. *Genes Dev.* 16, 1919–1933 (2002).

[444] A. A. Bertuch, V. Lundblad, EXO1 Contributes to Telomere Maintenance in Both Telomerase-Proficient and Telomerase-Deficient Saccharomyces cerevisiae. *Genetics*. 166, 1651–1659 (2004).

[445] J. M. Dewar, D. Lydall, Pif1- and Exo1-dependent nucleases coordinate checkpoint activation following telomere uncapping. *EMBO J.* 29, 4020–4034 (2010).

[446] D. Nakada, Y. Hirano, K. Sugimoto, Requirement of the Mre11 Complex and Exonuclease 1 for Activation of the Mec1 Signaling Pathway. *Mol. Cell. Biol.* 24, 10016–10025 (2004).

[447] J. Eccleston, C. Yan, K. Yuan, F. W. Alt, E. Selsing, Mismatch Repair Proteins MSH2, MLH1, and EXO1 Are Important for Class-Switch Recombination Events Occurring in B Cells That Lack Nonhomologous End Joining. *J. Immunol.* 186, 2336–2343 (2011).

[448] S. Sertic, R. Quadri, F. Lazzaro, M. Muzi-Falconi, EXO1: A tightly regulated nuclease. *DNA Repair*. 93, 102929 (2020).

[449] W. Eid, M. Steger, M. El-Shemerly, L. P. Ferretti, J. Peña-Diaz, C. König, E. Valtorta, A. A. Sartori, S. Ferrari, DNA end resection by CtIP and exonuclease 1 prevents genomic instability. *EMBO Rep.* 11, 962–968 (2010).

[450] S. D. Andersen, G. Keijzers, E. Rampakakis, K. Engels, P. Luhn, M. El-Shemerly, F. C. Nielsen, Y. Du, A. May, V. A. Bohr, S. Ferrari, M. Zannis-Hadjopoulos, H. Fu, L. J. Rasmussen, 14-3-3 checkpoint regulatory proteins interact specifically with DNA repair protein human exonuclease 1 (hEXO1) via a semi-conserved motif. *DNA Repair*. 11, 267–277 (2012).

[451] S. Li, Z. Lavagnino, D. Lemacon, L. Kong, A. Ustione, X. Ng, Y. Zhang, Y. Wang, B. Zheng, H. Piwnica-Worms, A. Vindigni, D. W. Piston, Z. You, Ca2+-Stimulated AMPK-Dependent Phosphorylation of Exo1 Protects Stressed Replication Forks from Aberrant Resection. *Mol. Cell*. 74, 1123-1137.e6 (2019).

[452] N. Tomimatsu, B. Mukherjee, M. C. Hardebeck, M. Ilcheva, C. V. Camacho, J. L. Harris, M. Porteus, B. Llorente, K. K. Khanna, S. Burma, Phosphorylation of EXO1 by CDKs 1 and 2 regulates DNA end resection and repair pathway choice. *Nat. Commun.* 5, 3561 (2014).

[453] N. Garcia-Rodriguez, M. Morawska, R. P. Wong, Y. Daigaku, H. D. Ulrich, Spatial separation between replisome- and template-induced replication stress signaling. *Embo J.* 37 (2018), doi:10.15252/embj.201798369.

[454] N. Tomimatsu, B. Mukherjee, J. L. Harris, F. L. Boffo, M. C. Hardebeck, P. R. Potts, K. K. Khanna, S. Burma, DNA-damage-induced degradation of EXO1 exonuclease limits DNA end resection to ensure accurate DNA repair. *J. Biol. Chem.* 292, 10779–10790 (2017).

[455] S. Bologna, V. Altmannova, E. Valtorta, C. Koenig, P. Liberali, C. Gentili, D. Anrather, G. Ammerer, L. Pelkmans, L. Krejci, S. Ferrari, Sumoylation regulates EXO1 stability and processing of DNA damage. *Cell Cycle*. 14, 2439–2450 (2015).

[456] T. F. S. Inc., Ed., SYBR Safe DNA Gel Stain Frequently Asked Questions (available at https://www.thermofisher.com/de/de/home/life-science/dna-rna-purification-analysis/nucleic-acid-gel-electrophoresis/dna-stains/sybr-safe/sybr-safe-faq.html).

[457] Guidelines for PCR Optimization with Phusion High-Fidelity DNA Polymerase | NEB, (available at https://www.neb.com/en/protocols/2012/06/01/guidelines-for-pcr-optimization-with-phusion-high-fidelity-dna-polymerase).

[458] D. G. Gibson, L. Young, R.-Y. Chuang, J. C. Venter, C. A. Hutchison, H. O. Smith, Enzymatic assembly of DNA molecules up to several hundred kilobases. *Nat. Methods*. 6, 343–345 (2009).

[459] C. Janke, M. M. Magiera, N. Rathfelder, C. Taxis, S. Reber, H. Maekawa, A. Moreno-Borchart, G. Doenges, E. Schwob, E. Schiebel, M. Knop, A versatile toolbox for PCR-based tagging of yeast genes: new fluorescent proteins, more markers and promoter substitution cassettes. *Yeast*. 21, 947--962 (2004).

[460] S. Fields, O. Song, A novel genetic system to detect protein–protein interactions. *Nature*. 340, 245–246 (1989).

[461] K. H. Young, Yeast Two-hybrid: So Many Interactions, (in) So Little Time…. *Biol. Reprod.* 58, 302–311 (1998).

[462] P. Trifilieff, M.-L. Rives, E. Urizar, R. A. Piskorowski, H. D. Vishwasrao, J. Castrillon, C. Schmauss, M. Slttman, M. Gullberg, J. A. Javitch, Detection of antigen interactions ex vivo by proximity ligation assay: endogenous dopamine D2-adenosine A2A receptor complexes in the striatum. *BioTechniques*. 51, 111–118 (2011).

[463] S. Y. Lee, J. J. Kim, K. M. Miller, HDAC/HAT Function Assessment and Inhibitor Development, Methods and Protocols. *Methods Mol Biology*. 2589, 345–360 (2022).

[464] S. Fredriksson, M. Gullberg, J. Jarvius, C. Olsson, K. Pietras, S. M. Gústafsdóttir, A. Östman, U. Landegren, Protein detection using proximity-dependent DNA ligation assays. *Nat. Biotechnol.* 20, 473–477 (2002).

[465] J. E. Noble, M. J. A. Bailey, Chapter 8 Quantitation of Protein. *Methods Enzym.* 463, 73–95 (2009).

[466] S. Wegmann, C. Meister, C. Renz, G. Yakoub, H.-P. Wollscheid, D. T. Takahashi, I. Mikicic, P. Beli, H. D. Ulrich, Linkage reprogramming by tailor-made E3s reveals polyubiquitin chain requirements in DNA-damage bypass. *Mol Cell*. 82, 1589-1602.e5 (2022).

[467] T. E. T. Mevissen, M. K. Hospenthal, P. P. Geurink, P. R. Elliott, M. Akutsu, N. Arnaudo, R. Ekkebus, Y. Kulathu, T. Wauer, F. E. Oualid, S. M. V. Freund, H. Ovaa, D. Komander, OTU deubiquitinases reveal mechanisms of linkage specificity and enable ubiquitin chain restriction analysis. *Cell*. 154, 169--184 (2013).

[468] Invitrogen, Ed., Bac-to-Bac® Baculovirus Expression System (2015), (available at https://tools.thermofisher.com/content/sfs/manuals/bactobac_man.pdf).

[469] F. Garzoni, C. Bieniossek, I. Berger, The MultiBac BEVS for producing proteins and their complexes. *Epigenesys* (2011), doi:10.13140/2.1.2039.3767.

[470] P. T. Tran, N. Erdeniz, S. Dudley, R. M. Liskay, Characterization of nuclease-dependent functions of Exo1p in Saccharomyces cerevisiae. *Dna Repair*. 1, 895--912 (2002).

[471] E. Cannavo, P. Cejka, S. C. Kowalczykowski, Relationship of DNA degradation by Saccharomyces cerevisiae exonuclease 1 and its stimulation by RPA and Mre11-Rad50-Xrs2 to DNA end resection. *Proc National Acad Sci*. 110, E1661-8 (2013).

[472] P. Cejka, S. C. Kowalczykowski, The full-length Saccharomyces cerevisiae Sgs1 protein is a vigorous DNA helicase that preferentially unwinds holliday junctions. *J Biol Chem*. 285, 8290--8301 (2010).

[473] M. A. Michel, D. Komander, P. R. Elliott, Enzymatic Assembly of Ubiquitin Chains. *Methods in molecular biology (Clifton, N.J.)*. 1844, 73--84 (2018).

[474] C. S. Hughes, S. Moggridge, T. Müller, P. H. Sorensen, G. B. Morin, J. Krijgsveld, Single-pot, solid-phase-enhanced sample preparation for proteomics experiments. *Nat. Protoc.* 14, 68–85 (2019).

[475] J. Rappsilber, Y. Ishihama, M. Mann, Stop and Go Extraction Tips for Matrix-Assisted Laser Desorption/Ionization, Nanoelectrospray, and LC/MS Sample Pretreatment in Proteomics. *Anal. Chem.* 75, 663–670 (2003).

[476] J. Cox, M. Mann, MaxQuant enables high peptide identification rates, individualized p.p.b.-range mass accuracies and proteome-wide protein quantification. *Nat. Biotechnol.* 26, 1367–1372 (2008).

[477] J. Cox, N. Neuhauser, A. Michalski, R. A. Scheltema, J. V. Olsen, M. Mann, Andromeda: A Peptide Search Engine Integrated into the MaxQuant Environment. *J. Proteome Res.* 10, 1794–1805 (2011).

[478] C. Zahnd, M. Kawe, M. T. Stumpp, C. de Pasquale, R. Tamaskovic, G. Nagy-Davidescu, B. Dreier, R. Schibli, H. K. Binz, R. Waibel, A. Pluckthun, Efficient tumor targeting with high-affinity designed ankyrin repeat proteins: effects of affinity and molecular size. *Cancer Res*. 70, 1595--1605 (2010).

[479] T. Strauch, thesis (2019).

[480] proteintech (ed.), WESTERN BLOTTING. *The complete guide to Western blotting*, (available at https://www.ptglab.com/media/sjhpf4gh/western-blot-protocol-by-proteintech.pdf).

[481] C. H. Emmerich, P. Cohen, Optimising methods for the preservation, capture and identification of ubiquitin chains and ubiquitylated proteins by immunoblotting. *Biochemical and biophysical research communications*. 466, 1--14 (2015).

[482] P. Elleringmann, Analysis of polyubiquitin conjugates in mammalian cells by DARPin-based affinity probes (2022).

[483] W. J. Cook, L. C. Jeffrey, E. Kasperek, C. M. Pickart, Structure of Tetraubiquitin Shows How Multiubiquitin Chains Can Be Formed. *J. Mol. Biol.* 236, 601–609 (1994).

[484] R. Beal, Q. Deveraux, G. Xia, M. Rechsteiner, C. Pickart, Surface Hydrophobic Residues of Multiubiquitin Chains Essential for Proteolytic Targeting. *Proc. Natl. Acad. Sci.* 40, 637–671 (1996).

[485] B. T. Bajar, E. S. Wang, S. Zhang, M. Z. Lin, J. Chu, A Guide to Fluorescent Protein FRET Pairs. *Sensors Basel Switz*. 16, 1488 (2016).

[486] D. E. Crone, Y.-M. Huang, D. J. Pitman, C. Schenkelberg, K. Fraser, S. Macari, C. Bystroff, State of the Art in Biosensors - General Aspects (2013), doi:10.5772/52250.

[487] R. B. Sekar, A. Periasamy, Fluorescence resonance energy transfer (FRET) microscopy imaging of live cell protein localizations. *J. Cell Biol.* 160, 629–633 (2003).

[488] B. A. Pollok, R. Heim, Using GFP in FRET-based applications. *Trends Cell Biol.* 9, 57–60 (1999).

[489] X. Sheng, Z. Xia, H. Yang, R. Hu, The ubiquitin codes in cellular stress responses. *Protein Cell*. 15, 157–190 (2023).

[490] A. Lopata, A. Kniss, F. Löhr, V. V. Rogov, V. Dötsch, Ubiquitination in the ERAD Process. *Int. J. Mol. Sci.* 21, 5369 (2020).

[491] Y. Wu, X. Li, J. Jia, Y. Zhang, J. Li, Z. Zhu, H. Wang, J. Tang, J. Hu, Transmembrane E3 ligase RNF183 mediates ER stress-induced apoptosis by degrading Bcl-xL. *Proc. Natl. Acad. Sci.* 115, E2762–E2771 (2018).

[492] M. Meerang, D. Ritz, S. Paliwal, Z. Garajova, M. Bosshard, N. Mailand, P. Janscak, U. Hübscher, H. Meyer, K. Ramadan, The ubiquitin-selective segregase VCP/p97 orchestrates the response to DNA double-strand breaks. *Nat. Cell Biol.* 13, 1376–1382 (2011).

[493] K. Ramadan, p97/VCP- and Lys48-linked polyubiquitination form a new signaling pathway in DNA damage response. *Cell Cycle*. 11, 1062–1069 (2012).

[494] L. Feng, J. Chen, The E3 ligase RNF8 regulates KU80 removal and NHEJ repair. *Nat. Struct. Mol. Biol.* 19, 201–206 (2012).

[495] W.-J. Zeng, C. Lu, Y. Shi, C. Wu, X. Chen, C. Li, J. Yao, Initiation of stress granule assembly by rapid clustering of IGF2BP proteins upon osmotic shock. *Biochimica Et Biophysica Acta Bba - Mol Cell Res*. 1867, 118795 (2020).

[496] M. A. M. Ali, H. Strickfaden, B. L. Lee, L. Spyracopoulos, M. J. Hendzel, RYBP Is a K63-Ubiquitin-Chain-Binding Protein that Inhibits Homologous Recombination Repair. *Cell Rep.* 22, 383–395 (2018).

[497] S. Chitale, H. Richly, Timing of DNA lesion recognition: Ubiquitin signaling in the NER pathway. *Cell Cycle*. 16, 163–171 (2017).

[498] M. Altun, H. B. Kramer, L. I. Willems, J. L. McDermott, C. A. Leach, S. J. Goldenberg, K. G. S. Kumar, R. Konietzny, R. Fischer, E. Kogan, M. M. Mackeen, J. McGouran, S. V. Khoronenkova, J. L. Parsons, G. L. Dianov, B. Nicholson, B. M. Kessler, Activity-based chemical proteomics accelerates inhibitor development for deubiquitylating enzymes. *Chem Biol*. 18, 1401--1412 (2011).

[499] R. E. Heap, M. S. Gant, F. Lamoliatte, J. Peltier, M. Trost, Mass spectrometry techniques for studying the ubiquitin system. *Biochem. Soc. Trans.* 45, 1137–1148 (2017).

[500] H. Wang, A. Matsuzawa, S. A. Brown, J. Zhou, C. S. Guy, P.-H. Tseng, K. Forbes, T. P. Nicholson, P. W. Sheppard, H. Häcker, M. Karin, D. A. A. Vignali, Analysis of nondegradative protein ubiquitylation with a monoclonal antibody specific for lysine-63-linked polyubiquitin. *Proc. Natl. Acad. Sci.* 105, 20197–20202 (2008).

[501] T. Hirano, O. Serve, M. Yagi-Utsumi, E. Takemoto, T. Hiromoto, T. Satoh, T. Mizushima, K. Kato, Conformational Dynamics of Wild-type Lys-48-linked Diubiquitin in Solution*. *J. Biol. Chem.* 286, 37496–37502 (2011).

[502] T. Satoh, E. Sakata, S. Yamamoto, Y. Yamaguchi, A. Sumiyoshi, S. Wakatsuki, K. Kato, Crystal structure of cyclic Lys48-linked tetraubiquitin. *Biochem. Biophys. Res. Commun.* 400, 329–333 (2010).

[503] Y. Ryabov, D. Fushman, Structural Assembly of Multidomain Proteins and Protein Complexes Guided by the Overall Rotational Diffusion Tensor. *J. Am. Chem. Soc.* 129, 7894–7902 (2007).

[504] Y. Ye, G. Blaser, M. H. Horrocks, M. J. Ruedas-Rama, S. Ibrahim, A. A. Zhukov, A. Orte, D. Klenerman, S. E. Jackson, D. Komander, Ubiquitin chain conformation regulates recognition and activity of interacting proteins. *Nature*. 492, 266–270 (2012).

[505] J. D. Wright, P. D. Mace, C. L. Day, Noncovalent Ubiquitin Interactions Regulate the Catalytic Activity of Ubiquitin Writers. *Trends Biochem. Sci.* 41, 924–937 (2016).

[506] S. Ko, G. B. Kang, S. M. Song, J.-G. Lee, D. Y. Shin, J.-H. Yun, Y. Sheng, C. Cheong, Y. H. Jeon, Y.-K. Jung, C. H. Arrowsmith, G. V. Avvakumov, S. Dhe-Paganon, Y. J. Yoo, S. H. Eom, W. Lee, Structural basis of E2-25K/UBB+1 interaction leading to proteasome inhibition and neurotoxicity. *J Biol Chem*. 285, 36070--36080 (2010).

[507] A. Ernst, G. Avvakumov, J. Tong, Y. Fan, Y. Zhao, P. Alberts, A. Persaud, J. R. Walker, A.-M. Neculai, D. Neculai, A. Vorobyov, P. Garg, L. Beatty, P.-K. Chan, Y.-C. Juang, M.-C. Landry, C. Yeh, E. Zeqiraj, K. Karamboulas, A. Allali-Hassani, M. Vedadi, M. Tyers, J. Moffat, F. Sicheri, L. Pelletier, D. Durocher, B. Raught, D. Rotin, J. Yang, M. F. Moran, S. Dhe-Paganon, S. S. Sidhu, A Strategy for Modulation of Enzymes in the Ubiquitin System. *Science*. 339, 590–595 (2013).

[508] Y. Sato, K. Okatsu, Y. Saeki, K. Yamano, N. Matsuda, A. Kaiho, A. Yamagata, S. Goto-Ito, M. Ishikawa, Y. Hashimoto, K. Tanaka, S. Fukai, Structural basis for specific cleavage of Lys6-linked polyubiquitin chains by USP30. *Nat Struct Mol Biol*. 24, 911--919 (2017).

[509] P. Wendler, C. Enenkel, Nuclear Transport of Yeast Proteasomes. *Frontiers Mol Biosci*. 6, 34 (2019).

[510] C. Enenkel, R. W. Kang, F. Wilfling, O. P. Ernst, Intracellular localization of the proteasome in response to stress conditions. *J. Biol. Chem.* 298, 102083 (2022).

[511] M. Fukuda, S. Asano, T. Nakamura, M. Adachi, M. Yoshida, M. Yanagida, E. Nishida, CRM1 is responsible for intracellular transport mediated by the nuclear export signal. *Nature*. 390, 308–311 (1997).

[512] N. L. Hindul, A. Jhita, D. G. Oprea, T. A. Hussain, O. Gonchar, M. A. M. Campillo, L. O'Regan, M. T. Kanemaki, A. M. Fry, K. Hirota, K. Tanaka, Construction of a human hTERT RPE-1 cell line with inducible Cre for editing of endogenous genes. *Biol. Open.* 11, bio059056 (2022).

[513] A. G. Bodnar, M. Ouellette, M. Frolkis, S. E. Holt, C.-P. Chiu, G. B. Morin, C. B. Harley, J. W. Shay, S. Lichtsteiner, W. E. Wright, Extension of Life-Span by Introduction of Telomerase into Normal Human Cells. *Science*. 279, 349–352 (1998).

[514] Alexa Fluor® 488 Alexa Fluor® 488 Anti-Ubiquitin (linkage-specific K48) antibody [EP8589] (AB204274) | Abcam, (available at https://www.abcam.com/en-de/products/primary-antibodies/alexa-fluor-488-ubiquitin-linkage-specific-k48-antibody-ep8589-ab204274#).

[515] High Affinity and Specificity Recombinant Ubiquitin K63 Monoclonal Antibody E-AB-81618 at Elabscience.com, (available at https://www.elabscience.com/p-recombinant_ubiquitin_k63_monoclonal_antibody-674128.html).

[516] P. Zhang, B. Fan, P. Yang, J. Temirov, J. Messing, H. J. Kim, J. P. Taylor, Chronic optogenetic induction of stress granules is cytotoxic and reveals the evolution of ALS-FTD pathology. *Elife*. 8 (2019), doi:10.7554/elife.39578.

[517] X. Xie, S. Matsumoto, A. Endo, T. Fukushima, H. Kawahara, Y. Saeki, M. Komada, *J Cell Sci*, in press, doi:10.1242/jcs.210856.

[518] D. Mateju, T. M. Franzmann, A. Patel, A. Kopach, E. E. Boczek, S. Maharana, H. O. Lee, S. Carra, A. A. Hyman, S. Alberti, An aberrant phase transition of stress granules triggered by misfolded protein and prevented by chaperone function. *Embo J*. 36, 1669--1687 (2017).

[519] T. Franzmann, S. Alberti, Ubiquitin protein helps cells to recover from stress. *Nature*. 597, 183–184 (2021).

[520] S. Kwon, Y. Zhang, P. Matthias, The deacetylase HDAC6 is a novel critical component of stress granules involved in the stress response. *Gene Dev*. 21, 3381--3394 (2007).

[521] N. Tolay, A. Buchberger, Comparative profiling of stress granule clearance reveals differential contributions of the ubiquitin system. *Life Sci Alliance*. 4 (2021), doi:10.26508/lsa.202000927.

[522] B. L. Lee, A. Singh, J. N. M. Glover, M. J. Hendzel, L. Spyracopoulos, Molecular Basis for K63-Linked Ubiquitination Processes in Double-Strand DNA Break Repair: A Focus on Kinetics and Dynamics. *J. Mol. Biol.* 429, 3409–3429 (2017).

[523] V. Chau, J. W. Tobias, A. Bachmair, D. Marriott, D. J. Ecker, D. K. Gonda, A. Varshavsky, A Multiubiquitin Chain Is Confined to Specific Lysine in a Targeted Short-Lived Protein. *Science*. 243, 1576–1583 (1989).

[524] S. Rahman, C. Wolberger, Breaking the K48-chain: linking ubiquitin beyond protein degradation. *Nat. Struct. Mol. Biol.* 31, 216–218 (2024).

[525] S. Manohar, S. Jacob, J. Wang, K. A. Wiechecki, H. W. L. Koh, V. Simões, H. Choi, C. Vogel, G. M. Silva, Polyubiquitin Chains Linked by Lysine Residue 48 (K48) Selectively Target Oxidized Proteins In Vivo. *Antioxid. Redox Signal.* 31, 1133–1149 (2019).

[526] J. J. Moser, M. J. Fritzler, Cytoplasmic ribonucleoprotein (RNP) bodies and their relationship to GW/P bodies. *Int J Biochem Cell Biology*. 42, 828--843 (2010).

[527] S. Hofmann, N. Kedersha, P. Anderson, P. Ivanov, Molecular mechanisms of stress granule assembly and disassembly. *Biochimica Et Biophysica Acta Bba - Mol Cell Res*. 1868, 118876 (2021).

[528] P. Anderson, N. Kedersha, Stress granules. *Curr Biol*. 19, R397-8 (2009).

[529] S. J. Seguin, F. F. Morelli, J. Vinet, D. Amore, S. de Biasi, A. Poletti, D. C. Rubinsztein, S. Carra, Inhibition of autophagy, lysosome and VCP function impairs stress granule assembly. *Cell Death Differ*. 21, 1838--1851 (2014).

[530] A. Turakhiya, S. R. Meyer, G. Marincola, S. Bohm, J. T. Vanselow, A. Schlosser, K. Hofmann, A. Buchberger, ZFAND1 Recruits p97 and the 26S Proteasome to Promote the Clearance of Arsenite-Induced Stress Granules. *Mol Cell*. 70, 906-919.e7 (2018).

[531] R. Nostramo, P. K. Herman, Deubiquitination and the regulation of stress granule assembly. *Curr Genet*. 62, 503--506 (2016).

[532] N. Kedersha, M. D. Panas, C. A. Achorn, S. Lyons, S. Tisdale, T. Hickman, M. Thomas, J. Lieberman, G. M. McInerney, P. Ivanov, P. Anderson, G3BP-Caprin1-USP10 complexes mediate stress granule condensation and associate with 40S subunits. *J Cell Biol*. 212, 845--860 (2016).

[533] S. Zhu, M. Yam, Y. Wang, J. D. Linton, A. Grenell, J. B. Hurley, J. Du, Impact of euthanasia, dissection and postmortem delay on metabolic profile in mouse retina and RPE/choroid. *Exp. Eye Res.* 174, 113–120 (2018).

[534] D. Laporte, A. Lebaudy, A. Sahin, B. Pinson, J. Ceschin, B. Daignan-Fornier, I. Sagot, Metabolic status rather than cell cycle signals control quiescence entry and exit. *J. Cell Biol.* 192, 949–957 (2011).

[535] D. Laporte, B. Salin, B. Daignan-Fornier, I. Sagot, Reversible cytoplasmic localization of the proteasome in quiescent yeast cells. *J. Cell Biol.* 181, 737–745 (2008).

[536] J. R. Buchan, R.-M. Kolaitis, J. P. Taylor, R. Parker, Eukaryotic stress granules are cleared by autophagy and Cdc48/VCP function. *Cell*. 153, 1461--1474 (2013).

[537] R. Nostramo, S. N. Varia, B. Zhang, M. M. Emerson, P. K. Herman, The Catalytic Activity of the Ubp3 Deubiquitinating Protease Is Required for Efficient Stress Granule Assembly in Saccharomyces cerevisiae. *Mol Cell Biol*. 36, 173--183 (2016).

[538] K. H. Shah, S. N. Varia, L. A. Cook, P. K. Herman, A Hybrid-Body Containing Constituents of Both P-Bodies and Stress Granules Forms in Response to Hypoosmotic Stress in Saccharomyces cerevisiae. *Plos One*. 11, e0158776 (2016).

[539] Y. Kawaguchi, J. J. Kovacs, A. McLaurin, J. M. Vance, A. Ito, T.-P. Yao, The Deacetylase HDAC6 Regulates Aggresome Formation and Cell Viability in Response to Misfolded Protein Stress. *Cell*. 115, 727–738 (2003).

[540] S. Qin, C. Jiang, J. Gao, Transcriptional factor Nrf2 is essential for aggresome formation during proteasome inhibition. *Biomed. Rep.* 11, 241–252 (2019).

[541] I. Kovacs, K. M. Lentini, L. M. Ingano, D. M. Kovacs, Presenilin 1 forms aggresomal deposits in response to heat shock. *J. Mol. Neurosci.* 29, 9–19 (2006).

[542] L. Catley, E. Weisberg, T. Kiziltepe, Y.-T. Tai, T. Hideshima, P. Neri, P. Tassone, P. Atadja, D. Chauhan, N. C. Munshi, K. C. Anderson, Aggresome induction by proteasome inhibitor bortezomib and α-tubulin hyperacetylation by tubulin deacetylase (TDAC) inhibitor LBH589 are synergistic in myeloma cells. *Blood*. 108, 3441–3449 (2006).

[543] H. An, A. V. Statsyuk, An inhibitor of ubiquitin conjugation and aggresome formation. *Chem. Sci.* 6, 5235–5245 (2015).

[544] H. LeVine, [18] Quantification of β-sheet amyloid fibril structures with thioflavin T. *Methods Enzym.* 309, 274–284 (1999).

[545] R. Hao, P. Nanduri, Y. Rao, R. S. Panichelli, A. Ito, M. Yoshida, T.-P. Yao, Proteasomes Activate Aggresome Disassembly and Clearance by Producing Unanchored Ubiquitin Chains. *Mol. Cell*. 51, 819–828 (2013).

[546] H. E. Johnston, R. S. Samant, Alternative systems for misfolded protein clearance: life beyond the proteasome. *FEBS J.* 288, 4464–4487 (2021).

[547] L. Dong, L. Liu, Y. Li, W. Li, L. Zhou, Q. Xia, E3 ligase Smurf1 protects against misfolded SOD1 in neuronal cells by promoting its K63 ubiquitylation and aggresome formation. *Hum. Mol. Genet.* 31, 2035–2048 (2022).

[548] J. A. Olzmann, L.-S. Chin, Parkin-mediated K63-linked polyubiquitination: A signal for targeting misfolded proteins to the aggresome-autophagy pathway. *Autophagy*. 4, 85–87 (2008).

[549] X. Kong, N. M. Wakida, K. Yokomori, Application of Laser Microirradiation in the Investigations of Cellular Responses to DNA Damage. *Front. Phys.* 8, 597866 (2021).

[550] M. Schmalz, X.-X. Liang, I. Wieser, C. Gruschel, L. Muskalla, M. T. Stöckl, R. Nitschke, N. Linz, A. Leitenstorfer, A. Vogel, E. Ferrando-May, Dissection of DNA damage and repair pathways in live cells by femtosecond laser microirradiation and free-electron modeling. *Proc. Natl. Acad. Sci.* 120, e2220132120 (2023).

[551] J. J. Kim, R. Kumbhar, F. Gong, K. M. Miller, DNA Repair, Methods and Protocols. *Methods Mol. Biol.* 1999, 61–74 (2019).

[552] A. Chansard, E. Pobega, P. Caron, S. E. Polo, Imaging the Response to DNA Damage in Heterochromatin Domains. *Front. Cell Dev. Biol.* 10, 920267 (2022).

[553] Q. Zhang, D. Karnak, M. Tan, T. S. Lawrence, M. A. Morgan, Y. Sun, FBXW7 Facilitates Nonhomologous End-Joining via K63-Linked Polyubiquitylation of XRCC4. *Mol. Cell*. 61, 419–433 (2016).

[554] I. K. Mandemaker, L. van Cuijk, R. C. Janssens, H. Lans, K. Bezstarosti, J. H. Hoeijmakers, J. A. Demmers, W. Vermeulen, J. A. Marteijn, DNA damage-induced histone H1 ubiquitylation is mediated by HUWE1 and stimulates the RNF8-RNF168 pathway. *Sci. Rep.* 7, 15353 (2017).

[555] B. N. Borsos, H. Majoros, T. Pankotai, Ubiquitylation-Mediated Fine-Tuning of DNA Double-Strand Break Repair. *Cancers*. 12, 1617 (2020).

[556] Y. Kodama, C.-D. Hu, Bimolecular fluorescence complementation (BiFC): A 5-year update and future perspectives. *BioTechniques*. 53, 285–298 (2012).

[557] C.-D. Hu, Y. Chinenov, T. K. Kerppola, Visualization of Interactions among bZIP and Rel Family Proteins in Living Cells Using Bimolecular Fluorescence Complementation. *Mol. Cell*. 9, 789–798 (2002).

[558] T. K. Kerppola, Design and implementation of bimolecular fluorescence complementation (BiFC) assays for the visualization of protein interactions in living cells. *Nat Protoc*. 1, 1278–1286 (2006).

[559] Y. J. Shyu, H. Liu, X. Deng, C.-D. Hu, Identification of new fluorescent protein fragments for bimolecular fluorescence complementation analysis under physiological conditions. *BioTechniques*. 40, 61–66 (2006).

[560] J. Reidel, Development of a K48/K63-branched ubiquitin chain sensor utilizing a bimolecular fluorescence complementation approach (2023).

[561] K. Baranes-Bachar, A. Levy-Barda, J. Oehler, D. A. Reid, I. Soria-Bretones, T. C. Voss, D. Chung, Y. Park, C. Liu, J.-B. Yoon, W. Li, G. Dellaire, T. Misteli, P. Huertas, E. Rothenberg, K. Ramadan, Y. Ziv, Y. Shiloh, The Ubiquitin E3/E4 Ligase UBE4A Adjusts Protein Ubiquitylation and Accumulation at Sites of DNA Damage, Facilitating Double-Strand Break Repair. *Mol. Cell*. 69, 866-878.e7 (2018).

[562] S. Panier, D. Durocher, Regulatory ubiquitylation in response to DNA double-strand breaks. *DNA Repair*. 8, 436–443 (2009).

[563] L. Inc., K48 TUBE HF (High Fidelity), FLAG® Catalog Number: UM607 (2004).

[564] C. Yan, F. Wu, R. L. Jernigan, D. Dobbs, V. Honavar, Characterization of Protein–Protein Interfaces. *Protein J.* 27, 59–70 (2008).

[565] C. Tsai, S. L. Lin, H. J. Wolfson, R. Nussinov, Studies of protein-protein interfaces: A statistical analysis of the hydrophobic effect. *Protein Sci.* 6, 53–64 (1997).

[566] M. Steinegger, J. Söding, MMseqs2 enables sensitive protein sequence searching for the analysis of massive data sets. 35, 1026–1028 (2017).

[567] R. Evans, M. O'Neill, A. Pritzel, N. Antropova, A. Senior, T. Green, A. Žídek, R. Bates, S. Blackwell, J. Yim, O. Ronneberger, S. Bodenstein, M. Zielinski, A. Bridgland, A. Potapenko, A. Cowie, K. Tunyasuvunakool, R. Jain, E. Clancy, P. Kohli, J. Jumper, D. Hassabis, *bioRxiv*, in press, doi:10.1101/2021.10.04.463034.

[568] J. J. Chen, C. A. Tsu, J. M. Gavin, M. A. Milhollen, F. J. Bruzzese, W. D. Mallender, M. D. Sintchak, N. J. Bump, X. Yang, J. Ma, H.-K. Loke, Q. Xu, P. Li, N. F. Bence, J. E. Brownell, L. R. Dick, Mechanistic Studies of Substrate-assisted Inhibition of Ubiquitin-activating Enzyme by Adenosine Sulfamate Analogues. *J. Biol. Chem.* 286, 40867–40877 (2011).

[569] S. McKenna, J. Hu, T. Moraes, W. Xiao, M. J. Ellison, L. Spyracopoulos, Energetics and Specificity of Interactions within Ub·Uev·Ubc13 Human Ubiquitin Conjugation Complexes †. *Biochemistry*. 42, 7922–7930 (2003).

[570] Y. Guo, Q. Liu, E. Mallette, C. Caba, F. Hou, J. Fux, G. LaPlante, A. Dong, Q. Zhang, H. Zheng, Y. Tong, W. Zhang, Structural and functional characterization of ubiquitin variant inhibitors for the JAMM-family deubiquitinases STAMBP and STAMBPL1. *J. Biol. Chem.* 297, 101107 (2021).

[571] M. E. Morrow, M. T. Morgan, M. Clerici, K. Growkova, M. Yan, D. Komander, T. K. Sixma, M. Simicek, C. Wolberger, Active site alanine mutations convert deubiquitinases into high-affinity ubiquitin-binding proteins. *EMBO Rep.* 19, e45680 (2018).

[572] D. No, T. P. Yao, R. M. Evans, Ecdysone-inducible gene expression in mammalian cells and transgenic mice. *Proc. Natl. Acad. Sci.* 93, 3346–3351 (1996).

[573] M. Schena, A. M. Lloyd, R. W. Davis, A steroid-inducible gene expression system for plant cells. *Proc. Natl. Acad. Sci.* 88, 10421–10425 (1991).

[574] D. I. Israel, R. J. Kaufman, Highly inducible expression from vectors containing multiple GRE's in CHO cells overexpressing the glucocorticoid receptor. *Nucleic Acids Res.* 17, 4589–4604 (1989).

[575] M. M. Corporatio, Ed., Anti-Ubiquitin, Lys48-Specific, clone Apu2, (available at https://www.merckmillipore.com/INTERSHOP/web/WFS/Merck-INTL-Site/en_US/-/USD/ShowDocument-File?ProductSKU=MM_NF-05-1307&;DocumentId=null&DocumentType=COA&Language=EN&Country=US&ProductBatchNo=2593165&Origin=PDP).

[576] S. Sigismund, S. Polo, Proteostasis, Methods and Protocols. *Methods Mol. Biol.* 1449, 143–151 (2016).

[577] A. Fu, V. Cohen-Kaplan, N. Avni, I. Livneh, A. Ciechanover, p62-containing, proteolytically active nuclear condensates, increase the efficiency of the ubiquitin–proteasome system. *Proc. Natl. Acad. Sci.* 118, e2107321118 (2021).

[578] S. Kageyama, S. R. Gudmundsson, Y.-S. Sou, Y. Ichimura, N. Tamura, S. Kazuno, T. Ueno, Y. Miura, D. Noshiro, M. Abe, T. Mizushima, N. Miura, S. Okuda, H. Motohashi, J.-A. Lee, K. Sakimura, T. Ohe, N. N. Noda, S. Waguri, E.-L. Eskelinen, M. Komatsu, p62/SQSTM1-droplet serves as a platform for autophagosome formation and anti-oxidative stress response. *Nat. Commun.* 12, 16 (2021).

[579] Y. Zhou, P. L. Kastritis, S. E. Dougherty, J. Bouvette, A. L. Hsu, L. Burbaum, S. Mosalaganti, S. Pfeffer, W. J. H. Hagen, F. Förster, M. J. Borgnia, C. Vogel, M. Beck, A. Bartesaghi, G. M. Silva, Structural impact of K63 ubiquitin on yeast translocating ribosomes under oxidative stress. *Proc. Natl. Acad. Sci.* 117, 22157–22166 (2020).

[580] K. G. Mark, M. Rape, Ubiquitin-dependent regulation of transcription in development and disease. *EMBO Rep.* 22, e51078 (2021).

[581] B. A. Maxwell, Y. Gwon, A. Mishra, J. Peng, H. Nakamura, K. Zhang, H. J. Kim, J. P. Taylor, Ubiquitination is essential for recovery of cellular activities after heat shock. *Science*. 372, eabc3593 (2021).

[582] Y. Gwon, B. A. Maxwell, R.-M. Kolaitis, P. Zhang, H. J. Kim, J. P. Taylor, Ubiquitination of G3BP1 mediates stress granule disassembly in a context-specific manner. *Science*. 372, eabf6548 (2021).

[583] S. Yasuda, H. Tsuchiya, A. Kaiho, Q. Guo, K. Ikeuchi, A. Endo, N. Arai, F. Ohtake, S. Murata, T. Inada, W. Baumeister, R. Fernández-Busnadiego, K. Tanaka, Y. Saeki, Stress- and ubiquitylation-dependent phase separation of the proteasome. *Nature*. 578, 296–300 (2020).

[584] L. J. Krause, M. G. Herrera, K. F. Winklhofer, The Role of Ubiquitin in Regulating Stress Granule Dynamics. *Front Physiol*. 13, 910759 (2022).

[585] C. Kielbassa, L. Roza, B. Epe, Wavelength dependence of oxidative DNA damage induced by UV and visible light. *Carcinogenesis*. 18, 811–816 (1997).

[586] C. Kielbassa, B. Epe, [39] DNA damage induced by ultraviolet and visible light and its wavelength dependence. *Methods Enzym.* 319, 436–445 (2000).

[587] N. W. Holton, J. F. Andrews, N. R. Gassman, Application of Laser Micro-irradiation for Examination of Single and Double Strand Break Repair in Mammalian Cells. *J. Vis. Exp. : JoVE*, 56265 (2017).

[588] D. Träutlein, M. Deibler, A. Leitenstorfer, E. Ferrando-May, Specific local induction of DNA strand breaks by infrared multi-photon absorption. *Nucleic Acids Res.* 38, e14–e14 (2010).

[589] Chromotek, Ed., Nano-Traps for superior immunoprecipitation (2022), (available at https://static.fishersci.eu/content/dam/fishersci/en_EU/Products/17707_Antibodies_page/17707_Chromotek_Nano_Trap_Brochure.pdf?cid=WEB_EXE_20220608_6O0DNF).

[590] R. H. Rose, S. J. Briddon, N. D. Holliday, Bimolecular fluorescence complementation: lighting up seven transmembrane domain receptor signalling networks. *Br. J. Pharmacol.* 159, 738–750 (2010).

[591] I. Anderie, A. Schmid, In vivo visualization of actin dynamics and actin interactions by BiFC. *Cell Biol. Int.* 31, 1131–1135 (2007).

[592] W. R. Algar, N. Hildebrandt, S. S. Vogel, I. L. Medintz, FRET as a biomolecular research tool — understanding its potential while avoiding pitfalls. *Nat. Methods*. 16, 815–829 (2019).

[593] C. Fang, Y. Huang, Y. Zhao, Review of FRET biosensing and its application in biomolecular detection. *Am. J. Transl. Res.* 15, 694–709 (2022).

[594] Ubiquitin K63 Selector - NanoTag Biotechnologies, (available at https://nano-tag.com/product/ubiquitin-k63-selector/).

[595] sdAb anti-Ubiquitin K48 - NanoTag Biotechnologies, (available at https://nano-tag.com/product/sdab-anti-ubiquitin-k48/).

[596] Lifesensor, K63 TUBE (FLAG) - ubiquitin interaction motifs - tagged antibody, (available at https://lifesensors.com/product/um604-k63-tube-flag/).

[597] S. J. Orcutt1, V. Zhukareva1, S. Kumar2, E. Martinez1, K. Longenecker1, J. E. Strickler, Selective Detection and Enrichment of K63-linked Polyubiquitin with K63-TUBEs (2019) (available at https://lifesensors.com/wp-content/uploads/2019/09/K63_TUBE_poster_final-1.pdf).

[598] T. Kalliokoski, C. Kramer, A. Vulpetti, P. Gedeck, Comparability of Mixed IC50 Data – A Statistical Analysis. *PLoS ONE*. 8, e61007 (2013).

[599] UM607: K48 TUBE HF (FLAG), (available at https://lifesensors.com/product/um607-k48-tube-hf-flag/).

[600] Y. Saeki, Ubiquitin recognition by the proteasome. *J Biochem*. 161, 113--124 (2017).

[601] S. Cabantous, H. B. Nguyen, J.-D. Pedelacq, F. Koraïchi, A. Chaudhary, K. Ganguly, M. A. Lockard, G. Favre, T. C. Terwilliger, G. S. Waldo, A New Protein-Protein Interaction Sensor Based on Tripartite Split-GFP Association. *Sci. Rep.* 3, 2854 (2013).

[602] H. D. Ulrich, Timing and spacing of ubiquitin-dependent DNA damage bypass. *Febs Lett*. 585, 2861--2867 (2011).

[603] E. C. Friedberg, Suffering in silence: the tolerance of DNA damage. *Nat Rev Mol Cell Bio*. 6, 943--953 (2005).

[604] N. Bowen, C. E. Smith, A. Srivatsan, S. Willcox, J. D. Griffith, R. D. Kolodner, Reconstitution of long and short patch mismatch repair reactions using Saccharomyces cerevisiae proteins. *Proc National Acad Sci*. 110, 18472--18477 (2013).

[605] T. Sokolsky, E. Alani, EXO1 and MSH6 Are High-Copy Suppressors of Conditional Mutations in the MSH2 Mismatch Repair Gene of Saccharomyces cerevisiae. *Genetics*. 155, 589–599 (2000).

[606] S. Moreau, E. A. Morgan, L. S. Symington, Overlapping Functions of the Saccharomyces cerevisiae Mre11, Exo1 and Rad27 Nucleases in DNA Metabolism. *Genetics*. 159, 1423–1433 (2001).

[607] P. Bichet, P. Mollat, C. Capdevila, E. Sarubbi, Endogenous Glutathione-Binding Proteins of Insect Cell Lines: Characterization and Removal from Glutathione S-Transferase (GST) Fusion Proteins. *Protein Expr. Purif.* 19, 197–201 (2000).

[608] M. S. Alphey, C. B. Wolford, S. A. MacNeill, Canonical binding of Chaetomium thermophilum DNA polymerase δ/ζ subunit PolD3 and flap endonuclease Fen1 to PCNA. *Front. Mol. Biosci.* 10, 1320648 (2023).

[609] N. Mailand, I. Gibbs-Seymour, S. Bekker-Jensen, Regulation of PCNA–protein interactions for genome stability. *Nat. Rev. Mol. Cell Biol.* 14, 269–282 (2013).

[610] W. Strzalka, T. Oyama, K. Tori, K. Morikawa, Crystal structures of the Arabidopsis thaliana proliferating cell nuclear antigen 1 and 2 proteins complexed with the human p21 C-terminal segment. *Protein Sci.* 18, 1072–1080 (2009).

[611] A. J. Horsfall, B. A. Vandborg, W. Kowalczyk, T. Chav, D. B. Scanlon, A. D. Abell, J. B. Bruning, Unlocking the PIP-box: A peptide library reveals interactions that drive high affinity binding to human PCNA. *J Biol Chem*. 296, 100773 (2021).

[612] A. Prestel, N. Wichmann, J. M. Martins, R. Marabini, N. Kassem, S. S. Broendum, M. Otterlei, O. Nielsen, M. Willemoës, M. Ploug, W. Boomsma, B. B. Kragelund, The PCNA interaction motifs revisited: thinking outside the PIP-box. *Cell. Mol. Life Sci.* 76, 4923–4943 (2019).

[613] S. Lee, Y. C. Tsai, R. Mattera, W. J. Smith, M. S. Kostelansky, A. M. Weissman, J. S. Bonifacino, J. H. Hurley, Structural basis for ubiquitin recognition and autoubiquitination by Rabex-5. *Nat. Struct. Mol. Biol.* 13, 264–271 (2006).

[614] J. W. Harper, B. A. Schulman, Structural Complexity in Ubiquitin Recognition. *Cell*. 124, 1133–1136 (2006).

[615] F. He, H.-P. Wollscheid, U. Nowicka, M. Biancospino, E. Valentini, A. Ehlinger, F. Acconcia, E. Magistrati, S. Polo, K. J. Walters, Myosin VI Contains a Compact Structural Motif that Binds to Ubiquitin Chains. *Cell Rep.* 14, 2683–2694 (2016).

[616] K. Choi, S. Batke, B. Szakal, J. Lowther, F. Hao, P. Sarangi, D. Branzei, H. D. Ulrich, X. Zhao, Concerted and differential actions of two enzymatic domains underlie Rad5 contributions to DNA damage tolerance. *Nucleic Acids Res*. 43, 2666–2677 (2015).

[617] B.-I. Lee, D. M. Wilson, The RAD2 Domain of Human Exonuclease 1 Exhibits 5′ to 3′ Exonuclease and Flap Structure-specific Endonuclease Activities*. *J. Biol. Chem.* 274, 37763–37769 (1999).

[618] D. M. Wilson, J. P. Carney, M. A. Coleman, A. W. Adamson, M. Christensen, J. E. Lamerdin, Hex1: a new human Rad2 nuclease family member with homology to yeast exonuclease 1. *Nucleic Acids Res*. 26, 3762--3768 (1998).

[619] M. Gioia, L. Payero, G. Pannafino, J. J. Chen, S. Salim, G. Fajith, A. F. Farnaz, S. Momoh, M. Scotland, V. Raghavan, C. Manhart, A. Shinohara, K. T. Nishant, E. Alani, *bioRxiv*, in press, doi:10.1101/2021.08.29.458102.

[620] M. Gioia, L. Payero, S. Salim, G. F. V., A. F. Farnaz, G. Pannafino, J. J. Chen, V. P. Ajith, S. Momoh, M. Scotland, V. Raghavan, C. M. Manhart, A. Shinohara, K. T. Nishant, E. Alani, Exo1 protects DNA nicks from ligation to promote crossover formation during meiosis. *PLOS Biol.* 21, e3002085 (2023).

[621] Z. Yan, C. Xue, S. Kumar, J. B. Crickard, Y. Yu, W. Wang, N. Pham, Y. Li, H. Niu, P. Sung, E. C. Greene, G. Ira, Rad52 Restrains Resection at DNA Double-Strand Break Ends in Yeast. *Mol. Cell*. 76, 699-711.e6 (2019).

[622] E. M. Boehm, M. T. Washington, R.I.P. to the PIP: PCNA-binding motif no longer considered specific. *BioEssays*. 38, 1117–1122 (2016).

[623] S. E. Liberti, S. D. Andersen, J. Wang, A. May, S. Miron, M. Perderiset, G. Keijzers, F. C. Nielsen, J.-B. Charbonnier, V. A. Bohr, L. J. Rasmussen, Bi-directional routing of DNA mismatch repair protein human exonuclease 1 to replication foci and DNA double strand breaks. *DNA Repair*. 10, 73–86 (2011).

[624] J. H. Hurley, S. Lee, G. Prag, Ubiquitin-binding domains. *Biochem J*. 399, 361--372 (2006).

[625] G. Yakoub, Y.-S. Choi, R. P. Wong, T. Strauch, K. J. Ann, R. E. Cohen, H. D. Ulrich, Avidity-based biosensors for ubiquitylated PCNA reveal choreography of DNA damage bypass. *Sci. Adv*. 9, eadf3041 (2023).

[626] E. Feuer, G. Zimran, M. Shpilman, A. Mosquna, A Modified Yeast Two-Hybrid Platform Enables Dynamic Control of Expression Intensities to Unmask Properties of Protein–Protein Interactions. *ACS Synth. Biol.* 11, 2589–2598 (2022).

[627] J. Hernandez, K. D. Ross, B. A. Hamilton, *bioRxiv*, in press, doi:10.1101/2021.07.01.450807.

[628] K. T. Powers, E. D. Lavering, M. T. Washington, Conformational Flexibility of Ubiquitin-Modified and SUMO-Modified PCNA Shown by Full-Ensemble Hybrid Methods. *J. Mol. Biol.* 430, 5294–5303 (2018).

[629] J. L. Parker, A. B. Bielen, I. Dikic, H. D. Ulrich, Contributions of ubiquitin- and PCNA-binding domains to the activity of Polymerase η in Saccharomyces cerevisiae. *Nucleic Acids Res.* 35, 881–889 (2007).

[630] J. L. Parker, H. D. Ulrich, Mechanistic analysis of PCNA poly-ubiquitylation by the ubiquitin protein ligases Rad18 and Rad5. *EMBO J.* 28, 3657–3666 (2009).

[631] T. S. Takahashi, H.-P. Wollscheid, J. Lowther, H. D. Ulrich, Effects of chain length and geometry on the activation of DNA damage bypass by polyubiquitylated PCNA. *Nucleic Acids Res* (2020), doi:10.1093/nar/gkaa053.

[632] S. Zhao, H. D. Ulrich, Distinct consequences of posttranslational modification by linear versus K63-linked polyubiquitin chains. *Proc National Acad Sci*. 107, 7704--7709 (2010).

[633] B. D. Freudenthal, L. Gakhar, S. Ramaswamy, M. T. Washington, Structure of monoubiquitinated PCNA and implications for translesion synthesis and DNA polymerase exchange. *Nat Struct Mol Biol*. 17, 479--484 (2010).

[634] C. Renz, E. Asimaki, C. Meister, V. Albanèse, K. Petriukov, N. C. Krapoth, S. Wegmann, H.-P. Wollscheid, R. P. Wong, A. Fulzele, J.-X. Chen, S. Léon, H. D. Ulrich, Ubiquiton—An inducible, linkage-specific polyubiquitylation tool. *Mol. Cell*. 84, 386-400.e11 (2024).

[635] L. Doerfler, L. Harris, E. Viebranz, K. H. Schmidt, Differential genetic interactions between Sgs1, DNA-damage checkpoint components and DNA repair factors in the maintenance of chromosome stability. *Genome Integr*. 2, 8 (2011).

6 Appendix

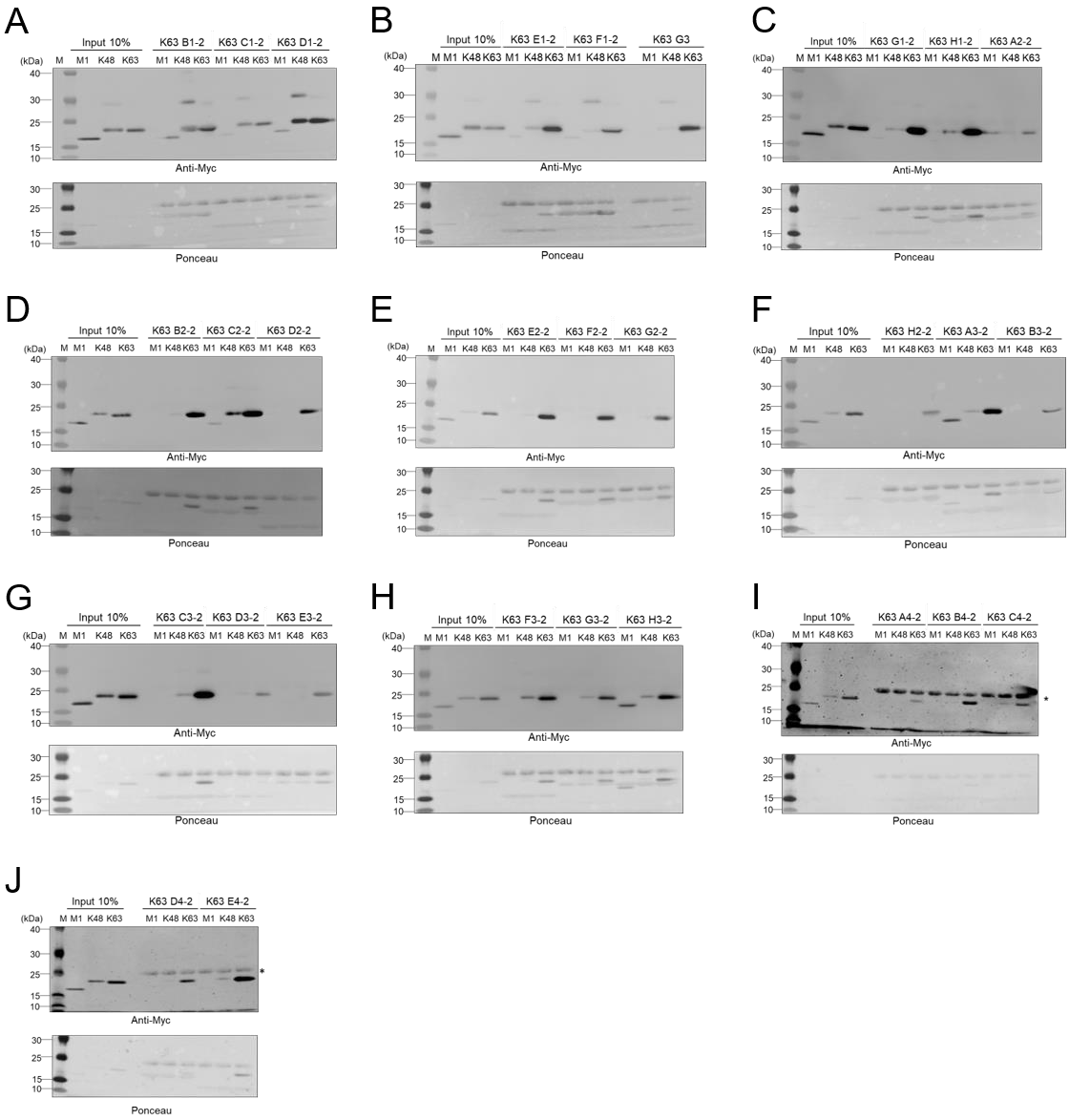

Figure 6.1: Full Western blots of first screen of Figure 3.2. (A-J) Pull-down results to validate selectivity of the indicated DARPins for the K63-linked ubiquitin dimer they were raised against, in comparison to 10% of the input. Flag-pull-down with the Flag-tagged DARPins and Myc-tagged ubiquitin dimers (specifically linked via M1, K48 and K63) was performed and analyzed by Western blotting against the Myc-tag of the ubiquitin dimers. Loading of the DARPins was analyzed by Ponceau staining. * = signal of light chain of M2 Flag-antibody from the beads used for pull-down. Related to Figure 3.2.

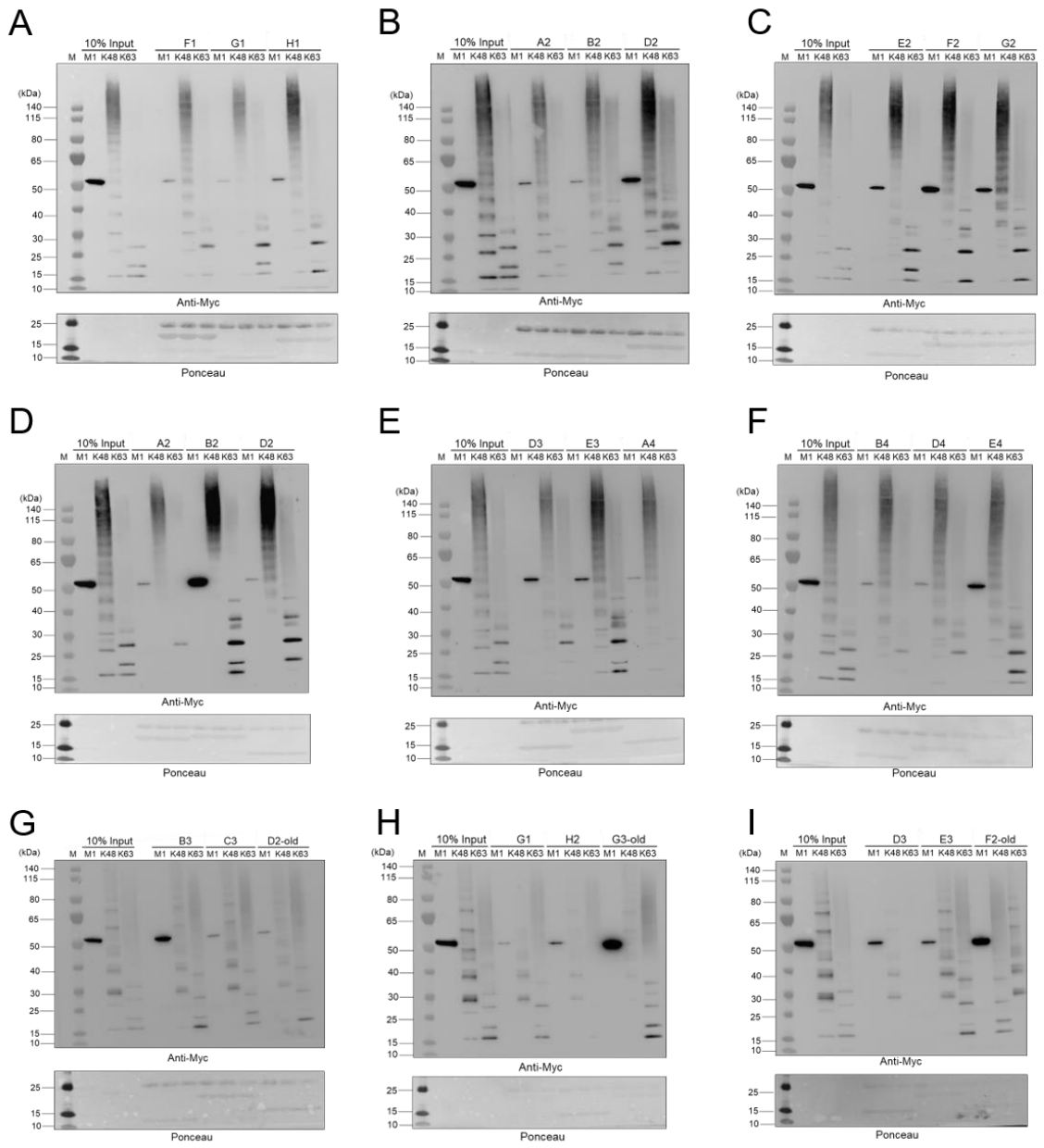

Figure 6.2: Full Western blots of validation of Figure 3.3. (A-I) Pull-down results to validate selectivity of the indicated DARPins (A-F) for K63-linked ubiquitin chains, in comparison to 10% of the input. Most selective DARPins of (A-F) were compared to previously selected anti-K63 DARPins, marked with "old" (G-I). Flag-pull-down with the Flag-tagged DARPins and Myc-tagged ubiquitin chains (specifically linked via M1, K48 and K63) was performed and analyzed by Western blotting against the Myc-tag of the ubiquitin chains. Loading of the DARPins was analyzed by Ponceau staining.

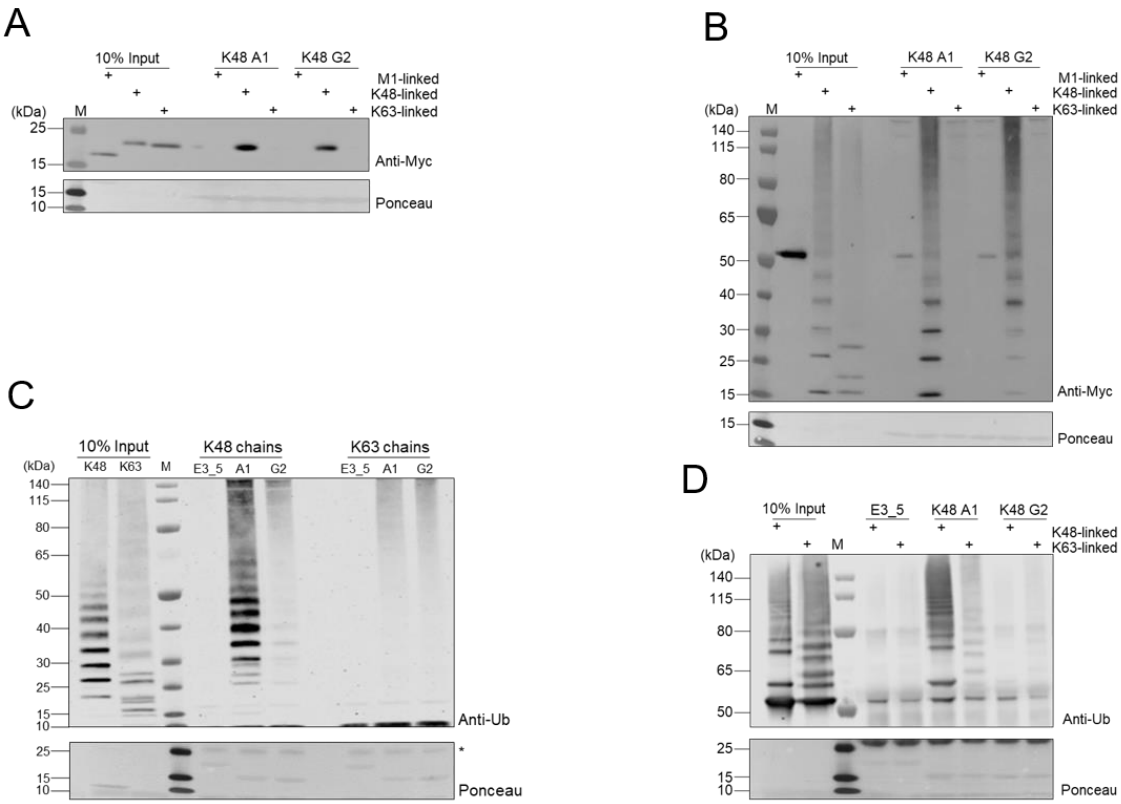

Figure 6.3: Specificity of anti-K48 DARPin G2 *in vitro*. (A+B) Pull-down results to validate selectivity of the anti-K48 DARPins A1 and G2 to K48-linked ubiquitin dimer (A) and chains (B), in comparison to 10% of the input. Flag-pull-down with the Flag-tagged DARPins and Myc-tagged ubiquitin dimers and chains (specifically linked via M1, K48 and K63) was performed and analyzed by Western blotting against the Myc-tag of the ubiquitin. (C+D) Western blot showing the interaction of the indicated DARPins with K48-/K63-linked ubiquitin chains free (C) or as conjugates on GFP (D) by pull-down. Equal loading of the DARPins was analyzed with Ponceau staining. Related to Figure 3.4.

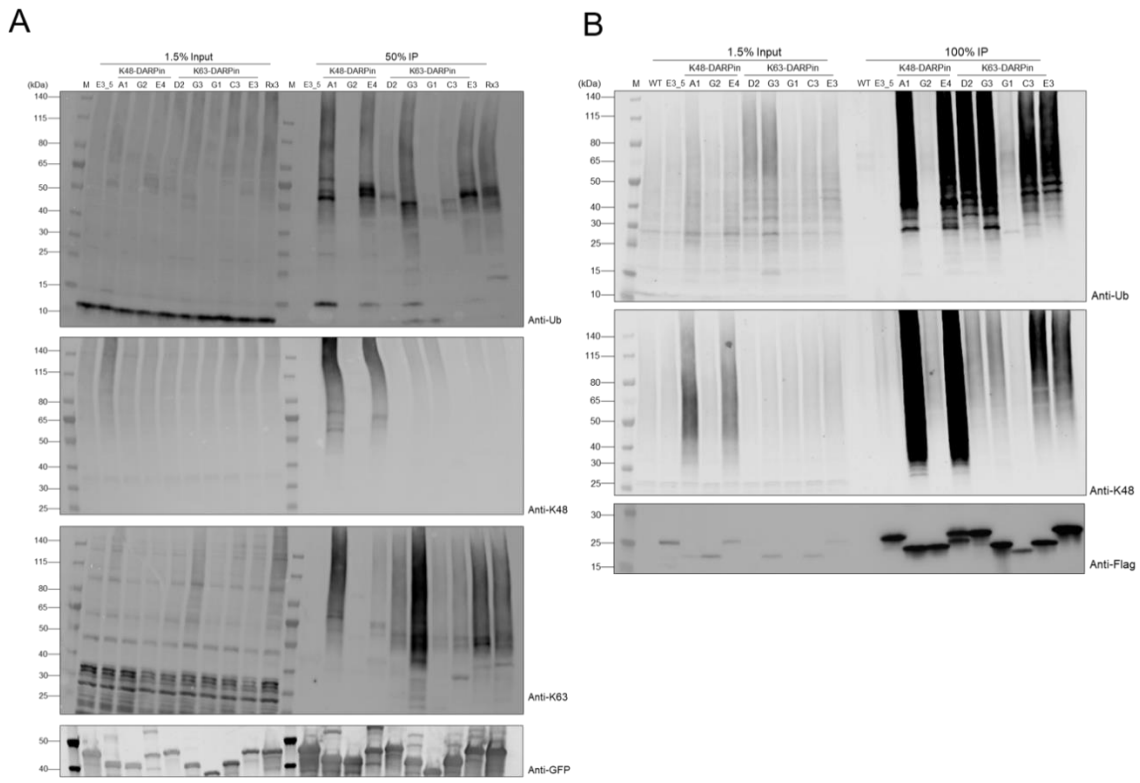

Figure 6.4: Specificity of anti-K48 and anti-K63 DARPins in cell extract. (E) Western blot showing the results of the pull-down of different GFP-tagged DARPins/TUBE expressed in HeLa cells and pulled-down using the GFP-Trap, analyzed with indicated antibodies. Conducted by Philipp Elleringmann. (F) Western blot showing the results of the pull-down of different Flag-tagged DARPins expressed in *S. cerevisae* and pulled-down using Flag-beads, analyzed with indicated antibodies. Related to Figure 3.4

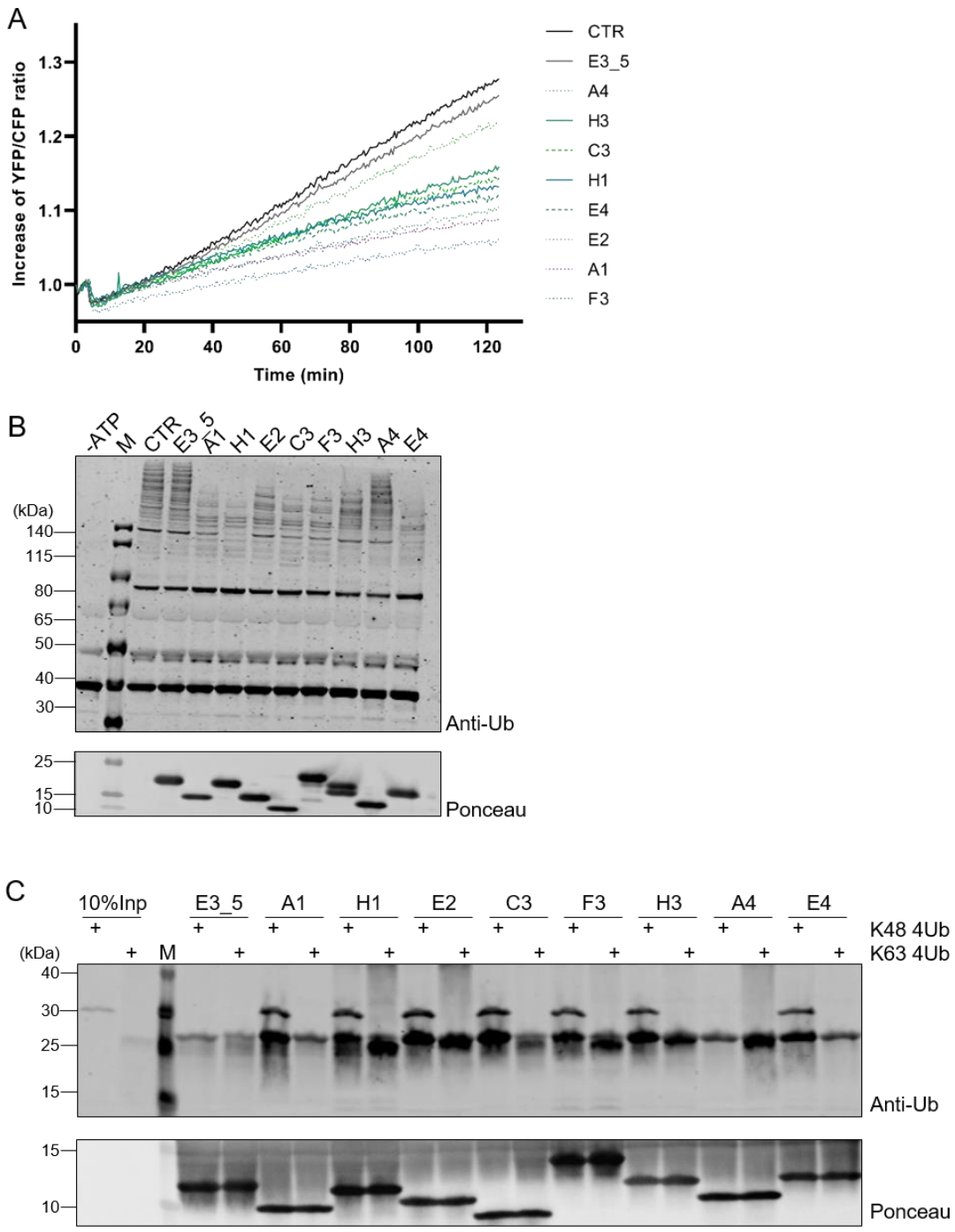

Figure 6.5: Second screening round for new selective anti-K48 DARPins. (A, B) Graph (A) and respective Western blot (B) showing the increase of the YFP/CFP-ratio over time as read out of the ubiquitin chain formation with YFP- and CFP-tagged ubiquitin in presence of the indicated K48-DARPin in two-fold excess. Western blots show the endpoint of this ubiquitin conjugation assay (C) Flag-pull-downs to test the affinity of the indicated anti-K48 DARPin (Flag-tagged) towards specifically-linked tetraubiquitin in comparison to the negative control DARPin E3_5. The pull-down was analyzed by Western blotting against ubiquitin. 10% of the input and 100% of the pull-down were loaded. Equal loading of the DARPins was confirmed by Ponceau staining.

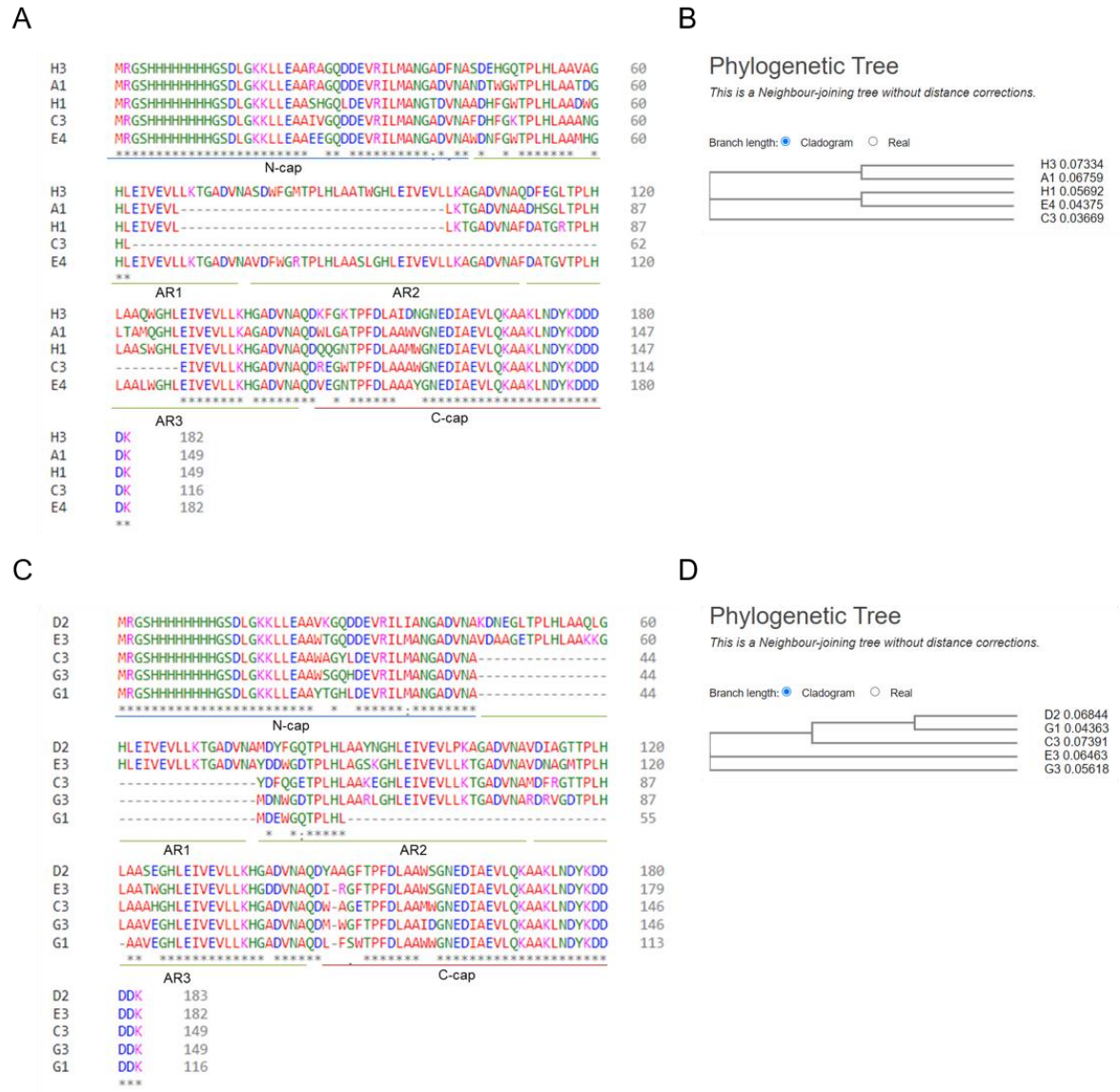

Figure 6.6: Alignments and phylogenetic tree of the anti-K48 and anti-K63 DARPins. (A, C) Alignment of the protein sequence of the selected five anti-K48 (A) and anti-K63 (C) DARPins by Clustal Omega. Hydrophobic amino acids are marked in red, polar in green, acidic in blue and basic in pink.Lines under the sequence indicate the DARPin modules: cap = capping module, AR =ankyrin repeat. (B, D) Phylogenic tree of the anti-K48 (B) and anti-K63 (D) DARPins by Clustal Omega.nes under the sequences locate the sequence to the DARPin structure: cap = capping module, AR =ankyrin repeat. (B, D) Phylogenic tree of the anti-K48 (B) and anti-K63 (D) DARPins by Clustel Omega.

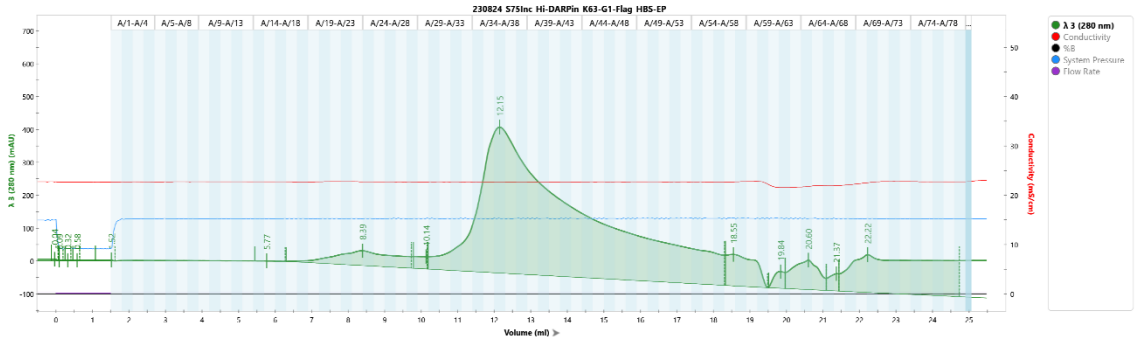

Figure 6.7: Size-exclusion chromatogram of the purification of anti-K63 DARPin G1. Superdex75 Inc (10/300 GL) was used and the protein concentration was monitored at 280 nm wavelength.

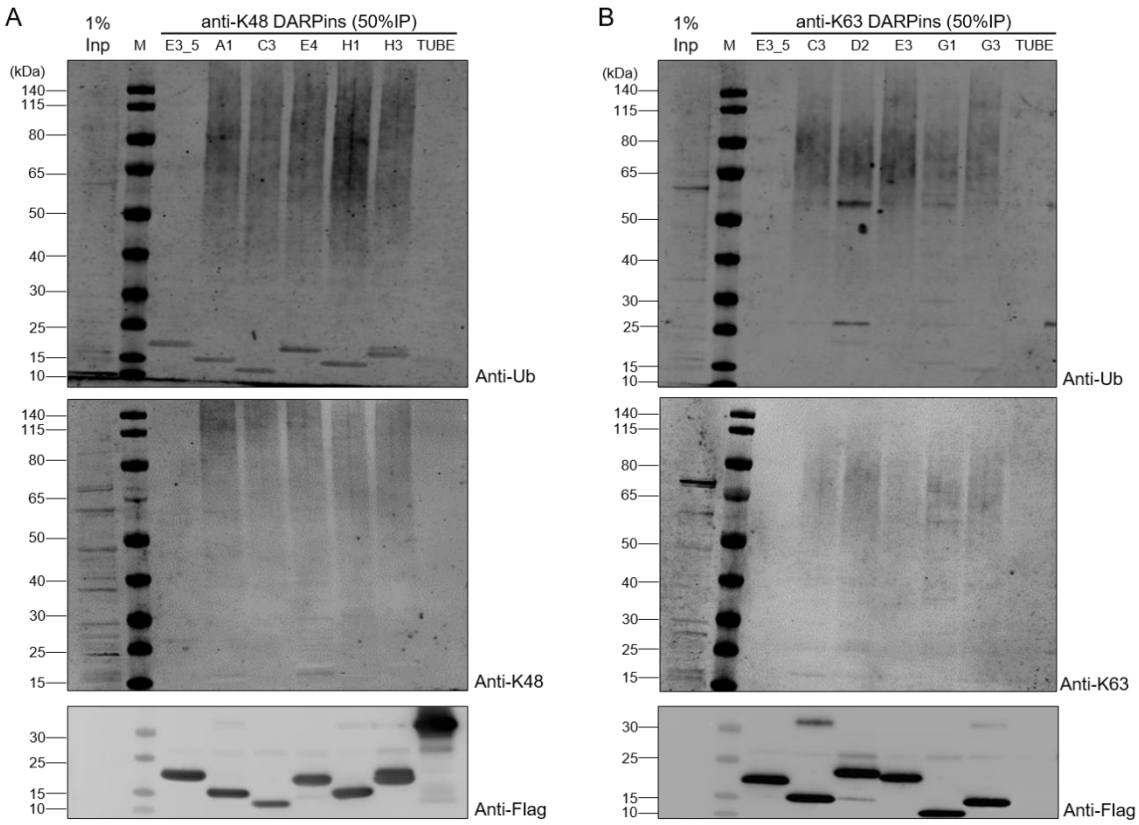

Figure 6.8 Specificity of DARPins in *S.cerevisiae* cell extract. (A, B) Flag-pull-down from *S. cerevisae* cell extract (1 mg total protein) with the indicated Flag-tagged K48-DARPins (A) or K63-DARPins (B), the respective TUBE and the control DARPin E3_5. 1% Input and 50% of the pull-down were analyzed by Western blot with antibodies against pan-ubiquitin, the specific ubiquitin linkage (K48 or K63) and the Flag-tag of the DARPins. Related to Figure 3.7.

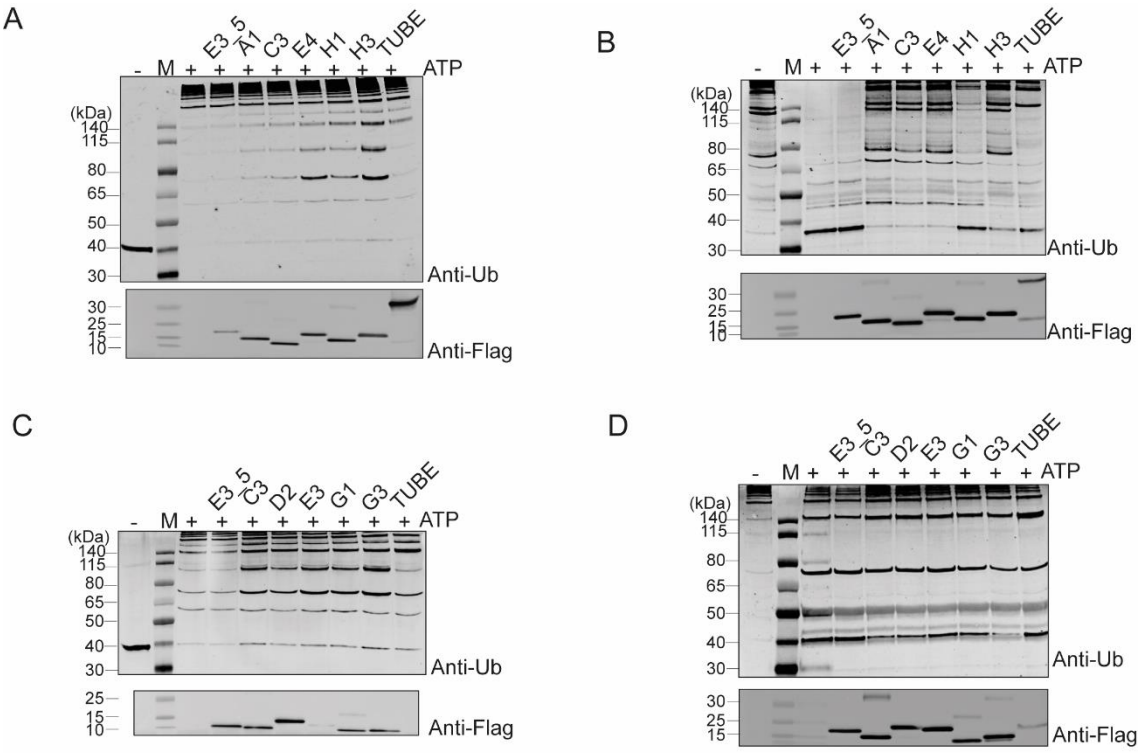

Figure 6.9: Western blots to FRET measurements of Figure 3.8. (A-D) Western blot showing the conjugation (A,C) and deconjugation (B,D) assay with the respective chains using the FRET-based assay with YFP- and CFP-tagged ubiquitin and the indicated K48-DARPin (A,B) or K63-DARPin (C,D). Endpoints of measurements were separated on Western blot and blotted with anti-Ub for checking the ubiquitin chain content and anti-Flag for the DARPin concentrations.

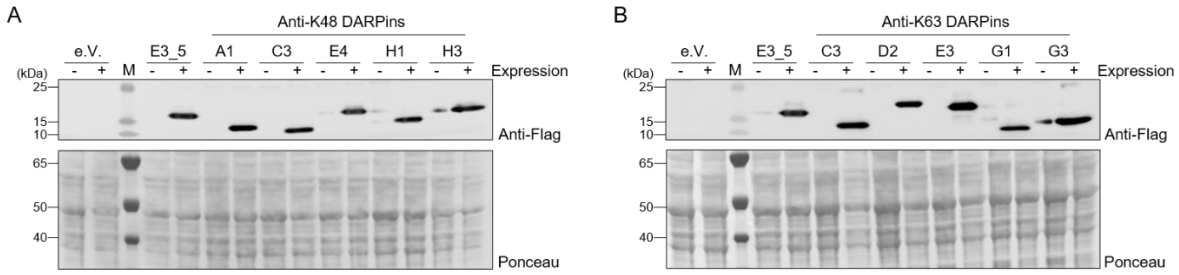

Figure 6.10: Expression levels of DARPins used for spot assays. (A, B) Western blots showing the expression levels of the anti-K48 (A) and anti-K63 DARPins (B) in the yeast cell lines used for the spot assays shown in Figure 3.9. DARPins were detected by the antibody against their Flag-tag, Ponceau staying as equal loading control**.**

Table 6.1: Raw data mass spectroscopy measurement. Related to Figure 3.11

	Summed intensities of ubiquitin peptides with GlyGly site / 10^{10}							
Link-age		HeLa 1	HeLa 2	E3_5	K48 A1	K48 TUBE	K63 G1	K63 TUBE
6	2.86	0.99	1.07	0	0.28	0.08	0	0.028
11	17.40	8.79	4.83	0	1.01	0.27	0.21	0.46
27	0.69	0.01	0.67	0	0	0	0	0.0054
29	2.18	1.59	0.54	0	0.01	0.13	0	0
33	0.12	0.05	0.04	0	0	0.0016	0	0
48	61.70	19.30	19.44	0.02	4.80	0.071	0.84	2.36
63	52.10	19.16	18.63	0.006	1.06	0.25	1.88	2.21

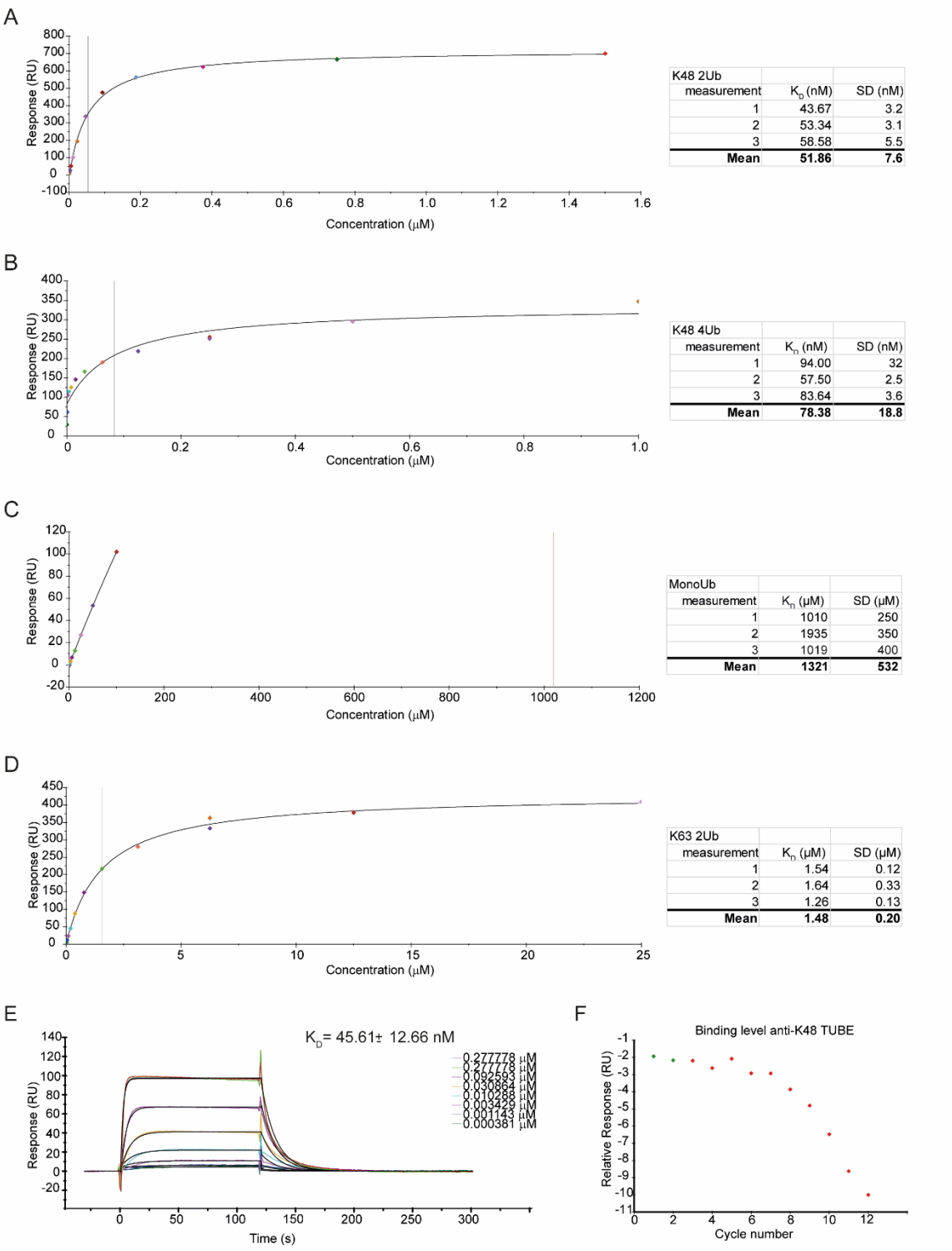

Figure 6.11: Affinity curves and equilibrium constant for anti-K48 DARPin A1. (A-D) Affinity curves fitted (1:1 binding model) the steady state binding against the increasing concentration of the indicated ubiquitin construct measured by SPR. Biotinylated anti-K48 DARPin A1 was captured on a SA-Chip to a density of 1000 RU, over which a two-fold series dilution of K48-linked diubiquitin (1.5 µM, A) K48-linked tetraubiquitin (1 µM, B), monoubiquitin (50 µM, C) or K63-linked diubiquitin (25 µM, D) were injected. Equilibrium constant (K_D) and their respective standard deviation were determined by the Biacore X100 evaluation software and is reported as the mean of three independent experiments (E) Kinetic curves of anit-K48 DARPin A1 interacting with K48-linked diubiquitin. Biotinylated anti-K48 DARPin A1 was captures on a CAP-chip to a density of 100 RU, over which a 3-fold serial dilution of indicated concentrations were injected. Equilibrium constant (K_D) and their respective standard deviation were determined by the Biacore X100 evaluation software. (F) No interaction was detectable between the anti-K48 TUBE and the K48-linked diubiquitin up to a concentration of 1 µM. Related to Table 3.1.

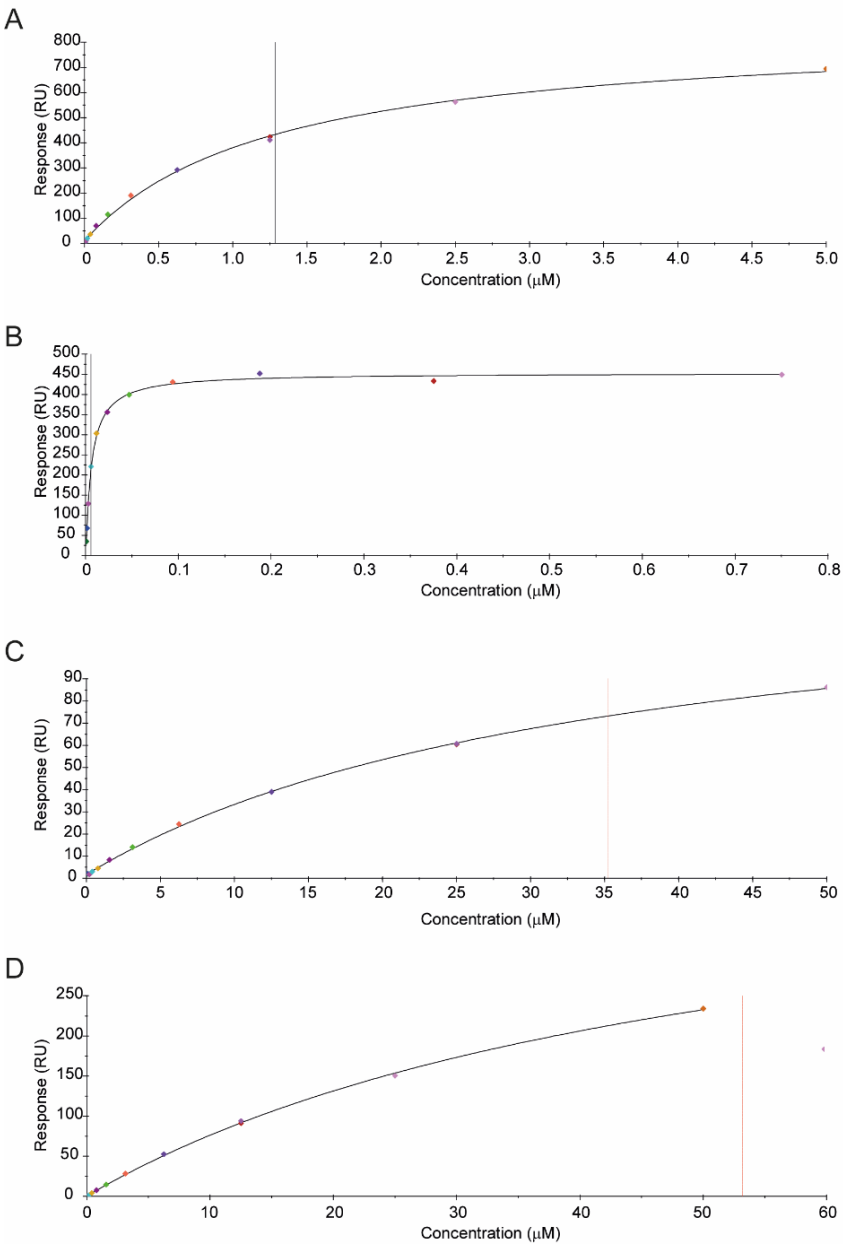

K63 2Ub		
measurement	K_D (μM)	SD (μM)
1	1.24	0.07
2	1.29	0.09
3	1.81	0.14
Mean	**1.45**	**0.32**

K63 4Ub		
measurement	K_D (nM)	SD (nM)
1	5.71	0.45
2	7.97	0.92
3	7.10	0.91
Mean	**6.93**	**1.14**

MonoUb		
measurement	K_D (μM)	SD (μM)
1	35.24	1.6
2	48.08	3.9
3	54.37	4.0
Mean	**45.90**	**9.8**

K48 2Ub		
measurement	K_D (μM)	SD (μM)
1	42.82	0.64
2	53.18	2.30
3	67.40	3.60
Mean	**54.47**	**12.34**

Figure 6.12 Affinity curves and equilibrium constant for anti-K63 DARPin G1. (A-D) Affinity curves fitted (1:1 binding model) the steady state binding against the increasing concentration of the indicated ubiquitin construct measured by SPR. Biotinylated anti-K63 DARPin G1 was captured on a SA-Chip to a density of 1000 RU, over which a two-fold series dilution of K63-linked diubiquitin (5 µM, A) K48-linked tetraubiquitin (0.75 µM, B), monoubiquitin (50 µM, C) or K48-linked diubiquitin (50 µM, D) were injected. Equilibrium constant (K_D) and their respective standard deviation were determined by the Biacore X100 evaluation software and is reported as the mean of three independent experiments. Related to Table 3.1.

Table 6.2: Data collection statistics. Data collection of the crystal structures of the DARPins with their corresponding ubiquitin dimers of Figure 3.11 and 3.12.

	K48-Ub2: DARPin-A1	K63-Ub2: DARPin-G1
Data Collection		
Beamline	ID23-2, ESRF	ID30-B, ESRF
Wavelength (Å)	0.873128	0.873128
Space group	C 2 2 21	P 1 21 1
Total reflections	572926 (29417)	81395 (8930)
Unique reflections	74344 (3717)	12258 (1288)
a,b,c (Å)	138.87 140.18 179.36	51.29 35.82 75.85
α,β,γ (°)	89.75 89.98 90.53	90.000 102.501 90.000
Resolution (Å)	64.337 - 2.446 (2.533 - 2.446)	35.82-2.30 (2.39-2.30)
R_{merge}	0.164 (0.794)	0099 (0.217)
I/σ(I)	7.5 (2.1)	12.2 (6.4)
Completeness (%)	93.2 (64.9)	99.8 (100.0)
Multiplicity	7.7 (7.9)	6.6 (6.9)
CC1/2	0.996 (0.905)	0.992 (0.975)
Refinement		
R-work	0.1932 (0.2411)	0.2121 (0.2133)
R-free	0.2398 (0.2977)	0.2693 (0.2706)
No. of Atoms		
Protein	1097	1940
Ligand	1	0
Water	193	38
Wilson B-factor	38.8	27.66
RMSDs		
Bond length (Å)	0.0096	0.0137
Bond angles (°)	1.19	1.96
Ramachandran Plot (%)		
Favored region	99.07	99.58
Allowed region	0.75	0.42
Outlier region	0.19	0

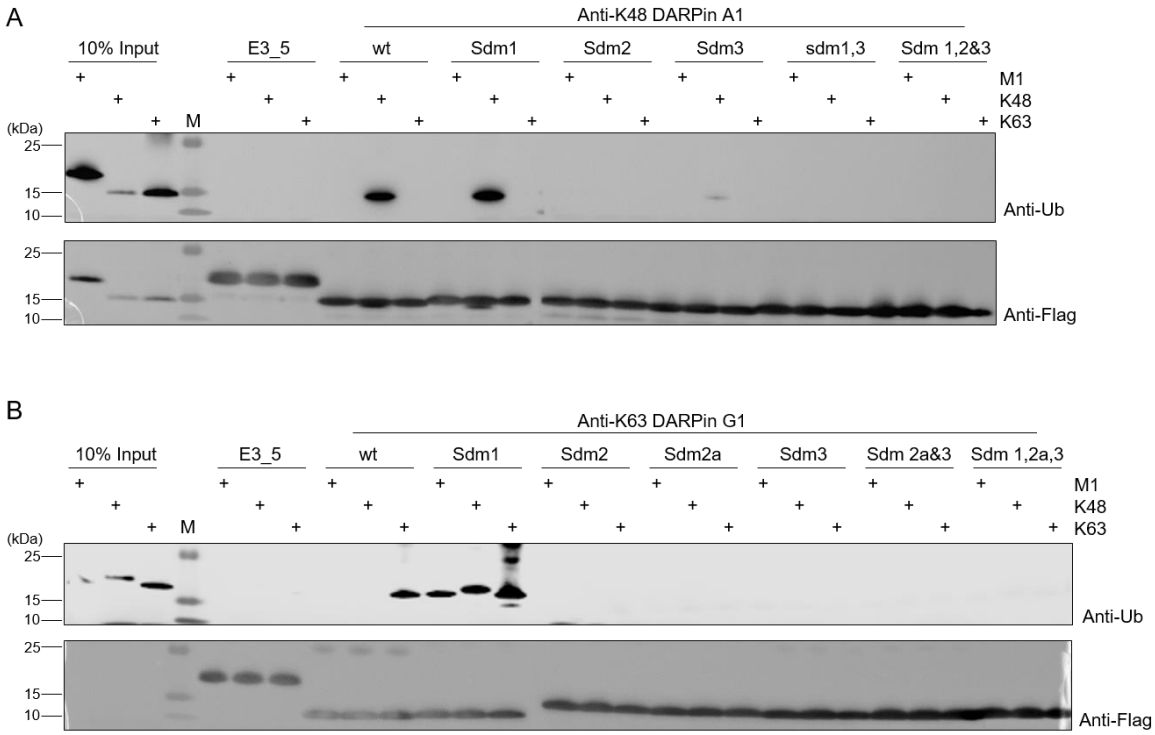

Figure 6.13: Interaction and specificity of structural mutants of anti-K48 DARPin A1 and anti-K63 DARPin G1. (A, B) Pull-down results to validate selectivity and interaction loss of the indicated anti-K48 A1 (A) and anti-K63 G1 (B) DARPin mutants, in comparison to the negative control DARPin E3_5 and 10% of the input. Flag-pull-down with the Flag-tagged DARPins and ubiquitin dimers (specifically linked via M1, K48 and K63) was performed and analyzed by Western blotting against ubiquitin. Loading of the DARPins was analyzed by anti-Flag. Related to Figure 3.12 and 3.13.

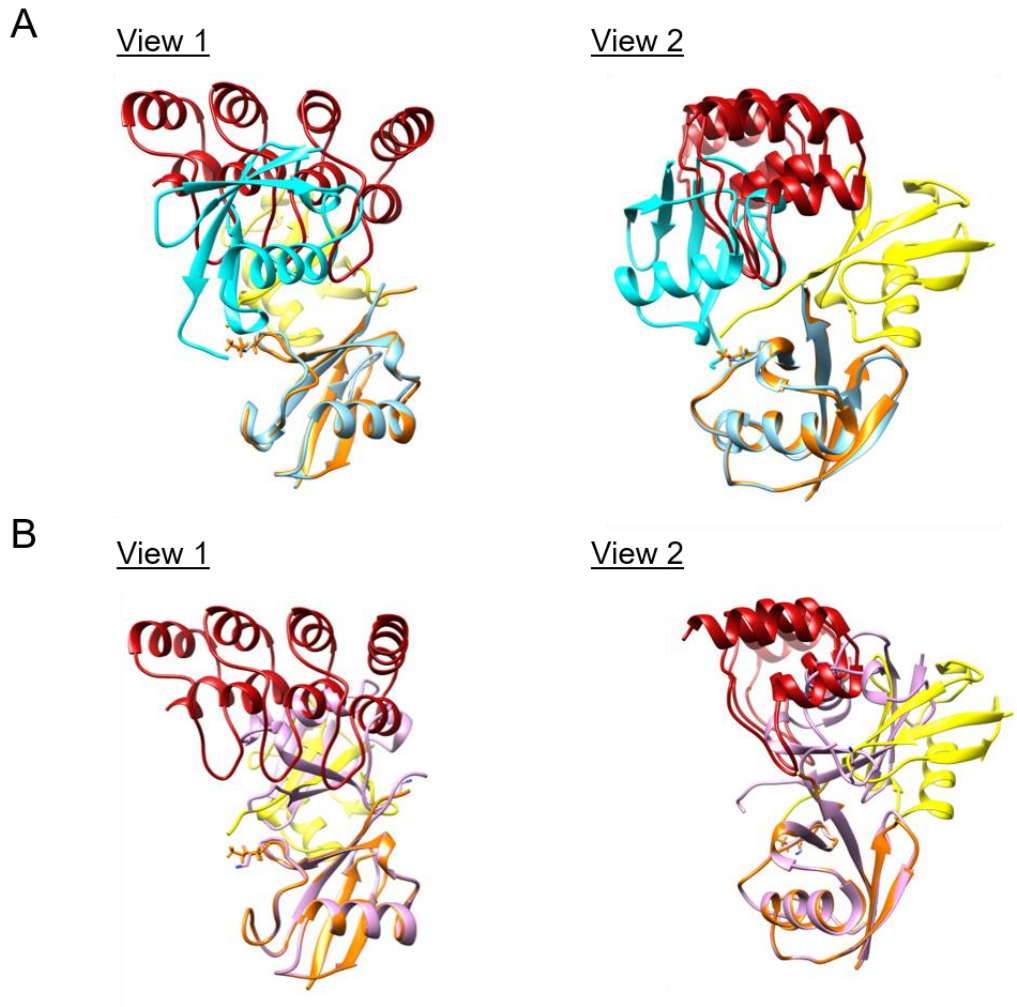

Figure 6.14: Comparison of K48-linked diubiqutin arrangement with open and closed conformations. (A, B) Overlay of the obtained crystal structure for the anti-K48 DARPin A1 (red) in complex with K48-linked diubiquitin (distal ubiquitin in yellow, proximal in orange) with the open (A, Pdb: 3AUL) and closed (B, Pdb: 3ALB) conformation of K48-linked diubiquitin.

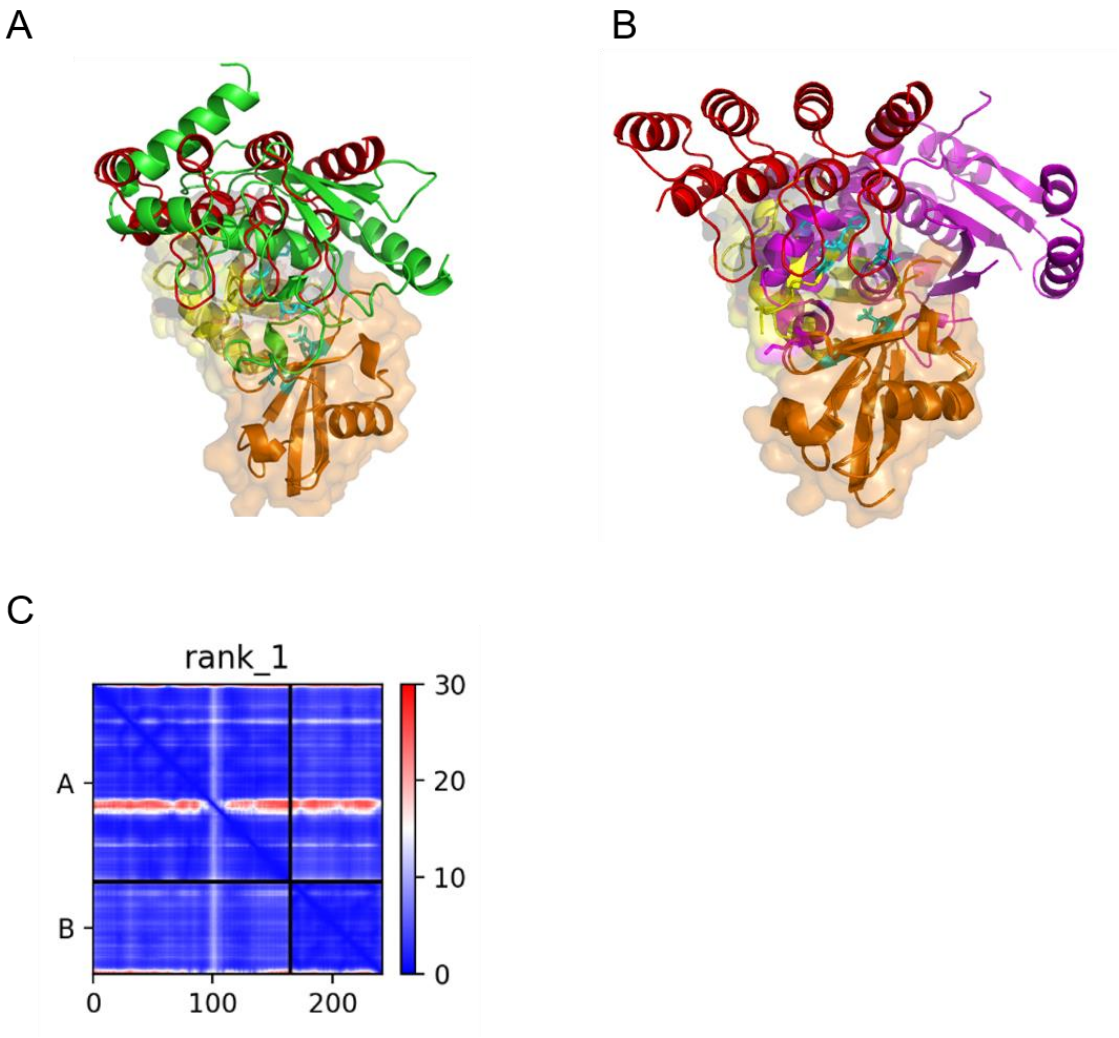

Figure 6.15: Overlay of anti-K48 DARPin A1 and K48-linked diubiquitin with specific writers and erasers. Overlay of the obtained crystal structure of the anti-K48 DARPin A1 (red) with K48-linked diubiquitin (distal ubiquitin in yellow, proximal in orange) with E2 Ubc7 (A, green, PDB: 2UCZ) or DUB OTUB1 (B, magenta, PDB: 2GMI). Ile44 patch marked in cyan. Alignment with Pymol, DeLano Scientific LLC. (C) Predicted Alignment Error (PAE) plots from the AlphaFold2 for the model of Ubc7 and ubiquitin shown in (A). Blue indicates a high model confidence.

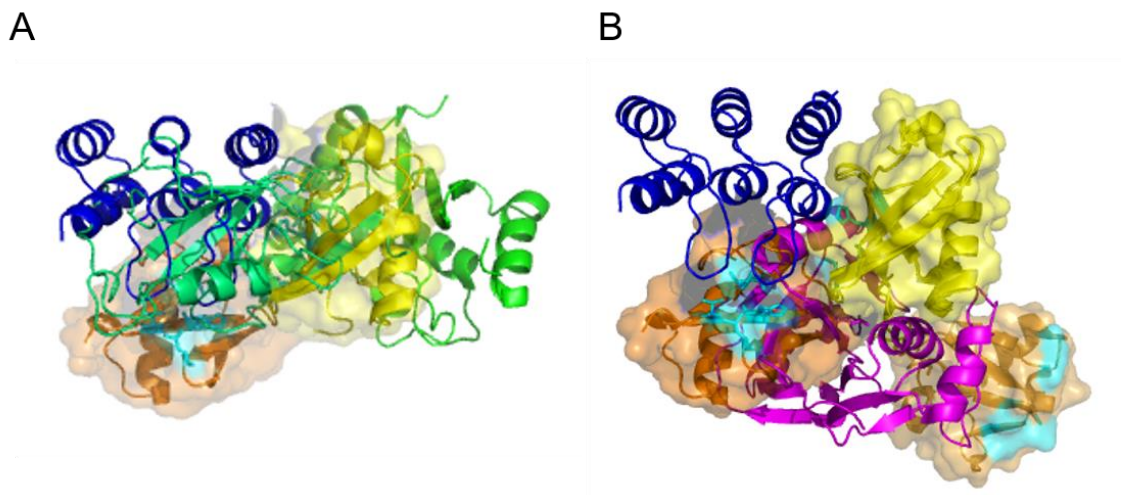

Figure 6.16: Overlay of anti -K63 DARPin G1 and K63-linked diubiquitin with specific writers and erasers. Overlay of the obtained crystal structure of the anti-K63 DARPin G1 (blue) with K63-linked diubiquitin (distal ubiquitin in yellow, proximal in orange) with E2 Ubc13 and Mms2 (A, green, PDB: 2GMI) or DUB AMSH (B, magenta, PDB: 2ZNV). Ile44 patch marked in cyan. Alignment with Pymol, DeLano Scientific LLC.

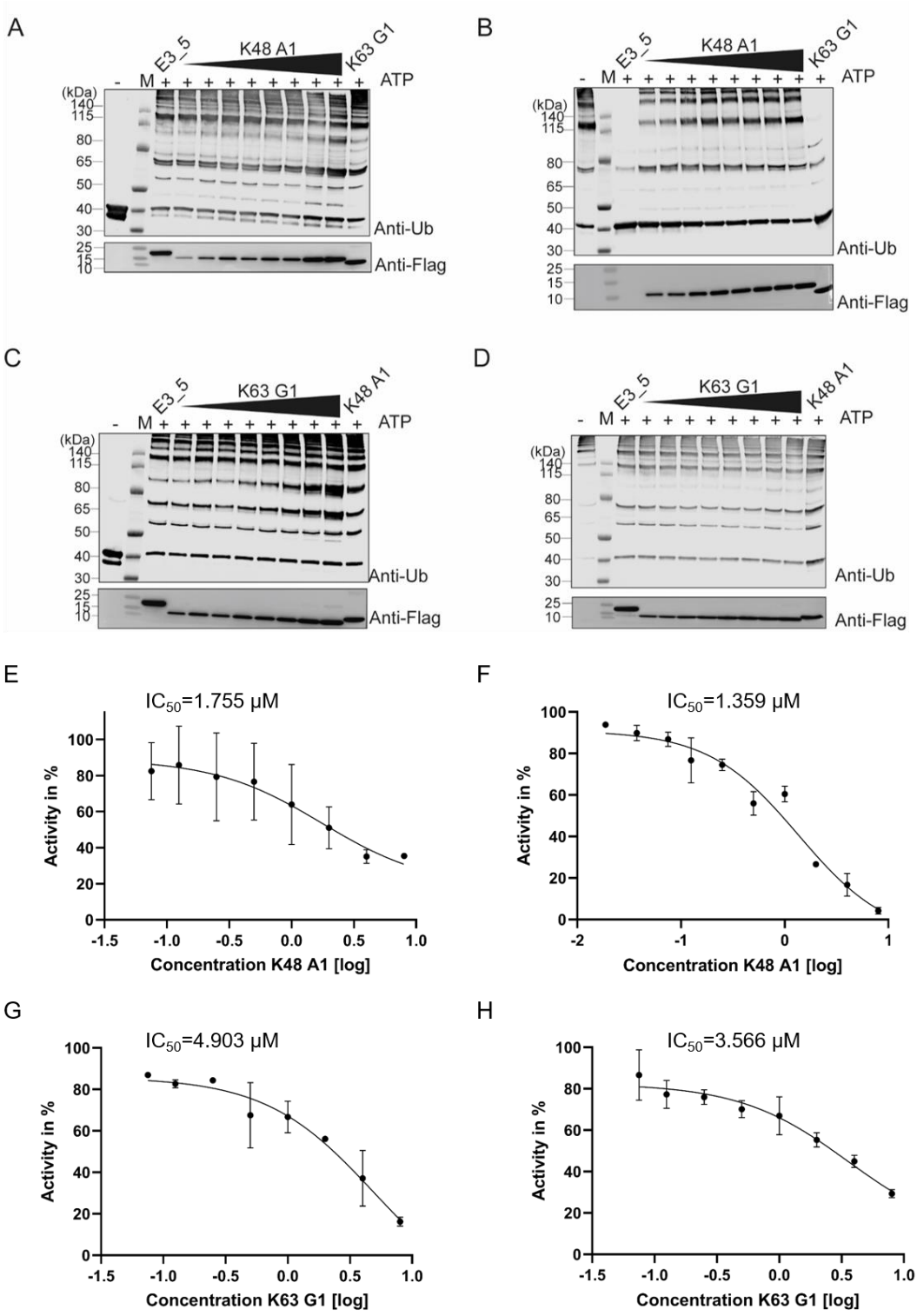

Figure 6.17: Western blots to FRET measurements of Figure 3.14 and graphs to IC_{50} values of Table 3.2. (A-D) To investigate if the effect is concentration dependent increasing concentrations of the indicated DARPin K48 A1 (A,B) or K63 G1 (C,D) were used in comparison to the highest concentration of the other DARPin. Endpoints of measurements were separated on Western blot and blotted with anti-Ub for checking the ubiquitin chain content and anti-Flag for the DARPin concentrations. (E-F)Graph with calculated IC_{50} values for the anti-K48 DARPin A1 (E,F) or anti-K63 DARPin G1 (G,H) on chain conjugation (E,G) or deconjugation (F, H). Calculated with Graph Pad Prism 8.3. Activity [%] based on the initial slope (first 60 min) of the measured FRET curves (compare Figure 3.14) is provided on vertical axis and log (concentration) on horizontal axis. The IC_{50} is the concentration at which the curve passes through the 50% inhibition level.

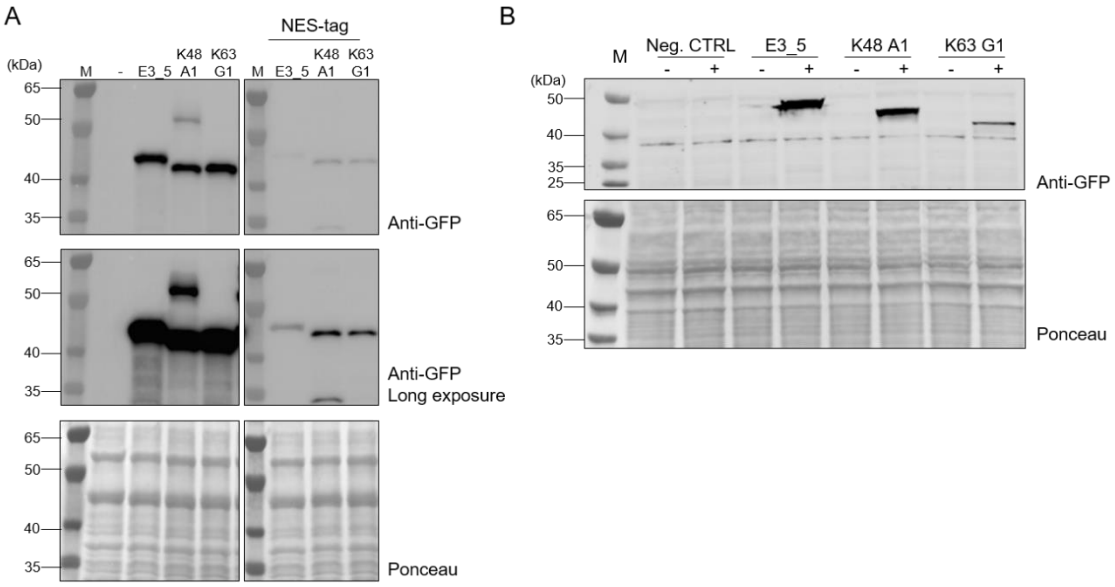

Figure 6.18: Expression levels of DARPins stably integrated in yeast and mammalian cells. (A, B) Western blots showing the expression levels of the anti-K48 and anti-K63 DARPin A1 and G1 as well as E3_5 stably integrated in *S.cerevisae* (A) or RPE-1 cells (B). DARPins were detected by the antibody against their GFP/YFP-tag, Ponceau staying as equal loading control. Related to Figure 3.15.

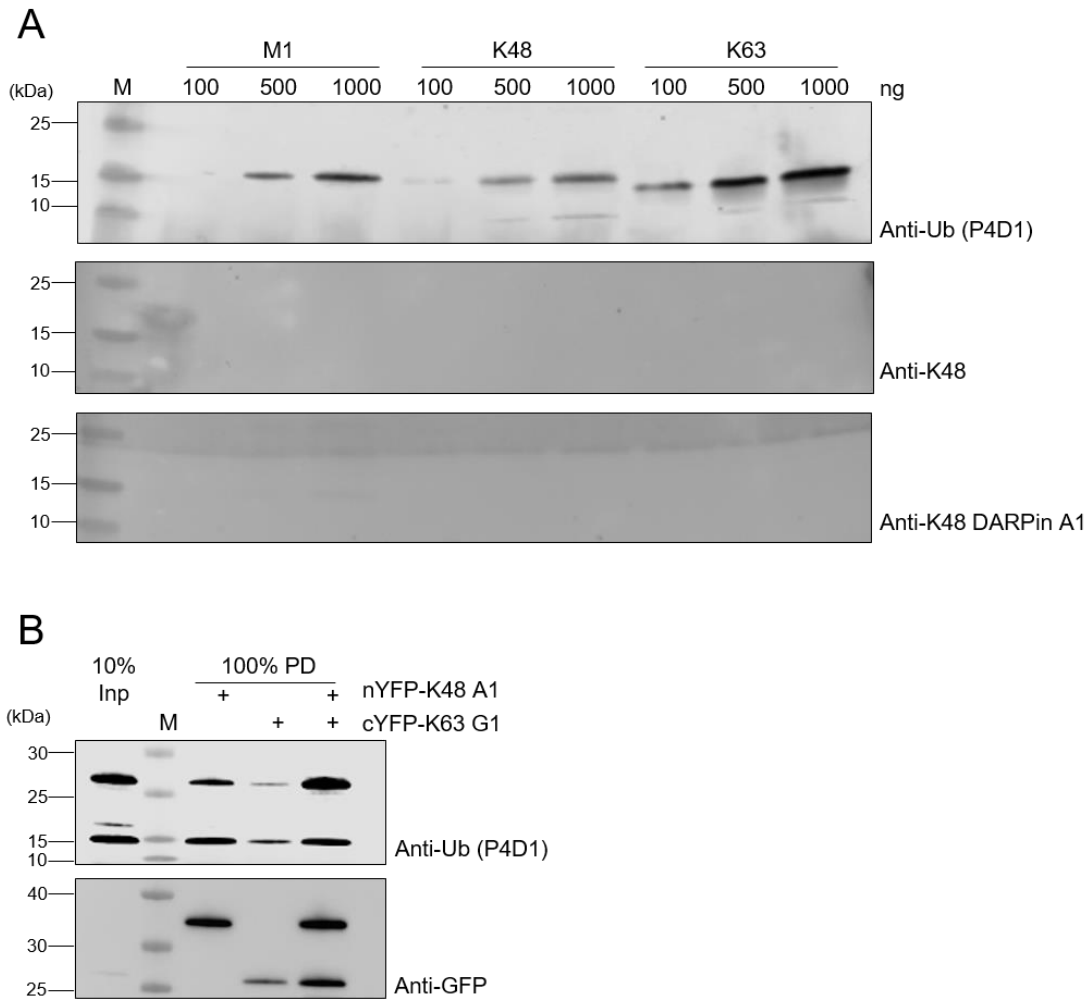

Figure 6.19: Testing anti-K48 DARPin A1 as antibody for Western blot and testing the K48-K63-branched chain sensor for its specificity in pull-downs. (A) Western blot with different with indicated amounts of specifically-linked ubiquitin dimers, detected by general ubiquitin antibody P4D1, the K48-linkage specific antibody Apu2 or the biotinylated anti-K48 DARPin A1. All detected with secondary antibody conjugated to HRP. (B) Western blot showing the pull-down result of the single fragments (nYFP-K48-DARPin A1 or cYFP-K63-DARPin G1) as well as the combined K48-K63-branched chain sensor. The input was an mixture of equal molar K48-linked and K63-linked ubiquitin dimers as well as the K48-K63-branched ubiquitin trimer. The pull-down was conducted with the Chromotek GFP-Trap and the capture of the fragments and the combined sensor were monitored by the anti-GFP blot.

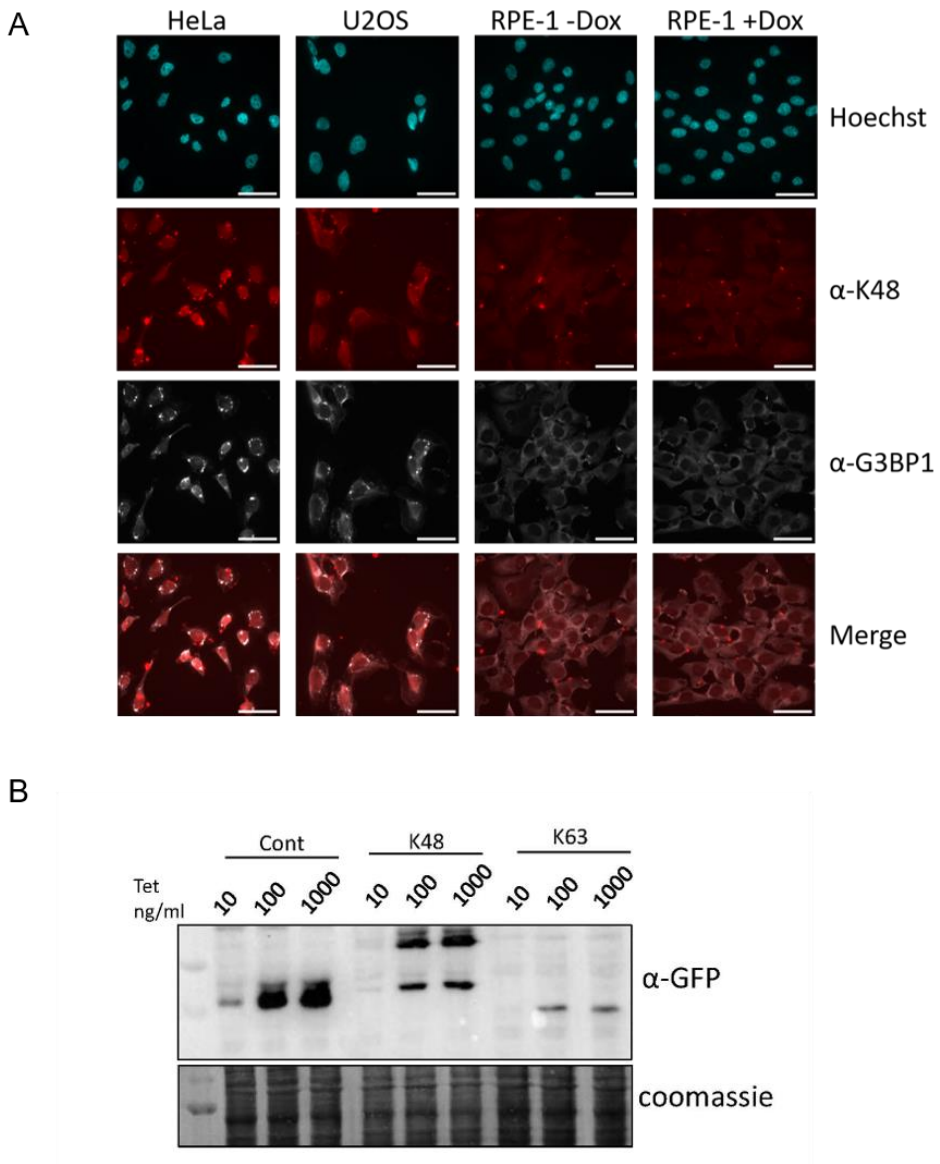

Figure 6.20: Stress granules formation in different cell lines and expression of DARPins in HeLa cells. (A) Fluorescence microscopy of different cell lines to visualize colocalization of K48-linked polyubiquitin and G3BP1 after heat stress (43°C, 2 h). Cells were fixed, permeabilized, stained with Hoechst33342 (blue) and antibodies against K48-linked polyubiquitin chains (red) and G3BP1 (grey) and imaged using the AF7000 microscope. Scale bar = 50 µm. Conducted by Philipp Elleringmann.[482] (B) Western blots showing the expression levels of the anti-K48 and anti-K63 DARPin A1 and G1 as well as E3_5 (Cont) stably integrated in HeLa cells induced by increasing tetracyclin concentrations. DARPins were detected by the antibody against their YFP-tag (alpha-GFP). Coomassie staying as equal loading control. Conducted by Nazife Tolay. Related to Figure 3.18.

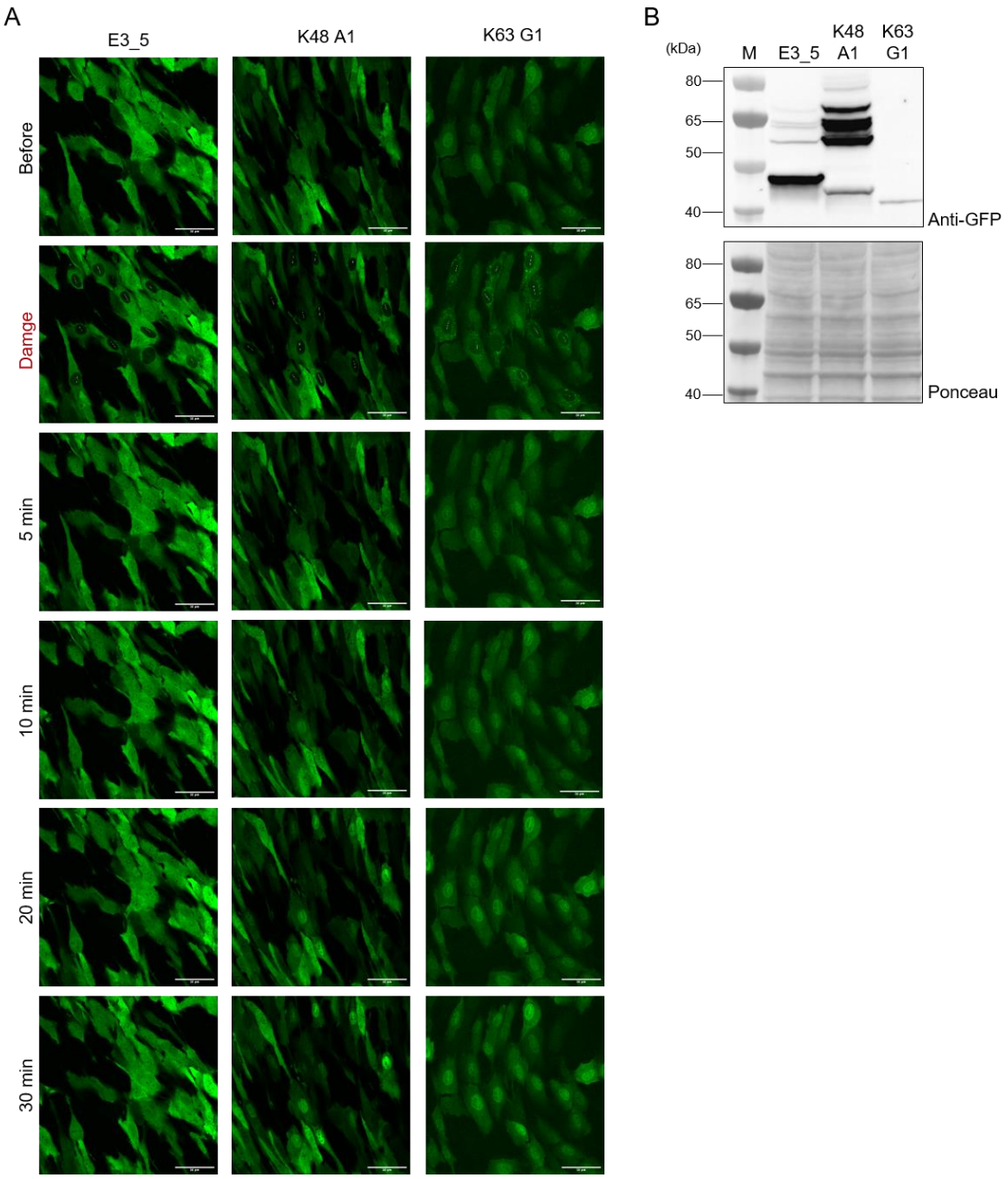

Figure 6.21: Whole microscopy images and expression levels of DARPins used in laser tracks of Figure 3.21. (A) Whole images showing the accumulation of YFP-tagged E3_5, K48 A1 or K63 G1 DARPin respectively at sites of laser-induced DNA damage in RPE-1 cells. Expression of DARPins was induced with 2 ng/µL doxycycline for 24h. The white lines indicates the laser path of the 355 nm laser (50% laserpower) and thereby represents the site of damage inside the living cell. Scale bar = 50 µM. (B) Western blots showing the expression levels of the anti-K48 and anti-K63 DARPin A1 and G1 as well as control E3_5 stably integrated in RPE-1 cells. DARPins were detected by the antibody against their YFP-tag, Ponceau staying as equal loading control. Related to Figure 3.21.

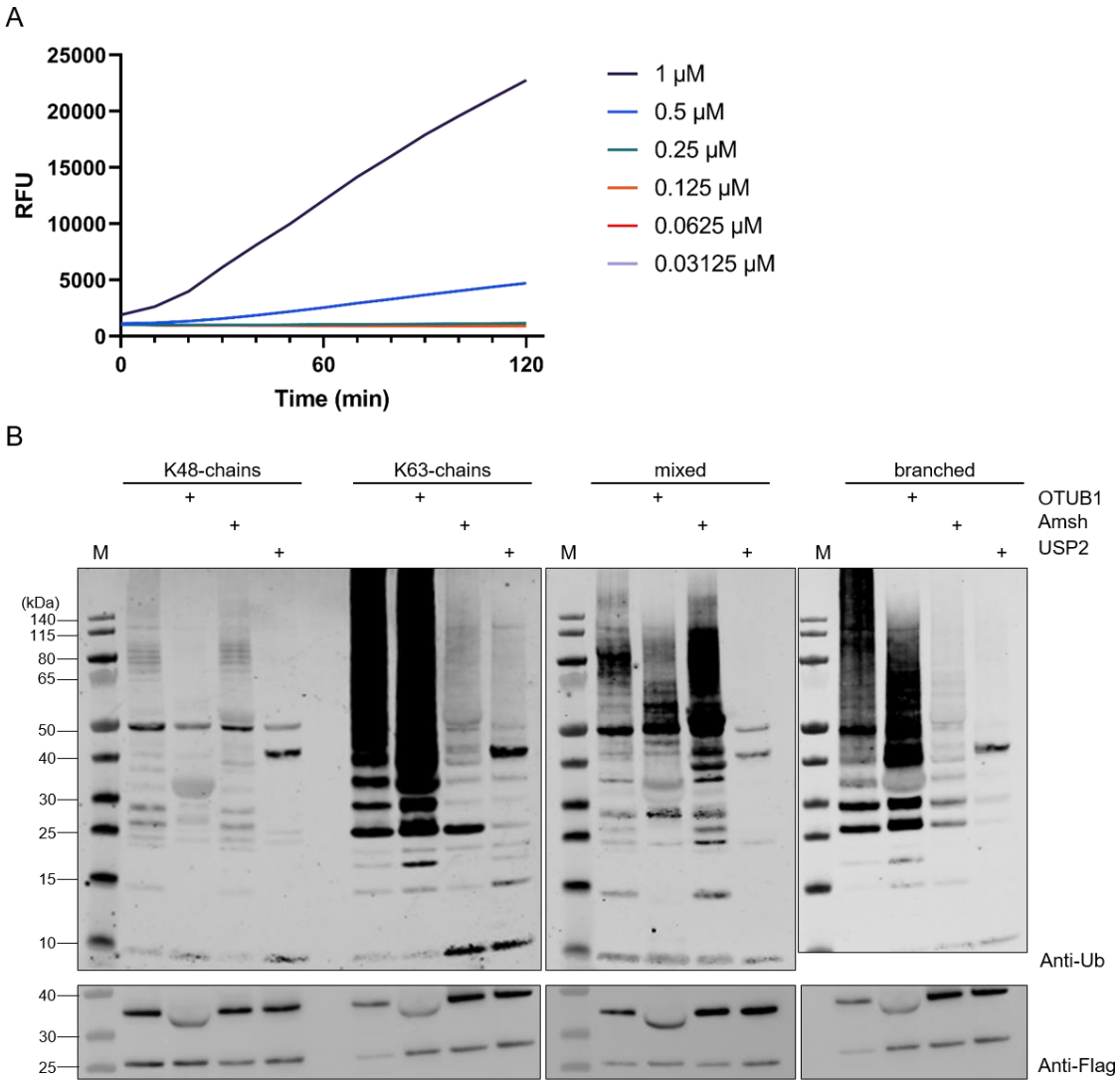

Figure 6.22: Spontaneous complementation screen and UbiCrest of BiFc assays. (A) The threshold concentration of the spontaneously reassociation of the nYFP-tagged DARPin K48 A1 and the cYFP-tagged DARPin K63 G1 was determined by incubating the mixture of the two DARPins in indicated concentrations and measuring the fluorescence signal every 10 min for 2 h using the Tecan Spark. Conducted by Jula Reidel.[560] (B) Western blot images of UbiCRest analyses of the different chains. Samples were after the measurement incubated for 3h with indicated DUB. For each sample, 5 µl were loaded. Equal loading of the DARPins was confirmed by anti-Flag blot. Abbreviations: M = Marker, RFU= relative fluorescence units. Related to Figure 3.22.

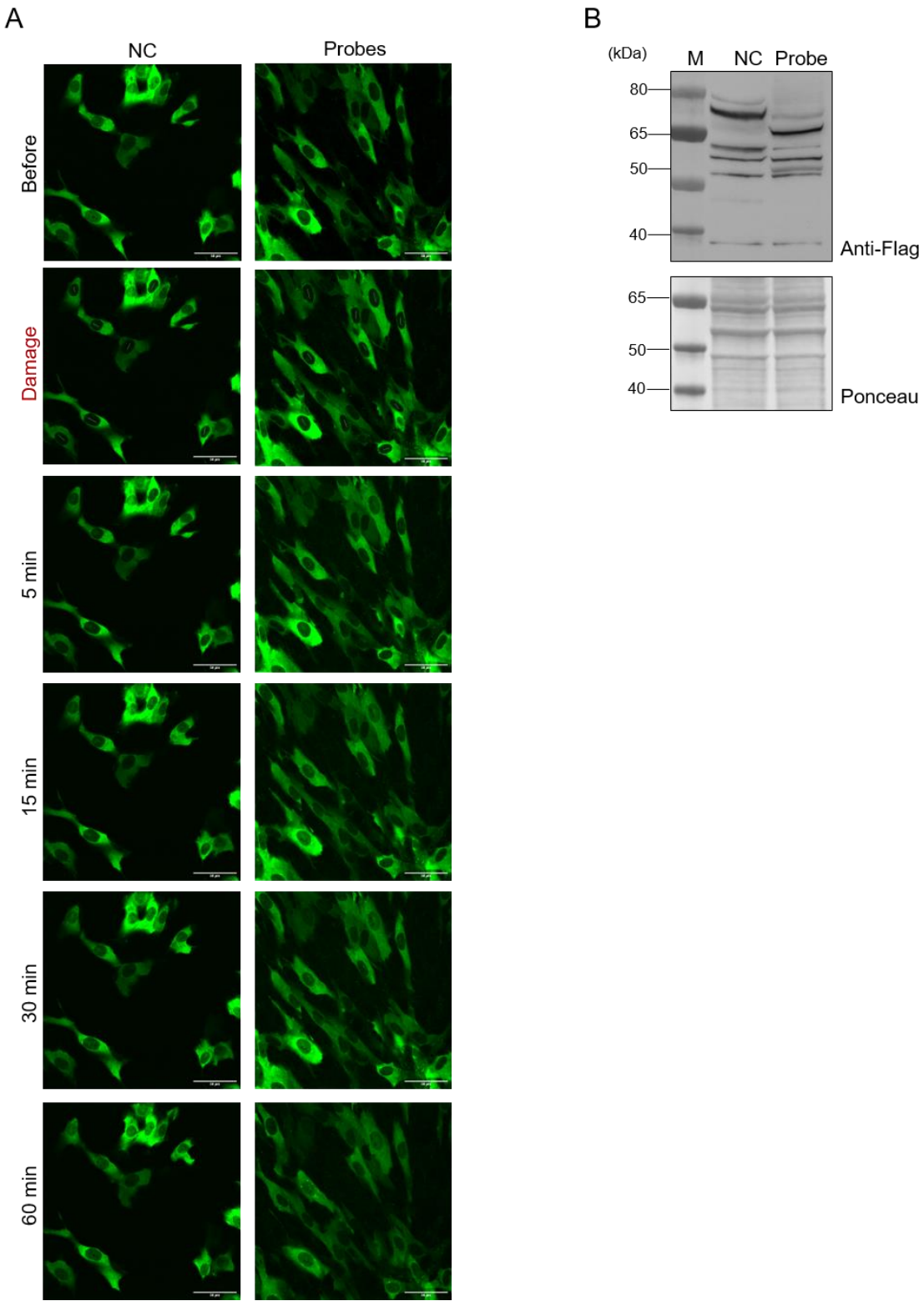

Figure 6.23: Whole microscopy images and expression levels of DARPins used in laser tracks of Figure 3.23. Whole image showing the accumulation of negtive control (nYFP-tagged K48 A1 + c-YFP-tagged E3_5) or BiFc probe (nYFP-tagged K48 A1+and cYFP-tagged K63 G1) respectively at sites of laser-induced DNA damage in RPE-1 cells. Expression of DARPins was induced with 2 ng/µL doxycycline for 24h. The white lines indicates the laser path of the 355 nm laser (50% laserpower) and thereby represents the site of damage inside the living cell. Scale bar = 10 µM. (B) Western blot showing the expression levels of the negative control and the probe (PC) stably integrated in RPE-1 cells. DARPins were detected by the antibody against their Flag-tag, Ponceau staying as equal loading control. Related to Figure 3.23.

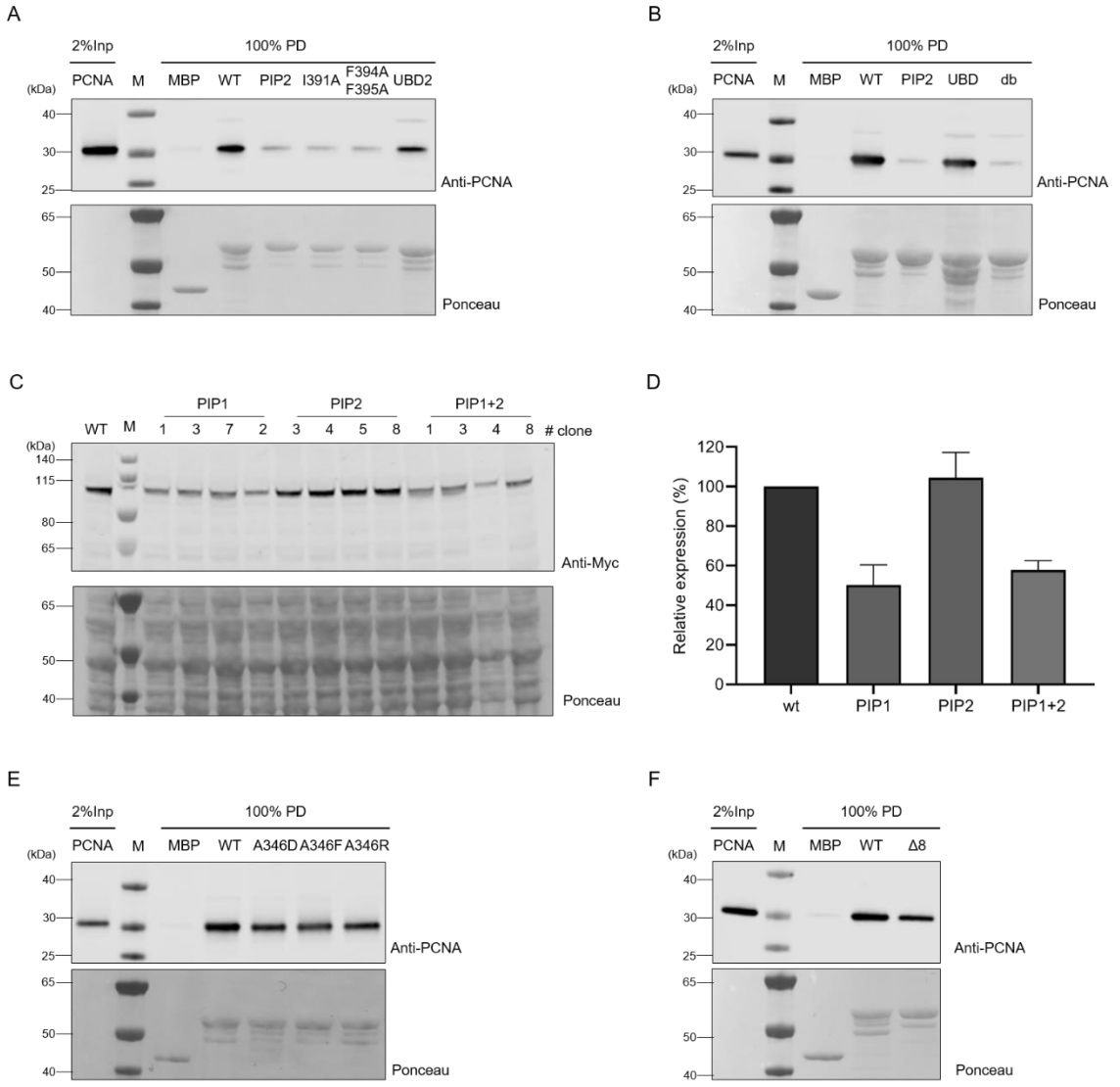

Figure 6.24: Effect of PIP mutations on interaction and expression. (A,B, E, F) Pull-downs to investigate the interaction of wild-type (WT) or indicated PIP or UBD mutants of Exo1 with PCNA. Amylose pull-down was performed with purified MBP-tagged minimal fragment of Exo1 (301-402) and analyzed by Western blotting against PCNA. Free MBP was used as negative control. Ponceau was used for validating equal loading. UBD= I345S and A346G, UBD3= H342A and Δ8 represents the deletion of aa339-346. (C) Western blot for investigating the expression of different clones of indicated PIP mutants tagged with 9-Myc. Ponceau as equal loading control. (C) Quantification of the expression signal according to the Western blot in (D). The signal of wild-type was set to 100%. Measured and analyzed by quantifying the band intensity using the Licore detector and Image Studio software. Related to Figure 4.4 and 4.6.

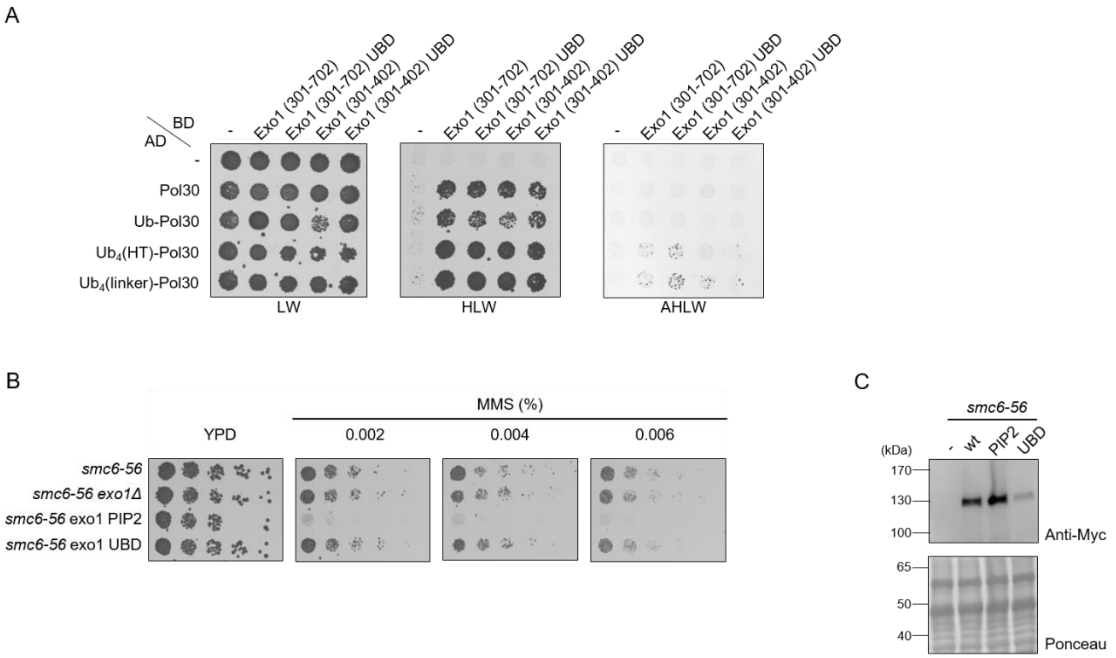

Figure 6.25: Studying influence of PIP and UBD mutations on interaction. (A) Yeast two-hybrid screen investigating the interaction of these different Exo1 wild-type and UBD mutant (BD) with differentially ubiquitylated Pol30 (AD), spotted on plates lacking leucine (L), tryptophan (W), histidine (H) and adenine (A) as indicated and grown for 4 days. Related to Figure 4.6. (B) Effect of MMS damage on a wild-type or MMS sensitive smc6-56 strain in which exo1 is deleted, expressed as wild-type or the indicated mutant. Serial dilutions of relevant strains were spotted onto plates containing the indicated concentrations of MMS. (C) Western blot showing the expression levels of the 9Myc-tagged Exo1 constructs used in (B). Exo1 was detected by the antibody against their 9Myc-tag, Ponceau staying as equal loading control. Related to Figure 4.7.

A

```
SP|P39875|EXO1_YEAST           LYLKDTESKRKRLYACIGFVIHRETQKKQIVHFDDDIDHHLHLKIAQGDLNPYDFHQPLA 360
TR|A0A0L8VIC3|A0A0L8VIC3_9SACH LYLKDTESKRKRLYACIGFVIHRETQKKQIVHFDDDIDHHLHLKIAQGDLNPYDFHQPLA 360
TR|G8ZMH9|G8ZMH9_TORDC         PHLLNCR-E---LYESIGYVVHKSTGSKGCVMNDDDIDHDLHLRIAIGDLNPNNVQKRLV 356
TR|A0A1Q3ACC0|A0A1Q3ACC0_ZYGRO QDLLKCE-K---LYQCIGNVIHKDTQEKQCVVDDCEIHHEKHTLVAMGELNPYNFHNRLV 356
TR|G0WC92|G0WC92_NAUDC         KDLNVES--LKLISQCIGCVIGLESQVKQEIVDENDIDHLLHSRLAFGELHPNDFHKRLV 358
TR|A0A4C2E6G8|A0A4C2E6G8_9SACH QDLLKCE-K---LYQCIGNVIHRDTGEKQCVVNDHEIHHEKHALVAMGELNPYNFHNRLI 356
TR|G0VHT0|G0VHT0_NAUCC         EEKFTAD-DLIILSQCIGNVIHRDSQVKQCVINDEDIDHELHARIANGDLNPYDFHRPLT 359
TR|H0H111|H0H111_SACCK         LHLRDTESKRKKLYECIGHVIHRETQKRQIVHFDNDIDHHLHFKIAQGDLNPYDFHQPLA 360
TR|A0A7G3ZBE6|A0A7G3ZBE6_9SACH EHLANCQ-E---LYDSIGHVIDRNTQVKECVMDDDRIHHDLHLKIAIGDLSPYDFRKRLV 356
TR|A0A7H9HUZ8|A0A7H9HUZ8_9SACH GHLTNCQ-E---LYDSIGHVIDRNTQIKECVMDDDKIHHDLHLKIAIGDLNPYDFRKRLV 356
UPI001458F090                  LYLKDTESKRKKLYECIGLVIHREAQKKQIVHFDDDIDHHLHLKIAQGDLNPYDFHQPLA 360
                                           :  .** *:  .:  :  :  :  *.*  *  :* *:* * :.:. *

SP|P39875|EXO1_YEAST           NREHKLQLASKSNIEFGKT----NTTNSEAKVKPIESFFQKMTKLDHNPKV--AN----- 409
TR|A0A0L8VIC3|A0A0L8VIC3_9SACH NREHKLQLASKSNIEFGKT----NSTNSEAKVKPIESFFQKMTKLDHNPKV--AN----- 409
TR|G8ZMH9|G8ZMH9_TORDC         NREHKLQLTSKSELQVE------NSKS-RPAVGSIDSFFSQATIDNKIPKL--T------ 401
TR|A0A1Q3ACC0|A0A1Q3ACC0_ZYGRO NREHKLQLSSKSEGPAVKA----FTGN-ASTASSVDSFFQKLGTPAT------Q------ 399
TR|G0WC92|G0WC92_NAUDC         NREHKLQLVSKSEAQISLTGELIDSTANKENNKPIDSFFRRIEKKSSSKAKNKSLISKNQ 418
TR|A0A4C2E6G8|A0A4C2E6G8_9SACH NREHKLQLSSKSEGPAVNI----STGN-VSTGSSIDSFFQKSGTLKT------Q------ 399
TR|G0VHT0|G0VHT0_NAUCC         NREQKLQLVSKSEMGIS-I----PSKN-QGETKGIDSFFKKTALKVTEKKA--VNVVQNK 411
TR|H0H111|H0H111_SACCK         NREHKLQLVSKSNLEFGNS----NINCTGVKNKPIESFFHKVQGGDHASKV--GT----- 409
TR|A0A7G3ZBE6|A0A7G3ZBE6_9SACH NREHKLQLSSKSDLQVE------LHDN-TPKKRSIDSFFSKKKD--SGAKE--N------ 399
TR|A0A7H9HUZ8|A0A7H9HUZ8_9SACH NREHKLQLSSKSDLQMG------LNDN-TPKNRSIDTFFSKQKD--NSAKE--N------ 399
UPI001458F090                  NREHKLQLASKSNLEFRKT----NTSSSEVKIKPIESFFQKMTKSDHTPKV--AN----- 409
                               ***:**** ***:                   :::** :
```

B

```
SP|P39875|EXO1_YEAST LNEIPLYLKDTESKRKRLYACIGFVIHRETQKKQIVHFDDDIDHHLHLKIAQGDLNPYDF 355
SP|P53695|EXO1_SCHPO LSPPERELSVHE------DAFIGSFFD----------------NQLAIDIAEGRSNPITK 331
SP|Q9UQ84|EXO1_HUMAN LNAYEDDVDPET------LSYAGQYVD----------------DSIALQIALGNKDINTF 335
SP|Q9QZ11|EXO1_MOUSE LNAYGDDVNPET------LTYAGQYVG----------------DSVALQIALGNRDVNTF 335
SP|Q24558|EXO1_DROME LCALEDYETDER-----YCSNAGTLLE---------------DSEQALHLALGNLNPFSM 339
                     *                 :  *  .                    :.:* *  :

SP|P39875|EXO1_YEAST HQPLANRE-HKLQLASKSNIEFGKTNTTNSEAKVKPIESFFQKMTK-------LDHNPKV 407
SP|P53695|EXO1_SCHPO CAFDIKDS--SMQSFTKTTITISKRK----GISKTDISNFFMKSIPPSKR-------PTK 378
SP|Q9UQ84|EXO1_HUMAN EQIDDYNPDTAMPAHSRS-HSWDDKT----CQKSANVSSIWHRNYSPRPESGTVSDAPQL 390
SP|Q9QZ11|EXO1_MOUSE EQIDDYSPDT-MPAHSRS-HSWNEKA----GQKPPGTNSIWHKNYCPRLEVNSVSHAPQL 389
SP|Q24558|EXO1_DROME KRLDSWTPEKAWP----------TPK----NVKRSKHKSIWQTNFQSENTHTP------K 379
                                              .    ..::

SP|P39875|EXO1_YEAST ANNIHSLRQAEDKLTMAIKRRKLSNANVVQET---LKDTRSKFFNKPS---MTVVENFKE 461
SP|P53695|EXO1_SCHPO S--TSLIDVTNV---K-VQRTHLANDISSEKQSI--KSANE---KAYVTPKSNSLKPGFG 427
SP|Q9UQ84|EXO1_HUMAN KENPSTVGVERV---ISTKGLNLPRKSSIVKRPRSAELSEDDLLSQYSLSFTKKTKKNSS 447
SP|Q9QZ11|EXO1_MOUSE KEKPSTLGLKQV---ISTKGLNLPRKSCVLKRPRNEALAEDDLLSQYSSVSKKIKENGCG 446
SP|Q24558|EXO1_DROME KENPCALFFKKV---D-FVGKTLNEEIEANQRLEQAKQTEAELFNMYSFKAKRRRSPSRE 435
                         :   .          * .     :       :.    .          .
```

Figure 6.26: Sequence alignments of Exo1 from different species. (A,B) The sequence of Exo1 from different yeast (A) and more broad species (B) was aligned using the align tool on UniProt (https://www.uniprot.org/).

7 Curriculum Vitae

Personal information

Name:	Tina Strauch
Date of birth:	18.06.1993
Place of birth:	Gelnhausen
Nationality:	German
Address:	Albert-Schweitzer Str. 17a, 55128 Mainz
E-mail	Strauch.tina@web.de

Education

09/2019 — present **PhD studies** (Dr. rer. nat.)
Institute of Molecular Biology (IMB), Mainz (Prof. Dr. Ulrich)
- *Functional analysis of polyubiquitin chain linkage in genome maintenance*
- Protein biochemistry
- Student of the International PhD Program (IPP)

10/2016 — 06/2019 **Master's degree program in biomedicine Chemistry**
Johannes Gutenberg University, Mainz
- **Master's thesis** at the Institute of Molecular Biology (IMB) (Prof. Dr. Ulrich): *Characterization of selective K48- and K63-polyubiquitin binders* (Final grade: 1.1)
- Grade point average: 1.8

10/2013 — 02/2017 **Bachelor's degree program in biomedicine Chemistry**
Johannes Gutenberg University, Mainz
- **Bachelor's thesis** at the institute of pharmacy and biochemistry (Prof. Dr. Hellmich): *Essential proteins of the parasitic iron- and thiolhomeostasis of T. brucei* (Finale grade: 1.0)
- Grade point average: 1.8

09/2003 — 06/2012 **Albert-Einstein-Schule** (High School), Schwalbach
- Abitur (A-levels) with grade 1.3

Publications

Yakoub G, Choi YS, Wong R, **Strauch T**, Ann KJ, Cohen RE, Ulrich HD. "Avidity-based biosensors for ubiquitylated PCNA reveal choreography of DNA damage bypass" *Science Advances*, **2023**; 9(36):eadf3041. (doi: 10.1126/sciadv.adf3041)

Shi J, Hauschulte K, Mikicic I, Maharjan S, Arz V, **Strauch T**, Heidelberger JB, Schaefer JV, Dreier B, Plückthun A, Beli P, Ulrich HD, Wollscheid HP. "Nuclear myosin VI maintains replication fork stability."*Nat Commun.* **2023**; 14(1):3787. (doi: 10.1038/s41467-023-39517-y)

Lueckerath T, **Strauch T**, Koynov K, Barner-Kowollik C, Ng DYW, Weil T "DNA-Polymer Conjugates by Photoinduced RAFT Polymerization." *Biomacromolecules* **2019**; 20(1), 212-221. (doi: 10.1021/acs.biomac.8b01328)